

FACULTY OF ENGINEERING TECHNOLOGY
DEPARTMENT OF CIVIL ENGINEERING
MATERIALS AND CONSTRUCTIONS, GHENT CAMPUS
Gebroeders De Smetstraat 1
9000 GHENT, BELGIUM
harry.hermawan@kuleuven.be
<https://iiw.kuleuven.be/onderzoek/Building-materials>



Harry Hermawan

OPTIMISED MIX DESIGNS FOR SELF-HEALING CONCRETE

December 2023

KU LEUVEN

ARENBERG DOCTORAL SCHOOL
FACULTY OF ENGINEERING TECHNOLOGY

A joint PhD thesis with



UNIVERSITAT
POLITÈCNICA
DE VALÈNCIA

Optimised Mix Designs for Self- Healing Concrete

Harry Hermawan

Dissertation presented in partial
fulfilment of the requirements for the
degree of Doctor of Engineering Technology
from KU Leuven and the degree of Doctor
from Universitat Politècnica de València

December 2023

OPTIMISED MIX DESIGNS FOR SELF-HEALING CONCRETE

Harry HERMAWAN

Examination committee:

Prof. Michael Kleemann, chair

Prof. Elke Gruyaert, supervisor

Prof. Pedro Serna, supervisor
(Universitat Politècnica de València)

dr. Virginie Wiktor (Cugla B.V.)

Prof. Veerle Vandeginste

Prof. Jean-Marc Tulliani (Politecnico di Torino)

Prof. Antonios Kanellopoulos (University of Hertfordshire)

Prof. Marta Roig Flores (Universitat Jaume I)

Dissertation presented in partial
fulfilment of the requirements for the
degree of Doctor of Engineering
Technology from KU Leuven and the
degree of Doctor from Universitat
Politècnica de València

December 2023

© 2023 HARRY HERMAWAN

Uitgegeven in eigen beheer, HARRY HERMAWAN, GENT - BELGIUM

Alle rechten voorbehouden. Niets uit deze uitgave mag worden vermenigvuldigd en/of openbaar gemaakt worden door middel van druk, fotokopie, microfilm, elektronisch of op welke andere wijze ook zonder voorafgaandelijke schriftelijke toestemming van de uitgever.

All rights reserved. No part of the publication may be reproduced in any form by print, photoprint, microfilm, electronic or any other means without written permission from the publisher.

ACKNOWLEDGEMENTS

Embarking this PhD journey is a very long, intensive and exhausting process and I cannot reach this milestone by myself. I am sincerely grateful to be surrounded by many positive and inspiring colleagues, friends and family that always encourage me for every path that I take and genuinely help me with everything both academically and socially. Therefore, I would like to appreciate all these people with my generous words.

First of all, I would like to express my deepest gratitude to Prof. Elke Gruyaert as my promotor that always supports me from the start until the end of my PhD. She has been a very nice and helpful professor, colleague and friend that I can rely on and she is always taking care of me like my mother in Belgium. Her comprehensive knowledge, patient guidance and constructive suggestions as well as professionalism are the ones that I learned a lot from her and I am grateful that she shapes me from an amateur to a skilled researcher. It has been an honor to share and work together in the laboratory and I cherish every moment I spent with her. Finally, I thank her for everything and wish her the best for the future.

Another biggest contributor in my research is Prof. Pedro Serna that I must gratefully acknowledge. I thank him for his inspiring guidance and broad experience in concrete technology. I enjoyed very much both working and networking with him especially during my research stay in Valencia despite my broken Spanish. He taught me how to be a good researcher and working hard is a success key. I appreciate his passion as a professor and his humble words that make me a better person. I should also acknowledge him for sincerely helping me to solve all difficulties that I encountered in Valencia starting from the administration, research barriers and any unfortunate events.

I wish to thank Prof. Dimitrios Aggelis, Prof. Antonios Kanellopoulos and Prof. Yaghoob (Amir) Farnam for being external reviewers and for their generosity in reviewing my dissertation. Their constructive feedback are very helpful to

enrich the quality of my dissertation and they are thanked for their contributions until I eventually finalize this dissertation.

I would like to thank dr. Virginie Wiktor, Prof. Veerle Vandeginste, Prof. Jean-Marc Tulliani, Prof. Antonios Kanellopoulos and Prof. Marta Roig Flores for their willingness in joining the Doctoral Examination Committee and their big effort in reviewing and discussing my research works. It was my honor having them as the jury of my PhD defences and their impactful suggestions are very much appreciated. Prof. Michael Kleemann is also thanked for his willingness to becoming a chair for my PhD defences and his leadership is very much appreciated.

I want to thank Prof. Maarten Vergauwen for his careful evaluation on my PhD milestones in KU Leuven – Gent. Thanks to him that I participated in many social events among our research groups.

A special thank is delivered to Peter Minne who is sharing the good time with me in the laboratory. He is the first person who taught me about the advanced concrete mix design with his well-developed tool. I gained a lot of insight about the concrete technology and he is always open for any fruitful discussion whenever I asked him. Also, I enjoy chatting random stuffs with him about the research, life, foods, jokes and future.

I wish to acknowledge Virginie Wiktor for her expertise during the 2 months secondment in Cugla, the Netherlands. It was totally a new world for me learning about the admixture for concrete and she always approaches me every time I work in the laboratory. She has been a very nice colleague to me and many thanks for your present on my last day in Cugla which was also coincidence with my 27th birthday. Also, other Cugla colleagues are thanked for their support such as Henriëtte Dikmans for allowing me to work in the renowned R&D company; Hans Huppertz for sharing his knowledge about the superplasticizers; and Guadalupe Sierra Beltran (Lupita) for her genuine assistance in running the experiments and thanks to her I had a chance to visit her coffee shop and tasted coffee from different countries.

I would like to express my gratitude to my beloved colleagues from Buzzi Unicem (BUILT), Italy. During my one-month secondment in Vercelli, I gained valuable knowledge and experience about the cement chemistry and the microstructural investigations. I wish to thank Fulvio Canonico for his leadership and hospitality; Daniela Gastaldi for her care and intensive training; Merlo Valentino for his great mentorship; Ippolito Mirko for being a nice buddy; Dell'Anno Gabriella for her exhaustive ride during our long trip

to the cement plant in Robilante; and all BUILT colleagues that I cannot mention one-by-one.

This acknowledgement would be incomplete without the recognition of amazing technicians that essentially contribute to the success of my experimental works.

I highly acknowledge the never-ending helps from Bram Gezels since the first time I came to KU Leuven – Gent. He is the most helpful colleague that I have ever met and I always consider him as a true model of a good colleague. His dedication to the work in the laboratory is praiseworthy. I always find him comfortable in every moment that I shared with him in the office and laboratory, and he handles all lab issues professionally where I learned this attitude thanks to him. I wish to appreciate Roger Pieri who has been a new technician in the KU Leuven – Gent campus. He is a very positive person who is always excited with his works and he is willing to help other colleagues although we do not ask any. It is my pleasure to work together with him and for sure his contribution to my research works should be appreciated. Bart de Vos, a former technician at KU Leuven – Gent, is also thanked for always making time for me whenever I need him in the laboratory. I would like to thank Francisco Martorell for his aid in fabricating the mould set and experimental setups during my secondment in UPV. Although I cannot communicate very well with him due to the language barrier, he always tries his best to aid me in any situations and I still remember that I spent most of my days in Valencia with him to test concrete specimens and he always makes sure that I am doing fine. A former PhD student from UPV which is now becoming an assistant professor in Universitat Jaume I, Marta Roig-Flores, is also thanked for her technical recommendations regarding the experimental tests for self-healing concrete.

I am able to survive throughout this PhD journey thanks to the continual support from my lab mates in KU Leuven – Gent: Zhuomin Zou, Suqin Liu, Hanne Vanoutrive and Eirini Mingou; my lab mates in UPV: Kiran Dabral, Hesam Doostkami and Marta Caballero; and all Early Stage Researchers (ESRs) from SMARTINCS: Yasmina Shields, Claire Riordan, Mustafa Mert Tezer, Sina Sayadi Moghadam, Suelen de Rocha Gomes, Priya Arul Kumar, Shan He, Gabriele Milone, Niranjan Prabhu, Vanessa Giaretton Cappellesso, Pardis Pourhaji, Kiran Dabral, Davide di Summa and Lais Bandeira Barros. They are the talented researchers that share the same path as myself to reach the PhD and I am lucky to have made such great friends. Specifically for SMARTINCS ESRs, a big thank for sharing your passion in doing research,

making deliverables together, developing collaborative works, exchanging ideas, travelling during the training schools, having great time whenever we meet and supporting each other for our success.

I wish to acknowledge SMARTINCS consortium for their wonderful feedback and togetherness that we spent for 3 years long. Specifically, I would like to thank Prof. Nele de Belie, Prof. Kim van Tittelboom and Tim van Mullem from Ghent University as they always give me valuable input to advance my PhD research. Also, I should thank Prof. Liberato Ferrara who acted as WP1 leader and his amazing works always inspire me to step further into my research.

I also should appreciate Gerda Friant from KU Leuven – Gent who is always ready to help me with the administration during my PhD period. Also, big thanks to my warm colleagues: Veerle de Swaef, Micheline Bekaert and Lies van Der Straeten for their open hands and assistance when I worked in their laboratory.

I have to appreciate the helps from my former Master students: Alicia Simons, Silke Teirlynck, Seppe van Der Sichel and Louis Lust for doing their best in performing experimental works related to my PhD topic. Few parts in this PhD thesis would not exist without their hard works. Guiding them for their Master theses allows me to get experience of being a co-supervisor and I had a good time teaching them in the laboratory.

The development of this thesis was made possible thanks to many collaborations from the academic and industrial worlds. I would like to acknowledge Prof. Paola Antonaci, Prof. Jean-Marc Tulliani and Giovanni Anglani from Politecnico di Torino for our nice collaboration on the use of macrocapsules. I wish to acknowledge Prof. Abir Al-Tabbaa from University of Cambridge, Dave Palmer and Claire Riordan from Micropore Technologies for the motivated collaboration to advance the utilization of microcapsules in the concrete composite. Next, I want to acknowledge Prof. Nele de Belie from Ghent University, Prof. Willy Verstraete and Mustafa Mert Tezer from Avecom for our great collaboration on the use of biomass agents for self-healing concrete. I would like to thank Prof. Henk M. Jonkers from TU Delft and Enricomaria Gastaldo Brac from Penetron Italia for the donation of their healing agents and for fruitful discussion until I could optimally use their materials. It has been my honor to work with these inspiring colleagues. For what concerns the industrial partner, I want to thank CBR, LafargeHolcim, Masaveu Industria and Buzzi Unicem for providing cements, Demula and Cugla for providing superplasticizers, InterBeton for providing coarse aggregate, ZEUS for providing polymeric tubes, Basilisk for providing

bacterial healing agent, Penetron Italia for providing crystalline admixture, Avecom for providing biomass agents and Micropore Technologies for providing microcapsules.

Working in Europe is one of the best experiences in my life and without the generous funding from the European Commission I would not be able to make it. It has been my honor to work in the SMARTINCS project as an ESR4. This project has received funding from the European Union's Horizon 2020 research and innovation programme under the Marie Skłodowska-Curie grant agreement No 860006. Thanks to this prestigious project and its consortium, I developed management skills that I never learned before. The SMARTINCS training schools were very helpful to develop my research activities in a very stimulating international environment and to do networking with many motivated colleagues.

I want to acknowledge emotional support and big encouragement from my Indonesian friends: Fariz Rifqi Zul Fahmi, Herry Suryadi Djayaprabha, Stefani Sitanggang, Deser Christian Wijaya, Vina Setiawan, Listia Rini, Nor Kamariah, Susana Endah, Suci Puspita Sari, Indria P. Sumardi, Anis R. Amna, Anik Juli, Satria Loka, Sekar Sedyana and all members of IndoSAG PPI Ghent.

Last but not least, this treasured thesis is dedicated to my beloved parents, Hendra Hermawan and Lilis Kusmiati who always give me never-ending support and prayer to wish me happy and healthy every day and also they always give me everything that I need. Their unconditional love has always been a source of strength and resilience for me. I also want to dedicate my thesis to my brother, Erik Hermawan who gives me a lot of enthusiastic support and advices.

Finally, I would like to thank KU Leuven and UPV for giving me opportunity to study and work in two of the best universities in the world and I am honored to be a joint PhD awardee from both universities.



Harry Hermawan



This project has received funding from the European Union's Horizon 2020 research and innovation programme under the Marie Skłodowska-Curie grant agreement No 860006.

ABSTRACT

(English version)

Concrete has been widely used as a major material for infrastructure works. The durable character and the advantageous price-quality ratio compared to other materials have made concrete indispensable in the modern era. However, cracks in concrete structures are inevitable and are known as one of the inherent weaknesses of concrete, thereby making a threat to the durability of infrastructure which can lead to unsafe conditions. There are many repair techniques to seal and heal the cracks, but these approaches are costly and time-consuming. Therefore, during past years, many researchers searched for alternatives to solve these problems by developing a new generation of concrete namely self-healing concrete. Self-healing technologies have proven to effectively close cracks partially or fully in the cementitious system. However, studies on the concrete level are still rather limited and in most cases, the mix designs were not optimized for the introduction of healing agents.

Based on a comprehensive literature, it was revealed that not all healing/sealing agents induce positive effects to the concrete properties. Consequently, an optimization of the mix designs is necessary to guarantee that these agents do not negatively affect the concrete properties to some extent. In this PhD dissertation, a wide range of healing/sealing agents were utilized such as bacteria (BAC), crystalline admixture (CA), biomasses, micro- and macro-encapsulated agents. Prior to the introduction of these agents into the concrete, the compatibility between healing/sealing agents and cementitious materials was evaluated to serve as a basic input for designing the concrete mixtures.

The optimizations of concrete mix designs were carried out depending on the choice of the agents and the research objectives. When using CA, it was found that increasing the CA dosage and cement content in the mix design

improved the healing efficiency (HE) and sealing efficiency (SE). Varying the water-cement ratio (w/c) did not give a remarkable improvement of HE and SE. A deep insight in the bond properties between the steel reinforcement and the self-healing concrete matrix was achieved. The inclusion of healing agents (i.e., BAC, CA, biomasses) possessed a bond strength improvement with the highest enhancement of 57% attained by the CA addition. Although the presence of a longitudinal crack critically reduced the bond strength, a bond restoration was achieved due to self-healing effects. Dual effects of using microcapsules were found, confirming a significant reduction of mechanical strength and a significant sealing improvement. Therefore, the mix design parameters were optimized to compensate the strength reduction via full factorial designs. With respect to the inert structure, the incorporation of macrocapsules tended to disturb the packing of aggregates. Hence, a modified particle packing model was developed to predict the voids ratio of aggregate-capsules mixtures.

All in all, the outcome of this PhD research can serve as a guidance to understand the contribution of mix design parameters affecting the self-healing concrete properties. This potentially helps researchers and engineers to formulate their concrete mixtures for self-healing application.

(Dutch version)

Beton wordt op grote schaal gebruikt als een belangrijk materiaal voor infrastructuurwerken. Het duurzame karakter en de gunstige prijs-kwaliteitverhouding ten opzichte van andere materialen hebben beton in de moderne tijd onmisbaar gemaakt. Scheuren in betonconstructies zijn echter onvermijdelijk en staan bekend als één van de inherente zwakheden van beton, waardoor ze een bedreiging vormen voor de duurzaamheid van infrastructuur, wat kan leiden tot onveilige omstandigheden. Er zijn veel reparatietechnieken om de scheuren af te dichten en te herstellen, maar deze interventies zijn duur en tijdrovend. Daarom hebben veel onderzoekers de afgelopen jaren gezocht naar alternatieven om deze problemen op te lossen door een nieuwe generatie beton te ontwikkelen, namelijk zelfhelend beton. Het is bewezen dat zelfhelende technologieën scheuren in het cementgebonden systeem gedeeltelijk of volledig dichten. Studies op het niveau van beton zijn echter nog vrij beperkt en in de meeste gevallen zijn de mengselontwerpen niet geoptimaliseerd voor de introductie van helende agentia.

Op basis van een uitgebreide literatuur werd onthuld dat niet alle helende/afdichtende middelen positieve effecten hebben op de betoneigenschappen. Bijgevolg is een optimalisatie van de mengselontwerpen nodig om te garanderen dat deze middelen de betoneigenschappen niet negatief beïnvloeden in mindere of meerdere mate. In dit doctoraatsproefschrift werd een breed scala aan helend agentia en afdichtingsmiddelen gebruikt, zoals bacteriën (BAC), kristallijne toevoegsels (CA), biomassa's, micro- en macro-ingekapselde middelen. Voorafgaand aan de introductie van deze middelen in het beton, werd de compatibiliteit tussen deze helende/afdichtende middelen en de cementgebonden materialen geëvalueerd om als basisinput te dienen voor het ontwerp van de betonmengsels.

De optimalisaties van de betonmengselontwerpen werden uitgevoerd afhankelijk van de keuze van de helende/afdichtende middelen en de onderzoeksdoelstellingen. Bij het gebruik van CA bleek dat het verhogen van de CA-dosering en het cementgehalte in het mengselontwerp leidde tot een verbetering van de zelfhelende efficiëntie (HE) en zelfafdichtende efficiëntie (SE). Het variëren van de water-cementverhouding (w/c) gaf geen opmerkelijke verbetering in HE en SE. Daarnaast werd een diepgaand inzicht verkregen in de hechtingseigenschappen tussen de wapening en de zelfhelende betonmatrix. De toevoeging van helende middelen (hier BAC, CA, biomassa) zorgde voor een verbetering van de hechtsterkte, waarbij de toevoeging van CA tot de hoogste verbetering van 57% leidde. Hoewel de aanwezigheid van longitudinale scheuren de hechtsterkte kritisch verminderde, werd een herstel van de hechting bereikt door zelfhelende effecten. Bij het gebruik van microcapsules werden duale effecten vastgesteld: een significante vermindering van de mechanische sterkte en een significante verbetering van de afdichting. Om de sterktevermindering te compenseren werden de parameters voor het mengselontwerp geoptimaliseerd via volledig factorieel ontwerp. Als laatste werd aangetoond dat de toevoeging van macrocapsules de neiging had om de pakking van de granulaten te verstoren. Een aangepast pakkingsmodel werd ontwikkeld om de holle ruimte ratio van mengsels van granulaten en capsules beter te voorspellen.

Globaal bekeken kan het resultaat van dit doctoraatsonderzoek dienen als leidraad om de bijdrage van mengselontwerpparameters die de eigenschappen van zelfhelend beton beïnvloeden beter te begrijpen. Dit kan onderzoekers en ingenieurs helpen bij het formuleren van hun betonmengsels voor zelfhelende toepassingen.

(Spanish version)

El hormigón es considerado como uno de los principales materiales de construcción más ampliamente utilizado en obras de infraestructuras. Su consideración como material de gran durabilidad y su ventajosa relación calidad-precio en comparación con otros materiales le ha hecho indispensable en la era moderna. Sin embargo, las fisuras son prácticamente inevitables en las estructuras de hormigón armado y se consideran como uno de sus puntos débiles, ya que comprometen la durabilidad de las infraestructuras y pueden generar condiciones inseguras. Hay muchas técnicas de reparación para sellar y sanar las fisuras, pero suelen ser costosas y requieren tiempo de intervención. Por esta razón, en los últimos años, se han realizado muchas investigaciones buscando alternativas para resolver estos problemas desarrollando una nueva generación de hormigones que se han denominado hormigones auto sanables. Se ha demostrado que las tecnologías de auto sanado cierran eficazmente las fisuras parcial o totalmente en un sistema cementoso. Sin embargo, los estudios a nivel del hormigón son todavía bastante limitados y en la mayoría de los casos las dosificaciones de la mezcla no fueron optimizados para la introducción de agentes de autosanado.

Del estudio amplio de la literatura se aprecia que la incorporación de agentes de autosanado no siempre conllevan efectos positivos en las propiedades del hormigón. En consecuencia, según el tipo de agente de sellado/sanado, será necesario optimizar la dosificación para garantizar que no reduce en alguna medida las prestaciones del hormigón colocado. Se analiza un amplio espectro de agentes de sanado/sellado: bacterias (BAC), adiciones cristalinas (CA), biomasas y agentes incorporados en micro o macro cápsulas. Previamente a su introducción en el hormigón se evaluó su compatibilidad con los materiales cementosos, como información básica para el diseño de las mezclas. La optimización del diseño de las mezclas de hormigón se llevó a cabo dependiendo del agente elegido y los objetivos de la investigación. Al utilizar CA, se encontró que aumentar su dosis y el contenido en cemento conducía a mejorar la eficiencia de curación (HE) y la de sellado (SE). La variación de la relación agua-cemento (a/c) no produjo una mejora notable de HE y SE. Se profundizó el conocimiento sobre las propiedades de adherencia entre las armaduras y la matriz de hormigón. La inclusión de agentes de sanado (BAC, CA, biomasas) conllevó la mejora de la adherencia con un crecimiento del 57% cuando se adiciona CA. Aunque la presencia de

fisuras longitudinales redujo críticamente la adherencia, se logró una recuperación importante gracias a los efectos del auto sanado. Se encontraron efectos contrapuestos del uso de microcápsulas. Se confirma una reducción significativa de la resistencia mecánica y una mejora significativa del sellado. Los parámetros de diseño de mezcla se optimizaron para compensar la reducción de resistencia, con un programa experimental con diseño factorial completo. Por la estructura inerte, las macrocápsulas tiende a perturbar el empaquetamiento de los áridos. Para la optimización de la mezcla se desarrolló un modelo de empaquetamiento de partículas modificado para predecir la proporción de huecos de las mezclas de áridos y cápsulas.

Con todo, el resultado de esta investigación puede servir como guía para comprender la contribución de los parámetros de diseño de mezclas que afectan las propiedades de auto sanado, que potencialmente ayudará a investigadores e ingenieros a formular mezclas de hormigón para aplicaciones de auto sanado.

(Valenciano version)

El formigó és considerat un dels principals materials de construcció més àmpliament utilitzat en obres d'infraestructures. La seua consideració com a material de gran durabilitat i la seua relació qualitat-preu avantatjosa en comparació amb altres materials l'ha fet indispensable en l'era moderna. Tot i això, les fissures són pràcticament inevitables en les estructures de formigó armat i es consideren com un dels seus punts febles, ja que comprometen la durabilitat de les infraestructures i poden generar condicions insegures. Hi ha moltes tècniques de reparació per segellar i curar les fissures, però solen ser costoses i requereixen temps d'intervenció. Per aquesta raó, en els darrers anys, s'han realitzat moltes investigacions buscant alternatives per resoldre aquests problemes desenvolupant una nova generació de formigons que s'han anomenat formigons auto sanables. S'ha demostrat que les tecnologies de auto curat tanquen eficaçment les fissures parcialment o totalment en un sistema de ciment. Tot i això, els estudis a nivell del formigó són encara força limitats i en la majoria dels casos les dosificacions no van ser optimitzades per a la introducció d'agents d'auto curat.

De l'estudi ampli de la literatura s'aprecia que la incorporació d'agents d'auto curat no sempre comporta efectes positius en les propietats del formigó. En

conseqüència, segons el tipus d'agent de segellat/curat, cal optimitzar la dosificació per garantir que no redueix en alguna mesura les prestacions del formigó. S'analitza un ampli espectre d'agents de curat / segellament: bacteris (BAC), addicions cristal·lines (CA), biomassa i agents incorporats en micro o macro càpsules. Prèviament a la seua introducció al formigó es va avaluar la compatibilitat amb els conglomerants, com a informació bàsica per al disseny de mescles. L'optimització del disseny de les mescles de formigó es va dur a terme depenent de l'agent elegit i els objectius de la investigació. En utilitzar CA, es va trobar que augmentar-ne la dosi i el contingut en ciment conduïa a millorar l'eficiència de curació (HE) i la de segellat (SE). La variació de la relació aigua-ciment (a/c) no va produir una millora notable de HE i SE. S'aprofundí el coneixement sobre les propietats d'adherència entre les armadures i la matriu de formigó. La inclusió d'agents de curació (BAC, CA, biomassa) va comportar la millora de l'adherència amb un creixement del 57% quan s'hi afegeix CA. Tot i que la presència de fissures longitudinals va reduir críticament l'adherència, es va aconseguir una recuperació important gràcies als efectes del auto curat. S'han trobat efectes contraposats de l'ús de microcàpsules. Es confirma una reducció significativa de la resistència mecànica i una millora significativa del segellat. Els paràmetres de disseny de mescla es van optimitzar per compensar la reducció de resistència, amb un programa experimental amb disseny factorial complet. Per la seua estructura inert, les macrocàpsules tendeixen a pertorbar l'empaquetament dels àrids. Per optimitzar la mescles es va desenvolupar un model d'empaquetament de partícules modificat per predir la proporció de buits de les mescles d'àrids i càpsules.

Amb tot, el resultat d'aquesta investigació pot servir com a guia per comprendre la contribució dels paràmetres de disseny de barreges que afecten les propietats de auto curat, que potencialment ajudarà investigadors i enginyers a formular barreges de formigó per a aplicacions de auto curat.

TABLE OF CONTENT

ACKNOWLEDGEMENTS	i
ABSTRACT	vi
TABLE OF CONTENT	xii
LIST OF ABBREVIATIONS	xix
LIST OF FIGURES AND TABLES	xxvii
Chapter 1 INTRODUCTION	1
1.1 Background and problem statement	1
1.2 Objectives and main contributions of the research	4
1.3 Organization of the text	6
Chapter 2 LITERATURE REVIEW	11
2.1 Novel self-healing agents	11
2.2 Comparative study on the inclusion of self-healing agents into the concrete mix.....	22
2.2.1 Effects of CA on concrete properties	24
2.2.1.1 Properties of the fresh concrete mixture	24
2.2.1.2 Properties of the hardened concrete	25
2.2.1.3 Self-healing properties	30
2.2.2 Effects of bacteria on concrete properties	32
2.2.2.1 Properties of the fresh concrete mixture	32
2.2.2.2 Properties of the hardened concrete	35
2.2.2.3 Self-healing properties	44
2.2.3 Effects of micro-encapsulated agent on concrete properties.....	45

2.2.3.1	Properties of the fresh concrete mixture	45
2.2.3.2	Properties of the hardened concrete	47
2.2.3.3	Self-healing properties	55
2.2.4	Effects of macro-encapsulated agent on concrete properties...	56
2.2.4.1	Properties of the fresh concrete mixture	56
2.2.4.2	Properties of the hardened concrete	59
2.2.4.3	Self-healing properties	63
2.3	Conclusions.....	65
Chapter 3 FRESH PROPERTIES OF THE MODIFIED CEMENT PASTE WITH INCLUSION OF HEALING AGENT AND ADMIXTURES		67
3.1	Introduction.....	67
3.2	Characterization of cement and healing agents.....	68
3.3	Initial assessment of the effect of healing agents on the cement paste.....	72
3.3.1	Testing methodologies.....	72
3.3.2	Influence of healing agents on water demand and setting time of cement paste	72
3.3.3	Water-reducing effect of superplasticizer on the cement paste	76
3.4	Compatibility study on the effect of SP dosage on workability and rheology of cement paste	77
3.4.1	Rheological test methods.....	78
3.4.2	Slump loss	80
3.4.3	Impact of SP dosage on pure cement paste.....	82
3.4.4	Impact of healing agents on superplasticized cement paste	85
3.4.5	Superplasticizer adsorption capacity of cement pastes with and without healing agents	88
3.4.6	Evolution of the early age setting of cement paste	92
3.5	Conclusions.....	96
Chapter 4 EVALUATION OF MODIFIED MIX DESIGNS OF CONCRETE CONTAINING CRYSTALLINE ADMIXTURES TOWARD SELF-HEALING AND SELF-SEALING PERFORMANCES.....		97

4.1	Introduction.....	97
4.2	Materials and methods	98
4.2.1	Materials	98
4.2.2	Modification of mix designs for self-healing concrete.....	100
4.2.3	Testing method	103
4.3	Results	106
4.3.1	Fresh properties	106
4.3.2	Strength development	106
4.3.3	Self-healing performance.....	108
4.3.3.1	Progress of crack closure after healing.....	108
4.3.3.2	Analysis of healing efficiency.....	114
4.3.3.3	Sealing performance by permeability measurement	122
4.4	Discussion.....	125
4.4.1	Relationship between crack width and permeability rate	125
4.4.2	Relationship between healing efficiency and sealing efficiency	127
4.4.3	Analysis of self-healing products.....	132
4.5	Conclusions.....	134
Chapter 5 EXPERIMENTAL INVESTIGATION ON THE BOND BEHAVIOUR OF STEEL REINFORCEMENT IN SELF-HEALING CONCRETE		136
5.1	Introduction.....	136
5.2	Materials and methods	137
5.2.1	Materials	137
5.2.2	Sample preparation.....	140
5.2.3	Test setup.....	142
5.2.4	Sample series	144
5.3	Results and discussion.....	146
5.3.1	Fresh properties	146
5.3.2	Hardened properties.....	147
5.3.3	Bond-slip response of uncracked (UNCR) concretes.....	149

5.3.4 Bond-slip response of cracked (CR) concretes	156
5.3.5 Phenomenon of crack closure.....	163
5.3.6 Bond-slip response of healed (HL) concretes.....	166
5.3.7 Failure mode	175
5.3.8 Characterization of healing products	177
5.4 Conclusions.....	180
Chapter 6 OPTIMIZATION OF CONCRETE MIX DESIGNS TOWARD THE BOND PROPERTIES OF STEEL REINFORCEMENT IN SELF-HEALING CONCRETE BY TAGUCHI METHOD	182
6.1 Introduction.....	182
6.2 Materials and methods	184
6.2.1 Raw materials.....	184
6.2.2 Experimental program	185
6.2.3 Test setup.....	188
6.3 Results and discussion.....	188
6.3.1 Fresh properties	188
6.3.2 Compressive strength	190
6.3.3 Bond properties of uncracked (UNCR) concretes	196
6.3.4 Bond properties of cracked (CR) concretes	207
6.3.5 Bond properties of healed (HL) concretes	217
6.3.6 Analysis of healing products	225
6.4 Conclusions.....	226
Chapter 7 MIX DESIGN OPTIMISATION OF SELF-SEALING CONCRETE CONTAINING MICROCAPSULES WITH PU SHELL AND WATER REPELLENT CARGO	228
7.1 Introduction.....	228
7.2 Preliminary study on the workability, mechanical and self-sealing properties of concrete containing microcapsules with PU shell and water repellent cargo	230
7.2.1 Materials	230
7.2.2 Testing program	233

7.2.3 Results and discussion	235
7.2.3.1 Fresh properties.....	235
7.2.3.2 Hardened properties	237
7.2.3.3 Self-sealing properties	241
7.2.3.4 Microcapsules' observation in the concrete matrix	244
7.2.4 Conclusions	245
7.3 Mix design optimization of microcapsule-based concrete using the full factorial design technique.....	246
7.3.1 Microcapsules	246
7.3.2 Design of experiment (DOE).....	247
7.3.3 Testing program	253
7.3.4 Results and discussion	257
7.3.4.1 Effect of the size and dosage of microcapsules on the fresh properties of cement paste	257
7.3.4.2 Compatibility study between microcapsules and cement type regarding the mechanical performance of mortar	259
7.3.4.3 Influence of different mixing procedure and pure WRA on the performance of MIC concrete	262
7.3.4.4 Fresh properties of MIC concretes	264
7.3.4.5 Hardened properties of MIC concretes	266
7.3.4.6 Self-sealing properties of MIC concretes.....	277
7.3.5 Microstructural observation	284
7.3.6 Conclusions	289
Chapter 8 EFFECT OF MACROCAPSULES IN THE INERT STRUCTURE OF SELF-HEALING CONCRETE: A PROOF OF CONCEPT	291
8.1 Introduction.....	291
8.2 Applicability of cementitious capsules in concrete production: initial assessment on capsule robustness, mechanical and self-sealing properties of concrete.....	292
8.2.1 Materials	292
8.2.2 Methods	293

8.2.2.1 Capsule survivability test	293
8.2.2.2 Mixing and casting procedure for capsule-based mixture	295
8.2.2.3 Test methods	296
8.2.3 Results and discussion	298
8.2.3.1 Capsule robustness	298
8.2.3.2 Fresh and hardened properties	298
8.2.3.3 Self-sealing properties	300
8.2.4 Conclusions	304
8.3 Prediction of aggregate packing with tubular (macro) capsules based on the Dewar's particle packing method	305
8.3.1 Particle packing model of Dewar	305
8.3.2 Polymeric and cementitious capsules	309
8.3.3 Physical properties of aggregates	311
8.3.4 Testing program	312
8.3.5 Packing of aggregates with and without macrocapsules	314
8.3.5.1 Voids ratio of aggregates	314
8.3.5.2 Interaction diagram of binary aggregate mixture (BAM) .	322
8.3.5.3 Interaction diagram of ternary aggregate mixture (TAM)	329
8.3.5.4 Validation of the voids ratio model	339
8.4 Modification of concrete mix designs for the introduction of macrocapsules.....	341
8.4.1 Mix design adaptations	341
8.4.2 Mixing and casting process	348
8.4.3 Testing program	349
8.4.4 Results and discussion	350
8.4.4.1 Effect of fine ratio in capsule-based concrete mixtures (in relation to the first program)	350
8.4.4.2 Effect of capsule size and capsule dosage in capsule-based concrete mixtures (in relation to the second program)	355
8.4.5 Qualitative evaluation	358

8.4.5.1 Capsule breakage	358
8.4.5.2 Bond between capsule shell and concrete matrix	360
8.4.6 Conclusions	362
Chapter 9 VALORIZATION PLANS	364
9.1 Identification of key exploitable results	364
9.2 Brief market analysis	365
9.3 Strategy for valorization	366
Chapter 10 CONCLUSIONS AND RECOMMENDATIONS FOR FUTURE RESEARCH	369
10.1 Summary	369
10.2 Suggestions for future research	376
REFERENCES.....	380
CURRICULUM VITAE.....	401

LIST OF ABBREVIATIONS

<i>112D</i>	112 days
<i>28D</i>	28 days
<i>a/b</i>	aggregate-to-binder
<i>AE</i>	air-entraining
<i>ANOVA</i>	analysis of variance
<i>ASR</i>	alkali silica reaction
<i>bwoc</i>	by weight of cement
<i>BAC</i>	Basilisk bacteria healing agent
<i>BAM</i>	binary aggregate mixture
<i>BRF</i>	bond reduction factor
<i>BSE</i>	backscattered electron
<i>c/d_b</i>	concrete cover to rebar diameter
<i>cfu</i>	cell or colony-forming unit
<i>cw/d_b</i>	ratio of crack width over rebar diameter
<i>C₂S</i>	dicalcium silicate, Belite
<i>C₃A</i>	tricalcium aluminate, Aluminate
<i>C₃S</i>	tricalcium silicate, Alite
<i>C₄AF</i>	tetracalcium aluminoferrite, Ferrite
<i>C</i>	carbon
<i>Ca²⁺</i>	calcium ion

CO_2	carbon dioxide
CO_3^{2-}	carbonate ion
CA	crystalline admixture
$CAPS$	capsules
CD	critical dosage
CEM	cementitious
$CEM23$	cementitious tubular capsules with the length of 23 mm
$CEM54$	cementitious tubular capsules with the length of 54 mm
CN	calcium nitrate
CP	continuous phase
CR	cracked
CS	colloidal silica
CSA	copper slag aggregate
CSH	calcium silicate hydrate
CV	coefficient of variation
CWA	capillary water absorption
Ca	calcium
$Ca(OH)_2$	calcium hydroxide, Portlandite
$CaCO_3$	calcium carbonate
d_b	diameter of rebar
d_{caps}	dosage of capsules
D_{50}	median size
D_{agg}	mean size of aggregate
D_{caps}	diameter of capsule
D_{fibre}	diameter of fibre
D	mean size of particle (Dewar)

<i>DOE</i>	design of experiment
<i>DP</i>	dispersed phase
$E_{1.0}$	area under the bond-slip curve up to a slip of 1.0 mm (= fracture energy)
<i>EDX</i>	energy dispersive X-ray
f'_c	compressive strength
<i>F</i>	adjustment factor
<i>FA</i>	fly ash
<i>FM</i>	fineness modulus
<i>FR</i>	fine ratio
<i>FRC</i>	fibre reinforced concrete
<i>FTIR</i>	Fourier transform infrared
<i>G</i>	geometric mean aggregate size
<i>GA</i>	gelatin/gum Arabic
<i>GGBFS</i>	ground granulated blast-furnace slag
<i>GNP</i>	graphite nanoplatelets
<i>GUL</i>	general used limestone
H_3PO_4	phosphoric acid
<i>HA</i>	healing agent
<i>HE</i>	healing efficiency
\overline{HE}	global healing efficiency
<i>HL</i>	healed
<i>HPFRC</i>	high performance fibre reinforced concrete
<i>HPFRCC</i>	high performance fibre reinforced cementitious composite
<i>HRWR</i>	high range water reducer
<i>ICDD</i>	international center for diffraction data

<i>ICSD</i>	inorganic crystal structure database
<i>ID</i>	internal diameter
<i>ION</i>	iron oxide nanoparticles
<i>IPDI</i>	isophorone diisocyanate
<i>ITZ</i>	interfacial transition zone
k_{int}	empirical factor used in Dewar's model
k_p	empirical factor used in Dewar's model
k	slope of the percentage change of U
L_{caps}	length of capsule
L_{fibre}	length of fibre
L	length
<i>LAC</i>	calcium lactate
<i>LBD</i>	loose bulk density
<i>LP</i>	limestone powder
<i>LVDT</i>	linear variable differential transformer
<i>LWA</i>	lightweight aggregate
<i>LWC</i>	lightweight aggregate concrete
m_1	mass of the empty container
m_2	mass of the container and oven-dried test specimen
m_3	mass of the container
m_{caps}	mass of added capsules
m	spacing factor
<i>MIC</i>	microcapsules
<i>MIC_56</i>	microcapsules with the mean size of 56 μm
<i>MIC_59</i>	microcapsules with the mean size of 59 μm
<i>MIC_88</i>	microcapsules with the mean size of 88 μm

<i>MIC</i> ₉₃	microcapsules with the mean size of 93 μm
<i>MICP</i>	microbial induced calcite precipitation
<i>MUC</i> ⁺	mixed ureolytic culture
<i>n</i>	fine fraction
<i>NSC</i>	normal strength concrete
<i>NZ</i>	natural zeolite
<i>O</i>	oxygen
<i>OD</i>	outer diameter
<i>OPC</i>	ordinary Portland cement
<i>ppmC</i>	parts per million carbon
<i>P(MMA/n – BMA)</i>	poly(methyl methacrylate/n-butyl methacrylate)
<i>PA</i>	paraffin
<i>PAW</i>	paraffin + PE wax
<i>PAWN</i>	paraffin + PE wax + Nano-SiO ₂
<i>PCE</i>	polycarboxylate ether
<i>PE</i>	polyethylene
<i>PEP</i>	peptone
<i>PEST</i>	political economical social technological
<i>PLA</i>	polylactic acid
<i>PLC</i>	Portland limestone cement
<i>PMMA</i>	poly(methyl methacrylate)
<i>POLY</i>	polymeric
<i>POLY35</i>	polymeric tubular capsules with the length of 35 mm
<i>POLY50</i>	polymeric tubular capsules with the length of 50 mm
<i>POLY65</i>	polymeric tubular capsules with the length of 65 mm
<i>PPM</i>	particle packing method

<i>PRA</i>	permeability-reducing admixture
<i>PS</i>	polystyrene
<i>PSD</i>	particle size distribution
<i>PU</i>	polyurethane
<i>PURE</i>	pure mass of material
<i>r</i>	ratio of mean sizes
R^2	coefficient of determination
R^2_{adj}	adjusted coefficient of determination
<i>RCM</i>	rapid chloride migration
<i>REF</i>	reference
<i>RH</i>	relative humidity
<i>RHA</i>	rice husk ash
<i>s/c</i>	sand-to-cement
S_{CR}	sorption coefficient of cracked concrete
S_{UNCR}	sorption coefficient of uncracked concrete
SE_{CR}	sealing efficiency of cracked concrete
SE_{UNCR}	sealing efficiency of uncracked concrete
S_u	slip corresponding to τ_u
<i>S</i>	sorption coefficient
<i>SAP</i>	superabsorbent polymer
<i>SCC</i>	self-compacting concrete
<i>SCM</i>	secondary cementitious material
<i>SD</i>	saturation dosage
<i>SE</i>	sealing efficiency
\overline{SE}	global sealing efficiency
<i>SED</i>	secondary electron detector

<i>SEM</i>	scanning electron microscopy
<i>SF</i>	silica fume
<i>SFA</i>	sintered fly ash
<i>SHR</i>	self-healing ratio
<i>SN</i>	signal-to-noise
<i>SOL</i>	mass of solution
<i>SP</i>	superplasticizer
<i>SRSCC</i>	steel reinforced self-compacting concrete
<i>SS</i>	sodium silicate
<i>TAM</i>	ternary aggregate mixture
<i>TC</i>	traditional concrete
<i>TEOS</i>	tetraethyl orthosilicate
<i>TGA</i>	thermogravimetric analysis
<i>TOC</i>	total organic carbon
<i>TSB</i>	tryptone soya broth
U_0	voids ratio of coarse particle
U_0''	effective voids ratio of coarse particle
U_1	voids ratio of fine particle
U_1''	effective voids ratio of fine particle
U_{AM_caps}	voids ratio of aggregate mixture after capsules' addition
$U_{AM_no\ caps}$	voids ratio of aggregate mixture without any capsules
U_{BAM_caps}	voids ratio of BAM after capsules' addition
$U_{BAM_no\ caps}$	initial voids ratio of BAM without any capsules
U_{TAM_caps}	voids ratio of TAM after capsules' addition
$U_{TAM_no\ caps}$	initial voids ratio of TAM without any capsules
U	voids ratio

<i>UHPC</i>	ultra-high performance concrete
<i>UNCR</i>	uncracked
<i>UPV</i>	ultrasonic pulse velocity
<i>UR</i>	urea
V_{caps}	volume of added capsules
V	volume
w/b	water-to-binder
w/c	water-cement ratio
w/p	water-to-powder
<i>WRA</i>	water-repellent agent
X	mean size of void
<i>XRD</i>	X-ray diffraction
<i>YE</i>	yeast extract
Z	notional width factor
α	empirical constant for BAM and TAM
β	empirical constant for BAM and TAM
ρ_b	loose bulk density
ρ_{rd}	oven-dried density of aggregates
τ_m	mean bond strength
$\overline{\tau_m}$	average value of mean bond strength
τ_u	ultimate bond strength
$\overline{\tau_u}$	average value of ultimate bond strength

LIST OF FIGURES AND TABLES

Figure 1-1. General overview of thesis outline and relation between different chapters	8
Figure 1-2. Detailed information of PhD chapters with their associated publications and contributions	9
Figure 1-3. Roles of early stage researchers (ESRs) in the framework of SMARTINCS project	10
Figure 2-1. XRD diffractogram of CA (Xypex) [26]	12
Figure 2-2. SEM micrograph of CA (Penetron Admix) [27]	13
Figure 2-3. (a) <i>Bacillus</i> bacteria cell under SEM [30], (b) isolation of bacteria colonies under a stereo microscope [42]	14
Figure 2-4. Optical microscopic images of produced microcapsules [59]	16
Figure 2-5. (a) Manual placement of two cementitious capsules in a small-scale mortar mould [22]; (b) manual placement of glass capsules onto a network of wires in a large-scale concrete beam mould [60]; (c) reconstructed CT scan of a sliced concrete core with a glass capsule crossed by a crack (left) and the 3D distribution of capsules in the concrete cores as a result of direct addition of capsules during concrete mixing (right) [56] ..	17
Figure 2-6. Main strategies to introduce healing agents in the recent application of self-healing concrete	23
Figure 2-7. Concrete strength increments due to the addition of CA at 28 days; data are taken from available literatures and the details of mix code can be seen in Table 2-3. The dot and dash-dot lines represent the value of compressive strength enhancement by using Xypex Admix (2–3% CA) and Penetron CA (0.8–1% CA), respectively, according to the technical data sheets [72,73].	26
Figure 2-8. Development of crack closing in the bacterial concrete after 30 days based on microscopic image [29]	45

Figure 2-9. The presence of large pores due to broken microcapsules in the cementitious matrix [52]	50
Figure 2-10. Compressive strength results of microcapsules-based concrete at various microcapsule concentrations (0.25, 0.50 and 1.00%) and mean sizes (22, 50 and 109 μm) [62].....	51
Figure 2-11. Capsule configuration within concrete railway sleeper: (a) short tubes at middle, (b) short tubes at rail seat, (c) long tubes at middle, and (d) long tubes at rail seat of sleepers [100]	61
Figure 3-1. Particle size distributions of cements and healing materials	71
Figure 3-2. SEM micrographs of cements and healing agents	71
Figure 3-3. Water demands of modified cement incorporated with (a) Basilisk bacteria and (b) Penetron crystalline admixture at different dosages (note: the empty markers represent the water demand values, while the filled markers represent the mean values).....	73
Figure 3-4. Setting times of modified cement pastes incorporated with (a) Basilisk bacteria and (b) Penetron crystalline admixture at different dosages	75
Figure 3-5. Effect of SP dosage on the water demand of powder mixtures: (a) CEM I + BAC, (b) CEM III/A + BAC, (c) CEM I + CA and (d) CEM III/A + CA.....	76
Figure 3-6. Sign of segregation on cement paste	78
Figure 3-7. (a) Mini slump cone, (b) Viscometer, (c) TOC device and (d) Ultrasonic test setup.....	80
Figure 3-8. Reduction of slump values over time on (a) CEM III/A pastes and (b) CEM I pastes	82
Figure 3-9. Slump life of superplasticized cement pastes ((a) CEM III/A and (b) CEM I) with different SP dosage and SP type (Fluivicon 801 for CEM III/A, Technofluid P175 for CEM I)	83
Figure 3-10. Determination of CD and SD in relation to a certain SP based on slump and viscosity results of (a) CEM III/A paste and (b) CEM I paste	84
Figure 3-11. Alteration of slump of (a) CEM III/A paste and (b) CEM I paste with various SP dosages (SP Fluivicon 801 and Technofluid P175 for CEM III/A and CEM I, respectively) due to the addition of healing agents.....	86
Figure 3-12. Alteration of viscosity of (a) CEM III/A paste and (b) CEM I paste with various SP dosages (SP Fluivicon 801 and Technofluid P175 for CEM III/A and CEM I, respectively) due to the addition of healing agents.....	87
Figure 3-13. Percentage of SP adsorbed on the (a) CEM III/A paste and (b) CEM I paste systems	89

Figure 3-14. Adsorption isotherms of SP on powders: (a) CEM III/A with/without healing agent and (b) CEM I with/without healing agent	91
Figure 3-15. Evolution of UPV in function of time in: (a) CEM III/A pastes and (b) CEM I pastes, both with and without healing agent	93
Figure 3-16. Effect of superplasticizer (Fluivicon 801) in the development of UPV on pastes with (a) pure CEM III/A, (b) CEM III/A + CA and (c) CEM III/A + BAC	94
Figure 3-17. Effect of superplasticizer (Technofluid P175) in the development of UPV on pastes with (a) pure CEM I, (b) CEM I + CA and (c) CEM I + BAC	95
Figure 4-1. Particle size distribution of aggregates	99
Figure 4-2. Methodology of crack measurement to quantify healing efficiency	104
Figure 4-3. Permeability test setup	105
Figure 4-4. Compressive strengths of all concrete mixtures (note: for each mix, the left, middle and right bars represent strength values at 7, 28 and 91 days, respectively)	108
Figure 4-5. The progress of crack closure on cracked specimens after healing for 21 and 121 days tested on various mixtures with a specific category, i.e. (a) effect of CA dosage, (b) effect of w/c ratio and (c) effect of cement content	113
Figure 4-6. (a) 21-day and (b) 121-day healing efficiencies of all concrete samples with different crack widths.....	116
Figure 4-7. Global healing efficiencies of all tested mixtures with different: (a) CA dosage, (b) w/c and (c) cement content and global sealing efficiencies of all tested mixtures with different: (d) CA dosage, (e) w/c and (f) cement content	121
Figure 4-8. Permeability rate (M7 mixture taken as an example).....	122
Figure 4-9. Relationship between permeability rate and crack width observed at 0, 21 and 121 days.....	126
Figure 4-10. Relationship between <i>HE</i> and <i>SE</i> after 21 healing days (grey markers) and 121 healing days (blue markers)	127
Figure 4-11. Some possibilities of different crack geometry	128
Figure 4-12. Some possibilities of the occurrence of precipitation products along the crack	129
Figure 4-13. Schematic representation of discrete correlations between <i>HE</i> and <i>SE</i> which may lead to a wrong interpretation	132

Figure 4-14. Collecting the healing products from the crack mouth.....	133
Figure 4-15. FTIR analysis of healing products	133
Figure 5-1. Pull-out mould set (left) and schematic of a pull-out specimen (right)	141
Figure 5-2. Splitting the pull-out specimen by means of a Brazilian splitting test.....	143
Figure 5-3. Schematic of pull-out test	143
Figure 5-4. A schematic representation of the bond-slip response	144
Figure 5-5. Flow chart of test series program	146
Figure 5-6. Slump and air content of all mixtures	147
Figure 5-7. Compressive strength of all concrete mixtures.....	149
Figure 5-8. Bond-slip responses of uncracked concrete with different healing agents	151
Figure 5-9. Comparison of different bond parameters based on the addition of healing agents	152
Figure 5-10. Microstructure of self-healing concrete.....	153
Figure 5-11. Void-filling effect of self-healing concrete containing CA and BAC	153
Figure 5-12. Relationship between the average ultimate bond strength and square root of average compressive strength.....	154
Figure 5-13. Relationship between ultimate bond strength, mean bond strength and fracture energy.....	154
Figure 5-14. Slip corresponding to ultimate bond strength	156
Figure 5-15. Bond-slip responses of cracked concrete with a specific crack width of (a) 200–300 μm , (b) 300–400 μm and (c) 400–500 μm	159
Figure 5-16. (a) Ultimate bond strengths, (b) mean bond strengths, (c) fracture energy and (d) slips corresponding to the ultimate bond strength of all series of specimens	161
Figure 5-17. Bond reduction factor as a function of the ratio of crack width-to-rebar diameter	163
Figure 5-18. Reduction of BRF with increasing cw/d_b as compared with existing models.....	163
Figure 5-19. (a) Self-healing phenomenon by the deposition of healing products in the cracks of REF specimens, and typical formation of healing	

products coming out from the crack observed after (b) 28 days and (c) 112 days of healing.....	165
Figure 5-20. Observation of crack closure by means of microscope.....	166
Figure 5-21. Bond-slip responses of 28d-healed concrete with a specific crack width of (a) 200–300 μm , (b) 300–400 μm and (c) 400–500 μm	169
Figure 5-22. Bond-slip responses of 112d-healed concrete with a specific crack width of (a) 200–300 μm , (b) 300–400 μm and (c) 400–500 μm	171
Figure 5-23. Development of the recovery of (a) the ultimate bond strength and (a) the mean bond strength in function of healing time	174
Figure 5-24. (a) Pull-out failure on UNCR specimens, (b) splitting failure on CR and HL specimens, and (c) the breakage of healing products on a healed crack due to splitting failure during a pull-out test (left: before testing, right: after testing).....	176
Figure 5-25. Concrete shear-off on pulled-out rebars.....	177
Figure 5-26. Inspection of healing products inside the crack of healed concrete	178
Figure 5-27. Observation of the structure of healing products by means of optical microscopy.....	178
Figure 5-28. FTIR spectra of healing products from different mixtures	180
Figure 6-1. Particle size distribution of cement, aggregates and healing agents	185
Figure 6-2. Series of pull-out specimens	188
Figure 6-3. Signal-to-noise ratios for (a) slump, (b) air content and (c) fresh density	190
Figure 6-4. Compressive strength of all different concrete mixtures.....	191
Figure 6-5. Signal-to-noise ratios for 28d compressive strength	193
Figure 6-6. Contour plots of 28d average compressive strength (in MPa) vs w/c and FR	195
Figure 6-7. Correlation between predicted and experimental results of compressive strength	196
Figure 6-8. Bond-slip curves on UNCR, CR and HL concretes (mixture M5 taken as example).....	199
Figure 6-9. Evaluation of various bond parameters on all concrete mixtures	200
Figure 6-10. Relationship between ultimate bond strength and compressive strength of UNCR concrete.....	200

Figure 6-11. Relationship between (a) ultimate bond strength and mean bond strength and (b) ultimate bond strength and fracture energy for UNCR concrete	201
Figure 6-12. Signal-to-noise ratios for (a) ultimate bond strength, (b) mean bond strength and (c) fracture energy of uncracked (UNCR) concretes	202
Figure 6-13. Contour plots of ultimate bond strength (in MPa) vs w/c and FR in uncracked concrete	205
Figure 6-14. Correlation between predicted and experimental results of ultimate bond strengths of (a) UNCR, (b) CR and (c) HL concretes	206
Figure 6-15. (a) Ultimate bond strengths, (b) mean bond strengths and (c) fracture energy of all series of concretes	211
Figure 6-16. Signal-to-noise ratios for ultimate bond strengths in cracked (CR) and healed (HL) concretes with specific crack width of (a) 200–300 μm , (b) 300–400 μm and (c) 400–500 μm	213
Figure 6-17. Signal-to-noise ratios for mean bond strengths in cracked (CR) and healed (HL) concretes with specific crack width of (a) 200–300 μm , (b) 300–400 μm and (c) 400–500 μm	214
Figure 6-18. Signal-to-noise ratios for fracture energy in cracked (CR) and healed (HL) concretes with specific crack width of (a) 200–300 μm , (b) 300–400 μm and (c) 400–500 μm	216
Figure 6-19. Relationship between the average ultimate bond strength of uncracked, cracked and healed concretes at a specific crack width of (a) 200–300 μm , (b) 300–400 μm and (c) 400–500 μm	217
Figure 6-20. Crack closure phenomenon with self-healing concretes	218
Figure 6-21. Self-healing ratio of the bond properties (note: for each HA factor, the left and right columns represent the bond results after 28 and 112 days of healing, respectively)	223
Figure 6-22. FTIR spectra analysis	226
Figure 7-1. Autonomic healing mechanism on the use of microcapsules [16]	229
Figure 7-2. Microscopic images of microcapsules as provided by the producer	231
Figure 7-3. Filtering process of microcapsules	232
Figure 7-4. Cracking the specimen and measuring the crack width	234
Figure 7-5. Configuration of the prism specimen and the setup of the capillary water absorption test	235

Figure 7-6. Fresh test results: (a) slump, (b) air content and (c) fresh density of all concrete mixtures with and without microcapsules' addition (note: single measurement for slump and air content results, while three measurements for fresh density result)	237
Figure 7-7. Hardened test results: (a) hardened density, (b) tensile splitting strength, (c) compressive strength and (d) ultrasonic pulse velocity of all concrete mixtures with and without microcapsules' addition	239
Figure 7-8. Comparison of strength changes of MIC concretes with different MIC dosage	241
Figure 7-9. Average crack width of all cracked prisms	242
Figure 7-10. Capillary water absorption capacity (note: UNCR – uncracked, CR – cracked, REF – reference concrete, MIC – microcapsule-based concrete)	243
Figure 7-11. Comparison of water ingress in the cracked reference and MIC concretes (both pictures were taken 15 min after the capillary water absorption test was performed).....	243
Figure 7-12. Observation of microcapsules in the concrete matrix via optical microscopy.....	245
Figure 7-13. Micrographs of freshly produced microcapsules using OM: (a) MIC_56 and (b) MIC_93. Micrographs of freshly produced microcapsules using SEM: (c) MIC_56 and (d) MIC_93.	247
Figure 7-14. Mixing procedures of MIC concretes: (a) procedure 1 (MP1) and (b) procedure 2 (MP2)	255
Figure 7-15. Capillary water absorption tests on CR and UNCR areas of a specimen.....	257
Figure 7-16. Water demands of cement incorporated with microcapsules (MIC_56 and MIC_93) at different dosages (note: single measurement per mixture)	258
Figure 7-17. Setting times of cement pastes incorporated with microcapsules (MIC_56 and MIC_93) at different dosages (note: average value is based on three repetitions per mixture).....	259
Figure 7-18. Compressive strength of mortars containing (a) MIC_56 and (b) MIC_93 with different cement types.....	261
Figure 7-19. Flexural strength of mortars containing (a) MIC_56 and (b) MIC_93 with different cement types.....	262
Figure 7-20. Fresh densities of all concrete mixtures (note: three measurements for each mixture)	265

Figure 7-21. Slumps of all concrete mixtures (note: single measurement for each mixture).....	265
Figure 7-22. Air contents of all concrete mixtures (note: single measurement for each mixture)	266
Figure 7-23. Hardened densities of all concrete mixtures (note: three measurements for each mixture)	267
Figure 7-24. Contour plots for the effect of (a) MIC dosage vs w/c for MIC_56, (b) MIC dosage vs w/c for MIC_93, (c) MIC dosage vs MIC size with a hold factor of w/c 0.50 and (d) MIC dosage vs MIC size with a hold factor of w/c 0.60, on compressive strength	270
Figure 7-25. Main effects plots for compressive strength	271
Figure 7-26. 3D plot of the alteration of compressive strength due to the addition of microcapsules in function of MIC size and MIC dosage	273
Figure 7-27. Contour plots for the effect of (a) MIC dosage vs w/c for MIC_56, (b) MIC dosage vs w/c for MIC_93, (c) MIC dosage vs MIC size with a hold factor of w/c 0.50 and (d) MIC dosage vs MIC size with a hold factor of w/c 0.60, on tensile splitting strength.....	274
Figure 7-28. Main effects plots for tensile splitting strength	275
Figure 7-29. Contour plots for the effect of (a) MIC dosage vs w/c for MIC_56, (b) MIC dosage vs w/c for MIC_93, (c) MIC dosage vs MIC size with a hold factor of w/c 0.50 and (d) MIC dosage vs MIC size with a hold factor of w/c 0.60, on UPV	276
Figure 7-30. Main effects plots for UPV	277
Figure 7-31. Variation of crack width for all mixtures (note: dash lines represent the range of target crack width between 200 and 300 μm)	278
Figure 7-32. Relationship between water uptake and time of water immersion on (a) w/c 0.40 mixtures, (b) w/c 0.50 mixtures and (c) w/c 0.60 mixtures (note: REF = reference (no microcapsules), UNCR = uncracked, CR = cracked)	279
Figure 7-33. Comparison between reference concrete (without microcapsules) and microcapsule-based concretes right after CWA tests	280
Figure 7-34. Effect of microcapsules on the sorption coefficient of uncracked and cracked concretes	281
Figure 7-35. Effect of w/c and microcapsules on the sealing efficiency of cracked concretes.....	283
Figure 7-36. Contour plots of SE: (a) MIC_56 and (b) MIC_93	283

Figure 7-37. The microstructure of the concrete matrix after the inclusion of 3% and 6% MIC_56 observed in mixtures with w/c of 0.60	284
Figure 7-38. EDX mapping analysis on the concrete surface with microcapsules	285
Figure 7-39. EDX regional analysis on the concrete surface with microcapsules	286
Figure 7-40. SEM micrographs on the bond between capsule shell and concrete matrix	287
Figure 7-41. SEM micrographs on the delamination between capsule shell and matrix and the formation of crystal needles on the fractured shell....	287
Figure 7-42. Wet spots in concrete indicating a release of sealing agent after mechanical testing on (a) cubical concrete and (b) cylindrical concrete....	288
Figure 7-43. Cracking of the embedded microcapsules in the concrete matrix	288
Figure 8-1. (a) Tilting drum mixer (Lescha SM 145 S) and (b) planetary mixer (Zyklos ZZ 75 HE).....	294
Figure 8-2. Capsule survivability test.....	294
Figure 8-3. Schematic design of the capsule-based prism	296
Figure 8-4. Hardened properties of the REF and CAPS concretes (notes: n = 3 for compression tests, n = 3 for tensile splitting tests and n = 3 for UPV tests)	299
Figure 8-5. Successful rupture of embedded capsules by releasing the sealing agent through the crack	301
Figure 8-6. Capillary water absorption results (note: n = 3 for capillary water absorption tests on each specimen series)	301
Figure 8-7. Sealing coverage area based on the water droplet test.....	302
Figure 8-8. Splitting the cube specimens to count the amount of broken capsules in a certain crack plane (note: the darkest concrete surface is the area covered by WRA)	303
Figure 8-9. Splitting the cylindrical specimens to count the amount of broken capsules in a certain crack plane (note: the darkest concrete surface is the area covered by WRA)	303
Figure 8-10. (a) Three dimensional model of a particle, associated void and related particles, (b) three-dimensional model of the dilated structure of coarse particles in a mixture containing fine particles	306
Figure 8-11. Theoretical relationship for voids ratio	307

Figure 8-12. Loosening and wall effects	307
Figure 8-13. Theoretical voids ratio diagram based on Dewar’s model	308
Figure 8-14. Several types of macrocapsules used in this study	310
Figure 8-15. PSD of aggregates.....	311
Figure 8-16. Schematic procedure of LBD test on a single type/fraction of aggregate	314
Figure 8-17. Schematic procedure of LBD test on aggregate mixtures	314
Figure 8-18. Voids ratio of different types and fractions of aggregates in function of the capsule dosage of (a) CEM23 and (b) CEM54	317
Figure 8-19. Capsule effect in the packing of aggregates.....	317
Figure 8-20. Changes in voids ratio due to the increase of capsule dosage with a certain aggregate: (a) sea sand 0/2.5, (b) gravel 4/8 and (c) gravel 8/16 320	
Figure 8-21. Relationship between k and L_{caps}/D_{caps} observed on the use of specific capsule types (note: black line/dot is based on CEM capsules, while red line/dot is based on POLY capsules).....	321
Figure 8-22. Relationship between k and mean aggregate size observed on the use of specific capsule type	321
Figure 8-23. Factor k versus $(D_{agg}/D_{caps})^2(L_{caps}/D_{agg})$	322
Figure 8-24. Voids ratio of BAM (without capsules): (a) original result, (b) Dewar result with adjustment factor $F = 1.3$	323
Figure 8-25. Voids ratios of BAM with CEM54 capsules at different dosages (note: Lab is experimental result (orange line), Dewar is Dewar’s result without adjustment factor (grey line), Dewar* is Dewar’s result with adjustment factor $F = 1.1-1.2$ (green line))	326
Figure 8-26. Voids ratios of BAM with (a) CEM54 capsules and (b) CEM23 capsules at different fine fraction (note: straight line with hollow dot represents Dewar* result and solid dot represents experimental/lab result)	327
Figure 8-27. Changes of voids ratio of BAM after the addition of (a) CEM54 capsules and (b) CEM23 capsules compared to initial voids ratio of BAM without capsules.....	328
Figure 8-28. Relationship between capsule dosage and percentage increase of voids ratio observed in BAM	329
Figure 8-29. Comparison between the actual U values and the predicted U values of BAM in function of capsules dosage and L_{caps}/D_{caps} ratio	329

Figure 8-30. Voids ratio of TAM (without capsules) (note: Lab is experimental result (orange line) and Dewar is Dewar’s result without adjustment factor (grey line)).....	330
Figure 8-31. Voids ratios of TAM with CEM54 capsules at different dosages (note: Lab is experimental result (orange line) and Dewar is Dewar’s result without adjustment factor (grey line))	331
Figure 8-32. Voids ratios of TAM with (a) CEM54 capsules, (b) CEM23 capsules, (c) POLY35 capsules, (d) POLY50 capsules and (e) POLY65 capsules at different fine fraction based on the lab results	334
Figure 8-33. Voids ratios of TAM with (a) CEM54 capsules, (b) CEM23 capsules, (c) POLY35 capsules, (d) POLY50 capsules and (e) POLY65 capsules at different fine fraction based on the Dewar results as compared to the lab results (note: straight line with hollow dot represents Dewar result and solid dot represents experimental/lab result)	335
Figure 8-34. Changes of voids ratio of TAM after the addition of (a) CEM54 capsules, (b) CEM23 capsules, (c) POLY35 capsules, (d) POLY50 capsules and (e) POLY65 capsules compared to initial voids ratio of TAM without capsules	337
Figure 8-35. Relationship between capsule dosage and percentage increase of voids ratio observed in TAM.....	338
Figure 8-36. Comparison between the actual U values and the predicted U values of TAM in function of capsules dosage and L_{caps}/D_{caps} ratio	338
Figure 8-37. Schematic illustration of concrete mix design modifications for the introduction of macrocapsules.....	348
Figure 8-38. Procedure of casting capsule-based concrete.....	349
Figure 8-39. (a) Slump, (b) air content and (c) fresh density of all mixtures from the first program; (d) fresh density of all mixtures from the second program	351
Figure 8-40. Evaluation of (a) hardened density, (b) compressive strength and (c) UPV of reference and capsule-based concretes tested at 28 days from the first program.....	353
Figure 8-41. Normalized ratio of compressive strength, voids ratio of TAM, UPV, hardened density of capsule-based mixtures (note: the ratio of 1.0 was considered at $n = 0.4$ where the lowest voids ratio was achieved).....	354
Figure 8-42. Correlation between compressive strength and voids ratio of TAM	355

Figure 8-43. Evaluation of (a) hardened density, (b) compressive strength and (c) UPV of reference and capsule-based concretes tested at 28 days from the second program.....	357
Figure 8-44. (a) Wet spots indicating that some capsules were broken inside the concrete during the compression test by releasing the sealing agent, (b) the spread of WRA via microcracks and capillary action.....	358
Figure 8-45. Observation of the broken capsules in a certain crack plane after splitting the cubes	359
Figure 8-46. Bond observation between the capsule shell and concrete matrix	361
Figure 8-47. Microstructure images at the interface between outer capsule shell and concrete matrix	361
Figure 8-48. EDX analysis on the interface of concrete matrix–outer capsule shell.....	362
Table 2-1. Different microcapsule materials with the corresponding parameters and characteristics used in concrete application.....	18
Table 2-2. Different macrocapsule materials with the corresponding parameters and characteristics used recently in mortar and concrete applications.....	19
Table 2-3. Summary of CA concrete composition and the scenario of self-healing assessment.....	27
Table 2-4. Comparison of various bacteria applications in normal strength concrete and their effects on the mechanical and durability properties	36
Table 2-5. Effect of nutritional admixtures on the compressive strength of the mortar (without bacteria) [15].	44
Table 2-6. Comparison of the strength changes of cementitious composite added with microcapsules at different size and dosage	52
Table 3-1. Chemical composition of the cements (provided by the manufacturer).....	69
Table 3-2. Quantitative XRD phase analysis on CEM I, CEM III/A and CA (note: * represents the indicative amount of compound below 1% that may be inaccurate).....	70
Table 3-3. Properties of superplasticizer (provided by the manufacturer) ..	71
Table 4-1. Physical properties of aggregates.....	99

Table 4-2. Concrete mix designs (note: the highlighted values relate to the adapted mix design parameters with respect to M1)	102
Table 4-3. Statistical analyses of data series of crack width with respect to the 21d healing efficiency	117
Table 5-1. Mix designs (note: (*) effective water included in the biomass agents)	138
Table 5-2. Comparison of BRV on different states of concrete (based on τ_u values).....	172
Table 5-3. Comparison of BRV on different states of concrete (based on τ_{tm} values).....	172
Table 6-1. Factors and levels adopted for the fractional factorial design ..	186
Table 6-2. Mix designs	187
Table 6-3. Response table for SN ratios for 28d compressive strength	193
Table 6-4. Analysis of variance of SN ratios for 28d compressive strength	194
Table 6-5. Response table for SN ratios for ultimate bond strength, mean bond strength and fracture energy of UNCR concretes	203
Table 6-6. Statistical evaluation of the bond properties by ANOVA based on p-values of SN ratios (note: the p-value of 0.05 was set as a significance threshold and the highlighted 'green' cells represent significant p-values)	203
Table 6-7. Statistical evaluation of the effect of crack width in the bond properties (note: the p-value of 0.05 was set as a significance threshold and the highlighted 'green' cells represent significant p-values).....	222
Table 6-8. Statistical evaluation of the SHR of bond properties by ANOVA (note: p-value of 0.05 as a significance threshold)	224
Table 7-1. Background information of microcapsules.....	231
Table 7-2. Mix designs of reference and microcapsule-based concretes ..	233
Table 7-3. Self-sealing results based on the CWA tests	244
Table 7-4. Background information of freshly produced microcapsules ...	246
Table 7-5. Main composition of binder with and without microcapsules..	248
Table 7-6. Mix proportion of mortars with and without microcapsules (note: capsule concentrations of MIC_56 and MIC_93 solutions are 30 and 50 wt%, respectively)	249
Table 7-7. Factors and levels adopted for the full factorial design	250
Table 7-8. Mix designs	252

Table 7-9. Description of mixing procedures	254
Table 7-10. Effect of capsule mixing and pure WRA on the fresh and hardened properties of concrete	263
Table 7-11. Measured values for mechanical properties of hardened concrete (note: the reductions in red are relative to the corresponding reference concrete without capsules)	268
Table 7-12. Analysis of variance for 28d compressive strength (note: DF = degree of freedom, Adj SS = adjusted sum of square, Adj MS = adjusted mean square).....	271
Table 7-13. Analysis of variance for 28d tensile splitting strength.....	275
Table 7-14. Analysis of variance for UPV	277
Table 7-15. Analysis of variance for S_{UNCR}	282
Table 7-16. Analysis of variance for S_{CR}	282
Table 7-17. Analysis of variance for SE.....	284
Table 8-1. Mix designs	293
Table 8-2. Capsule survivability (results based on a single test)	298
Table 8-3. Fresh properties (note: single measurement for slump and air content tests).....	299
Table 8-4. Parameters for the change points in Dewar’s model	309
Table 8-5. Detailed geometry of the macrocapsules (based on the average values from sampling)	310
Table 8-6. Properties of aggregates	311
Table 8-7. Number of capsules used for LBD tests.....	313
Table 8-8. Assessment on the change of voids ratio of coarse aggregates due to the presence of CEM capsules (note: the increment of S (CEM54 vs CEM23) = $(S_{CEM54} - S_{CEM23})/S_{CEM23}$).....	317
Table 8-9. Empirical constants for U_{AM_caps}	339
Table 8-10. Composition of new aggregate mixtures for validation	340
Table 8-11. Validation results.....	340
Table 8-12. The first proposed aggregate composition ratio for capsule-based mix designs	343
Table 8-13. The first proposed mix designs of capsule-based concrete	344
Table 8-14. The second proposed aggregate composition ratio for capsule-based mix designs.....	346

Table 8-15. The second proposed mix designs of capsule-based concrete	347
Table 8-16. Probability of capsule breakage in a certain crack plane	359
Table 9-1. IPR strategy proposed	366
Table 9-2. PEST analysis for valorization	367
Table 9-3. Risks identified	367

Chapter 1

INTRODUCTION

1.1 Background and problem statement

Concrete is one of the most consumed materials all over the world and it is regarded as an essential construction material in the global construction and infrastructure sector. The ability of concrete to withstand high compressive stresses contributes to its high load-bearing capacity. In contrast, concrete is relatively weak in tension and needs reinforcement to withstand tensile forces and to make it more ductile. Even with embedded reinforcement inside the concrete, the cracks may inevitably occur due to numerous factors such as climate-related exposure, high tensile stresses, etc. Cracks continuously grow from the micro size to the macro size and they can emerge in different locations. The formation of these cracks is one of the major causes of concrete degradation. The ingress of water, harmful liquids, acidic gaseous pollutants and other substances into the crack can jeopardize the internal structure of concrete elements by corroding the steel reinforcement and/or deteriorating the microstructure of concrete. Efforts have been spent to patch existing cracks using different techniques; however, they are costly, cause indirect costs (e.g., economic losses from traffic jams which occur due to the repair works in the field), and in a lot of cases the repair is temporary. Therefore, there is a need to find a sustainable way of healing cracks. To mitigate this issue, over the last decade, self-healing technologies have received great attention from researchers due to their effectiveness in closing cracks. These aforementioned technologies enable the cementitious composite to repair cracks independently, without human intervention, by stimulating autogenous healing and autonomous healing mechanisms.

Crystalline admixture (CA), bacteria and encapsulated agents are some types of promising healing agents that have been introduced lately. CA is defined as a type of permeability-reducing admixture (PRA), as reported by the ACI Committee 212 [1], with a hydrophilic nature, reacting easily with water. The self-healing phenomenon of mortar containing CA (Xypex Admix C-1000NF) was studied earlier by Sisomphon et al. [2] and they found that cracks with a width up to 250 μm were completely healed. Calcium carbonate (CaCO_3) was found to be the major healing product. The healing capacity of CAs (Harbin CA, citric acid, silica dioxide, sodium silicate, sodium carbonate) for micro cracks ($< 300 \mu\text{m}$) is relatively effective, but macro cracks ($> 300 \mu\text{m}$) are hard to be healed [3]. García-Vera et al. [4] reported an improvement in the durability behaviour of mortar containing CA (Xypex Admix C-1000NF) (a greater compressive strength, a lower mass loss and a lower reduction of Young's modulus than the control mortar after 90 days of sulphuric acid attack). Ferrara et al. [5] upscaled the utilization of CA (Penetron Admix) to produce high-performance, fibre-reinforced cementitious composites and revealed that the mechanical performances (the load capacity, stiffness, ductility and toughness) of cracked specimens were significantly recovered after a short healing period of about one month under water at 20°C.

On the other hand, the implementation of bacteria as a self-healing agent in the concrete matrix emerges as one of the most promising approaches in healing cracks. Jonkers et al. [6] started to investigate the viability of bacteria spores (*Bacillus pseudofirmus* and *Bacillus cohnii*) in cement paste with the addition of calcium precursor compounds as nutrient for bacteria growth. This showed that the number of viable bacterial cells (vegetative cells plus bacterial spores) significantly decreased with increasing specimen age, indicating the low viability under a highly alkaline environment. To address the issue of bacteria vulnerability, several encapsulation techniques were proposed to protect the bacteria using hydrogels [7–9], nanoparticles [10], aggregates [11] or capsules [12]. Furthermore, Mondal et al. [13] suggested the optimal bacterial (*Bacillus subtilis*) concentration of 10^5 cells/mL for strength enhancement and 10^7 cells/mL for durability purposes (reduction in water absorption and water penetration depth). Pei et al. [14] supported the fact that the incorporation of *Bacillus subtilis* into the mortar mixtures improved the compressive strength and decreased the porosity at a specific dosage. The properties of the fresh cement paste/mortar mixture containing bacteria are still unclear. Previous work of Schreiberová et al. [15] showed, for instance, that the

addition of nutritional admixtures, that bacteria need for their growth, resulted in an increased fluidity of the fresh cement paste.

The concept of encapsulation technology was first introduced by White et al. [16] in polymer systems. Encapsulation can be defined as an advanced technique to entrap the healing agent inside a capsule-like material. The encapsulated agents are present in the composite and when a crack penetrates into it, the inert shell of the encapsulated material is ruptured, releasing the healing agent from the core to start the healing action. Based on their size, macrocapsules and microcapsules can be distinguished. Giannaros et al. [17] developed microcapsules with mean sizes of 130 and 500 μm for autonomic self-healing of hardened cement paste. The microcapsules were successfully added into the fresh cement paste and an increased viscosity was noticed in the paste containing microcapsules. As a proof of concept, Kanellopoulos et al. [18] performed a three-point bending test on hardened cement paste prisms with the addition of microcapsules. After loading, the specimens were fractured and, from the split sections of cracked specimens, it was observed that there were an unquantified number of 'wet' spots, indicating the ruptured microcapsules. A substantial reduction in compressive strength and Young's modulus of mortar containing organic microcapsules (with urea formaldehyde and epoxy as shell and core materials, respectively) as compared with the control mortar was reported by Wang et al. [19]. However, after being subjected to a healing scenario, the porosity and total pore volume of mortar were reduced remarkably.

To utilise macrocapsules in self-healing mortar/concrete, the capsules should be able to break when the specimen is subjected to cracking while the capsules should not be destroyed during the mixing. Hilloulin et al. [20] suggested that the brittleness of (polymeric) capsules should be designed as high as possible but also allowing to be mixed in. Van Tittelboom et al. [21] used different types of glass and ceramic capsules in mortar specimens as a proof-of-concept. After the capsules were ruptured and specimens were subjected to healing, an improved strength regain and a reduction in water permeability were noticed due to the activation of a suitable healing agent (two-compound system of a prepolymer of polyurethane (PU) and accelerator). Cementitious capsules were also successfully experimented in previous works [22–25] and positive results with regard to healing efficiency were shown. The properties of the fresh concrete mixture as well as the mechanical strengths were in most cases not evaluated as the research focussed first on the quantification of the self-healing capacity.

Self-healing concrete promotes a longer life-span of concrete structures and reduces maintenance costs. During the past decade, there have been many publications reporting the feasibility of different healing agents in the application of cementitious mortars, while very limited publications have reported on upscaling to the concrete level. In fact, it remains rather unclear on how the results observed in the mortars will be transferrable to the concrete. In most cases, the healing agents are simply added to the normal mix, without making any adaptations to the design of the concrete mix. In other words, the mix design for self-healing concrete still keeps maintaining the same proportion of each component from the reference mix design. Although researchers have demonstrated the crack healing achieved by self-healing concrete, it is very important to examine the workability of self-healing concrete mixtures and assess the long-term performance of the hardened self-healing concrete before healing to guarantee that the healing agents do not negatively affect the concrete properties to some extent. Knowledge on the consequences of incorporating healing agents in concrete will allow to define adequate mitigation strategies.

1.2 Objectives and main contributions of the research

The main objectives of this doctoral study are listed below:

- to develop a robust methodology for the design of optimized self-healing concrete mixes to be used in ready-mixed concrete applications which should overcome the problems arising from the current practice where self-healing agents are added just 'on top' of the normal concrete mixes
- to compensate the possible strength reduction due to the inclusion of self-healing additives by an enhanced mix design
- to understand the key parameters affecting mechanical properties, consistency and self-healing efficiency
- to facilitate the valorization of self-healing concrete by mix design optimization fulfilling the demands with regard to workability, self-healing efficiency and mechanical performance considering the objectives of the specific engineering application.

To achieve at these objectives, numerous concrete mix designs are developed, employing various healing or sealing agents. Different strategies are presented for mix design optimization based on the selection of agents, test methods and research objectives. The fresh, hardened and self-healing or self-sealing properties of concrete are primarily investigated.

The original contributions are summarized as follows.

1. Self-healing technologies are often applied in cementitious pastes and mortars and to a small extent they are applied into concrete. Upscaling self-healing technologies to the concrete-level is necessary as there are still many concerns arising to successfully incorporate healing agents into the concrete mix without changing the concrete properties. Therefore, this research contributes to apply several self-healing technologies at concrete level. Preliminary investigations at paste and mortar levels were performed to ensure the compatibility between healing agents, cement and chemical admixture.
2. A full insight on the specific alteration of fresh and hardened properties of self-healing concrete caused by the incorporation of various healing agents is obtained. There are six healing agents studied in this research including crystalline admixture, bacteria, bacteria-based biomass, fungi-based biomass, microcapsules (water-repellent agent as cargo) and macrocapsules (water-repellent agent as cargo). Different healing agents induce different effects on concrete properties and understanding the consequences of incorporating healing agents opens the possibility to do the optimization by eliminating the negative effects induced by the healing agents.
3. Optimization techniques for self-healing concrete are introduced depending on the selection of healing agent and their considered effects on concrete properties. The optimization process is essentially based on large experimental data sets (e.g., compressive strength, tensile splitting strength, ultimate bond strength, healing efficiency, sealing efficiency and workability) using full and fractional factorial design approaches. Mix design modifications are also considered to optimize the performance of self-healing concrete.
4. Almost no studies are found in the literature where the bond between the reinforcement and self-healing concrete matrix is investigated. The capabilities of various healing agents towards the bond behavior of steel reinforcement in self-healing concrete are further explored in this research. Results give insight on the possibility of improving the bond properties with the aid of healing agents.
5. At the time this thesis is written, there is no official standard for testing self-healing concrete. Hence, several methodologies / procedures to quantify the healing and sealing efficiencies of concrete are used for the lab-scale experiments. First, the crack width measurement was done via optical microscopy to assess the healing efficiency in terms of crack closure. Second, the permeability test was performed to assess the sealing efficiency by measuring the water flow rate in function of healing

time (in relation to the formation of healing products inside the crack). Third, the pull-out test for self-healing concrete was performed to understand the healing efficiency mechanically as showcased by the bond restoration. Fourth, capillary water absorption test was performed to assess the sealing efficiency of cracked/sealed concretes.

1.3 Organization of the text

The outline of the thesis is divided into ten chapters and Figure 1-1 presents how the different chapters interact with each other and which healing agents are considered in each of the chapters. In general, the content of each chapter can be summarized as follows:

Chapter 1 introduces the thesis by providing background, problem statement and objectives of the PhD research. This chapter is concluded by presenting an overview of original contributions of the research.

Chapter 2 presents the state-of-the-art on the impacts of healing agents on the fresh and hardened properties of self-healing concrete. Several types of healing agents are considered including crystalline admixture, bacteria, micro-encapsulated and macro-encapsulated agents. The main strategies of incorporating healing agents into the concrete mixture are discussed. In addition, pros and cons of using different healing agents towards concrete properties are discussed.

Chapter 3 provides a detailed evaluation of the fresh properties of cement paste with specific healing agents (i.e., crystalline admixture and bacteria) on. The effects of healing agents in different cement environments are investigated in terms of water demand, setting time, mini slump and plastic viscosity. The compatibility between cement, healing agent and superplasticizer is explored in this chapter.

Chapter 4 describes the modification of mix designs of self-healing concrete to improve the healing and sealing performances. Commercial healing agents (i.e., crystalline admixture and bacteria) are mainly used in this chapter. Dosage of healing agent, water-cement ratio (w/c) and cement content are selected as the main mix design parameters. The healing performance is assessed by monitoring the crack closure phenomenon while the sealing performance is evaluated by means of permeability testing. Statistical tests are aided to understand the obtained results. The relationship between healing and sealing efficiencies in self-healing concrete is discussed in detail.

Chapter 5 deals with the investigation on the bond behavior of steel reinforcement in self-healing concrete. Four healing agents are utilized namely crystalline admixture, bacteria, bacteria-based biomass and fungi-based biomass. Different series of specimens are made including uncracked, cracked and healed. The bond-slip behavior of reinforcement is investigated by means of a well-developed pull-out test setup. Several bond parameters (i.e., ultimate bond strength, mean bond strength, fracture energy and slip) are investigated. The inclusion of healing agent into the concrete possesses a slight bond strength recovery after healing. Moreover, healing products, confirmed to be calcium carbonate, are found inside the crack and their morphologies are characterized by means of Fourier transform infrared (FTIR) spectroscopy.

Chapter 6 is a continuation of Chapter 5 with the optimization of concrete mix designs towards the bond properties of steel reinforcement. Specifically here, crystalline admixture and bacteria are used. Nine concrete mix designs are developed and statistically analyzed by the Taguchi method. This method analyses the results based on the signal-to-noise (SN) ratio for process optimization. Three mix design factors (i.e., water-cement ratio (w/c), fine ratio (FR) and healing agent (HA)) are investigated with three levels for each factor. Ultimate bond strength, mean bond strength and fracture energy are taken as main bond parameters. Depending on the size of the crack, an improvement of the bond strength can be attained after undergoing a long healing (i.e., water immersion for 121 days at 20°C).

Chapter 7 discusses the effects of microcapsules on the fresh, hardened and self-sealing properties of concrete. The shell and cargo of the microcapsules are made of polyurethane and water-repellent agent, respectively. A preliminary study is conducted to monitor the changes of fresh and mechanical properties of concrete when microcapsules are added. Furthermore, the influence of microcapsules in cement pastes is evaluated in relation to the water demand and setting time. Then, the mechanical properties of mortar made of different cement types and containing microcapsules are investigated. Based on these preliminary studies, a mix design optimization is performed using the full factorial design technique. Three mix design factors are opted including water-cement ratio, size of microcapsules and dosage of microcapsules. Contour plots are developed to visually show the relationship between mix design parameters and to carefully select the parameters for desired properties.

Chapter 8 explores the effects of macrocapsules on the inert structure of self-healing concrete. The particle packing model of Dewar is implemented in this research. Cementitious capsules and polymeric capsules are used at different dosages and sizes to evaluate their influences on the packing of aggregates. Formulas to predict the voids ratio of aggregates after macrocapsules' addition are proposed. Initial assessments on capsule robustness towards mixing forces are performed and mechanical and self-sealing properties of capsule-based concrete are determined. Based on the modelling section, modifications of the mix design are studied by demonstrating the capsules' effect in different inert structures of concrete.

Chapter 9 elaborates the valorization plans related to this research. Exploitable research results are identified and a strategy for valorization is proposed. A roadmap for commercialization has been considered.

Chapter 10 concludes the work by summarizing the most important research findings and recommendations for future research are suggested.

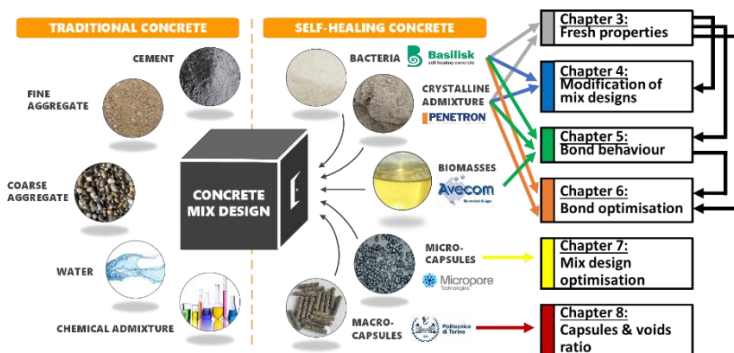


Figure 1-1. General overview of thesis outline and relation between different chapters

Furthermore, Figure 1-2 elaborates the specific title of each chapter with its associated publications (journal and/or congress) and the authors' contribution. All publications are based on the current PhD works where the authors are Harry Hermawan (author of the current PhD) and Elke Gruyaert and Pedro Serna (supervisors of the current PhD work). In chapters corresponding to papers where there are other authors, the main author is Harry Hermawan and no other co-authors will use the same paper in another PhD. The main author worked for his PhD as an early stage researcher 4 (ESR4) in the framework of SMARTINCS project delving into the mix design of self-healing concrete. The global overview of the SMARTINCS project and the main topic of each ESR can be found in Figure 1-3.

PHD CHAPTER	ASSOCIATED PUBLICATIONS	AUTHORS' CONTRIBUTION
CHAPTER 1 INTRODUCTION		
CHAPTER 2 LITERATURE REVIEW	This chapter is based on the following paper: Hermawan H , Minne P, Serna P, Gruyaert E. Understanding the Impacts of Healing Agents on the Properties of Fresh and Hardened Self-Healing Concrete: A Review. <i>Processes</i> . 2021; 9(12):2206.	Conceptualization, H.H. and E.G.; Methodology, H.H. and E.G.; Formal analysis, H.H.; Investigation, H.H.; Data curation, H.H.; Writing—original draft preparation, H.H.; Writing—review and editing, H.H., P.M., P.S. and E.G.; Supervision, P.M., P.S. and E.G.; Project administration, E.G.; Funding acquisition, E.G.
CHAPTER 3 FRESH PROPERTIES OF THE MODIFIED CEMENT PASTE WITH INCLUSION OF HEALING AGENT AND ADMIXTURES	This chapter is based on the following papers: (1) Hermawan H , Minne P, Brac EG, Wiktor V, Serna Ros P, Gruyaert E. Influence of Crystalline Admixtures and Bacteria on the Fresh Properties of Self-healing Concrete. In: Proceedings of the 75th RILEM Annual Week 2021, RW 2021 Springer International Publishing; 2023. p. 451-60; and (2) Hermawan H , Beltran GS, Wiktor V, Serna P, Gruyaert E. Effect of healing agents on the rheological properties of cement paste and compatibility with superplasticizer. <i>MATEC Web Conf</i> 2022;5008(361).	Conceptualization, H.H., V.W. and E.G.; Methodology, H.H., V.W. and E.G.; Formal analysis, H.H.; Investigation, H.H., V.W. and G.S.B.; Data curation, H.H.; Writing—original draft preparation, H.H.; Writing—review and editing, H.H., V.W., G.S.B., P.M., E.G.B., P.S. and E.G.; Supervision, V.W., G.S.B., P.M., P.S. and E.G.; Project administration, E.G.; Funding acquisition, E.G.
CHAPTER 4 EVALUATION OF MODIFIED MIX DESIGNS OF CONCRETE CONTAINING CRYSTALLINE ADMIXTURE TOWARD SELF-HEALING AND SELF-SEALING PERFORMANCES	This chapter is based on the following paper: Hermawan H , Wiktor V, Serna P, Gruyaert E. Experimental investigation on the novel self-healing properties of concrete mixed with commercial bacteria-based healing agent and crystalline admixtures. In: Proceedings of the SynerCrete'23, Springer International Publishing; 2023. https://doi.org/10.1007/978-3-031-33187-9_77	Conceptualization, H.H., P.S. and E.G.; Methodology, H.H. and P.S.; Formal analysis, H.H.; Investigation, H.H. and E.G.; Data curation, H.H.; Writing—original draft preparation, H.H.; Writing—review and editing, H.H., V.W., P.S. and E.G.; Supervision, V.W., P.S. and E.G.; Project administration, E.G.; Funding acquisition, E.G.
CHAPTER 5 EXPERIMENTAL INVESTIGATION ON THE BOND BEHAVIOUR OF STEEL REINFORCEMENT IN SELF-HEALING CONCRETE	This chapter is based on the following papers: (1) Hermawan H , Wiktor V, Gruyaert E, Serna P. Experimental investigation on the bond behaviour of steel reinforcement in self-healing concrete. <i>Constr Build Mater</i> 2023;383:131378. https://doi.org/10.1016/j.conbuildmat.2023.131378 ; and (2) Hermawan H , Tezer MM, Verstraete W, Belie N De, Serna P, Gruyaert E. Bond behaviour evaluation between steel reinforcement and self-healing concrete containing non-axenic biofilms. In: <i>MATEC Web of Conferences EDP Sciences</i> ; 2023. https://doi.org/10.1051/mateconf/202337802009	Conceptualization, H.H. and P.S.; Methodology, H.H. and P.S.; Formal analysis, H.H.; Investigation, H.H. and P.S.; Data curation, H.H.; Writing—original draft preparation, H.H.; Writing—review and editing, H.H., M.M.T., W.V., N.D.B., V.W., P.S. and E.G.; Supervision, V.W., P.S. and E.G.; Project administration, E.G.; Funding acquisition, E.G.
CHAPTER 6 OPTIMIZATION OF CONCRETE MIX DESIGNS TOWARD THE BOND PROPERTIES OF STEEL REINFORCEMENT IN SELF-HEALING CONCRETE BY TAGUCHI METHOD	This chapter is based on the following paper: Hermawan H , Wiktor V, Gruyaert E, Serna P. Optimization of concrete mix designs toward the bond properties of steel reinforcement in self-healing concrete by Taguchi method. <i>J Build Eng</i> 2023;107294. https://doi.org/10.1016/j.jobe.2023.107294	Conceptualization, H.H. and P.S.; Methodology, H.H. and P.S.; Formal analysis, H.H.; Investigation, H.H. and P.S.; Data curation, H.H.; Writing—original draft preparation, H.H.; Writing—review and editing, H.H., V.W., P.S. and E.G.; Supervision, V.W., P.S. and E.G.; Project administration, E.G.; Funding acquisition, E.G.
CHAPTER 7 MIX DESIGN OPTIMISATION OF SELF-SEALING CONCRETE CONTAINING MICROCAPSULES WITH PU SHELL AND WATER REPELLENT CARGO		
CHAPTER 8 EFFECT OF MACROCAPSULES IN THE INERT STRUCTURE OF SELF-HEALING CONCRETE: A PROOF OF CONCEPT	This chapter is based on the following paper: Hermawan H , Simons A, Teirylnck S, Serna P, Minne P, Anglani G, Tulliani JM, Antonaçi P, Gruyaert E. Applicability of cementitious capsules in concrete production: initial assessment on capsule robustness, mechanical and self-sealing properties of concrete. In: <i>MATEC Web of Conferences EDP Sciences</i> ; 2023. https://doi.org/10.1051/mateconf/202337802013	Conceptualization, H.H. and E.G.; Methodology, H.H.; Formal analysis, H.H., A.S. and S.T.; Investigation, H.H., A.S. and S.T.; Data curation, H.H., A.S. and S.T.; Writing—original draft preparation, H.H.; Writing—review and editing, H.H., P.S., P.M., G.A., J.M.T., P.A. and E.G.; Supervision, E.G.; Project administration, E.G.; Funding acquisition, E.G.
CHAPTER 9 VALORIZATION PLANS		
CHAPTER 10 CONCLUSIONS AND RECOMMENDATIONS FOR FUTURE RESEARCH		

Figure 1-2. Detailed information of PhD chapters with their associated publications and contributions

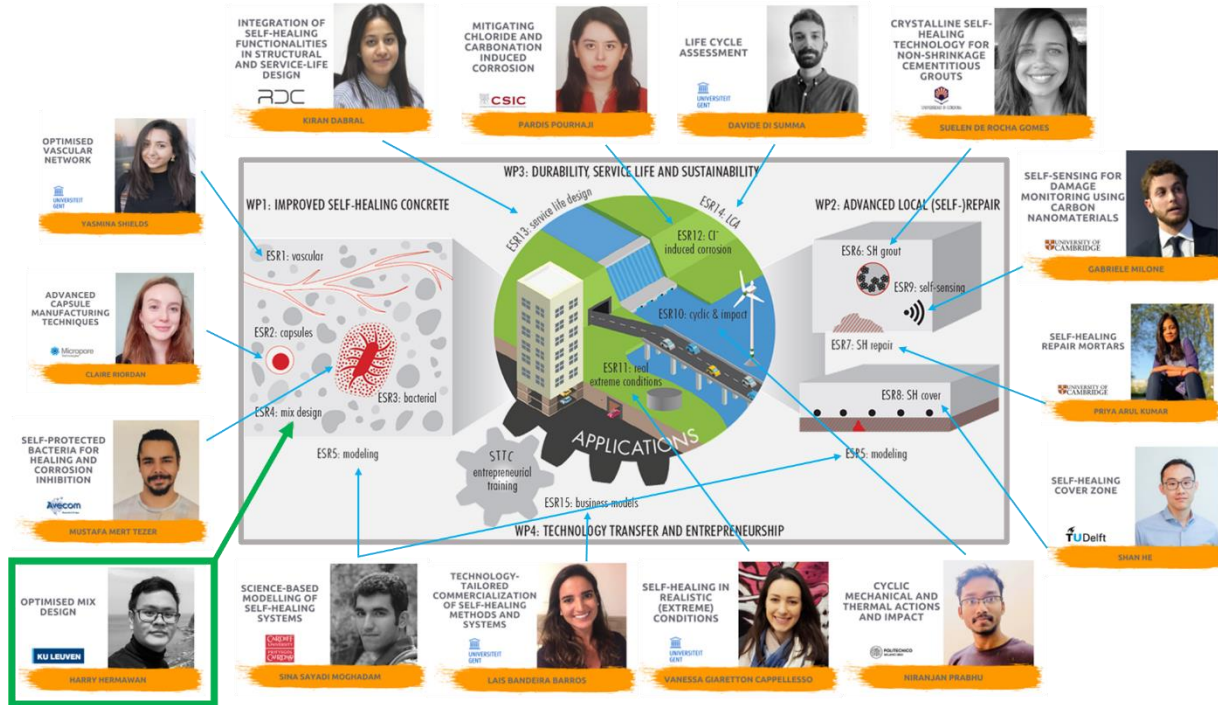


Figure 1-3. Roles of early stage researchers (ESRs) in the framework of SMARTINCS project

Chapter 2

LITERATURE REVIEW

2.1 Novel self-healing agents

Stimulated autogenous healing as well as autonomous healing of concrete primarily occur due to the incorporation and activation of healing agents. In general, the healing agents can be added directly, via a vascular system or after encapsulation. Crystalline admixture (CA), bacteria and micro- or macro-encapsulated agents, such as polymers, minerals, etc., are some types of acknowledged healing agents that have been introduced lately in the application of cementitious composites. The detailed descriptions of these healing agents are summarized below.

CA (Xypex Admix C-1000NF) mainly consists of active chemicals, reactive silica and some catalysts [2]. According to an XRD diffractogram as shown in Figure 2-1, the main constituents of CA (Xypex) are brucite, gypsum, calcite, and quartz, in addition to C_3S , C_2S , C_3A and C_4AF , similar to the clinker minerals in ordinary Portland cement (OPC) [26]. Figure 2-2 shows a scanning electron microscopy (SEM) image of CA. The morphology of CA (Penetron Admix) is similar to cement grains and their sizes are typically in the range of 1–20 μm with irregular shape [27]. Due to the proprietary nature of this admixture, the chemical composition of CA is kept confidential by all producers. CAs are commercially available in the form of dry powder or liquid. The product was originally used as a waterproofing agent for an

*) This chapter is based on the following paper: **Hermawan H, Minne P, Serna P, Gruyaert E.** *Understanding the Impacts of Healing Agents on the Properties of Fresh and Hardened Self-Healing Concrete: A Review. Processes.* 2021; 9(12):2206.

exposed concrete surface. These admixtures will block water from any direction because the concrete itself becomes the water barrier.

In practice, there are three methods to apply the CA as a waterproofing system: (1) coating on the surface of existing concrete, (2) adding the admixture at the time of batching and (3) dry-shaking to the surface of fresh concrete [4]. Adding CA into the mixes leads additionally to stimulated autogenous healing of cracks. When combined with water during concrete production, these chemicals react with calcium hydroxide and the other products resulting from cement hydration to form millions of needle-shaped crystals within the concrete. The crystalline structures continuously grow and fill pores and capillaries in the concrete in the presence of moisture [4]. The crystalline products increase the density of the calcium silicate hydrate (C-S-H) phase [5]. In this way, they become an integral part of the concrete matrix and the crystals block the passages, thus preventing the ingress of water and other liquids that may deteriorate the concrete. The capability of the CA to stay dormant and then become active again in the presence of water promotes the self-healing ability to the concrete [28]. If a crack forms, any water ingress triggers the formation of crystals to fill and block this crack. The benefits of the concrete treated with CA are (1) improved water tightness, (2) good immunity to damage and (3) high effectiveness against hydrostatic pressure. Additionally, CA offers an advantage as no encapsulation is needed, reducing sample preparation time. The functionality of CA can also be combined with other healing agents, for instance, superabsorbent polymer (SAP), to seal macro-cracks more efficiently [3].

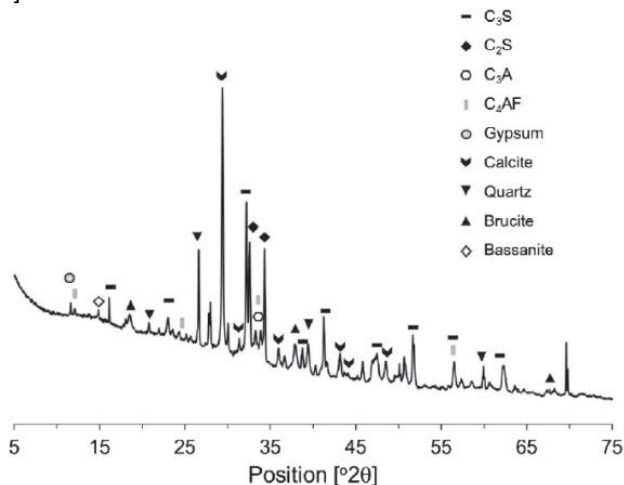


Figure 2-1. XRD diffractogram of CA (Xypex) [26]

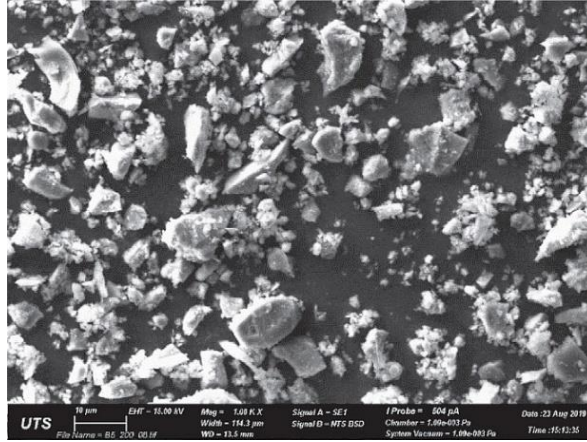


Figure 2-2. SEM micrograph of CA (Penetron Admix) [27]

Bacteria are microscopic unicellular organisms which live everywhere and exist in many forms. The bacteria are typically isolated from a medium such as soil and they are extracted through serial cultivation processes. The presence of a nutrient source is a prerequisite to fully stimulate the growth of the bacteria. The selection of the nutrient is mainly based on the mode of metabolic activity of the used bacteria [15]. For instance, ureolytic bacteria are known as one of the exceptional species of microorganisms in producing excessive amount of carbonates, and bacteria such as *Sporosarcina pasteurii* need urea and calcium sources to precipitate CaCO_3 [29]. On the other hand, *Bacillus* is a genus of bacteria which is frequently used in the research field due to the fact that they can precipitate calcite crystals as a result of the biomineralization process [30]. Figure 2-3 depicts the rod shaped structure of *Bacillus* bacteria in a solution taken by SEM and optical microscopy. According to the available reports, some prospective bacteria that have been used extensively in concrete are *Bacillus sphaericus* [10,31], *Bacillus subtilis* [32–34], *Bacillus aerius* [35], *Bacillus megaterium* [30], *Bacillus cohnii* [36–39], *Sporosarcina pasteurii* [29,40–42], *Shewanella oneidensis* [43], and a mixed ureolytic culture (MUC^+) [44].

Bacteria are often proposed as a healing agent to promote an autonomous self-healing repair system based on a biotechnology approach. When cracks appear in the concrete and water penetrates through cracks, the metabolic activation of the dormant bacteria induces the precipitation of CaCO_3 into the pores and cracks, leading to a densification of the concrete

matrix. The rate of CaCO_3 precipitation is dependent upon the type of bacteria and the concentration of bacteria. A higher concentration of bacteria typically generates higher precipitation of calcite, which is beneficial for the purpose of concrete protection. In general, there are three proposed techniques to incorporate bacteria into the concrete: (1) bacteria are added directly without carriers at the time of batching [35,42,43], (2) bacteria are impregnated into pellets or aggregates [11,45,46] and (3) bacteria are encapsulated via capsules or a vascular network [23,47,48]. The utilization of carriers is regarded as one of the most promising solutions to enhance the possibility of bacterial survival [33] because the concrete's high pH and the shear stress during the mixing stage may lower the viability of bacteria [10]. Concrete treated with bacteria offers generally a wide variety of advantages, such as (1) self-repair of cracks without any external aids, (2) good improvement in mechanical properties and (3) more sustainable and durable concrete.

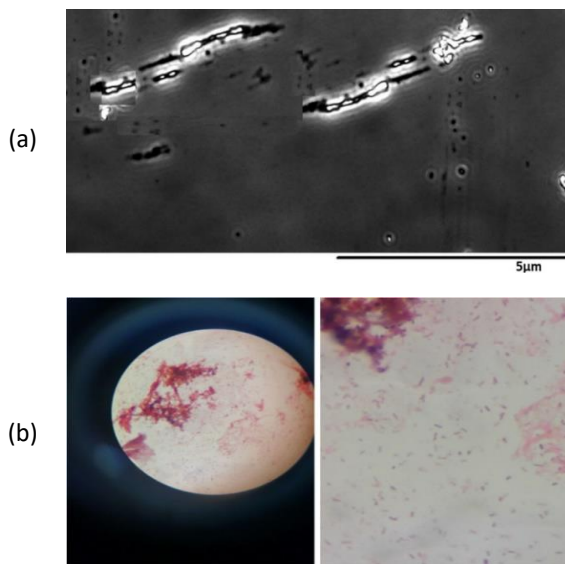


Figure 2-3. (a) *Bacillus* bacteria cell under SEM [30], (b) isolation of bacteria colonies under a stereo microscope [42]

The encapsulation method is constantly developed in the field of concrete technology, ranging from the microscale to the macroscale. In this chapter, the encapsulation of healing/sealing agents considers the use of capsule-like carriers. The encapsulation of agents such as bacteria via pellets or aggregates is not considered in this review.

- (1) Microcapsules have a nominal size of no more than 1 mm and are produced with a variety of production methods (i.e., interfacial polymerization, in situ polymerization, spray drying, ionic gelation and complex coacervation—as discussed by Kanellopoulos et al. [18]). Table 2-1 shows the different types of microcapsules which have been successfully applied in concrete. Morphologically, microcapsules have mostly a spherical shape, as shown in Figure 2-4. The production of microcapsules has to be carefully performed because many parameters may change the physical properties of the final product. Three important design parameters are capsule size/diameter, shell thickness and surface texture [49]. Other parameters such as type of formation, materials and volume will certainly affect the size distribution. The size of microcapsules significantly affects self-healing efficacy. Comparing the same amount of healing agent in smaller or larger capsules, smaller microcapsules open the possibility to heal more scattered cracks due to their high distribution inside the matrix, while larger microcapsules carry more healing agents that may cover a larger healed area, which are effective to seal wider cracks and can simultaneously heal smaller cracks in a nearby region. Hence, it is still unclear what would be the best size of the microcapsules in order to achieve optimal self-healing performance. In general, thin-walled microcapsules would fail during the production process and concrete mixing, while thick-walled microcapsules are reluctant to break as the propagated crack will hardly penetrate [17]. The size and morphology of prepared microcapsules are dependent on numerous factors including temperature, pH and agitation rate [17,18,50,51]. Microcapsules are typically stored in a preserving solution to prevent shrinkage and the premature hardening of microcapsules as may occur in a dry condition. To incorporate the microcapsules in concrete, direct addition during the mixing stage has been investigated in several studies [49,52,53].
- (2) Macrocapsules are bigger in size (>1 mm) and can store a larger amount of healing agents than microcapsules. Macrocapsules can be also produced with the same methods used for microcapsules, however specifically here the tubular macrocapsules will be further discussed. Macrocapsules can be prepared by cutting the long tubes into short tubes or the capsules can be manufactured by means of an extruder through an extrusion process [22,23,54]. Table 2-2 presents various types of capsules used in the application of self-healing concrete. The physical appearance of some tubular capsules is shown in Figure 2-5. Glass capsules could affect negatively the concrete durability due to the

undesired alkali-silica reaction (ASR) [55,56], while polymeric capsules could cause premature curing of an entrapped agent such as PU [54]. To avoid these drawbacks, ceramic capsules [57] and cementitious capsules [22–25] were successfully experimented. To incorporate the capsules into the concrete, other aspects such as capsule dimensions (i.e., diameter, thickness and length) also play an important role in the self-healing scenario because the capsule should be able to break when a crack propagates. Thin-walled capsules are effective for capsule breakage during cracking of the concrete as they are relatively fragile; however, they would fail when the capsules are added during the mixing. Conversely, thick-walled capsules are highly resistant to withstand mixing forces, but they are reluctant to break as the propagated crack will hardly penetrate through the planar surface of the capsules and this might lead to a lower self-healing efficiency. The same problem occurs with the length of capsules. Short capsules may cause a slippage [54,58] when a crack appears, while long capsules will be more challenging to be incorporated into the concrete because of the interaction with aggregates which will disturb the packing system. Thus, the optimal design of macrocapsules remains an interesting topic of research. To author's knowledge, there are two methodologies to incorporate macrocapsules in concrete mixes, namely manual placement and direct addition. In the first method, the most practical application is manually placing the capsules in the cover zone of mortar/concrete (as shown in Figure 2-5a,b), while in the second method, a previous work [56] attempted to incorporate the capsules directly into the fresh mixture during the mixing stage. The random distribution of mixed-in capsules was observed in the hardened concrete core, as shown in Figure 2-5c.

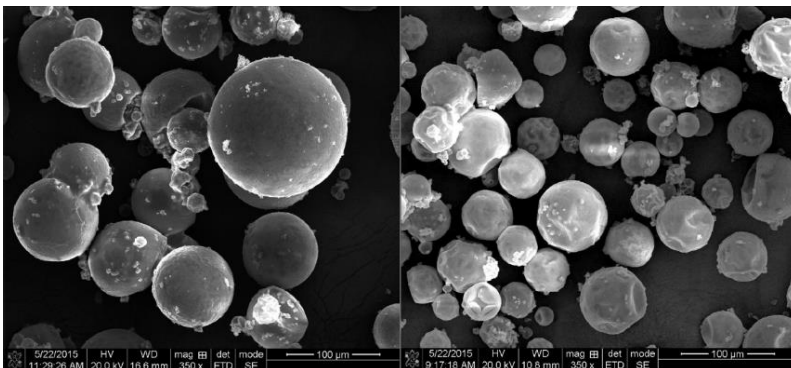


Figure 2-4. Optical microscopic images of produced microcapsules [59]

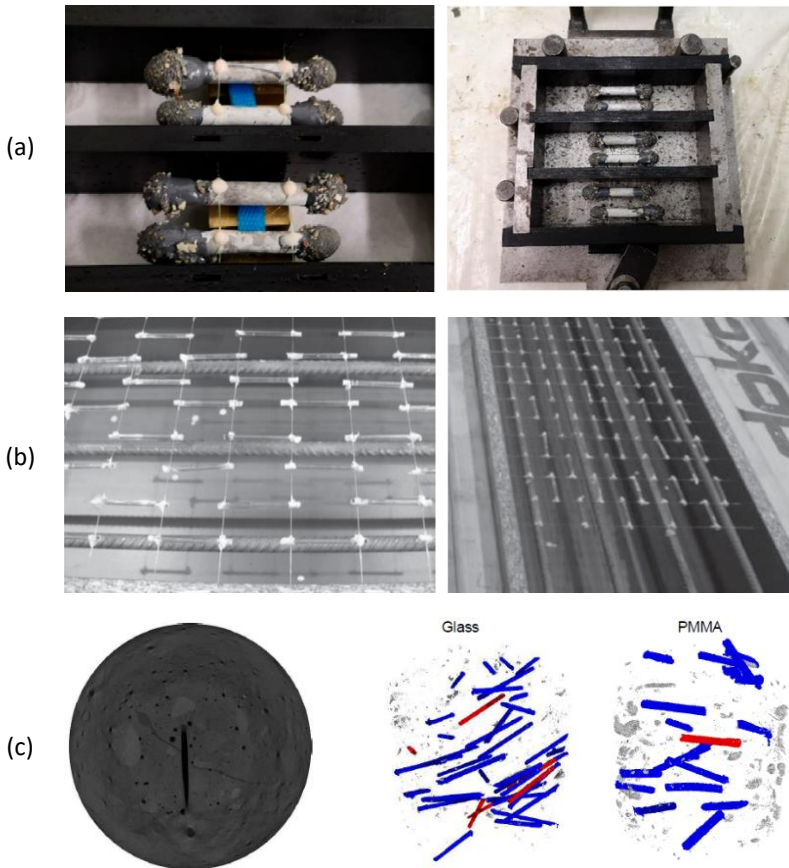


Figure 2-5. (a) Manual placement of two cementitious capsules in a small-scale mortar mould [22]; (b) manual placement of glass capsules onto a network of wires in a large-scale concrete beam mould [60]; (c) reconstructed CT scan of a sliced concrete core with a glass capsule crossed by a crack (left) and the 3D distribution of capsules in the concrete cores as a result of direct addition of capsules during concrete mixing (right) [56]

Table 2-1. Different microcapsule materials with the corresponding parameters and characteristics used in concrete application

Ref.	Production Method	Microcapsule Shell	Cargo	Capsule Diameter (μm)	Shell Thickness (μm)	Remarks
[50]	In situ polymerization	Polyurethane/urea-formaldehyde	Sodium silicate	Not specified	Not specified	Spherical double-walled microcapsules with rough surface
[49]	Interfacial polymerization	Polyurethane	Sodium silicate	Not specified	Not specified	Self-synthesized microcapsules with rough surface
[18,61]	Complex coacervation	Gelatin/gum Arabic shell	Sodium silicate	290	5–20	Microcapsules with the shape of “rugby-ball” which have switchable mechanical properties
[19]	In situ polymerization	Urea-formaldehyde	Epoxy resin	45–185	5.46	Spherical-shaped organic microcapsules that can produce ductility for the cementitious composites
[52]	In situ polymerization	Urea-formaldehyde	Epoxy resin	110–190	Not specified	Round-shaped microcapsules with non-smooth surface which have a good thermal stability
[59]	In situ polymerization	Urea-formaldehyde	Calcium nitrate	22–59	Not specified	Smooth surface and non-porous texture
[62]	In situ polymerization	Urea-formaldehyde	Calcium nitrate	22–109	Not specified	Smooth exterior surface coated with Span60 emulsifier
[51]	In situ polymerization	Urea-formaldehyde	Calcium nitrate	41–107	0.60–1.31	Spherical-shaped microcapsules with smooth exterior surface and rough interior surface

[53]	In situ polymerization	Urea-formaldehyde	Dicyclopentadiene	80–600	0.20–0.25	Rough permeable outer layer and smooth interior shell free of cavities; more uniform
	In situ polymerization	Polyurethane/urea-formaldehyde	Sodium silicate	450–550	0.45–0.70	Rough permeable outer layer and smooth interior shell free of cavities; less uniform

Table 2-2. Different macrocapsule materials with the corresponding parameters and characteristics used recently in mortar and concrete applications

Ref.	Type of Composite	Specimen Size (mm)	Macrocapsules					Cargo	Dosage of Capsules	Placement Method	Remarks
			Shell	OD (mm)	ID (mm)	L (mm)	Coat				
[60]	SR-SCC	150 × 250 × 3000	Glass	3.35	3	50	-	PU	350 caps/beam	Manual	Capsules started to break when the crack width amounted to 50 μm.
[56]	SR-SCC	200 × 400 × 2500	PMMA	6.5	5.1	50	-	WRA	22 caps/L of concrete	Direct addition	Survival probability of the PMMA capsules increased as the wall thickness of the capsules increased. Capsules were able to rupture at crack width of 116 μm.

	SR-SCC	200 × 400 × 2500	Glass	5	3.4	50	-	WRA	22 caps/ L of concrete	Direct addition	Good survivability with thick-walled capsule and more uniform distribution using glass capsules than PMMA capsules. Capsules were able to rupture at a crack width of 30 μm.
[57]	FRC	100 × 100 × 650	Glass, ceramic	Not specified	3	60, 400	Mortar layer, cement paste bar	PU	Not specified	Manual, direct addition	Capsules broke during the mixing stage, while they remained intact when the capsules were placed manually using wires.
	TC	120 × 120 × 500	Glass	2.3	1.7	25, 50	-, Ethyl cellulose	PU	2% v/v	Direct addition	The dip-coated capsules showed a higher survivability than the uncoated capsules. Capsules were able to rupture at a crack width of 400 μm.
[54]	Mortar	40 × 40 × 160	Ethyl cellulose	5	3	50	-	PU	2 caps/prism	Manual	Some capsules were not broken after complete cracking and polymeric capsules showed an incompatibility issue as the stored healing agent is prematurely cured inside the capsule.

[63]	Mortar	50 × 50 × 220	Glass	7.05	6.15	50	Thin PVC film	TEOS, SS, CS, C	2 caps/prism	Manual	Capsules and its corresponding cargo could survive in a high pH solution (pH = 12) similar to cement, except cyanoacrylate (C) which started to harden within 4 days after encapsulation.
[20]	Mortar	40 × 40 × 160	Polymers –PLA, PS, P(MMA/n-BMA)	5	3	50, 100	-	Water	2–4 caps/prism	Manual, direct addition	Moderate resistance during the mixing stage. P(MMA/n-BMA) capsules showed a high brittleness and they ruptured when subjected to a relatively small deformation.
[23]	Mortar	40 × 40 × 160	Cementitious	10	7.5	50	Epoxy	WRA, PU, bacteria	1–2 caps/prism	Manual	Cementitious capsules were able to sequester and release the healing agents. They showed a good protection between agents and harsh environment of the matrix.

Note: OD = outer diameter, ID = internal diameter, L = length, SR-SCC = steel reinforced self-compacting concrete, TC = traditional concrete, FRC = fibre reinforced concrete, PMMA = poly(methyl methacrylate), PLA = poly(lactic acid), PS = polystyrene, P(MMA/n-BMA) = poly(methyl methacrylate/n-butyl methacrylate), PU = polyurethane, WRA = water-repellent agent, SS = sodium silicate, TEOS = tetraethyl orthosilicate, CS = Colloidal silica, C = Cyanoacrylate.

2.2 Comparative study on the inclusion of self-healing agents into the concrete mix

Following the development of novel self-healing agents, different agents induce different effects on cementitious composites. In the initial phase, the self-healing ability was mostly monitored on paste and mortar matrices. In fact, the influence of agents on concrete level might be different. Prior to the activation of the self-healing effect, it is vital to guarantee that the agents do not negatively affect the concrete properties. To understand the concrete behaviour as a consequence of incorporating healing agents, it is necessary to highlight some key parameters that affect the properties of fresh and hardened self-healing concrete. The main aspects covered in this review are:

- The main strategies of incorporating healing agent with or without capsules into the self-healing concrete mixes, as described in Figure 2-6;
- Effect of addition of healing agents on the properties of fresh and hardened concrete before healing (especially for micro- and macro-encapsulated agents, these properties will be evaluated based on the physical presence of capsules in the concrete matrix);
- Brief evaluation of the self-healing phenomenon in cracked concrete after healing (Note: the term of healing efficiency/ratio refers to the crack width reduction or crack closure by microscopic investigation, while the sealing efficiency/ratio refers to a reduction in water flow rate tested via a permeability test or a reduction in sorption rate tested via a capillary water absorption test). Testing methods to evaluate self-healing/sealing capacity of the concrete will not be addressed in this review, but can be found in [64].





Healing agent (HA)	Main strategies of incorporating HA into concrete (current practices)	Parameters and materials considered
<p>Crystalline admixture (CA)</p> 	<ul style="list-style-type: none"> Utilization of CA as: <ul style="list-style-type: none"> + a direct addition on top of normal concrete mix (without changing the mix design) + a partial replacement of filler (e.g. limestone powder) + a partial replacement of cement + a partial replacement of aggregate 	<ul style="list-style-type: none"> Effective dosage of CA (typically 0.8–4.5% by weight of cement)
<p>Bacteria</p> 	<ul style="list-style-type: none"> Direct addition of bacteria on top of normal concrete mix (without changing the mix design) Encapsulation of bacteria to improve the cell viability (e.g. immobilization, impregnation, etc.) 	<ul style="list-style-type: none"> Bacteria genus and species; and the concentration of bacteria (typically 10^3–10^{10} cfu/ml) Selection of a suitable nutrient/precursor and its dosage Selection of compatible chemical admixtures
<p>Micro-encapsulated HA</p> 	<ul style="list-style-type: none"> Direct addition of microcapsules on top of normal concrete mix (without changing the mix design) 	<ul style="list-style-type: none"> Size and concentration of microcapsules (typically 0.5–10% by weight of cement) Shell material of microcapsules and its cargo
<p>Macro-encapsulated HA</p> 	<ul style="list-style-type: none"> Direct addition of macrocapsules on top of normal concrete mix (without changing the mix design) Instalment of the capsules (in relation to the capsule distribution): <ul style="list-style-type: none"> + manual placement in the mould by means of wires (capsules are not added during mixing stage) + random distribution and orientation of the capsules (capsules are added during mixing stage) 	<ul style="list-style-type: none"> Type of capsule material and the dimension of the capsule (length, diameter and thickness) Survivability of capsules during mixing stage: (1) evolving capsule brittleness by plasticizing agents or by heating and (2) increasing capsule thickness Dosage (or number) of capsules added into the concrete Selection of healing agent stored inside the capsule

Figure 2-6. Main strategies to introduce healing agents in the recent application of self-healing concrete

2.2.1 Effects of CA on concrete properties

2.2.1.1 Properties of the fresh concrete mixture

Based on previous studies [65,66], workability of fresh CA-based concrete, termed as CA concrete, is mostly assessed by its slump value (at least for traditional concrete mixes), determined in accordance with EN 12350-2:2009. It should be mentioned in this regard that for most studies, the CAs were just added to the reference mix, while only a small number of studies have made modifications to the self-healing concrete mix design.

Roig-Flores et al. [66] characterized the workability of fresh fibre-reinforced concretes between two mix batches (control and CA) with 4% addition of CA (unspecified) by weight of cement. According to their mix design, the amount of CA was opted as a replacement of limestone powder (LP), while the total quantity of the powder materials (cement + LP + CA) was kept constant for both mixes. A slight adjustment was made to the nominal amount of aggregates. For instance, in the composition of CA concrete, the amount of gravel 4/12 increased from 950 to 959 kg/m³ as compared with the control concrete, while the amount of natural sand decreased from 899 to 875 kg/m³. Steel fibre was added equally for all mixtures with the purpose of controlling crack width during the self-healing test. The slump values for control concrete and CA concrete were 130 mm and 150 mm, respectively. The difference of slump test results between these two mixes was minor because the slump was deliberately maintained in a similar value (140 ± 20 mm) by adjusting the dosage of superplasticizer. In another study by the same authors [65], the same concept of adding CA as an LP replacement was applied on precast concrete C45/55 and standard concrete C30/37. The results showed that slump values for all mixes were identical because the amount of superplasticizer was adjusted to reach a similar slump value (~150 mm), and thus the effect of CA was not apparent.

The application of CA on high performance fibre reinforced concrete (HPFRC) was introduced by Escoffres et al. [67]. The amount of CA (Sika WT-250) was fixed at 2% by weight of cement (equivalent to 11 kg/m³), while all concrete components, including steel fibres, were kept constant with respect to the reference mixture except for the aggregates. The amounts of both fine and coarse aggregates were slightly reduced to compensate for the addition of CA. The amount of sand was reduced from 814 to 808 kg/m³, while coarse aggregates from 658 to 653 kg/m³. Chemical admixtures, such as a superplasticizer and viscosity agent, were added in the same amount. The workability of the concrete mixtures was measured by the slump flow test

and the results showed that the HPFRC mixtures without and with CA had slump flow values of 530 and 540 mm, respectively. There was no considerable effect of CA addition on the flowability of concrete.

Moreover, Azarsa et al. [68] investigated the properties of fresh normal strength concrete mixtures with two different cement classes named OPC and Portland Limestone Cement (PLC). CA (Kryton) in powder form was added in addition to the normal mix with a dosage of 2% by weight of cement. No superplasticizer was introduced in these mixes. In the case of the OPC mixtures, the inclusion of CA resulted in a reduction of the slump value from 130 to 110 mm and the air content was slightly increased by 0.2%. On the other hand, the slump value decreased considerably on the PLC mixtures from 130 to 85 mm and a 0.3% increase of the air content was observed. One possible reason for the reduced workability can be associated with the nature of the CA as a hydrophilic material. Azarsa et al. [68] claimed that due to its unique characteristics, in the initial stage of mixing the concrete, CA tends to absorb water which results in a lower workability. Although the addition of CA showed a reduction in slump values and a slight increase in the air void content, the plastic densities between CA concretes and reference concretes were found to be similar. It is noteworthy to mention that different studies use different types of CAs, with varying chemical composition and physical properties. However, most CA producers argue that the addition of their commercial CAs shows little or no effect on the workability aspect.

2.2.1.2 Properties of the hardened concrete

While an introduction of CA into the concrete mix is designated to enhance autogenous self-healing [27], the mechanical properties of concrete treated with CA show a considerable improvement regardless of the type of concrete, as can be seen from Figure 2-7 which is compiled based on [65,66,68–71]. The compressive strength of CA-based concrete is directly associated with the addition of CA and the proportioning of concrete constituents. Figure 2-7 shows the 28-day strength improvement of CA concretes with respect to the corresponding reference concretes. In addition, Table 2-3 shows the description of each mix code including concrete type, type of cement, water-to-cement ratio (w/c), CA dosage and the role of CA.

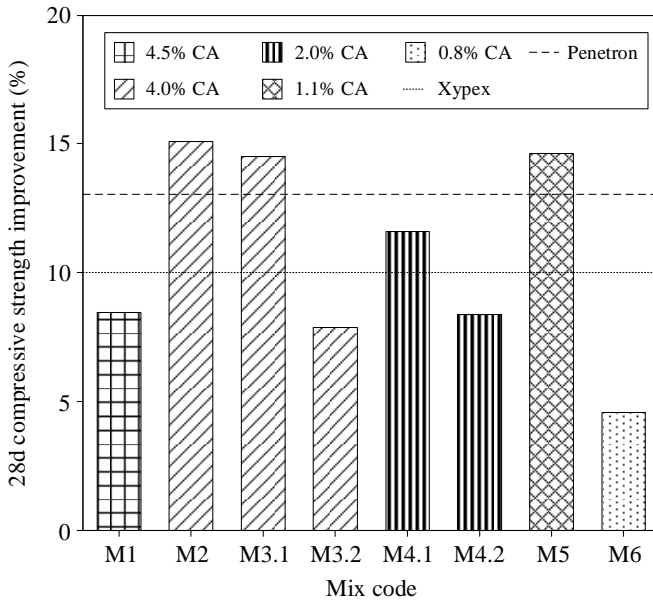


Figure 2-7. Concrete strength increments due to the addition of CA at 28 days; data are taken from available literatures and the details of mix code can be seen in Table 2-3. The dot and dash-dot lines represent the value of compressive strength enhancement by using Xypex Admix (2–3% CA) and Penetron CA (0.8–1% CA), respectively, according to the technical data sheets [72,73].

Table 2-3. Summary of CA concrete composition and the scenario of self-healing assessment

Ref.	Mix Code	Concrete Type	Cement Type	w/c	CA Dosage (wt% cement)	Role of CA	Age of Cracking	Healing Time	Crack Width (mm)	Healing Ratio (Scale 0–1)	Exposure
[69]	M1	LWC	Not specified	0.45	4.5%	Cement replacement	7 days	28 days	0.150	-	Water immersion
[66]	M2	FRC	II 42.5R	0.45	4%	Limestone powder replacement	2 days	42 days	≤0.3	0.90–1.00	Water immersion
[65]	M3.1	Precast FRC	II 42.5R	0.45	4%	Limestone powder replacement	2 days	42 days	0.1–0.4	0.80–1.00	Water immersion
	M3.2	FRC	II 42.5R	0.60	4%	Limestone powder replacement	2 days	42 days	0.1–0.4	0.80–1.00	Water immersion
[68]	M4.1	NSC	I 42.5R	0.53	2%	Direct addition (on top of concrete mix)	28 days	4–5 days	0.1–0.4	0.98–1.00	Water immersion
	M4.2	NSC	GUL	0.53	2%	Direct addition (on top of concrete mix)	28 days	4–5 days	0.1–0.4	0.97–0.99	Water immersion
[70]	M5	FRC	OPC 53	0.45	1.1%	Cement replacement	2 days	42 days	≤0.4	-	Water immersion
[71]	M6	NSC	II 32.5R	0.64	0.8%	Direct addition (on top of concrete mix)	-	-	-	-	Curing chamber (20 °C, RH >98%)

[74]	M7	NSC	OPC 43	0.40	2%	Direct addition (on top of concrete mix)	3 days	42 days	≤0.4	-	Water immersion
[5]	M8	HPFRCC	II 42.5R	0.63	1%	Direct addition (on top of concrete mix)	42 days	365 days	0.2	0.60	Open air
[75]	M9	UHPC	I + III	0.29	0.9%	Direct addition (on top of concrete mix)	10 months	1-6 months	0.01-0.2	0.72-1.00	Freeze-thaw cycle (-20 to 38°C; 20 cycles of 20 hours each) + Water immersion
[76]	M10	UHPC	I 52.5R	0.33	0.8%	Direct addition (on top of concrete mix)	1 year	1-6 months	0.15	0.50-1.00	Wet-dry cycle (4 days of water immersion + 3 days in lab environment (20 °C, RH >98%))
[77]	M11	UHPC	I 52.5	0.33	0.8%	Direct addition (on top of concrete mix)	> 1 year	1-6 months	0.25	0.30-1.00	Water immersion

Note: LWC = lightweight aggregate concrete, FRC = fibre-reinforced concrete, NSC = normal strength concrete, HPFRCC = high performance fibre reinforced cementitious composite, UHPC = ultra-high performance concrete, GUL cement (General Used Limestone) = Portland Limestone cement which follows Canadian standard for cement.

Wang et al. [69] studied the strength characteristics of lightweight concrete (mix code M1) produced by incorporating CA (Xypex) up to 4.5% as a cement replacement and found that after 28 days of curing, the mean compressive strength enhanced from 29 to 31.5 MPa. Additionally, the flexural strength of this concrete slightly increased from 8.19 to 8.62 MPa. Mix codes of M2, M3.1 and M3.2 were casted by Roig Flores et al. [65,66] to produce fibre-reinforced concretes with the addition of 4% CA by the weight of cement and the addition of CA partially replaced the amount of limestone powder to keep the binder amount constant. The strength improvements of M2 and M3.1 mixtures were recorded at 15.1% and 14.5%, respectively, while the M3.2 mixture had a small increment approximately at 7.9% which may be explained by the influence of higher w/c and lower binder content. Another study [70] also fabricated fibre reinforced concrete (mix code M5) with a lower CA dosage. Here, CA (unspecified) was added as a cement replacement by 1.1% and the strength of the CA-based concrete was 14.6% higher than for the reference concrete.

Moreover, the mix codes of M4.1, M4.2 and M6 are basically classified as normal strength concretes with a relatively low CA dosage in the range of 0.8–2%. Azarsa et al. [68] investigated the influence of different cement classes as OPC type I (mix code M4.1) and PLC type GUL (mix code M4.2) in combination with CA (Kryton) on the compressive strength of self-healing concrete. CA was directly added to the reference mix and the mix composition was featuring the same cement content, w/c and aggregates proportions. The result showed that the highest strength improvement of approximately 11.6% was achieved by the M4.1 mixture while an improvement of 8.4% was observed on the M4.2 mixture. Sideris et al. [71] incorporated 0.8% CA (Penetron Admix) by the weight of cement in addition to the C20/25 mixtures (mix code M6). As can be seen from Figure 2-7, the addition of CA at a low percentage of 0.8% slightly increased the compressive strength by 5.5%.

Generally, it can be observed that the addition of CA in the range of 0.8–4.5% by weight of cement increases the compressive strength up to 15%. However, it is interesting that the gradual CA addition does not linearly increase the strength in the same way. It might be explained by the fact that each study selected different variables, dosages and materials which accordingly makes it difficult to compare the results. On the other hand, commercial CA producers such as, for instance, Xypex and Penetron indicated that the addition of their CA, named Xypex Admix [72] and Penetron Admix [73], resulted in 10% and 13% increase of compressive

strength at 28 days, respectively. The recommended dosages suggested by the CA producers are 2–3% by weight of cement for Xypex Admix and 0.8–1.0% by weight of cement for Penetron Admix. For instance, the mix code of M1 used 4.50% Xypex Admix CA and the concrete had a better compressive strength of 8.4% [69]. One interesting result was found by Pazderka et al. [28] discussing the influence of two types of CAs on the C20/25 concrete mixture. They utilized Penetron Admix and Xypex Admix C-1000NF at the constant dosage of 2% of the cement weight. The compressive strengths of concrete without CA, concrete with Penetron Admix and concrete with Xypex Admix were 36.8, 36.2 and 36.3 MPa. The results were almost identical for all specimens and, in fact, it was in contrast with other results presented earlier. Pazderka et al. [28] hypothesized that the addition of CA in an amount of 2% caused a mild deceleration of the hardening of concrete.

The phenomenon of strength enhancement might be explained by three reasons: (1) the filling effect of CA [65,66], (2) the role of CA as cement hydration activator by promoting the further densification of the microstructure [68] and (3) the production of CaCO_3 by CA inside the concrete matrix upon presence of moisture [74]. Microstructural analysis based on XRD and SEM revealed the presence of CaCO_3 , $\text{Ca}(\text{OH})_2$, C-S-H, crystalline Mg-phase and ettringite in CA concrete specimens [69]. The utilization of CA has a great potential to make concrete more durable and impermeable due to its waterproofing effect to plug the pores by depositing precipitated CaCO_3 crystals. Incorporation of CA also reduces the water penetration depth remarkably. For concrete treated with CA (Kryton), the penetration depth of water can be reduced by 40–50%, indicating the superior water-tightness effect of this admixture [68]. It was also reported that commercial CAs from Xypex and Penetron reduced the water vapor permeability by 16% and 20%, respectively [28]. In addition, CA helped the cementitious matrix to withstand chloride attack and induces lower carbonation depth, thus enhancing the concrete durability and prolonging the service life of the structure [71].

2.2.1.3 Self-healing properties

The healing ability of CA is beneficial for extending the lifetime of concrete. In fact, the evaluation of the self-healing phenomenon is generally dependent on many variables, such as the age of cracking, healing time, crack width and curing condition. Some researchers have performed cracking of specimens at different ages by doing splitting tests or three-point bending

tests and the healing period was varied from around 1 to 6 months. It was suggested by Roig-Flores et al. [66] to crack the specimens during early ages (~2 days) to prevent initial cracking due to shrinkage. In general, the initial crack width is typically controlled in the range of 0.10–0.40 mm. The maximum crack width that can be healed with CA varies between 0.15 and 0.30 mm [5,65–69,78], and if combined with other techniques, such as CA with expansive agents, the healed crack width can be increased up to 0.40 mm [2]. There are some exposure scenarios that have been applied to CA concrete, such as water immersion, water contact, wet-dry cycles, and storage in a humidity chamber and open air; however, the best exposure to effectively stimulate autogenous healing seems to be the water immersion [65,66].

Due to the diversity of testing methods and their associated parameters, it is not easy to compare the results presented in different studies. In general, Table 2-3 summarizes the research programs and parameters used to evaluate the self-healing efficiency. As a note, the healing ratio is assessed by measuring the value of crack width after and before healing by means of microscopic investigation. The crack width reduction vs. the original crack width is considered as the healing ratio. The crack widths reduced considerably in the samples which were fully immersed in water when compared with other exposures. Healing ratios in the range of 0.80–1.00 were obtained [65,66] for concretes treated with CA (unspecified), while the reference concrete can achieve a healing ratio between 0.50–1.00 [65]. When the cracked concrete specimens were subjected to air exposure as a curing condition, interestingly, CA (Penetron Admix) were still able to promote crack healing by up to 60% after several months [5]. It is evident that the presence of moisture plays a key role in activating the CA to further encourage the crystallization process. Kannikachalam et al. [75] exposed their concrete specimens to freeze-thaw cycles (see Table 2-3) for 17 days, and the freeze-thaw exposure certainly damaged the specimens with some cracking. After the exposure, the specimens were immersed in water for healing. After one month of healing, the healing ratio reached 0.72–0.84 and with a long healing period up to three months, the cracks were completely closed for the average crack width of 20–50 μm . UHPC added with CA (Penetron Admix) was claimed to be able to heal cracks up to 300 μm in width. In [76], the wet-dry cycling was also found to be beneficial in activating the CA (Penetron Admix) to close the cracks.

As a visual observation, normally, there were whitish formations near the mouth of the crack and they were confirmed to be calcite crystals with a

rhombohedral morphology mainly containing Ca, C and O [69]. The CaCO_3 precipitation, as the self-healing product, in the presence of CA is coherent with the observations of Sisomphon et al. [2], Roig-Flores et al. [65,66], and Escoffres et al. [67]. In addition, the use of CA is also beneficial for the recovery of mechanical properties that could achieve more than 78% strength regain as reported by [74]. Kannikachalam et al. [77] also reported a restoration of the mechanical properties of cracked UHPC after being healed by CA (Penetron Admix) and an improvement of the stiffness that can potentially extend the fatigue life of the structure. Consequently, CA acts as a stimulator of the autogenous healing mechanism of concrete [55] and simultaneously may promote a durable concrete. Sideris et al. [71] estimated that the service life of their concrete slabs without CA (Penetron Admix) was about 40 years, while concrete slabs treated with 0.8% CA could reach 48 years and even more than 50 years in case an improved curing regime was applied.

2.2.2 Effects of bacteria on concrete properties

2.2.2.1 Properties of the fresh concrete mixture

The workability of fresh bacterial concrete is an important property that should be investigated thoroughly. The inclusion of bacteria is normally combined with a suitable nutrient to supply the food for their growth inside the concrete matrix. On the one hand, nutrients play an important role for bacteria activation as long as water and moisture are present, while, on the other hand, this additive may also affect the properties of the fresh concrete mixture to a certain extent. According to previous studies, bacteria are often implemented as an additional agent placed into the normal concrete mixes, while the mix composition remains the same as for the reference concrete. From the author's point of view, this concept might raise a concern as changes in the properties of the fresh concrete might be expected. It is still uncertain whether the water demand and setting time of the concrete mix with a fixed dosage of bacteria will change abruptly or still remain stable. Thus, a comprehensive review, as presented below, is needed to investigate the workability issues due to the addition of bacteria and nutrients.

Vijay et al. [32] studied the combination effect of *Bacillus subtilis* bacteria spore powder and calcium lactate on the workability of two concrete mixes, i.e., normal concrete and basalt-fibre reinforced concrete. The concentration of bacteria was fixed at 10^5 cfu/mL (cfu = cell or colony-forming unit) with the purpose of improving the strength of concrete, and

calcium lactate was used as nutrient source for bacteria at the dosage of 0.5% by weight of cement. Both bacteria and nutrient were added to the normal mix while maintaining the volume of aggregates and no superplasticizer was used in the mix design. Coarse aggregate with the nominal size of 20 mm and fine aggregate were used. The results showed that the addition of *Bacillus subtilis* together with calcium lactate increased the slump value of normal concrete. The workability of bacterial concrete improved due to the role of calcium lactate as a retarding agent in the concrete that may increase the setting time and fluidity of the concrete. Furthermore, basalt fibres were introduced in the bacterial concrete mix and the slump value was nearly the same as for the normal concrete without bacteria. Due to the internal friction between fibres and cement, the traditional bacterial concrete is more workable than the fibre-reinforced bacterial concrete.

Siddique et al. [35] added isolated ureolytic bacteria *Bacillus aerius* strain AKKR5 with a concentration of 10^5 cfu/mL to the normal concrete mix, while the nutrient for bacteria growth was not incorporated in the mixture. The w/c and aggregate-to-binder (a/b) ratios were kept constant at 0.50 and 4.44, respectively, and superplasticizer was not utilized in this study. Coarse aggregate with a maximum size of 12.5 mm and fineness modulus (FM) of 6.38 and fine aggregate with an FM of 2.58, were used in the mix design. The results indicated that no effect was found on the slump value of bacterial concrete as compared with the reference concrete. A similar result was also found by Mohammed et al. [43]. The inclusion of iron-respiring bacteria, which was cultured in Tryptone Soya Broth (TSB), showed no effect on the fresh density and slump value of CEM I concretes. However, different behaviour was observed on the CEM III concretes as there was a small reduction in the concrete density and a 9% reduction of slump value. Nevertheless, all concrete mixes achieved medium workability, which was classified as S3 according to EN 12350-2:2009.

Ameri et al. [42] performed the evaluation of self-compacting concrete (SCC) mixtures with different *Bacillus pasteurii* cell concentrations by performing slump flow, T_{50} , V-funnel, U-flow, and L-box tests. Calcium lactate was selected as the nutrient source and added to the mixtures at a dosage of 5% by weight of cementitious materials. Here, the concrete mixes were designed using the optimum rice husk ash (RHA) content (15% by weight of cement) and three bacteria cell concentrations of 10^3 , 10^5 and 10^7 cells/mL. This optimum RHA dosage achieved the highest strength among the used dosage between 5–30% by weight of cement. The water content for all mixtures was kept constant with a water-to-binder ratio (w/b) of 0.40.

Pumice was used as coarse aggregate with a maximum aggregate size of 19 mm, while natural sand was used as fine aggregate with a particle size between 0 and 4.75 mm. Superplasticizer was incorporated in all mixes with a dosage of 2.5% by weight of cementitious materials. To obtain comparative results, reference concrete was made with the same composition as bacterial concrete with RHA as secondary cementitious material (SCM), only without adding bacteria and nutrients. It is worth noting that for all workability tests, all mixes showed identical results despite different bacteria concentrations. For instance, the slump flows of reference concrete and bacteria concretes with cell concentrations of 10^3 , 10^5 , and 10^7 cells/mL were 680, 684, 689 and 690 mm. This result is in contrast to the results found by Vijay et al. [32] regarding the influence of bacteria and nutrient on workability aspect.

While it is difficult to judge which parameter influences workability, interesting research undertaken by Nguyen et al. [34] can be taken into account to understand the impact of nutrients and bacteria with nutrients in concrete applications. In their study, three concrete mix designs were formulated, maintaining the same proportions of cement, water, aggregates and superplasticizer. In other words, two parameters of interest were chosen, i.e., nutrients and bacteria cells. (1) The first mix was the control concrete with a slump target about 180 ± 20 mm (or consistency class of S4) without nutrients and bacteria. (2) The second mix consisted of control concrete with the addition of two types of nutrients. Peptone and yeast extract were incorporated to the mixing water with a dosage of 1.00% and 0.50%, respectively. Lastly, (3) the third mix was the bacterial concrete which was the combination of the second mix and *Bacillus subtilis* bacteria with a concentration of 1.82×10^{10} cells/m³. Both nutrients and bacteria with nutrients were just added to the control mix. Based on the slump test results, comparing the second mix and the first mix, the addition of nutrients increased the slump value from 185 to 205 mm, while, comparing the third mix and the first mix, the combination of bacteria and nutrients increased the slump value from 185 to 195 mm. Eventually, it can be concluded that, in this case, the nutrients used as growth media for culturing bacteria were mainly responsible for the changes of workability, while the addition of bacteria in the fresh concrete with nutrients slightly decreased the slump value but still maintained the same consistency class as the control concrete.

Cappellesso et al. [39] used commercial bacterial healing agent from Basilisk which was composed of bacterial spores (*Bacillus cohnii*) and calcium lactate as nutrient for the production of self-compacting concrete. The reference concrete mixture was made with a w/c of 0.45 and cement content

of 360 kg/m³. The healing agent was added with a dosage of 10 kg/m³ of concrete (approximately 2.8% by weight of cement) and the mix design of bacteria-based concrete was slightly adapted for the inclusion of healing agent to comply a 1-m³ volumetric design based. The fresh density and air content of reference concrete were 2325 kg/m³ and 1.4%, respectively. The addition of bacteria slightly increased the fresh density to 2337 kg/m³ and the air content was almost doubled (2.9%) with respect to the reference mixture. The slump flows of reference and bacteria-based mixtures were 716 and 687 mm, respectively. Nevertheless, on the use of the same healing agent (Basilisk), Rossi et al. [79] previously investigated its effect on the fresh properties of mortar. Results showed that the chemical interaction between bacterial healing agent and cement caused a decrease of heat developed by the hydration of the Portland cement, confirming a retardation effect.

2.2.2.2 Properties of the hardened concrete

A general overview of the recent application of bacteria at the concrete level assessed by compressive strength, flexural strength, tensile splitting strength and water absorption is presented in Table 2-4. The changes in mechanical and durability properties in relation to the control concrete without bacteria, nutrients and SCMs are expressed in percentage. The performance of concrete embedded with the different genus of bacteria and suitable nutrient(s) normally shows an improvement on the mechanical properties due to the precipitation of calcite. As a note, no adaptations in the mix designs were done for the introduction of bacteria-based healing agents.

One of the main issues in introducing bacteria into concrete mixes is the limited cell viability when the bacteria are directly incorporated to the fresh concrete due to the concrete's high pH and the shear forces occurring during the mixing stage. To address this issue, Seifan et al. [10] designed immobilized bacteria cells with magnetic iron oxide nanoparticles (IONs). *Bacillus sphaericus* was selected as the microorganism which was cultured in calcium chloride, urea and yeast extract. The designed healing agent was added to their normal concrete mix and superplasticizer was not used. As compared with the reference concrete, the compressive strength of bacterial concrete was enhanced by 43% and 15% at 7 and 28 days, respectively. The optimum improvement of mechanical properties of bacterial concrete based on *Bacillus sphaericus* was found by Reddy et al. [31] for a cell concentration of 10⁵ cells/mL. However, the inclusion of a bacterial agent led to a higher free shrinkage due to the chemical reaction of nutrients during cement hydration [10].

Table 2-4. Comparison of various bacteria applications in normal strength concrete and their effects on the mechanical and durability properties

Ref.	Bacteria	Bacteria Concentration	Nutrient	SCM	Changes at 28 Days			Water Absorption	
					Compressive Strength	Flexural Strength	Tensile Splitting Strength	Control Concrete	Bacterial Concrete
[10]	<i>Bacillus sphaericus</i>	250 µg/mL	YE, UR, CaCl	-	↑ 15%	-	-	-	-
[31]	<i>Bacillus sphaericus</i>	10 ³ cells/mL	YE, UR	-	↑ 10%	↑ 2%	↑ 16%	-	-
		10 ⁵ cells/mL	YE, UR	-	↑ 20%	↑ 35%	↑ 25%	-	-
		10 ⁷ cells/mL	YE, UR	-	↑ 17%	↑ 22%	↑ 19%	-	-
[32]	<i>Bacillus subtilis</i>	10 ⁵ cells/mL	LAC	-	↑ 21%	↑ 17%	-	-	-
[33]	<i>Bacillus subtilis</i>	3 × 10 ⁸ cells/mL	LAC	-	↑ 12%	-	-	-	-
[34]	<i>Bacillus subtilis</i>	10 ⁸ cells/mL	YE, PEP	-	-	-	-	6.3%	5.3%
[35]	<i>Bacillus aerius</i>	10 ⁵ cells/mL	Not specified	-	↑ 11%	-	-	2.3%	1.2%
		10 ⁵ cells/mL	Not specified	10% SF	↑ 31%	-	-		0.8%
[30]	<i>Bacillus megaterium</i>	10 ³ cells/mL	LAC, UR	-	↑ 3%	-	-	-	-
		10 ⁵ cells/mL	LAC, UR	-	↑ 5%	-	-	-	-
		10 ⁷ cells/mL	LAC, UR	-	↓ 5%	-	-	-	-

[80]	<i>Bacillus megaterium</i>	10 ⁴ cells/mL	LAC	-	↑ 4%	-	-	6.0%	5.3%	
		10 ⁵ cells/mL	LAC	-	↑ 9%	-	-		4.6%	
		10 ⁶ cells/mL	LAC	-	↑ 7%	-	-		5.1%	
		10 ⁷ cells/mL	LAC	-	↑ 6%	-	-		5.1%	
[81]	<i>Bacillus licheniformis</i>	10 ⁴ cells/mL	YE, PEP	-	↑ 12%	-	↑ 20%	-	-	
		10 ⁵ cells/mL	YE, PEP	-	↑ 15%	-	↑ 26%	-	-	
		10 ⁶ cells/mL	YE, PEP	-	↑ 19%	-	↑ 29%	-	-	
		10 ⁷ cells/mL	YE, PEP	-	↑ 21%	-	↑ 32%	-	-	
		10 ⁸ cells/mL	YE, PEP	-	↑ 16%	-	↑ 26%	-	-	
[82]	<i>Bacillus safensis</i>	6 × 10 ⁷ cells/mL	LAC	-	↑ 22%	-	↑ 24%	-	-	
		<i>Bacillus pumilus</i>	6 × 10 ⁷ cells/mL	LAC	-	↑ 39%	-	↑ 25%	-	-
		<i>Arthrobacter luteolus</i>	6 × 10 ⁷ cells/mL	LAC	-	↑ 12%	-	↑ 16%	-	-
		<i>Chryseomicrobium imtechense</i>	6 × 10 ⁷ cells/mL	LAC	-	↑ 8%	-	↑ 19%	-	-
		<i>Corynebacterium efficiens</i>	6 × 10 ⁷ cells/mL	LAC	-	↑ 8%	-	↑ 14%	-	-
[29]	<i>Sporosarcina pasteurii</i>	10 ⁷ cells/mL	Not specified	-	↑ 5%	-	↑ 11%	-	-	
		10 ⁷ cells/mL	Not specified	10% NZ	↑ 20%	-	↑ 20%	-	-	

[40]	<i>Sporosarcina pasteurii</i>	10 ³ cells/mL	Not specified	-	↑ 4%	-	-	17.7%	14.0%
		10 ⁵ cells/mL	Not specified	-	↑ 17%	-	-		13.0%
		10 ⁷ cells/mL	Not specified	-	↑ 8%	-	-		13.7%
		10 ³ cells/mL	Not specified	10% FA	No changes	-	-	17.7%	4.0%
		10 ⁵ cells/mL	Not specified	10% FA	↑ 15%	-	-		3.3%
		10 ⁷ cells/mL	Not specified	10% FA	↑ 4%	-	-		3.7%
[41]	<i>Sporosarcina pasteurii</i>	10 ³ cells/mL	Not specified	10% SF	↑ 52%	-	-	17.5%	0.1%
		10 ⁵ cells/mL	Not specified	10% SF	↑ 66%	-	-		0.1%
		10 ⁷ cells/mL	Not specified	10% SF	↑ 45%	-	-		0.8%
[42]	<i>Sporosarcina pasteurii</i>	10 ³ cells/mL	LAC	15% RHA	↑ 13%	↑ 23%	↑ 21%	4.8%	3.2%
		10 ⁵ cells/mL	LAC	15% RHA	↑ 20%	↑ 29%	↑ 29%		1.4%
		10 ⁷ cells/mL	LAC	15% RHA	↑ 17%	↑ 26%	↑ 25%		1.1%
[43]	<i>Shewanella oneidensis</i>	2.3 × 10 ⁸ cells/mL	TSB	-	↑ 3%	-	-	-	-
	<i>Bacillus sphaericus</i>	2.3 × 10 ⁸ cells/mL	TSB	60% GGBS	↓ 10%	-	-	-	-

Note: LAC = calcium lactate, YE = yeast extract, UR = urea, PEP = peptone, TSB = tryptone soya broth, FA = fly ash, SF = silica fume, NZ = natural zeolite, RHA = rice husk ash, GGBS = ground granulated blast-furnace slag

The introduction of *Bacillus subtilis* with calcium lactate as the nutrient source in concrete applications was experimented by Vijay et al. [32] and Khaliq et al. [33]. As observed at 28 days, the compressive strength of concrete with *Bacillus subtilis* at a cell concentration of 10^5 cells/mL is at least 20% higher than that of concrete without bacteria [32]. From the microstructure findings, it was revealed that the strength enhancement occurred due to the formation of calcite which filled in the voids.

Khaliq et al. [33] designed bacterial concretes with three different approaches. (1) In the first mix, bacteria were added directly into the fresh concrete without any protective carriers. (2) In the second mix, lightweight aggregates (LWA) were used as a protective carrier of bacteria, replacing the natural coarse aggregates. LWA were soaked in the bacterial solution for 24 h prior to mixing. (3) In the same way as the second mix, the third mix used graphite nanoplatelets (GNP), instead of LWA, as a bacteria carrier compound. The reference mix without bacteria was designed for a compressive strength of 28 MPa. The concrete mix designs for bacterial concretes were not adapted and still maintained the same proportion as the reference mix. Retarding admixture and superplasticizer were added into the mixes at 1% by weight of cement to produce free-flowing concrete for the application in hot climates. The results showed that the compressive strengths of all mixes were increased for all bacterial incorporation techniques. The highest strength improvement of 12% was achieved by the bacterial concrete specimens containing LWA as compared to the control concrete. One possible reason for this improvement is attributed to the smaller size of LWA in comparison to regular sized coarse aggregates which may have resulted in better packing and compaction of the concrete matrix. The use of GNP induced a positive effect as the compressive strength increased by about 9.8%. It was claimed that the small size of GNP decreased the formation of a weak interfacial transition zone (ITZ) in the concrete by filling the porous and crystalline microstructure within the ITZ. A decrease in ITZ makes the mortar matrix denser and more compact, resulting in a higher compressive strength [33]. This may be explained by the fact that the ITZ has a significantly higher porosity and shows multiple microcracks, leading to the common view of the ITZ as the weak link in concrete [83]. Nevertheless, the direct inclusion of *Bacillus subtilis* bacteria without carrier also showed an approximately 5% enhancement of compressive strength. The presence of bacteria and its organic precursor densify the internal structure of the concrete due to the bacterial activity producing CaCO_3 .

Andalib et al. [30] formulated concrete mix designs with a target compressive strength of 30 MPa by using several dosages of *Bacillus megaterium* with the purpose of obtaining the optimum concentration for strengthening structural concrete. One single parameter was initially chosen namely cell concentration in the range of 10^3 – 10^7 cells/mL. The mix design for bacterial concrete was not adapted, thus maintaining the same proportions as the control one. To effectively germinate the bacteria, 5% of mixing water as bacterial broth medium culture was added during the mixing stage. The results showed that the compressive strength of bacterial concrete increased optimally (7.8% improvement) at a cell concentration of 10^5 cells/mL, whereas a higher concentration showed a negative effect resulting in a lower strength with respect to the reference concrete. This result was supported by SEM micrographs showing that the bacterial concentration of 10^7 cells/mL yielded a higher porosity of the concrete microstructure. Furthermore, a more detailed investigation in the narrower range between 10×10^5 and 50×10^5 cells/mL was executed to find the optimal concentration in relation to the strength improvement. The highest strength was achieved with the bacterial concentration of 30×10^5 cells/mL for the application of structural concrete. However, as a matter of fact, there was no big difference on the compressive strength of bacterial concrete at 10 – 50×10^5 cells/mL. Similar findings were also found by Sadeghpour et al. [80] on the use of *Bacillus megaterium* with a cell concentration between 10^4 – 10^7 cells/mL, confirming a minimal strength improvement in the range of 4-9%, as compared with reference concrete.

One interesting study by Shaheen et al. [82] utilized several newly identified bacterial strains that are able to precipitate calcite in harsh alkaline environment including *Bacillus safensis*, *Bacillus pumilus*, *Arthrobacter luteolus*, *Chryseomicrobium imtechense* and *Corynebacterium efficiens*. The cell concentration of all bacterial solutions was fixed at 6×10^7 cells/mL and calcium lactate was used as food source for the bacteria. Six concrete mixtures were developed to assess the performance of bacterial concrete. The w/c was fixed at 0.30 for all mixtures and the SP was used at 0.7% by weight of cement to improve the workability. For bacteria-based mixtures, the bacterial solution was used to partially replace the mixing water, nevertheless, the w/c was still the same as reference. As shown in Table 2-4, the inclusion of all types of bacterial strains enhanced the mechanical properties of concrete by a maximum of 39% and 25% (with *B. pumilus*) as compared to reference concrete in compression and tensile splitting strength, respectively. A significant rise in mechanical strength of concrete with the addition of *B. pumilus* was also found by Akhtar et al. [84],

supporting the findings of [82]. The densification of the microstructure due to the calcite precipitation was responsible for pore refinement in the matrix and the bacteria cells provided nucleation sites for MICP in the cementitious matrix that ultimately leads into strength improvement. In addition, the cell surface of bacteria was negatively charged and attracted positive ions that also contributed to the concrete strength.

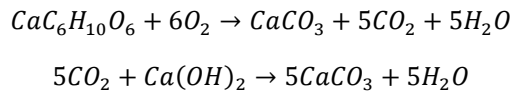
Many studies frequently utilized *Sporosarcina pasteurii*, which is also known as *Bacillus pasteurii* from older taxonomies, for the application of self-healing concrete due to the fact that this bacteria has the ability to solidify organic nitrogen source through the process of biological cementation [40]. Due to its high urease activity, urease catalyzes the hydrolysis of urea to form ammonia and carbonic acid, in which ammonia later forms ammonium and hydroxide ions in water, while carbonic acid also forms bicarbonate and hydrogen ions in water. This leads to the formation of carbonate ions. In the presence of calcium ions in the cement system, CaCO_3 crystals can be precipitated [85]. The role of *Sporosarcina* bacteria as a bio-based healing agent has been known to exhibit significant improvement from the perspective of mechanical properties [29,40–42] at the concrete level by utilizing the most frequently proposed cell concentrations of 10^3 , 10^5 and 10^7 cells/mL. For instance, Chahal et al. [40] designed concrete mixtures to have a compressive strength of 28 MPa at 28 days. Cement was partially replaced with 0, 10%, 20%, and 30% fly ash by weight of cement and *Sporosarcina pasteurii* bacteria was cultured to obtain different concentrations of cells. Nutrient broth was also prepared in advance prior to the mixing stage, but the ingredients of this nutrient were not specified. Similarly to other studies, the mix designs were not adapted for the introduction of bacteria. For bacterial concrete specimens without cement substitution, the compressive strength improvement was 4%, 17% and 8% for a cell concentration of 10^3 , 10^5 and 10^7 cells/mL, respectively. Moreover, from a durability point of view, the utilization of fly ash in combination with bacteria greatly improved the water tightness of the concrete as in fact, the water absorption was found to be reduced nearly four times [40]. Based on another report by the same authors [41], 10% cement substitution by silica fume greatly boosted the compressive strength of bacterial concrete up to 52%, 66% and 45% with the corresponding cell concentrations of 10^3 , 10^5 and 10^7 cells/mL, respectively, compared to control concrete without the bacteria and silica fume. A similar pattern was also found when substituting the cement with rice husk ash [42] or natural zeolite [29]. Microstructure analysis by means of SEM confirmed the presence of CaCO_3 in the bacterial concrete.

Mohammed et al. [43] attempted to produce bacterial concrete with *Shewanella oneidensis* and high cement replacement by blast furnace slag of up to 60%; however, a substantial drop of the concrete's strength was observed. In Siddique's experiment [35], self-healing concrete mixes were designed using *Bacillus aerius* bacteria in combination with silica fume as a partial replacement of cement. The advantage of the *Bacillus* species is high pH tolerance, thus increasing the viability under alkaline environments. The *w/b* was fixed at 0.47 and the aggregate proportions were maintained the same for all mixes. With no cement substitution and the inclusion of 10^5 cells/mL *Bacillus aerius* bacteria, an 11% enhancement in compressive strength in comparison to the normal strength concrete was observed. By using the same bacteria cell concentration and 10% cement replacement by silica fume, there was a steep increase of the strength up to 31%, which was mainly due to microbial calcite precipitation and a denser microstructure.

The results based on the flexural strength and the tensile splitting strength basically follow the same trend as the compressive strength [29,31,32,42]. Moreover, as shown in Table 2-4, the concretes containing bacteria are more durable than the normal concrete as a reduction in water absorption was clearly observed [34,35,40–42,80]. The reduction was more pronounced when SCMs (e.g., fly ash, silica fume, natural zeolite and rice husk ash) were utilized in the bacterial concrete mixes as cement replacement. The highest reduction of water absorption was observed in the bacterial concrete containing *Sporosarcina pasteurii* bacteria and 10% silica fume. The deposition of CaCO_3 in the concrete capillary pores caused the reduction in water absorption and porosity which in turn increases the durability of the concrete [35,40–42]. It is noteworthy to highlight that the optimum bacteria cell concentration for strengthening the concrete was achieved at 10^5 cells/mL. A higher bacterial cell concentration would be more efficient where protection of concrete is more important than strength [13].

Additionally, the nutritional admixtures for the growth of bacteria may also affect the strength of concrete considerably. However, due to the fact that a limited number of studies in this domain on concrete is available, a review of impact of different nutrients was done at the mortar level. Schreiberová et al. [15] fabricated mortar specimens which were combined with the most frequently proposed nutrients including calcium lactate, calcium nitrate, calcium formate, yeast extract and urea; bacteria were not incorporated in the mortar mixtures. As shown in Table 2-5, it was observed that the pre-selected calcium sources did not endanger the strength values at any ages except calcium nitrate at 28 days. Moreover, the inclusion of

calcium lactate and calcium formate increased the compressive strength. It is evident that based on the available results presented in Table 2-5, the addition of calcium lactate [30,32,33,42] with the relevant bacteria has a similar tendency to enhance the strength of the concrete. One possible reason of strength enhancement by calcium lactate may be explained in the following reactions [6]:



As a result of metabolic conversion of calcium lactate, minerals are formed and are likely CaCO₃-based. Further, the produced CO₂ molecules react with Ca(OH)₂ which results in more production of CaCO₃-based minerals. Chaerun et al. [86] also argued that Ca²⁺ ion from calcium lactate likely contributed to the generation of calcium silicate hydrate, calcium hydroxide, and calcium carbonate on cementitious materials through hydration and carbonation reaction. Vijay et al. [87] mentioned that the reaction by-products of calcium lactate help in filling the pores in concrete and densifying the microstructure. Nevertheless, there was an optimum dosage of calcium lactate to achieve this positive behaviour because if the dosage is too high, the reduction of compressive strength can be attained due to the excess production of calcium carbonate.

Furthermore, the addition of urea exhibited a positive result during the early ages while at the later age of 28 days the mortar strength was similar to the control [15]. On the contrary, a drastic drop of the mortar compressive strength was observed when the yeast extract was added into the mix, which is in agreement with the result reported by Jonkers et al. [6]. Chen et al. [88] proved that the addition of yeast extract (0.06% by weight of cement) into the mortar mixes lowered the compressive strength, approximately from 38 to 32 MPa. This may be explained due to the fact that the air content of mortar containing yeast extract was almost doubled in relation to the reference mortar without nutrients; increasing from 2.1 to 3.8%. The result suggests that the addition of nutritional admixtures will have a considerable effect on the performance of concrete and the appropriate dosage should be optimized in order to not negatively affect the mechanical properties while still maintaining the ability to supply the “food” for the bacteria’s consumption.

Table 2-5. Effect of nutritional admixtures on the compressive strength of the mortar (without bacteria) [15].

Nutrient	Dosage (% Weight of Cement)	Mean Values of Compressive Strength					
		3 Days		7 Days		28 Days	
		(MPa)	(%)	(MPa)	(%)	(MPa)	(%)
Control	-	22.88	100	28.93	100	45.31	100
Calcium lactate	3.00	27.70	121	36.02	125	58.76	130
Calcium nitrate	3.00	26.44	116	33.47	116	41.13	91
Calcium formate	3.00	37.96	166	44.23	153	57.63	127
Yeast extract	0.85	10.65	47	19.61	68	35.12	77
Urea	2.50	30.80	135	34.77	120	44.39	98

2.2.2.3 Self-healing properties

The incorporation of bacteria into the concrete mixture with a suitable nutrient source essentially promotes an autonomous healing mechanism. The precipitation of calcite crystals in the cracks takes place upon the presence of water, hence, blocking the passage of water and other liquids that may jeopardize the structure of the concrete. In order to simulate the self-healing capability, in laboratory conditions, concrete specimens treated with bacteria were typically cracked at the age of 28 days and the healing time was varied depending on the experimental programs done by past studies [32–34]. After a healing period under water immersion, it can be observed visually that the crack mouth was filled with white sedimentation, identified as CaCO_3 crystals. The morphology of calcite was observed in tetrahedron and pyramid shapes by [32]. In [29], concrete containing *Sporosarcina pasteurii* bacteria, cracked to a width of 0.28 mm, was nearly fully healed after 30 days of curing in aqueous molar solution of urea and calcium chloride, as shown in Figure 2-8. The sealing efficiency of the bacterial concrete was recorded at 90% when the cracked specimens were immersed in water for 27 weeks [44]. The incorporation of *Bacillus subtilis* bacteria by the use of LWA and GNP, which act as protective carriers to ensure the viability of bacteria, was effective to stimulate crack closing up to 0.52 mm and 0.38 mm, respectively [33]. As a matter of fact, the need for liquid water is vital to activate the dormant bacteria in producing CaCO_3 . In [13], the best performance of bacteria concrete in terms of self-healing capacity was achieved by using the bacteria cell concentration of 10^7

cells/mL, where it possessed maximum reduction in water absorption and maximum surface crack and pore healing. Cappellesso et al. [39] demonstrated the beneficial self-healing effect of commercial bacterial agent (Basilisk) in concrete exposed to extreme environments where 90% higher frost salt scaling resistance and 46% reduction of chloride penetration were achieved as compared with normal concrete.

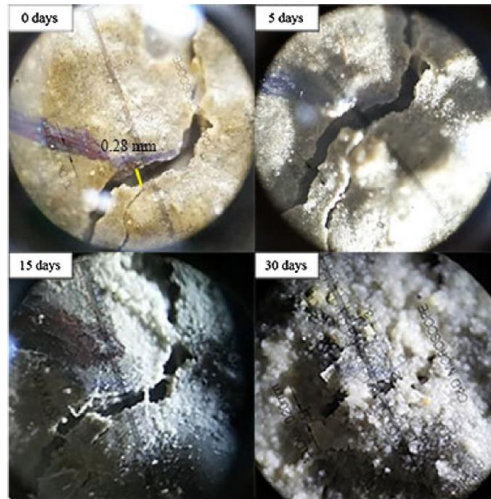


Figure 2-8. Development of crack closing in the bacterial concrete after 30 days based on microscopic image [29]

2.2.3 Effects of micro-encapsulated agent on concrete properties

2.2.3.1 Properties of the fresh concrete mixture

Microcapsules are regarded as ‘vessels’ for healing agents which are fabricated through serial synthesis by, for instance, emulsification and polymerization to entrap the core in a shell structure. The final product of the microencapsulated healing agent normally exists in a liquid or slurry form containing a certain amount of microcapsules. These microcapsules are added during the mixing process into the concrete in a small dosage for self-healing purposes. However, the presence of microcapsules may affect the properties of the fresh concrete mixture.

Only a few studies investigated the effects of microcapsules on the properties of the fresh concrete mixture. Sidiq et al. [49] designed the concrete mixes with a w/c and sand-to-cement ratio (s/c) of 0.54 and 1.83, respectively. The coarse aggregates were chosen with two nominal sizes of 7 mm and 10 mm. The microcapsules were prepared with two different dosages of 2.5% and 5% by weight of cement and in fact, the mix designs were not adapted for the introduction of microcapsules. The microcapsules were mainly composed of sodium silicate solution as core material and PU as shell material. To prevent high damage on microcapsules, the healing agent solution was added into the concrete mixer after three minutes of mixing, followed by one more minute after the addition. It was reported that the fresh concrete mixture experienced a loss of plasticity as a result of incorporating the microcapsules at the time of batching. This phenomenon may be explained by two reasons: (1) the microcapsules were regarded as powder-like material thus increasing the ratio of powder material to the water content of the mix and (2) a partial reduction of water content due to the hydrophilic character of the PU as shell material. Despite this unsatisfactory effect, both mixes still remained workable.

Milla et al. [59] incorporated the microcapsules carrying calcium nitrate with urea-formaldehyde as shell material in the production of steel fibre reinforced concrete. Calcium nitrate was claimed to enhance the autogenous healing capacity in concrete. The microcapsules were technically produced with and without Span 60 emulsifier and the characteristics were assessed by means of slump and air content tests. The dosages of all microcapsules were fixed at 0.50% and 0.75% by weight of cement. The proportions of the concrete mixes were kept constant for all mixes with w/c of 0.41. Limestone was used as coarse aggregate with the maximum aggregate size of 19 mm, while sand was used as fine aggregate with the maximum particle size of 4.76 mm. Superplasticizer was used to ensure workability and a defoaming agent was also used to counter the increase of air content when combining microcapsules with superplasticizer. The results showed that the air content values were low for all concretes and no considerable difference could be found in the air content between the reference concrete and the microcapsule-based concrete. Based on the slump test, by using one type of microcapsules with emulsifier, the workability showed a declined trend owing to the agglomerations and difficulties in dispersing the microcapsules throughout the concrete matrix, resulting in stiff mixtures. In contrast, another type of microcapsules without emulsifier showed a higher slump value than the reference concrete indicating a better workability. However,

the difference in workability in the presence of microcapsules (with and without emulsifier) is not yet fully understood.

It should be emphasized that a handful of reports did not explicitly address the influence of microcapsules on the properties of the fresh concrete mixture, despite its superior ability to heal the cracks. Logically, it is plausible that the microcapsules will not entirely survive during the mixing process and there is a certain amount of microcapsules that rupture due to the collision with the aggregates [49,89]. Subsequently the broken microcapsules would release the healing agent, reacting immediately with the cement blend and influencing the hydration process. To date, the compatibility between the microencapsulated healing agents and the cementitious matrix is not yet completely understood. Hence, evaluating the influence of microcapsules on the properties of the fresh concrete mixture is of great importance to realize its application in the fieldwork in the future.

2.2.3.2 Properties of the hardened concrete

One of the main issues by adding the microcapsules into the mixture is the unfavourable tendency on the mechanical properties of the concrete. In view of the previously reported findings [49,52,61,62,90], the compressive strength of the concrete was reduced considerably at any dosage. Two major parameters discussed in this state-of-art review are the concentration and the size of the microcapsules, while the cargo material as healing agent will not be considered in detail owing to the fact that the properties of the hardened concrete in this part are assessed before being subjected to a cracking and healing scenario.

Al-Tabbaa et al. [61] demonstrated the first field application of microencapsulation technology in the UK by fabricating concrete wall panels using gelatin gum-Arabic shell microcapsules containing sodium silicate in the slurry form. The mean diameter of these microcapsules was approximately 290 μm . The design of ready mixed concrete was formulated to achieve the strength class of C40/50 with an effective w/c of 0.45. Cement type I, limestone aggregates with a nominal size of 10 mm, limestone fines and marine sand were included in the design. A plasticizer and retarder were also used as concrete admixtures. The addition of microcapsules was limited to 2.67% by weight of cement or approximately 0.47% of the total volume of concrete. Before being added into the concrete mixer, the microcapsules were initially washed with water and then filtered from the preserving

solution. With regard to the compressive strength before healing, it was confirmed that at 28 days, the strengths of concrete samples without and with microcapsules were 59 MPa and 42 MPa, respectively. This result was in contrast with their previous research in the laboratory field. It was hypothesized that the poor workability and honeycombing during casting resulted in a significant drop in strength. Similarly, an 8% decrease in the concrete stiffness value was attributed to the presence of the microcapsules. On the other hand, Sidiq et al. [49] proposed their concrete mix design based on microcapsules, which has been introduced previously in the Section 2.2.3.1. As a result of doubling the microcapsules dosage from 2.5% to 5.0% by the weight of cement, the reduction of compressive strength was recorded at 26.51%. Such reduction may be caused by a higher porosity content and less adhesion/interlocking between cementitious particles due to the presence of microcapsules. As demonstrated in the work of Al-Ansari et al. [90], even at a low dosage (0.75% by weight of cement), both compressive strength and flexural strength were reduced by 11% and 14%, respectively.

Litina et al. [91] also validated the practical application of microcapsules in the real construction of reinforced concrete slabs at the University of Cambridge. Gelatin/gum Arabic shell microcapsules containing sodium silicate, produced via complex coacervation, were developed with a mean diameter of 290 μm . The ready-mix C32/40 concrete was supplied by the company (Tarmac, UK) and was delivered on site. The concrete mix design was defined by the contractor with a cement type of CEM I, 20-mm maximum aggregate size, target slump of S2, w/c of 0.45, cement content of 340 kg/m^3 and exposure class of XF4. The fresh concrete mixture delivered to the site was divided into several containers. Next, the microcapsules were added in slurry form at 12 and 16% by volume of cement (corresponding to 4 and 5.3% by weight of cement or 0.66 and 0.88% of the total concrete volume, respectively) and the mixture was manually hand mixed on site. Concrete cubes were casted on site for 28-day strength characterization. Their study confirmed a negative influence of microcapsules on strength development and the effect was dependent on the volumetric content of microcapsules. The addition of 12 and 16 vol.% microcapsules reduced the compressive strength by 15 and 13%, respectively. Although an initial strength reduction was found (before exposure to freeze-thaw), Litina et al. [91] reported that the microcapsules induced a strength retention after the concrete was subjected to freeze-thaw cycles. The cube specimens were immersed in 3% sodium chloride solution and exposed to freeze-thaw regime (28 cycles consisting of 16h of freezing at -18°C and 8h of thawing at 20°C). After the

exposure, the specimens were tested by compression tests. Reference concrete (without microcapsules) experienced 38% strength reduction while concrete containing 12 vol.% microcapsules had slightly lower reduction at 32%. Specifically for concrete added with 16 vol.% microcapsules, a complete immunity was attained after 28 cycles as no reduction of compressive strength was found. They confirmed the resistance of the concrete to freeze-thaw, increasing the long-term durability with the microcapsules addition.

A research conducted by Wang et al. [52] attempted to use a higher concentration of the microcapsules (10% by weight of cement) for application in a tunnel construction project in Shenzhen, China. The microcapsules were prepared in the laboratory and consisted of epoxy resin as cargo material and urea-formaldehyde resin as shell material with mean diameter of 152.4 μm . All concrete specimens with and without microcapsules were designed with the same w/b of 0.32 and the cement content was partially replaced by slag and fly ash. Other agents such as expansive agent and superplasticizer were employed during proportioning. Especially for concrete with microcapsules, a curing agent was added at 5% by weight of the total binders to effectively activate the healing mechanism when the broken microcapsules release the healing agent. Compressive strength tests on specimens at 60 days showed that the strength of the microcapsule-based concrete was approximately 70% of the control concrete. This negative effect was attributed to the presence of the microcapsules which modified the microstructure of the self-healing concrete. At the microscopic level, as shown in Figure 2-9 from the SEM image, it was clear that the broken microcapsules still remained in the matrix and they took up some large pore spaces that ultimately decreased the density and homogeneity of the concrete matrix. This finding was supported by the fact that the addition of microcapsules led to a greater porosity value of the concrete [49]. In terms of compressive strength, the presence of the microcapsules can be regarded as harmful pores which are not able to withstand the compression load during mechanical tests [52].

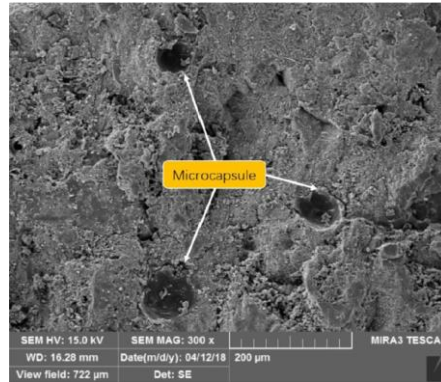


Figure 2-9. The presence of large pores due to broken microcapsules in the cementitious matrix [52]

In general, the geometry of microcapsules will indirectly affect the performance of the concrete. This fact was addressed in the research of Milla et al. [62], discussing another parameter aside from microcapsules concentration, specifically the average size of microcapsules. During the production process, the size of the microcapsule was controlled by the agitation rate during synthesizing. Higher agitation rates led to smaller microcapsules and vice versa. Three batches of microcapsules were prepared with varying agitation rates of 450, 800 and 1500 rpm, and the mean particle size for each batch was found to be 109, 50 and 22 μm , respectively. The concentrations of microcapsules were tested at 0.25, 0.50 and 1.00% by weight of cement. After the preparation of the microcapsules, the optimal mix designs of concrete were composed in accordance to their previous studies to achieve workable mixtures with low w/c . Hence, superplasticizer was used and the w/c was fixed at 0.41. Due to the fact that the combination of microcapsules and superplasticizer generated a higher air content, a defoamer was utilized. Limestone and sand were employed as coarse and fine aggregates, respectively, with the maximum particle size of 19 mm and 4.76 mm. The microcapsules were added to the normal mix, thus no adaptations on concrete compositions. Figure 2-10 shows the compressive strength result of the self-healing concrete with two design parameters namely average microcapsule size (22, 50 and 109 μm) and microcapsule concentration (0.25, 0.50 and 1.00%). The result confirmed that the highest strength was achieved for the control concrete without microcapsules, while mix 50–0.25% attained the highest compressive strength among microcapsules-based specimens. In contrast, specimens made with 22 μm microcapsules at the dosage of 1% showed the lowest strength. It may be

explained by the fact that microcapsules prepared with a higher agitation rate (smaller capsules in size) tended to agglomerate more than the other microcapsules with lower rates [44]. However, the strength differences of the microcapsule-based concretes were relatively low, ranging up to 5.1 MPa. Furthermore, the lowest strength was observed on the concretes with the highest microcapsule concentration of 1% for all microcapsules sizes. The aforementioned results suggested that the embedded microcapsules yielded a substantial reduction in mechanical strength due to the porous microstructure of the concrete and an appropriate concentration should be defined in order to not affect negatively on concrete properties.

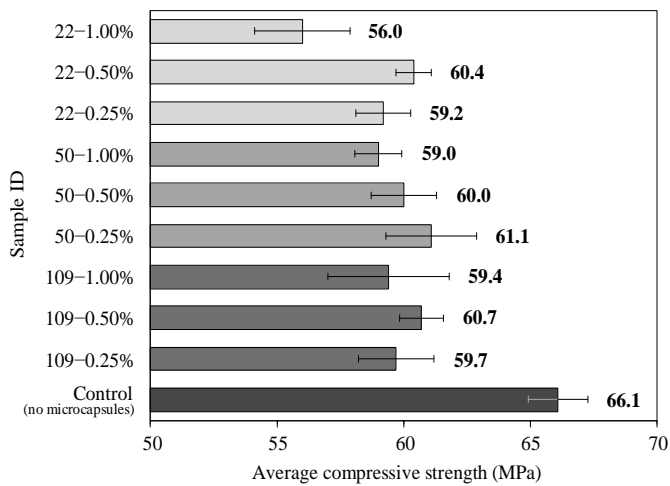


Figure 2-10. Compressive strength results of microcapsules-based concrete at various microcapsule concentrations (0.25, 0.50 and 1.00%) and mean sizes (22, 50 and 109 μm) [62]

To conclude, Table 2-6 summarizes the effect of microcapsules on the compressive strength of cementitious composite (including paste, mortar and concrete) and the reasoning behind the alteration of the mechanical properties.

Table 2-6. Comparison of the strength changes of cementitious composite added with microcapsules at different size and dosage

Ref.	Composite	MIC		Average MIC size (μm)	MIC dosage (% bwoc)	Changes of 28d comp. strength *)	Reasoning
		Shell	Cargo				
[17]	Paste	GA	SS	500	1	↑ 7%	Ability of microcapsules to absorb water
					2	↑ 1%	
					3	↓ 3%	
					4	↓ 3%	
		PU	SS	130	1	↓ 6%	Ability of microcapsules to absorb water
					2	↓ 9%	
					3	↓ 11%	
					4	↓ 14%	
[92]	Paste	PU	SS	110	2.5	↓ 14%	Lower stiffness of microcapsules compared to cement matrix, hence creating weak spots in the matrix
					5	↓ 20%	
					7.5	↓ 26%	
[93]	Mortar	GA	SS	290	0.8	↑ 2%	The presence of microcapsules in the matrix and their contribution in increasing the viscosity of the mixture
					1.6	↓ 1%	
					2.3	↓ 17%	
					3.1	↓ 25%	
					4.6	↓ 24%	
					6	↓ 27%	
[19]	Mortar	UF	EP	122	3	↓ 5%	Not specified

					6	↓ 8%	
					9	↓ 14%	
[94]	Mortar	UF	EP	206	5	↓ 7%	The microcapsule wall may be broken during the mixing due to its low strength and rigidity, hence, release of the healing agent and formation of defects similar to holes in specimens
					10	↓ 14%	
					15	↓ 19%	
[95]	Mortar	PA	TDI	90	3	↑ 28%	The appropriate dosage of microcapsules could fill the internal pores of mortar
		PAW	TDI	320	3	↓ 3%	The large size of MICs enlarges the internal pore of mortars
		PAWN	TDI	480	3	↓ 6%	
[96]	Mortar	PA	TDI	90	1.5	↑ 16%	A suitable dosage of microcapsules can fill the internal voids of mortar
					3	↑ 28%	
					4.5	↓ 7%	Low strength of microcapsules and they are prone to break
					6	↓ 23%	
[61]	Concrete	GA	SS	290	2.7	↓ 29%	Significantly deteriorated workability and honeycombing
[91]	Concrete	GA	SS	290	4	↓ 15%	Not specified
					5.3	↓ 13%	
[97]	Concrete	UF	EP	248	3	↓ 7%	Microcapsules increase the porosity of the specimen, thus decreasing its compactness
					6	↓ 10%	
[52]	Concrete	UF	EP	152	10	↓ 30%	Change in microstructure and hydration degree
[62]	Concrete	UF	CN	22	0.25, 0.5, 1	↓ 9–15%	Agglomeration of microcapsules creating weak links in the concrete matrix
				50	0.25, 0.5, 1	↓ 8–11%	
				109	0.25, 0.5, 1	↓ 8–10%	

[90]	Concrete	UF	CN	60	0.75	↓ 11%	Not specified
[98]	Concrete	PA	IPDI	90	3	↑ 15%	Small-sized capsules improve the gradation and compactness of concrete and the pores in concrete can be filled with these capsules
		PAW	IPDI	300	3	↓ 4%	Large-sized capsules reduce the compactness of concrete
		PAWN	IPDI	500	3	↓ 9%	

Note: *) as compared with reference (0% microcapsules), MIC = microcapsules, PU = polyurethane, WRA = water-repellent agent, SS = sodium silicate, UF = urea-formaldehyde, EP = epoxy, CN = calcium nitrate, GA = gelatin/gum Arabic, PA = paraffin, PAW = paraffin + PE wax, PAWN = paraffin + PE wax + Nano-SiO₂, PE = polyethylene, CS = colloidal silica, IPDI = isophorone diisocyanate

2.2.3.3 Self-healing properties

The introduction of microcapsules significantly enhances the autonomous crack healing/sealing ability of self-healing concrete as compared with the normal concrete. In order to effectively activate the healing mechanism, capsules should be broken so the healing agent can be released. Therefore, in laboratory studies, cracks are created by means of three-point bending tests [17,18,59] or by applying 60–70% of maximum compressive strength to the samples [49,52]. Depending on the healing agent, these tests are done at a young or later age; and the curing conditions differ. Sidiq et al. [49], for instance, damaged the concrete specimens at 28 days by 70% of maximum compressive strength, and then the specimens were subjected to a healing scenario in a humidity chamber up to 56 days. It was found that after 56 days of healing, the concrete containing a microcapsule content of 2.5% (sodium silicate as the cargo) was fully recovered, meaning the compressive strength of the damaged specimen after healing equals or exceeds the maximum 28-day compressive strength. For the samples with 5% microcapsules, a full recovery was observed at 14 days of healing and the compressive strength was improved by 38% at the age of 56 days [49]. In other words, the strength recovery was greatly enhanced on the specimens with the higher amount of microcapsules.

Similar findings have been found in other studies confirming the positive impacts of the micro-encapsulated healing agents on the mechanical performance after undergoing a healing scheme [51,52,59,61,62,90]. Sidiq et al. [49] found that cracks with a width up to 122 μm were effectively healed with embedded microcapsules containing sodium silicate and the crack healing ratio achieved up to 60%. It can be concluded that the inclusion of microcapsules generated dual effects on the mechanical properties of self-healing concrete [52]. Firstly, before the healing period, the addition of microcapsules undeniably induced an adverse effect on the mechanical performance due to the large pores in the cementitious matrix. Secondly, after being subjected to the healing scenario, the healing efficiency of the concrete was significantly increased in terms of mechanical strengths.

Moreover, Wang et al. [52] and Al-Ansari et al. [90] reported on the durability performance of the self-healing concrete which improved remarkably with increased healing time. Wang et al. [52] performed the rapid chloride migration (RCM) test on concrete disc specimens containing 10% microcapsules (urea-formaldehyde as the shell and epoxy resin as the core) by weight of binders. Initially, the 60 days old concrete specimens were

subjected to a compressive load with 30% of the maximum compressive strength to induce microcracks. Then, cracked specimens were stored and healed in a curing room (60°C, 95% RH) for 3, 5, 7, 14 and 28 days; after each respective healing time, the RCM test was conducted. After healing at a specific age, the specimens were split in half and a silver nitrate solution was sprayed on the freshly split specimens to measure the average chloride penetration depth. During the first week of healing, the chloride migration coefficient decreased rapidly from 5.4 to 4.6 ($\times 10^{-12}$ m²/s) and then the reduction rate slowed reaching a value of 4.2 ($\times 10^{-12}$ m²/s) after 28 days.

Another study by Al-Ansari et al. [90] found a significant reduction of air permeability of the concrete samples containing 0.75% microcapsules (urea-formaldehyde as the shell and calcium nitrate as the core) by weight of cement. At first, the hardened concretes were loaded up to 60% of their ultimate load at 28 days, and the air permeability test was executed. After that, the specimens were healed under water curing and the air permeability was re-measured after 3 and 7 days of healing. The results showed that the air permeability coefficients of self-healing concrete were 0.98×10^{-16} m² after loading, 0.62×10^{-16} m² after 3 days of healing and 0.03×10^{-16} m² after 7 days of healing. In addition, the air permeability coefficient of control concrete without microcapsules decreased slightly from 0.57×10^{-16} m² (after loading) to 0.43×10^{-16} m² (after 7 days of healing). Despite the negative effects of the microcapsules in view of mechanical strengths before the healing period, the concrete with micro-encapsulated healing agent showed a better improvement after the specimens were healed. It is feasible to explain that the healing agent released from the broken microcapsules filled the defects and sealed the microcracks, which decreased the concrete's permeability and promoted a more durable concrete.

2.2.4 Effects of macro-encapsulated agent on concrete properties

2.2.4.1 Properties of the fresh concrete mixture

To date, macrocapsules are mostly included by pre-installment of the capsules [57,60,99] in the mould and a fresh mix is later poured after a sufficient time of mixing. Only in a limited number of studies, the macrocapsules have been added during the mixing process. In these cases, the mix design is generally not adapted. Here, a review is made to observe

the characteristics of fresh concrete mixes containing capsules and the evaluation of survivability of capsules after undergoing the mixing scenario.

Hilloulin et al. [20] started to investigate the resistance of several types of polymeric capsules including PLA, P(MMA/n-BMA) and PS capsules (the abbreviations are described in Table 2-2) towards concrete mixing. All capsules were prepared with a length of 50 mm and filled with water. The outer diameters of PLA, P(MMA/n-BMA) and PS capsules were 3.5, 6.6 and 7.2 mm, respectively. In order to test the survival rate of capsules during concrete mixing, small concrete batches (~10 L) containing 10 capsules per batch were prepared. The mixing techniques were divided into two parts: hot mixing and cold mixing. As the capsules were made from polymers with a low glass transition temperature, the change in temperature of the constituents was sought to modify the mechanical properties of the capsules and subsequently adjust the brittleness of the capsules with temperature, aiming to improve the survivability of the capsules during mixing. As a matter of fact, the physical properties of polymers change considerably around their glass transition temperature (i.e., 50 °C, 60 °C and 100 °C for P(MMA/n-BMA), PLA, and PS, respectively). Specially for the concrete hot mixing test, cement was not added, while only using pre-heated aggregates (85–105 °C) and boiling water (100 °C) during mixing. The amount of boiling water was kept the same as the water needed in the cold mixing. Additionally, capsules were pre-heated in an oven (85–120 °C) during 20–40 min prior to addition into hot mixes. The cold mixing scheme followed the traditional concrete mixing procedure. The results showed that the survivability ratio of all capsules used in the hot mixing was higher than in the cold mixing. More than 8 capsules out of 10 capsules could survive during the hot mixing. This might be explained due to the fact that the capsules showed more flexible behaviour after pre-heating. In the cold mixing, PS capsules showed the highest resistance (2–3 broken capsules), followed by P(MMA/n-BMA) capsules (7 broken capsules) and PLA capsules (10 broken capsules). It is logical that the PS capsules were able to survive in the cold mixing rather well due to the bigger diameter and wall thickness. However, the treatment for pre-heated capsules seems complicated from an industrial point of view.

Gruyaert et al. [54] investigated the idea to use polymeric capsules with evolving brittleness (flexible at first and brittle enough in contact with hardened concrete environment) in the concrete application. During the capsule production, capsules were made with two different dosages of plasticizing agent, at 10% and 25%, through a serial extrusion process. Plasticizing agents were added to obtain capsules with evolving brittleness.

To measure the resistance of capsules during concrete mixing, 10 capsules (5 mm outer diameter, 1 mm thickness and 50 mm in length) were prepared and tested with a 10 L of fresh concrete. The concrete mix design was formulated with a w/c of 0.47 and employing sand 0/4 and crushed limestone with two fractions of 2/6 and 6/20. Capsules were added during the last 2 min of mixing. The results showed that the capsules with 25% plasticizing agent performed better (9 out of the 10 capsules remained intact) in comparison to capsules with 10% plasticizing agent. However, these polymeric capsules tend to react chemically with the healing agent (e.g., PU), resulting in a premature hardening of the precursor inside the capsules before healing takes place. On top of that, the capsules did not break upon crack appearance, indicating less suitability for self-healing concrete application.

Araujo et al. [56] studied the survivability of other types of capsules in two different concrete mixes, prior to the final production of large concrete beams with mixed-in capsules. Initially, two types of capsules were utilized including glass capsules with a wall thickness of 0.8 mm and poly(methyl methacrylate) (PMMA) capsules with different wall thicknesses of 0.2, 0.4 and 0.7 mm. The length of all capsules was fixed at 50 mm, while the external diameters slightly varied in the range of 5.0–6.5 mm. In general, two concrete mix designs were formulated to observe the behaviour of mixed-in capsules in relation to the survivability of capsules towards mixing forces. (1) The first mixture was designed for traditional concrete containing crushed stones as coarse aggregates with two size fractions of 2/6 and 6/20. The w/c was fixed at 0.47 and no admixtures were added. (2) The second mixture was designed for SCC containing gravel with the fractions of 2/8 and 8/16. The w/c was higher than the first mixture (0.55) and superplasticizer was added. The mixing procedure was kept constant for all mixtures where the capsules were added directly into the fresh mixture in the last two minutes of the mixing time. By using their developed techniques, the survival ratios of capsules were evaluated. It was reported that the concrete composition had an exceptional influence on the resistance of capsules. The stresses induced on the capsules were lower in an SCC mix than a traditional mix. This was clearly reflected in the survival percentages of thin-walled PMMA capsules which was higher in the SCC mix. For instance, the survival ratios of PMMA capsules with the thickness of 0.4 mm were 20% and 83% in the traditional and SCC mixtures, respectively. Additionally, the survival ratio of thick-walled glass capsules increased from 70% in the traditional mix to 100% in the SCC mix. The aforementioned results may also indicate that the capsules could have a better survivability and less damage when they are incorporated into the

concrete mixes with the use of gravel as coarse aggregates. Since crushed limestones are angular in shape and characterized by their sharp and pointy edges, they will critically damage the capsules during mixing and possess a higher impact than gravel [54]; while gravels are naturally rounded aggregates. Based on these findings, three large concrete beams were fabricated using an SCC mixture: (1) reference concrete, (2) self-healing concrete with PMMA capsules (wall thickness = 0.7 mm, outer diameter = 6.5 mm, length = 50 mm) and (3) self-healing concrete with glass capsules (wall thickness = 0.8 mm, outer diameter = 5.0 mm, length = 50 mm). Both types of capsules were added with a dosage of 22 capsules per liter of concrete (equivalent to 3250 capsules in 150 L of concrete). However, due to the tendency of PMMA capsules to float, the casting of concrete beam was divided into two steps: (1) an SCC mix containing capsules was cast and poured into the mould forming a cover layer of 120 mm, and (2) another SCC mix without capsules was prepared and placed on top of the previous layer. The properties of these fresh concrete mixes were not evaluated.

2.2.4.2 Properties of the hardened concrete

As mentioned previously, the mix designs of the self-healing concretes are identical to the mix designs of their reference concretes; the capsules are either placed manually in the moulds or are added to the concrete mix during mixing. Simultaneously, the evaluation of the properties of the hardened capsule-based concrete is rarely done and the main focus of applying the capsules lies on the assessment of self-healing capabilities. In this chapter, a small number of studies reporting on the alteration of the properties of the hardened capsule-based concrete before being subjected to a healing scenario is reviewed.

Formia et al. [25] performed a preliminary test on the use of cementitious capsules to evaluate the changes on compressive strength of SCC due to the presence of capsules inside the concrete matrix. The cementitious capsules having a volume of 4000 mm³ (10 mm in diameter, 50 mm in length) were not filled with healing agent to avoid any possible contributions to the compressive strength and also to simulate the condition of empty capsules. The capsules were added with the dosage of 1.6% by volume of concrete (or in a proportion of four capsules per liter of concrete). In general, these capsules were embedded in the concrete cubes (100 × 100 × 100 mm) with three different orientations: (1) horizontal orientation, (2) vertical orientation and (3) random orientation. For horizontal and vertical

orientations, the first layer of SCC was poured in the mould, then one tube was put on the fresh concrete surface. Hence, a second layer of SCC was poured and a second tube was placed; and so on until filling completely the mould with concrete including four capsules. Especially for random orientation, the capsules were installed in each concrete layer with a random position and inclination. In this case, during casting, the capsules were placed by pressing them into the fresh concrete mix in order to guarantee a random orientation in space. SCC was designed using CEM I 52.5R, calcareous aggregates with five different fractions (with a maximum diameter of 10 mm), limestone powder, and plasticizer. The effective w/c was fixed at 0.46. The compressive strengths of concrete specimens with different capsule orientation were investigated after curing for 28 days at 90% relative humidity. The SCC without capsules had a mean compressive strength of 36.55 MPa; while the mean compressive strengths of SCC with horizontally oriented capsules, SCC with vertically oriented capsules, and SCC with randomly distributed capsules were 36.45, 35.95 and 33.45 MPa, respectively. The results showed that the incorporation of capsule with the dosage of 1.6 vol% did not significantly influence the compressive strength. Concrete with randomly distributed capsules experienced a 8.5% strength reduction due to the poor manual placement of the capsules which led to worse interfacial properties between the concrete matrix and the capsules. However, it was observed that these cementitious capsules had a good bonding system with the concrete matrix because neither slipping nor debonding of the capsules was found at the end of the compression test, indicating a promising usage of cementitious capsules for a future research.

In the research of Van Tittelboom et al. [60], two SCC beams were fabricated with the same dimension of $150 \times 250 \times 3000 \text{ mm}^3$. The mix design consisted of cement CEM I 52.5 N, sand 0/5, gravel with two size fractions (2/8 and 8/16), limestone filler and superplasticizer. Both mix designs of reference concrete and capsule-based concrete were kept the same. The major difference lies on the self-healing concrete beam where about 350 glass capsules (3.35 mm outer diameter and 50 mm in length) were placed inside the mould using a network of plastic wires at a cover depth of 10 mm. The density of the hardened concrete was approximately 2320 kg/m^3 , and the mean compressive strength at 28 days was recorded at 59.2 MPa. Both reference and capsule-based concrete beams were loaded in four-point bending to reach an average crack width of $250 \mu\text{m}$, controlled by means of linear variable differential transformers (LVDTs). During testing, the vertical displacements in the middle of the beam were found to be 20.76 and 22.91 mm for the reference concrete and capsule-based concrete, respectively. At

the end of crack formation, the total load was registered around 36 kN for both concretes. No difference was found between reference and capsule-based concretes in this test.

Siahkouhi et al. [100] demonstrated the first real application of macrocapsules (i.e., glass capsules filled with PU) in railway concrete sleepers. Two types of glass capsules were fabricated: (1) long capsules with outer diameter, wall thickness and length of 9, 1, 200 mm, respectively, and (2) short capsules with outer diameter, wall thickness and length of 4, 0.5, 50 mm, respectively. The configuration of capsules within the concrete sleepers can be found in Figure 2-11. The first sleeper was designed with incorporating 10 long capsules in the middle section, while in another section of the sleeper called as rail seat, another 10 long capsules were also placed. The second sleeper was designed with using 54 short capsules (instead of 10 long capsules) at both middle and rail seat sections. The capsules were pre-installed in the sleeper mould with the aid of plastic wires. The glass networks, located in the concrete cover zone, for both long and short capsules covered at least 500 mm in the middle of the sleeper and 600 mm at the rail seat (both in length). The concrete mixture with a w/c factor of 0.33 was then cast and the 28d mean compressive strength of the concrete was 81 MPa. The sleepers were subjected to a bending moment (flexural test) twice: (1) one test at the middle (negative bending) and (2) another test

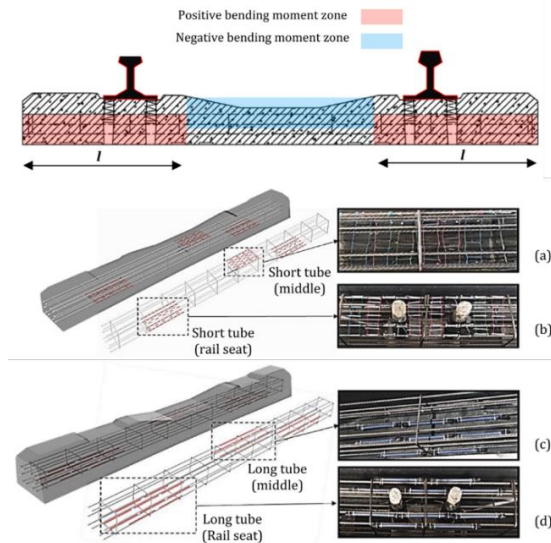


Figure 2-11. Capsule configuration within concrete railway sleeper: (a) short tubes at middle, (b) short tubes at rail seat, (c) long tubes at middle, and (d) long tubes at rail seat of sleepers [100]

on rail seat (positive bending). Based on three repetitions, it was reported that the average flexural load for sleepers with no capsules, short capsules and long capsules in the middle were 73, 81 and 72 kN, respectively, and for the rail seat, 224, 235 and 247 kN, respectively. Their results suggested that there was no severe effect of incorporating capsules in the concrete cover zone in terms of flexural strength which is an important design parameter for railway sleeper structure.

In addition to (tubular) macrocapsules that have been explained above, spherical macrocapsules can also be used for encapsulation. Sinha et al. [101], for instance, developed spherical and elliptical lignin-based capsules that are manufactured via 3D printing. The capsules were injected with sodium silicate as healing agent. Gravel-sized lignin capsules, having a diameter between 9.5–14.25 mm and shell thickness of 0.4 mm, were fabricated in accordance with the nominal size of gravel used in concrete. A volume fraction of 5% was employed for these capsules to assess their effect on mechanical strength. However, the author did not describe whether the capsules are treated as a replacement of gravel or as a direct addition to the concrete. Reference concrete was initially made with w/c of 0.4 and cement:sand:gravel ratio of 1:2:3. For capsule concrete, the capsules were added during mixing to obtain a random capsule distribution with an additional 5 min of mixing after capsules' addition. Both reference and capsule concretes were casted into cylindrical moulds and they were tested at 28 days. The results showed that the addition of 5 vol% lignin capsules significantly reduced the compressive strength and splitting tensile strength by 48% and 20%, respectively, as compared with reference concrete. The reasons for this strength reduction were due to (1) the high capsule volume fraction, (2) the degradation of the lignin capsules creating weak zones inside the concrete matrix, and (3) the capsules are lighter than the regular gravels and tended to move up during casting resulting in a less homogeneous distribution. The same author performed similar tests and methods in another study [102], but with changing the capsule material from lignin to polylactic acid (PLA). The diameter of PLA capsules was slightly bigger (9.5–19.05 mm) than for the lignin capsules and 5 vol.% PLA capsules were also added into the concrete. Sodium silicate was also injected into PLA capsules. The mixing procedure stayed the same as of using lignin capsules. After 28 days, the capsule-based concrete experienced a 18.5% reduction of compressive strength and a 8.4% increment of splitting tensile strength. Two hypotheses were elaborated to further explain the compressive strength loss: (1) the degradation of the capsules inside the concrete causes possible pathways of crack propagation under loading and (2) the capsules serve as

large inclusions in the matrix of concrete creating larger potential defects for stress concentration under loading.

There have been many publications [20,21,54,56,57,99] reporting the positive results of introducing the macrocapsules in the application of concrete. However, the results are only limited to the healing efficiency and thus the properties of the hardened capsule-based concrete are often neglected. Similar to the case of microcapsules, the addition of macrocapsules in the concrete matrix may induce a considerable effect in respect to the mechanical properties. The consequence of adding capsules in the concrete may also 'downgrade' other concrete properties before the healing ability is triggered upon cracking and rupture of the embedded capsules. One may argue that the properties of the hardened concrete such as the compressive strength of capsule-based concrete may experience a loss as compared with the control concrete without capsules. It is logical that the notion is presumed by two possible reasons: (1) the presence of macrocapsules, which even have a much larger volume than microcapsules, takes a partial volume of concrete and (2) the presence of macrocapsules disturbs the packing of aggregates which increases the volume of voids; both reasons may lead to a reduction of concrete strength. Therefore, the real application of macrocapsules in the concrete is still a bottleneck and more advancements in research are needed to mitigate potential problems induced by the presence of capsules in the concrete matrix. Hence, the application of the macrocapsules should be carefully considered and optimized to not affect negatively the properties of the hardened concrete.

2.2.4.3 Self-healing properties

The major notion of the encapsulated self-healing mechanism is based on the ability of the capsules to rupture when a crack generates and simultaneously release the healing agent into the crack, promoting in situ repair. The selection of the healing agent is also of great importance as the cargo should not be hardened during the entrapment inside the capsule. Thus, the suitability between the capsule material and healing agent is essential to be understood. The self-healing approach using an encapsulation technology steadily rises in the research field; however, most applications stay in the mortar level. Some studies upscale the utilization of capsules at the concrete level as discussed in this section.

The self-healing performance of concrete containing glass capsules was studied by Hu et al. [103]. The capsules with an internal diameter of 8 mm and length of 40 mm were filled with PU and were embedded manually in the concrete. The concrete specimens were cracked under a controlled three-point bending test until a crack width of approximately 300 μm was reached. Cracked specimens were cured in the curing chamber (20°C, 90% RH) until the testing day. After 2 days of healing, the strength recovery rate and the healing efficiency were recorded at 75% and 67%, respectively. Based on SEM micrographs at the interface between concrete and PU, large amounts of the PU curing products were identified and found to be cemented together with fine sand as well as with the C_3S and C_2S on the concrete surface [103]. In another large-scale test [60], Van Tittelboom et al. incorporated 350 glass capsules (3.35 mm outer diameter and 50 mm in length) with a cargo of PU in a concrete beam using a network of plastic wires at a depth of 10 mm. The agent was chosen due to the fact that it can harden in contact with humidity inside the concrete matrix. After the beam was initially cracked to achieve an average crack width of 250 μm , the beam was stored in standard laboratory climate and was sprayed with water during 6 weeks as a curing condition in order to allow a fair comparison with the other beams tested in that research. As a result of the 6 weeks of showering, a combined effect of autonomous healing (immediately) and autogenous healing (in time) was detected. At the end of the healing period, the crack closing ratio was obtained in the range of 10–40%. The wider the crack width, the lower the crack closing ratio. The highest portion of crack healing occurred at the moment of crack formation and capsule rupture. It should be noted that not all cracks were filled with PU.

Similar work was conducted by Araujo et al. [56] comparing the self-healing efficiency of two concrete beams (200×400×2500 mm^3) with the direct addition of glass capsules (5.0 mm outer diameter and 50 mm in length) and PMMA capsules (6.5 mm outer diameter and 50 mm in length). A water-repellent agent was injected into the capsule by means of a syringe and the both ends were sealed with hot glue or epoxy resin. All beams were stored in a standard laboratory environment until the time of testing. At the age of 14 days, a three-point bending test was performed in each beam by creating six localized cracks. The cracks were created consecutively (one crack per day) by moving the test set-up over the length of the beam. The crack widths were measured at six positions using an optical microscope and found in the range of 0.36–0.67 mm. During the loading of the beams, leaking of agents was noticed, indicating that the crack crossed and broke some capsules inside the beam. In order to evaluate the self-healing efficiency of

the concrete beams with the addition of macrocapsules, chloride ingress tests were conducted. To do this test, the beams were positioned slightly tilted in order to allow a 3% NaCl solution to flow over the beams during 24 h per week. The cracked surface was positioned upwards, and thus exposed to the 3% NaCl solution. After the first day of testing, the beams were left in the dry cycle for 6 days and the chloride test was repeated during 6 weeks. At the end of testing, to determine the chloride ingress, two concrete cores with a diameter of 150 mm (with a crack inside) were obtained from each beam. Then, each core was split along the crack surface and by following the testing procedures, concrete powders were collected by grinding in 2 mm layers perpendicular to the crack face at various depths. The total chloride concentration was measured by titration against silver nitrate. The result showed that the chloride concentrations of healed samples were approximately constant at every depth. When compared with the reference concrete (without capsules), the chloride content of healed concrete was considerably reduced due to the release of the healing agent from the capsules.

2.3 Conclusions

The importance of this PhD study is to understand the effect of the addition of healing agents on the behaviour of concrete in the fresh and hardened state as well as in relation to its self-healing capacity. This chapter explores three prospective self-healing materials including CA, bacteria and encapsulated healing agents that can be used for repairing the cracks and improving the self-healing efficiency of concrete. Based on the literature studies, the following conclusions can be drawn as follows:

1. There is still no clear explanation regarding the workability of concrete due to the addition of healing agents. Some studies claimed that the addition of CA, bacteria or capsules did not show negative effects on the workability, while other studies argued that they contributed to a longer setting time, loss of plasticity, higher air content and a decrease in slump value. Consequently, there is a need to further investigate the consistency and workability of self-healing concrete and understand the underlying mechanisms leading to the changes and formulate mitigation plans.
2. The addition of CA and bacteria with suitable nutrients generally enhances the compressive strength of concrete composites. This may be

attributed to: (1) the filling and water-barrier effects of CA as well as the role of CA as hydration activator to promote the further densification of the concrete microstructure and (2) pores clogging phenomenon by microbial calcite precipitation leading to a denser microstructure and the notable effect of suitable nutritional admixtures to react and help producing more CaCO₃-based materials.

3. The incorporation of microcapsules caused a steep decrease of the strength value due to the high pore volume as a result of capsules presence inside the concrete matrix. The properties of the hardened concrete with macrocapsules are still not well understood, while, in fact, the presence of macrocapsules may disturb the packing of aggregates.
4. The inclusion of healing agents demonstrates adequate healing capabilities to a great extent and the durability performance of self-healing concrete is remarkably improved upon healing activation.

This state-of-art review has shown that self-healing technologies offer a new advancement of using smart materials to preserve the longevity of the concrete structures. However, to date, findings show that the inclusion of healing agents at the concrete level is very limited, suggesting that many improvements are needed in this research. One of the major drawbacks in the current practice is that no adaptations are made in original mix designs for self-healing concrete. Consequently, mix design optimization is highly required and more interdisciplinary works should aim at developing the self-healing concrete composition, selecting the optimum dosage of healing agents, and determining some key parameters that affect the engineering properties of self-healing concrete. Finally, it may be hoped that in the near future there would be technical standards and specifications to optimally compose the mix designs for self-healing concrete in a similar way as designing the conventional concrete in accordance with international standards.

Chapter 3

FRESH PROPERTIES OF THE MODIFIED CEMENT PASTE WITH INCLUSION OF HEALING AGENT AND ADMIXTURES

3.1 Introduction

As discussed in Section 2, the two main goals of adding healing agent into the concrete are to activate the healing mechanism and to improve the healing efficiency, however, the evaluation of fresh properties of concrete mixes with the inclusion of healing agents is often neglected [104]. Workability is an important aspect for fresh concrete to ensure that it can be easily placed and handled in the field. Furthermore, chemical admixture such as superplasticizer is often added to improve the workability of the mixture. The adsorption behaviour of superplasticizer in cementitious materials has been previously studied [105–108], while the compatibility between cement, superplasticizer and healing agents is still unknown. Therefore, understanding the influence of healing agents in relation to the rheological properties is of great importance. Before going into the concrete level, the effect of healing agents should be clearly identified starting from the paste level to serve as a basic input for formulating the mix design of self-healing

**) This chapter is based on the following papers: (1) Hermawan H, Minne P, Brac EG, Wiktor V, Serna Ros P, Gruyaert E. Influence of Crystalline Admixtures and Bacteria on the Fresh Properties of Self-healing Concrete. In: Proceedings of the 75th RILEM Annual Week 2021, RW 2021 Springer International Publishing; 2023. p. 451–60; and (2) Hermawan H, Beltran GS, Wiktor V, Serna P, Gruyaert E. Effect of healing agents on the rheological properties of cement paste and compatibility with superplasticizer. MATEC Web Conf 2022;5008(361).*

concrete. In this chapter, two commercial healing agents (i.e. Basilisk bacteria healing agent and Penetron Admix crystalline admixture) are introduced into the fresh paste to investigate the effects on the consistency and setting time of the paste. The effect of healing agents on the dispersing ability of PCE-based superplasticizer in the paste is also analyzed to understand the adsorption behaviour.

3.2 Characterization of cement and healing agents

Two types of cements from CBR (Belgium) (CEM I 52.5N and CEM III/A 42.5N, abbreviated as CEM I and CEM III/A) and demineralized water were used to make the fresh pastes. The chemical compositions of these cements are presented in Table 3-1. Penetron Admix crystalline admixture (CA) and Basilisk bacteria spores (BAC), both in powder form, were utilized as healing agents. The particle size distributions (PSDs) of cements, bacteria and crystalline admixtures are presented in Figure 3-1. The PSDs were obtained by laser diffraction particle size analysis via FRITSCH Analysette 22 COMPACT (Germany). Specifically for the bacteria healing agent, laser diffraction analysis was complemented with sieve analysis because particles larger than 300 μm were present, exceeding the upper size limit of the laser diffraction apparatus. The PSD of CA is in the range of the cements, but a bit broader. The median sizes (D_{50}) of CEM I, CEM III/A, CA and BAC are 17.16, 11.73, 15.20 and 490.24 μm . The scanning electron microscopy (SEM) micrographs of these materials can be found in Figure 3-2, tested via PhenomXL Desktop SEM (Thermo Fisher Science, US). The material was initially placed on the carbon-coated sample holder and the sample were further coated with gold for the imaging. The micrographs were finally taken using the secondary electron detector (SED).

The XRD analysis was performed on the powdery materials. The samples were back loaded in the sample holders to mitigate preferred orientation effects for XRD data collection. A PANalytical CubiX3 diffractometer in conventional Bragg-Brentano θ - θ geometry with a 200-mm goniometer radius was used for data collection. Cu K-alpha X-rays were generated using a standard X-ray tube operated at 40 kV accelerating voltage and 45 mA filament current. Finally, the phase identification and Rietveld analysis were carried out using X'Pert High Score plus v4.8 software package by PANalytical. As a note, 4 ICDD cards and 15 ICSD cards were used for the phase identification in the XRD instrument (note: ICDD = International Center for Diffraction Data, ICSD = Inorganic Crystal Structure Database).

Table 3-2 shows the phase composition of cements and CA. CEM I has a similar C_3S content as CA, while it is nearly half for CEM III/A. This is attributed due to the low clinker content in CEM III/A where this cement type is blended with blast furnace slag (48%). C_3S has been known as the key source of the main hydration product named calcium silicate hydrates (C-S-H) and is responsible for the setting and initial strength development of cement [109]. The fact that CA contains a high C_3S compound is due to the fact that the CA itself is partly composed of Portland cement. In case of C_3A , the total C_3A compound (aluminate cubic + aluminate ortho) of CEM I and CEM III/A are 3.12 and 4.02%, respectively. It is interesting to see that the total C_3A compound of CA is much higher than CEM I by a factor of 3.3 (10.44%). C_3A is the most highly reactive phase in clinker and the one with the greatest affinity for superplasticizer admixtures. The fresh properties of cement paste are also influenced by the amount of calcium sulfate (i.e. gypsum, hemihydrate and anhydrite) in cement. Calcium sulfate is added to control the hydration of C_3A to avoid flash setting and to induce the optimum hydration of C_3S [110]. The total calcium sulfate (gypsum + hemihydrate + anhydrite) of CEM I, CEM III/A and CA are 3.35, 5.92 and 4.73%, respectively. Alkali sulfates also play an important role in cement hydration and setting. With high amount of alkali sulfates, the hydration rate of C_3A increases, which may lead to rapid setting [111].

Table 3-1. Chemical composition of the cements (provided by the manufacturer)

Chemical composition (%)	CEM I 52.5N	CEM III/A 42.5N
CaO	64.35	53.58
SiO ₂	21.00	27.39
Al ₂ O ₃	4.22	6.83
Fe ₂ O ₃	2.72	1.82
SO ₃	3.29	3.02
CO ₂	1.00	1.04
Cl	0.07	0.05
MgO	2.04	4.66
K ₂ O	0.80	0.59
Na ₂ O	0.24	0.27
P ₂ O ₅	0.49	0.22

According to the manufacturer, the recommended dosage of healing agent is in the range of 0.8–1.0% by weight of cement for Penetron crystalline admixture and 1.0–4.0% by weight of cement for Basilisk bacteria healing agent. However, an attempt was made to use a higher dosage of healing agent to possibly increase the self-healing efficiency without lowering other properties such as workability. Healing agents, both CA and BAC, were finally added in the range of 0.8–5.0% by weight of powder. The incorporation of healing agents is mostly carried out on top of the normal mix, without any adaptation in the mix design. In this study, the healing agents are added into the cement paste by changing the powder proportion of the mixture. For instance, the powder composition of the paste CEM I + 3% BAC is composed of 97% CEM I and 3% Basilisk bacteria. Additionally, the polycarboxylate-ether (PCE) based superplasticizer (SP) of Demula Technofluid P175, supplied by Cugla B.V., was also used as a high-range water reducer (HRWR). The properties of this superplasticizer are given in Table 3-3.

Table 3-2. Quantitative XRD phase analysis on CEM I, CEM III/A and CA (note: * represents the indicative amount of compound below 1% that may be inaccurate)

ICDD/ICSD card number	Phase	CEM I 52.5N	CEM III/A 42.5N	PENETRON CA
ICSD 64759	C ₃ S - Alite	60.23	29.29	61.50
ICSD 21	C ₂ S - Belite	17.48	6.13	9.47
ICSD 81097	C ₂ S - Belite alpha*	1.95	-	0.00*
ICSD 245646	C ₄ AF - Ferrite	6.73	5.44	3.86
ICSD 4	C ₃ A - Aluminate cubic	2.34	1.27	8.34
ICDD 04-012-8663	C ₃ A - Aluminate ortho	0.78*	2.75	2.10
ICSD 5	Free Lime - CaO	1.48	0.00*	0.38*
ICSD 7	Portlandite - Ca(OH) ₂	0.47*	0.11*	5.38
ICSD 6	Periclase - MgO	1.39	0.24*	2.07
ICSD 20	Arcanite - K ₂ SO ₄	0.72*	0.09*	0.19*
ICSD 26014 / ICDD 00-020-0928	Aphthitalite - K ₃ Na(SO ₄) ₂	0.66*	0.09*	0.54*
ICDD 04-008-8637	Calciolangbeinite - K ₂ Ca ₂ (SO ₄) ₃	0.16*	0.05*	0.00*
ICSD 7	Gypsum - CaSO ₄ ·2H ₂ O	0.19*	0.27*	2.21
ICSD 79528	Hemihydrate - CaSO ₄ ·0.5H ₂ O	0.00*	0.29*	2.52
ICSD 15876 / ICDD 00-037-1496	Anhydrite - CaSO ₄	3.16	5.36	0.00*
ICSD 73446	Calcite - CaCO ₃	1.96	0.53*	1.44
ICSD 5	Quartz - SiO ₂	0.30*	0.08*	0.00*
	Slag	-	48.01	-

Table 3-3. Properties of superplasticizer (provided by the manufacturer)

SP type	Chemical type	Density (kg/dm ³)	Solid content (%)	pH
Demula	Polycarboxylate	1.07	30	2.0 – 8.0
Technofluid P175	ether			

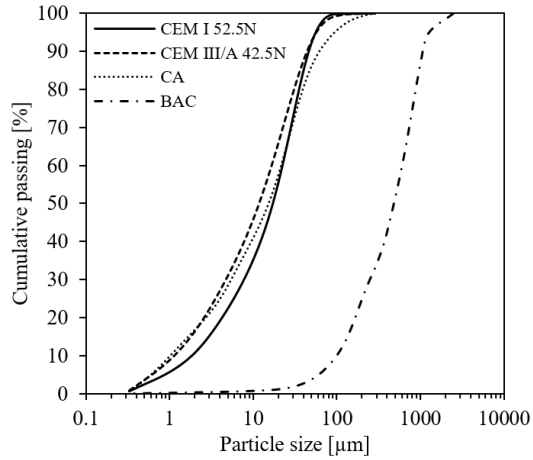


Figure 3-1. Particle size distributions of cements and healing materials

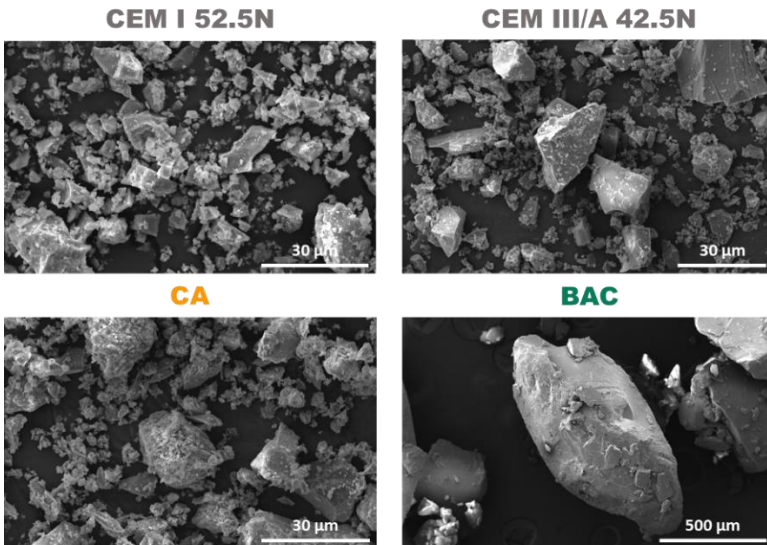


Figure 3-2. SEM micrographs of cements and healing agents

3.3 Initial assessment of the effect of healing agents on the cement paste

3.3.1 Testing methodologies

In this study, initial tests on the fresh cement paste in combination with healing agents were performed. To start, the standard consistency test and setting time test in accordance with EN 196-3:2016 were carried out. The standard consistency test is performed by use of the manual Vicat apparatus (with the use of a plunger) to determine the water demand of each modified powder mixture in comparison to pure cement without a healing agent. On the other hand, the automatic Vicat apparatus is also used to measure the initial and final setting time of the pastes at standard consistency. As a note, a circulation bath was used to maintain constant temperature during the tests. In practice, superplasticizers are widely used in concrete mixtures to improve the workability. Consequently, an additional experiment was executed to investigate the effect of superplasticizer in relation to the reduction of water demand. The superplasticizer is added in the dosage of 0.1–2.0% by weight of powders (cement + healing agent).

3.3.2 Influence of healing agents on water demand and setting time of cement paste

The results on water demand of cement in combination with BAC and CA at standard consistency are presented in Figure 3-3. It shows that the gradual addition of BAC slightly reduced the water demand. The combination of CEM III/A with 5% BAC reduces the water demand from 29.5 (pure CEM III/A) to 27.7% (CEM III/A + 5% BAC). In combination with CEM I, the reduction induced by the presence of BAC is apparently minor as the water demand reduces only from 28 to 27%. As shown in Figure 3-3b, the behavior of CA is completely different on the use of different cement types which is also in contrast with the result of using BAC. The result shows that the water demand is higher in presence of CA (for all dosages from 0.8 to 5% by the weight of powder). On the use of CEM III/A, the amount of water needed to achieve a standard consistency raises from 29.5 to 34.5%. Although it is clear that, in combination with this type of cement, the water demand in case of 4% CA is higher than in case of 5% CA, a linear regression line was plotted (Figure 3-3b). Contrarily, the result of combining CA and CEM I shows a different behavior. The tendency seems to be a parabolic regression where

the gradual addition of CA up to 3% increases the water demand by 3%, while the higher dosage of CA shows a declined trend as the water demand reduces from 31 to 29.5% when the CA dosage is increased from 3 to 5%. By comparing these two results on water demand, in fact, the addition of CA showed a similar behavior on both types of cements when the dosage was limited to 3%.

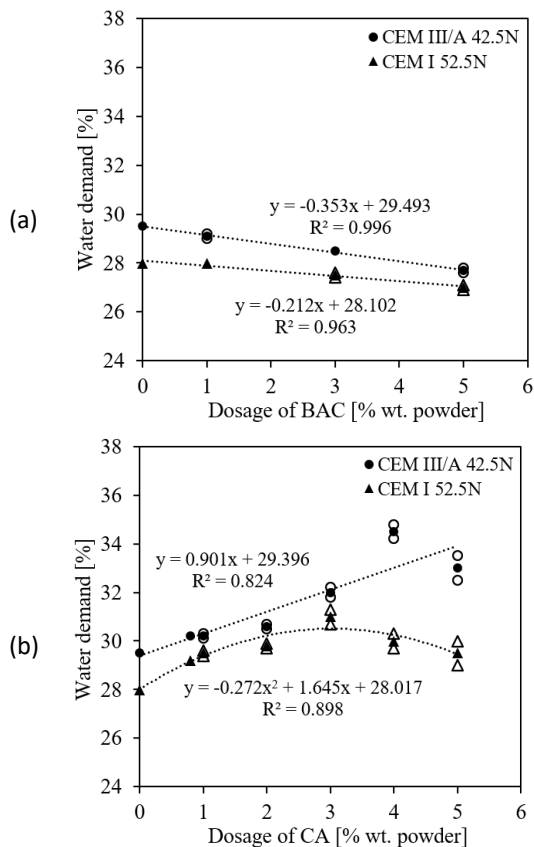


Figure 3-3. Water demands of modified cement incorporated with (a) Basilisk bacteria and (b) Penetron crystalline admixture at different dosages (note: the empty markers represent the water demand values, while the filled markers represent the mean values)

As a matter of fact, as reported by [112], in case CA is used, it is important to make a judicious selection regarding the type of cement. Cement with a high content of clinker, such as CEM I, is preferred because CA needs an appreciable amount of calcium hydroxide, which is a typical hydration

product of Portland cement, to react. In the case of blended cement like CEM III/A, less calcium hydroxide is produced and can be even consumed.

Moreover, the setting time test was evaluated and results are shown in Figure 3-4. In spite of the rather small effect by BAC on water demand, the setting time of these pastes considerably increases as a consequence of incorporating BAC into the fresh mix. Based on Figure 3-4a, both initial and final setting times are delayed regardless the cement type. However, a considerable effect is identified on the mixture containing 5% BAC and CEM I. The final setting times of cement pastes (with CEM I) are 175, 221, 311 and 660 min with the addition of 0, 1, 3 and 5% BAC, respectively. It is clear that the setting time of cement paste with 5% BAC is roughly doubled in comparison with cement paste with 3% BAC. Moreover, this exceptional result is not observed in the paste with CEM III/A. On the use of CEM III/A, the addition of BAC from 1 to 5% gradually increases the setting time of the paste. The final setting times of cement pastes (with CEM III/A) amount to 227, 256, 333 and 430 min with the addition of 0, 1, 3 and 5% BAC, respectively. In general, the mean gap time between initial and final setting time of paste containing BAC is approximately 63 ± 9 min. Rossi et al. [79] investigated the cement hydration with the addition of Basilisk bacteria healing agent by means of an isothermal calorimetry test and they found that the addition of BAC caused a decrease of heat developed by the hydration of cement, resulting in the retardation effect. Due to the reason that BAC is composed of organic compounds, the alkaline degradation of these compounds into molecules containing the α -hydroxy carboxyl group may be responsible for the delay in the setting time of the cement pastes [79,113].

The setting time of paste containing different CA dosage (0.8–5% by weight of powder) is presented in Figure 3-4b. Similar with the consistency test results, the inclusion of CA in combination with CEM I and III shows different behavior. On the use of CEM I, the 1% CA addition increases the initial and final setting time of the paste by approximately 63 and 77 min, respectively. The higher the addition of CA the faster the setting time of the paste. Specifically the gradual addition of CA from 1 to 5% shortens the final setting time from 252 to 183 min. A significant effect in using high dosage of CA was the fast setting of the paste. By using the high CA dosage at 4 and 5% by weight of powder, the initial setting times were found to be at 68 and 22 min, respectively. From the visual observation by the author, the cement paste incorporated with a high dosage of CA was quickly stiffened after the mixing process. This may be attributed to a chemical reaction occurring when the CA came into contact with water and cement, resulting into a fast setting

time. This was supported by the fact that the white powder present in CA particles which presumed to be active chemicals immediately dissolved in water. From the experiment, it was observed that when the CA came into contact with water, the mixing water turned into greenish color, indicating an immediate reaction and a hydrophilic character of CA which can react easily with water [65]. However, further investigations should be conducted to analyze these results in detail. Furthermore, it is clear that the addition of CA in combination with CEM III/A shows similar setting times regardless the dosage. As a matter of fact, the use of high CA dosage at 4–5% has a comparable result with the low dosage at 1% in the terms of setting time.

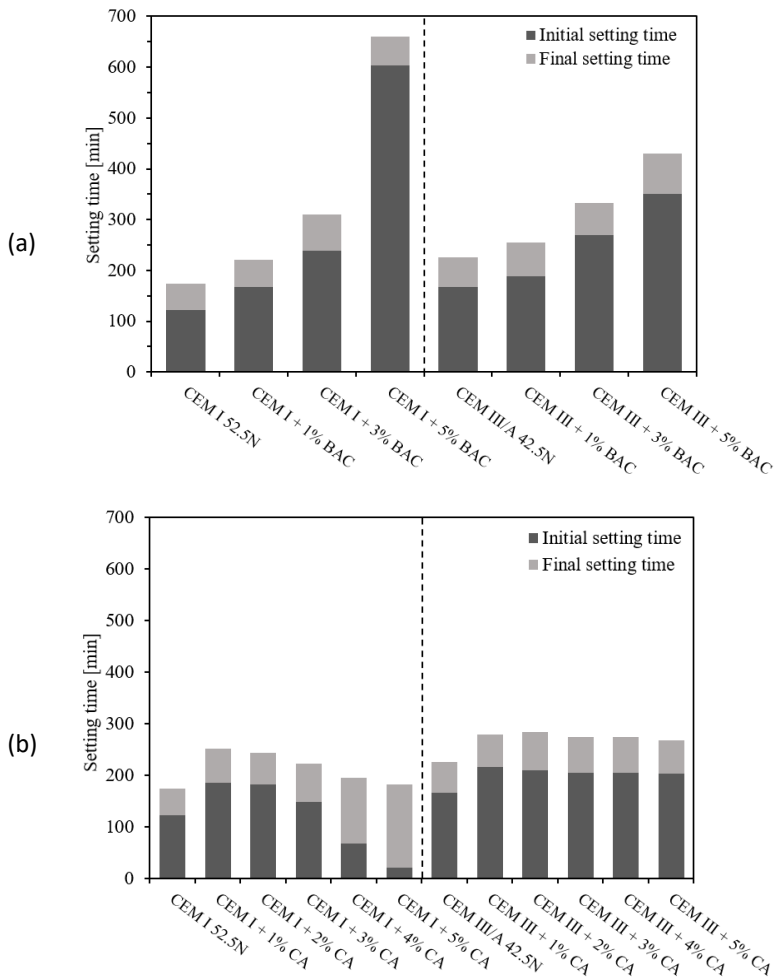


Figure 3-4. Setting times of modified cement pastes incorporated with (a) Basilisk bacteria and (b) Penetron crystalline admixture at different dosages

3.3.3 Water-reducing effect of superplasticizer on the cement paste

Additionally, the SP was added into the modified cement paste with healing agent, either BAC or CA, at the dosage between 0.1 and 2.0% by weight of powders (cement + healing agent) to measure the water reduction of the paste at normal consistency and to observe the compatibility aspect between healing agent and superplasticizer. Figure 3-5 shows the relationship between SP dosage and total water demand in combination with different dosages of healing agent. The BAC was fixed at dosages up to 5%, while the dosage of CA was limited up to 3% to eliminate the unfavorable effect on the use of a higher dosage as explained in the previous results. As a note, the water demand was increased with the water contained in the SP solution, and is further defined as total water demand.

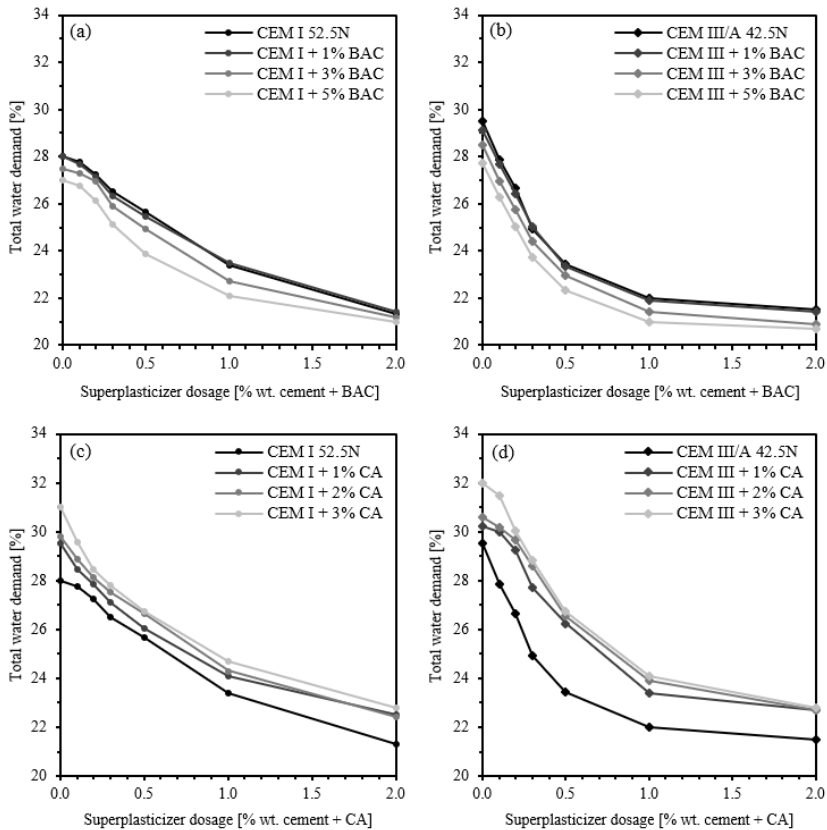


Figure 3-5. Effect of SP dosage on the water demand of powder mixtures: (a) CEM I + BAC, (b) CEM III/A + BAC, (c) CEM I + CA and (d) CEM III/A + CA

According to Figure 3-5a and Figure 3-5b, the reduction rate of the water demand is relatively similar for control paste and paste containing BAC. As shown in Figure 3-5c, there is an immediate reduction of the water demand of cement pastes with CEM I containing CA at a low SP dosage. However, the reduction rate of the water demand with varying SP dosages of all pastes with HA was quite similar with the control paste. Contrarily, this was not the case for the modified paste with CEM III/A and CA. As shown in Figure 3-5d, the water demands of CA and CEM III/A are always higher than the pure cement and in addition, the changes in water demand of CA and CEM III/A upon increasing SP dosage do not follow the behavior of water demand reduction of the pure CEM III/A. Nevertheless, the incorporation of the superplasticizer decreases the water demand at all dosages of healing agents (CA or BAC), while the variations in the water demand are generally lower at a higher dosage of SP.

3.4 Compatibility study on the effect of SP dosage on workability and rheology of cement paste

Moreover, cement pastes were made of CEM III/A and CEM I in combination with CA and BAC. The dosages of CA and BAC were fixed at 1% and 2% by weight of powder, respectively, as recommended by the producers. Previously in Section 3.3, Technofluid P175 was used for all pastes. However, after several considerations of SP usage related to the concrete application, two types of SP were used here depending on cement type and its purpose:

- For CEM III/A (aimed for ready mixed concrete application), Fluvicon 801 was used as a PCE-based SP with a solid concentration of 20%.
- For CEM I (aimed for precast concrete application), Technofluid P175 was used as a PCE-based SP with a solid concentration of 30%.

The dosage of both SPs was fixed in the range of 0–0.8% by weight of powder (i.e. powder means 100% cement for control paste, 99% cement + 1% CA for CA paste, and 98% cement + 2% BAC for BAC paste). Finally, all pastes were made with a water to powder (w/p) ratio of 0.40. For the mixing procedure, the dry components (cement and healing agents) and water (without and with diluted SP) were initially mixed for 1 min in the Hobart mixer with a low speed. Then, the mixer was stopped for 30 sec and the bowl was scraped to ensure homogeneity and ensure no dry components remained on the wall

and bottom part of the bowl. Next, the paste was mixed again for 2 min in the Hobart mixer with a low speed. Thus, the total mixing time was 3 min.

3.4.1 Rheological test methods

In order to evaluate the fresh properties of the paste, several experimental tests were executed including:

➤ Mini slump test

The mini-slump test was performed to evaluate the workability of the fresh paste. Another aim of this test was to determine the critical dosage and saturation dosage of the SP. The critical dosage (CD) is defined as the minimum SP dosage to start improving the workability, while the saturation dosage (SD) corresponds to the dosage at which the effectiveness of the SP reaches the maximum limit, as beyond this dosage, water reduction is not possible or segregation occurs. The indication of segregation can be found in Figure 3-6. To do this test, a truncated conic mould (70 mm in top diameter, 100 mm in bottom diameter and 60 mm in height – see Figure 3-7a) was placed on an acrylic plate, filled with the paste and lifted upward. The resulting spread diameter of the paste was the mean value of two measurements made in two perpendicular directions. The slump tests were performed at 5, 30, 60 and 90 min after mixing time. As a note, prior to all slump tests, the paste was pre-mixed for 30 sec. The slump spread was recorded and regarded as a consistency parameter. A single measurement was considered for this test on each mixture. Specifically for CEM I, the slump tests were only continued until 60 min considering in practice the transport time for precast concrete is generally shorter than ready-mixed concrete.

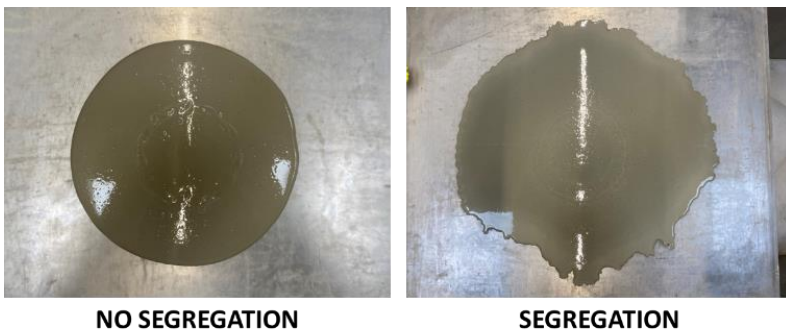


Figure 3-6. Sign of segregation on cement paste

➤ Viscosity test (visco-test)

The visco-test was carried out to measure the plastic viscosity of the paste in relation to the rheology of the fresh paste which could not be quantified in the mini slump test. The paste was poured into the cup with the constant mass of paste between 210–220 g. Then, the container was installed in the HAAKE Viscotester 550 (see Figure 3-7b) together with a spindle. The apparatus was programmed to measure the paste viscosity at 5, 30, 60 and 90 min after mixing time. On each measurement, the shear rate was gradually increased from 0 to 50 s⁻¹ for about one minute. In this study, the shear rate of 15 s⁻¹ was considered for further analyses. This shear rate mimics the concrete mixing during rotation inside the truck mixer and pouring the fresh concrete from 1 meter height. A single measurement was considered for this test on each mixture.

➤ Total organic carbon (TOC) test

The TOC test was executed to analyse the adsorption capacity of SP on cement and healing agent particles. After mixing the powder and water for 3 min, the paste was immediately poured into plastic tubes with ~50 g of paste per tube and centrifuged for 10 min to separate the solid from the pore solution. The supernatant was then extracted and diluted (6 mL) with phosphoric acid (H₃PO₄) (6 mL) to remove inorganic matters in the solution. The solution was then centrifuged for another 10 min in order to allow sedimentation of the impurities. The solution was finally diluted (1–6 mL, depending on the SP concentration) with demineralized water to meet the calibration range of the TOC analyzer and poured into vials to be tested on the Lotix TOC Combustion Analyzer (see Figure 3-7c). The carbon content of pure SP and control paste without SP was also measured in order to calculate the total amount of SP adsorbed. A single measurement was considered for this test on each mixture.

➤ Ultrasonic test (ultra-test)

Ultrasonic wave transmission was used in this test to monitor the setting process of the cementitious materials. The Ultratest IP8 device (Germany) measures the velocity of ultrasonic longitudinal waves transmitting through cement paste (Ø40×52 mm) with a travel distance of 40 mm and a frequency of 30 kHz (in compliance with EN 12504-4). Ultrasonic pulse velocity (UPV) is also closely related to the physical and mechanical properties of materials [114]. The development of the ultrasonic velocity with respect to time was recorded starting from the fresh paste (right after mixing) to the hardened paste (after 24 hours). The setting behaviour of material can be evaluated

from the UPV curve considering its first derivative of UPV (or called as acceleration in $\text{m}/\text{min}\cdot\text{s}$ or m/min^2) [115]. Ye et al. [116] suggested that when UPV rapidly increased in fresh cement paste, it corresponds to the end of the dormant stage which is related to the initial solid percolation. When cement hydrates percolated through the specimen, a complete path for the UPV was formed. A quick increase of the UPV followed the rapid change of the connectivity of the solid phase. Finally, when all the solid phase was connected, the slow increase of the UPV followed the evolution of the total solid fraction. Figure 3-7d shows the setup of the ultrasonic test. A single measurement was considered for this test on each mixture.

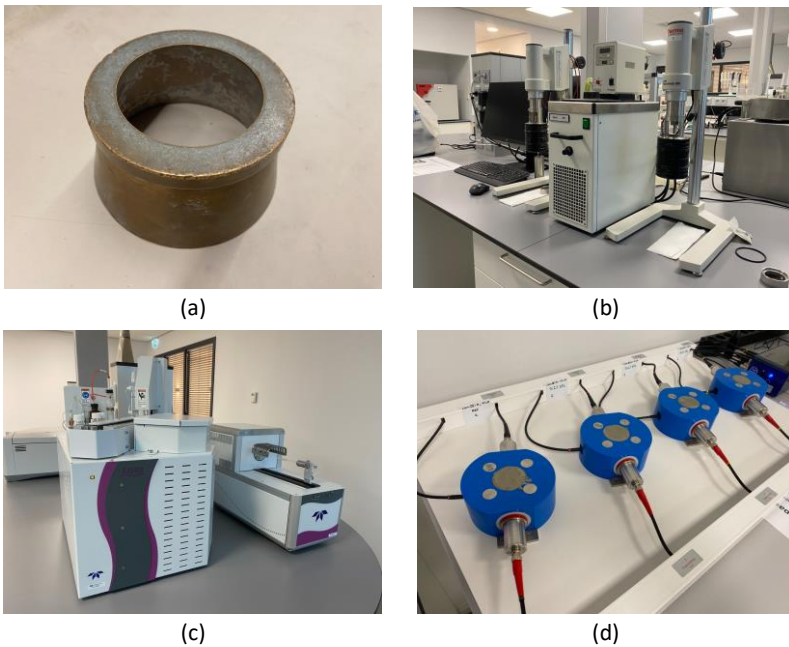


Figure 3-7. (a) Mini slump cone, (b) Viscometer, (c) TOC device and (d) Ultrasonic test setup

3.4.2 Slump loss

Figure 3-8 illustrates the slump changes over time on pure cement paste and cement pastes with healing agents.

- Based on Figure 3-8a, the first slump of pure CEM III/A paste was measured at 135 mm. The slump gradually decreased as time increased,

reaching 118 mm after 90 min. The influence of CA and BAC was noticeable. The slump values at 5 min for CA paste and BAC paste were 120 and 145 mm, respectively. In comparison to the pure CEM III/A paste, it showed that the CA reduced the slump by 11.1% while the slump increased by 7.4% due to BAC. The tendency of slump reduction over time was also clear on these pastes. Especially for CA paste, the reduction was less significant as compared with pure and BAC pastes and was almost constant. It was attributed to the very low slump value at the beginning which almost reached the boundary of the mini slump cone. Thus, further reduction was not possible over 100 mm. It is interesting to observe that the initial slump of the pure CEM III/A paste corresponded to the slump of the BAC paste after 60 min.

- Based on Figure 3-8b, the first slump of pure CEM I paste was measured at 212 mm, which is much higher than the initial slump of pure CEM III/A paste (135 mm). As expected, the slump of cement paste continuously decreased as increasing the time, reaching 205 mm after 60 min. The addition of CA reduced the initial slump to 196 mm. However, it is interesting to see that at 15 and 30 min, the slump of CA paste suddenly increased to 206 and 209 mm, respectively. It shows that there is a thixotropic behaviour of the cement paste due to the addition of CA. It means that the CA paste is viscous under normal condition after mixing, while it remains fluid when agitated during mixing. After 45-60 min, the thixotropic behaviour of CA paste disappeared as the slump decreased gradually over time. The addition of BAC slightly increased the initial slump of cement paste. The slump reduction over time of BAC paste follows a similar trend as pure CEM I paste.

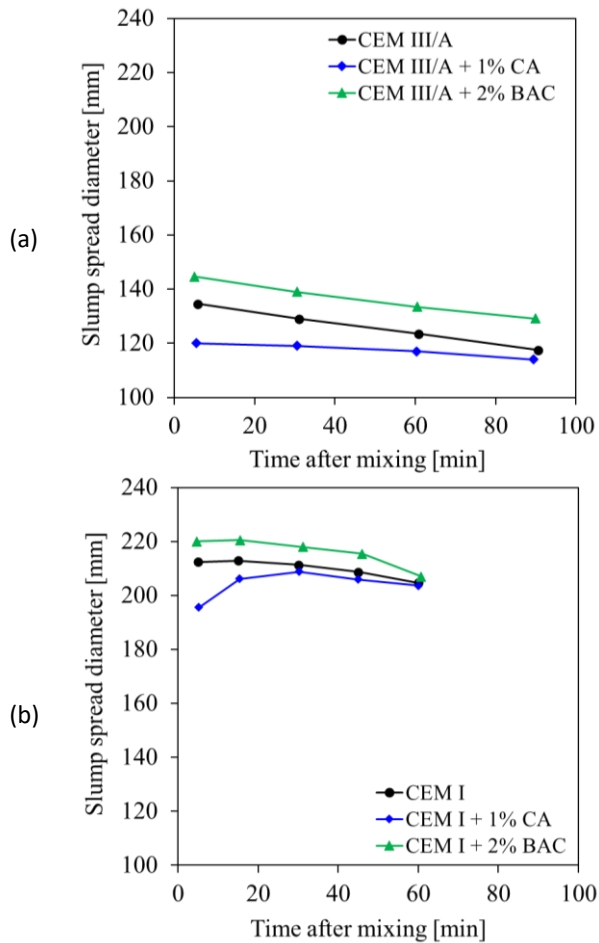


Figure 3-8. Reduction of slump values over time on (a) CEM III/A pastes and (b) CEM I pastes

3.4.3 Impact of SP dosage on pure cement paste

From Figure 3-8, it was evident that there is a need to introduce the SP to improve the workability of the cement paste. The SP was initially introduced to the pure cement paste from 0.1 to 0.6% by weight of powder. Initially the slump life of the cement paste with the addition of SP was evaluated as shown in Figure 3-9.

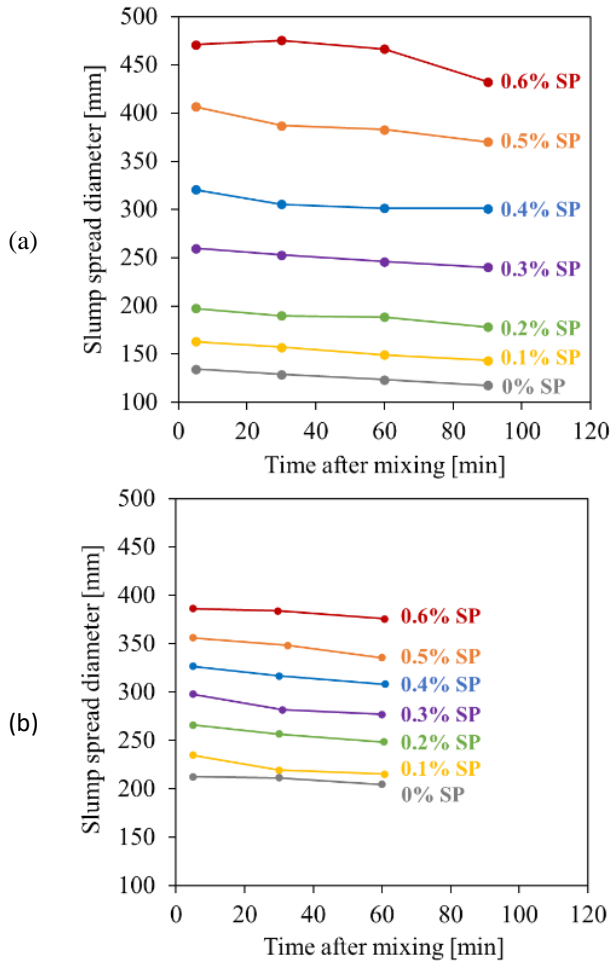


Figure 3-9. Slump life of superplasticized cement pastes ((a) CEM III/A and (b) CEM I) with different SP dosage and SP type (Fluviscon 801 for CEM III/A, Technofluid P175 for CEM I)

- Based on Figure 3-9a, the slump spread reduction of CEM III/A paste as a function of time was relatively small by the addition of SP dosage $\leq 0.3\%$ by powder weight. The slump retention was clearly identified when the SP was introduced at the dosage of 0.4% by powder weight, maintaining the existing slump after a long period (in this case, from 30 to 90 min). CEM III/A paste containing 0.6% SP showed segregation.
- Based on Figure 3-9b, the slump spread reduction of CEM I paste as a function of time was also minor by the addition of SP at any dosages. The slump retention was already seen when added with 0.1% SP. It should

be noted that the SP used for CEM I (Technofluid P175) is different with the SP for CEM III/A (Fluvison 801). The SP addition from 0.1 to 0.6% gradually increased the initial slump spread (at 5 min) with the interval of approximately 30 mm. CEM I paste containing 0.6% SP showed segregation.

Further analysis was done to establish the relationship between slump spread and SP dosage by considering the slump results from the first slump test (5 min after mixing). Figure 3-10 shows that, as expected, the slump spread diameter increases with an increasing dosage of SP. It can also be seen that increasing the SP dosage results in a decrease in the viscosity.

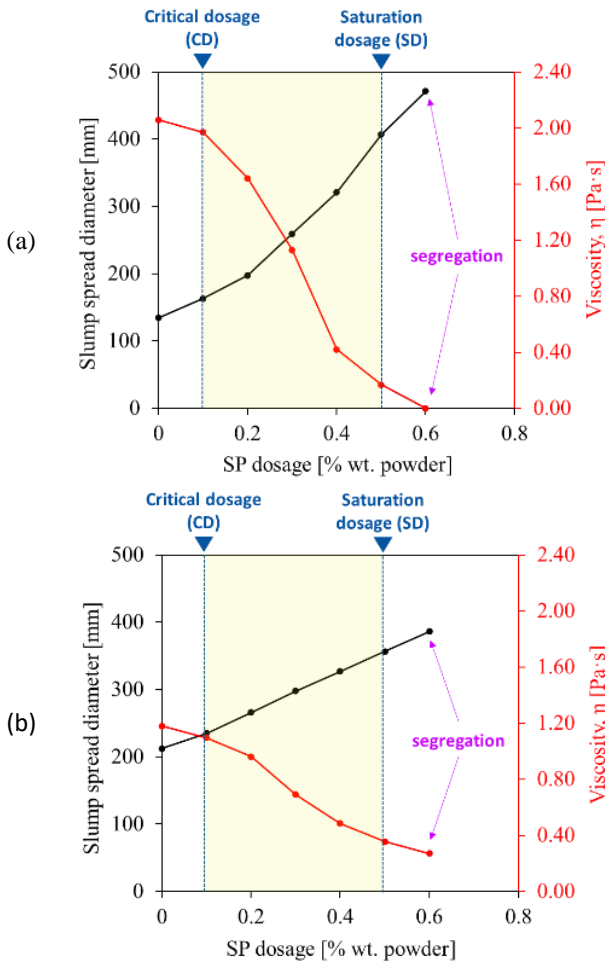


Figure 3-10. Determination of CD and SD in relation to a certain SP based on slump and viscosity results of (a) CEM III/A paste and (b) CEM I paste

As can be seen in Figure 3-10, when a high SP dosage (0.6 wt% powder) was introduced, segregation was observed from visual inspection. It was also clear that the slump spread still increased with a high SP dosage but the viscosity of the paste was considerably low. Therefore, the CD and SD were determined at 0.1% and 0.5%, respectively, for both CEM III/A and CEM I pastes. In this range between 0.1–0.5%, the addition of SP can be regarded as effective to improve the paste workability.

3.4.4 Impact of healing agents on superplasticized cement paste

The CA and BAC pastes were evaluated in the same way as the pure cement paste and the results are depicted in Figure 3-11 and Figure 3-12.

- *On the use of CEM III/A:* As can be seen in Figure 3-11(a), the introduction of BAC slightly increased the slump values as compared with pure CEM III/A paste. Nevertheless, both BAC paste and pure CEM III/A paste exhibited a very similar tendency in terms of workability changes by the gradual SP addition from 0 to 0.6% by powder weight. It suggests that (1) the BAC did not considerably affect the rheology of superplasticized cement paste and (2) BAC did not interfere with the dispersing ability of SP in the paste. In contrast, the incorporation of CA considerably affected the slump value. The CA paste, in fact, showed an initial improvement of the workability after 0.3% SP was introduced. Above this dosage, the slump started to increase gradually. It is noteworthy to mention that the pure CEM III/A and BAC pastes showed segregation at 0.6% SP, while for CA paste, it occurred at 0.8% SP. It was clear that the CA paste needs more SP than the other two systems. On the other hand, Figure 3-12(a) showed that the viscosity of BAC paste was identical with the viscosity of pure CEM III/A paste, despite the minor differences which were observed at 0 and 0.1% SP. It indicates no considerable effect of bacteria on the fresh properties of the paste, which is in line with the mini slump test result. Specifically on the use of CA, the CEM III/A paste showed a thixotropic behaviour. In order to eliminate this behaviour, the CA paste was pre-sheared at the highest shear rate (50 s^{-1}) before testing as suggested by Wallevik et al. [117]. The viscosity of CA paste without SP was recorded at 2.5 Pa·s, which was approximately 21% higher than the viscosity of pure cement paste. However, regardless the SP dosage, the CA paste always showed a higher viscosity as compared with other pastes. All in all, the CD and SD of BAC paste were

determined at 0.1 and 0.5% by powder weight, respectively. The CD and SD of CA paste showed higher values at 0.2% and 0.7% by powder weight.

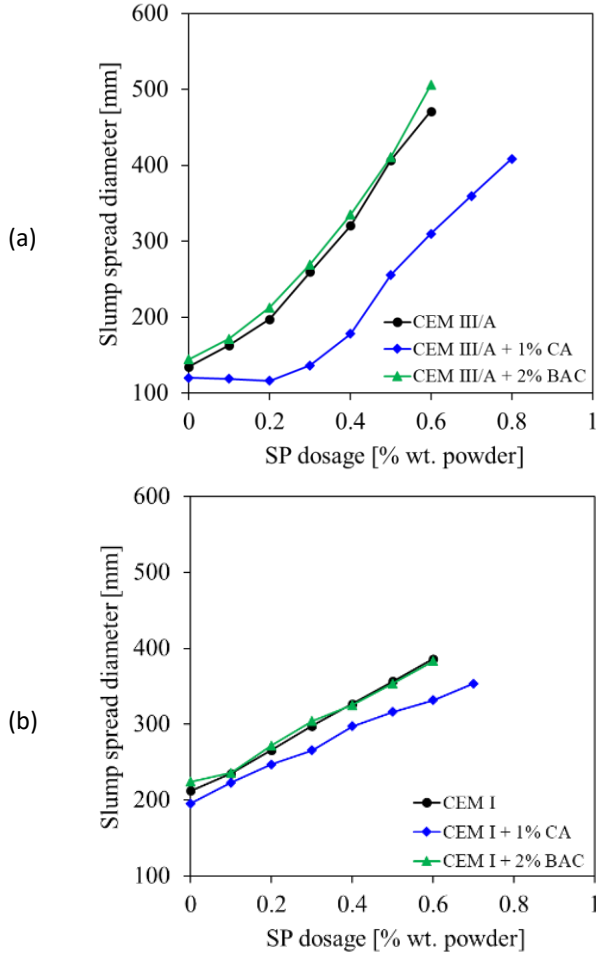


Figure 3-11. Alteration of slump of (a) CEM III/A paste and (b) CEM I paste with various SP dosages (SP Fluvicon 801 and Technofluid P175 for CEM III/A and CEM I, respectively) due to the addition of healing agents

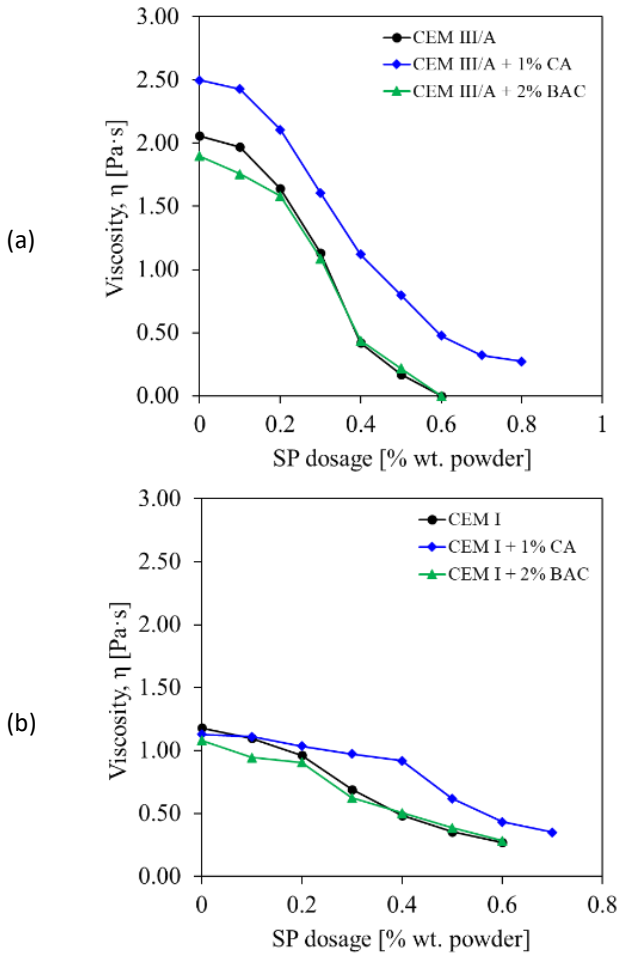


Figure 3-12. Alteration of viscosity of (a) CEM III/A paste and (b) CEM I paste with various SP dosages (SP Fluvicon 801 and Technofluid P175 for CEM III/A and CEM I, respectively) due to the addition of healing agents

- *On the use of CEM I:* As can be seen in Figure 3-11(b), there was no effect of BAC in terms of slump values as the workability between pure CEM I and BAC paste was almost same. Contrarily, the addition of CA reduced the slump value as compared with pure CEM I paste. The same conclusion as the previous observation from CEM III/A on the incorporation of BAC and CA is also valid for CEM I. Unlike the behaviour of CEM III/A paste in combination with CA where the slump remained constant until being added with 0.2% SP, the slump of CEM I paste added with CA gradually increased as increasing the SP dosage from 0.1 to

0.7%. It is noteworthy to mention that the pure CEM I and BAC pastes showed segregation at 0.6% SP, while for CA paste, it occurred at 0.7% SP. It was also evident that the CA paste needs a higher SP demand than pure CEM I and BAC pastes. Figure 3-12(b) showed that the viscosity of BAC paste was also comparable with the viscosity of pure CEM I paste, despite the minor differences which were observed at 0 and 0.1% SP. It implies that no negative effect occurred on the fresh properties of CEM I paste after the addition of BAC. The viscosities of CEM I, BAC and CA pastes without SP were identical. The CA paste showed a higher viscosity as compared with other pastes after being introduced with the SP above 0.2%. All in all, the CD and SD of BAC paste were determined at 0.1 and 0.5% by powder weight, respectively. The CD and SD of CA paste showed higher values at 0.1% and 0.6% by powder weight, respectively.

3.4.5 Superplasticizer adsorption capacity of cement pastes with and without healing agents

Initially, the total organic carbon of all pastes without SP was measured. The total organic carbon of pure CEM III/A paste and pure CEM I paste were 161 and 255 ppm C (parts per million carbon), respectively. When the healing agents (CA and BAC) were added, a significant amount of organic carbon was released into the pore solution. The additions of CA and BAC contributed roughly 600 ppm C to the CEM III/A paste, while the contribution was much higher, around 740 ppm C, when they were applied to the CEM I paste. A specific SP type was then introduced to each paste (with specific cement type) with the SP dosage between 0.1–0.5%. The result is shown in Figure 3-13.

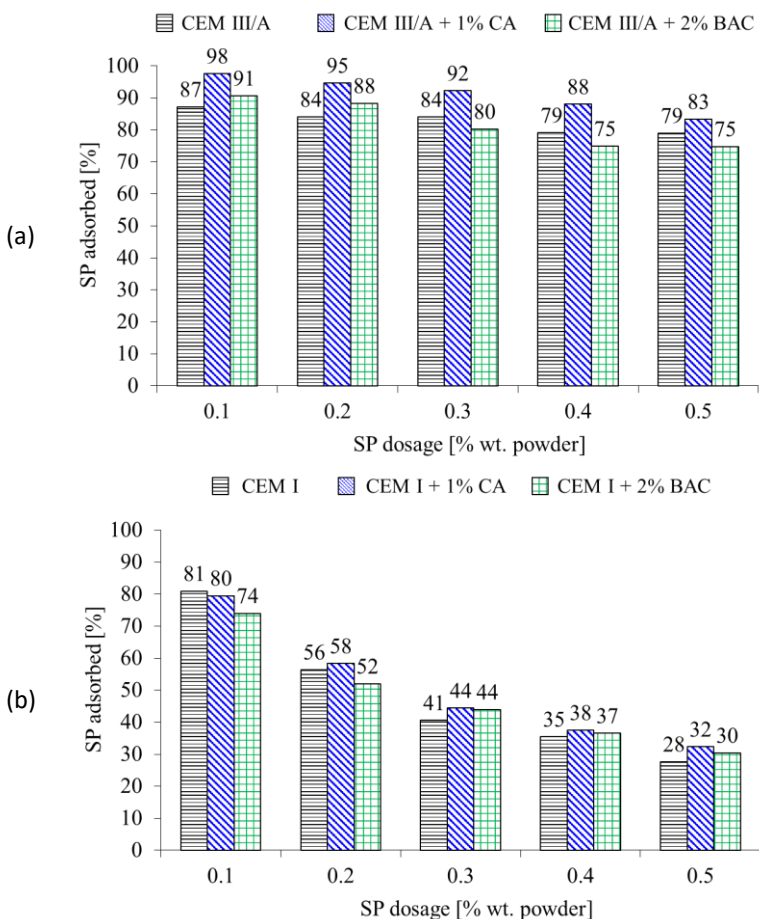


Figure 3-13. Percentage of SP adsorbed on the (a) CEM III/A paste and (b) CEM I paste systems

- Based on Figure 3-13(a), by adding 0.1% SP (Fluvison 801) on pure CEM III/A paste, it showed 87% SP adsorbed on the paste (immediately after mixing), while 13% remained in the pore solution. The further additions of SP in the range of 0.2–0.3% and 0.4–0.5% slightly reduced the amount of SP adsorbed at 84 and 79%, respectively. In case of CA paste, a higher amount of SP is adsorbed indicating that the SP also adsorbs on the surface of the CA healing agent particles. XRD analysis revealed that the CA contains a significant amount of C_3A (see Table 3-2). SP is known to have a high affinity for C_3A and it determines the paste rheology. Alonso et al. [118] reported that since C_3A has a higher zeta potential than the silicate phases, the admixture tends to adsorb onto the aluminate. The

hydration products of C_3A such as C_4AH_{19} and calcium monosulfoaluminate hydrate (C_4AsH_{12}) are able to take up admixtures in their laminate structures. Therefore, in this case, the SP is adsorbed by the C_3A phase and a higher SP demand is needed when the CA is introduced into the cementitious system to reach the same dispersion as the system without CA. Moreover, the incorporation of BAC slightly altered the adsorption capacity of the SP. The addition of 0.1% SP dosage showed that 91% SP was consumed and a gradual reduction of the amount of SP adsorbed was observed as the SP dosage increased. The same trend was attained in control and BAC pastes.

- Based on Figure 3-13(b), by adding 0.1% SP (Technofluid P175) on pure CEM I paste, it showed 81% SP adsorbed on the paste, while 19% remained in the pore solution. However, increasing the SP dosage seems to lower the amount of adsorbed SP. Only 56% SP was consumed when the SP was added at 0.2% SP. When the SP dosage was increased from 0.3 to 0.5%, the adsorbed SP was accounted for 41 to 28%. The addition of CA into the paste required a slightly higher SP demand than pure CEM I paste due to the fact that CA could adsorb on CA particles. The addition of BAC into the superplasticized cement paste follows similar behaviour as pure CEM I and CA pastes. Comparing the combination of CEM I + SP Technofluid and CEM III/A + SP Fluvicon, the SP Technofluid seems to not optimally adsorb with cement type I when a high SP dosage is used. This is because the adsorbed SP Technofluid in CEM I paste was less than SP Fluvicon in CEM III/A paste. It may be associated with the compatibility between cement-superplasticizer interaction. However, this compatibility study is out of scope in this PhD study, thus further study is needed to find and select the most suitable admixture which depends on the characteristic of the cement used.

Furthermore, the adsorption isotherm can be calculated from the amount of the superplasticizer adsorbed on a cement component mineral in an equilibrated solution [119]. The adsorption isotherm is defined as the relationship between the adsorbate in the liquid phase and the adsorbate adsorbed on the surface of the adsorbent at equilibrium at constant temperature [120]. The SP adsorption isotherms on powders (cement + healing agent) are illustrated in Figure 3-14. As a matter of fact, this relationship follows a Langmuir adsorption isotherm. After constantly introducing SP into the paste, at one point, addition of extra SP will not result in additional adsorption because all adsorption sites at the surface of cement particles are occupied, as shown by plateau curves. Thus, the non-adsorbed

SP will stay in the pore solution. To summarize, by incorporating CA into the superplasticized cement paste, the SP was also adsorbed by the CA. It means the SP is not sufficiently available to disperse the cement particles thus lower workability and high viscosity were observed. Conversely, the utilization of BAC as a healing agent showed a comparable result with the pure cement paste.

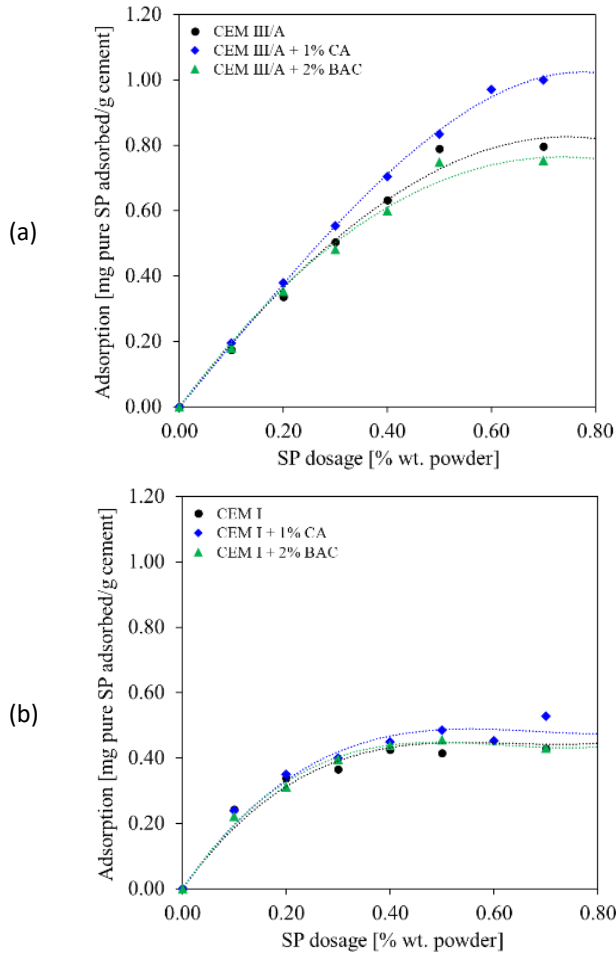


Figure 3-14. Adsorption isotherms of SP on powders: (a) CEM III/A with/without healing agent and (b) CEM I with/without healing agent

3.4.6 Evolution of the early age setting of cement paste

Figure 3-15 shows the evolution of ultrasonic pulse velocity (UPV) in function of the setting/hardening time of cement pastes (left figure) and the acceleration of UPV (right figure). Based on the observations from CEM III/A and CEM I pastes, the development of UPV of CA pastes follows a similar pattern as the pure cement pastes, while for the BAC pastes, the UPV is lower than the other pastes. As a matter of fact, this UPV measurement is also associated with the early strength development of cementitious materials [121,122] and the acceleration curves can predict the setting behaviour of the cementitious paste [115]. It seems that the early strength of BAC paste is basically lower than CA and pure cement pastes. The maximum acceleration of CEM III/A paste occurred at around 110 min. Based on the acceleration results from Figure 3-15a, it is clear that there is a delayed setting with the addition of CA and BAC. The maximum accelerations of CA and BAC pastes were around 170 and 270 min, respectively. The same observation was also found in CEM I pastes (Figure 3-15b) where the maximum accelerations of pure CEM I, CA and BAC pastes were around 100, 200 and 250 min. These results support the previous finding (see Figure 3-4) that the addition of healing agents tends to delay the setting of cement paste (either CEM III/A or CEM I).

Furthermore, the influence of the SP in the cementitious paste related to the UPV development was investigated. The SP was added at the dosage of 0.2 and 0.4% by weight of cement. The result was shown in Figure 3-16 with considering CEM III/A as an example. It is evident that the inclusion of SP lowered the UPV of the cementitious paste and it seems that the higher SP dosage the lower the velocities. This tendency was constantly found in the CEM III/A paste with and without healing agent. By looking into the acceleration curvature, it is also clear that the incorporation of SP delays the setting of cement paste at any dosages. For instance, in the case of pure CEM III/A paste, the maximum acceleration was recorded at around 110 min and the addition of SP at 0.2 and 0.4% delayed the maximum acceleration to around 300 and 360 min, respectively. This retarding effect is also associated with the delayed hydration capacity of cement due to the admixture. Lothenbach et al. [123] investigated the liquid and solid phases of hydrating Portland cement in the absence and presence of a PCE-based SP and found that the SP retarded the dissolution of alite during the first 30 hours and further delaying the formation of portlandite and C-S-H. Although the SP adsorbed strongly on aluminates, the retardation of the formation of ettringite was less distinct. They also reported that in the presence of SP a

little amount of ettringite has precipitated after 6 hours of hydration while after 16 hours the same amount of ettringite has formed in the absence of SP. The results on the use of CEM I, CA, BAC and SP Technofluid P175 can also be found in Figure 3-17.

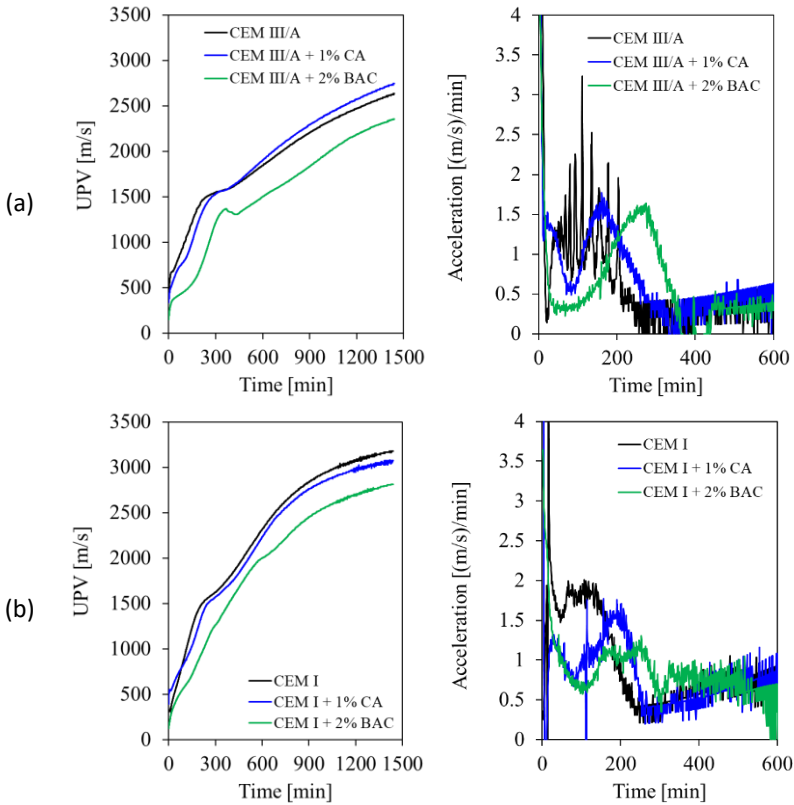


Figure 3-15. Evolution of UPV in function of time in: (a) CEM III/A pastes and (b) CEM I pastes, both with and without healing agent

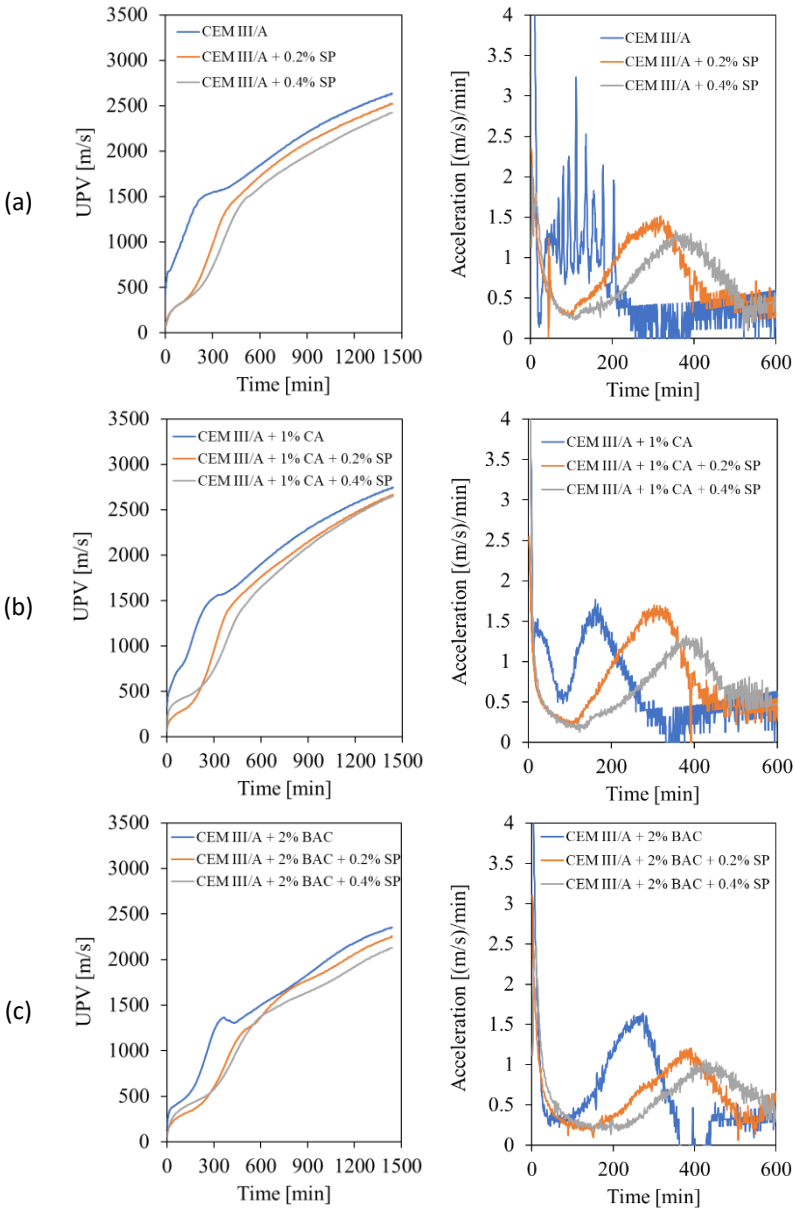


Figure 3-16. Effect of superplasticizer (Fluvison 801) in the development of UPV on pastes with (a) pure CEM III/A, (b) CEM III/A + CA and (c) CEM III/A + BAC

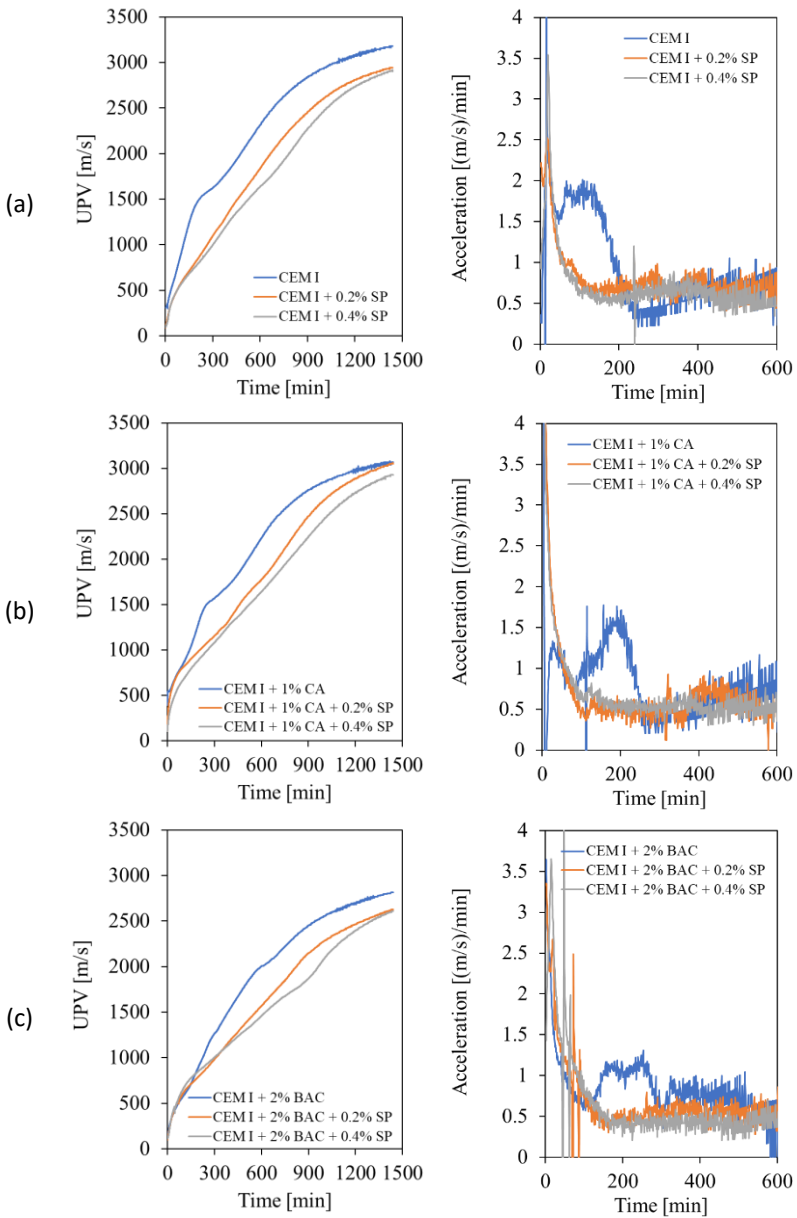


Figure 3-17. Effect of superplasticizer (Technofluid P175) in the development of UPV on pastes with (a) pure CEM I, (b) CEM I + CA and (c) CEM I + BAC

3.5 Conclusions

The effects of incorporating bacteria (BAC) and crystalline admixtures (CA) in relation to the rheological properties of cement pastes were evaluated based on several fresh tests. Two types of cement were used namely CEM I 52.5N and CEM III/A 42.5N. The compatibility between PCE superplasticizer (SP), cement and healing agents was also studied. The major conclusions are presented as follows:

1. The water demand of cement with BAC slightly reduces as the bacteria dosage increases up to 5%, while the water demand of cement with CA increases as the CA dosage increases up to 3%.
2. The addition of BAC prolongs both initial and final setting time and the higher the BAC dosage, the longer the setting time. In contrast, the gradual addition of CA from 1 to 5% by weight of powder into the cement paste with CEM I tends to shorten the setting time. The impact of using a high CA dosage on fresh CEM I paste is a rapid initial setting and loss of plasticity. However, the initial and final setting times of paste containing CA and CEM III/A are relatively similar at any CA dosage.
3. As a consequence of incorporating a PCE-based SP into fresh pastes, the water demand of cement and healing agent reduces with increasing SP dosage.
4. The incorporation of BAC did not affect the rheological properties of the paste and no negative interaction with superplasticizers (Fluvison 801; Technofluid P175) was found.
5. The incorporation of CA considerably influenced the rheological properties of the paste by reducing the workability and increasing the viscosity of the paste.
6. The CA paste showed a thixotropic behavior and required a higher SP dosage to achieve the same workability as the pure cement paste because the SP could adsorb on CA particles.
7. The critical and saturation SP (Fluvison 801) dosages of pure CEM III/A and CEM III/A+BAC pastes were the same (0.1% and 0.5% by powder weight, respectively); while for the CEM III/A+CA paste, they were higher (0.2% and 0.7% by powder weight, respectively).
8. The critical and saturation SP (Technofluid P175) dosages of pure CEM I and CEM I+BAC pastes were also the same (0.1% and 0.5% by powder weight, respectively); while for the CEM I+CA paste, the CD remained the same at 0.1% while the SD was higher at 0.6% by powder weight.
9. The inclusion of healing agents and superplasticizer into cement paste tended to lowering the ultrasonic velocity of cementitious materials.

Chapter 4

EVALUATION OF MODIFIED MIX DESIGNS OF CONCRETE CONTAINING CRYSTALLINE ADMIXTURES TOWARD SELF-HEALING AND SELF-SEALING PERFORMANCES

4.1 Introduction

In relation to the available concrete mix designs from literature review (Chapter 2), in most cases, the healing agents are added just 'on top' of the normal concrete mixes, meaning that no adaptations of concrete mix designs are made for the introduction of healing agents. The rare existing demonstrators up-scaled in concrete structures sometimes show insufficient [56,124] or not yet proven [36,44] self-healing efficiency. Furthermore, this may lead to a research question on the effect of variability in the mix design parameters related to the self-healing ability. De Belie et al. [55] elaborated the importance of selecting the mix design parameters towards the intrinsic healing performance. First, the clinker content, in relation to the cement type, determines the supply of Ca^{2+} and subsequently the ability to develop the precipitation products. Second, the silicate additions determine the duration of the healing mechanism due to the characteristic pozzolanic

**) This chapter is based on the following paper: Hermawan H, Wiktor V, Serna P, Gruyaert E. Experimental investigation on the novel self-healing properties of concrete mixed with commercial bacteria-based healing agent and crystalline admixtures. In: Proceedings of the SynerCrete'23, Springer International Publishing; 2023. https://doi.org/10.1007/978-3-031-33187-9_77*

reactions and the consumption rate of the calcium hydroxide. Third, aggregate type may induce an effect on the cracking pattern which indirectly influences the healing process. Fourth, concrete class may also contribute to the healing effect. In case of a high strength concrete with a low water-cement ratio, it contains important resources of unhydrated cement grains that can easily develop significant quantities of new calcium silicate hydrate (C-S-H) products as a result of ongoing hydration. Fifth, the concrete age is another important parameter with respect to the healing mechanism. Young concrete contains more unhydrated binder particles that is important for the crack closure. These facts lead to the awareness that the mix design itself influences the healing performance and the addition of the healing agent may induce different effects on different mix designs.

This chapter attempts to modify the mix designs of self-healing concrete in order to potentially enhance the self-healing and self-sealing performances. Crystalline admixture (Penetron Admix) is chosen as the healing agent in this study. Three mix design parameters are proposed, namely the dosage of healing agent, water-cement (w/c) ratio and cement content, which involves three levels for each parameter. The methodology used in this research is based on the initial evaluation of the fresh and hardened concrete properties, and is continued to the inspection of crack closure by optical microscopy and the measurement of water flow by permeability tests. Moreover, statistical tests are employed to aid in understanding the comparison between the obtained results and finally, a recommendation for optimized mix design is proposed based on the optimum parameters. The results based on the healing and sealing efficiencies are further discussed and the healing products formed in the cracks are clearly identified.

4.2 Materials and methods

4.2.1 Materials

CEM III/A 42.5N, supplied by LafargeHolcim, was used in this study with the target of ready-mixed concrete application. Penetron Admix Crystalline Admixture (labelled as CA) was used as a healing agent to stimulate the autogenous healing mechanism. This admixture consists of cement and various active chemicals, while the detailed composition is kept confidential by the producer. The dosage of CA was fixed at 1–2% bwoc. It should be noted that the recommended dosage of CA was actually 1% bwoc, while in

this study, a higher dosage (2% bwoc) was also studied to evaluate its effect on concrete properties and also to investigate whether the healing efficiency can be improved. Fine aggregates (white sand 0/2 and red sand 0/4) and coarse aggregates (limestone 2/6, limestone 6/16 and limestone 16/20) were used as inert components. The physical properties of the aggregates are presented in Table 4-1. The mean size of aggregate was determined by sieving test (EN 933-1), the voids ratio of aggregate was determined by loose bulk density test (EN 1097-3) and both oven-dry density and water absorption of aggregate were determined by particle density test (EN 1097-6). The particle size distribution (PSD) of the aggregates is depicted in Figure 4-1 based on the sieving test (EN 933-1).

Table 4-1. Physical properties of aggregates

Aggregate	Mean size [mm]	Voids ratio [-]	Oven-dry density [g/cm ³]	Water absorption [%]
White sand 0/2	0.274	0.795	2.695	0.682
Red sand 0/4	0.799	0.592	2.637	0.792
Limestone 2/6	4.301	0.952	2.627	1.169
Limestone 6/16	8.475	0.877	2.641	1.098
Limestone 16/20	18.005	0.905	2.662	0.790

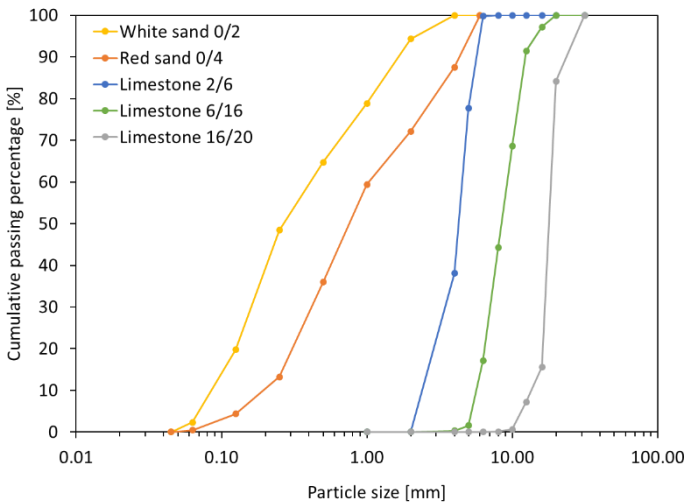


Figure 4-1. Particle size distribution of aggregates

Moreover, Demula Technofluid P175 and Demula LR-7000 superplasticizers (SP), supplied by CUGLA B.V., were used as admixtures to improve the workability of fresh concrete. These SPs were in fact different with the one that was investigated previously in Chapter 3 (i.e., Demula Fluvicon 801 for CEM III/A) because the workability of the mixture did not improve when using SP Fluvicon 801. This was hypothesized due to the aggregates used during casting (in Spain) seemed containing clay that may entrap superplasticizer. Following a considerable number of trials, it was decided to use two types of SP to maintain a good workability for all mixtures.

4.2.2 Modification of mix designs for self-healing concrete

Seven concrete mixtures (denoted as M1-7) were prepared as shown in Table 4-2. The reference concrete (M1) was designed for the application of reinforced concrete exposed to two exposure classes, including XC4 (corrosion induced by carbonation where concrete is exposed to the cyclic wet and dry) and XF3 (freeze/thaw attack where concrete is exposed to a high water saturation without de-icing agent) according to NBN EN 206. These exposure classes were related to an environmental class of EE3 (frost, exposure to rain or splashing water) according to the Belgian standard NBN B15-001 [125], and to a concrete type of T(0.50) with the following specifications: (1) maximum water-cement (w/c) ratio of 0.50, (2) minimum cement content of 320 kg/m³ and (3) minimum strength class of C30/37; in accordance with NBN EN 206 [126] and NBN B15-001 [125]. The target consistency class was S4 (target slump = 200 mm) and the entrapped air was estimated at 3.0% in the mix design phase and the maximum aggregate size was 20 mm. Based on Table 4-2, three series of modifications of concrete mix designs are developed:

- The first series, involving M1 – M2 – M7, aims to study the effect of CA dosage towards self-healing properties. M2 and M7 mixtures used the CA dosage at 1% and 2% bwoc, respectively. The CA was added on top of reference mixture M1, thus in this case there is no major adaptation on mix designs. The water-cement (w/c) ratio was fixed at 0.49 for all mixtures.
- The second series, involving M3 – M2 – M4, is basically targeted to study the effect of w/c ratio towards self-healing properties with a constant CA addition at 1% bwoc and a constant cement content at 340 kg/m³. The w/c ratios of M3, M2 and M4 were fixed at 0.46, 0.49 and 0.52,

respectively. The mix designs were modified to ensure a 1 m³ volumetric design for each specific w/c.

- The third series, involving M5 – M2 – M6, is designed to investigate the effect of cement content towards self-healing properties with a constant CA dosage at 1% bwoc and a constant w/c at 0.49. The cement contents of M5, M2 and M6 were 320, 340 and 360 kg/m³, respectively. The mix designs were modified to ensure a 1 m³ volumetric design for each specific cement content.

All concrete mixtures were cast with a volume of 70 L and the mixing and casting procedures were described as follow:

- 1) The fine and coarse aggregates were poured with a small amount of mixing water and were mixed homogenously until reaching a pre-wetting condition (approximately 15-30 min).
- 2) The pre-wetted fine aggregates (i.e., white sand and red sand) and dry cement were added into a planetary mixer and they were mixed for 20 sec. In case of self-healing mixtures (M2-7), CA was also added at this stage.
- 3) A partial amount of mixing water (with diluted SPs) was added and mixing was continued for 2 min.
- 4) The pre-wetted coarse aggregates (i.e., all limestones) were added into the mixer and mixing was continued. After one minute, the remaining water (with diluted SPs) was poured and mixing was continued for 4 min.
- 5) Right after mixing for about 7.5 min, approximately 50 L of fresh concrete was taken out of the mixer. This fresh mixture was partially used to perform the slump and air content tests (in accordance with EN 12350-2,7); and partially cast into nine cubic moulds of 150 mm in side.
- 6) After finishing the tests, the remaining mixture of ~20 L in the mixer was continuously mixed and steel fibers (Dramix 35/65) were added in the last stage of mixing at the dosage of 40 kg/m³ with the purpose of obtaining crack control during splitting of hardened cylindrical specimens.
- 7) The fresh mix with fibers was mixed for an additional 2-3 min. A small amount of superplasticizers was added to make the leftover mixture (more or less 20 L) workable again because a loss of workability was detected during post-mixing.
- 8) Finally, the fiber-reinforced concrete (FRC) mixture was poured into six cylindrical moulds of Ø100×200 mm.
- 9) All specimens were demoulded after 24 h and were cured in the curing chamber with a temperature of 20°C and RH > 90%.

Table 4-2. Concrete mix designs (note: the highlighted values relate to the adapted mix design parameters with respect to M1)

Material	Unit	Concrete Mixture						
		M1	M2	M3	M4	M5	M6	M7
CEM III/A 42.5N	kg/m ³	340	340	340	340	320	360	340
White sand 0/2	kg/m ³	334	333	342	331	345	328	333
Red sand 0/4	kg/m ³	371	368	374	362	376	358	367
Limestone 2/6	kg/m ³	239	239	243	235	245	233	239
Limestone 6/16	kg/m ³	567	567	577	558	581	552	566
Limestone 16/20	kg/m ³	313	313	318	308	321	305	313
Effective water	kg/m ³	166	167	156	177	156	177	167
Effective w/c	-	0.49	0.49	0.46	0.52	0.49	0.49	0.49
SP Demula Technofluid P175	kg/m ³	2.22	2.22	2.99	1.73	2.52	1.75	2.49
SP Demula LR-7000	kg/m ³	0.75	0.75	0.75	0.75	0.75	0.75	0.75
Penetron CA	kg/m ³	-	3.40	3.40	3.40	3.20	3.60	6.80
DRAMIX fibers 35/65	kg/m ³	40	40	40	40	40	40	40
Additional SP for FRC	kg/m ³	-	-	0.71	0.65	1.60	0.64	1.34
Fresh properties (for non-fibered mixes)								
Slump	mm	200	210	145	170	165	185	150
Air content	%	2.5	2.3	2.2	2.6	2.5	2.5	2.5
Fresh density	kg/m ³	2393 ± 6	2352 ± 4	2401 ± 8	2348 ± 7	2382 ± 10	2363 ± 16	2385 ± 9

4.2.3 Testing method

The fresh properties of concrete were evaluated by means of slump, air content and fresh density tests (in accordance with EN 12350-2,6,7), while the hardened properties of concrete were determined by compression strength tests at 7, 28 and 91 days (in accordance with EN 12390-3). Moreover, the self-healing properties of concrete were assessed by (1) a crack measurement by optical microscopy and (2) a permeability test, both at 0 days (as a reference), 21 days and 121 days after healing. The detailed procedure for the self-healing and self-sealing tests is given below:

- For each mixture, the 7-days old concrete cylindrical specimens with a size of 200 mm in height and 100 mm in diameter were cut by sawing, turning into five discs: one disc with a height of 25 mm (top part), three discs with a height of 50 mm (middle part) and another disc with the height of 25 mm (bottom part). The top and bottom parts of the discs were discarded due to uneven surfaces (trowelled and sliced), thus three discs from the middle section were collected. All discs were stored under water for one day. In the next day, the discs were cracked by means of a Brazilian splitting test. It was initially aimed to obtain a similar crack width for all specimens, however it was relatively difficult to control the cracks. Thus, later it was decided to have the crack widths in the range of 100–500 μm . Crack measurement was performed by means of an optical microscope. For each mixture, 6–8 out of 15–18 cracked concrete discs were selected for further self-healing considering the crack width, crack line, crack consistency between the two sides of a concrete disc, etc. Per concrete disc, 6 white marks were indicated along the crack line on two sides (3 marks on the top surface, 3 marks on the bottom surface – both given at random locations). For each white mark, five locations were chosen to measure the crack width. So 30 measurements were taken to determine the initial crack width at 0 day per specimen. After healing, the same locations as the first measurement at 0 day (as indicated by blue lines, see Figure 4-2) were used to study the crack closure. An example of a crack measurement is depicted in Figure 4-2. Hence, healing efficiency (HE) per specimen was calculated as follows:

$$HE = \left(1 - \frac{\text{Final crack width at } i \text{ day}}{\text{Initial crack width at 0 day}}\right) \times 100\% \quad (4.1)$$

where i is the healing period, either at 21 or 121 days.

As previously mentioned, in a single mixture, there were 6-8 concrete discs selected. Thus, a global healing efficiency for a single mixture (\overline{HE})

was calculated based on the average of *HEs* from all specimens, as follows:

$$\overline{HE} = \frac{\sum_{j=1}^k HE_j}{k} \quad (4.2)$$

where *k* is number of concrete discs from a single mixture and *j* is a summation index (*j* = 1, 2, 3, ..., *k*).

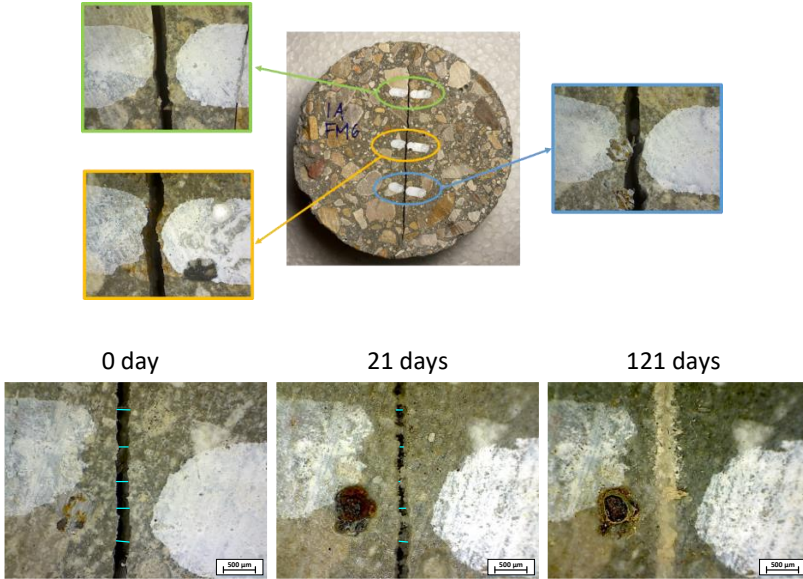


Figure 4-2. Methodology of crack measurement to quantify healing efficiency

- After the initial crack measurement was done, the permeability test was executed to evaluate the rate of water permeability. The setup of the permeability test was developed as described by the Round Robin Testing Programme in the framework of “SARCOS” COST Action CA 15202 [127]. The same specimens were used from the crack measurement. Initially, the concrete disc was partially inserted into a hollow PVC tube for approximately half of the height of the disc. Hence, in order to eliminate the water leaking from the gap between the disc and inner wall of the tube, a sealant was applied on the outer surface (non-inserted part) of the disc and also the outer-bottom part of PVC tube. In that way, during the test, the water will only flow through the crack. After the sealant was dried for one day, a small amount of water was initially poured in order to check the quality of the sealant (to avoid

water leaking from the sealant) and also to make the discs stay in a wet condition. After the check was completed, the water was added until it reached more or less 20 cm from the top surface of the specimen. A ruler was placed inside the tube to check the height of the water. Then, the permeability test was finally performed by monitoring the reduction of water height from ~20 cm as a function of time, which is later called as a permeability rate. The measurement was done with two repetitions on the same specimen and the average permeability rate was recorded at day 0. The actual setup of the permeability test can be seen in Figure 4-3. After the tests at day 0, the specimens kept in the tubes were completely submerged in the water tank with a temperature of $20 \pm 2^\circ\text{C}$ with a horizontal position, thus the cracks on the top and bottom surfaces of the specimens were in contact with water. The permeability rate was measured again at 21 days (after a short healing) and 121 days (after a long healing). The sealing efficiency was calculated by Equation (4.3) and the global sealing efficiency of a mixture was computed by Equation (4.4).

$$SE = \left(1 - \frac{\text{Permeability rate at } i \text{ days}}{\text{Permeability rate at 0 day}}\right) \times 100\% \quad (4.3)$$

$$\overline{SE} = \frac{\sum_{j=1}^k SE_j}{k} \quad (4.4)$$

where SE is the sealing efficiency of a specimen, \overline{SE} is global sealing efficiency of a single mixture [%], i is the healing period, either at 21 or 121 days, k is the number of concrete discs from a single mixture, and j is summation index ($j = 1, 2, 3, \dots, k$).

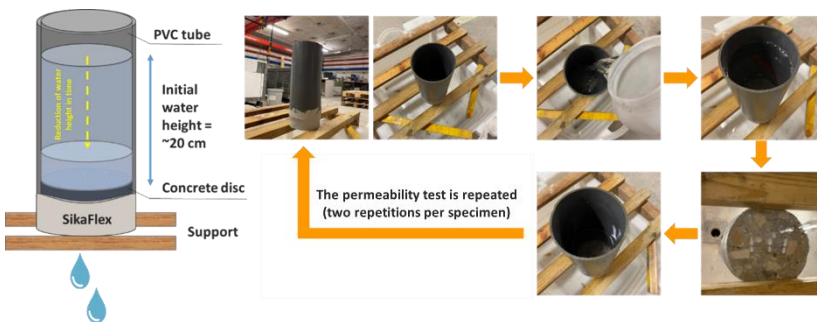


Figure 4-3. Permeability test setup

Moreover, statistical evaluations based on the analysis of variance (ANOVA) (either parametric or non-parametric tests – depending on type of data) were

employed to determine the significant parameters with p-value of 0.05 as a significance threshold.

4.3 Results

4.3.1 Fresh properties

The fresh results based on slump, air content and fresh density tests were summarized in Table 4-2. The reference mixture (M1) initially had a slump of 200 mm, and when the CA was introduced at 1% bwoc as demonstrated in M2, the slump was comparable at 210 mm. Moreover, when the dosage was scaled up to 2% bwoc (M7), the slump reduced considerably to 150 mm although the SP demand had been slightly increased as compared with M1 and M2 mixtures. When the w/c was changed to 0.46 (M3) and 0.52 (M4), the SP was adjusted to meet the same slump class of S4 as M2. However, M3 gave a slump of 145 mm which is classified as S3, and this indicates that the SP demand at 2.99 kg/m^3 is insufficient to improve the workability of the mixture considering the w/c of this mixture is relatively low. For M4, due to a high w/c at 0.52, a lower SP demand at 1.73 kg/m^3 is adequate to achieve a target slump class of S4. Especially for the M2, M5 and M6 mixtures on the effect of cement content, the SP demands were also adjusted and all mixtures achieved a S4 slump class. In terms of air content, there is less variation among all mixtures as the results are relatively identical. The lowest air content was attained by M3 due to the contribution of a low w/c which makes a denser mixture, while the highest air content was found on M4 due to the high w/c . The fresh densities of all mixtures were recorded in Table 4-2 and it was clear that a lower w/c led to a higher fresh density, and vice versa.

4.3.2 Strength development

The evaluation of strength development of self-healing concrete employed with different mix designs is important to be analysed to understand the effects of healing agent on different concrete compositions. Figure 4-4 shows the compressive strengths of hardened concretes at 7, 28 and 91 days.

- In the first series on the effect of CA dosage (M1 – M2 – M7), the compressive strengths of 7 days-old concretes were similar for all mixtures. It shows that the addition of CA (regardless its dosage) did not

contribute to the strength improvement for a relatively young concrete. At this stage, it is presumed that the CA is not active yet to help enhancing the strength of concrete. However, the effect of CA is more pronounced on mature concretes. At 28 days, the addition of CA by 1% bwoc had a small improvement on compressive strength from 51.7 to 53 MPa. However, the difference between M1 and M2 is statistically not significant ($p = 0.61 > 0.05$), meaning that the addition of 1% CA did not contribute a lot on the 28d compressive strength. With 2% CA, an 8.7% strength improvement was noticed as compared with M1 (0% CA). It is also interesting that there is a sudden strength increment of M7 concrete by approximately 22% from 7 to 28 days. This might be attributed to the activation of CA at a high dosage after concrete maturation. At 91 days, the compressive strengths of concretes were 55, 57 and 59.5 MPa for M1, M2 and M7, respectively. It is clear that the gradual addition of CA results in an increase of compressive strength of concrete at later age.

- In the second series on the effect of w/c (M3 – M2 – M4), it is logic that a lower w/c results in a higher compressive strength of concrete at all ages. At 28 days, the compressive strengths of concretes with w/c of 0.46, 0.49 and 0.52 were 56, 53 and 45.7 MPa, respectively. By looking into the strength development from 28 to 91 days, it is interesting to observe that the compressive strengths of M3 and M2 concretes increased up to 7.5% from 28 to 91 days, while the strength increment of M4 concrete was doubled at 15%. In case of comparing the M3 and M7 concretes, it is also noteworthy to mention that the addition of 2% CA on a mixture with w/c of 0.49 (M7) showed a similar compressive strength with the addition of 1% CA on a mixture with w/c of 0.46 (M3). It indicates that instead of using a high CA dosage (2% bwoc), the mixture can be further adapted to use a normal CA dosage at 1% bwoc but with a lower w/c (and more SP needed) in order to obtain a similar strength. As a matter of fact, the usage of 2% CA will directly concern the material cost, and based on this result, it is more cost-effective to use a lower dosage (e.g. 1% CA) aided with an adaptation on concrete mix design. This finding will potentially help to design the CA mixes in an optimal way.
- In the third series on the effect of cement content (M5 – M2 – M6), there were no significant differences in terms of compressive strengths at all ages due to the reason that all mixtures had the same w/c ratio at 0.49 and CA dosage at 1% bwoc. From the environmental point of view,

it is recommended to use a low-and-appropriate cement content (which follows the minimum cement amount based on the standards and specifications) to reduce the carbon footprint and the emission of carbon dioxide (CO₂).

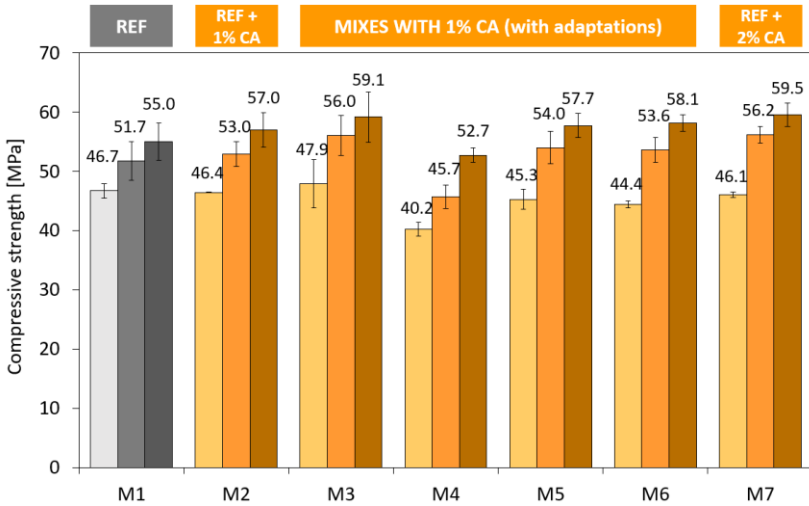


Figure 4-4. Compressive strengths of all concrete mixtures (note: for each mix, the left, middle and right bars represent strength values at 7, 28 and 91 days, respectively)

4.3.3 Self-healing performance

4.3.3.1 Progress of crack closure after healing

The evaluation of self-healing properties of hardened concretes was performed on cracked specimens before and after being subjected to a healing scenario. The phenomenon of crack closure based on the measurement by optical microscopy was investigated. Figure 4-5 shows the relationship between initial crack width at 0 day (after cracking) and final crack width after 21 and 121 days of healing for each mixture.

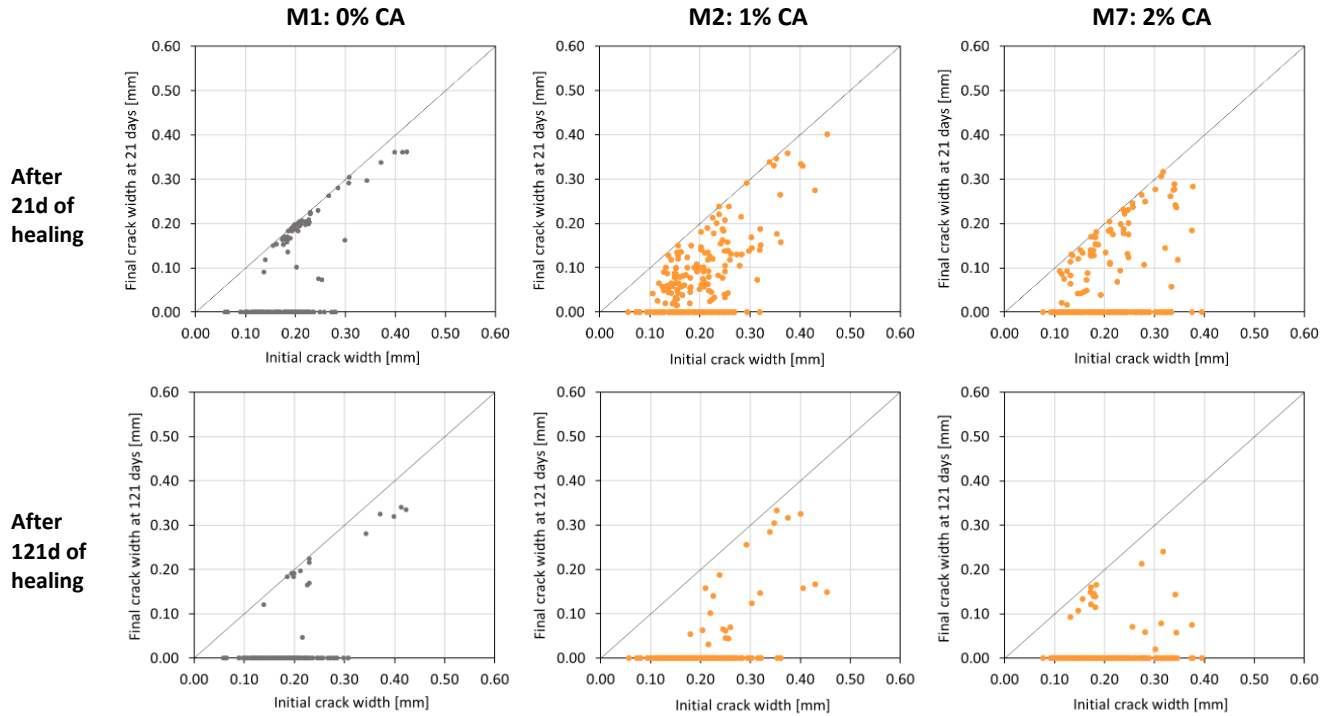
- Figure 4-5a shows the first series of mixtures on the effect of CA dosage from 0 to 2% bwoc with respect to the progress of crack closure after healing. It is clear from M1 (0% CA) that there are two tendencies in crack closure phenomena after undergoing a short healing (21 days),

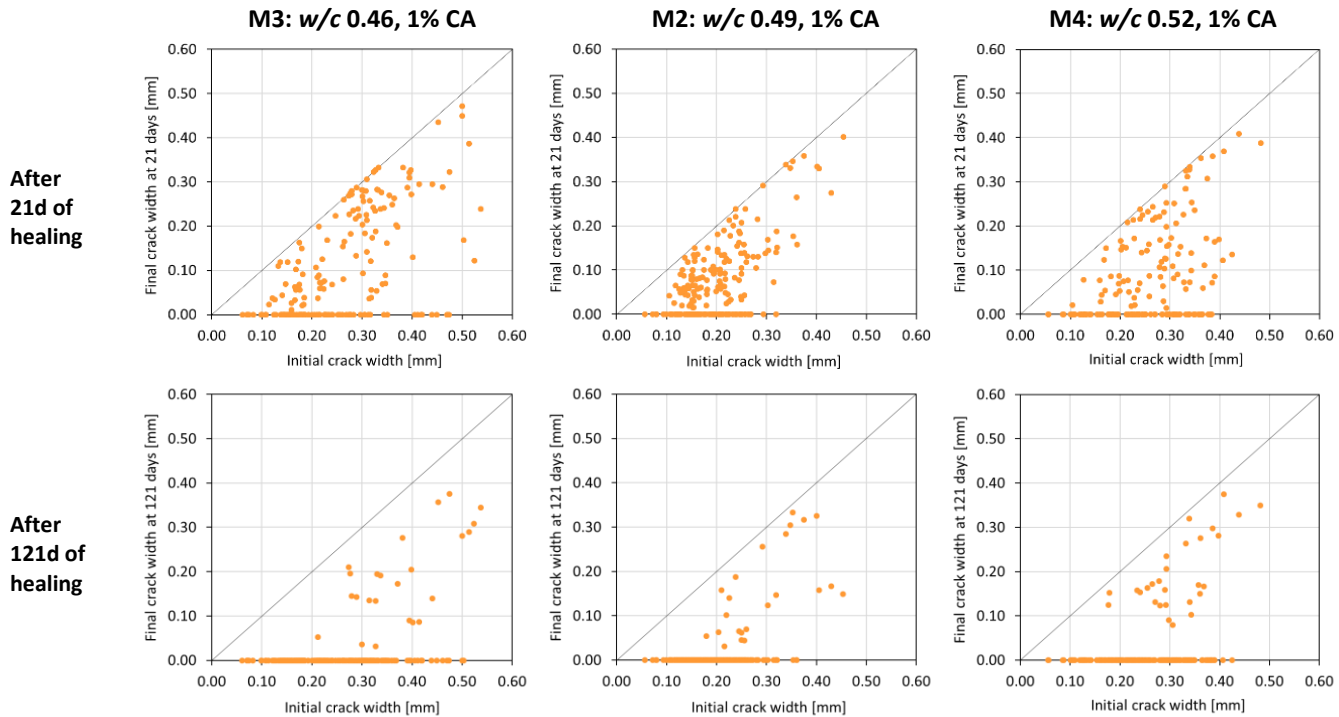
either the crack is fully healed or not fully healed; while a very few cracks are partially healed. In fact, in this case most of the cracks having a width of around 200 μm are concentrated near the bisector line, meaning that these cracks were not really healed. Although less data points are available for cracks with a bigger size ($\geq 300 \mu\text{m}$), it seems that they were even hardly healed. In case of M2 and M7, it is evident that by the addition of CA, the stimulated autogenous healing mechanism worked as the initial cracks showed some progresses in crack closing. This notion is shown by the fact that the data points are scattered below the bisector line, meaning that the original crack width is getting narrower due to the deposited healing products surrounding the crack. On the other hand, some cracks were already fully healed. Based on the observation, it seems that the addition of 2% CA leads to a faster healing than 1% CA because there are more data points between the bisector line and x-axis (see Figure 4-5a) on M2 than M7, meaning the progress of crack closing of M2 is relatively slower than M7, but faster than M1. After 121 days of healing, most of unhealed and partially-healed cracks at 21 days were completely healed as only a few data points were seen between the bisector line and x-axis. On M1, the progress of autogenous healing was noticeable especially for cracks with a width of less than 300 μm , while the bigger cracks were still hardly healed even after a long healing exposure. However, considering the number of data points was very limited for crack widths of 300–500 μm , it needs further investigations. On M2 and M3, the same tendency as M1 was observed where the small cracks with a width between 100–300 μm were mostly healed. Cracks in the range of 300–500 μm also showed an advancement in terms of crack closure, although not all cracks were completely healed.

- Figure 4-5b shows the second series of CA mixtures on the effect of w/c from 0.46 to 0.52 with respect to the progress of crack closure after healing. As previously seen in Figure 4-5a on CA mixes at 21 healing days, the M3 and M4 also show the same behaviour where the scattered data points are noticed between the bisector line and x-axis. However, it should be noted that the cracks from M2 were mostly concentrated in the range of 100 to 300 μm , while M3 and M4 were more distributed up to 400 μm . This occurs due to the fact that controlling the same or similar crack width for all specimens was very difficult, thus there might be a variation in the values. After a longer healing period (121 days), most of cracks were fully healed while a few cracks were partially healed. However at this stage, the effect of w/c

with respect to the progress of crack closure is not quite clear because all representative mixtures have a similar behaviour.

- Figure 4-5c shows the third series of CA mixtures on the effect of cement content from 320 to 360 kg/m³ with respect to the progress of crack closure after healing. After 21 days of healing, the data points of M5 and M6 are more distributed within 100 to 500 μm, as compared with M2 within 100 to 400 μm. Nevertheless, it is interesting to see that especially on M5 with the cement content of 320 kg/m³, there are a high number of cracks which stay close to the bisector line as compared with M2 and M6 (cement content of 340 and 360 kg/m³, respectively). It indicates that these cracks did not show a considerable progress of crack healing and the observed crack widths at 21 days were almost similar to the original crack widths at 0 days. Although this case is sometimes observed in other mixtures, M5 still shows the least healing development especially in the crack range of 200–400 μm. After the specimens were healed for 121 days, most of cracks were again completely healed. However, in case of M5, there are still a lot of cracks near the bisector line and apparently the number of partially-healed cracks is higher than M2 and M6. In general, by dividing the number of fully-healed cracks over the total number of cracks (in percentage), the result shows that after 21 days of healing, 21%, 37% and 27% of all cracks are completely healed for M5, M2 and M6 (cement content of 320, 340 and 360 kg/m³), respectively. While after 121 days, these values increase to 73%, 89% and 88% for M5, M2 and M6, respectively. It is also interesting to see that in the crack range of 100 to 300 μm, the best healing advancement is achieved by M6 (cement content of 360 kg/m³), followed by M2 (cement content of 340 kg/m³) and M5 (cement content of 320 kg/m³). Based on this observation, it is clear that with the use of low cement content, e.g. 320 kg/m³, aided with 3.2 kg/m³ of CA, a slower healing progress is obtained than for the other mixtures with a higher cement content (e.g. 340 or 360 kg/m³) aided with the same CA dosage at 1% bwoc.





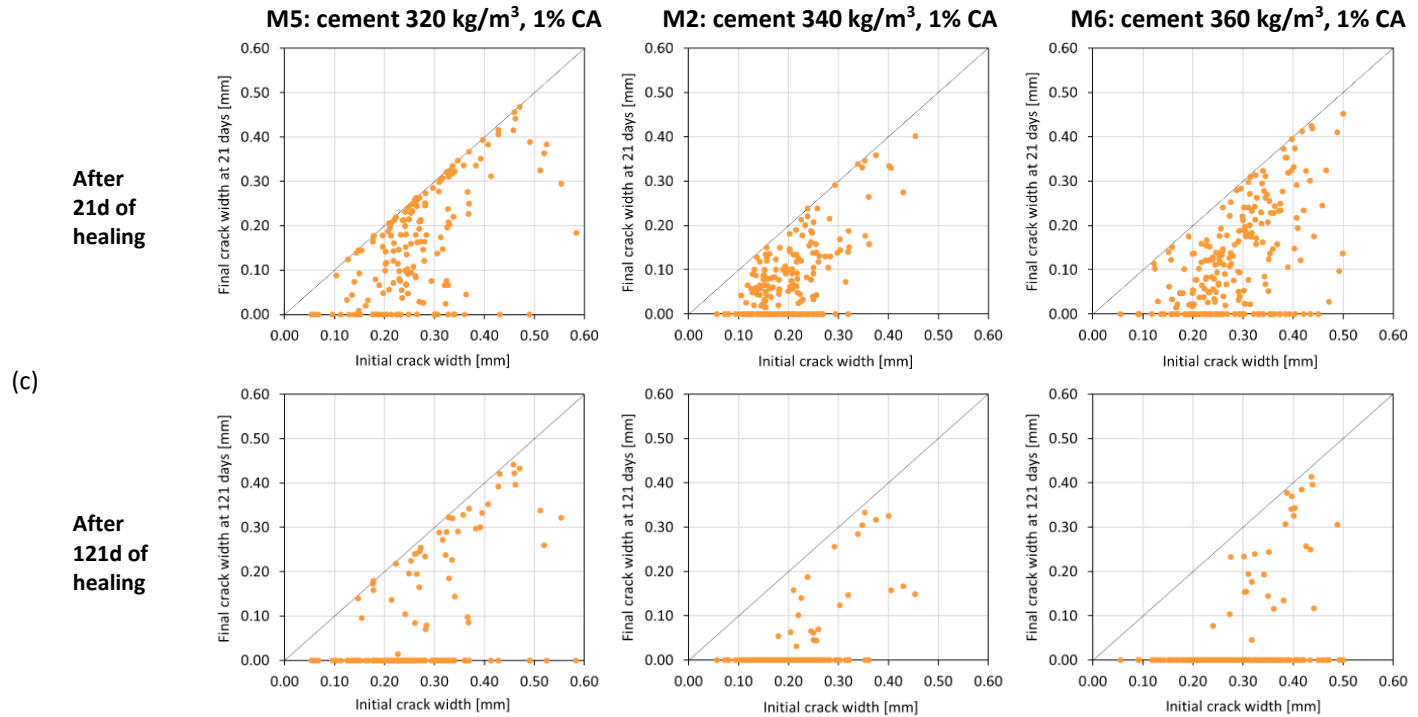


Figure 4-5. The progress of crack closure on cracked specimens after healing for 21 and 121 days tested on various mixtures with a specific category, i.e. (a) effect of CA dosage, (b) effect of w/c ratio and (c) effect of cement content

4.3.3.2 Analysis of healing efficiency

In order to quantify the healing efficiency of mixtures, based on Figure 4-5, the analysis was done by categorizing the crack width into a range with an interval of 100 μm (e.g. 0–100, 100–200, ..., 500–600 μm). Per crack width range, all data points are taken to calculate the healing efficiency by using Equation (4.1). The 21d healing efficiency per crack width range for all mixtures is summarized in Figure 4-6. The result showed that all mixtures (M1–7) exhibited an 100% healing efficiency on samples with a small crack of less than 100 μm . This finding is supported by the fact that the autogenous healing mechanism normally works best with a small crack width as reported by [55]. When the cracks were larger than 100 μm , there were large variabilities of the healing results and this happens due to several reasons. First, different crack patterns on all specimens lead to a variety of crack sizes. Second, the number of data per crack range is not the same for each mixture (also can be seen in Figure 4-5), leading to unequal sample sizes to make a fair comparison. In fact, this is unavoidable considering difficulties in controlling the crack width during the splitting test and the random selection of measuring points along a crack. Thus, it is very hard to obtain a similar or even the same crack width for all specimens with equal sample size.

Following the above limitations, the HE results, as presented in Figure 4-6, cannot be compared directly by mean values from one mixture to another mixtures. Hence, a series of statistical tests ran by Minitab to understand the interpretation of the data and whether a significant difference is detected among all representative mixtures in the same series. In this case, the data analysis is limited up to 300–400 μm because on a higher level of crack width, some mixtures sometimes do not have data (e.g. M7 samples did not have cracks between 400–500 in width and only M3 and M5 samples had cracks around 500–600 μm in width) and the sample size is rather insufficient. Initially, the raw data generated from Figure 4-6a were tabulated and categorized into different series (e.g. M1–2–7, M3–2–4, and M5–2–6) to investigate the interaction between those mixtures in the same series. Two statistical tests were initially performed, namely (1) a normality test by the Shapiro-Wilk test to check whether the data set follows a normal distribution and (2) a variance test by the Levene's test to assess the equality of variances for groups. The results are summarized in Table 4-3 and based on the evaluation of the p-value for each test, it is confirmed that not all data from representative mixtures for each series follow a normal distribution (significance level = 0.05, $p < 0.05$) and have an equal variance (significance level = 0.05, $p > 0.05$). As a result of several boundaries (i.e. unequal variance,

non-normal distribution and unbalanced sample size), a non-parametric test is suitable to analyse the current data. In this case, the Kruskal-Wallis test is employed, which is basically a similar approach as a one-way ANOVA but it is based on the ranks of the data. Because the mean values cannot be compared to analyse the results with these specific boundaries, this Kruskal-Wallis test can be used to determine whether the medians of groups are statistically different (with p -value < 0.05). Next, if a significant result is detected, the Kruskal-Wallis test basically could not tell which group(s) is statistically different. Thus, a post hoc test is necessary to be executed. Amongst all available post hoc tests for non-parametric tests, the Dunn's test is mostly used to assist the results obtained from the Kruskal-Wallis test in order to evaluate if there are statistically significant differences between two or more mixtures. Eventually, for each data set of crack width (e.g. 100–200, 200–300 and 300–400 μm), each mixture series is analysed by the Kruskal-Wallis and Dunn's tests and the results are recorded in Table 4-3. Based on a series of statistical tests, the key findings are described below.

- For 'small' cracks between 100–200 μm in width, the addition of CA from 1 to 2% bwoc and the change of cement content for CA mixes from 320 to 360 kg/m^3 did not show a considerable improvement of healing efficiency, but with the increase of w/c from 0.46 (M2) to 0.52 (M4), there was a significant difference of HE. This may lead to the notion that for small cracks, a higher w/c will induce a better healing mechanism.
- For 'medium' cracks between 200–300 μm in width, there were significant differences between M5-M2 and M5-M6 in the series of cement content. It shows that an increase of cement content from 320 to 340 (or 360) kg/m^3 seems to effectively enhance the healing performance by crack closure. It is also clear from Figure 4-6a that the mean of HE values from M5 is lower than the other mixtures. In this case, the adaptation of mix design in terms of w/c and CA dosage seems to not give a real contribution to improve the healing efficiency.
- For 'large' cracks between 300–400 μm in width, a significance difference of HE was also detected between M1 (0% CA) and M7 (2% CA). The adaptation of w/c also exhibited the same tendency where a gradual increase of w/c from 0.46 (M3) to 0.49 (M2) and 0.49 (M2) to 0.52 (M4) showed a better improvement on the healing efficacy. Moreover, the effect of cement content on the healing efficiency for large cracks is not apparent.

The aforementioned results are mainly based on experimental results observed during 21 days of healing, and the same approach is also applied to statistically analyse the data (from Figure 4-6) after the healing is prolonged to 121 days. Our analysis confirms that there are no significant differences (p -values > 0.05) for all HE results at any crack widths, CA dosage, w/c and cement content. Therefore, in the view of mix design parameters (i.e., CA dosage, w/c and cement content), the modification of mix designs is more important to boost the healing efficiency at early ages than at later ages.

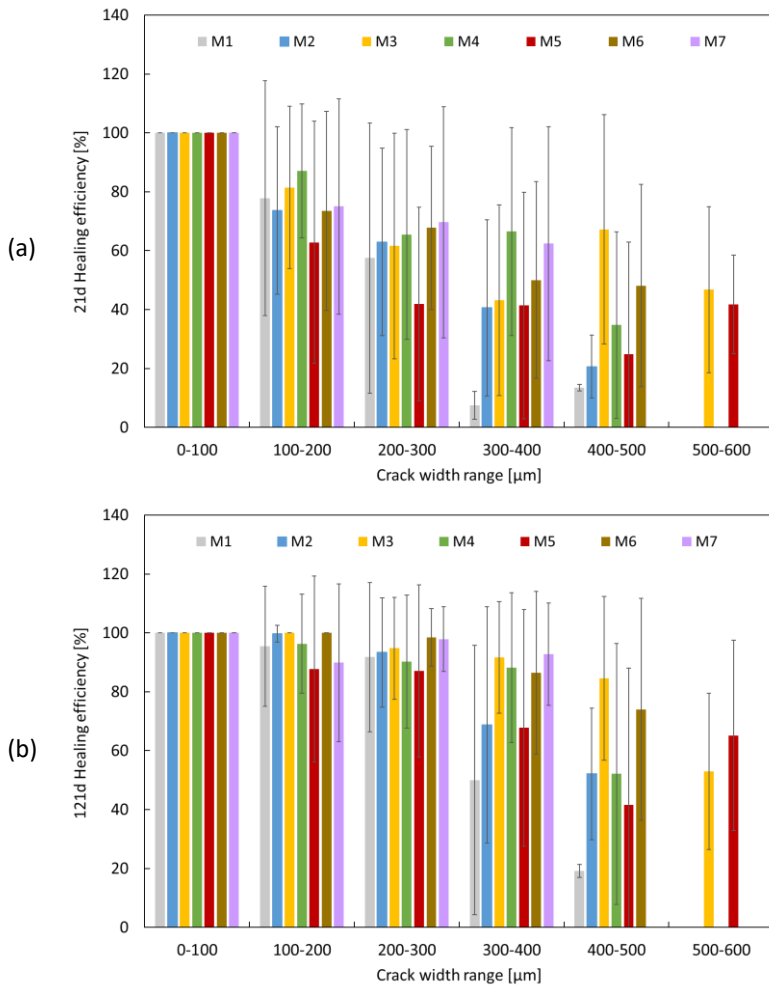


Figure 4-6. (a) 21-day and (b) 121-day healing efficiencies of all concrete samples with different crack widths

Table 4-3. Statistical analyses of data series of crack width with respect to the 21d healing efficiency

Crack width	Series	Mixture	Normality test	Variance test	Non-parametric test	Post hoc test
			Shapiro-Wilk test	Levene's test	Kruskal-Wallis test	Dunn's test
			p-value (*)	p-value (**)	p-value (***)	p-value (***)
100–200 µm	Effect of CA dosage	M1 (0% CA)	< 0.010	0.805	0.057	-
		M2 (1% CA)	> 0.100			
		M7 (2% CA)	< 0.010			
	Effect of w/c	M3 (0.46)	< 0.010	0.007	0.018	M2 vs. M4 p = 0.004
		M2 (0.49)	> 0.100			
		M4 (0.52)	> 0.100			
	Effect of cement content	M5 (320 kg/m ³)	< 0.010	0.024	0.537	-
		M2 (340 kg/m ³)	> 0.100			
		M6 (360 kg/m ³)	< 0.010			
200–300 µm	Effect of CA dosage	M1 (0% CA)	< 0.010	0.037	0.169	-
		M2 (1% CA)	> 0.100			
		M7 (2% CA)	0.032			
	Effect of w/c	M3 (0.46)	0.074	0.155	0.808	-
		M2 (0.49)	> 0.100			
		M4 (0.52)	0.024			
	Effect of cement content	M5 (320 kg/m ³)	< 0.100	0.155	0.000	M5 vs. M2 p = 0.000 M5 vs. M6 p = 0.000
		M2 (340 kg/m ³)	> 0.100			
		M6 (360 kg/m ³)	0.032			

300–400 μm	Effect of CA dosage	M1 (0% CA)	> 0.100	0.001	0.008	M1 vs. M7 p = 0.003
		M2 (1% CA)	> 0.100			
		M7 (2% CA)	> 0.100			
	Effect of w/c	M3 (0.46)	< 0.010	0.542	0.001	M3 vs. M4 p = 0.001 M2 vs. M4 p = 0.013
		M2 (0.49)	> 0.100			
		M4 (0.52)	0.095			
	Effect of cement content	M5 (320 kg/m ³)	< 0.010	0.285	0.286	-
		M2 (340 kg/m ³)	> 0.100			
		M6 (360 kg/m ³)	< 0.010			

Note: (*) p-value < 0.05 means that the null hypothesis is rejected and the distribution is not normal, (**) p-value < 0.05 means that the null hypothesis is rejected and the variances are not equal, (***) p-value < 0.05 means the null hypothesis is rejected and the difference is statistically significant, as indicated by **blue fonts**.

In order to quantify the self-healing results for all mixtures, by considering the mean values of all healing efficiencies from the crack widths in the range of 0–400 μm (from Figure 4-6), the global healing efficiency for each mixture can be calculated by Equation (4.2) to establish a robust comparison. Figure 4-7 shows the global healing efficiency of all mixtures with the different parameters of interest, i.e. CA dosage, w/c and cement content.

- Based on Figure 4-7a, the \overline{HE} increases as increasing the CA dosage at any healing period. It is clear that with the addition of CA, the variability of the results reduces considerably, meaning that a more reliable result most likely can be achieved with a less spread-out of the data. This also suggests that the formation of crystalline products by CA is noticeable in the crack, thus when the crack measurement is executed, the crack width becomes narrower due to the deposited crystals nearby the cracks. It may be argued that a higher CA dosage leads to a higher crystal formation. According to Figure 4-7a and considering the mean values at 21 days, the addition of 1% CA (M2) enhances the healing efficiency by 14%. As a result of doubling the CA dosage to 2% (M7), the improvement is also almost doubled, recorded at 26% with respect to M1. At 121 days of healing, the healing efficiency of mixtures with 1% and 2% CA also improved by 7% and 13%, respectively. In this case, a high dosage of CA is potentially beneficial to fasten the healing process.
- Based on Figure 4-7b, after a short healing, the increase of w/c from 0.46 (M3) to 0.49 (M2) shows a similar healing efficiency and when the w/c is increased to 0.52 (M4), a 10% improvement of \overline{HE} is noticed. Nevertheless, after 121 days of healing, the healing efficiency did not show any considerable improvement as increasing the w/c . It may be attributed due to the fact that a long healing period for 121 days is already sufficient for all these mixtures to almost fully heal the cracks with a high healing efficiency. This is supported by the results from Figure 4-7b where the values of \overline{HE} are already between 90–100%, being the highest level of \overline{HE} amongst other series where some other mixtures still show around 80% by average.
- Based on Figure 4-7c, the effect of cement content on CA mixes shows the same tendency as the effect of CA dosage. The healing efficiency of CA mixes increases with increasing the cement content. The 21d \overline{HE} s of mixtures with cement contents of 320 (M5), 340 (M2) and 360 (M6) kg/m^3 were 61, 69 and 72%, respectively (by mean values). This might be attributed to a higher CA amount for mixtures with a higher cement

content and also a higher cement content relates to a higher supply of calcium ions leading to a higher precipitation [128]. In the concrete mix design of this series, a constant CA dosage at 1% bwoc was used and the w/c was fixed at 0.49. It means that mixtures with cement content of 320–360 kg/m³ have a CA amount of 3.2–3.6 kg/m³. It has been mentioned previously that a higher CA content leads to a higher healing efficiency. This finding is in line with the observation from the first series of mixtures on the effect of CA dosage. The results observed after a long healing also show the same trend as the case of short healing. It can be argued that the effect of crack closing by CA for stimulating autogenous healing is more pronounced in the mixtures with a high cement content. At one side, it is potentially beneficial for a fast healing progress that high amounts of CA and cement are used, but a high cement content will have a negative implication in terms of environmental impacts such as carbon foot print, CO₂ emission, etc. Thus, the optimisation of mix designs of self-healing concrete should take into account the performance of mixtures in terms of healing and sealing besides other fresh and hardened properties (e.g. workability, strength, etc.) as well as the sustainability issues. To give a confidence level for selecting certain mix design parameters, the permeability test was also conducted in this scenario to evaluate the performance of the mixtures in terms of sealing, and eventually the optimum parameters can be further opted.

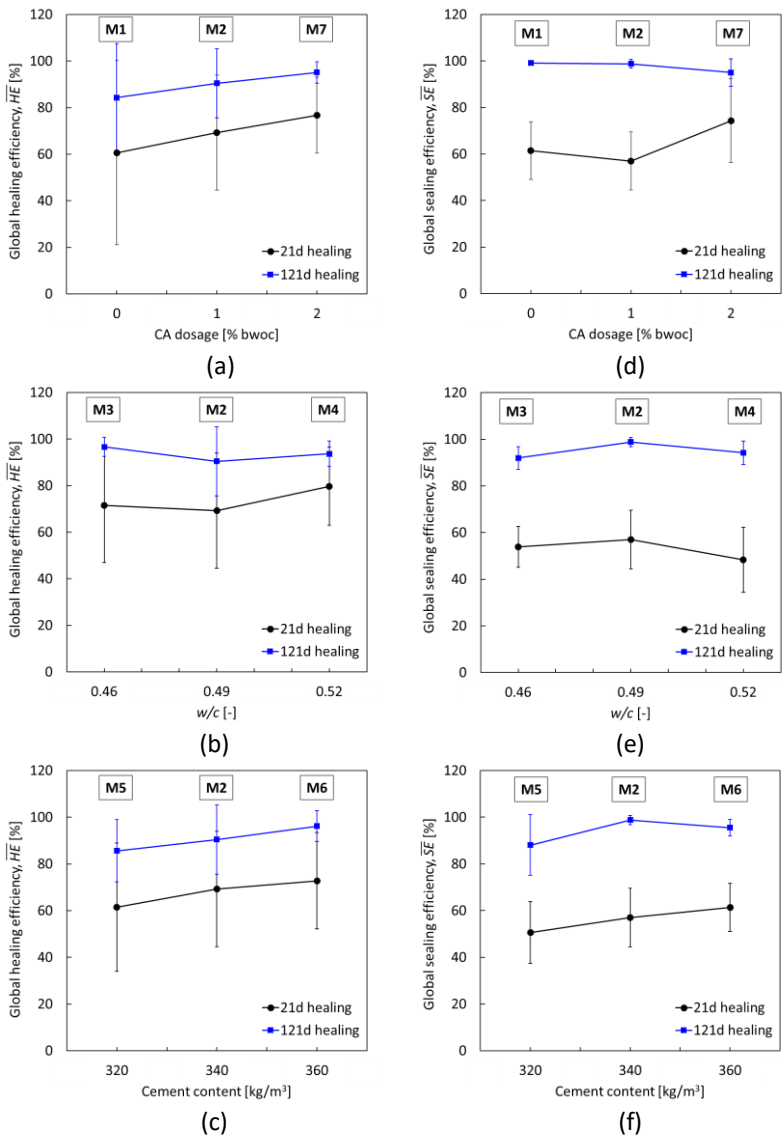


Figure 4-7. Global healing efficiencies of all tested mixtures with different: (a) CA dosage, (b) w/c and (c) cement content and global sealing efficiencies of all tested mixtures with different: (d) CA dosage, (e) w/c and (f) cement content

4.3.3.3 Sealing performance by permeability measurement

To evaluate a self-sealing phenomenon of the concrete, a permeability test was complemented before and after healing, as explained previously in Section 4.2.3. An example of the results from the permeability test on M7 specimens is depicted in Figure 4-8. It is clear that after the specimens were cracked at 0 days and subsequently tested by the permeability test, the water flowed rapidly through the crack as the slopes had steep inclinations. It is noteworthy to mention that there is a high variability in permeability results which is attributed to the variety of crack width. The cracked specimens were not differentiated based on the crack width range and a mix of cracks between 100 and 500 μm was available in all tested specimens, which eventually may affect the permeability results. In this regard, the slope represents the permeability rate, determined as the water height reduction over time. However, after healing for 21 days, there were good improvements as the reductions of water height were relatively slow, as compared with the initial test at 0 days. This means that the cracks became narrower after healing due to the formation of healing products inside the crack. However, the cracks were not completely closed in this scenario as in most specimens, the water reductions were still apparent. With a longer healing time up to 121 days, in some specimens, the water level remained constant, meaning no further reduction of water height that indicates a 100% sealing efficiency. Some specimens still showcased a water reduction in time, meaning that the cracks on top and bottom sides were still not completely closed, but the results showed a better permeability if compared with results from 0 and 21 days. Thus, an improvement in sealing efficiency was certainly attained.

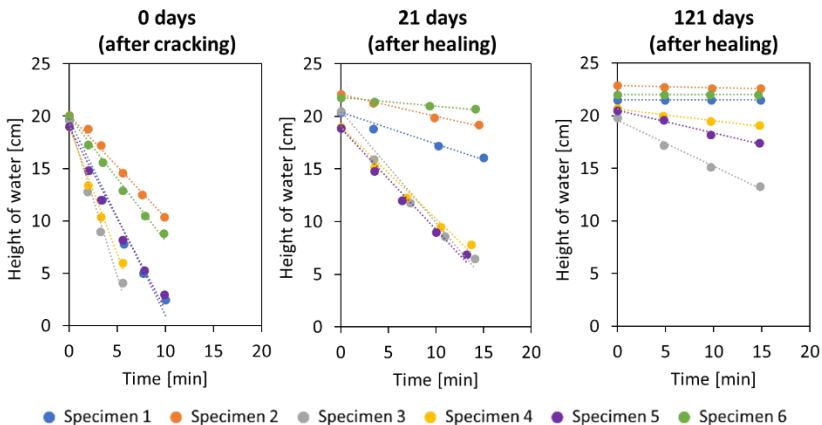


Figure 4-8. Permeability rate (M7 mixture taken as an example)

As previously mentioned in Section 4.2.3, the measurement was done in duplicate for each specimen and the average permeability rate per specimen was obtained. The sealing efficiency was calculated for each specimen after healing and the global sealing efficiency was determined based on SE results from all specimens in one single mixture. Figure 4-7 shows the global sealing efficiency of all mixtures with different parameters of interest, i.e. CA dosage, w/c and cement content.

- Based on Figure 4-7d, the effect of CA dosage was evident at a relatively short healing. With the addition of 1% CA (M2), apparently there is no improvement of sealing efficiency as compared with the mixture without CA (M1). When the CA was increased up to 2%, there is a considerable improvement from 61 to 74%. It indicates that the healing products were highly formed inside the cracks, thus when the permeability test was performed, the rate of water flow decreased due to the presence of the crystals. This notion is supported by the previous findings [112] where they found an excessive formation of white crystals on the concrete containing a high dosage of crystalline admixture. However, after 121 days of healing, there is no significant difference on the global sealing efficiency of all mixtures because all values are reaching close to 100% \overline{SE} . Although there is a slightly bigger variation on M7 results with respect to M1 and M2, the trend of \overline{SE} results is relatively stable. It suggests that after a long healing exposure, the use of a high dosage of CA is not effective anymore as compared with a short healing. Also in this case, the use of 1% CA did not show a considerable improvement on sealing efficiency at any healing time. Thus, a selection of 2% CA is recommended where self-healing and self-sealing are needed at a relatively short time, but with a long exposure time, 1% CA can be a wise choice considering a higher CA amount leads to a higher material cost. In case the mixture of 1% CA is opted for projects where a quick healing is required, an adaptation of mix designs (either with varying w/c or cement content) is needed to enhance the healing and sealing performances.
- The effect of w/c on global sealing efficiency is shown in Figure 4-7e. At a relatively short healing, the \overline{SE} results of M3, M2 and M4 were relatively comparable and statistically there are no significant difference on these values ($p = 0.46 > 0.05$), although a slightly lower \overline{SE} was found on M4. A major improvement is observed after the specimens are healed for 121 days. The global sealing efficiencies of mixtures with w/c ratios of 0.46, 0.49 and 0.52 were 92, 99 and 94%,

respectively. A one-way ANOVA analysis revealed that an increase of w/c from 0.46 to 0.49 on CA mixtures gave a significant impact ($p = 0.01 < 0.05$) in terms of sealing efficiency, however an increase of w/c to 0.52 did not significantly improve the sealing efficiency ($p = 0.06 > 0.05$) even though a small increment was noticed in relation to w/c of 0.46 (M3). Based on this finding, a low w/c seems to give a lower sealing performance after a long healing exposure. This may be explained by the concept of hydration degree of the cement where the hydration is prolonged with increasing w/c ratio [129]. It might be possible that there is more formation of healing products inside the crack from ongoing hydration in M2 and M4 rather than M3, because with the w/c of 0.46, a slower long-term hydration is expected which results in less dense precipitation due to more unhydrated cement particles are still available in the matrix. However, further investigation is needed to confirm this hypothesis. Based on our findings, among w/c ratios of 0.46–0.52, the healing and sealing performances of CA concrete can be optimised by the w/c of 0.49.

- Lastly, the effect of cement content on sealing efficiency is depicted in Figure 4-7f. After 21 days of healing, the results showed that a gradual increase of cement content from 320 to 360 kg/m^3 increases the sealing ability linearly. This effect is attributed to a high CA amount and a high cement content. Thus, it is expected that a greater formation of healing products occurs in the mixture with a higher CA content (M6) than the other mixtures with a lower CA amount (M5 and M2). However, it seems that there is a change of \overline{SE} trend after 121 days of healing. A large variation of the results from M5 is clearly noticed, while the results of M2 and M6 appear with a small variation. Considering the mean values of \overline{SE} , M5 with cement content of 320 kg/m^3 still showed a lower \overline{SE} (88%) than other mixtures and the highest \overline{SE} at 99% is attained by M2 with cement content of 340 kg/m^3 , followed by M6 with cement content of 360 kg/m^3 at 95%. In general, this result shows that an adaptation of mix designs of CA concretes in terms of cement content will affect the sealing performance. The cement content of 340 kg/m^3 (among 320–360 kg/m^3) can be selected as the optimum amount of cement to produce better self-sealing properties of CA concrete and a fairly good healing performance after undergoing a long healing. In case a rapid healing/sealing ability is needed, a high cement content can be further used with careful considerations towards sustainability, or a higher CA dosage up to 2% bwoc can also be used with lowering cement content.

4.4 Discussion

4.4.1 Relationship between crack width and permeability rate

Figure 4-9 presents a possible correlation between crack width and permeability rate observed before and after healing. Three parameters of interest were employed including (1) average crack width from top and bottom surfaces, (2) average crack width at top surface and (3) average crack width at bottom surface. At 0 days (right after cracking), a Power regression was used to define the relationship between initial crack width and permeability rate. Out of three parameters, the best correlation was obtained by taking into account the average crack width from top and bottom surfaces of the specimen. It suggests that the water flow rate strongly depends on the third order power of the initial crack width. This observation was also found and supported by previous studies [130–132]. On the other hand, the correlation between permeability rate and average crack width from top or bottom side is less reliable and those parameters cannot indicate the level of damage of the cracked specimen as tested by a permeability test. Roig-Flores et al. [66] also argued that selecting the top or bottom crack as a parameter did not show any stable results and the average crack width from top and bottom surfaces was considered as the best parameter. However, it seems that the third order power trend is only valid during the first observation on cracked concrete. As for healed concrete, it is difficult to set the trend considering the reduced crack width. Also, it is difficult to know whether the deposited healing products in the interior of cracks are distributed evenly. Thus, the observation of crack width from the surface of healed concrete by optical microscope could not be linked with the permeability results. Nevertheless, based on Figure 4-9, the results observed from 0 to 121 days show that the self-healing and self-sealing effects are noticeable with reducing the crack width and lowering the permeability rate, respectively, as increasing the time of healing.

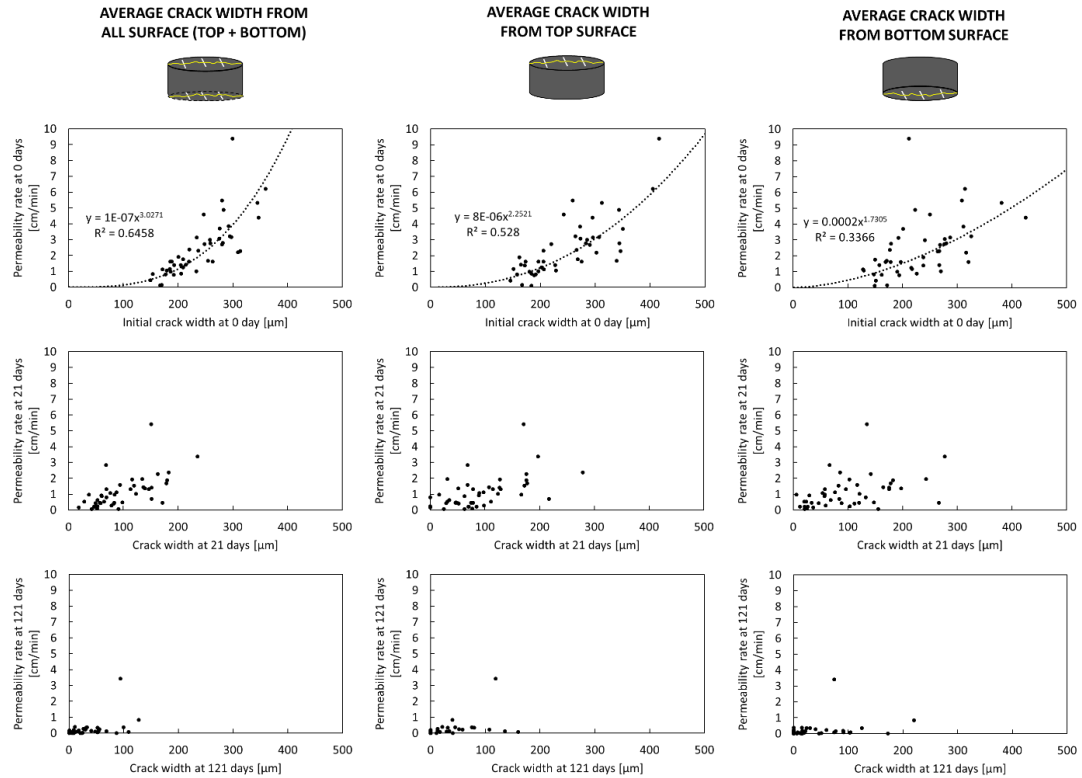


Figure 4-9. Relationship between permeability rate and crack width observed at 0, 21 and 121 days

4.4.2 Relationship between healing efficiency and sealing efficiency

Figure 4-10 depicts a relationship between healing efficiency and sealing efficiency of all mixtures after being subjected to different healing periods. At a relatively short healing of 21 days (see Figure 4-10, grey markers), there is no definite relationship between *HE* and *SE* as the data points are randomly scattered far from the bisector line. At a long healing period of 121 days (see Figure 4-10, blue markers), the points of interest are moving concentrated to the left-top corner. This tendency occurs because a longer healing period will have a better healing/sealing efficiency as a result of the further precipitation of healing products inside the crack. Apparently, no definite trend between *HE* and *SE* at 121 days can be drawn which is attributed to several factors such as different measurements, variability of test results, etc., as explained below.

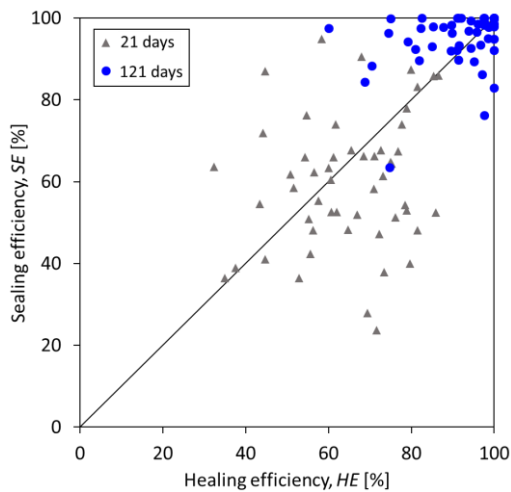


Figure 4-10. Relationship between *HE* and *SE* after 21 healing days (grey markers) and 121 healing days (blue markers)

The morphology of the crack inside the specimens will undeniably affect the *SE* result as it will certainly not be the same for each specimen, for instance it can be a uniform linear crack, pyramidal frustum, convex or concave form (see Figure 4-11). Nevertheless, the pattern of precipitated crystals on the crack mouth and (inner) crack sides is also a point of interest. To grasp a better understanding of the precipitation sites, Figure 4-12 shows some possible locations of precipitation which may take place along the crack after being subjected to healing. As a note, the pictures before (0 day) and

after healing (21 days) were taken from the top surface of cracked specimens.

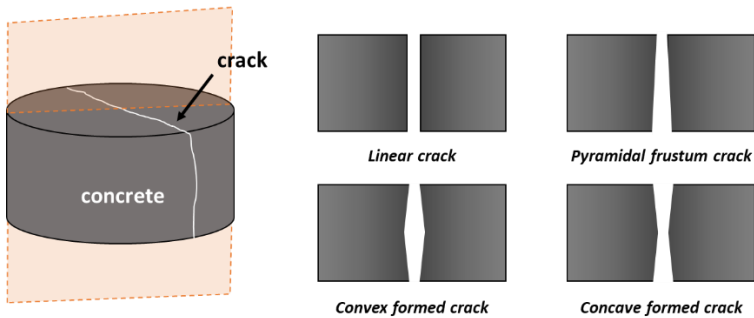


Figure 4-11. Some possibilities of different crack geometry

- In the first case (Figure 4-12a), no precipitates are formed on the crack mouth thus the observation from microscope will lead to a 0% HE. Because the crack occurs on the aggregate side, rather than on the mortar matrix, healing products are most likely not prone to be formed. It may also be assumed that along the crack, there are rather low precipitations or even no products formed.
- In the second case (Figure 4-12b), the crack partially cuts the interfacial transition zone (ITZ) between mortar and aggregate and also a partition between aggregate-aggregate on top side and mortar-mortar on bottom side. In this regard, after 21 days of healing, the precipitation, which is confirmed to be calcium carbonate (as explained later in Section 4.4.3), takes place on the crack mouth. However, from the microscopy observation, the crack area appearing in dark colour is slightly covered by a thin layer of the healing products. It might indicate that the healing products are not dense yet and still are in the process of closing the cracks.
- In the third case (Figure 4-12c), it is evident on the pictures before and after healing that the white precipitates are well formed inside the crack, but did not start initially from the crack mouth. It may probably be due to the reason that the crack size inside the crack is smaller than the crack size from the surface. Thus, healing products may effectively form starting from the inner side.
- The fourth case (Figure 4-12d) might be an ideal case of a self-healing phenomenon where at the beginning the crystallisation takes place on

the crack mouth and probably also along the crack wall showing a growth of healing products from the crack sides to slowly close the entire crack as healing time increases.

- The last case (Figure 4-12e) demonstrated a 100% healing efficiency where the crack is fully healed by the healing products and the dense precipitation is clearly observed. Nevertheless, it is still questioned whether the healing products are fully formed only near the crack mouth or the entire crack has been fully filled with the white crystals. Moreover, the crack closure on the crack mouth has been suggested as a good indication of self-healing as no further substances may penetrate into the crack, thus the concrete degradation can be potentially avoided.

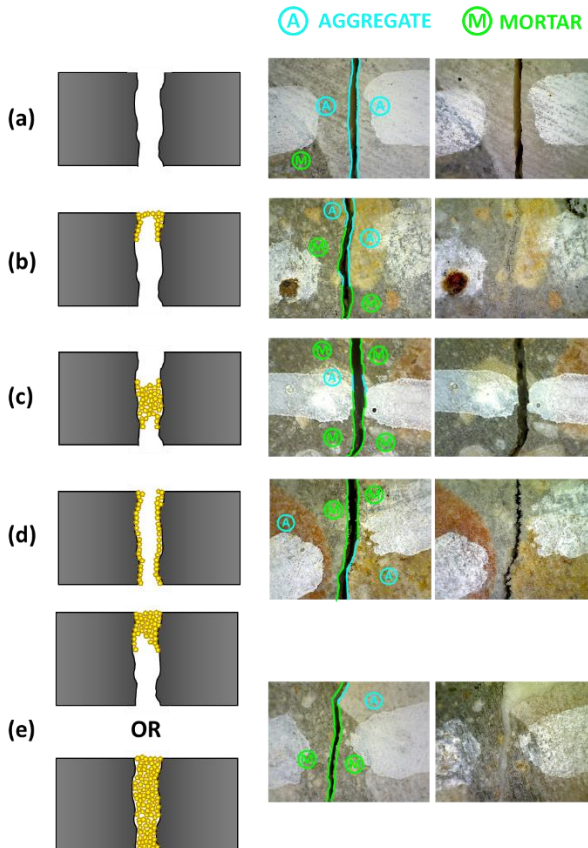


Figure 4-12. Some possibilities of the occurrence of precipitation products along the crack

Moreover, as previously shown in Figure 4-10, the correlation between healing efficiency (from optical microscope) and sealing efficiency (from permeability test) is relatively complicated because there are many possibilities which may occur naturally during the healing process. As a note, ongoing hydration and CaCO_3 precipitation are both considered in this case. The self-healing phenomenon could also occur inside the crack as crystallization could start easily in the zones with smaller crack width. This may lead to a different interpretation when constructing the link between *HE* and *SE*, because one may argue that the *HE* is assessed based on the measurement on the crack mouth and to date, the measurement of crack size inside the crack seems difficult to do by means of a microscope. Figure 4-13 depicts some possible conditions which make that the *SE* and *HE* could not be linked together, as described below.

- According to Figure 4-13a, which is similar with the previous case according to Figure 4-12b, the precipitation layer on the concrete surface is relatively thin and flat. Based on an analysis of the crack measurement, in this case, the healing efficiencies on top and bottom sides are approximately 100% and 0%, respectively. While this case is being simplified in a two-dimensional shape, the mean healing efficiency is accounted for 50%. However, when performing the permeability test, it may be possible that during pouring the water into the test setup until it reaches ~20 cm in height, the thin-layered healing product is broken and being washed away with the water. This phenomenon will result in a low *SE* if the precipitated products are not strong enough.
- Figure 4-13b depicts a condition where the crack on the top side is fully healed with a high densified healing product while on the bottom side the crack is not completely healed. During performing the permeability test, it is highly possible that the water height will remain stable around ~20 cm meaning the water does not penetrate into the crack. Here the *SE* is accounted for ~100%, however the average *HE* is calculated about ~50% as both top and bottom sides are taken into consideration. It shows an indirect link between *HE* and *SE*, indicating no relationship can be established.
- Figure 4-13c shows a critical interpretation between *HE* and *SE*, as from microscopy observation, the *HE* on both sides is 0% because there are no healing products near the crack mouth. However, it might be possible that the healing products are already available inside the crack (see Figure 4-12c), thus the permeability test will give a quite high *SE* as the water

can be entrapped in the middle of crack. Consequently, the water height will not decrease considerably. In this case, again the relationship between *HE* and *SE* is difficult to be concluded.

- On the other hand, Figure 4-13d and Figure 4-13e present two ideal cases where the *HE* and *SE* can be correlated. In Figure 4-13d, the healing scenario is relatively similar at top and bottom sides ($HE < 100\%$), and the *SE* also will be lower than 100%. In this case, it is expected that there is a relationship as shown in Figure 4-10. In addition, Figure 4-13e illustrates a complete healing and sealing where both *SE* and *HE* equal to $\sim 100\%$, showing a perfect correlation.

The assessments of *HE* and *SE* are both important parameters to determine the efficacy of the self-healing and self-sealing phenomenon which has been receiving a great interest from researchers. However, the analysis and interpretation of healing and sealing efficiencies might be tricky, depending on the specific test method, healing condition, proposed parameters, etc. In this research, the *HE* and *SE* did not exhibit a definite relationship which might be attributed to the assumption of various crack patterns/morphologies and different precipitation locations. Nevertheless, optical microscopy is always beneficial to measure the crack closure as the crack mouth should eventually be healed to guarantee that no liquid or any substances penetrate into the crack that may jeopardize the concrete matrix. In contrast, one major disadvantage of using a microscope is that the precipitation inside the crack cannot be clearly identified. A permeability test is also a relevant test to evaluate the self-sealing ability of the concrete. This test can indirectly “sense” the existence of healing products inside the crack which is presented by a reduction of the rate of water permeability. The more healing products are available inside the crack, the slower the water flows through the crack due to the reason that the healing products are making the crack narrower with time. Nevertheless, both techniques either measuring crack width by optical microscope or water flow rate by permeability test can be used to assess the healing or sealing efficiency of healed concrete.

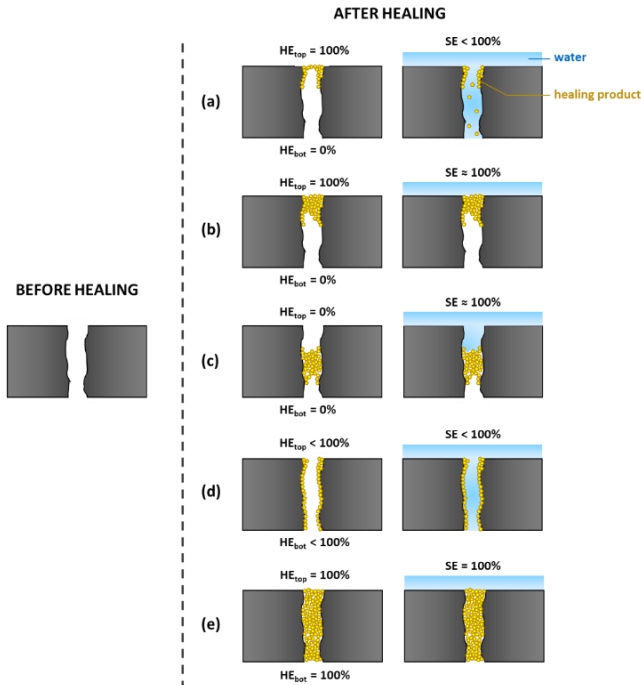


Figure 4-13. Schematic representation of discrete correlations between HE and SE which may lead to a wrong interpretation

4.4.3 Analysis of self-healing products

An additional study was conducted to investigate whether the healing products coming out from the crack differ for each mix design. Initially, the healing products from each mixture were collected by carefully scraping the precipitates near the crack mouth (see Figure 4-14). Then, a Fourier transform infrared (FTIR) spectroscopy (UATR Spectrum Two, PerkinElmer, US) was used to analyse the composition of the self-healing products and the FTIR band results are shown in Figure 4-15. Apparently, there is a high degree of similarities in FTIR spectra of all samples taken from different mixtures as they superposed perfectly. A low intensity band at 3690 cm^{-1} corresponds to O–H bond, while the bands at $1448\text{--}1467$, 854 and 712 cm^{-1} correspond to the three different elongation modes of C–O bonds [133]. A strong and intense band at $1448\text{--}1467\text{ cm}^{-1}$ is associated to the carbonate C–O bonds. Based on previous studies [133,134], the fundamental peaks of calcium carbonate (CaCO_3) can be seen around $1448\text{--}1467$ and 854 cm^{-1} . CaCO_3 in the form of calcite has two bands characteristic in the out of bending plane

at 873–878 cm^{-1} and doubly degenerate planar bending around 712–713 cm^{-1} as reported by [135–140], while CaCO_3 in the form of aragonite displays a characteristic symmetric carbonate stretching vibration at 1081–1087 cm^{-1} , a carbonate out-of-plane bending vibration at 844–858 cm^{-1} , and a double degenerate planar bending at 712–713 cm^{-1} in its FTIR spectrum [136,139,141]. Based on this observation, it can be confirmed that the mineral coming outside from the crack is composed of CaCO_3 in the polymorph of aragonite for all mixtures. This observation is also supported by previous studies [67,78] mentioning a favourable formation of aragonite on the use of CA on cementitious composites.

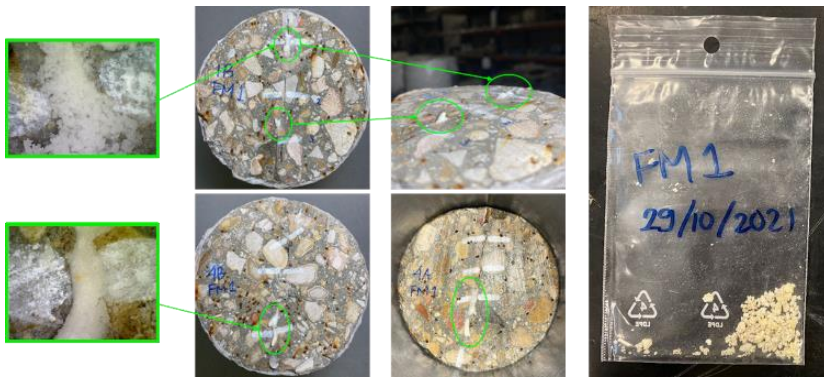


Figure 4-14. Collecting the healing products from the crack mouth

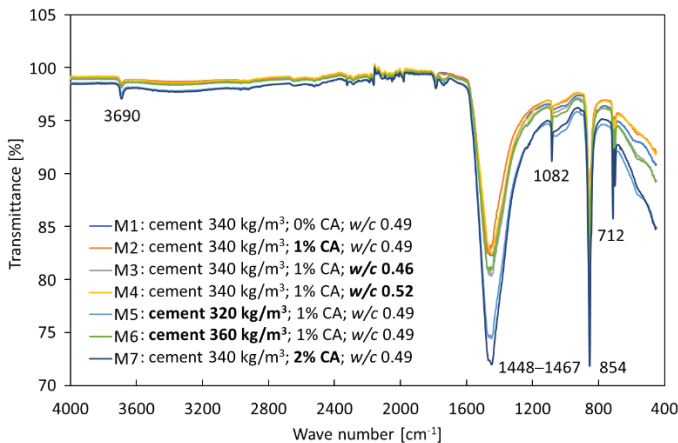


Figure 4-15. FTIR analysis of healing products

4.5 Conclusions

This study investigated the effect of concrete mix design modifications in terms of self-healing and self-sealing performances. The mix design parameters used include: (1) dosages of healing agent at 0, 1 and 2% bwoc, (2) w/c ratios at 0.46, 0.49 and 0.52, and (3) cement contents at 320, 340 and 360 kg/m^3 . In this work, Penetron Admix crystalline admixture (CA) is utilised as a healing agent which is available in the market. For self-healing purpose, the 7-days old concretes were cracked and subsequently healed for 0, 21 and 121 days under full water immersion. Based on the aforementioned results, the following conclusions can be drawn from this specific study:

1. The addition of CA at an appropriate dosage at 1% bwoc did not affect the workability of normal mixture, while a considerable reduction was found at 2% bwoc.
2. The compressive strength of hardened concrete containing CA increases as increasing the CA dosage. The strength improvements at later age (91 days) were recorded at 3.6 and 8.1% with the use of CA at 1 and 2% bwoc, respectively, with respect to reference mixture without CA. The mixture containing 2% CA and w/c of 0.49 (M7) had a comparable compressive strength at all ages with the mixture containing 1% CA and w/c of 0.46 (M3). Thus, instead of using a high CA content which directly relates to the high material cost, the mixture can be further adapted to obtain a similar strength by changing the w/c and keeping a normal CA dosage at 1% bwoc.
3. With respect to the progress of crack closure, the introduction of CA into the mixes helps to stimulate the autogenous healing mechanism by reducing the crack width even after a short healing. In this case, without the use of CA, most of the cracks in the normal mix (M1) did not show any healing progress. A long healing (e.g. 121 days) is effective to heal a high portion of the cracks with and without the help of healing agent.
4. Depending on the size of the crack that needs to be healed, the optimum parameter of mix design can be selected to achieve a better healing after exposed to 21 days of healing. For small cracks between 100–200 μm , the healing efficiency improves with increasing w/c from 0.49 to 0.52, while for medium cracks between 200–300 μm , the increase of cement content from 320 to 360 kg/m^3 enhances the healing efficiency of mixtures containing 1% CA. In case of large cracks between 300–400 μm , the use of 2% CA seems more effective to improve the healing than 1% CA, and the gradual increase of w/c from

0.46 to 0.52 continuously increases the healing efficiency. Additionally, for cracks in the range of 0–100 μm , a 100% healing efficiency is achieved by all mixtures, regardless any CA additions or any adaptations of mix designs.

5. Based on the analyses of global healing (\overline{HE}) and sealing (\overline{SE}) efficiencies, the key findings are listed below:
 - The \overline{HE} increases with increasing the CA dosage and as a result of doubling the CA dosage from 1 to 2% bwoc, the improvement of \overline{HE} is almost doubled by average with respect to reference mixture without CA. Moreover, after a short healing for 21 days, only the addition of 2% CA gives a considerable contribution by increasing the \overline{SE} . However, after a long healing at 121 days, the sealing performance of mixtures with and without CA shows a comparable result.
 - The effect of w/c on CA mixtures is visible at short healing where the mean \overline{HE} of the mixture with w/c of 0.52 increases by 10% as compared with the mixture with w/c of 0.46. However, the variation of w/c did not show a remarkable improvement on the \overline{HE} after undergoing a long healing. The best \overline{SE} improvement is attained by the mixture with the w/c of 0.49 at any healing time.
 - A gradual increase of cement content from 320 to 360 kg/m^3 leads to a continuous improvement of both \overline{HE} and \overline{SE} . However, a high cement content strongly relates to environmental and sustainability issues. Thus, it is suggested to only use a high cement content in the case of a rapid healing or sealing is needed or a low cement content aided with a high CA dosage up to 2% bwoc can be further used.
6. The healing products taken from the crack mouth, both in the healed concretes with and without CA, are confirmed to be calcium carbonate in the polymorph of aragonite.

Chapter 5

EXPERIMENTAL INVESTIGATION ON THE BOND BEHAVIOUR OF STEEL REINFORCEMENT IN SELF-HEALING CONCRETE

5.1 Introduction

With many positive outcomes on the use of healing agents with regard to their ability to heal cracks, the research is limited to mortar and unreinforced concrete. A few studies [60,61] also used reinforcement bars to make large-scale concrete structures like beams and walls, but the investigations were mainly aimed to crack the specimens and to evaluate the healing performance. Almost no studies were found where the bond between the reinforcement and the self-healing concrete matrix is investigated. Mousavi et al. [142–144] however studied the effect of the addition of SAP on the bond at the rebar-concrete interface. Results showed that the addition of SAP accelerated the healing process and improved the bond properties in uncracked and healed concretes with respect to the

**) This chapter is based on the following papers: (1) Hermawan H, Wiktor V, Gruyaert E, Serna P. Experimental investigation on the bond behaviour of steel reinforcement in self-healing concrete. *Constr Build Mater* 2023;383:131378. <https://doi.org/10.1016/j.conbuildmat.2023.131378>; and (2) Hermawan H, Tezer MM, Verstraete W, Belie N De, Serna P, Gruyaert E. Bond behaviour evaluation between steel reinforcement and self-healing concrete containing non-axenic biomasses. In: *MATEC Web of Conferences EDP Sciences*; 2023. <https://doi.org/10.1051/mateconf/202337802009>*

normal concrete without SAP. A large SAP particle size was more effective in enhancing the bond properties than a small SAP particle size. An SAP dosage of 0.25% by mass of cement was selected as the most appropriate and effective content to improve the bond strength, while a higher SAP dosage led to a higher healing efficiency on crack closing. This research eventually aimed to further explore the capabilities of various healing agents towards the bond behaviour of steel reinforcement in self-healing concrete. The research questions defined in the current study include:

- (1) What are the effects of adding healing agents into the concrete in relation to the fresh, mechanical and bond properties?
- (2) How big is the influence of a splitting crack on the hardened specimen in relation to the bond-slip behaviour?
- (3) Are the self-healing effects only useful to close the crack or may they contribute to improve the bond system?
- (4) What is the efficiency of different healing agents used in terms of a potential improvement on the bond performance?

This chapter aims to investigate the effects of self-healing agents on the bond response between the steel rebar and the concrete. The influence of the presence of splitting cracks is also considered. Four healing agents were used to stimulate the healing mechanism and to assess their contribution to the bond properties, and their contribution to recover the loss of bond properties due to splitting cracks. A modified pull-out test was performed to monitor the bond-slip responses in confined specimens, while a splitting test was executed to generate a splitting crack in the confined specimens with controlled crack widths in the concrete specimens. Two healing periods were opted to assess the bond performance of healed concrete: a short healing for 28 days (1 month) and a long healing for 112 days (4 months). Water immersion was selected as the curing and healing condition for all concretes.

5.2 Materials and methods

5.2.1 Materials

In order to study the effects of healing agents on the fresh and hardened concrete properties, five mixtures were produced in the laboratory. CEM III/A 42.5N was used as a binder component. The used aggregates were: (1) fine aggregates with two size fractions namely white sand 0/2 and red sand 0/4 having specific gravities of 2.69 and 2.64, respectively; and (2) two fractions of coarse aggregates namely limestone 4/6 and limestone 6/12

having specific gravities of 2.64 and 2.62, respectively. The sand-to-aggregate ratio was fixed at 0.44 for all mixtures based on the optimum packing of the inert skeleton from the Dewar model [145] with the minimum voids ratio and the water-to-cement (w/c) ratio was fixed at 0.50 for all mixtures. A PCE-based superplasticizer with a solid concentration of 20%, supplied by Cugla B.V., was used to improve the workability of the fresh concrete. The reference concrete mixture (REF) was designed for the application in reinforced concrete with the w/c of 0.50 and the cement content of 350 kg/m³. The mix designs are summarized in Table 5-1.

Table 5-1. Mix designs (note: (*) effective water included in the biomass agents)

Material	Mixture Type (kg/m ³)				
	REF	HTN*	YEAST*	CA	BAC
CEM III/A 42.5N	350	350	350	350	350
White sand 0/2	244	244	244	244	242
Red sand 0/4	547	547	547	546	543
Limestone 4/6	539	539	539	538	535
Limestone 6/12	462	462	462	461	458
Effective water	175	-	-	175	175
Superplasticizer	5.25	5.25	5.25	5.25	5.25
AVECOM bacteria	-	175	-	-	-
AVECOM fungi	-	-	175	-	-
Penetron CA	-	-	-	3.50	-
Basilisk bacteria	-	-	-	-	7.00

Four types of healing agents were employed in this study. The first two healing agents are non-axenic biomass agents, produced and developed by AVECOM, which are originally obtained from waste water treatment, called as HTN and YEAST (as named by the producer). The difference between these two agents lies on their microorganisms: HTN is a bacteria-based healing agent, while YEAST is a fungi-based healing agent. These materials are classified as non-axenic agents, meaning the liquid agent contains different species for each microorganism, not strictly limited to a single species. For HTN, the bacterial consortium is dependent on CO₂, H₂ and acetate. HTN may resist against high pH environment, and it is an alkali tolerant culture. A

consortium of HTN may produce a small amount of nitrite and as it is heterotrophic nitrifier, a denitrification may occur to achieve the microbial-induced calcite precipitation. On the other hand, a fungal consortium of YEAST has the ability to supply urease enzyme, which is useful for urea hydrolysis to favour calcium carbonate precipitation. However, since the agents are in development stage, the exact mechanisms for the microbially induced precipitation is being elucidated. Although these agents are still under development and in preparation to enter the market, preliminary studies by producers on mortar level revealed promising outcomes in terms of crack healing efficiency and durability improvement. Thus, it was decided to study further the impacts of adding these biomass agents by scaling up into concrete level. It should be noted that the YEAST agent used in this study is literally different from the well-known yeast product (e.g., yeast extract) and it is not regarded as nutrient, instead it is a type of healing agent containing a fungal consortium. The main composition of these biomass agents is kept confidential by the producer.

Penetron Admix crystalline admixture (labelled as CA) was also used in this study. It is mainly composed of Portland cement and active chemicals, while the detailed composition is kept confidential by the producer. Penetron Admix has been entering the market as a crystalline waterproofing admixture aiming to improve the durability of structures as well as to promote the self-healing effect. CA is a hydrophilic material that reacts with water and concrete minerals creating crystals in the crack. Roig-Flores et al. [66] reported a 95% healing efficiency of concrete containing CA (unspecified type) having a crack width of 250 μm .

The last healing agent considered in the current study is a commercial bacteria-based healing agent produced by Basilisk (labelled as BAC). It contains dormant bacterial spores from alkaliphilic spore-forming *Bacillus cohnii* which is encapsulated into polylactic acid (PLA) particles and being mixed with other materials such as inorganic salts, calcium lactate (as a nutrient), limestone powder, etc. One of the advantages of this product is that during the healing process the active microorganism will consume oxygen which will decrease the corrosion process during the process of autonomous crack repair [146]. This healing agent has been successfully applied in mortar samples by Roy et al. [147] and a big crack width of around 500 μm could be completely healed. Rossi et al. [79] also confirmed that the self-healing capacity of mortar containing BAC improved by a factor of 4 as compared with normal mortar without BAC.

In order to compare the best abilities of the four healing agents in concrete application, the dosage recommended by the respective producer of each agent was used. In this study, the dosages of CA and BAC (in powder form) were opted at 1.00% and 2.00% by weight of cement, respectively. The biomass agents of HTN and YEAST were used in the form of solutions and they were treated as a complete replacement of the mixing water (see Table 5-1). The solution itself already contains water (as mixing water) and microorganisms in which the active dry contents of the microorganisms were fixed at 0.05% by weight of cement for HTN and 0.45% by weight of cement for YEAST. The pH of YEAST and HTN agents were 7 and 9, respectively. On the other hand, CA and BAC were used in powder form and they were added on top of the normal concrete mix. The cement content for all mixes was deliberately the same (350 kg/m^3) and the composition of the aggregates was not changed for the introduction of healing agents except for CA and BAC mixes where a slight adaptation was made to ensure a 1 m^3 -volumetric design. The amount of superplasticizer was also kept the same as for the REF mix, so the effect of healing agents on the consistency of the fresh concrete can be clearly seen.

5.2.2 Sample preparation

All concrete mixtures were cast with a volume of 80 L from which approximately 15 L was used to assess the properties of the fresh concrete by means of slump, air content and fresh density tests (in accordance with EN 12350-2,6,7), approximately 10 L was cast into three cubic moulds of 150 mm in side for an assessment of the compressive strength at 28 days (in accordance with EN 12390-3), and the other 55 L was cast into pull-out moulds (see Figure 5-1). PVC tubes with an inner diameter, height and wall thickness of 105, 100 and 2 mm, respectively, were used as moulds for pull-out specimens. Later, this tube remained attached to the concrete (cylinders were not demoulded) because this tube can act as a confinement for the concrete in order to control the crack width upon crack creation. Preliminary studies showed that for concrete manually cracked with a splitting test, unconfined specimens tend to have a sudden splitting failure due to the concrete brittleness. A study by Desnerck et al. [148] also demonstrated the successful use of plastic tubes to control the crack. Steel rebars with a diameter (d_b) of 10 mm and rib pattern were used. It was found by [148] that the crack orientation with respect to the reinforcing bar's rib pattern did not influence the bond performance, thus this factor was eliminated in our study.

The ratio of concrete cover to rebar diameter (c/d_b) was fixed at 5.25 and this ratio was sufficient to ensure a pull-out failure for uncracked specimens. As the rebar was inserted into a mould with a height of 100 mm, the bond (or embedded) region was strictly limited to $5d_b$ (or 50 mm), while the other length of 50 mm was regarded as unbonded region to reduce the confinement effect of the loading plate. To get that, in this length the rebar was covered with a small PVC tube. This program was intended to perform a short pull-out test to determine the local bond slip behaviour. As with the small embedded length of the rebar, a relatively constant slip along the bonded part of the bar can be achieved [149]. Figure 5-1 shows the custom-made mould set and the dimensions of the pull-out specimen.

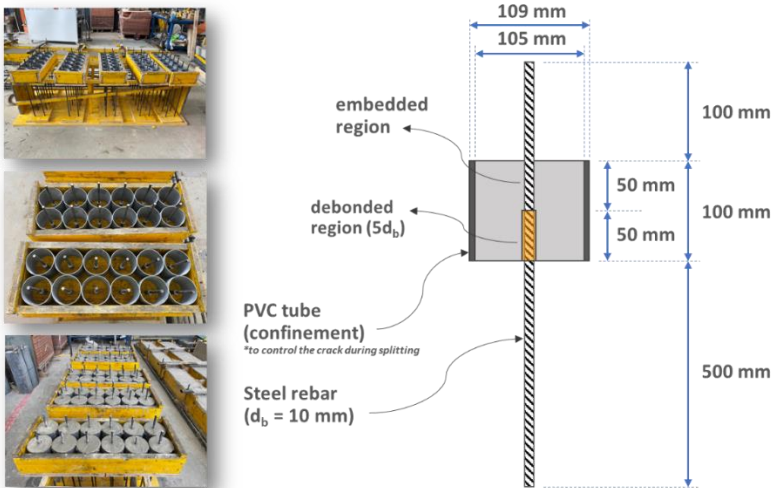


Figure 5-1. Pull-out mould set (left) and schematic of a pull-out specimen (right)

24h after concrete casting, all specimens were demoulded. Cube specimens for compressive strength were stored in a curing chamber with a temperature of 20°C and relative humidity of >90% for 28 days. The pull-out specimens were directly stored under water in tanks with a temperature of 22±1°C. Five water tanks were used in order to store the specimens from the different mixtures separately, so a possible leaching of healing agents to the curing water and contamination to other mixtures can be eliminated. The pull-out specimens in the water tanks were positioned vertically, meaning the top side of specimens faced the water surface, while the bottom side faced the base of the water tank. The position was kept the same for all

specimens to avoid that a different position may affect the formation of healing products. Since all pull-out specimens were cured under water, the protruding steel rebar was fully covered with aluminium tape in order to prevent corrosion due to the direct contact with water.

5.2.3 Test setup

In order to crack the specimens, a Brazilian splitting test was performed. As soon as a crack was formed (see Figure 5-2), the specimen was unloaded and the crack width was measured by means of an optical microscope at the two sides of the specimen. It was targeted to achieve a specific crack width between 200 to 500 μm (crack series with an interval of 100 μm are considered later). The specimen was placed back to the machine to be reloaded if the crack was too small, while if the crack width was out of the range ($>500 \mu\text{m}$ by average), the specimen was rejected. The loading rate was not registered during the test as the loading was manually controlled.

The pull-out test was finally performed by means of an Instron machine as shown in Figure 5-3. The pull-out specimen was initially placed in the support plate in which both support and reaction plates had a central hole to allow the passage of the rebar. At the bottom of the reaction plate, the load cell with a nominal capacity of 500 kN was mounted onto the steel rebar and the rebar anchorage was used to chain the rebar and to fix the load cell to the reaction plate. Next, the linear variable differential transformers (LVDTs) were placed in the setup. LVDT 1 was attached to the rebar on top of the specimen to measure the relative slip of the rebar from the concrete specimen surface. LVDT 2 was also attached to the rebar on the bottom of the support plate to measure the displacement on the active side.

The load was applied to the rebar and transferred to the specimen along the embedded rebar surface. The test was controlled at 0.05 mm/s (related to the movement of the crosshead of the press machine). The results are presented by a bond stress (load / embedded surface) vs. slip and the slip was measured by LVDT 1 from the passive side (Figure 5-3). The test was stopped when reaching a slip at 2 mm.

The aforementioned pull-out tests were adopted from the following standards: RILEM-RC6:1983 and EN 10080:2005. In general, these guidelines define a short pull-out test with the recommendations as follows: an embedded rebar length of $5d_b$, a rebar diameter ≤ 32 mm, concrete cube specimens with at least $10d_b$ in side, a slip measuring device mounted on the

top of the rebar tip, the loading rate of $0.56d_b^2$ (N/s) and the applied tension force on the long-end part of the rebar. The actual pull-out test within this study deviates slightly from the above standards including: (i) $\text{Ø}105 \times 100$ confined cylindrical specimens (while maintaining $5d_b$ as embedded length and an appropriate rebar diameter of 10 mm), (ii) different pull-out test setup (using Instron device, not a standardized bond test setup), (iii) the concrete specimen was pulled-out from the rebar (while the original standards define to pull out the rebar from the concrete), (iv) the loading rate was not controlled in function of rebar diameter and (v) the slip was measured from LVDT 1 (Figure 5-3) which was placed on the concrete surface (while the standards recommend to position the LVDT on the tip of the rebar). Although some deviations were implemented, the (modified) pull-out tests were successfully performed on all specimens, generating bond stress-slip relationships.



Figure 5-2. Splitting the pull-out specimen by means of a Brazilian splitting test

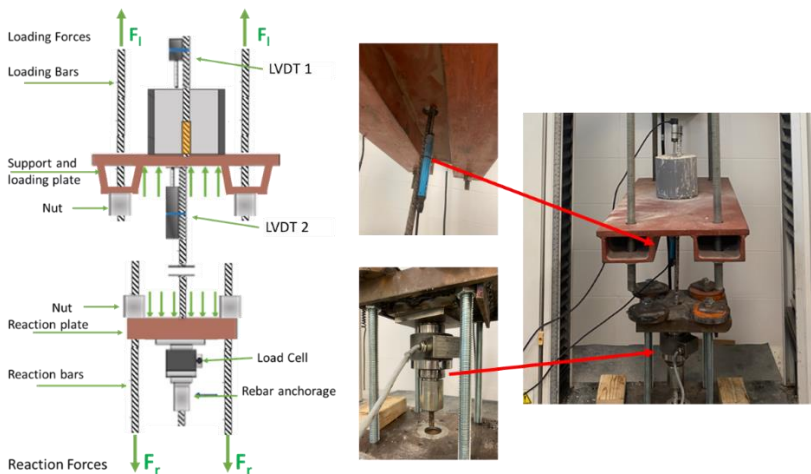


Figure 5-3. Schematic of pull-out test

A typical bond stress-slip response from the pull-out test is presented in Figure 5-4. In this study, four parameters were taken into account for further analysis, including:

- 1) the ultimate bond strength (τ_u): the bond stress corresponding to the maximum load
- 2) the mean bond strength (τ_m): the average value of the bond stresses corresponding to a slip of 0.01, 0.1 and 1.0 mm ($\tau_{0.01}$, $\tau_{0.1}$, and $\tau_{1.0}$) as defined by RILEM [150]
- 3) the slip corresponding to τ_u (S_u): the slip at the ultimate bond strength with respect to the ductility of the bond failure
- 4) the area under the bond-slip curve up to a slip of 1.0 mm ($E_{1.0}$): this area is often called as the fracture energy of the bond mechanism [151]

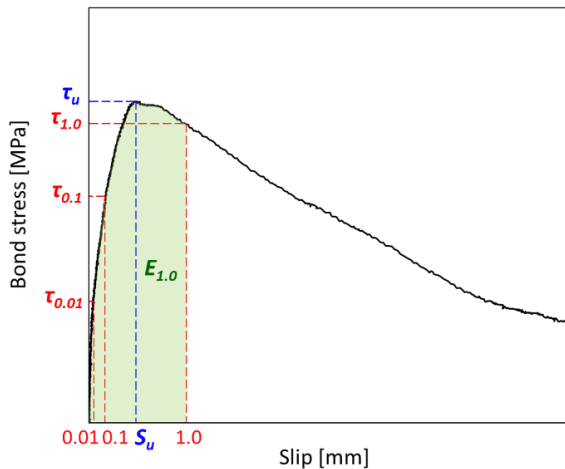


Figure 5-4. A schematic representation of the bond-slip response

5.2.4 Sample series

For a single mix, sixty pull-out specimens were produced. The specimens were later divided into several categories in order to assess the healing efficiency of different mixtures towards bond properties:

- 1) A series of uncracked (UNCR) specimens: The pull-out test on UNCR specimens was performed at 49 days. At least 5 uncracked specimens were tested.
- 2) A series of cracked (CR) specimens: In this series, the 49 days-old specimens were cracked by a Brazilian splitting test. As it is impossible to

exactly crack the specimens with the same crack width, it was decided to distinguish between small (200–300 μm), medium (300–400 μm) and large (400–500 μm) crack sizes (denoted as CR200-300, CR300-400 and CR400-500, respectively). Immediately after cracking, the pull-out tests were executed on the cracked specimens. Three to five repetitions were considered in this series for each crack size.

- 3) A series of healed (HL (28D)) specimens: In this series, 21 days-old specimens were cracked by a Brazilian splitting test. Again the specimens were categorized according to their crack width (denoted as HL200-300, HL300-400 and HL400-500, respectively). After cracking, the specimens were stored under water with a temperature of $22\pm 1^\circ\text{C}$ for 28 days. After a short healing time (28 days), the pull-out test was carried out considering the specimens reached 49 days which was the same as the condition of the UNCR and CR series. Three to five repetitions were considered in this series for each crack size.
- 4) A series of healed (HL (112D)) specimens: This series is prepared in a similar way like the (HL (28D)) series with a main difference in terms of the healing time. In this series, the cracked specimens were healed under water for 112 days. It should be noted that the age of the specimens in this series reached 133 days during the pull-out tests. Three to five repetitions were considered in this series for each crack size.

After cracking the specimens, the crack measurement by means of optical microscope was executed to measure the actual width of the crack. The assessment of crack measurement was done at both sides of the specimen and the average crack width was obtained from four measured crack widths. Also, after the specimens were subjected to a specific healing time, crack measurements and visual inspections were executed to evaluate the crack closure by the precipitation of healing products. A full schematic test series program is provided in Figure 5-5.

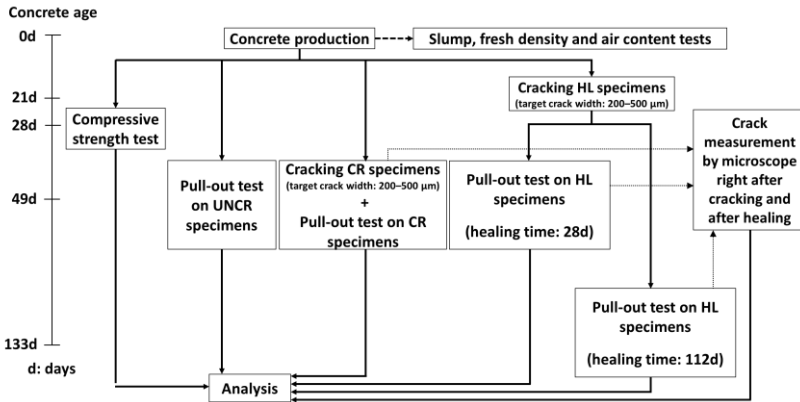


Figure 5-5. Flow chart of test series program

5.3 Results and discussion

5.3.1 Fresh properties

Figure 5-6 exhibits the slump and air content results of all mixtures. The REF mixture had a slump of 170 mm which was classified as S4 class in accordance with NBN EN 206 [126]. As shown in Figure 5-6, different healing agents induced a different effect on the consistency of the fresh concrete mixture. On the use of HTN, the slump was considerably decreased up to 130 mm and this was a downgrade of slump class to S3. The introduction of YEAST slightly increased the slump to 190 mm, however it was still in the same S4 class as the REF mix. Thus, the addition of YEAST did not negatively affect the workability of the normal mix. On the use of 1% CA by weight of cement, the slump was reduced to 150 mm and was classified as S3 class. Moreover, the addition of BAC at 2% by weight of cement greatly increased the slump to 220 mm and according to the standard, this was categorized as S5 class. The tendency of CA to lower the workability can be explained by the fact that the superplasticizer was adsorbed by the CA particles. According to XRD analysis, the CA contains a significant amount of C_3A and it has been known that superplasticizer has a high affinity for C_3A . Thus, the addition of CA causes a reduction in the workability aspect and an increase in the viscosity of the mixture. Therefore, a higher superplasticizer demand is needed in case of the CA mix to achieve the same consistency as the mixture without CA addition.

The average fresh densities of all mixtures were almost identical at 2340, 2350, 2350, 2330 and 2340 kg/m^3 for REF, HTN, YEAST, CA and BAC mixtures,

respectively. With respect to the air content, the REF mix showed a 2.50% air content which was the highest among all mixtures. The lowest air content was achieved by the CA mix and amounted to 1.90%. The addition of HTN, YEAST and BAC led to an identical air content of the concrete mixtures (2.20–2.30%), which was slightly lower than the air content of the REF mix. It may be concluded that the additions of YEAST and BAC increased the workability of the fresh mixture without showing any sign of segregation, while a considerable reduction of air content was achieved by the addition of CA but with a lower slump. All in all, with the obtained workability, the casting of specimens was done with guaranty of a good production for the test program.

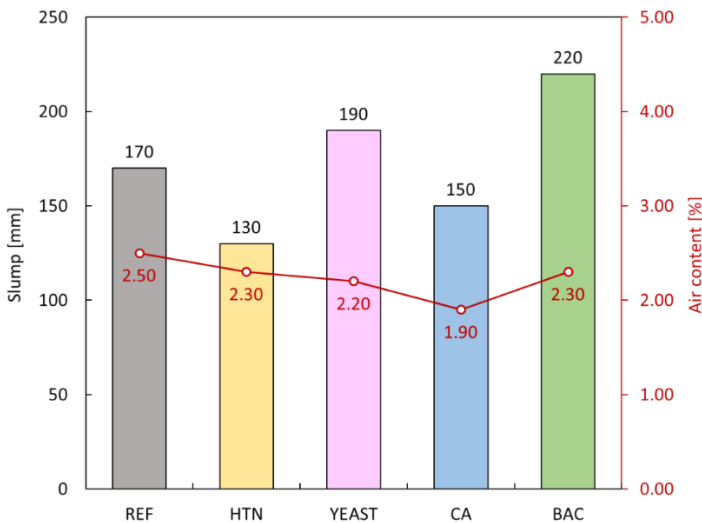


Figure 5-6. Slump and air content of all mixtures

5.3.2 Hardened properties

The hardened properties of reference and self-healing concretes were assessed by hardened density and compressive strength tests on 28 days-old specimens. The average hardened densities of all mixtures were also almost identical at 2290, 2310, 2310, 2290 and 2300 kg/m³ for REF, HTN, YEAST, CA and BAC mixtures, respectively, which were in line with the results from fresh density tests. The compressive strengths of all concretes are depicted in Figure 5-7. Without the addition of any healing agents, the REF mix achieved an average compressive strength of 47.1 MPa. The additions of biomass

agents, HTN and YEAST, increased the strength by 5.8 and 0.8%, respectively. This result meets with expectations from the author because according to the claims by the producers, the biomass agents did not aim to improve the compressive strength, but did rather aim to improve the healing efficiency. The highest compressive strength was obtained by the CA mix at 50.9 MPa with an 8.0% improvement as compared with the REF mix. An improvement of the mechanical strength of the CA concrete is expected as PENETRON [73] claimed a 13% strength improvement by using CA at the dosage of 0.8–1.0% by weight of cement. A strength improvement by CA can be potentially explained by an SEM analysis conducted by García-Vera et al. [4] where they found the crystalline structures in the pores of CA-based mortar as a result of reaction between crystalline chemicals, calcium hydroxide and other by-products of cement hydration. These crystalline formations filled and clogged pores, capillaries and microcracks of the cementitious materials. The introduction of BAC also showed a slightly higher compressive strength than the REF mix with 4.5% increment. This finding is in line with a study by Rossi et al. [79] where they also found a small improvement of compressive strength of the cement paste mixed with Basilisk healing agent at 2.6% by mass of cement. All in all, the addition of these four types of healing agents did not induce any harmful effects on the mechanical properties of normal concrete, indicating a positive outcome to introduce the healing agents in real applications. Statistical analysis by one-way Analysis of Variance (ANOVA) aided with Dunnett's post hoc test reveals that the strength differences between REF and CA ($p = 0.03$) are statistically significant by considering a significance level at 0.05. On contrary, there is no significant difference on the compressive strength for the addition of HTN ($p = 0.12$), YEAST ($p = 0.99$) and BAC ($p = 0.27$), in comparison with REF.

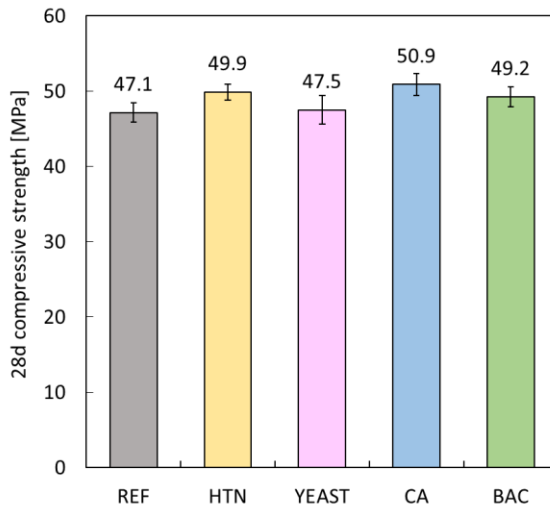


Figure 5-7. Compressive strength of all concrete mixtures

5.3.3 Bond-slip response of uncracked (UNCR) concretes

The bond behaviour of reinforcement with different concrete mixtures is presented in Figure 5-8. The bond-slip responses follow the trend as previously explained in Figure 5-4. As shown in Figure 5-8, the bond-slip responses of the REF mix had a good repetition within five specimens. The ultimate bond strength of the REF mix was in the range of 11–16 MPa. The introduction of HTN into the normal mix seems to give an improvement on the bond capacity as the average ultimate bond strength reached 17.10 MPa. Nevertheless, 2 out of 5 specimens gave exceptional low values which were comparable with the ultimate bond strength of REF mix. The addition of YEAST did not induce a noticeable enhancement on the bond strength as the ultimate bond strength was recorded at 15.28 MPa by average. Comparing the REF mix and the other two mixes of CA and BAC, the addition of these commercial agents considerably increased the bond strength. On the use of CA, a good repetition was achieved with the improvement of the ultimate bond strength by 57.1%, while with BAC, it was found to be 46.9%, with respect to REF.

In order to completely understand the results of ultimate bond strength, a one-way ANOVA and Dunnett's test were performed. The statistical analysis revealed that a significant difference was observed between REF–CA mixes ($p = 0.01 < 0.05$) and also REF–BAC mixes ($p = 0.03 < 0.05$). By using the

same level of significance (0.05), the p-values of REF–HTN and REF–YEAST were 0.55 and 0.98, respectively, indicating no significant differences on the bond strengths of reference mix and the mixes with the addition of biomasses. Thus, in this case, the addition of Penetron crystalline admixture gave the highest improvement on the bond strength, which is then followed by Basilisk bacteria healing agent. This may be attributed to the formation of a dense interfacial transition zone (ITZ) by the addition of specific healing agents into the mix, thus enhancing the bond between the concrete matrix and steel rebar.

Further investigation was done by analysing the other two parameters of interest so called mean bond strength and fracture energy. Figure 5-9 summarizes all important results based on τ_u , τ_m , and $E_{1.0}$. The mean bond strengths of REF, HTN, YEAST, CA and BAC mixes were 8.30, 15.86, 12.93, 19.42 and 19.25 MPa, respectively. Although the initial result revealed no significant difference on the use of biomasses, these agents interestingly gave a better improvement in terms of mean bond strength. The results based on fracture energy showed the same trend as on ultimate bond strength with CA being the promising agent to improve the bond strength amongst other agents studied in this research. In general, the trend of bond improvement was in line with the observation based on the result of compressive strength.

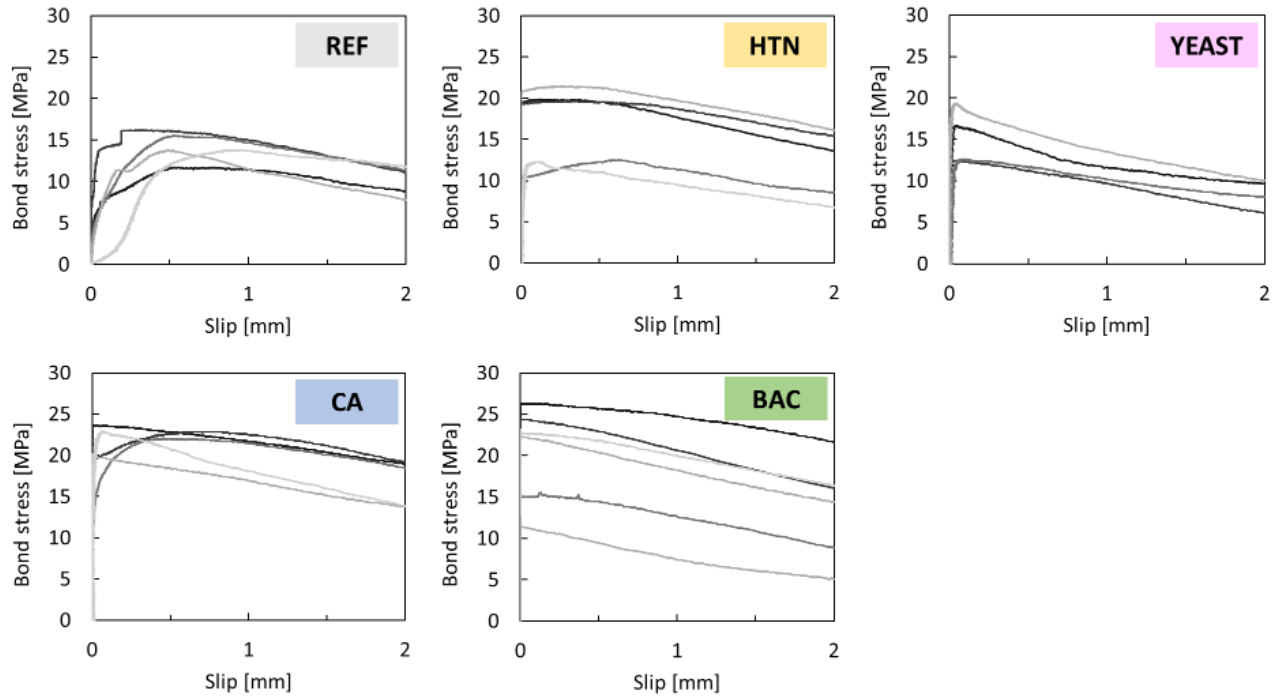


Figure 5-8. Bond-slip responses of uncracked concrete with different healing agents

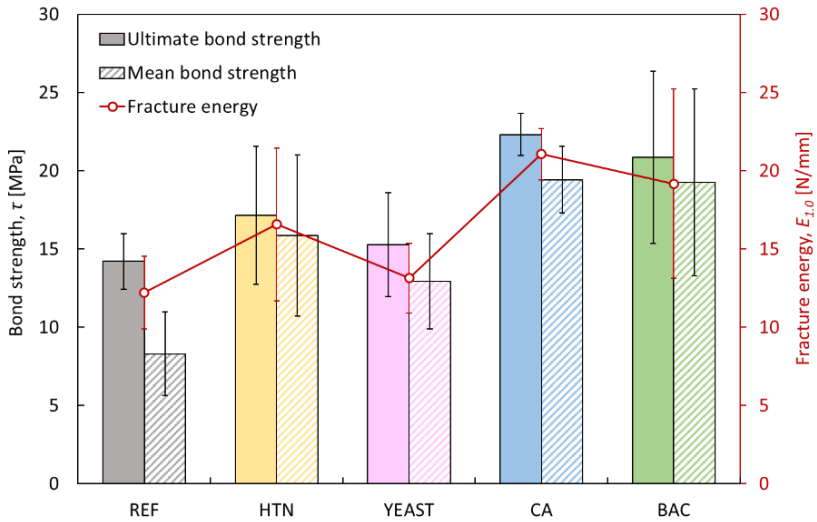


Figure 5-9. Comparison of different bond parameters based on the addition of healing agents

Concrete fragments were later taken from each mixture and scanning electron microscopy (SEM) (PhenomXL Desktop SEM, Thermo Fisher Science, US) was conducted to monitor the microstructure of the concrete via a secondary electron detector (SED). Figure 5-10 shows the microstructure of reference and self-healing concretes. It is seen that there was a modification of microstructure with the introduction of CA and BAC (as compared with REF) where a massive needle-like structure formed in the matrix. However, this observation was not found in HTN and YEAST concretes, rather their microstructures were similar to REF. Figure 5-11 also shows the void-filling effect by the inclusion of CA and BAC. Therefore, the modification of microstructure and filling effect of CA and BAC seems contributing to the improvement of the hardened concrete properties which supports the results from the compressive strength and bond strength.

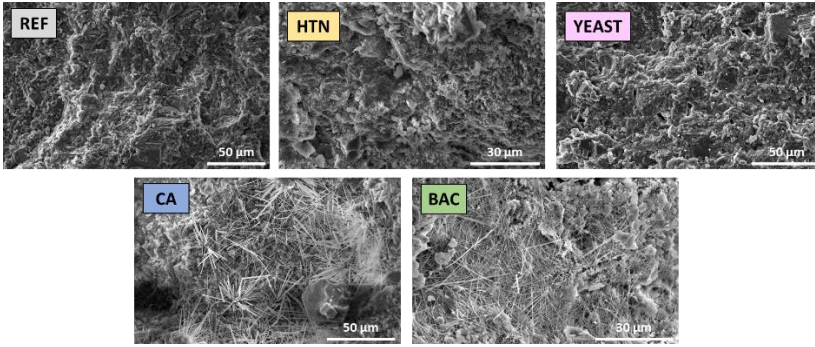


Figure 5-10. Microstructure of self-healing concrete

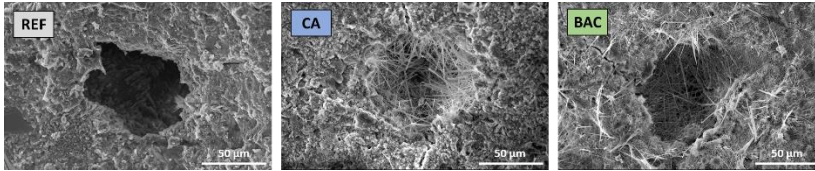


Figure 5-11. Void-filling effect of self-healing concrete containing CA and BAC

According to past studies [152–154], the bond strength is closely related to the square root of the concrete compressive strength called the normalized bond ratio ($\tau_u/(f'_c)^{1/2}$) and this relationship can be drawn as presented in Figure 5-12. Adjusted R-squared (R_{adj}^2) was used in order to evaluate the corrected goodness-of-fit of the linear model. With a fairly good result, the ultimate bond strength can be predicted as a function of compressive strength as follows:

$$\tau_u = 26.57\sqrt{f'_c} - 167.91 \quad (5.1)$$

A relationship between ultimate bond strength, mean bond strength and fracture energy can be constructed as shown in Figure 5-13. It is clear that there is a strong relationship ($R_{adj}^2 \geq 0.84$) to define the mean bond strength and fracture energy as a function of ultimate bond strength as proposed below.

$$\tau_m = 1.25\tau_u - 7.27 \quad (5.2)$$

$$E_{1.0} = 1.07\tau_u - 2.73 \quad (5.3)$$

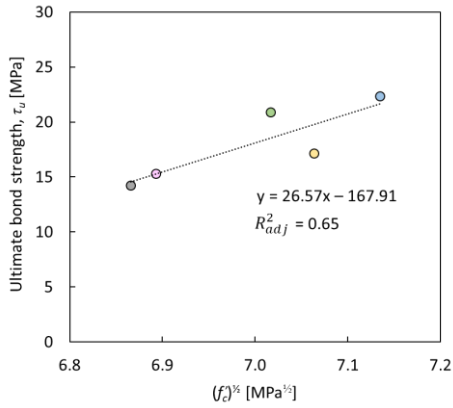


Figure 5-12. Relationship between the average ultimate bond strength and square root of average compressive strength

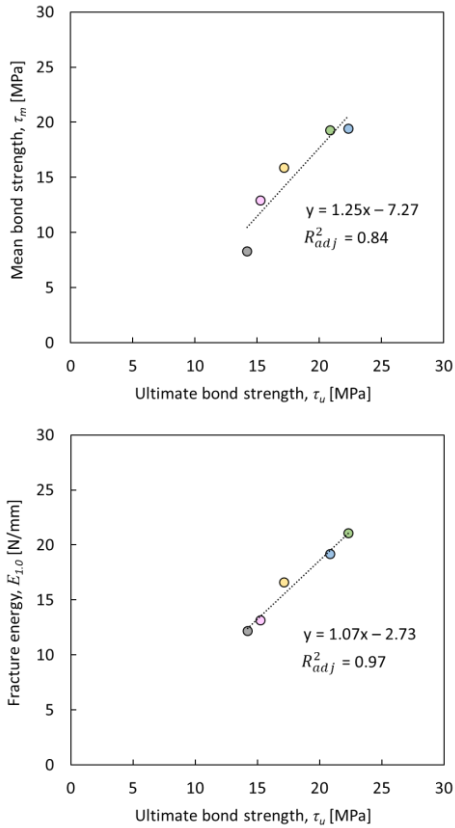


Figure 5-13. Relationship between ultimate bond strength, mean bond strength and fracture energy

The aforementioned results from the compression and pull-out tests suggested no detrimental effect of the addition of healing agents to the hardened concrete (in uncracked state) as a slight increase of compressive strength and a meaningful bond strength improvement were found. For CA, there are three potential reasons to explain the strength improvement: (1) the filling effect of CA [65,66], (2) the role of CA as cement hydration activator [68] and (3) the production of calcium carbonate by CA in the concrete matrix [74]. García-Vera et al. [4] supported the finding where the crystalline products filled and plugged the pores, capillaries and microcracks of the cementitious materials. In case of BAC, the reasons for strength enhancement may be attributed to the effect of calcium lactate. Many studies [15,32,33,42,86,87] have demonstrated the positive outcome of utilizing this type of nutrient and the addition of calcium lactate to the cementitious composite tended to increase the compressive strength. There are three possible reasons to explain this behaviour: (1) Ca^{2+} ions from calcium lactate contribute to the generation of calcium silicate hydrate, calcium hydroxide and calcium carbonate through hydration and carbonation reaction [86], (2) these reaction by-products help in filling the pores in concrete [32,87], and (3) calcium lactate as organic precursor densifies the internal structure of concrete [33,87]. Considering the HTN and YEAST, there is no significant effect on the compressive and bond strengths. It should be noted that these biomass agents are not developed to increase the strength, but rather to promote a robust autonomous healing mechanism.

The last parameter of slip corresponding to ultimate bond strength, S_u , was also analysed and the result was depicted in Figure 5-14. Apparently, there was a high variation on the S_u values. It was also initially observed in Figure 5-8 that the bond-slip responses were not always constant and the maximum bond stress occurred at a slip with a relatively different value. For instance, on REF mixes, the S_u happened at 0.47 ± 0.09 mm which were comparable. However, for other mixes, the slips occurred sometimes close to 0 mm, meaning that once the bond interface between reinforcement and concrete matrix went off at a maximum stress level, the reinforcement bar suddenly slipped. This can be explained because the slip was measured in the passive phase which only starts having movements after the bond surface shows degradation. On top of that, the relationship between the maximum bond stress and slip in all specimens may demonstrate a logical brittle behaviour when the strength increases by generating an abrupt failure. Moreover, the softening phase after reaching the peak stress was able to be controlled, indicating a good repeatability of the test responses.

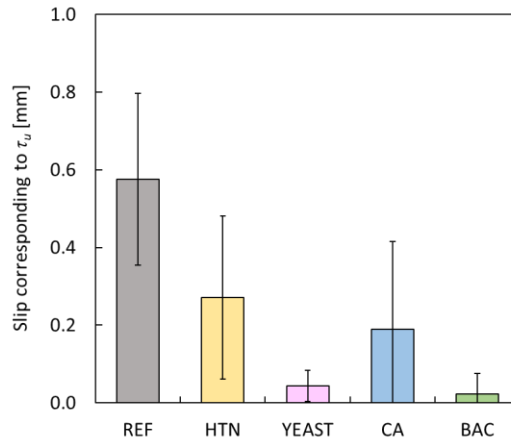


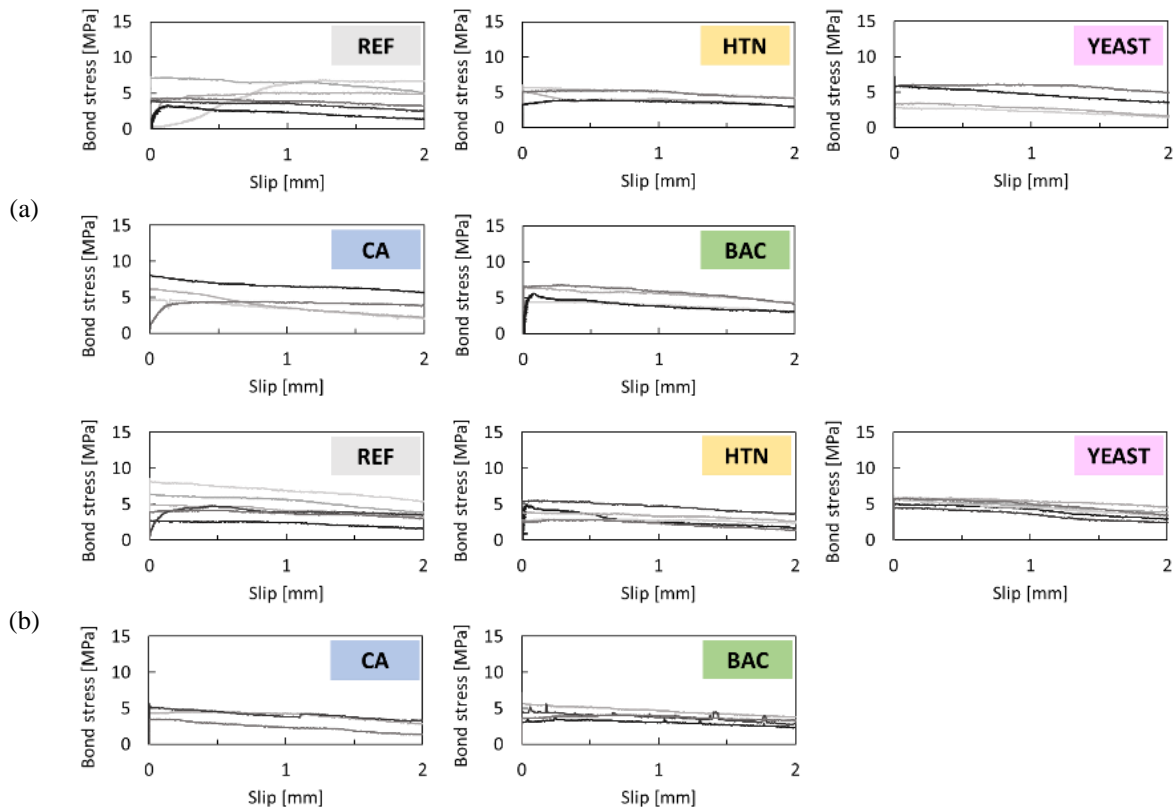
Figure 5-14. Slip corresponding to ultimate bond strength

5.3.4 Bond-slip response of cracked (CR) concretes

The hardened concretes, cracked at 49 days with different crack widths, were subjected to pull-out tests in order to evaluate the effect of splitting cracking on the bond behaviour with respect to uncracked concrete. Figure 5-15 shows the bond-slip responses of cracked concrete with a specific crack width range from 200–300, 300–400 and 400–500 μm . It is clear that there is a significant difference between the bond stress-slip responses of uncracked and cracked concretes. In case of concrete in cracked condition, the bond-slip curves were relatively low, indicating a significant reduction of bond strength and the bond brittleness. At first, it was expected that the increase of crack width will cause a gradual reduction of bond strength. However, our results interestingly showed that the ultimate bond strengths were relatively similar regardless variations on crack width range as well as addition of different healing agents. Nevertheless, the cracking phenomenon still causes a critical effect on the bond performance. This finding contradicts with a study by Mousavi et al. [142] where they found a gradual reduction of bond strength with increasing crack width. This may be attributed to the fact that different mix designs, a different pull-out test setup and cracking method were used.

Figure 5-16(a) summarises the results of ultimate bond strength of cracked concretes (CR series). Generally, 60–80% strength reduction was observed on the bond performance of the cracked concrete with respect to the uncracked one. Desnerck et al. [148] in their study also found a 44% bond

strength reduction for specimens having a single crack even with a small crack size between 10–70 μm , while for double cracked specimens, the reduction reached 54%. Apparently, in this study there is no clear tendency on the effect of healing agents on the bond strength of cracked concretes. This implies that the combined effect of the crack and the confining tube is much higher than the effect of the healing agents' addition. It is logic that no effect of healing agents can be found at this stage because the specimens were just cracked, thus the healing activation was not yet started. Moreover, statistical tests were conducted to validate the variation within the obtained results. It was confirmed that there is no significant difference of ultimate bond strength within the groups of cracked concretes with the sizes of 200–300 μm ($p = 0.75 > 0.05$), 300–400 μm ($p = 0.36 > 0.05$) and 400–500 μm ($p = 0.07 > 0.05$); and also no significant difference between all cracked concretes regardless of their crack sizes ($p = 0.17 > 0.05$). The results based on τ_m (see Figure 5-16(b)) and $E_{1.0}$ (see Figure 5-16(c)) exhibited similar responses as the ultimate bond strength. No effect of the crack size on τ_m and $E_{1.0}$ of CR concretes was detected as the τ_m values stayed below 10 MPa and the $E_{1.0}$ were below 10 N/mm. As shown in Figure 5-16(d), there was, also for the cracked concretes and regardless of the crack sizes, a high variation on the S_u of rebar as has been previously discussed for the uncracked series.



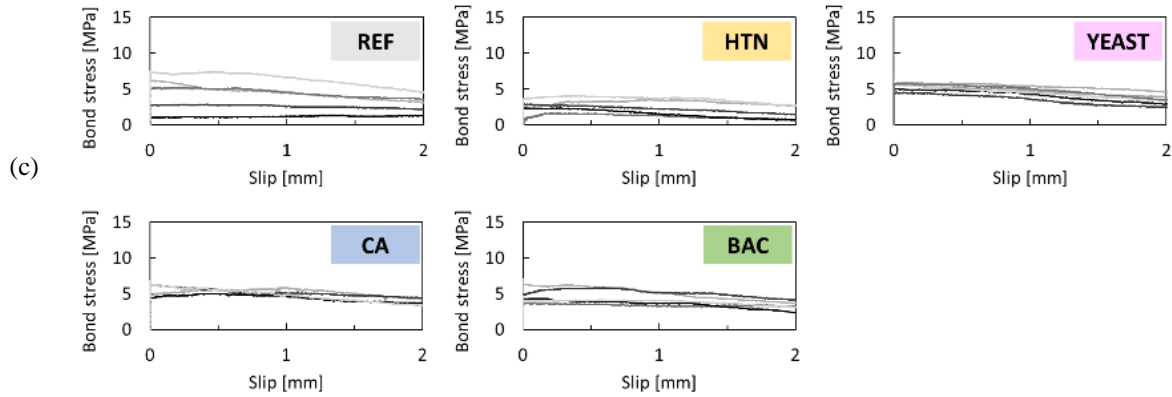
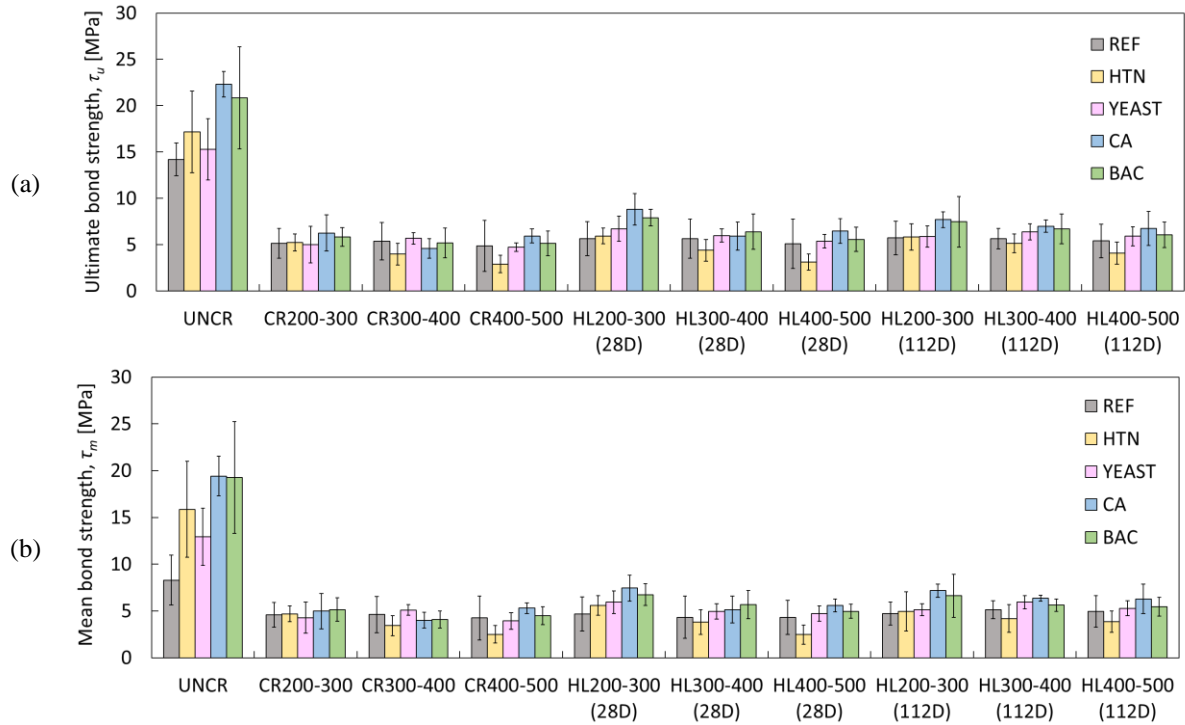


Figure 5-15. Bond-slip responses of cracked concrete with a specific crack width of (a) 200–300 μm , (b) 300–400 μm and (c) 400–500 μm



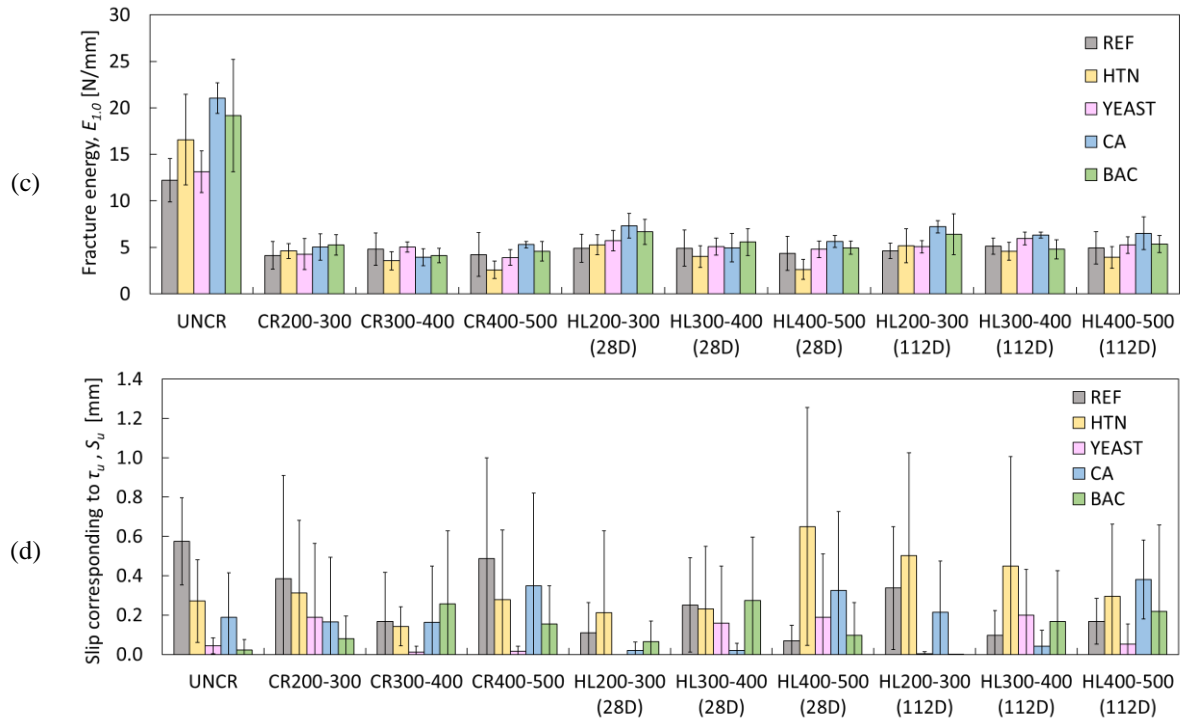


Figure 5-16. (a) Ultimate bond strengths, (b) mean bond strengths, (c) fracture energy and (d) slips corresponding to the ultimate bond strength of all series of specimens

To better understand the relation between the results of cracked and uncracked concrete, a bond-reduction factor (BRF) is defined as follows:

$$BRF = \frac{\tau_{u_CR}}{\tau_{u_UNCR}} \quad (5.4)$$

According to literature, the bond reduction factor is described as a function of the ratio of crack width-to-rebar diameter, cw/d_b . Based on the data series collected from bond-slip responses (Figure 5-15), a relationship between BRF and cw/d_b is established for different healing agents as illustrated in Figure 5-17. Logarithmic regression was selected as the best fitting curve for all mixes. The regression employed on this current data was compared with existing models from the literature database as shown in Figure 5-18. Based on the current data, a similar trend can be observed following the models from Idda [155] and Purainer [156]. However, the trend is apparently far from the other models from Gambarova et al. [157,158], Mahrenholtz [159] and Mousavi et al [160]. This may be attributed due to the fundamentally different approaches used by each author. As reported by [151], a significant scatter arose amongst the proposed models which is justified by the fact that the available equations mainly have an empirical background, thus depending mostly on the performed test, a customized test setup, consideration of several rebar types, embedded region of rebar, concrete type, etc. The stiffness of the confining tube can be also an influential factor to be considered in determining the relationship between cw/d_b and BRF. Furthermore, based on Figure 5-17 and Figure 5-18, it seems that there is a sudden fall of BRF as soon as a small crack appears on the concrete. Although there are no data points available for cw/d_b below 0.02 in our study, it has been previously confirmed by [148] that minor cracks of 30–40 μm in width caused 44% reduction on the bond strength. It indicates that even a small crack on concrete will strongly affect the bond strength. From Figure 5-17, the REF and YEAST mixes gave similar trend, while another similar trend with lower values was observed on HTN, CA and BAC mixes. Nevertheless, judging by the slopes of the trendlines for all mixes within the crack width ranges studied (200 to 500 μm), the slopes were relatively identical with the value of 3.36–3.97. This supports the aforementioned finding that there is no significant difference on bond strengths for cracked concretes within the crack width range of 200–500 μm .

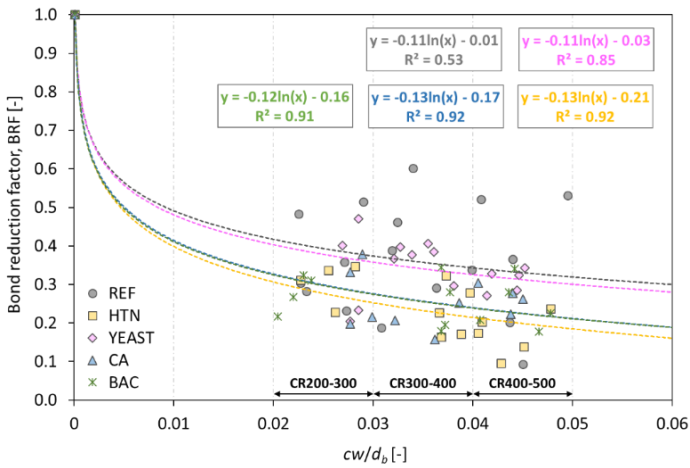


Figure 5-17. Bond reduction factor as a function of the ratio of crack width-to-rebar diameter

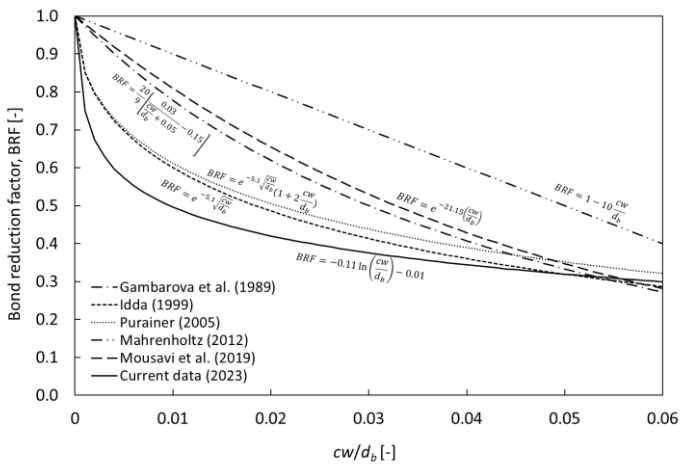


Figure 5-18. Reduction of BRF with increasing cw/d_b as compared with existing models

5.3.5 Phenomenon of crack closure

Before pull-out tests were executed on a series of HL specimens, a visual inspection and microscopic observation were done to understand the self-healing effect. Figure 5-19(a) shows four examples of REF specimens with the appearance of healing products on the crack mouth after undergoing a 28

days of healing under water. Interestingly, even without the use of any healing agents, the autogenous healing seemed quite robust. Although the cracks were not fully closed, at this stage, the healing products already covered a portion of the crack lines.

Figure 5-19(b) shows a typical formation of healing products at the crack mouth on the use of different healing agents after 28 days of healing. On the REF specimens, healing products were formed but with a relatively low density. Based on a visual inspection conducted by the author, the healing products could be easily broken and the crack was not really filled with the precipitation. Potentially it indicates that the autogenous healing process was relative slow (during short healing of 28 days), and the precipitation was not quick enough to completely fill the crack. So the healing efficiency can be improved by adding healing agents to boost the healing process. It was also found that on REF specimens, the healing products existed in the form of fine granulates, expected to be calcium carbonate (CaCO_3). On the use of biomass agents such as HTN and YEAST, a clustering of healing products was visible near the crack mouth. However, the structure of these products was similar as for the REF specimens. There was a high discrepancy with the healing products formed in the CA and BAC specimens as there were many stalactites formed at the crack mouth (see Figure 5-19(b)). Based on author's inspection, the stalactites were relatively sturdy. Although the CA and BAC are completely different materials (one with crystalline admixtures and another one with bacterial spores), they induce a prominent effect in terms of crack closure by a high precipitation of healing products. This may confirm that the PLA particles of BAC agent were broken during cracking by releasing dormant bacteria to produce calcium carbonates from the metabolic activation.

Figure 5-19(c) shows the evolution of healing products after undergoing a long healing period up to 112 days. On REF specimens, it seems that the healing products were much denser than the ones observed after 28 days (see Figure 5-19(a,b) – REF). On the use of HTN and YEAST, interestingly, there was an evolution of the minerals coming out from the crack from the short to the long healing period. After 112 days of healing, long stalactites were massively formed in most of the specimens. It can be associated with a strong production of minerals at later time as this observation was not apparent during a short healing time (see Figure 5-19(b,c) – HTN, YEAST). More formations of stalactites along the crack lines were observed on CA and BAC specimens after a long healing. An observation by optical microscope was also done as shown in Figure 5-20. In general, when a crack was limited to around 200–300 μm in width, the healing products were precipitated

abundantly by overfilling the crack and it completely blocked the crack. When the crack was made bigger, having a width of 300–400 or 400–500 μm , the cracks were not completely healed but a sufficient amount of precipitation was observed.

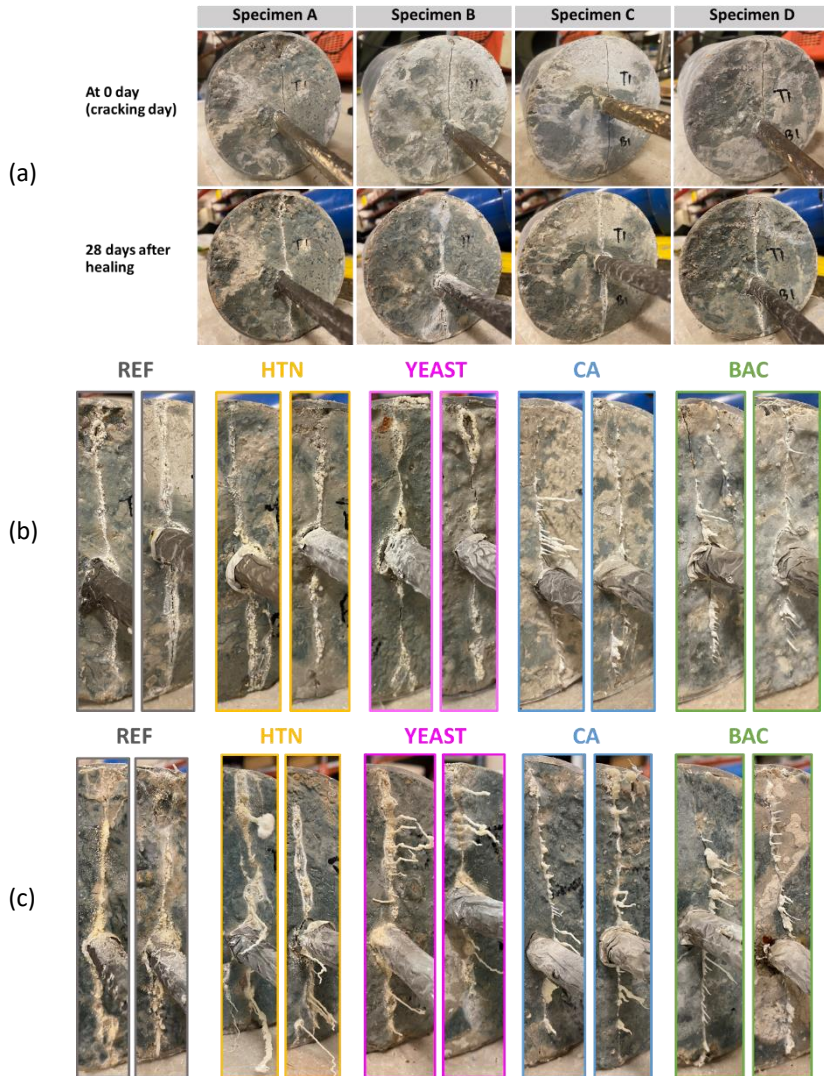


Figure 5-19. (a) Self-healing phenomenon by the deposition of healing products in the cracks of REF specimens, and typical formation of healing products coming out from the crack observed after (b) 28 days and (c) 112 days of healing

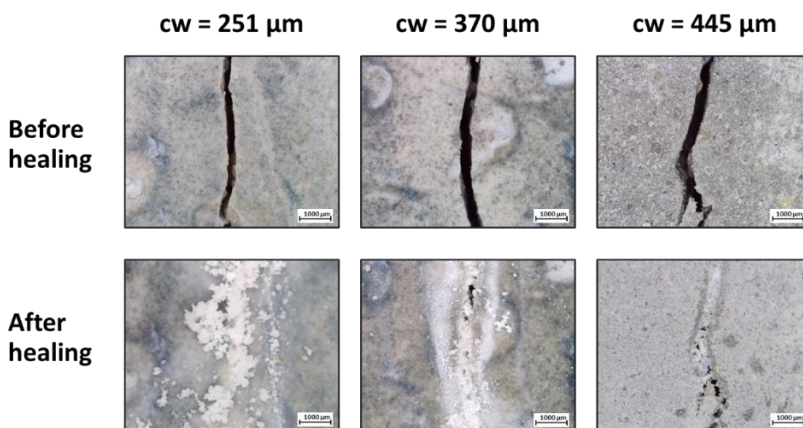


Figure 5-20. Observation of crack closure by means of microscope

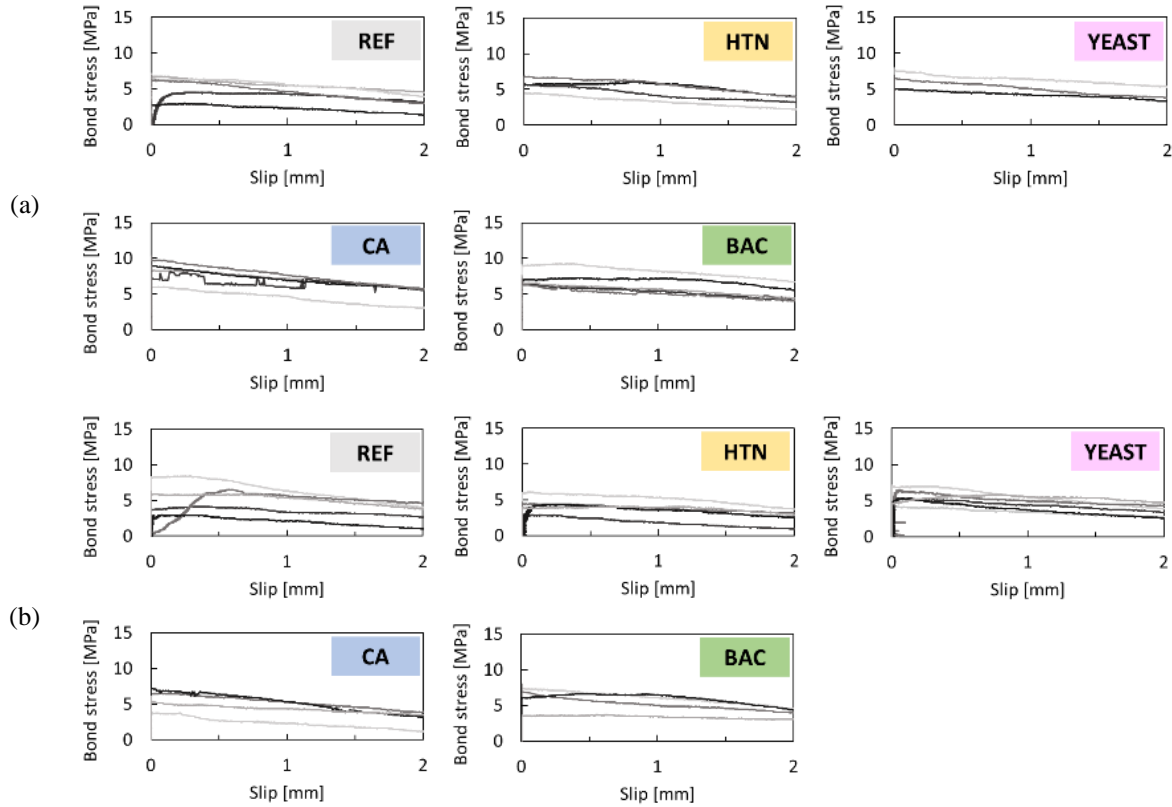
5.3.6 Bond-slip response of healed (HL) concretes

The pull-out tests on HL specimens after 28 days of healing were performed and the bond-slip responses with a specific healed crack width between 200–300, 300–400 and 400–500 μm are illustrated in Figure 5-21. Similarly like CR concrete series, the bond-slip curves were still relatively low showing the bond strength mostly went under 10 MPa. At least three repetitions were tested on each series and the results were relatively comparable. However, a research question comes whether there is a bond improvement due to the self-healing effect. To understand about the outcomes, the ultimate bond strengths from Figure 5-21 are summarized in Figure 5-16(a). A one-way ANOVA was performed to analyse the variations among the obtained results. Unlike the group series of CR200-300, statistical analysis revealed that there was a significant difference among HL200-300 series ($p = 0 < 0.05$). Based on Dunnett's test, it was found that the comparison between REF and CA mixes showed a statistically significant difference with the p-value of 0.01 (level of significance = 0.05). The HTN, YEAST and BAC mixes did not show a significant difference with respect to REF mix with the p-values of 0.99, 0.71 and 0.07, respectively. Afterwards, the group series of HL300-400 and HL400-500 were also checked by ANOVA and it was reported that there were no significant differences amongst these groups. The result suggests that only the inclusion of CA improves the bond strength of healed concrete with a relatively small crack width in the range of 200–300 μm ($\bar{\tau}_u = 8.8 \text{ MPa}$), as compared with reference healed concrete

with the same crack size ($\bar{\tau}_u = 5.7$ MPa). In case of bigger healed cracks (300–500 μm), the addition of healing agents seems not to improve the bond strength with respect to the REF mix.

The final pull-out tests with the last series of HL specimens after being healed for 112 days were executed and the bond stress-slip behaviour can be found in Figure 5-22. The curves still stayed low, specifically below 10 MPa. Similarly like HL (28D) series, it seems that a long healing did not change the ductility of the healed specimens. The ultimate bond strengths of the HL (112D) specimens series are recorded in Figure 5-16(a). Initially, ANOVA was conducted on each crack size group i.e. HL200-300 (112D), HL300-400 (112D) and HL400-500 (112D) and the statistical analysis revealed that no significant differences were found among all healed specimens regardless of their crack size ($p\text{-value} = 0.07 > 0.05$). The results based on the mean bond strength, fracture energy and slips of rebar in all healed concretes can be found in Figure 5-16(b-d). In general, both τ_m and $E_{1,0}$ followed the same trend as the responses of τ_u , in the same way as UNCR and CR series. The S_u of rebar also varied in healed concretes and there was no clear relationship of the slip in relation to the cracking and healing.

The bond-reduction factor (BRF) can also be calculated by using Equation (5.4) on healed specimens by adopting the $\bar{\tau}_u$ and $\bar{\tau}_m$ values, and the results are presented in Table 5-2 and Table 5-3, respectively. After 28 days of healing, the BRF of cracked concretes slightly increased with a maximum increment of 0.11 for $\bar{\tau}_u$ and 0.13 for $\bar{\tau}_m$. In most cases, an insignificant improvement of BRF in the range of 0.01–0.06 was noticed. Furthermore, a noticeable increment of BRF was observed on the use of YEAST, CA and BAC in the series of HL200-300 (28D) specimens. It may indicate that these three agents may be effective to slightly improve the ultimate bond strength of healed concrete with small cracks up to 300 μm in comparison to cracked concrete. Nevertheless, the BRF values of healed concretes after 112 days of healing were, in most cases, comparable to the BRF values of HL concrete after 28 days of healing. This means that a long healing time could not help to strongly recover the bond strength.



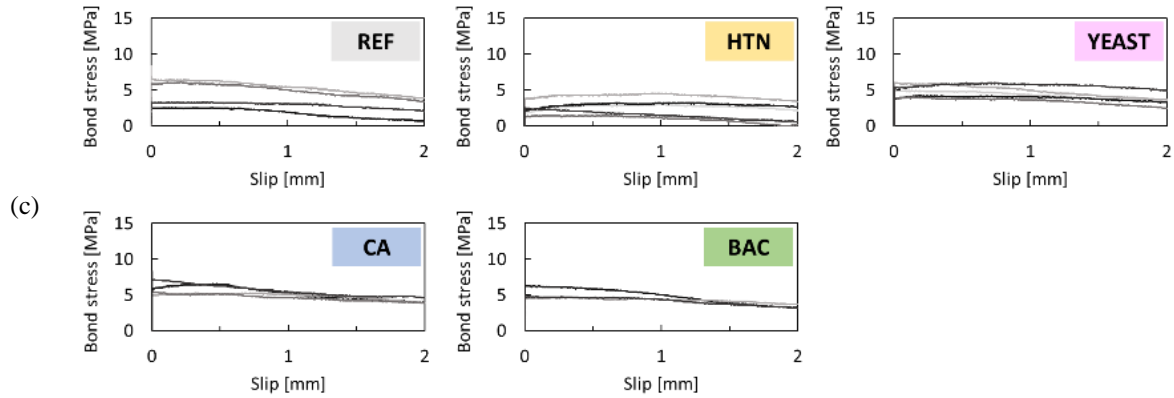
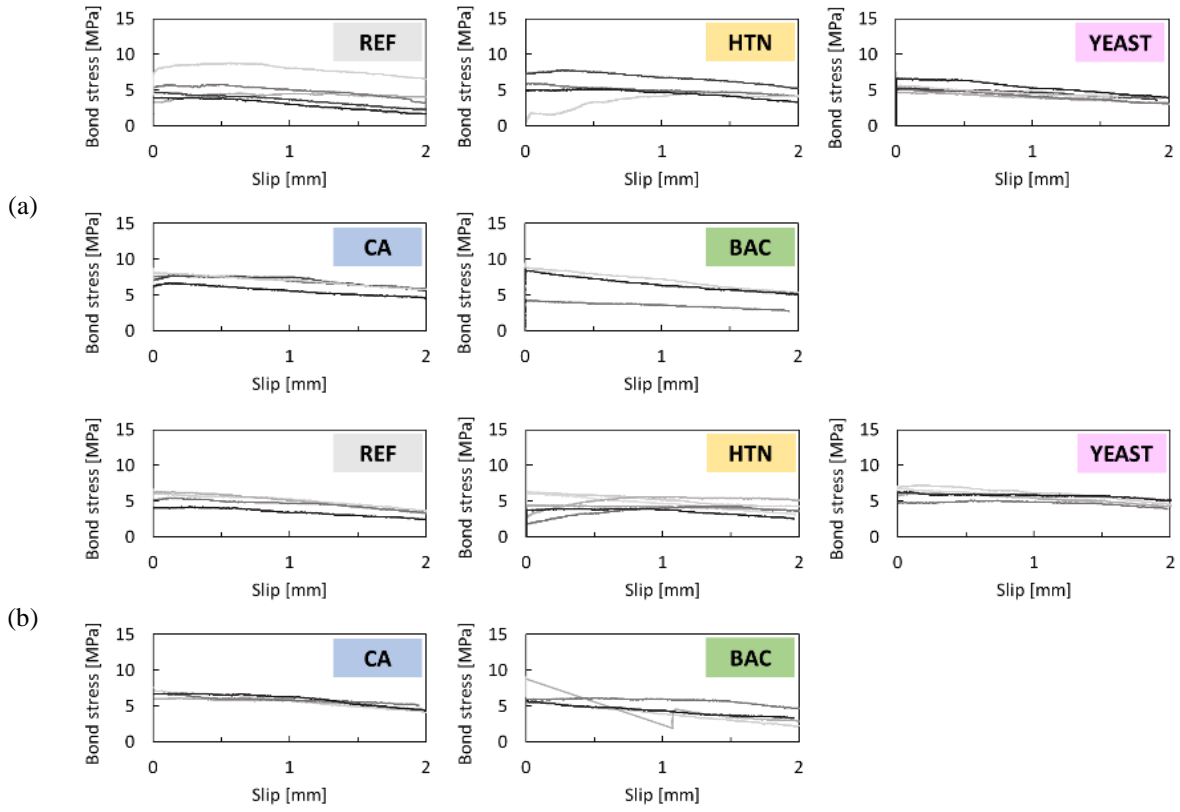


Figure 5-21. Bond-slip responses of 28d-healed concrete with a specific crack width of (a) 200–300 μm , (b) 300–400 μm and (c) 400–500 μm



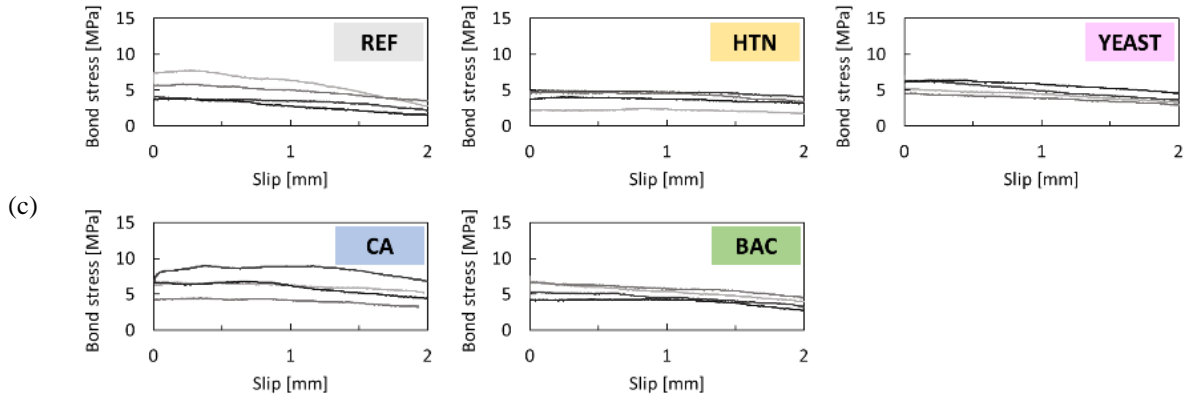


Figure 5-22. Bond-slip responses of 112d-healed concrete with a specific crack width of (a) 200–300 μm , (b) 300–400 μm and (c) 400–500 μm

Table 5-2. Comparison of BRF on different states of concrete (based on $\bar{\tau}_u$ values)

Crack width:	200–300 μm			300–400 μm			400–500 μm		
Series:	CR	HL (28D)	HL (112D)	CR	HL (28D)	HL (112D)	CR	HL (28D)	HL (112D)
REF	0.36	0.40	0.40	0.38	0.40	0.40	0.34	0.36	0.38
HTN	0.31	0.35	0.34	0.23	0.26	0.30	0.17	0.18	0.24
YEAST	0.33	0.44	0.38	0.37	0.39	0.42	0.31	0.35	0.39
CA	0.28	0.39	0.35	0.21	0.27	0.31	0.27	0.29	0.30
BAC	0.28	0.38	0.36	0.25	0.31	0.32	0.25	0.27	0.29

Table 5-3. Comparison of BRF on different states of concrete (based on $\bar{\tau}_m$ values)

Crack width:	200–300 μm			300–400 μm			400–500 μm		
Series:	CR	HL (28D)	HL (112D)	CR	HL (28D)	HL (112D)	CR	HL (28D)	HL (112D)
REF	0.55	0.56	0.57	0.56	0.52	0.62	0.51	0.52	0.60
HTN	0.30	0.35	0.31	0.22	0.24	0.26	0.16	0.16	0.24
YEAST	0.33	0.46	0.40	0.39	0.38	0.46	0.30	0.36	0.41
CA	0.26	0.38	0.37	0.21	0.26	0.33	0.27	0.29	0.32
BAC	0.27	0.35	0.34	0.21	0.30	0.29	0.23	0.26	0.28

Moreover, based on all aforementioned results observed on three different conditions (cracked and healed after 28 days and healed after 112 days), the developments of the ultimate bond strength and the mean bond strength in function of healing time can be constructed as presented in Figure 5-23. As a note, the relationship between fracture energy and healing time is not presented as the result follows the same agreement as the recovery of ultimate bond strength and mean bond strength. From Figure 5-23, there were large variations in all results as the areas of standard deviations overlapped on top of each other's results. This was previously detected by the ANOVA analysis where there were no significant differences among CR, HL (28D) and HL (112D) series. Nevertheless, it is interesting to evaluate the tendencies of the results based on the average values.

- Based on Figure 5-23(a), in case of REF, the $\bar{\tau}_u$ was relatively constant starting from the cracking day (0 day of healing) to 112 days of healing with the values from 5.1 to 5.6 MPa. In case of HTN, the $\bar{\tau}_u$ values were always lower than REF, but it possessed a bond strength recovery. The bond strength slightly increased with increasing the healing time and this can be established with a linear relation. In case of YEAST, there was also a little bond strength recovery from 5.2 (0 day) to 5.9 MPa (28 days). However, above 28 days, it seems that the $\bar{\tau}_u$ remained constant. After 112 days of healing, the $\bar{\tau}_u$ was approximately 6.0 MPa. Interestingly, there was a better increment of the $\bar{\tau}_u$ from 0 to 28 days which was attained by CA and BAC, as compared with other mixtures. The $\bar{\tau}_u$ values were slightly recovered from 5.7 to 7.2 MPa and 5.4 to 6.8 MPa for CA and BAC, respectively. Similarly like YEAST, when the healing time was prolonged to 112 days, there was no further bond recovery above 28 days both for CA and BAC. Eventually, the precipitated healing products, previously shown in Figure 5-19(c), could not be an indication of the bond recovery of the steel reinforcement in the healed concrete although it possessed the crack closure ability.
- Based on Figure 5-23(b), in general, the recovery of the $\bar{\tau}_m$ follows a similar trend as the $\bar{\tau}_u$ (Figure 5-23(a)). In case of REF, there was no recovery of the $\bar{\tau}_m$ after a short healing (28 days). Nevertheless, a scant increase of $\bar{\tau}_m$ was found from 28 to 112 days. The $\bar{\tau}_m$ recovery of HTN was pronounced where the $\bar{\tau}_m$ increased linearly from 3.5 (0 day) to 4.3 MPa (112 days). However, the $\bar{\tau}_m$ of HTN was found to be lower than REF. Similarly like HTN, YEAST also promoted a $\bar{\tau}_m$ recovery from 4.5 (0 day) to 5.1 MPa (28 days) after a short healing, and with a longer healing time (112 days), the $\bar{\tau}_m$ slightly increased up to 5.5 MPa. A notable bond

strength recovery was found after a short healing on the use of CA and BAC. The $\bar{\tau}_m$ slightly improved from 4.8 to 6.2 MPa (for CA) and from 4.6 to 5.9 MPa (for BAC). Apparently, BAC did not show any further recovery after the healing time was prolonged to 112 days. In contrast, CA showcased a further bond recovery after 112 days with the $\bar{\tau}_m$ of 6.6 MPa (6% improvement as compared with $\bar{\tau}_m$ after 28 healing days).

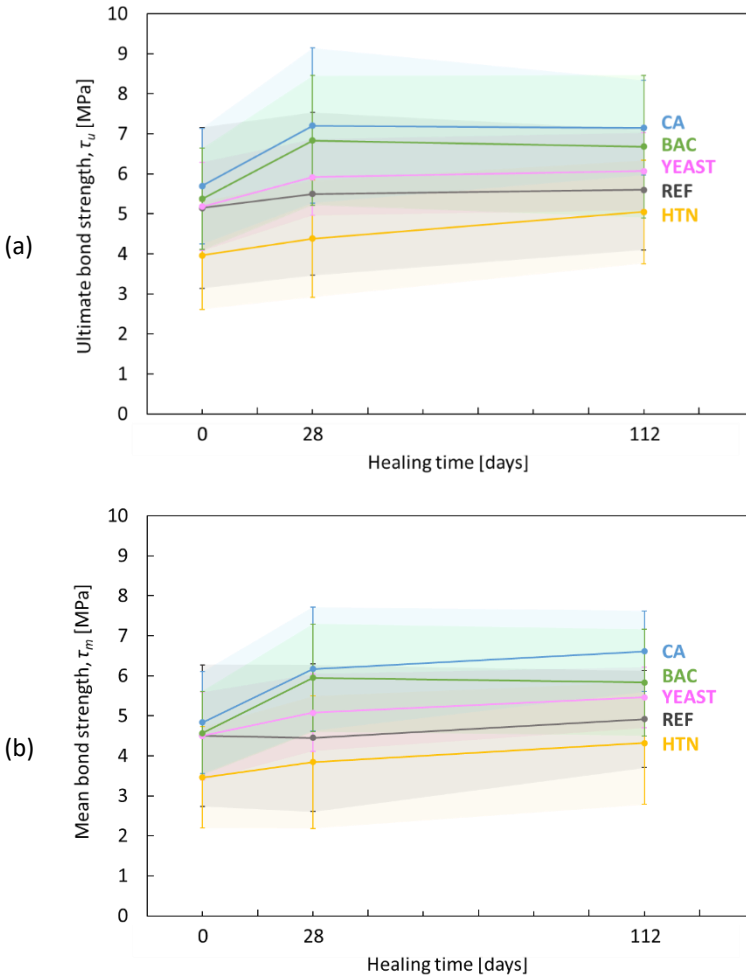


Figure 5-23. Development of the recovery of (a) the ultimate bond strength and (a) the mean bond strength in function of healing time

5.3.7 Failure mode

In general, there are two failure modes for pull-out specimens namely pull-out failure and splitting failure. In this study, the pull-out failure always occurred on UNCR specimens as shown in Figure 5-24(a), while splitting failure occurred on CR and HL specimens regardless the size of the crack width (see Figure 5-24(b)). The pull-out failure on UNCR has been estimated during the design stage with the use of a sufficient concrete cover ratio (c/d_b) at 5.25. Desnerck et al. [148] studied the effect of concrete cover ratio towards the failure mode of specimens and it was reported that for a cover $c/d_b = 2.5$, the failure mode of uncracked concrete shifted from a pull-out failure to a splitting failure. When a bigger cover was used ($c/d_b = 4.8$ based on [148] or 7.5 based on [160]), the pull-out failure for uncracked concrete always occurred. In addition, when the concrete cover ratio was reduced from 4.8 to 2.5 mm, the residual bond strength after cracking was reduced as well [148]. The failure of CR specimens was always splitting because the specimens were just split by the Brazilian splitting test at the same day as the pull-out test, so no failure shifting was expected. On HL specimens, it was also noticed that the splitting failure constantly happened. Figure 5-24(c) shows the condition of a HL specimen before and after a pull-out test. It was obvious that the precipitated healing products, which originally healed or closed the crack, broke during the pull-out test resulting in a re-opening of the existing crack. This may indicate that the healing products are not strong enough to sustain the tensile stress and they are not able to transform the failure mode from splitting failure to pull-out failure.



(a)



(b)



(c)

Figure 5-24. (a) Pull-out failure on UNCR specimens, (b) splitting failure on CR and HL specimens, and (c) the breakage of healing products on a healed crack due to splitting failure during a pull-out test (left: before testing, right: after testing)

The failure mechanisms of uncracked, cracked and healed concretes can also be potentially identified at rebar surfaces on the bonded region as demonstrated in Figure 5-25. The rebars bounded to the specimen were completely pulled out and the level of concrete shear-off can be clearly seen. On the UNCR specimens, there was a high shearing off of the concrete on the ribs of the rebars. In case of CR specimens, the failure was more like a crushing of the concrete in shear due to the wedging action of the ribs as described by [161]. With the crack width of around 200–300 μm , the level of concrete shear-off was still relatively high but it is slightly lower than the uncracked series. However as increasing the crack width, the level of concrete shear-off was gradually decreased. This is evident on the pulled-out rebars from CR/HL400-500 specimens where a very low level of concrete shear-off on the ribs of the rebars was observed. It suggests that the bond between rebar and concrete is influenced by the crack width, where increasing the crack width will result in a gradual reduction of the bond system and the level of concrete shear-off on rebar surfaces.

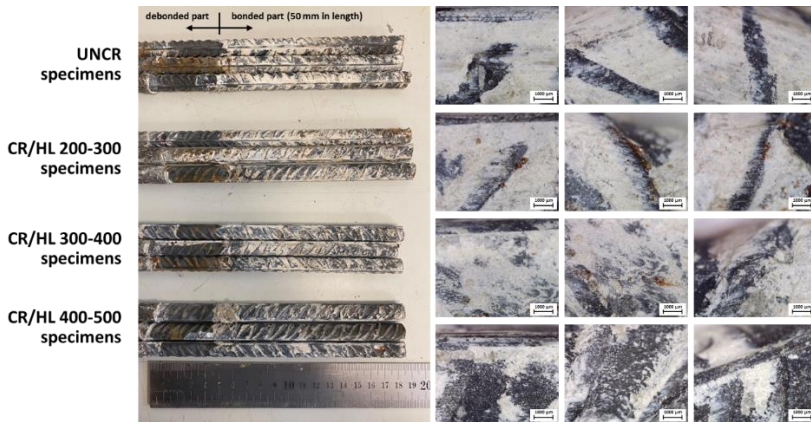


Figure 5-25. Concrete shear-off on pulled-out rebars

5.3.8 Characterization of healing products

An additional investigation was conducted to evaluate whether there is a formation of healing products inside the crack. In this case, a few healed specimens were prepared after being tested by pull-out tests. The PVC tube attached to the specimen was initially removed and then the specimen was carefully split into two parts by hand which turned into two sections: one section without rebar and another section with embedded rebar. An inspection of the healing products was executed by means of optical microscope on the crack plane by dividing into two different locations: (i) the crack at the top surface and (ii) the crack plane. Two observations were performed on the pull-out specimen, observations after being healed for 28 days and others after being healed for 112 days (see Figure 5-26). As shown in the figure, after the specimens were healed for 28 days, the healing products were obviously located at the crack as indicated by yellow lines. However, the healing products were hardly seen in the crack plane, meaning the healing products have not yet formed inside the crack after a short healing. After the healing was prolonged to 112 days, other pull-out specimens were split and Figure 5-26 shows a representative specimen. At the top crack as indicated by yellow lines, the healing products were still available. Interestingly, as highlighted in blue lines, the healing products were found in the crack plane, in a zone up to 20–50 mm from the bottom crack mouth. It confirms that the deposition of healing products also takes place inside the crack when the healing time is prolonged. It seems that the healing

products will be initially and actively formed from the crack mouth and then going deeper inside the crack.

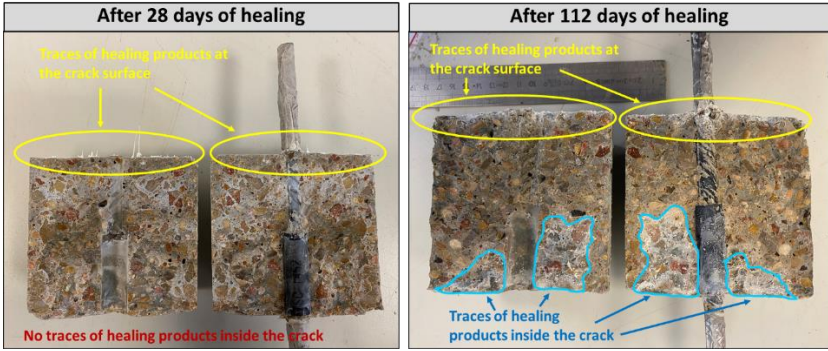


Figure 5-26. Inspection of healing products inside the crack of healed concrete

The healing products situated in the area of blue lines were observed by means of optical microscopy as shown in Figure 5-27 for all five mixtures. On the REF specimen, the white healing products had amorphous shape and they were in the form of fine granulates. In the case of the HTN specimen, the healing products were available in the form of needle-like crystals. The YEAST specimen had a similar form of healing products as the HTN specimen and they looked like crystal clear needles. The healing products of CA were also existing in the form of flowery needles and it seemed that the needles

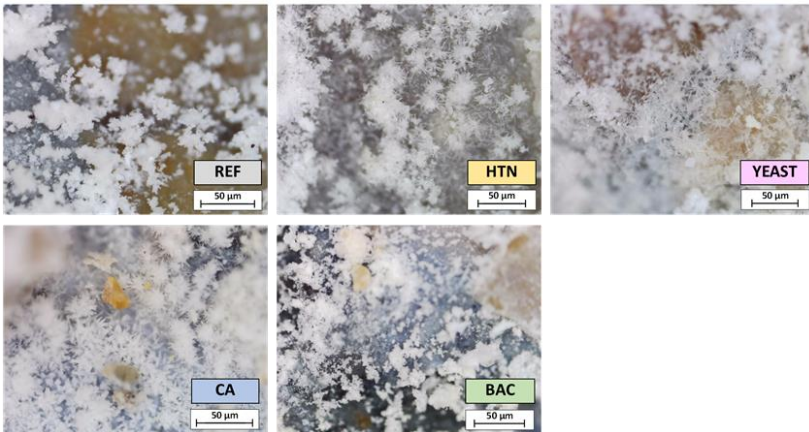


Figure 5-27. Observation of the structure of healing products by means of optical microscopy

were relatively thick by judging on how solid the white needles were, in comparison with crystal clear needles observed in HTN and YEAST specimens. On the other hand, the healing products found in BAC specimen were comparable as the REF specimen in the form of white fine granulates. Based on Figure 5-27, it is interesting to see that the structures of healing products were different depending on the selection of healing agent. In order to confirm this result, an additional test was performed to characterize the mineral compound and the morphology of the healing products by means of Fourier transform infrared (FTIR) spectroscopy (UATR Spectrum Two, PerkinElmer, US). Since only a low amount of healing products was found inside the crack, the healing products coming out from the crack (as previously shown in Figure 5-19(c)) were carefully scraped and collected, for each mixture.

The FTIR tests were carried out and the obtained results are depicted in Figure 5-28. The FTIR fundamental peaks from all mixtures showed the presence of calcium carbonates (CaCO_3) existing in different morphologies. In general, the CaCO_3 in the form of calcite has two absorption bands in the out-of-bending plane at 872 cm^{-1} and a double degenerate planar bending at 712 cm^{-1} [135,137–140]. Aragonite displays a characteristic symmetric carbonate stretching vibration at 1083 cm^{-1} , a carbonate out-of-plane bending vibration at 854 cm^{-1} and a double degenerate planar bending at 712 cm^{-1} [136,137,139,141]. Based on Figure 5-28, both REF and BAC mixtures had identical FTIR spectra, except one peculiar peak at 1005 cm^{-1} in BAC mixture. There was one shoulder peak around 900 cm^{-1} in BAC products that may confirm the presence of aragonite. Thus, there might be a formation of both calcite and aragonite in BAC products. It was revealed that the dominant healing products of REF and BAC were found to be calcite. Moreover, the healing products taken from HTN, YEAST and CA mixtures had very similar spectra and they were confirmed to be aragonite. The results based on the FTIR analysis (Figure 5-28) were in line with the observations of healing products via optical microscopy (Figure 5-27). Both results positively confirmed that the addition of BAC did not change the morphology of healing products from the reference concrete, while the addition of HTN, YEAST and CA modified the healing products from calcite (REF) to aragonite.

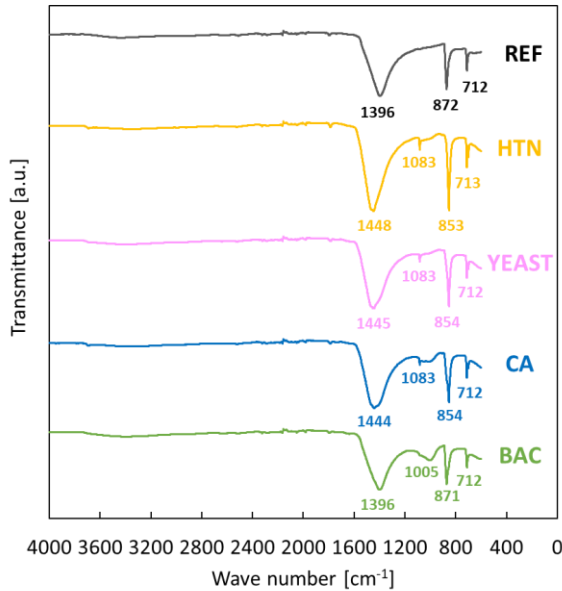


Figure 5-28. FTIR spectra of healing products from different mixtures

5.4 Conclusions

This chapter discusses the effects of several healing agents on the bond properties between steel reinforcement and self-healing concrete. Four healing agents were utilized namely two biomass agents (one containing a non-axenic bacterial consortium (called as HTN) and another one with a non-axenic fungal consortium (called as YEAST)) and two commercial agents namely Penetron Admix crystalline admixture (CA) and Basilisk bacteria healing agent (BAC). The fresh and mechanical properties of concrete mixtures were initially evaluated, and then pull-out specimens were fabricated. Three different conditions for pull-out specimens were defined: uncracked (UNCR), cracked (CR) and healed (HL). Both CR and HL series have three levels of interest namely crack width range of 200–300, 300–400 and 400–500 μm . On HL series, two healing periods were designed: a short healing period of 28 days and a long healing period of 112 days, both under full water immersion. Pull-out tests were eventually carried out on all series of specimens to determine the bond properties. The key findings of this extensive experimental investigation are summarized below.

1. The additions of HTN and CA reduced the workability of the normal concrete mixture, while the addition of BAC resulted in a more workable concrete. On the other hand, the introduction of YEAST did not change the consistency of the fresh concrete.
2. The compressive strength of normal concrete was increased by 8.0% with the addition of CA. The additions of HTN, YEAST and BAC slightly increased the compressive strength by 5.8, 0.8 and 4.4%, respectively. In a C30/37 concrete, a strength increment by 8% (in case of CA) will not change the concrete grade and this is an acceptable variability in a standard concrete production.
3. The highest improvement of the ultimate bond strength between steel reinforcement and concrete in uncracked state was achieved by the addition of CA (57% enhancement), and then followed by BAC (47% enhancement), with respect to the REF concrete. The addition of HTN and YEAST also possessed 21% and 7% ultimate bond strength increment, respectively.
4. The presence of a longitudinal crack strongly affected the bond strength and 60–80% of bond strength reduction was found with the crack size between 200 and 500 μm in width. There were no positive improvements on the bond strength of cracked concrete with the inclusion of healing agents with respect to the reference cracked concrete.
5. The healing agents used in this study tended to promote a little bond strength recovery after 28 days of healing (27, 27, 14 and 11% ultimate bond strength recovery with the addition of CA, BAC, YEAST and HTN, respectively). No clear self-healing recovery was further detected in the bond strength of steel reinforcement in healed specimens after 112 days of healing. Nevertheless, the effect of healing agents on the bond strength of reinforcement may vary depending on the size of the crack width that needs to be elucidated in further research.
6. Although no significant improvement in the bond strength recovery was found after healing, the phenomenon of crack closure by the formation of healing products was strongly evident. It positively opens the way to the durability protection.
7. The healing products of REF and BAC mixtures were confirmed to be calcite. The addition of other healing agents (HTN, YEAST and CA) modified the healing products from calcite crystals to aragonite crystals.

Chapter 6

OPTIMIZATION OF CONCRETE MIX DESIGNS TOWARD THE BOND PROPERTIES OF STEEL REINFORCEMENT IN SELF-HEALING CONCRETE BY TAGUCHI METHOD

6.1 Introduction

There are many possible ways to perform an optimisation of the mix designs based on the experimental and statistical approaches. The Taguchi method [162] is one of the robust techniques for optimising the performance characteristics through the setting of design parameters. In order to design efficient experiments, orthogonal arrays are implemented and the relationship among the experimental factors and their levels can be investigated [163]. The Taguchi method analyses the results based on the signal-to-noise (SN) ratio for process optimization. The SN ratios take into account both the variability in the response data and the closeness of the average response to the target [164]. The Taguchi method has been frequently applied in the field of concrete technology for optimisation purpose. Dhemla et al. [165] examined the effects of sintered fly ash (SFA) proportion, extra water demand and vibration time for lightweight concrete.

) This chapter is based on the following paper: **Hermawan H, Wiktor V, Gruyaert E, Serna P. Optimization of concrete mix designs toward the bond properties of steel reinforcement in self-healing concrete by Taguchi method. *J Build Eng* 2023:107294. <https://doi.org/10.1016/j.jobe.2023.107294>*

An L_9 orthogonal array (9 experimental runs, employing 3 factors each at 3 levels) was used to implement the experiments. Analyses by the Taguchi method revealed that the extra water demand and proportion of SFA affected the compressive strength substantially, while the segregation index was significantly influenced by the proportion of SFA and vibration time. Panda et al. [166] applied the Taguchi design to optimise the mix design variables toward abrasion resistance of copper slag aggregate (CSA) concrete. It was found that the wear depth of CSA concrete increased significantly as the amount of copper slag replacement and curing period increased. Durgun et al. [167] employed the L_{16} orthogonal array (16 experimental runs, employing 4 factors each at 4 levels) for the experimental design to determine the effectiveness of four mineral additives against sodium and magnesium sulphate attack in concrete. Optimal factor levels were determined through the main effects plots of SN ratio and ANOVA. Zhang et al. [168] used the Taguchi-based grey relational analysis to study the defrosting behaviour of the concrete in relation to the temperature, size of specimen and ice content. Results showed that size played an important role in determining the defrosting behaviour. Chokkalingam et al. [169] investigated factors affecting the compressive strength of geopolymer concrete using the Taguchi method. The optimum mixture was obtained using main effects plots of SN ratio to achieve the highest strength. Bakhbergen et al. [170] and Sharifi et al. [171] also demonstrated a successful implementation of the Taguchi method to optimise the mix designs of reactive powder concrete and self-consolidating concrete, respectively. Many researchers used the Taguchi method for optimisation in other applications such as machinery [172,173], medical [174], biology [175], agriculture [176], electrochemical [177], etc. However, this method has not been employed in optimising the mix design of self-healing concrete in relation to the bond properties of embedded steel reinforcement.

This chapter is basically a continuation of Chapter 5 with the aim to optimize the concrete mix designs towards the bond properties of steel reinforcement in self-healing concrete. Two types of healing agents were used namely bacterial healing agent (Basilisk) and crystalline admixture (Penetron Admix). The bond performance was evaluated by pull-out tests on three different states of concretes (uncracked, cracked and healed). For mix design optimisation purpose, the grading of aggregates based on the fine ratio (FR) and the water to cement ratio (w/c) were analysed. To cover a wide range of concretes frequently used in construction, the w/c was considered at three levels, i.e. 0.40, 0.50 and 0.60, and the FR defined as the ratio of fine aggregate over total (fine + coarse) aggregate in the mixture was analysed at

three levels namely 0.34, 0.44 and 0.54. As analysing all those variables and levels in all the possible combinations leads to a too wide experimental program, it was decided to run the program with a fractional factorial design based on the Taguchi method. This way the number of experimental tests program can be smaller than the full design without losing any vital information and the interactions between experimental factors as well as the effects of the individual factors (main effects) can be studied.

6.2 Materials and methods

6.2.1 Raw materials

This study used the same raw materials (i.e., cement, aggregates, superplasticizer) as described in Chapter 5. The PSDs of aggregates are depicted in Figure 6-1. However, only two commercial healing agents were used namely Basilisk bacterial healing agent (BAC) and Penetron Admix crystalline admixture (CA). The bacterial agent was supplied by Basilisk B.V. (the Netherlands) and the BAC mainly consists of bacterial spores of *Bacillus cohnii*-related strains which are encapsulated into polylactic acid (PLA) particles together with an inorganic salts mixture, calcium lactate and limestone powder [146]. The density of BAC was 1200 kg/m^3 and the product was introduced at a dosage of 2% by weight of cement (bwoc). Crystalline admixture was originally used as a waterproofing agent, while here its functionality shifts from permeability reducer to stimulator of autogenous healing [178]. This healing agent was supplied by Penetron Italia (Italy). CA is mainly composed of Portland cement and proprietary active chemicals. The density of CA was 2730 kg/m^3 and the recommended dosage of CA for concrete application was used at 1% bwoc. It should be noted that these dosages of both BAC and CA are the recommended dosages as suggested by the producers for the ideal concrete application. The particle size distributions (PSD) of BAC and CA can also be seen in Figure 6-1. It is visible that the PSD of cement is finer than the PSD of CA, while the BAC particles are much coarser than cement and CA due to the presence of PLA capsules. As a note, the amount of superplasticizer was later adjusted for all mixtures in order to achieve a comparable consistency of the fresh concrete with a slump class of S4 or close to S5.

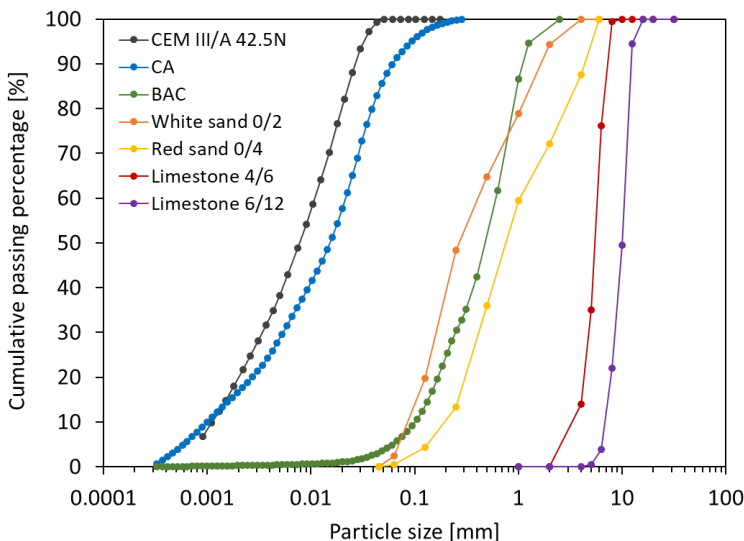


Figure 6-1. Particle size distribution of cement, aggregates and healing agents

6.2.2 Experimental program

In order to optimise the mix designs for self-healing concrete oriented to improving the self-healing efficiency over the mechanical and bond properties, an experimental program was developed. Three factors of interest were employed for optimisation including: (1) water-cement ratio (w/c), (2) fine ratio (FR) and (3) healing agent (HA), and each factor was run at three levels as shown in Table 6-1. Those factors were analysed in a broad margin of variability to cover most of the possible concretes used in practice. It is assumed that other factors like cement type or dosage, type of aggregate, etc., can also be influencer in the bond properties, but it was decided to keep it out of this study. The w/c was considered as an important factor in terms of mechanical performance of hardened concrete. This factor is further studied in this chapter with opting three levels, i.e. 0.40, 0.50 and 0.60. The FR is defined as the ratio of fine aggregate over total (fine + coarse) aggregate in the mixture. The content of fine aggregate influenced the bond properties of reinforcement in the concrete as reported by Mousavi et al. [179]. Hence, this FR ratio is selected as one of the criteria to evaluate the bond behaviour of steel rebars. The FR ratio was originally fixed at 0.44 based on the optimum packing of the inert skeleton from the Dewar model [145] with the minimum voids ratio. In order to study the effect of FR ratio, one

level below and above this original value were opted to make the mixture coarser and finer, respectively. Therefore, three levels of FR ratio were selected namely 0.34, 0.44 and 0.54. The last parameter is the selection of the healing agent, which is based on the use of three materials: (1) BAC, (2) CA, and (3) no healing agent (REF).

Table 6-1. Factors and levels adopted for the fractional factorial design

Factor	Level (-1)	Level (0)	Level (1)
w/c	0.40	0.50	0.60
FR	0.34	0.44	0.54
HA	BAC	CA	REF

The statistical model for this design includes k as the number of factors (i.e., 3) studied and the numbering (i.e., 3) as the levels of each factor. The full factorial design is the most robust one that requires $3^3 = 27$ experiments. However, this leads to a high consumption of raw materials, a low cost-effective and a time-consuming experimental program. Thus, it was decided to run the program with the fractional factorial design (3^{k-1}) where the number of experiments was greatly reduced to 9 experiments. Nine different mix designs of self-healing concrete were developed and produced in the laboratory as shown in Table 6-2. The design parameters were determined by Minitab® statistical software by use of the Taguchi design with employing L_9 orthogonal array. This array is used to analysed three factors each at three levels with nine experimental runs. The design of experiment (DOE) coded levels and the detailed mix designs are presented in Table 6-2 which are designed as to the requirements of a statistical fractional factorial cube plot.

Each concrete mixture was cast with a volume of 80 L where roughly 15 L was used to monitor the fresh properties, 10 L for casting into three cubic moulds of 150 mm in side, and the remaining volume (~55 L) for casting into pull-out moulds. The design of pull-out moulds and specimen preparations can be found in Chapter 5.

Table 6-2. Mix designs

Mix code	Coded levels			Mixture design								Fresh properties					
	w/c	FR	HA	CEM III/A 42.5N [kg/m ³]	Effective water [kg/m ³]	w/c [-]	White sand 0/2 [kg/m ³]	Red sand 0/4 [kg/m ³]	Limestone 4/6 [kg/m ³]	Limestone 6/12 [kg/m ³]	FR [-]	SP [kg/m ³]	CA [kg/m ³]	BAC [kg/m ³]	Slump [mm]	Air content [%]	Fresh density [kg/m ³]
M1	-1	-1	-1	350	140	0.40	197	441	661	566	0.34	7.03	-	7.00	210	1.8	2370
M2	-1	0	0	350	140	0.40	255	572	564	483	0.44	8.25	3.50	-	210	1.2	2400
M3	-1	1	1	350	140	0.40	315	705	463	397	0.54	8.25	-	-	220	1.8	2400
M4	0	-1	0	350	175	0.50	189	423	633	542	0.34	5.41	3.50	-	160	2.3	2380
M5	0	0	1	350	175	0.50	244	547	539	462	0.44	5.25	-	-	170	2.5	2340
M6	0	1	-1	350	175	0.50	297	666	438	375	0.54	6.68	-	7.00	230	2.3	2330
M7	1	-1	1	350	210	0.60	180	403	605	518	0.34	2.45	-	-	170	2.2	2310
M8	1	0	-1	350	210	0.60	230	516	509	436	0.44	3.00	-	7.00	210	1.7	2310
M9	1	1	0	350	210	0.60	285	638	420	360	0.54	3.57	3.50	-	200	2.5	2320

Note: w/c = water-cement ratio, FR = fine ratio, HA = healing agent, SP = superplasticizer, CA = crystalline admixture, BAC = bacteria

6.2.3 Test setup

The test methods and sample series also maintained the same as previously described in Chapter 5. Figure 6-2 shows a quick overview of sample series including uncracked (UNCR), cracked (CR) and healed (HL) concretes.

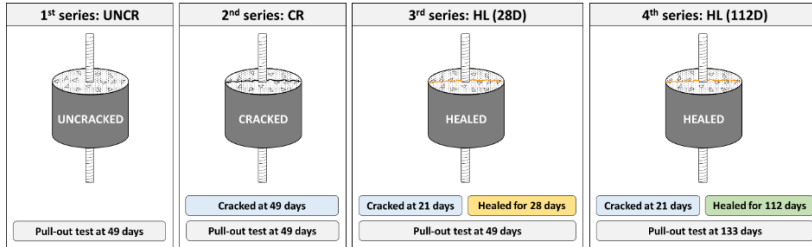


Figure 6-2. Series of pull-out specimens

6.3 Results and discussion

6.3.1 Fresh properties

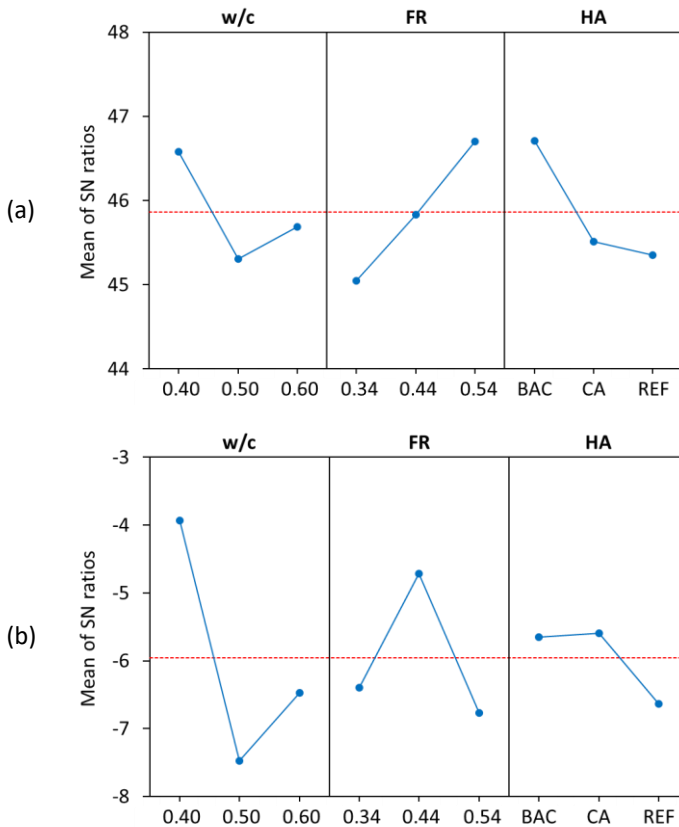
The fresh results based on the slump, air content and fresh density tests (in accordance with EN 12350-2,6,7) were summarized in Table 6-2. The Taguchi analysis was done on the fresh results to understand the main effects and interactions between levels for each factor in terms of SN ratio.

The main effects plot of SN ratios for slump is displayed in Figure 6-3(a) with “larger is better” approach. As a result of the adjustment on the amount of superplasticizer to achieve a workable mixture, the slump classes of all mixtures were relatively similar, mostly in class S4 and few mixtures were in class S5. This explains the unclear tendency on the effect of w/c in slump from Figure 6-3(a) as different amounts of SP were used in different mixtures.

The main effects plot of SN ratios for air content is shown in Figure 6-3(b) with “smaller is better” approach. There were variations on the results of air content from different mixtures. The inclusion of healing agents seems to decrease the air content of the fresh mixture. The gradual increase of w/c from 0.40 to 0.60 and FR from 0.34 to 0.54 did not give a clear tendency on the air content results. This might be occurred due to the fact that the air content test was performed only once for each mixture after mixing the concrete, thus more repetitions should be executed to give a more clear picture.

The main effects plot of SN ratios for fresh density is showcased in Figure 6-3(c) with “larger is better” approach. It has been clear that the lower w/c leads to the higher fresh density due to the packing. Apparently, the influence of FR from 0.34 to 0.54 did not affect the fresh density as indicated by the flat line in Figure 6-3(c). Similarly for HA, there were no effects of BAC and CA on the fresh density of concrete considering they were added at low amount in powder form.

The aforementioned results are in agreement with the recent studies [180–183] on the use of BAC and CA (at the same dosages) confirming no negative effects of these healing agents on the fresh concrete properties.



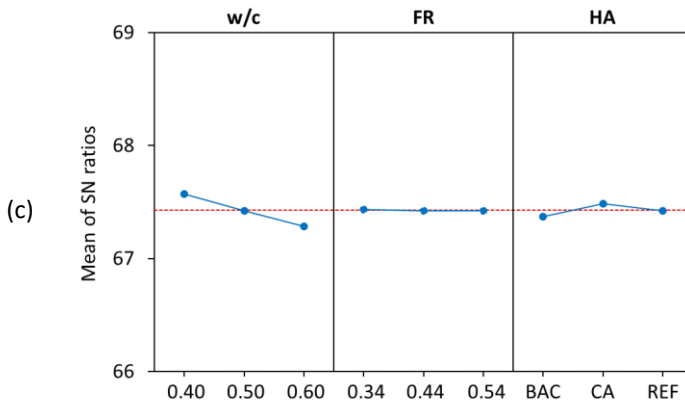


Figure 6-3. Signal-to-noise ratios for (a) slump, (b) air content and (c) fresh density

6.3.2 Compressive strength

The hardened cubical concrete specimens were subjected to compression tests at the age of 28 days (in accordance with EN 12390-3) and the result is depicted in Figure 6-4. It is interesting to see on the series of mixtures with w/c of 0.40 (M1-3) that although the contents of fine aggregate were different, the addition of healing agents did not considerably affect the compressive strength of the concrete as the strengths of M1-3 were relatively comparable. In another example on the series of mixtures with w/c of 0.50 (M4-6), the M6 achieved the highest compressive strength among these mixtures which basically showed a significant increment. On the series of mixtures with w/c of 0.60 (M7-9), the bacterial mixture M8 and a CA mixture M9 showed higher compressive strengths than the mixture without healing agent (M7).

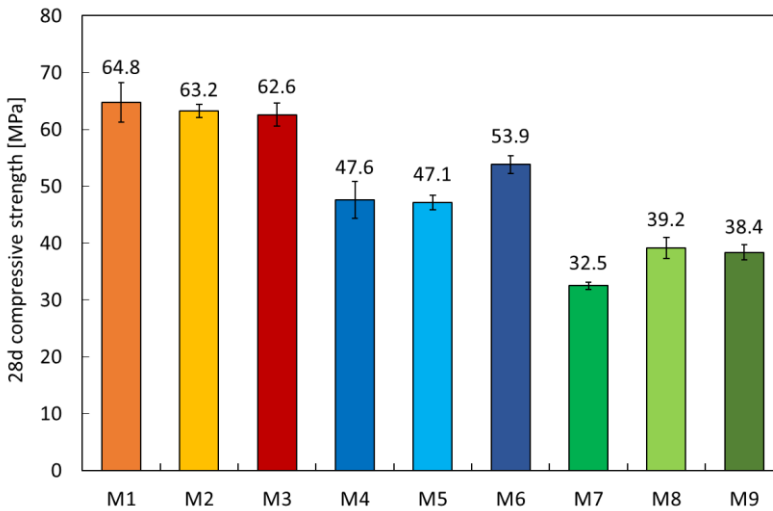


Figure 6-4. Compressive strength of all different concrete mixtures

To compare all results in a more statistical way, the Taguchi method was employed with the approach of "larger is better" since a high strength is preferred. The main effects plots are shown in Figure 6-5. In the case of w/c ratio, it has been clear that a lower w/c leads to a higher strength. The factor of FR also shows a gradual strength increment with increasing fine ratio from 0.34 to 0.54. Although the FR shows a positive effect on the strength enhancement, the slope of the FR curve is less steep than the slope of the w/c curve. It means that the improvement of strength with increasing FR ratio is not as significant as with w/c ratio. Looking at the HA-factor, the highest strength was achieved for the mixture with the addition of BAC, followed by CA and REF. This confirms that the addition of healing agent, either BAC or CA, increases the compressive strength of concrete. This finding is partly supported by the fact that the addition of healing agent tends to reduce the air content of the mix as previously discussed in Figure 6-3.

The producer of CA, Penetron, claimed that the incorporation of their product can increase the concrete strength up to 13% [73]. The same CA product (Penetron Admix) has been used by few researchers in past studies. Cadersa et al. [184] used CA at a dosage of 0.8% bwoc on traditional concrete and a strength increment up to 15% was found. In another study by Neverkovic et al. [185], there was a minor improvement on the compressive strength (~2%) with employing 1% CA. Pazderka et al. [28] and Ferrara et al. [186] supported the finding that there was a scant effect on the addition of

CA with regard to the compressive strength development. The different outcomes may strongly depend on the formulation of mix designs in each of these studies which may affect the performance of the crystalline admixture. In our study, the addition of CA shows an improvement of compressive strength, despite the increment is not as significant as the slope of w/c. García-Vera et al. [4] studied the microstructure of CA-based mortar and they confirmed that the formation of crystals filling the pores, capillaries and microcracks is one of the possible reasons for strength enhancement by the addition of this admixture.

Previous studies utilized the same BAC material for self-healing investigations, however the applications were limited to the paste or mortar level. Rossi et al. [79] investigated the compressive strength of OPC mortar mixed with 2.6% by mass of cement of BAC and they interestingly found that the inclusion of BAC on OPC mortar caused a strength reduction of 20–35% on 7-days-old specimens due to a chemical interaction between the PLA particles and cement hydration at early ages. Nevertheless, at 28 days, the compressive strength slightly increased from 36.5 (control) to 39.5 MPa (control + BAC), suggesting no detrimental effect on the long-term properties. In contrast, He et al. [38] reported that the inclusion of BAC into strain hardening cementitious composite (SHCC) resulted in strength reduction at any BAC dosages (1.25–5.00% by weight of binder). It was hypothesized that the hydrolytic degradation of PLA capsules and the consumption of alkalinity by the bacterial agent caused this detrimental effect. It is noteworthy to mention that He et al. [38] formulated the mix designs of SHCC by using blast furnace slag cement CEM III/B, while Rossi et al. [79] used CEM I for cement paste. This might be an indication that the performance of BAC can be interfered by the selection of binder component. Mors et al. [37] developed a bacterial healing agent which was basically composed of basic ingredients or derivatives of the BAC core materials, i.e. lactate derivatives, calcium source, bacterial spores (of *Bacillus cohnii*-related strains), and activation nutrients. This agent was introduced into CEM I and CEM III/B concrete mixtures with a dosage of 4% bwoc. Results confirmed that a negligible effect on compressive strength was observed upon healing agent addition to OPC concrete (CEM I), and even a 7% strength improvement was noticed. However, for slag-based concrete on CEM III/B, a significant reduction on compressive strength at 28 days of around 50% was observed as compared with reference concrete without healing agent. The addition of healing agent to CEM III/B based material also showed a significant reduction of the slag reaction.

Based on the literature above, the inclusion of BAC seems more compatible in CEM I based materials and less suitable for CEM III/B based materials. For CEM III/A, a limited effect on strength, hydration energy and slag reaction occurred for the addition of bacterial healing agent (*Bacillus cohnii*) [37]. In our study, CEM III/A was used and it was confirmed from the compressive strength results as well as the main effects plots that the addition of BAC induced a positive impact on the concrete strength. Table 6-3 shows the response table of SN ratios on the compressive strength employing a statistical analysis by the Taguchi method. It was revealed that the most significant factor affecting the compressive strength of concrete was w/c, then followed by the HA. The FR was regarded as the least factor affecting the compressive strength.

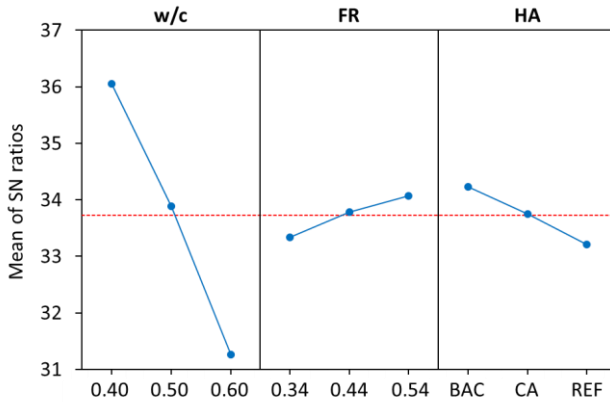


Figure 6-5. Signal-to-noise ratios for 28d compressive strength

Table 6-3. Response table for SN ratios for 28d compressive strength

Level	w/c	FR	HA
-1	36.06	33.34	34.24
0	33.88	33.78	33.75
1	31.26	34.08	33.21
Δ	4.80	0.74	1.03
Rank	1	3	2

Based on the obtained results, the analysis of variance (ANOVA) was performed on the SN ratios of strength responses as shown in Table 6-4. It shows that the factors of w/c and HA showed significant influences on the

compressive strength (p -values < 0.05). A relationship between w/c and FR is constructed by the contour plots as shown in Figure 6-6. The vertical contours observed in Figure 6-6 reaffirm the significant effect of w/c on the compressive strength and also the influence of the healing agent as the contours shift after the addition of healing agents from REF to CA or BAC, showing a notable effect on strength enhancement. The contour plots were based on the general linear model with the proposed mathematical model as follows:

$$f'_c = \alpha - 134.13 \cdot w/c + 16.47 \cdot FR \quad (6.1)$$

where f'_c is the compressive strength at 28 days, α is the fixed constant (107.22 for REF, 109.56 for CA and 112.41 for BAC), w/c is the water-cement ratio and FR is the fine ratio. A correlation between the proposed strength model based on Equation (6.1) and the actual strength values obtained from experiments was established. Figure 6-7 confirms a good prediction of the model with the adjusted coefficient of determination (R^2_{adj}) of 0.99, indicating the optimum results estimated by the Taguchi method are highly accurate.

Table 6-4. Analysis of variance of SN ratios for 28d compressive strength

Source	Degree of Freedom	Adjusted Sum of Square	Adjusted Mean Square	F-value	P-value
w/c	2	34.6142	17.3071	671.18	0.001
FR	2	0.8214	0.4107	15.93	0.059
HA	2	1.5809	0.7905	30.65	0.032
Error	2	0.0516	0.0258		
Total	8	37.0681			

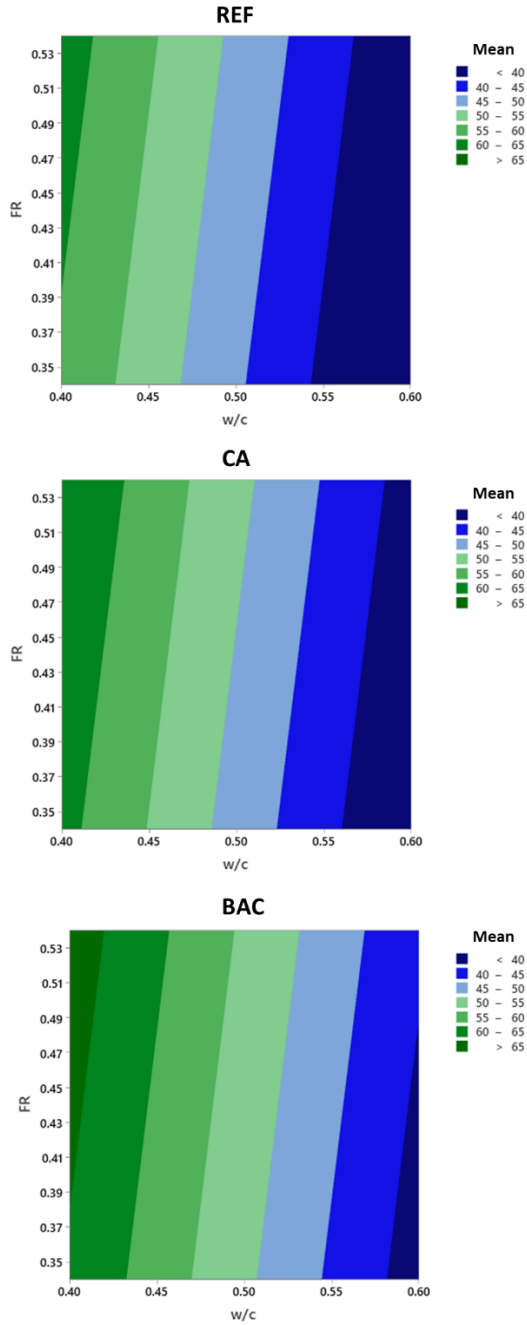


Figure 6-6. Contour plots of 28d average compressive strength (in MPa) vs w/c and FR

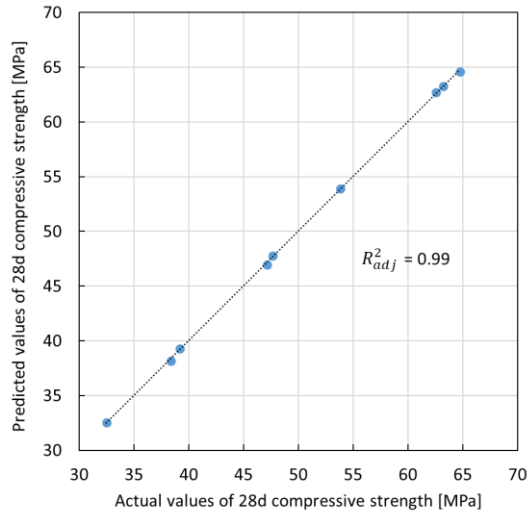


Figure 6-7. Correlation between predicted and experimental results of compressive strength

6.3.3 Bond properties of uncracked (UNCR) concretes

The pull-out tests were performed on 49-days-old pull-out specimens in uncracked condition. The bond-slip behaviour of steel reinforcement in the concrete is shown in Figure 6-8 with M5 taken as an example. Five to six repetitions were used to obtain a reliable average value for the ultimate bond strength for each mixture. According to the bond slip response, several parameters were analysed such as τ_u , τ_m and $E_{1.0}$. The results of these parameters were depicted in Figure 6-9. In terms of ultimate bond strength, it is obvious that a series of mixtures with a lower w/c (M1-3) tends to have a higher bond strength as compared with mixtures with a higher w/c (M4-9). This tendency is also observed on the results of compressive strength. According to available literature [152–154], the ultimate bond strength is related to the square root of compressive strength as shown in Figure 6-10. Hence, the ultimate bond strength of the uncracked concrete can be further predicted with an acceptable R^2_{adj} of 0.85 by using Equation (6.2). The other bond parameters such as τ_m and $E_{1.0}$ can also be predicted by its ultimate bond strength as shown in Figure 6-11. It is confirmed that there is a strong relationship ($R^2_{adj} \geq 0.90$) to define the mean bond strength and fracture

energy as a function of ultimate bond strength as proposed in Equations (6.3) and (6.4).

$$\tau_u = 6.82\sqrt{f'_c} - 27.71 \quad (6.2)$$

$$\tau_m = 0.91\tau_u - 1.00 \quad (6.3)$$

$$E_{1.0} = 0.87\tau_u + 0.33 \quad (6.4)$$

Considering all mixtures have different compositions, the Taguchi analysis was employed to understand the effects of each factor towards the bond strength with the approach of "larger is better" as a high bond strength is desired. The main effects plots of ultimate bond strength are presented in Figure 6-12. The factor of w/c again shows a steep curve where the ultimate bond strength reduces with increasing the w/c in the mixture. Moreover, the factor of FR did not give a clear relationship on the ultimate bond strength as the FR of 0.44 showcased a lower SN ratio than FRs of 0.34 and 0.54. Nevertheless, a high FR of 0.54 seems to give a better ultimate bond strength among other FRs. Mousavi et al. [179] stressed that the proportion of fine aggregate influenced the bond strength of the embedded reinforcement, which was attributed due to the filling effect. However, increasing the fine aggregate content can also reduce the aggregate interlock mechanism in the mixture, thus an optimum content should be used. In the case of HA, similarly like the trend observed in compressive strength, the addition of healing agents contributed to an enhancement on ultimate bond strength. It is found that the inclusion of BAC had a higher contribution than CA, but both of these agents have higher SN ratios than REF. It suggests that aside of the purpose of adding the healing agents to improve the healing efficiency, the incorporation of these healing agents interestingly improves the bond properties. As a matter of fact, there were very limited studies discussing the effect of healing agents on the bond properties. Only one research [142] studied the bond properties of reinforcement in self-healing concrete containing superabsorbent polymers (SAP). The effect of SAP on the bond strength was greatly dependent on its dosage. The addition of 0.25% bwoc of SAP did not affect the ultimate bond strength as compared with the control mixture, however the addition of 0.50 and 1.00% caused ultimate bond strength reductions of approximately 40 and 58%, respectively. It was found that the formation of macro voids generated by SAP particles was responsible for this degradation. In our study, different healing agents were used and the dosages were added as recommended by the producers. Thus, it might be possible that the dosages of BAC and CA were already optimum to induce positive effects on the concrete properties.

According to Table 6-5, the factors affecting the ultimate bond strength of reinforcement in uncracked concrete were in a following order: $w/c > FR > HA$. The w/c was selected as the most significant factor in relation to the bond strength, while the effects of FR and HA were quite comparable judging from the delta values in Table 6-5. This is reflected from the ANOVA results (see Table 6-6) where the p-values of w/c , FR and HA were 0.042, 0.318 and 0.386, respectively. The interaction between w/c , FR and HA with respect to the ultimate bond strength was established in contour plots as shown in Figure 6-13. The proposed mathematical model was given as follows:

$$\tau_u = \alpha - 65.9 \cdot w/c + 8.1 \cdot FR \quad (6.5)$$

where τ_u is the ultimate bond strength, α is a fixed constant (48.29 for REF, 49.33 for CA and 51.06 for BAC), w/c is the water-cement ratio and FR is the fine ratio. The proposed strength model for uncracked concretes was tested with a confirmation test as shown in Figure 6-14(a). The same method was later applied for the cracked and healed concretes as shown in Figure 6-14(b) and Figure 6-14(c), respectively. With the good R_{adj}^2 of 0.94–0.96, a high accuracy of predicting the ultimate bond strength by Taguchi method can be achieved.

The same methodologies were applied to analyse the results based on the mean bond strength and fracture energy. In Figure 6-9, the observations of τ_m and $E_{1.0}$ followed a similar trend as τ_u . It is interesting to see that the fracture energy of the series of mixtures with w/c of 0.60 (M7-9) was stable regardless variations in FR and HA, while in other series (M1-3, M4-6), the effect of mix design parameters was more pronounced. To better understand the results, the main effects plots of these factors were also constructed in Figure 6-12(b-c). As compared with Figure 6-12(a), the effects of the other parameters (τ_m , $E_{1.0}$) had the same agreement as τ_u . As tabulated in Table 6-5, the delta values of both FR and HA were similar, while the delta value of w/c was always the highest, indicating the most influential factor in determining the bond properties.

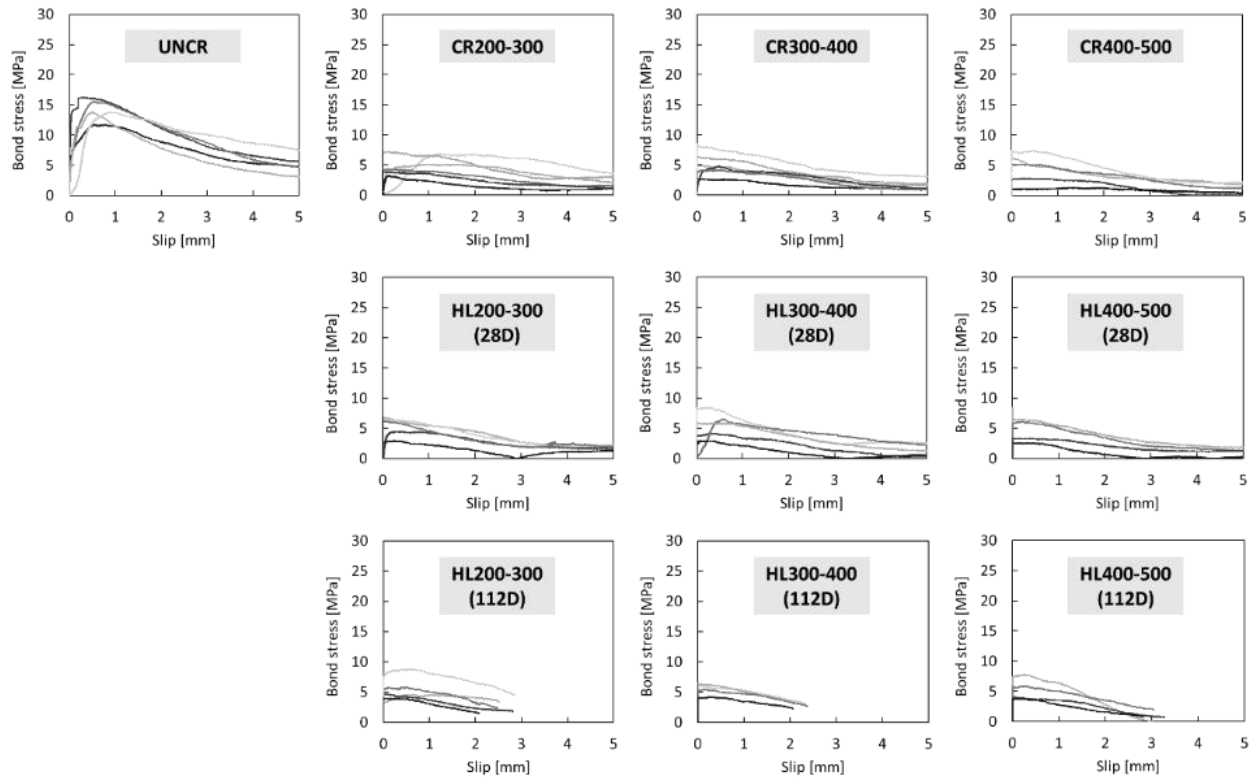


Figure 6-8. Bond-slip curves on UNCR, CR and HL concretes (mixture M5 taken as example)

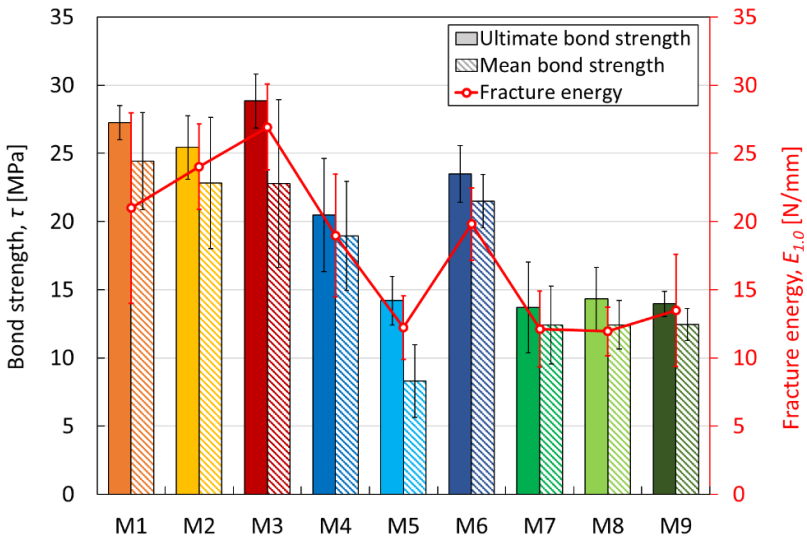


Figure 6-9. Evaluation of various bond parameters on all concrete mixtures

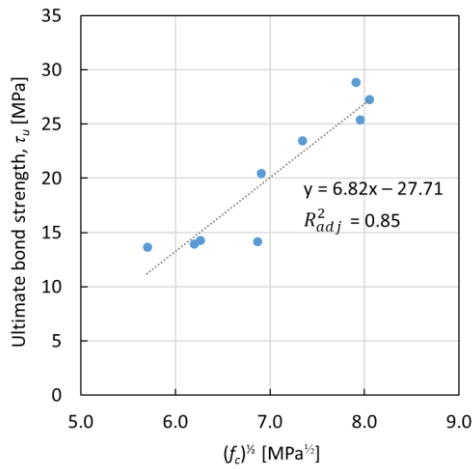


Figure 6-10. Relationship between ultimate bond strength and compressive strength of UNCR concrete

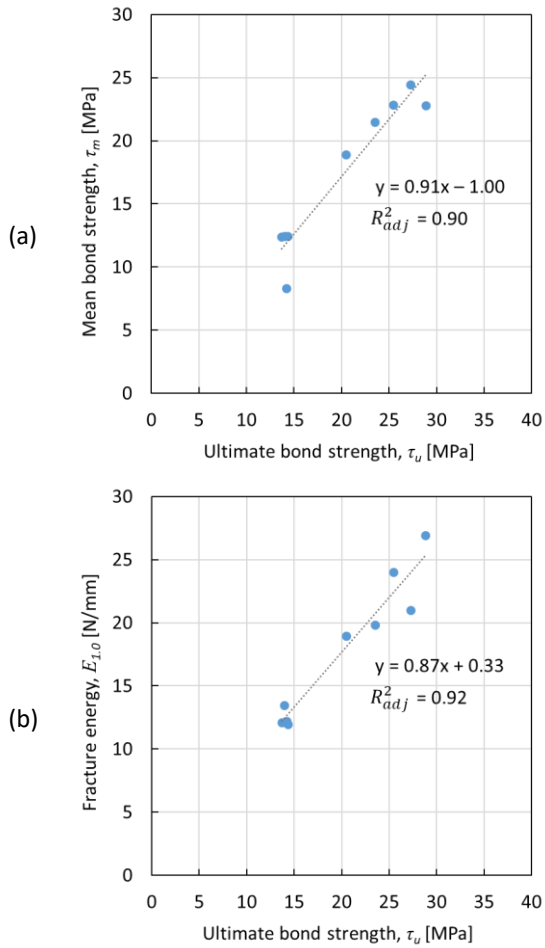


Figure 6-11. Relationship between (a) ultimate bond strength and mean bond strength and (b) ultimate bond strength and fracture energy for UNCR concrete

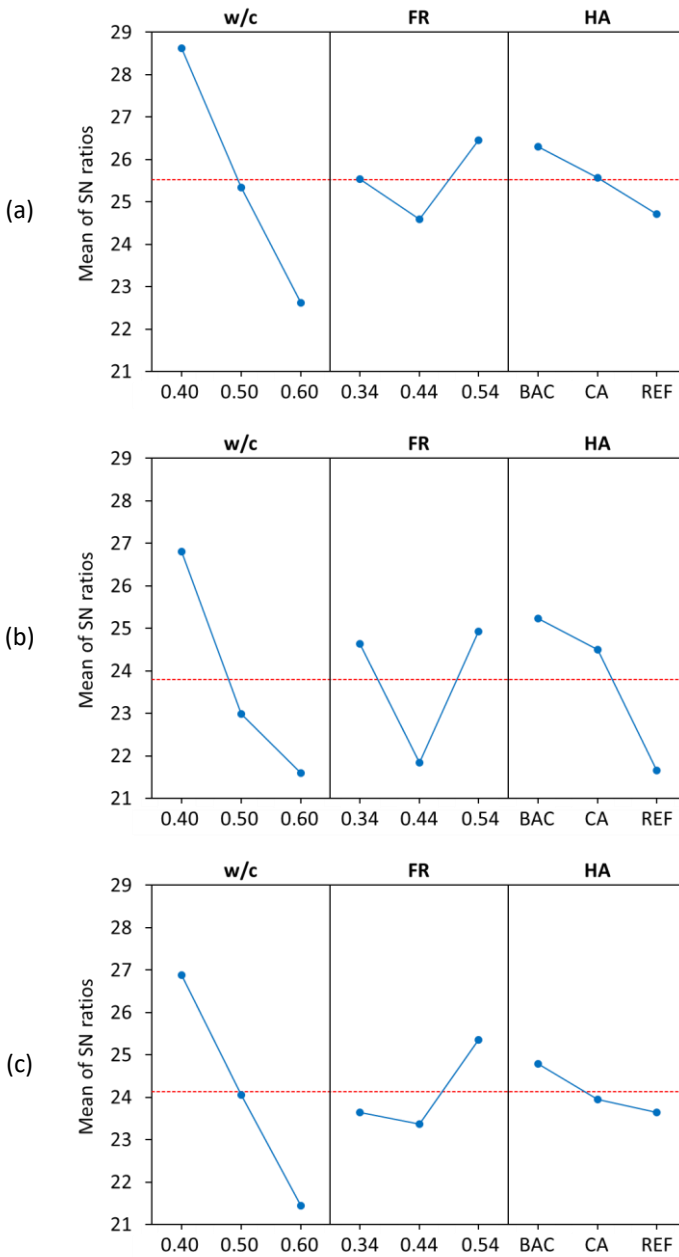


Figure 6-12. Signal-to-noise ratios for (a) ultimate bond strength, (b) mean bond strength and (c) fracture energy of uncracked (UNCR) concretes

Table 6-5. Response table for SN ratios for ultimate bond strength, mean bond strength and fracture energy of UNCR concretes

Level	Ultimate bond strength			Mean bond strength			Fracture energy		
	w/c	FR	HA	w/c	FR	HA	w/c	FR	HA
-1	28.62	25.54	26.31	26.80	24.63	25.23	26.88	23.65	24.79
0	25.34	24.60	25.56	22.99	21.84	24.50	24.06	23.37	23.95
1	22.62	26.45	24.71	21.60	24.92	21.66	21.44	25.36	23.64
Δ	6.00	1.85	1.59	5.20	3.09	3.57	5.45	1.99	1.14
Rank	1	2	3	1	3	2	1	2	3

Table 6-6. Statistical evaluation of the bond properties by ANOVA based on p-values of SN ratios (note: the p-value of 0.05 was set as a significance threshold and the highlighted 'green' cells represent significant p-values)

Series	Factor	p-value (based on SN ratios)		
		τ_u	τ_m	$E_{1.0}$
UNCR	w/c	0.042	0.219	0.179
	FR	0.318	0.412	0.582
	HA	0.386	0.363	0.822
CR200-300	w/c	0.001	0.238	0.273
	FR	0.038	0.437	0.275
	HA	0.039	0.400	0.321
CR300-400	w/c	0.111	0.188	0.294
	FR	0.605	0.679	0.927
	HA	0.774	0.861	0.968
CR400-500	w/c	0.144	0.363	0.287
	FR	0.642	0.754	0.463
	HA	0.442	0.456	0.521
HL200-300 (28D)	w/c	0.025	0.323	0.124
	FR	0.186	0.233	0.630
	HA	0.490	0.469	0.406
HL300-400 (28D)	w/c	0.004	0.112	0.056
	FR	0.182	0.302	0.626
	HA	0.376	0.866	0.786

HL400-500 (28D)	w/c	0.141	0.307	0.016
	FR	0.562	0.063	0.067
	HA	0.558	0.487	0.065
HL200-300 (112D)	w/c	0.284	0.240	0.211
	FR	0.711	0.235	0.379
	HA	0.838	0.544	0.505
HL300-400 (112D)	w/c	0.156	0.125	0.146
	FR	0.634	0.377	0.539
	HA	0.782	0.865	0.690
HL400-500 (112D)	w/c	0.101	0.111	0.179
	FR	0.771	0.714	0.677
	HA	0.890	0.655	0.854

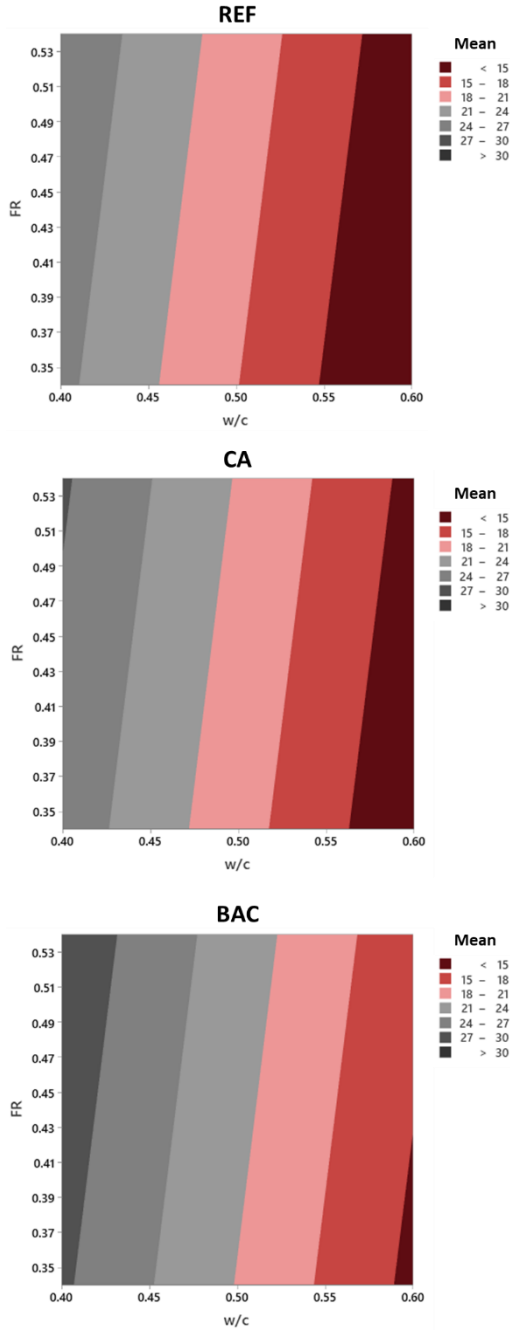


Figure 6-13. Contour plots of ultimate bond strength (in MPa) vs w/c and FR in uncracked concrete

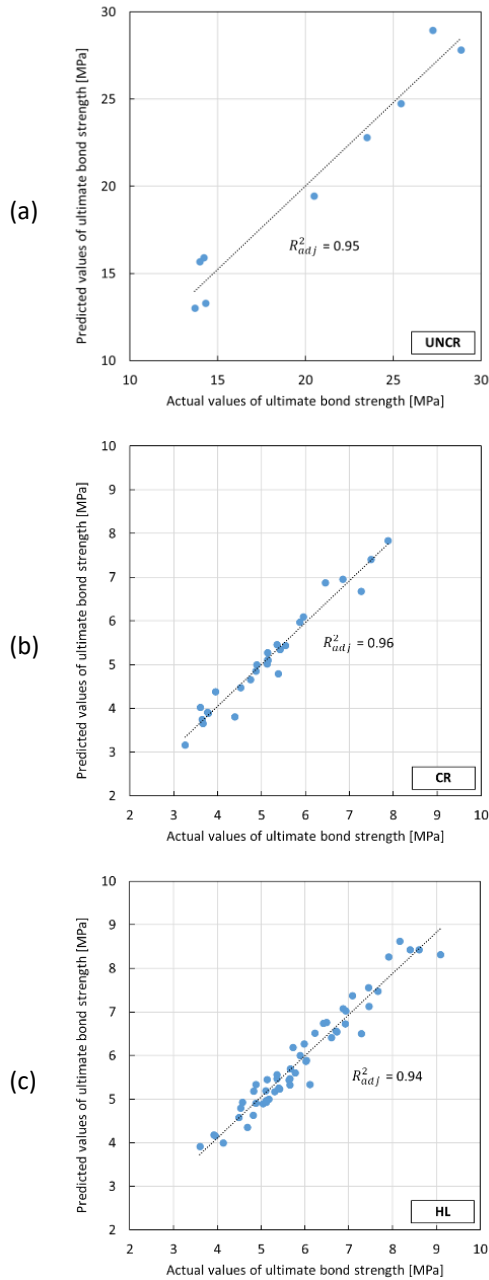


Figure 6-14. Correlation between predicted and experimental results of ultimate bond strengths of (a) UNCR, (b) CR and (c) HL concretes

6.3.4 Bond properties of cracked (CR) concretes

The cracked concretes with various crack widths were tested by means of pull-out tests at 49 days. As shown in Figure 6-8 (example for mix M5), the bond-slip curves of CR series were much lower than the UNCR series due to the cracking. The ultimate bond strengths of all CR concretes were recorded and summarized in Figure 6-15(a). It shows that a significant reduction of ultimate bond strength from uncracked to cracked condition was observed. The bond strength reduction was recorded in the range of 60–82%. This indicates that the formation of a crack gives a critical effect on the bond of steel reinforcement and concrete. Although the cracks were distinguished from small to big sizes, the ultimate bond strengths seemed comparable for all CR concretes with values lower than 10 MPa. In fact, this finding is in contrast with the previous report made by Mousavi et al. [142] where they found a gradual bond strength reduction with increasing crack size from 100 to 500 μm . This may be explained by a different method that was used to induce cracks in the concrete as well as the design of the pull-out specimen. In [142], the specimens were fabricated in an unconfined condition with a ratio of concrete cover to rebar diameter of 7.5. The cracking was simulated by a controlled splitting test on the unconfined specimens with the aid of crack gauges. In our study, the specimens were produced in a confined condition with the use of PVC tubes and the ratio of concrete cover to rebar diameter was fixed at 5.25.

A Brazilian splitting test was used to crack the specimens while the actual crack width was measured by means of optical microscopy. Preliminary tests showed that without the use of a PVC tube as a confinement, the concretes experienced a sudden failure during cracking stage. As the bond stress reaches a maximum limit, the crack width increases considerably leading to a brittle failure of the bond. While on the use of confinement, the size of the cracks can be easily controlled. However, it seems that the use of PVC tube also influences the bond result. Desnerck et al. [148] reported similar bond strength values between the confined and unconfined specimens in an uncracked state. However, when the specimens were in a cracked state, an additional bond strength reduction of 11% was confirmed in unconfined specimens as compared with confined specimens. This beneficial effect of the external confinement was also reported by Gambarova et al. [157,158]. According to Figure 6-15(a), it is visible that the average ultimate bond strengths of M1-M3 mixtures were higher than the other mixtures. This is attributed to the contribution of a lower w/c (= 0.40) which results in a higher strength. On the other hand, the mixtures with w/c of 0.50 and 0.60 had a

similar level of ultimate bond strength. The results of mean bond strength and fracture energy had a similar pattern as the ultimate bond strength as shown in Figure 6-15(b) and Figure 6-15(c), respectively.

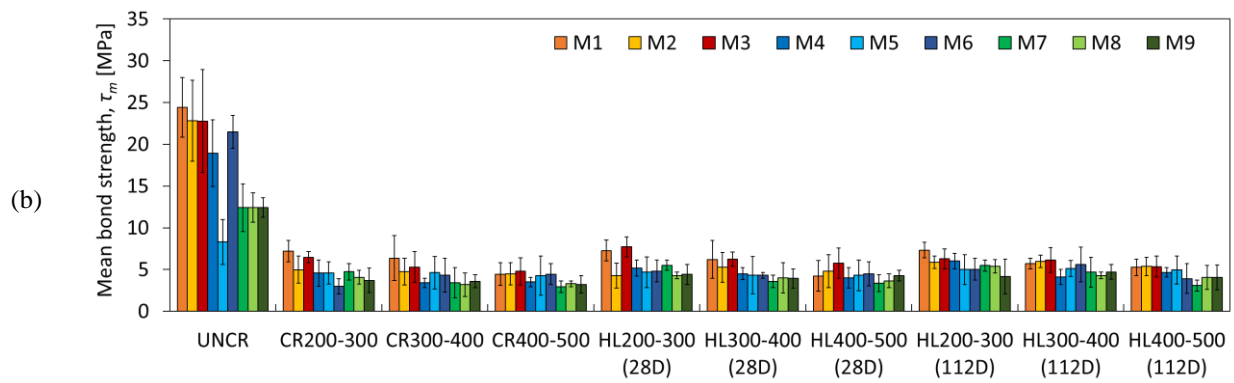
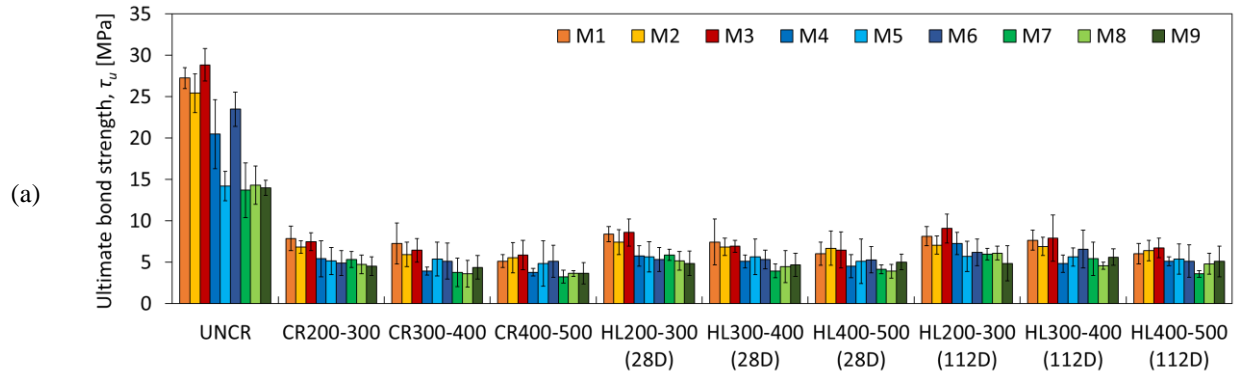
The Taguchi analysis was employed in this dataset to understand the influences of mix design factors toward the ultimate bond strength of cracked concretes. The main effects plots based on the SN ratios were depicted in Figure 6-16 as observed in three different crack width ranges. Figure 6-16(a) with the cracks of 200–300 μm shows the w/c of 0.40 as a dominant factor with the highest SN ratio, while the SN ratios for w/c of 0.50 and 0.60 were identical. In terms of FR, the slope of the plots is not steep indicating the effect of this factor is not significant. In case of HA, the SN ratios of BAC, CA and REF were rather similar, showing an insignificant effect of HA for the bond strength of CR concrete. It is logic to mention that at this cracked condition, the healing agents such as BAC or CA will not give a positive effect as the self-healing ability is not yet activated at the time of cracking. This healing effect will be explained in the next section.

When the cracks were enlarged to 300–400 μm (see Figure 6-16(b)), it is more clear that the SN ratio had a linear relationship with the factor w/c where the SN ratios increase with decreasing w/c. In this regard, the w/c of 0.40 showcased the highest SN ratio. The FR factor in this case did not give a clear picture as the FR of 0.54 obtained the highest SN ratio, followed by 0.34 and 0.44. The factor of HA follows the previous interpretation where the effect of HA will potentially be clear after the specimens are healed. Based on Figure 6-16(c), for the crack width of 400–500 μm , the effect of w/c was also clear with a higher SN ratio for a lower w/c (in this case, w/c of 0.40). All in all, Figure 6-16(a-c) confirms that one factor level leads to the optimum bond strength in cracked condition which is the w/c of 0.40 with a consistent trend. A low w/c in concrete can improve the bond strength between the concrete and reinforcement materials, even when the concrete is cracked. The main reason for this is that a lower w/c results in a more densely packed cement matrix. This denser matrix provides more surface area for the concrete to bind with the reinforcement material. Additionally, the lower porosity of the concrete resulting from a lower w/c may reduce the ingress of water and other harmful substances, which can weaken the bond between the concrete and reinforcement material. Figure 6-19 shows the relationship between the average ultimate bond strength of UNCR and CR concretes and it is noteworthy to mention that the higher the ultimate bond strength of uncracked concrete, the higher the ultimate bond strength of cracked concrete which is constructed with a linear regression. The adjusted

coefficient of determination (R_{adj}^2) between τ_{u_UNCR} and τ_{u_CR} is relatively good to give a possible insightful trend on the changes of bond strength from uncracked to cracked condition, and furthermore to healed condition.

The other bond parameters such as mean bond strength (τ_m) and fracture energy ($E_{1.0}$) were also analysed by the Taguchi method and the main effects plots can be found in Figure 6-17 and Figure 6-18, respectively. In general, the trend of SN ratios for each combination of factor-level had a similar tendency as the τ_u results (see Figure 6-16). In case of τ_m , the change of FR from 0.34 to 0.54 was more pronounced than the τ_u for small cracks (200–300 μm). The FR of 0.34 achieved the highest SN ratio, followed by the FR of 0.44 and 0.54. Nevertheless, when the cracks were enlarged up to 300–400 or 400–500 μm , the highest SN ratio was achieved by the FR of 0.54. It seems that there is a transition of FR for mean bond strength where a low value of FR seems beneficial for small cracks and a high value of FR is more suitable for big cracks. The τ_m was not improved by the addition of HA as the REF achieved the highest SN ratio for small cracks, while for big cracks, for instance 400–500 μm , the addition of HA, either BAC or CA, had a higher SN ratio than REF. This observation was also found in the $E_{1.0}$ (see Figure 6-18a-c).

Statistical evaluation by ANOVA was conducted on the influence of mix design factors as presented in Table 6-6. It was found that w/c ratio is the most influential factor (p-value < 0.05) in the ultimate bond strength for uncracked specimens and specimens with small cracks, and other mix design factors show some influences. But with medium and big cracks, the effect of these factors were rather not significant (p-value >> 0.05). For big cracks and for other bond parameters (τ_m , $E_{1.0}$), the influences of the mix design factors are hidden by the effect of the crack geometry. Considering a small crack, there seems to be a contribution of the matrix quality on the crushed concrete at steel ribs during the first pull-out affecting the bond strength results. When a large crack was made or at a larger slip state, the effect of the confinement setup can be more influential than the concrete matrix.



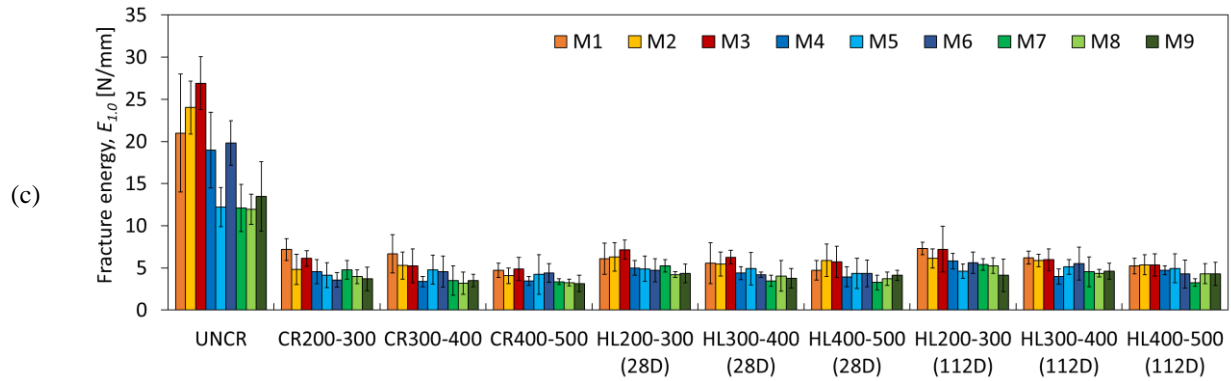
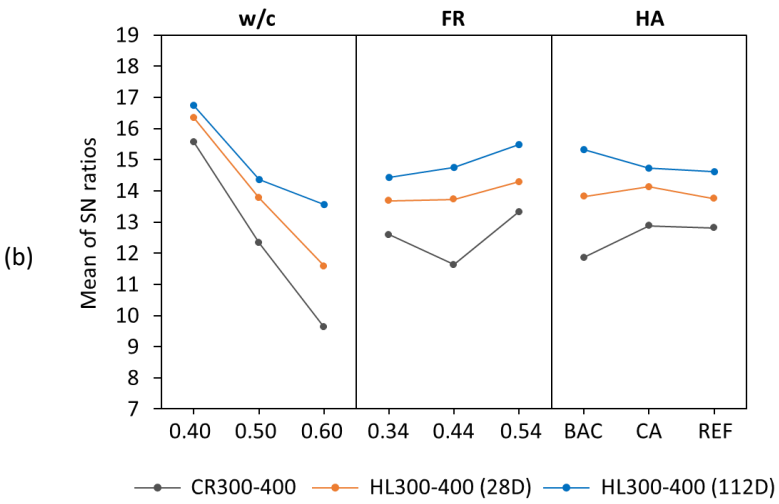
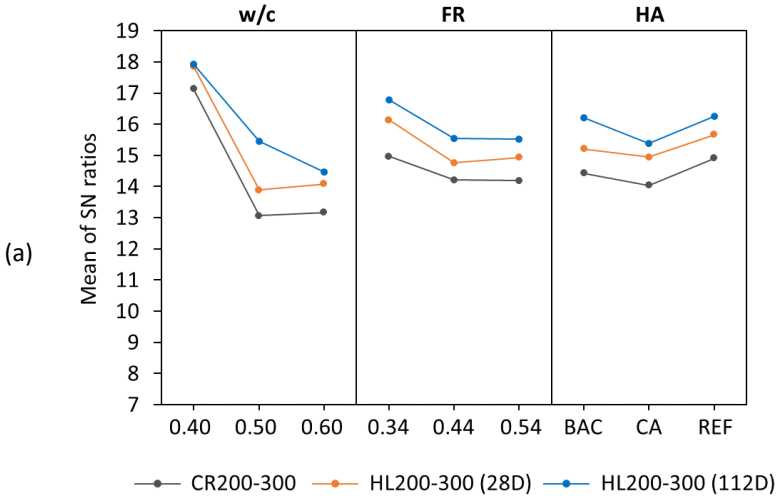


Figure 6-15. (a) Ultimate bond strengths, (b) mean bond strengths and (c) fracture energy of all series of concretes



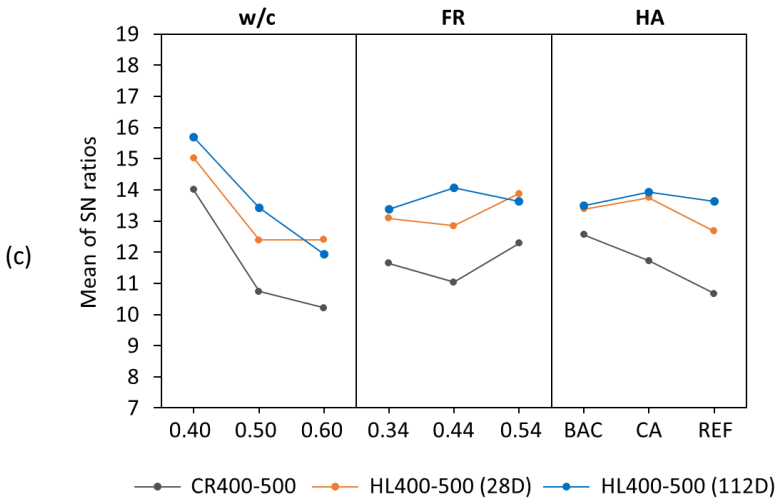
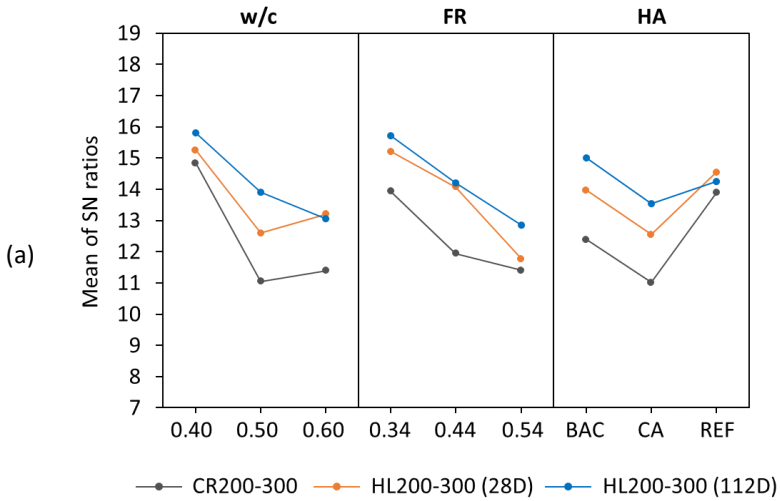


Figure 6-16. Signal-to-noise ratios for ultimate bond strengths in cracked (CR) and healed (HL) concretes with specific crack width of (a) 200–300 μm, (b) 300–400 μm and (c) 400–500 μm



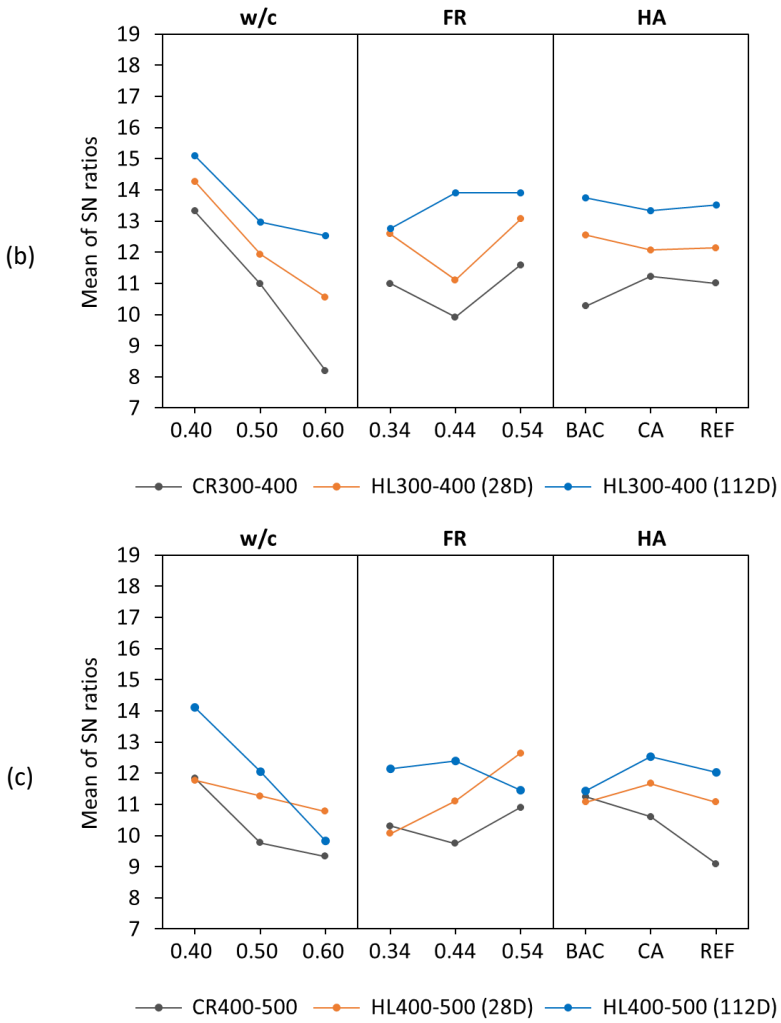
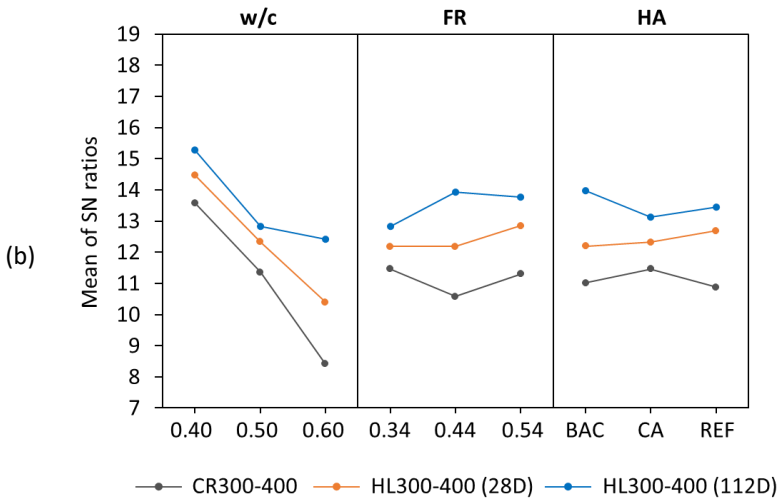
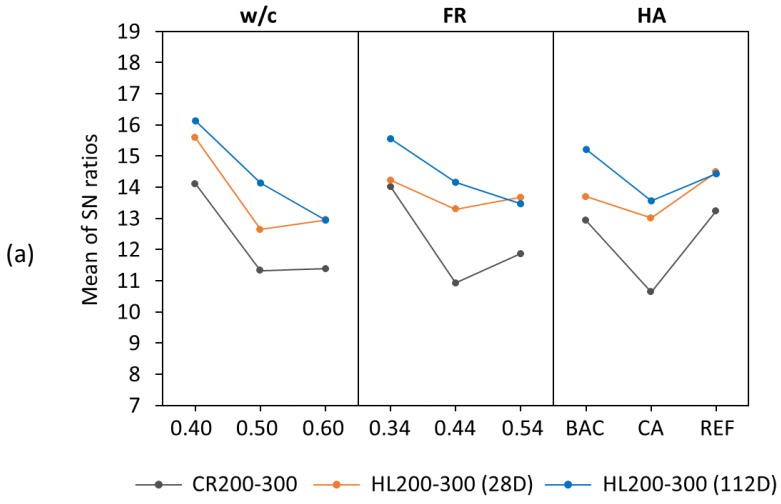


Figure 6-17. Signal-to-noise ratios for mean bond strengths in cracked (CR) and healed (HL) concretes with specific crack width of (a) 200–300 μm , (b) 300–400 μm and (c) 400–500 μm



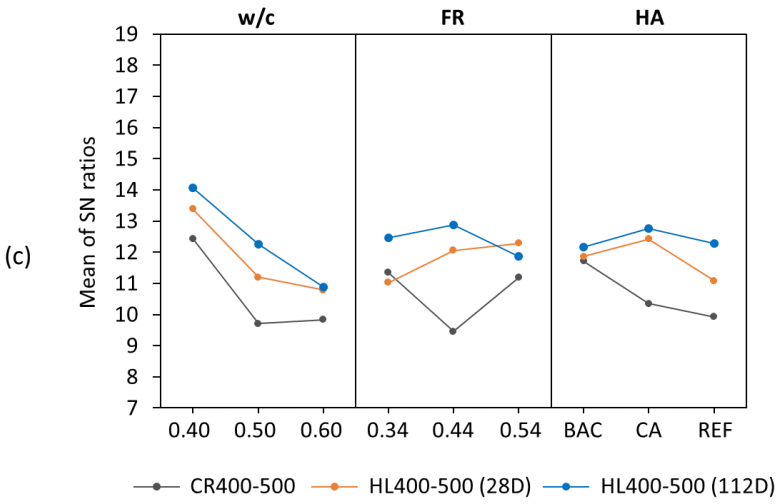
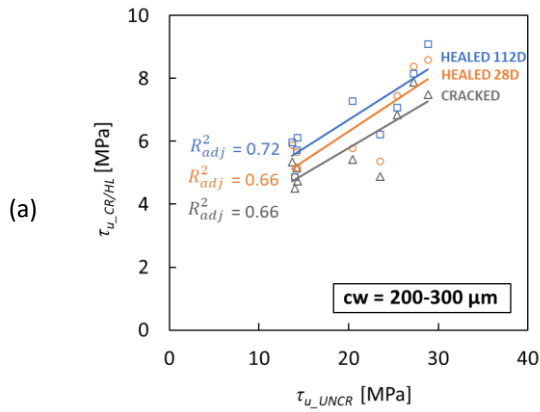


Figure 6-18. Signal-to-noise ratios for fracture energy in cracked (CR) and healed (HL) concretes with specific crack width of (a) 200–300 μm , (b) 300–400 μm and (c) 400–500 μm



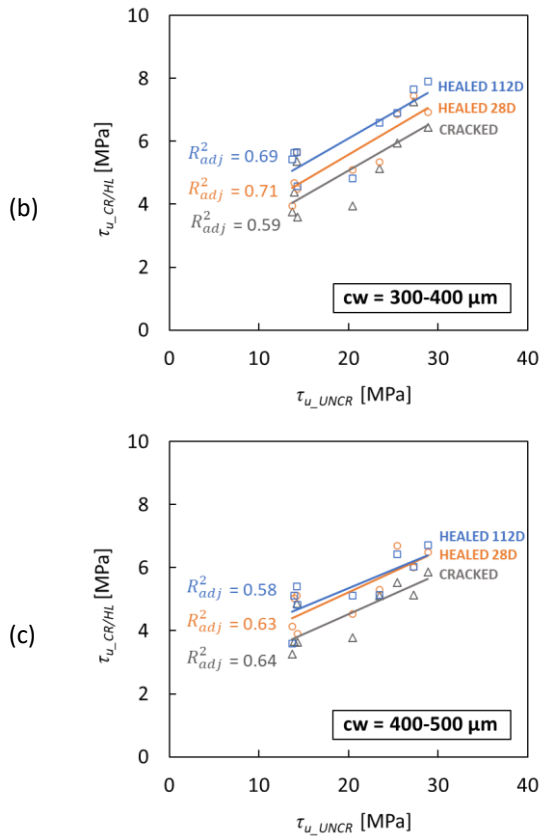


Figure 6-19. Relationship between the average ultimate bond strength of uncracked, cracked and healed concretes at a specific crack width of (a) 200–300 μm , (b) 300–400 μm and (c) 400–500 μm

6.3.5 Bond properties of healed (HL) concretes

Two series of HL concretes were investigated: (1) healed concretes after 28 days of healing (HL (28D)) and (2) healed concretes after 112 days of healing (HL (112D)). Figure 6-20 shows the phenomenon of crack closure on self-healing concretes. Comparing the CR and HL concretes, there was a white formation of minerals at the crack mouth in the HL concretes and these healing products were already available after a short healing period of 28 days. Without the aid of healing agents, the REF concrete has demonstrated the autogenous healing by the precipitation of healing products. These healing products seemed like a grouping of fine granulates and in addition, there were some fine fragments scattering nearby the crack mouth. When

the BAC or CA was introduced, there was a peculiar formation of healing products coming out from the crack in the structure of stalactites. These formations were observed both at 28 and 112 days. After a long healing period of 112 days, it seems that the formed stalactites were more abundant.

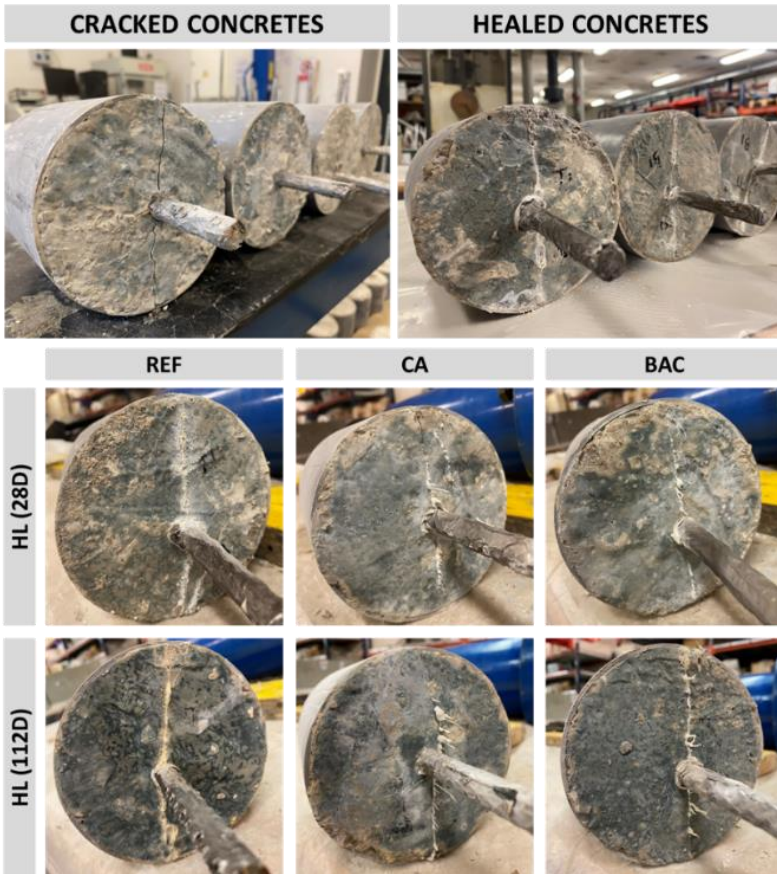


Figure 6-20. Crack closure phenomenon with self-healing concretes

A typical bond-slip behaviour was depicted in Figure 6-8 with mixture M5 taken as an example. As a note, especially for the HL (112D) series, the pull-out tests were stopped after reaching a slip of 2–3 mm, while for the other series, the tests were stopped after reaching a slip of 5 mm. Nevertheless, this difference did not alter the bond performance as the slip will continuously increase after reaching the maximum load with increasing the testing time. Moreover, Figure 6-8 shows that there were no big differences on the bond-slip responses between CR and HL series. The bond-slip curves

stayed at low level, below 10 MPa, which is similar as the cracked concretes. The results of several bond parameters of HL concretes were summarized in Figure 6-15. The parameters of τ_u , τ_m and $E_{1.0}$ exhibited a similar tendency. The average ultimate bond strengths of M1-3 were always higher than other mixtures due the low w/c of 0.40, which is similar as for the UNCR and CR series. The main results from Figure 6-15 were further analysed by the Taguchi method and the main effects plots were presented in Figure 6-16, Figure 6-17 and Figure 6-18. In general, interesting tendencies of SN ratios for the bond properties (i.e. τ_u , τ_m and $E_{1.0}$) of HL concretes in function of design factors, crack width and healing time were observed.

Firstly, the factor of w/c again showed the steepest curve in main effect plots (see Figure 6-16, Figure 6-17, Figure 6-18) that means the w/c strongly affects the bond properties on healed concrete. The w/c of 0.40 always achieved the highest SN ratio regardless of crack width and healing time. In most cases, increasing w/c from 0.40 to 0.60 resulted in a gradual decrease of SN ratio. Based on the statistical evaluation on HL (28D) series from Table 6-6, a significant effect of w/c was only clear in the ultimate bond strength for small cracks (200–300 μm , p-value = 0.025) and medium cracks (300–400 μm , p-value = 0.004). In case of mean bond strength, there was no significant contribution of the bond properties with all design factors. Statistical results based on fracture energy follow the same conclusion as mean bond strength, expect one series namely HL400-500 (28D) indicated w/c as a significant factor. Furthermore, in the series of HL (112D), none of the design factors showed their significant effects to the bond properties after a long healing.

Secondly, the SN ratios of HL series (28D and 112D) were always higher than the CR series. Since the SN ratio is directly related to the bond properties, it is evident that a higher SN ratio leads to a higher properties. Although a considerable improvement of the bond properties is not really apparent in Figure 6-15, the SN ratios results confirm that there was actually an improvement of the bond properties from the cracked to healed condition. For the results obtained from 28 days of healing (HL (28D)), this improvement is potentially still minor as the cracks inside the specimens may not be covered by the healing products. This is evident from the observation by the author where the healed specimens (after pull-out test) were split and the healing products were found not covering the internal wall of the crack, but rather available near the crack mouth. As a matter of fact, these healing products could not form a strong connection in a gap between the concrete and embedded steel rebar. It is noteworthy to mention that the HL (28D) and HL (112D) concretes had different maturity level. Specimens, at the time of

pull-out tests, were 49 and 133 days old for the concretes healed after 28 and 112 days, respectively. The SN ratios of HL (112D) were always higher than HL (28D) which is potentially due to the concrete ageing. The mechanical strength of concrete will slightly increase after 28 days as increasing the curing time/age of specimens due to a continuous hydration. This notion can also support the fact that the bond strength of healed concrete after 112 days of healing is slightly higher than the ones after 28 days.

Thirdly, by looking into the values of SN ratios in different crack width, the SN ratios of bond properties with small cracks (200–300 μm) were, in most cases, higher than the SN ratios for medium cracks (300–400 μm) and big cracks (400–500 μm). This confirms that there is a gradual reduction of the bond properties as increasing the crack width.

The influence of crack width can also be analysed by ANOVA considering p-values from each sample series as shown in Table 6-7. The Tukey's test was aided as post hoc test to detect the significance difference between mixture series. The results showed that crack width apparently showed a significant influence on the ultimate bond strength regardless of cracked and healed condition. The difference of τ_u with the crack width range between 200–300 and 400–500 μm were statistically significant. This may be attributed due to the big cracks such 400–500 μm cause more reduction of the bond strength as compared with small cracks such 200–300 μm . Similarly like τ_u , the significant difference was also detected on the τ_m and $E_{1.0}$ results between the crack width of 200–300 and 400–500 μm but only in healed specimens. This suggests the importance of considering the size of crack width to evaluate the bond properties in cracked and healed concretes.

Finally, the most significant factor affecting the bond properties was w/c with the w/c of 0.40 as the optimum parameter (with respect to other w/c in this study). In terms of FR, there was an unclear tendency on the effect of its level from 0.34 to 0.54. For the selection of HA, it seems that the inclusion of HA (CA or BAC in this case) would not really help to enhance the bond strength of cracked / healed concretes. It should be noted that the addition of HA may help to heal the crack by crack closure effect but it does not mean that the crack healing would give an extra bond strength recovery to the reinforcement inside concrete. As a matter of fact, by reducing a little amount of water (w/c) in the mixture, the same effect as using HA can be attained in terms of the bond strength which means that the cost is clearly lower. Furthermore, Figure 6-19 visually shows the changes of ultimate bond

strengths of reinforcement in different concrete conditions from the cracked to healed condition (both after 28 and 112 days of healing) observed in several crack width ranges. It is found that the healing process affects positively to slightly increase the bond strength of rebar in the cracked concrete. This is valid for the healing time of both 28 and 112 days and at any crack widths between 200 and 500 μm . Nevertheless, interestingly, for the crack width of 200–300 and 300–400 μm , a longer healing time of 112 days exhibits a better bond strength recovery than a short healing time of 28 days. With the crack width of 400–500 μm and the increase of healing time from 28 to 112 days, the bond strength recovery was rather limited and less apparent than the other crack width ranges.

Table 6-7. Statistical evaluation of the effect of crack width in the bond properties (note: the p-value of 0.05 was set as a significance threshold and the highlighted 'green' cells represent significant p-values)

Variable	Series	p-value (based on raw data)		
		τ_u	τ_m	$E_{1.0}$
Crack width (200–500 μm)	CR	0.010	0.072	0.118
	HL (28D)	0.016	0.025	0.014
	HL(112D)	0.001	0.001	0.002
Remarks (mixture series that show significant difference in bond results as detected by Tukey's test)		<ul style="list-style-type: none"> • CR200-300 vs. CR400-500 • HL200-300 (28D) vs. HL400-500 (28D) • HL200-300 (112D) vs. HL400-500 (112D) 	<ul style="list-style-type: none"> • HL200-300 (28D) vs. HL400-500 (28D) • HL200-300 (112D) vs. HL400-500 (112D) 	<ul style="list-style-type: none"> • HL200-300 (28D) vs. HL400-500 (28D) • HL200-300 (112D) vs. HL400-500 (112D)

The self-healing effect on the bond properties can be analysed by the following equation:

$$SHR = \frac{i_{HL(x)}}{i_{CR}} \quad (6.6)$$

where SHR is self-healing ratio, i is the bond parameter (i.e., τ_u , τ_m or $E_{1.0}$), HL is healed concrete, CR is cracked concrete, x is the number of healing days (i.e., 28D or 112D). In case of SHR equals to or below than 1.0, it means that there is no improvement of the bond properties. Based on the large data set of nine mixtures, the SHR can be calculated with considering the self-healing effect for each healing agent as shown in Figure 6-21.

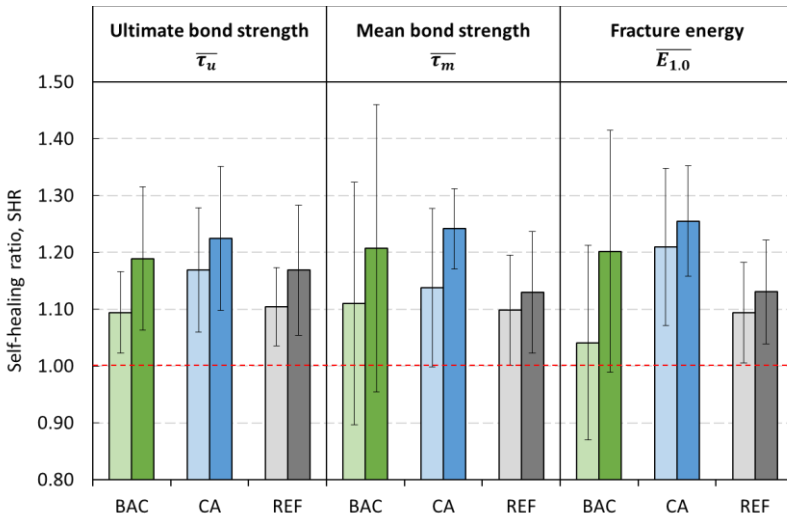


Figure 6-21. Self-healing ratio of the bond properties (note: for each HA factor, the left and right columns represent the bond results after 28 and 112 days of healing, respectively)

As expected, there is a big variation of the SHR results which is previously detected in the raw data (see Figure 6-15). Nevertheless, in general, there is an improvement of bond properties by the addition of healing agent from the cracked to healed condition. For instance, in τ_u , the average SHR (28D) for BAC was similar to the REF (around 1.10), but the average SHR (28D) of CA is slightly higher at 1.17. Furthermore, after 112 days of healing, the SHR (112D) of CA still showed the highest value at 1.23, followed by BAC (1.19) and REF (1.17). It is interesting to observe that the SHR of τ_u REF after 112

days of healing can be achieved with the CA with only 28 days of healing. In terms of τ_m and $E_{1.0}$, a big variation of BAC results was observed which may be attributed to the discrepancy in the bond-slip curvatures. Nevertheless, there is a similar trend of both τ_m and $E_{1.0}$ as compared with τ_u where the average of SHR for all bond properties increases after the addition of healing agent and increases from 28D to 112D. Eventually, the good behaviour of self-healing concrete is demonstrated in addition to the ability of self-healing concrete to heal and seal the cracks. This behaviour is possibly due to the crack-filling and pore-filling effects of self-healing concrete matrix portions bonded to the interface of the steel reinforcement. Moreover, Table 6-8 shows the statistical evaluation of the SHR based on the design factors (i.e., w/c, FR, HA) and the results suggest that the influence of mix design factor toward SHR on the bond properties is found to be insignificant are above 0.05 due to the high variability.

Table 6-8. Statistical evaluation of the SHR of bond properties by ANOVA (note: p-value of 0.05 as a significance threshold)

Series	Factor	p-value (based on SHR)		
		τ_u	τ_m	$E_{1.0}$
HL200-300 (28D)	w/c	0.678	0.269	0.768
	FR	0.322	0.134	0.402
	HA	0.198	0.418	0.681
HL300-400 (28D)	w/c	0.927	0.963	0.917
	FR	0.764	0.994	0.952
	HA	0.676	0.812	0.865
HL400-500 (28D)	w/c	0.210	0.227	0.550
	FR	0.355	0.292	0.460
	HA	0.162	0.202	0.170
HL200-300 (112D)	w/c	0.670	0.427	0.672
	FR	0.961	0.879	0.736
	HA	0.932	0.483	0.709
HL300-400 (112D)	w/c	0.430	0.410	0.198
	FR	0.707	0.779	0.733
	HA	0.954	0.870	0.939
HL400-500 (112D)	w/c	0.672	0.932	0.931
	FR	0.978	0.735	0.599
	HA	0.510	0.551	0.285

6.3.6 Analysis of healing products

A qualitative analysis on the healing products can be useful to identify the deposited minerals in the crack. Since it is difficult to take the healing products located inside the crack, the healing products coming out from the crack (see Figure 6-20) were collected by carefully scrapping the powders, stalactites and white granulates at the crack surface. In general, the healing products were divided into three different batches: (1) REF series from M3, M5 and M7 mixtures, (2) CA series from M2, M4 and M9 mixtures and (3) BAC series from M1, M6 and M8 mixtures. Fourier transform infrared (FTIR) spectroscopy (UATR Spectrum Two, PerkinElmer, US) was used to characterize the mineral compounds and the morphology of the healing products based on the spectra analysis. Figure 6-22 shows the FTIR spectra of the tested materials. The FTIR spectra of the precipitates showed the typical vibrational bands for calcium carbonates (CaCO_3), as further explained below:

- *REF mixtures*: A low intensity band at 1795 cm^{-1} corresponds to the C=O bonds from carbonates, while a band at 872 cm^{-1} corresponds to Ca-O bonds [133]. The typical bands centered at 712 and 872 cm^{-1} reveal the presence of calcite [135,137–140]. In this case, the dominant phase of the healing product of REF is found to be calcite.
- *CA mixtures*: A low intensity band at 3694 cm^{-1} corresponds to the O-H bonds from hydroxides, while a low band at 1788 cm^{-1} corresponds also to the C=O bonds from carbonate [133]. The peculiar peaks at 1083 and 1444 cm^{-1} are diagnosed as vaterite if these bands are accompanied with a specific band at $745\text{--}747\text{ cm}^{-1}$ [138,139]. However, as stated by [136,141], the intense bands at 854 and 1083 cm^{-1} are attributed to aragonite phase. The specific intense bands at 712 and 854 cm^{-1} confirm the aragonite form [139]. Therefore, it can be concluded that the dominant phase of the healing product of CA is aragonite.
- *BAC mixtures*: The FTIR spectrum of BAC mixtures has the same agreement as the FTIR spectrum of REF mixtures, except one peculiar peak at 1005 cm^{-1} . A shoulder peak at 900 cm^{-1} may confirm the presence of aragonite, but dominantly the intense peaks confirm the calcite formation in the same way as REF. Furthermore, the healing products of BAC are confirmed to be calcite.

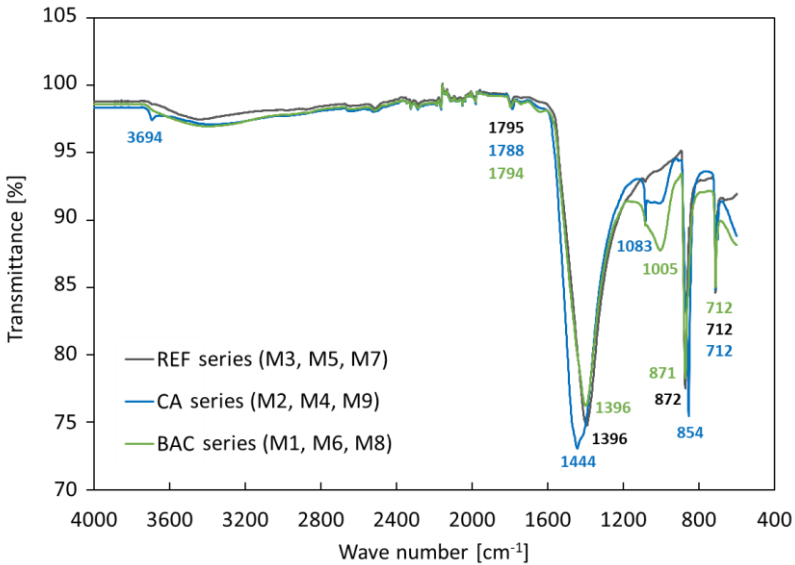


Figure 6-22. FTIR spectra analysis

6.4 Conclusions

In this chapter, several mix design parameters were studied in relation to the fresh and mechanical properties of concrete and mainly the bond properties of steel reinforcement in self-healing concrete. Three mix design factors with employing three levels for each factor were selected namely (1) water-cement ratio (w/c) at 0.40, 0.50, 0.60; (2) fine ratio (FR) at 0.34, 0.44, 0.54; and (3) healing agents with bacteria (BAC), crystalline admixture (CA) and reference (REF). The pull-out specimens were designed in three states of uncracked (UNCR), cracked (CR) and healed (HL). For the CR and HL series, the cracks were made in different widths of 200–300, 300–400 and 400–500 μm . Specifically for HL series, the specimens were healed under water for 28 and 112 days. The test results were processed by the use of a statistical software and the optimisation by the Taguchi method was employed. The following conclusions are listed below:

1. The compressive strength of concrete was found to increase with lowering the w/c, increasing the FR and adding the healing agent of either BAC or CA. Statistical results showed that the w/c and HA were the most significant factors affecting the compressive strength.
2. The bond strength of embedded steel reinforcement in the uncracked concrete was highly influenced by the w/c, followed by HA and FR. A

good correlation between compressive strength and ultimate bond strength was established with an adjusted coefficient of determination of 0.85.

3. The presence of a longitudinal crack along the rebar caused a significant bond strength reduction in the range of 60–82%. Statistical analysis revealed that the variation of crack width from 200 to 500 μm , in fact, influenced the bond properties of rebars in cracked concretes. The effect of mix design factors and levels was only evident in the ultimate bond strength specifically for small cracks (200–300 μm) and the effect of w/c is more superior than all other factors.
4. The crack closure phenomenon was noticeable in all healed concretes after healing for 28 and 112 days. However, the self-healing effect by the healing agents did not significantly improve the bond strength. A longer healing period exhibited a better improvement for concretes with small-to-medium cracks of 200–400 μm .
5. The healing products coming out from the crack were confirmed to be calcium carbonates in the polymorph of calcite for REF and BAC mixtures and aragonite for CA mixtures.

Chapter 7

MIX DESIGN OPTIMISATION OF SELF-SEALING CONCRETE CONTAINING MICROCAPSULES WITH PU SHELL AND WATER REPELLENT CARGO

7.1 Introduction

Microencapsulation is a recent advanced self-healing technology that enables storing agents in a tiny vessel called as microcapsule. In many applications, healing or sealing agents are encapsulated in order to ensure the viability of the agent, homogenous distribution throughout the matrix, and to facilitate localised repair where cracks are occurring and capsules are triggered. The encapsulation technique for self-healing applications was firstly introduced in 2001 by White et al. [16] in polymers where a microencapsulated healing agent was embedded in a structural composite matrix containing a catalyst. When the matrix was damaged by the presence of cracks, the microcapsules broke and released the healing agent into the crack plane through capillary action. The healing agent contacted the catalyst, triggering polymerization that eventually closed the crack. The schematic illustration of this mechanism is presented in Figure 7-1 taken from [16].

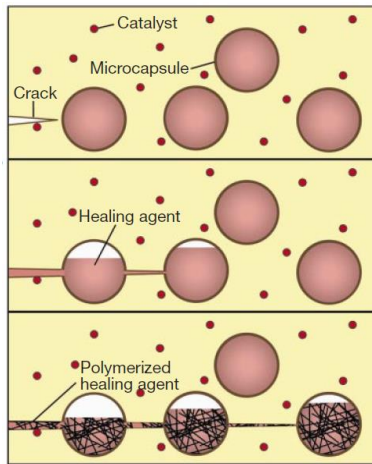


Figure 7-1. Autonomic healing mechanism on the use of microcapsules [16]

Since then, more technological developments of encapsulation are made by researchers and industrial experts with several production methods such as *situ* polymerization and complex coacervation. The quality of microcapsules strongly depends on the shell material, shell thickness, size of capsule, suitable cargo, chemical formulation, manufacturing process, etc. The microcapsules are typically produced in bulk and stored in solution for preservation. A variety of microcapsules has been developed in recent years. A list of several microcapsule materials with the corresponding parameters and characteristics used in concrete application can be found in Table 2-1.

There are both pros and cons related to the use of microcapsules in cementitious materials. Microcapsules were found to be beneficial in terms of healing/sealing efficiency [50,59,95,187], strength recovery [49,52,62] and improved durability [17,90,188], as previously reported in many publications. These benefits were often observed after the specimens were damaged. However, the inclusion of microcapsules, of various sizes and dosages, can reduce the tensile and compressive strength in a non-damaged composite, meaning that the mechanical performance of cementitious composite declined due to the incorporation of microcapsules before damage or cracking of the specimens. Capsule agglomeration [62], capsule breaking during mixing [94,96], increased porosity [95,97] and change of the microstructural matrix [52,92] are some potential explanations that may be responsible for the strength reduction. Therefore, it will be necessary to modify the mix design to compensate this flaw, as reaching the target strength is a mandatory condition.

This chapter is essentially divided into two programs. The first program (Section 7.2) aimed to assess the effect of microcapsules in terms of fresh, hardened and self-sealing properties of the concrete, to get acquainted with the materials. This preliminary study was executed with a limited quantity of microcapsules. In the second program (Section 7.3), after understanding the performance of microcapsule-based concrete from the first program, the mix design optimisation is implemented with employing three mix design parameters including w/c, capsule dosage and capsule size. The main objective of the optimisation is to compensate the strength reduction induced by the inclusion of microcapsules, as well as to optimise the sealing performance. The newly produced microcapsules with varying size and varying dosage are used for optimisation at concrete level. In addition, the influence of microcapsules on the fresh and mechanical properties of cement paste and mortar are further investigated.

7.2 Preliminary study on the workability, mechanical and self-sealing properties of concrete containing microcapsules with PU shell and water repellent cargo

7.2.1 Materials

Two batches of microcapsules (MIC) in slurry state were provided by Micropore Technologies Ltd (referred as producer) namely MIC_59 and MIC_88. These microcapsules were produced through a membrane emulsification process, followed by interfacial polymerization. The median sizes (d50) of the microcapsules were 59 and 88 μm for MIC_59 and MIC_88, respectively. The capsule shell was made of polyurethane (PU) and the synthesis of this PU was done by using a monomeric building block (isophorone diisocyanate (IPDI)) after undergoing a chemical reaction. The cargo of the capsules was water-repellent agent (WRA, Sikagard 705L). The detailed information of the microcapsule batches is given in Table 7-1 and the microscopic images of MIC_59 and MIC_88 can be found in Figure 7-2.

Table 7-1. Background information of microcapsules

Microcapsule batch	MIC_59	MIC_88
Continuous phase (CP)		
PVA	2% aqueous solution	1% aqueous solution
Dispersed phase (DP)		
Sikagard 705L	80 wt%	70 wt%
Isophorone Diisocyanate	20 wt%	30 wt%
Membrane		
Size	10 × 200 μm	10 × 200 μm
Size information		
d10 (μm)	49.29	73.84
d50 (μm)	59.45	88.15
d90 (μm)	70.83	102.58
Span	0.36	0.33
CV	14.99	16.22
Active core content		
Core content (%)	15	35

Note: Span is a statistical measurement which refers to the width (or span) of the size distribution, CV is coefficient of variation

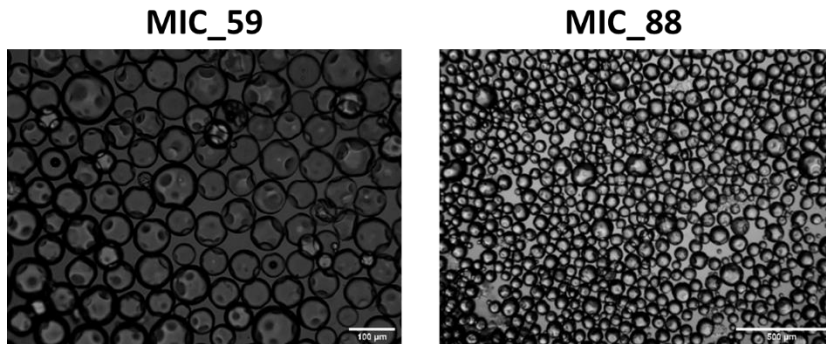


Figure 7-2. Microscopic images of microcapsules as provided by the producer

Prior to the concrete production, all batches of microcapsules were filtered by means of filter paper (5-13 μm) for 24 hours in the lab environment at 20°C. Then, in order to remove the excess water present in the capsules, the dry capsules were stored in the oven at 35°C. As discussed with the producer, the thermal degradation of the capsules seems to show that there is no major mass change at 40°C and there should not be any shrinkage considering the shell was made of PU. After drying, the capsules were present in the form of powder and flakes as shown in Figure 7-3. The pure (dry) capsules of MIC_59

and MIC_88 were weighed at 261 and 118 g, respectively. The preliminary investigation was aimed to gain a first understanding on the effects of microcapsules on the concrete properties.



Figure 7-3. Filtering process of microcapsules

The C30/37 concrete mix design is proposed in Table 7-2. The reference concrete (REF) had the cement content of 330 kg/m^3 and the water-cement (w/c) ratio was fixed at 0.50. CEM III/A 42.5 was used in this study, having 52% clinker and 48% blast furnace slag. Sea sand with the fraction of 0/2.5 was used as fine aggregate, while two fractions of gravels (4/8 and 8/16) were used as coarse aggregates. The specific gravities of sand 0/2.5, gravel 4/8 and gravel 8/16 were 2.67, 2.59 and 2.60, respectively. Polycarboxylate-ether (PCE) superplasticizer (Fluivicon 801, supplied by CUGLA B.V.) with a 20% solid content was used to improve the workability of the fresh mixture. Due to the limited amount of materials, the dosages of microcapsules were restricted. For MIC_59, the used dosages were 0.5, 1.0 and 1.5% by weight of cement (bwoc), while for MIC_88, only one dosage was done at 1.5% bwoc due to the limited amount of material. The microcapsules were added on top of the normal mixes, thus no adaptations of the mix designs were made for the introduction of the capsules. The mixing procedure was proposed as follows:

1. Prior to mixing, the dry microcapsules were added and diluted to the mixing water until homogeneous

2. All raw materials (cement, sand, gravels) were put into the mixer and were mixed for 30 s
3. Mixing water (with dry microcapsules which have been diluted) was added to the mixer and the mixing was continued for 2 min
4. Superplasticizer was added into the mix, then the mixing was continued until reaching a total mixing time of 6 min
5. Eventually, the fresh mix was tested and then cast into cubical moulds, cylindrical moulds and prismatic moulds. It should be noted that 20 liters of fresh concrete was produced for all mixtures
6. 24h after casting, the specimens were demoulded. The cubes and cylinders were stored under water at $20\pm 2^{\circ}\text{C}$, while the prisms were stored in the curing chamber at $20\pm 2^{\circ}\text{C}$ and 60% RH

Table 7-2. Mix designs of reference and microcapsule-based concretes

Material	Unit	REF	0.5% MIC_59	1.0% MIC_59	1.5% MIC_59	1.5% MIC_88
CEM III/A 42.5N	kg/m ³	330	330	330	330	330
Sea sand 0/2.5	kg/m ³	740	740	740	740	740
Gravel 4/8	kg/m ³	702	702	702	702	702
Gravel 8/16	kg/m ³	378	378	378	378	378
Effective water	kg/m ³	165	165	165	165	165
Effective w/c	-	0.50	0.50	0.50	0.50	0.50
SP Fluvicon 801	kg/m ³	0.90	0.90	0.90	0.90	0.90
Microcapsules (MIC) dosage	kg/m ³	0	1.65	3.30	4.95	4.95

7.2.2 Testing program

A series of tests was programmed to evaluate several concrete properties after the introduction of microcapsules. In terms of fresh properties, the slump, air content and fresh density tests (EN 12350-2,6,7) were executed after mixing. In terms of hardened properties, on three hardened cube samples of $150\times 150\times 150\text{ mm}^3$ per concrete mixture the hardened density test (EN 12390-7), ultrasonic pulse velocity (UPV) test (EN 12504-4) and compression test (EN 12390-3) were executed; and for one cylindrical sample of $\text{Ø}100\times 200\text{ mm}$ per mixture the tensile splitting strength (EN 12390-6) was determined. In terms of self-sealing properties, capillary water absorption tests were performed on two reinforced prisms of $100\times 100\times 400\text{ mm}^3$ (see Figure 7-5) for the reference concrete (one for the

uncracked series (UNCR) and one for the cracked series (CR)), while for the other four mixtures containing microcapsules, only one prism per mixture was used for the CR series. As a note, the cube and cylindrical specimens were stored in a water tank at a temperature of $20\pm 2^{\circ}\text{C}$, while the prismatic specimens were stored in a curing chamber at $20\pm 2^{\circ}\text{C}$ and 60% RH. There were two steel rebars $\varnothing 5$ mm embedded in the upper part of the prism to ensure that no sudden failure occurred during cracking. The prisms of the CR series were cracked by means of a three-point bending test at the age of 14 days. The target crack width for this test was around $200\ \mu\text{m}$. After cracking, the crack width was measured by means of an optical microscope. Five marks along the crack line at the bottom side of prism were selected and in each mark, five measurements of crack width were done. Thus, the average crack width was calculated based on the average measurement of 25 data points (5 marks \times 5 measurements). The cracking test and the crack measurement are depicted in Figure 7-4.

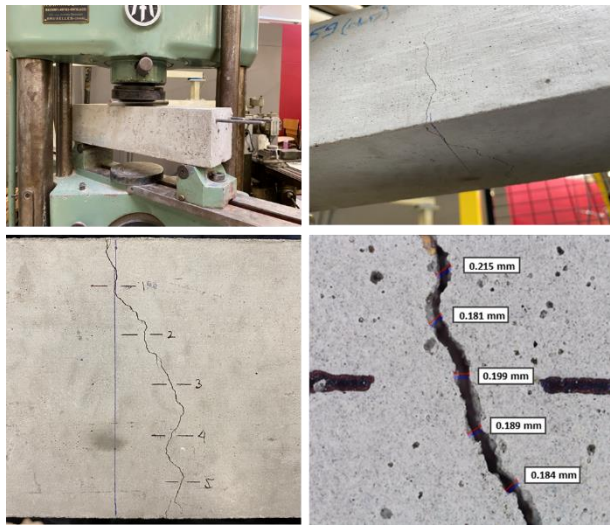


Figure 7-4. Cracking the specimen and measuring the crack width

After crack formation, the cracked prisms were stored in the oven at 40°C for 10 days until constant weight achieved. Constant weight was considered to be achieved when the change in mass over a period of 24 hours was less than 0.2%. Next, the sides and the bottom of the specimens were partially covered with epoxy resin (Episol Designtop SF) as shown in Figure 7-5. The prisms were later returned to the oven for 3 days and the capillary water absorption test was finally conducted. A small area around the crack (20 mm in width)

was left uncovered which was assigned as a contact area for this test (see Figure 7-5). The specimens were immersed in water with the water level at 3 mm from the bottom surface of the prisms. The weight of the specimens was recorded at 10, 20, 30, 60, 90, 120, 180, 240, 360, 480, and 1440 min. During the capillary water absorption test, it was ensured that the water level remained constant. The CWA test procedure remained the same for UNCR specimens from reference concrete (only without cracking).

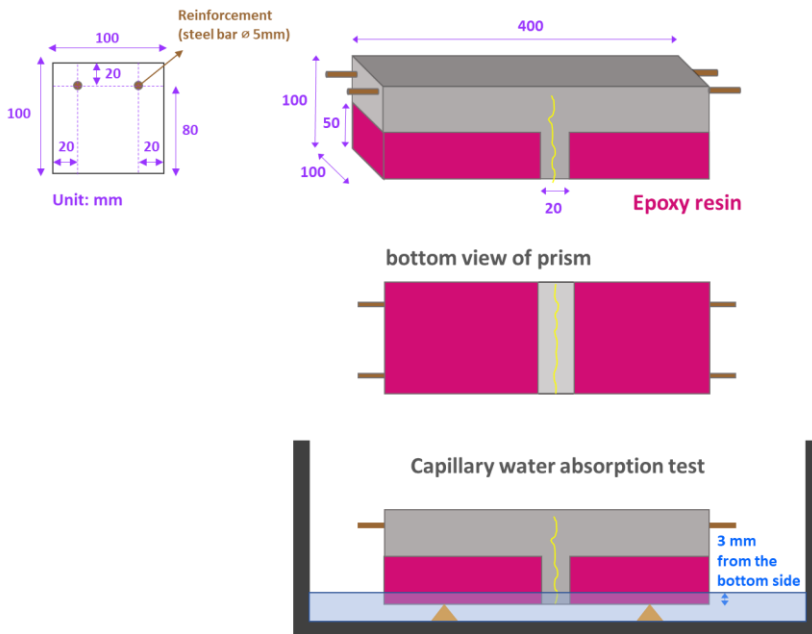


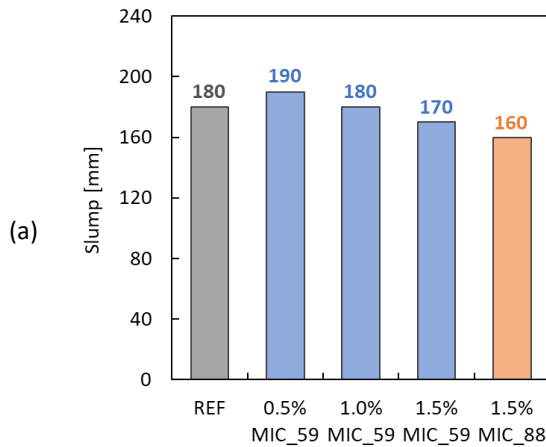
Figure 7-5. Configuration of the prism specimen and the setup of the capillary water absorption test

7.2.3 Results and discussion

7.2.3.1 Fresh properties

The fresh properties of all concrete mixtures are given in Figure 7-6. As shown in Figure 7-6(a), the slump of reference concrete was 180 mm which was classified as a slump class of S4 in accordance with EN 12350-2. The slump values of fresh concretes added with MIC_59 at 0.5%, 1.0% and 1.5% bwoc were 190, 180 and 170 mm (S4 slump class), respectively, while the addition of MIC_88 at 1.5% bwoc had a slump of 160 mm (S4 slump class). In

general, the addition of microcapsules did not considerably affect the slump. Regardless of the capsules dosage (from 0.5 to 1.5% bwoc) and the capsule size (in this case, either 59 or 88 μm), the slump class of these mixtures was the same as the reference mixture. The air content was evaluated and the result is depicted in Figure 7-6(b). The air content of reference concrete was recorded at 3.0%. The incorporation of microcapsules clearly increased the air content of the fresh mixture. The addition of MIC_59 from 0.5 to 1.5% bwoc caused an increase of air content in the range of 1.1–1.3%, while the addition of MIC_88 at 1.5% bwoc exhibited a 1% increase in air content. In terms of fresh density, the addition of microcapsules did not really influence the fresh density of the normal mixture as the fresh densities of all mixtures were identical as shown in Figure 7-6(c).



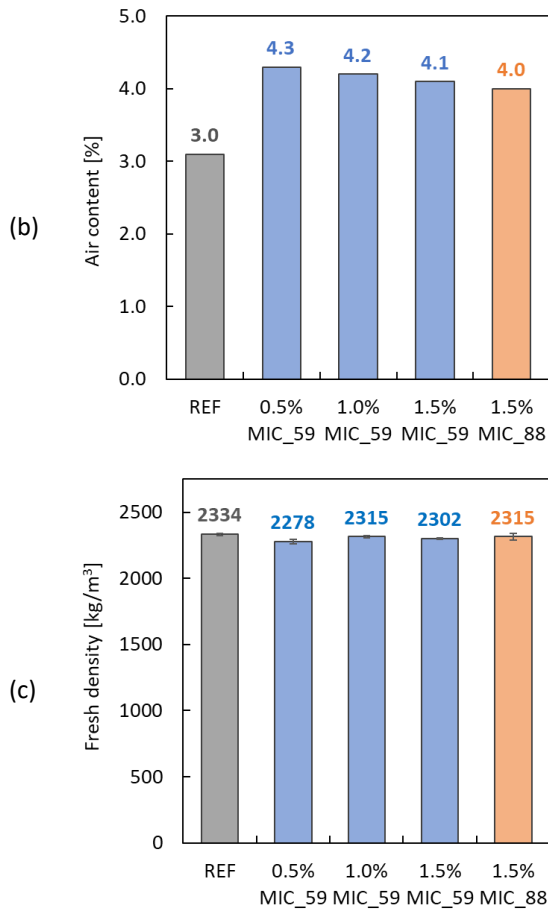
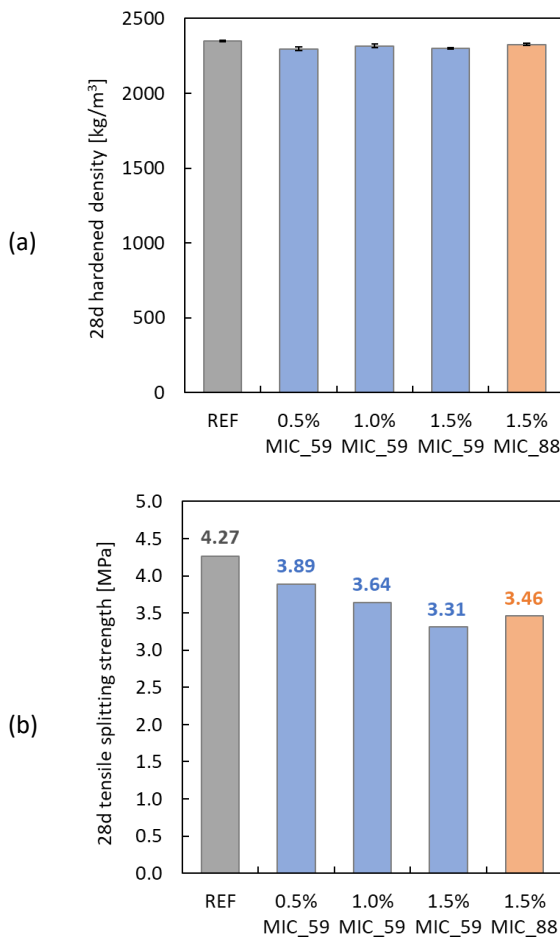


Figure 7-6. Fresh test results: (a) slump, (b) air content and (c) fresh density of all concrete mixtures with and without microcapsules' addition (note: single measurement for slump and air content results, while three measurements for fresh density result)

7.2.3.2 Hardened properties

The hardened concrete properties were mainly evaluated at the age of 28 days. The hardened densities of all concrete mixtures with and without microcapsules were comparable around 2300 kg/m³ as shown in Figure 7-7(a), which is in line with the observation from fresh density (see Figure 7-6(c)). According to Figure 7-7(b), the tensile splitting strength of the reference concrete was recorded at 4.27 MPa. It was found that increasing

the dosage of microcapsules from 0.5 to 1.5% bwoc led to a gradual reduction of the tensile splitting strength. The additions of MIC_59 reduced the tensile splitting strength by 9, 15 and 22% with the specific dosage at 0.5, 1.0 and 1.5% bwoc, respectively. The addition of 1.5% MIC_88 also caused a 19% reduction in tensile splitting strength, which is similar with the addition of 1.5% MIC_59. However, it should be noted that there is no possibility for repetition during testing the tensile splitting strength due to the limited amount of pure capsules which led to a limited concrete volume (or sampling). Further investigation is needed to re-confirm this result with more repetitions.



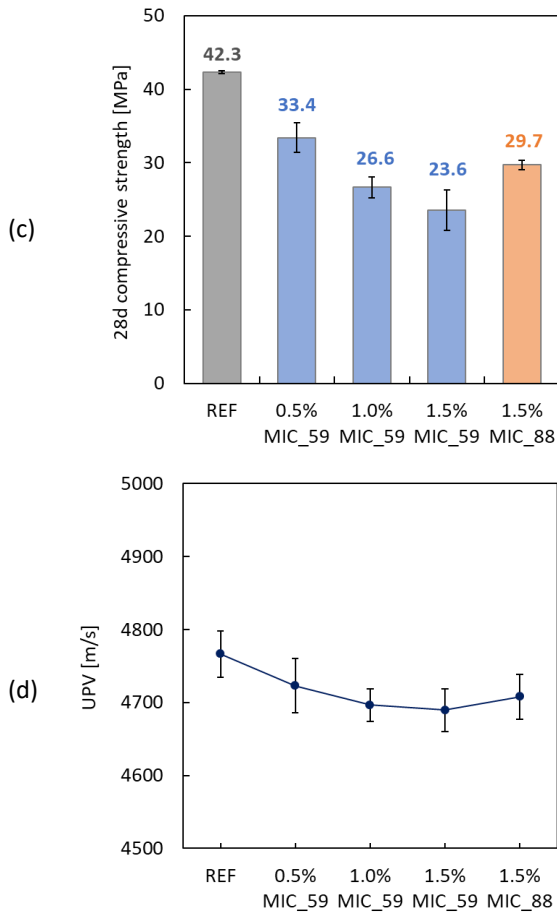


Figure 7-7. Hardened test results: (a) hardened density, (b) tensile splitting strength, (c) compressive strength and (d) ultrasonic pulse velocity of all concrete mixtures with and without microcapsules' addition

The 28d compressive strength of the concrete is presented in Figure 7-7(c). The reference concrete had an average compressive strength of 42.3 MPa. A significant reduction of the compressive strength was found with the inclusion of microcapsules. Similarly like the tensile splitting strength results, the gradual reduction of compressive strength was attained with increasing the capsules' dosage. The additions of MIC_59 at a very low dosage of 0.5% greatly reduced the compressive strength by 21%. Doubling the dosage of MIC_59 from 0.5 to 1.0% caused a higher strength reduction to 37%. A 47% reduction of compressive strength was noticed after adding the MIC_59 at the dosage of 1.5%. Moreover, the addition of 1.5% MIC_88 caused a 30%

strength reduction with respect to the reference concrete. Interestingly, comparing the MIC_59 and MIC_88 at the same dosage (1.5% bwoc), the reduction was more severe on the use of MIC_59 than MIC_88. As depicted in Figure 7-7(d), the compactness of the concrete matrix evaluated by means of the UPV device followed the same trend as the compressive strength results. The average ultrasound velocity of REF was 4766 m/s, while the addition of either MIC_59 or MIC_88 slightly reduced the velocity values. It seems that the higher the addition of microcapsules, the higher the reduction in velocity. However, it should be noted that the differences in velocities for all concretes were not significant (p -value > 0.05, tested by one-way ANOVA).

In fact, the negative effect of using microcapsules in the cement-based composite has been reported in Section 2.2.3.2. Specifically here, by selecting the capsule dosage as the main parameter, the current results are compared with the available results from the literature as shown in Figure 7-8. As expected, past studies also found a strength reduction after introducing microcapsules into the concrete. Although different studies use different types of capsule materials (e.g. shell, core, etc.), the capsule dosage plays a critical role in downgrading the mechanical properties. In any case, the strength reduction of concrete with the use of MIC_59 and MIC_88 is at a higher level than the observations from past studies. One interesting result was obtained by Litina et al. [91] where the incorporation of Gelatin/gum Arabic shell microcapsules (with sodium silicate as a cargo) exhibited a minor effect in the concrete strength: 10% strength reduction for a microcapsule dosage of 4.0% bwoc, and even less than 20% strength reduction at a microcapsule dosage of 5.3% bwoc. Figure 7-8 implies that the type of microcapsules itself contributes to lowering the strength of concrete and the chemical composition and other aspects of the microcapsules may affect the performance. A wide range of capsule parameters should be investigated in future works to achieve an optimum design. The heterogeneous distribution of capsules in the matrix, leading to the clustering of the capsules, may also be responsible for this drawback and this will be elaborated in the section 7.2.3.4.

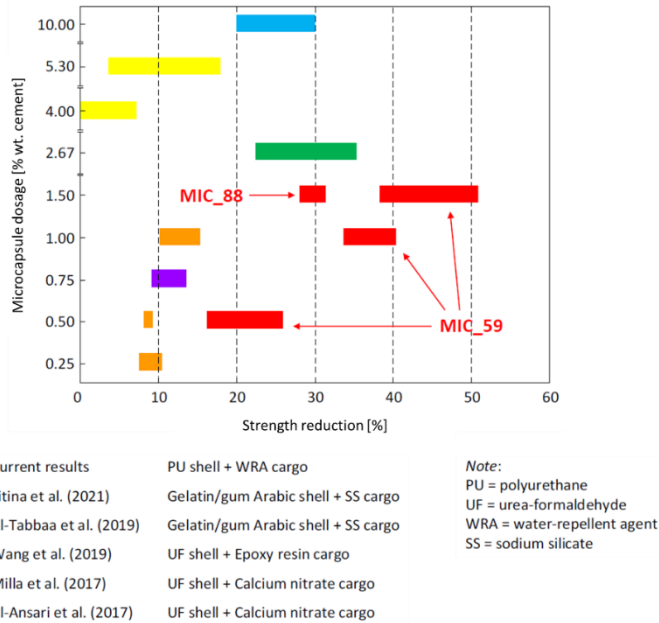


Figure 7-8. Comparison of strength changes of MIC concretes with different MIC dosage

7.2.3.3 Self-sealing properties

In order to perform the self-sealing test, the 14-days-old prisms were initially cracked by means of the three point bending test. The loading of the machine was manually controlled until a crack appears at the mid bottom side of the prism. Figure 7-9 shows the average crack width of all specimens from different mixtures. The average crack widths of all cracked specimens were relatively comparable (~ 0.200 mm) and the difference in crack widths is statistically not significant. The prisms were later tested by means of the capillary water absorption test and the result is depicted in Figure 7-10. There is a significant difference in the development of water uptake in function of time between the UNCR and CR series of reference concretes. In the UNCR series, the water uptake was rather low considering there were no cracks available in the contact area, thus the water entered via capillaries at the concrete surface. In the CR series, as shown by the blue line in Figure 7-10, there is a high water uptake by the cracked REF concrete due to the ingress of water via the crack. At the end of the measurement (after 24h), the final water uptake values of reference UNCR and CR concretes were 5.4 and 35.4

kg/m², respectively. It shows that the presence of a crack strongly affects the capillary water absorption with a factor of 6.5 at 24 hours. The cracked concretes containing microcapsules were also tested and it was interesting that the water uptake of these concretes was much lower than the water uptake of cracked reference concrete, and actually comparable to the water uptake of the uncracked reference concrete. Figure 7-11 shows a fast water ingress in the first 15 min via crack and capillaries in the cracked reference concrete and no sign of water ingress in the cracked MIC concrete. There are two hypothesis that can explain this behavior:

- The capsules present in the crack zone may rupture and release the sealing agent after cracking. This agent will seal the concrete matrix by giving a water-barrier effect, thus less water ingress via crack is expected.
- It might be possible that a certain amount of microcapsules is already ruptured even during the concrete mixing. The capsules may break due to the collision with aggregates and blade mixer. In this way, the broken capsules will release the sealing agent to the concrete matrix even before cracking happens. In other words, it can be that the MIC concrete matrix itself is already water repellent.

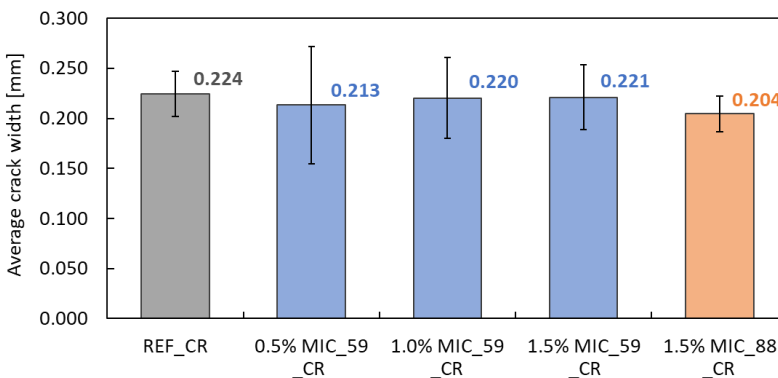


Figure 7-9. Average crack width of all cracked prisms

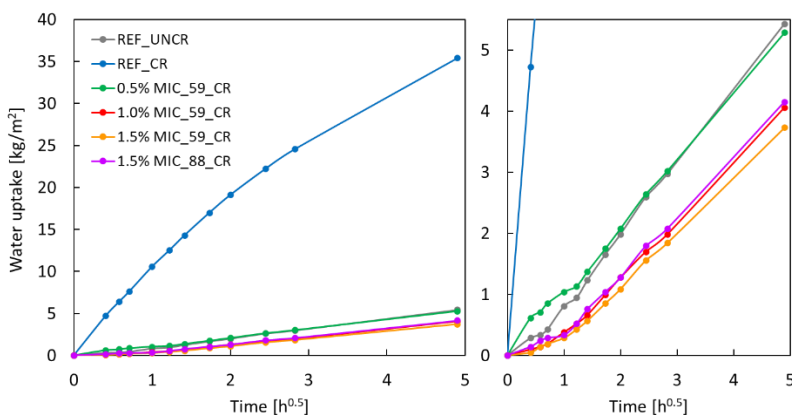


Figure 7-10. Capillary water absorption capacity (note: UNCR – uncracked, CR – cracked, REF – reference concrete, MIC – microcapsule-based concrete)

REFERENCE CONCRETE (CRACKED)



MIC CONCRETE (CRACKED)



Figure 7-11. Comparison of water ingress in the cracked reference and MIC concretes (both pictures were taken 15 min after the capillary water absorption test was performed)

In accordance with EN 13057, the sorption coefficient (S) was determined and the results are tabulated in Table 7-3. It seems that there is a little improvement of the sealing ability of MIC concrete with increasing the capsule dosage where the S of 1.5% MIC_59 < 1.0% MIC_59 < 0.5% MIC_59. The S of 1.5% MIC_88 was higher than the S of 1.5% MIC_59, but was comparable with 1.0% MIC_59. Moreover, the sealing efficiency (SE) is calculated with Equation (7.1) to determine the efficiency of the microcapsules. The results showed that regardless of capsule dosage and capsules size, the addition of microcapsules gives a good sealing system to the concrete. The ability of microcapsules to seal the concrete cracks is

evident with the high sealing efficiency (80–90%), showing a considerable improvement in terms of durability.

$$SE = \left(1 - \frac{S_{MIC_CR}}{S_{REF_CR}}\right) \times 100\% \quad (7.1)$$

Table 7-3. Self-sealing results based on the CWA tests

Specimen	Sorption coefficient, <i>S</i> (kg/(m ² h ^{0.5}))	Sealing efficiency, <i>SE</i> (%)
REF_UNCR	1.11	-
REF_CR	7.22	-
0.5% MIC_59_CR	1.08	85
1.0% MIC_59_CR	0.83	89
1.5% MIC_59_CR	0.76	89
1.5% MIC_88_CR	0.85	88

7.2.3.4 Microcapsules' observation in the concrete matrix

An additional investigation was conducted to observe the presence of microcapsules in the concrete matrix. As the fluorescence dye has been previously added to the slurry of microcapsules by the producer, the microcapsules will 'shine' under the fluorescence light. In this test, a split cylindrical MIC specimen (1.5% MIC_59) was taken as a representative sample and the optical microscopy aided with fluorescence light was used to monitor the capsules. Figure 7-12 shows few locations of capsules found in the matrix. It should be noted that it was quite difficult to find the capsules, considering the dosage of capsules was very low (1.5% bwoc). Apparently, many 'clumped' microcapsules were clearly observed in the concrete matrix, meaning that the capsules are not well dispersed within the mixture. It was later found that the drying process of microcapsules during the preparation stage was responsible for the capsule agglomeration. As a consequence, the capsules are not mixed homogeneously in the fresh mix and it can be one of possible reasons of strength reduction. In this work, capsule agglomeration is not intended and should be prevented in the future and this can be done by using the capsules in slurry form. Consequently, in order to avoid the capsule agglomeration, the capsules were further added in slurry as later discussed in Section 7.3.

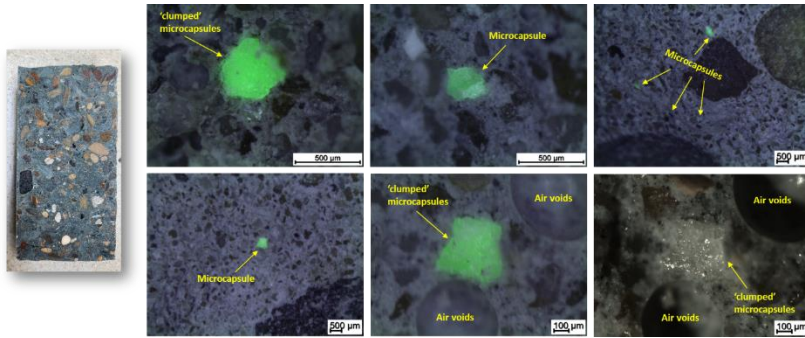


Figure 7-12. Observation of microcapsules in the concrete matrix via optical microscopy

7.2.4 Conclusions

This preliminary work was aimed to understand the effects of microcapsules on the concrete properties. Two capsule parameters were chosen namely (1) capsule size (59 and 88 μm) and (2) capsule dosage (0.5, 1.0 and 1.5% by weight of cement for MIC_59). Microcapsules were added into the fresh mixture in a dry form. Fresh, hardened and self-sealing tests were executed to evaluate the performance of concrete with and without the addition of capsules. The key conclusions are listed below:

1. The addition of microcapsules into the fresh mix did not affect the slump, but it increased the air content.
2. The inclusion of microcapsules provided a better sealing system to the concrete as compared to the traditional concrete.
3. The non-uniform distribution of capsules throughout the mix certainly has contributed to the large decrease in mechanical performance. Moreover, a decrease in the compressive strength with increasing capsule dosage was also observed.

7.3 Mix design optimization of microcapsule-based concrete using the full factorial design technique

7.3.1 Microcapsules

Another two batches of freshly produced microcapsules (MIC) in slurry state were provided namely MIC_56 and MIC_93. These microcapsules were produced through a membrane emulsification process, followed by interfacial polymerization [189]. The median sizes (d50) of microcapsules for MIC_56 and MIC_93 were 56 and 93 μm , respectively. The capsule shell was made of polyurethane (PU) and the synthesis of this PU was done by using a monomeric building block (isophorone diisocyanate (IPDI)) after undergoing a chemical reaction. The core content of the capsules was water-repellent agent (WRA, Sikagard 705L). The detailed information of the microcapsules batches is given in Table 7-4. Capsule morphology was characterized using optical microscopy (OM) (Meiji GXCAM-U3-5, Meiji Techno, UK) and scanning electron microscopy (SEM) (PhenomXL, Thermo Fisher Scientific, US). As seen in Figure 7-13, the microcapsules are spherical with a smooth shell with some dimpling formed during the shell synthesis process.

Table 7-4. Background information of freshly produced microcapsules

Microcapsule batch	MIC_56	MIC_93
Continuous phase (CP)		
PVA	2% aqueous solution	0.5% aqueous solution
Dispersed phase (DP)		
Sikagard 705L	70 wt%	70 wt%
Isophorone Diisocyanate	30 wt%	30 wt%
Membrane		
Size	10 × 200 μm	10 × 200 μm
Size information		
d10 (μm)	45.37	75.50
d50 (μm)	55.77	92.70
d90 (μm)	77.37	114.96
Span	0.57	0.43
CV	22.07	17.96
Active capsule content		
Core content	70%	70%
Capsule concentration in solution	30 wt%	50 wt%

Note: PVA is poly(vinyl alcohol), Span is a statistical measurement which refers to the width (or span) of the size distribution, CV is coefficient of variation

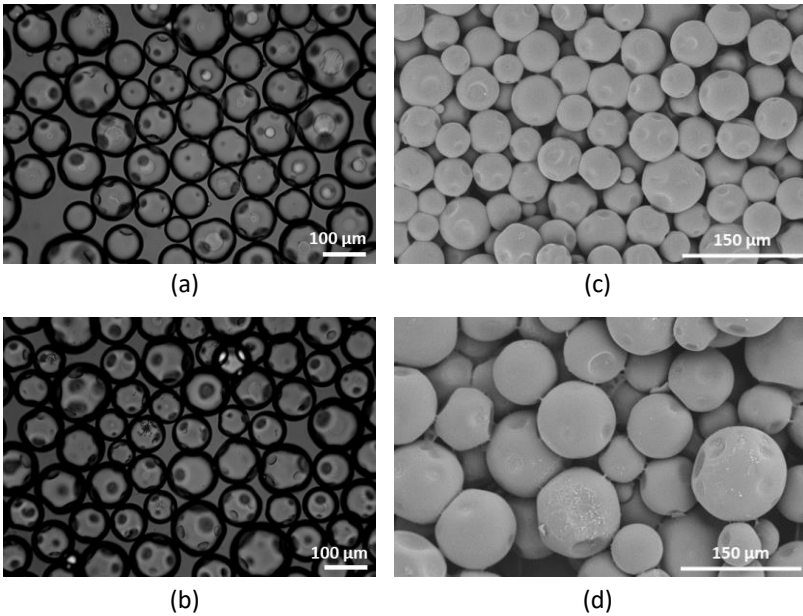


Figure 7-13. Micrographs of freshly produced microcapsules using OM: (a) MIC_56 and (b) MIC_93. Micrographs of freshly produced microcapsules using SEM: (c) MIC_56 and (d) MIC_93.

As a note, the capsule concentrations of MIC_56 and MIC_93 solutions were 30 and 50% by weight of solution (slurry), respectively. Unlike the capsule handling from the previous experiment by filtering, the current capsules were added into the fresh concrete mixture in slurry state. Thus, no drying process was executed in order to avoid the capsule agglomeration and to ensure a homogeneous distribution of the microcapsules within the mixture. It should be noted that the solution contains pure amount of microcapsules and deionized water, and the ratio between capsules and water depends on the given batch (see Table 7-4). Therefore, the amount of deionized water in the solution was considered as a part of the mixing water for cement-based mixtures.

7.3.2 Design of experiment (DOE)

The design of experiment for capsule-based mixtures was basically divided into three main parts, depending on the matrix of the composite starting from the paste level to mortar and concrete levels.

At paste level:

The fresh properties of the self-sealing concrete containing microcapsules are neglected in many studies. In fact, it is very important to understand the effect of microcapsules starting from the paste level and to assess whether there is an incompatibility issue between cement and microcapsules. In this experiment, CEM I 52.5N was used as a main binder component for the paste (in the same way as the binder used for concrete production in the next sections). The microcapsules, both MIC_56 and MIC_93, were added into the cement paste with a specific dosage of 0, 1.5, 3.0 and 6.0% bwoc. The detailed composition of the cement pastes is presented in Table 7-5. For instance, the mixture notation of CP_56_1.5 means cement paste with the addition of 56- μ m microcapsules at 1.5% bwoc. The demand of water was investigated to reach the standard consistency per designated mixture.

Table 7-5. Main composition of binder with and without microcapsules

No	Mixture	Mass of material (g)				
		CEM	MIC_56		MIC_93	
			PURE	SOL	PURE	SOL
1	CP_0	2000	0	0	0	0
2	CP_56_1.5	2000	30	100	0	0
3	CP_56_3.0	2000	60	200	0	0
4	CP_56_6.0	2000	120	400	0	0
5	CP_93_1.5	2000	0	0	30	60
6	CP_93_3.0	2000	0	0	60	120
7	CP_93_6.0	2000	0	0	120	240

Note: PURE = pure mass of microcapsules, SOL = mass of microcapsules' solution (pure microcapsules + deionized water in the solution)

At mortar level:

An initial study was conducted to assess the compatibility between microcapsules and cement type in terms of mechanical performance of the mortar. This study is initiated due to the fact that (1) a reduction of compressive strength was found in the CEM III/A concrete based on the preliminary study (Section 7.2.3.2) and (2) few studies within the SMARTINCS project reported a different behavior of microcapsules depending on the cement type. Therefore, in this experiment, a compatibility study was performed to assess the mechanical performance of mortars mixed with microcapsules, specifically on the use of three cement types including CEM III/A 42.5N, CEM I 52.5N and CEM I 52.5R.

The composition of reference mortar (without microcapsules) consists of one part of cement and three parts of CEN standard sand (cement:sand = 1:3), and one half part of water (w/c = 0.50), which is in accordance with EN 196-1:2016. Three dosages of microcapsules were fixed at 0, 3 and 6% bwoc. The mix proportion of mortars can be found in Table 7-6. For instance, the mixture notation of CEM3_56_3 means CEM III/A mortar with the addition of 56- μ m microcapsules at 3% bwoc. Pure MIC is the pure amount of microcapsules at a specific dosage, while Sol MIC is the mass of solution containing pure MIC and deionized water (which depends on the active capsule concentration). Water in Sol MIC is the exact amount of deionized water in the solution (Sol MIC), which will be taken into account to calculate the amount of effective water. It is noteworthy to mention that the w/c of all mortar mixtures were deliberately made the same at 0.50.

Table 7-6. Mix proportion of mortars with and without microcapsules (note: capsule concentrations of MIC_56 and MIC_93 solutions are 30 and 50 wt%, respectively)

Mixture	Cement (g)	CEN sand (g)	Pure MIC (g)	Sol MIC (g)	Water in Sol MIC (g)	Additional water (g)	Effective water (g)
CEM3_0	450	1350	0	0	0	225	225
CEM3_56_3	450	1350	13.5	45	31.5	193.5	225
CEM3_56_6	450	1350	27	90	63	162	225
CEM3_93_3	450	1350	13.5	27	13.5	211.5	225
CEM3_93_6	450	1350	27	54	27	198	225
CEM1N_0	450	1350	0	0	0	225	225
CEM1N_56_3	450	1350	13.5	45	31.5	193.5	225
CEM1N_56_6	450	1350	27	90	63	162	225
CEM1N_93_3	450	1350	13.5	27	13.5	211.5	225
CEM1N_93_6	450	1350	27	54	27	198	225
CEM1R_0	450	1350	0	0	0	225	225
CEM1R_56_3	450	1350	13.5	45	31.5	193.5	225
CEM1R_56_6	450	1350	27	90	63	162	225
CEM1R_93_3	450	1350	13.5	27	13.5	211.5	225
CEM1R_93_6	450	1350	27	54	27	198	225

At concrete level:

To optimise the mix designs for self-sealing concrete, the full factorial design was implemented to model the performance of concrete. The full factorial design is a robust technique to formulate all combinations of desired mix design parameters. Three factors of interest were employed for optimization including: (1) capsule size (labelled as MIC size), (2) capsule dosage (labelled as MIC dosage) and (3) w/c ratio, and each factor was run at 2-3 levels as

shown in Table 7-7. In this case, MIC size and MIC dosage were selected as the two important capsule-related factors affecting the concrete properties. It is important to note that other factors, such as shell thickness, shell material, and cargo type, will also influence the concrete properties. However, for this study, they will not be considered. The w/c was also considered as an important factor as it greatly affects the mechanical performance of hardened concrete and allows further investigation of the behavior of microcapsules in different w/c.

Table 7-7. Factors and levels adopted for the full factorial design

Factor	Level (-1)	Level (0)	Level (1)
MIC size	-	56 μm	93 μm
MIC dosage	0% bwoc	3% bwoc	6% bwoc
w/c ratio	0.40	0.50	0.60

The statistical model for a full factorial design, such as 2^k or 3^k , includes k as number of factors studied and the numbering (i.e. 2 or 3) as the levels of each factor. However, as shown in Table 7-7, there is an unbalanced factor-level for all combinations as only two MIC sizes were used. Thus, the complete 3^3 full factorial design could not be achieved. However, the effects of all parameters can still be investigated by dividing the full factorial design into two approaches, as explained below. For both factorial designs, Minitab software (Minitab, LLC, US) was used to generate the contour plots for all measured properties and the statistical analyses based on the analysis of variance (ANOVA) and main effects plots were employed to determine the significant parameters (p -value of 0.05 as a significance threshold) and to examine the contribution of different factor-level, respectively.

- 3^2 full factorial design

This design uses two factors, namely (1) MIC dosage and (2) w/c ratio, each with three levels (levels -1, 0, 1) per factor. The design was then divided into two parts: one with a hold factor of 56- μm microcapsules and another with a hold factor of 93- μm microcapsules. Thus, the main objective of this design is to investigate the effect of w/c and MIC dosage on concrete properties assuming a constant MIC size.

- 2^3 full factorial design

This design employs three factors, namely (1) MIC size, (2) MIC dosage and (3) w/c ratio, each with two levels (levels 0 and 1) per factor. Unlike the

previously described 3^2 design, there is no hold factor in this design. The main drawback of this approach is that, as two adjacent levels are investigated, a linear relation between the levels will be assumed. This is may not be as accurate and thus a 2^3 design is less robust than a 3^2 one. However, when used in tandem, the two factorial designs will better illuminate the effect of MIC size on concrete properties.

To carry out the two factorial designs detailed above, 26 concrete mixtures were required. However, after removing the overlapping mixtures of the 2^3 and 3^3 designs, 15 concrete mixtures remained. All of the mixes are presented in Table 7-8. The cement content for all mixes was fixed at 350 kg/m^3 . When comparing the SP demand of the different mixes, specifically those with different w/c ratios, the amount of SP added was adjusted to ensure good workability. To note, mixes which had the same w/c ratio had a consistent amount of SP added, whether or not microcapsules were added. This allowed the effects of microcapsules in the fresh properties of concrete to be investigated. As an exception, the mixes with a w/c of 0.60 did not have any SP added as a good workability has been achieved (no segregation/bleeding).

Table 7-8. Mix designs

Coded levels			Mixture design								
MIC size	MIC dosage	w/c	CEM I 52.5N [kg/m ³]	Sand 0/2.5 [kg/m ³]	Gravel 4/8 [kg/m ³]	Gravel 8/16 [kg/m ³]	Effective water [kg/m ³]	w/c [-]	SP [kg/m ³]	MIC_56 (pure) [kg/m ³]	MIC_93 (pure) [kg/m ³]
0, 1	-1	-1	350	765	727	392	140	0.40	5.93	-	-
0	0	-1	350	765	727	392	140	0.40	5.93	10.5	-
0	1	-1	350	765	727	392	140	0.40	5.93	21	-
1	0	-1	350	765	727	392	140	0.40	5.93	-	10.5
1	1	-1	350	765	727	392	140	0.40	5.93	-	21
0, 1	-1	0	350	740	684	370	175	0.50	0.77	-	-
0	0	0	350	740	684	370	175	0.50	0.77	10.5	-
0	1	0	350	740	684	370	175	0.50	0.77	21	-
1	0	0	350	740	684	370	175	0.50	0.77	-	10.5
1	1	0	350	740	684	370	175	0.50	0.77	-	21
0, 1	-1	1	350	702	649	351	210	0.60	-	-	-
0	0	1	350	702	649	351	210	0.60	-	10.5	-
0	1	1	350	702	649	351	210	0.60	-	21	-
1	0	1	350	702	649	351	210	0.60	-	-	10.5
1	1	1	350	702	649	351	210	0.60	-	-	21

7.3.3 Testing program

Several test programs were employed depending on the matrix of the composite. At paste level, the effect of microcapsules was evaluated by means of standard consistency and setting time tests, following the EN 196-3 standard. At mortar level, the flexural and compressive strength tests of mortar specimens with and without capsules' addition were evaluated in accordance with EN 196-1. At concrete level, the influence of mixing process towards the performance of microcapsule-based concrete was initially investigated. Two mixing procedures (MP) were considered, namely MP1 and MP2, as shown in Figure 7-14. Both mixing procedures were described in Table 7-9 and the main difference lies in the mixing time of the microcapsules with concrete materials (1 min capsule mixing for MP1; 5.5 min capsule mixing for MP2). Two mixtures were used for this assessment namely w/c 0.60 as reference (REF) concrete and w/c 0.60 + 6% MIC_93 as MIC concrete. The fresh and mechanical properties of these concrete mixtures were evaluated to understand the effect of capsule mixing.

In order to confirm the effect of pure WRA (non-encapsulated), two additional mixtures were made with the direct addition of WRA. Considering a 70% core content of capsules, it means that 3% and 6% bwoc of MIC (pure content, either 56 or 93 μm) were equivalent to 2.1% and 4.2% bwoc of WRA, respectively (further labelled as '3% eq. WRA' and '6% eq. WRA'). These two pure WRA dosages were introduced in the concrete mixture with the same w/c of 0.60. In this case, the mixing procedure MP1 was employed (note: WRA was added 1 min prior to the total mixing time). The fresh and mechanical properties of these concrete mixtures were also evaluated to understand the effect of pure WRA.

Table 7-9. Description of mixing procedures

MP1	MP2
<p>(1) Raw materials (i.e. cement, aggregates, water, microcapsules, SP) were prepared in advance</p> <p>(2) From the prepared mixing water, a small amount of water was taken for rinsing the bottle in which capsules are in a later step (6) to make sure all capsules are in the mix</p> <p>(3) Aggregates and cement were put into the mixer and were mixed for 30 sec</p> <p>(4) Mixing water was put into the mixer and mixing was continued</p> <p>(5) For some mixes, SP was added after 2.5 min of mixing</p> <p>(6) After 5 min of mixing, microcapsules (in solution) were added, together with a small amount of water for rinsing the capsules</p> <p>(7) Mixing was stopped after reaching 6 min</p>	<p>(1) Raw materials (i.e. cement, aggregates, water, microcapsules, SP) were prepared in advance</p> <p>(2) The microcapsules (in solution) were poured onto the mixing water and they were mixed until homogeneous (around 2–3 min)</p> <p>(3) Aggregates and cement were put into the mixer and were mixed for 30 sec</p> <p>(4) Mixing water which has been combined with microcapsules was put into the mixer and mixing was continued</p> <p>(5) For some mixes, SP was added after 2.5 min of mixing</p> <p>(6) Mixing was stopped after reaching 6 min</p>



(a)

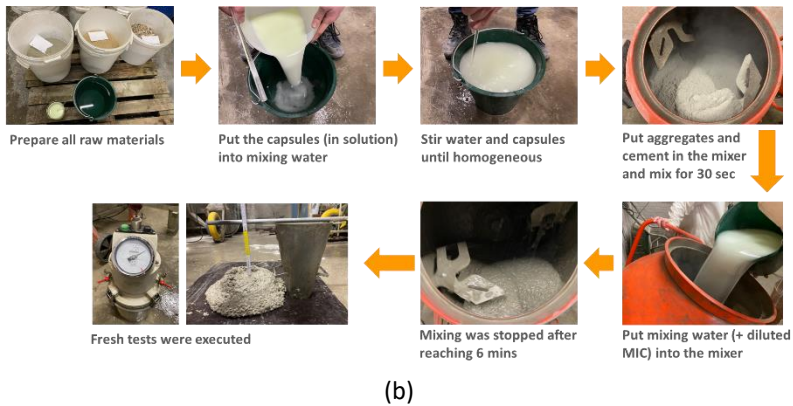


Figure 7-14. Mixing procedures of MIC concretes: (a) procedure 1 (MP1) and (b) procedure 2 (MP2)

Following the optimisation of the mixing procedure, the fifteen concrete mixtures were cast using MP1, each with a volume of 30 L. All reference concrete mixes without microcapsules were prepared using MP1 and cast in the same way as MIC concretes. For each concrete mixture, three cubic moulds ($150 \times 150 \times 150 \text{ mm}^3$), three cylindrical moulds ($\varnothing 100 \times 200 \text{ mm}$), and three prismatic moulds of ($100 \times 100 \times 400 \text{ mm}^3$) were cast. Two rebars ($\varnothing 5 \text{ mm}$) were embedded 20 mm from the top of the prismatic samples (see Figure 7-15) to allow greater specimen stability required for the testing explained below. The cube and cylindrical specimens were stored in a water tank at a temperature of $20 \pm 2^\circ\text{C}$, while the prismatic specimens were stored in a curing chamber at $20 \pm 2^\circ\text{C}$ and 60% RH.

The fresh tests, such as slump, air content and fresh density, were evaluated after concrete mixing in accordance with EN 12350-2,6,7. The hardened concrete specimens were evaluated by means of ultrasonic pulse velocity (UPV) tests (EN 12504-4), compression tests (EN 12390-3) and tensile splitting tests (EN 12390-6). To measure the self-sealing effectiveness, prismatic specimens' sorptivity was measured via a capillary water absorption (CWA) test. Prior to the CWA test, the prisms were cracked by means of three-point bending tests (UTM, Mohr & Federhaff A.G., Germany) at the age of 14 days. The loading of the instrument was manually controlled with a relatively slow loading rate to generate a crack between 200 and 300 μm . The rebars within the specimens ensured that there was no sudden failure during cracking. As soon as a crack occurred, observed via visual assessment, it was unloaded. Furthermore, the achieved crack width was measured by means of an optical microscope. Five marks along the crack were selected and, at each mark, four crack width measurements were

taken. Thus, the average crack width was calculated based on the average of 20 data points (5 marks × 4 measurements) per specimen.

After crack formation, the cracked prisms were stored in an oven at 35°C for 21 days until constant weight was achieved. Constant weight was achieved when the change in mass over a period of 24 hours was less than 0.2%. Next, the sides and the bottom of the specimens were partially covered with epoxy resin (Episol Designtop SF, Belgium) as depicted in Figure 7-15. The prisms were later returned to the oven for 14 days to ensure the specimens stayed in the dry state prior to conducting the CWA test. Two small areas (20 mm in width) were left uncovered as the contact areas for this test (see Figure 7-15). One of these areas was located in an uncracked zone (UNCR) while the other one contained the crack (CR). This allows to investigate the influence of UNCR and CR conditions on sorptivity in both reference and MIC concretes. The two areas were tested one at a time. For the first CWA test, the CR area was tightly covered with aluminum tape leaving only the UNCR area exposed. The specimens were immersed in water with a water level of 3 mm above the bottom of the prism. The weight of the specimens was recorded at 10, 20, 30, 60, 90, 120, 180, 240, 360, 480, and 1440 min. During the CWA test, it was ensured that the water level remained constant (3 ± 1 mm). After the first CWA test was done, the aluminum tape covering the CR area was removed and all specimens were returned to the oven at 35°C for 7 days to let the specimens dry and attain the constant weight condition. Following this, the specimens were taken out from the oven and the second CWA test was performed. In this test, the UNCR area was covered with aluminum tape and the CR area was left uncovered. Despite the different contact area, the CWA test procedure was kept constant for both tests. Following CWA testing, SEM of the concrete fragments was performed, visualizing the microcapsules' integration, rupture, and bond with the cementitious matrix.

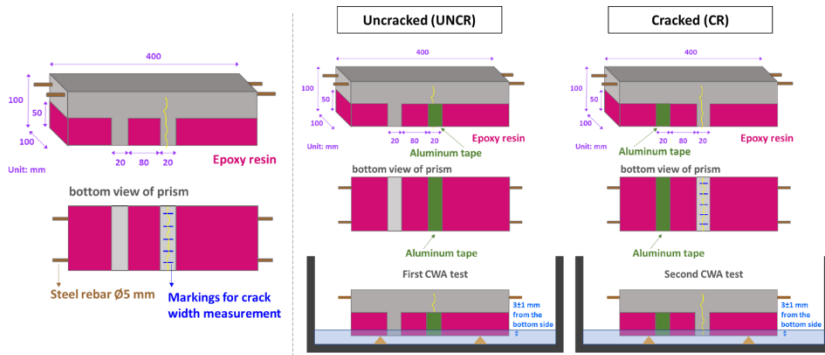


Figure 7-15. Capillary water absorption tests on CR and UNCR areas of a specimen

7.3.4 Results and discussion

7.3.4.1 Effect of the size and dosage of microcapsules on the fresh properties of cement paste

The water demand of cement (CEM I 52.5N) mixed with microcapsules was initially investigated and the results are depicted in Figure 7-16. The water demand of reference cement was recorded at 33%. The addition of microcapsules, regardless of size and dosage, did not really change the water demand of cement. This is in contrast with other healing agents such as Penetron crystalline admixture and Basilisk bacteria, which influenced the water demand of the cement depending on the given dosage (see Chapter 3, Section 3.3.2). Although the increase of MIC dosage from 1.5 to 6.0% bwoc seems to lower the water demand of cement slightly, the differences were rather minor. The variation of MIC size also did not induce any substantial effects to the water demand of cement.

Figure 7-17 shows the setting time of cement pastes with and without addition of microcapsules. The average initial and final setting times of reference cement paste (CEM I 52.5N) were 195 and 349 min, respectively. It is clear to see that the addition of microcapsules delays the setting time of the cement paste. This retardation effect increased with increasing the MIC dosage. The incorporation of MIC_56 from 1.5 to 6.0% bwoc caused a delay in initial setting time by almost 1–2 hours and a delay in final setting time up to one hour, as compared with setting times of reference cement paste. On the other hand, the incorporation of MIC_93 at the dosage of 1.5% bwoc also

prolonged the setting time. Nevertheless, no considerable differences in both initial setting time (~260 min) and final setting time (~380 min) were observed when comparing the pastes with 1.5 and 3.0% MIC_93. Furthermore, a higher MIC dosage at 6% bwoc induced a longer delay of setting time by approximately 100 min (for initial) and 80 min (final), as compared with reference cement paste. Comparing the size of microcapsules (MIC_56 and MIC_93) at the same dosage, there were little differences observed in terms of setting time. Based on the initial setting time, only additions of 3.0% and 6.0% of microcapsules showed minor differences with a gap of between $\frac{1}{4}$ and $\frac{1}{2}$ hour. From the final setting time, the addition of 3.0% MIC, both MIC_56 and MIC_93, showed identical values at 390 min. However, there were little differences at other dosages. Specifically at the dosage of 1.5%, there was an almost 1-hour difference in final setting time between the addition of MIC_56 and MIC_93 and at the dosage of 6.0%, the gap was monitored for around $\frac{1}{2}$ hour.

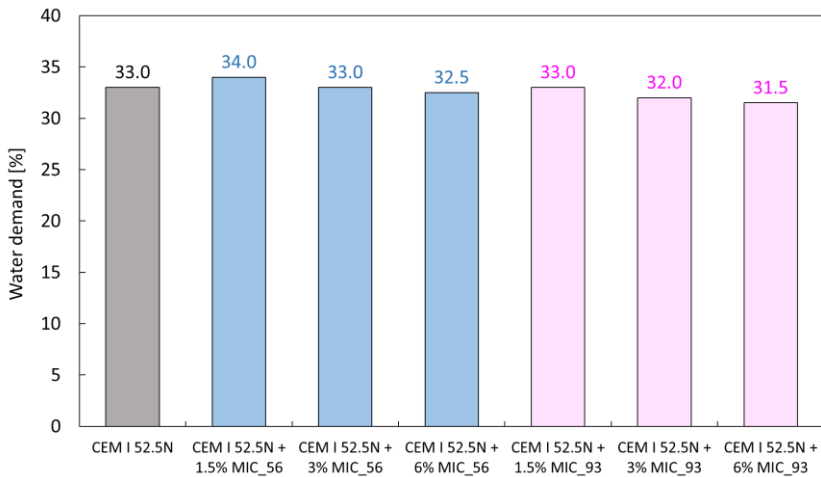


Figure 7-16. Water demands of cement incorporated with microcapsules (MIC_56 and MIC_93) at different dosages (note: single measurement per mixture)

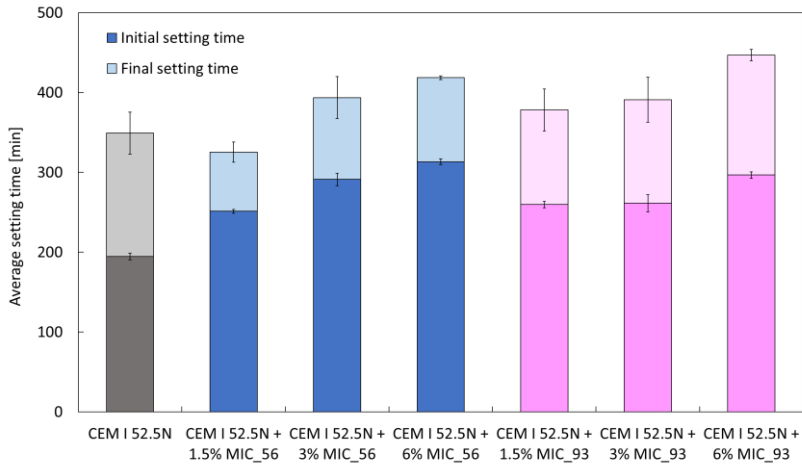


Figure 7-17. Setting times of cement pastes incorporated with microcapsules (MIC_56 and MIC_93) at different dosages (note: average value is based on three repetitions per mixture)

7.3.4.2 Compatibility study between microcapsules and cement type regarding the mechanical performance of mortar

Preliminary tests on the synergetic effect of microcapsules and cement type toward the mechanical properties of mortar were conducted. The 28d compressive strengths of mortars containing microcapsules (MIC_56 and MIC_93) with different cement types are presented in Figure 7-18. The compressive strengths of reference CEM III/A, CEM I(R) and CEM I(N) mortars were 49.5, 56.9 and 56.4 MPa, respectively. The percentage of strength reduction of mortars containing microcapsules was calculated with respect to the reference mortar without microcapsules for each respective cement type.

- Based on Figure 7-18a on the addition of MIC_56, there was a 49% and 45% strength reduction relative to the strength of CEM III/A mortar after the addition of 3 and 6% MIC_56 by weight of cement, respectively. On the CEM I(R) mortar, the strength reductions were interestingly found at similar levels as for CEM III/A mortar namely 42% for 3% MIC_56 and 49% for 6% MIC_56. With the use of CEM I(N) for mortar specimens, the additions of MIC_56 at 3 and 6% bwoc induced less reductions than the other cement types. The additions of 3 and 6% MIC_56 reduced the strength of CEM I(N) mortar by 32 and 37%, as compared with reference CEM I(N) mortar.

- Comparing Figure 7-18a and Figure 7-18b, the effect of MIC_93 on the compressive strength of mortar was found to be lower than MIC_56, which was observed from all mortars, while the influence of MIC_93 in terms of compressive strength reduction of mortar with different cement environments follows a similar behavior as MIC_56. It was found that the strengths of CEM III/A mortars reduced by 21 and 32% after the addition of 3 and 6% MIC_93, respectively. On CEM I(R) mortars, the strength reductions were recorded at 10 and 24% with the introduction of 3 and 6% MIC_93, respectively. Furthermore, there were only 13–15% strength reductions of CEM I(N) mortars with the inclusion of 3–6% MIC_93.
- The flexural strength of mortars, in fact, follows the same tendency as the compressive strength. According to Figure 7-19a, the addition of MIC_56 from 3.0 to 6.0% bwoc to CEM III/A and CEM I(R) mortars induced 35–39% strength reduction with respect to the reference mortars. With the same range of MIC_56 dosage, less reduction (between 22–25%) was found on CEM I(N) mortars. On the use of MIC_93, the flexural strength of CEM III/A mortars was reduced by 28% when added with 3.0–6.0% MIC_93. The inclusion of 3.0% MIC_93 into CEM I(R) and CEM I(N) mortars induced the same effect, where the mortars experienced 14% flexural strength reduction. With a high MIC_93 dosage (6.0% bwoc), the flexural strengths of CEM I(R) and CEM I(N) mortars reduced by 18 and 21%, respectively.

It is interesting to observe that there is a distinct effect of microcapsules in various cement environments. Based on the observations above, in general, the strength of mortar was greatly affected by the microcapsules and the strength reduction was higher in a combination between microcapsules (regardless of their size and dosage) and CEM III/A or CEM I(R) and lower on the use of CEM I(N). This may lead to a better compatibility between CEM I(N) and the microcapsules than the other cement types, specifically in terms of mechanical performance. No clear explanation could be given for this behavior and further research will be needed. By considering the preliminary results from this test, it was decided to proceed with CEM I(N) for the concrete production.

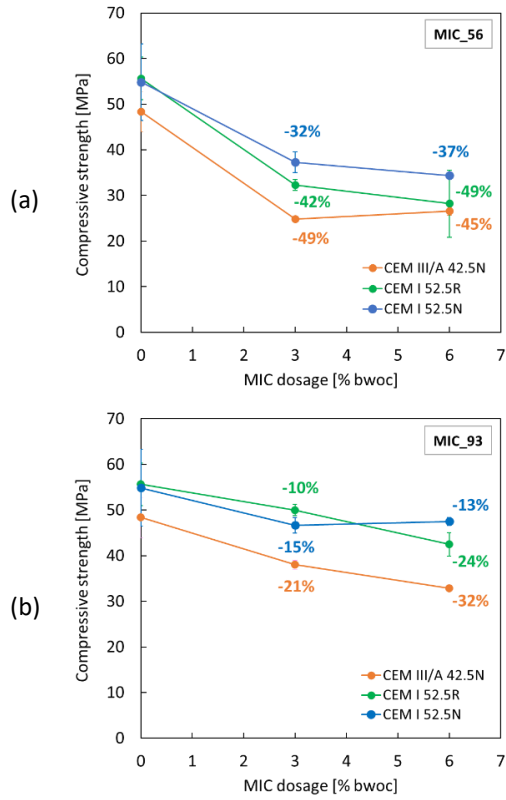
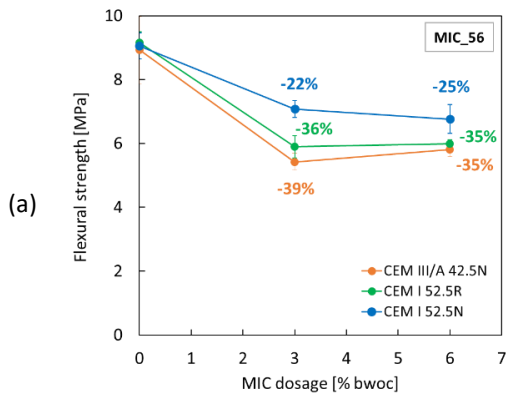


Figure 7-18. Compressive strength of mortars containing (a) MIC_56 and (b) MIC_93 with different cement types



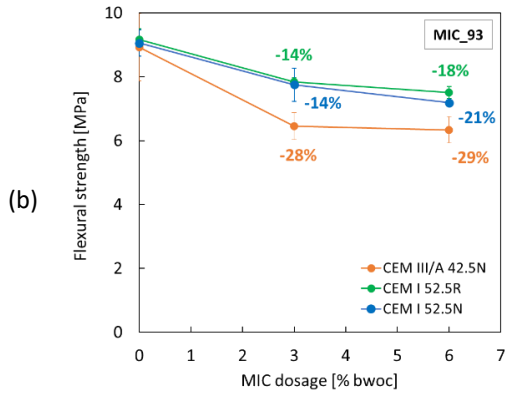


Figure 7-19. Flexural strength of mortars containing (a) MIC₅₆ and (b) MIC₉₃ with different cement types

7.3.4.3 Influence of different mixing procedure and pure WRA on the performance of MIC concrete

The effect of two different mixing procedures was initially evaluated on the fresh and hardened properties on one representative mix, namely w/c 0.60 + 6% MIC₉₃. This mix was fabricated via mixing procedures MP1 and MP2. One reference mixture without capsules namely w/c 0.60 + 0% MIC₉₃ was also made for comparison, employing one mixing procedure. Table 7-10 summarizes the fresh and mechanical properties of these concrete mixtures. In terms of fresh properties, there was no difference between the results from using MP1 and MP2 as the slump, fresh density and air content were identical. However, for hardened properties, the compressive strengths of w/c 0.60 + 6% MIC₉₃ reduced by 22% when using MP1 and 34% when using MP2, meaning the extension of the capsule mixing time from 1 to 5.5 min reduced the strength by a further 12%. For the tensile splitting strength of the capsule-based mixtures, using MP1 resulted in a reduction of 14%, while MP2 resulted in a reduction of 17%. The ultrasonic velocities of capsule-based mixtures were slightly reduced compared to the reference mixture but, the differences of UPV values between MP1 and MP2 were not significant. The aforementioned results confirm that the mixing procedure considerably affects the performance of hardened concrete. The concrete fabricated using mixing procedure MP1 showed considerable better hardened strength properties than the concrete produced using MP2. This may be attributed to the longer capsule mixing time used in mixing

procedure MP2. As the capsules were added at the beginning of the mixing process, the probability of capsule breakage increases. It is hypothesised that capsule breakage occurs for two main reasons: (i) collisions between capsules, aggregates, and the mixer blade resulting in a premature triggering of the capsules and (ii) high shear stress during mixing, increasing the strain placed on the shell wall. Although the capsules added in mixing procedure MP1 may also experience the above mentioned collisions and stress, their reduced mixing time (from 5.5 min (MP2) to 1 min (MP1)) may increase the capsules' survivability. Based on these results, the mixing procedure MP1 was selected for the fabrication of all further mixtures. It is important to note that the reasoning behind the reduction in hardened properties due to microcapsule addition will be discussed further in Section 7.3.4.5.

Table 7-10. Effect of capsule mixing and pure WRA on the fresh and hardened properties of concrete

Concrete properties	Reference	Effect of mixing procedure		Effect of pure WRA	
	w/c 0.60 (REF)	w/c 0.60 + 6% MIC_93 (MP1)	w/c 0.60 + 6% MIC_93 (MP2)	w/c 0.60 + 3% eq. WRA	w/c 0.60 + 6% eq. WRA
Fresh properties					
Slump [cm]	25	26	26	23	25
Fresh density [kg/m ³]	2339 ± 5	2239 ± 19 (↓ 4%)	2269 ± 8 (↓ 3%)	2312 ± 11 (↓ 1%)	2294 ± 16 (↓ 2%)
Air content [%]	1.1	3.2 (↑ 190%)	3.2 (↑ 190%)	-	-
Hardened properties					
28d hardened density [kg/m ³]	2339 ± 11	2265 ± 8 (↓ 3%)	2278 ± 7 (↓ 3%)	2332 ± 18 (↓ 0%)	2320 ± 1 (↓ 1%)
28d compressive strength [MPa]	39.3 ± 0.3	30.7 ± 1.8 (↓ 22%)	25.9 ± 0.6 (↓ 34%)	30.0 ± 0.3 (↓ 24%)	27.8 ± 0.3 (↓ 29%)
28d tensile splitting strength [MPa]	3.67 ± 0.52	3.17 ± 0.38 (↓ 14%)	3.04 ± 0.27 (↓ 17%)	-	-
UPV [m/s]	4776 ± 10	4566 ± 69 (↓ 4%)	4509 ± 46 (↓ 6%)	-	-

The effect of pure WRA can also be found in Table 7-10. The addition of 3 and 6% eq. WRA did not considerably affect the slump and fresh density of

reference mixture. Furthermore, the 28d compressive strength of concrete was found to be significantly affected by the inclusion of pure WRA with a reduction of 24–29% by using 3–6% eq. WRA. The result implies that the potential release of WRA from the capsules happening during mixing can induce an additional strength reduction. Comparing the mixtures between w/c 0.60 + 6% MIC_93 (MP1) and w/c 0.60 + 6% eq. WRA, it is interesting to observe that the density of concrete mixture with encapsulated WRA had a lower value than the mixture with non-encapsulated WRA. It suggests that the presence of microcapsules physically occupies a small volume of concrete that may also be partly responsible for the strength reduction. Apparently, the above results confirm that both intact capsules and release of WRA cause a decline in concrete strength.

7.3.4.4 Fresh properties of MIC concretes

The fresh densities of the reference and MIC concretes are shown in Figure 7-20. On average, the fresh densities of MIC concretes were lower than the fresh densities of the reference mixes due to the high percentage addition of microcapsules (in this case at 3 and 6% bwoc). However, there was no substantial effect of MIC size on the fresh density of the concrete mixtures using the same w/c and MIC dosage, with an exception on w/c 0.4 mixtures where there was a difference.

The workability of fresh concrete was evaluated by the slump values (Figure 7-21). During the mix design process, a slump class of S4 or S5 was targeted for all reference mixes. From Figure 7-21, the slump values for reference mixtures with w/c of 0.40, 0.50 and 0.60 were 210, 230 and 250 mm, respectively. Results from this test show that the addition of microcapsules to the fresh concrete, regardless of their size or dosage, do not affect the slump classification with only minor (10–20 mm) increases to the slump height seen. Moreover, there was no segregation/bleeding in any of these mixtures. Thus, the addition of MIC does not negatively influence the workability.

Nevertheless, the inclusion of MIC induces a considerable effect on the air content of the fresh mixture (see Figure 7-22). There was a clear relationship between air content and percentage MIC addition (0 to 6% bwoc) for mixtures containing a w/c of 0.6. Note that these mixes did not contain any SP in order to keep the workability constant. Concrete mixes with either a w/c of 0.4 or 0.5 exhibited various trends. These inconsistencies may be caused by (1) an interaction between the microcapsules and the

superplasticizer and (2) a lack of test repetitions (only one measurement per mixture). This compatibility study will be further investigated in future work. Overall, however, the inclusion of MIC_56 increased the air content of all mixes with the exception of one outlier (6% MIC_56 in the w/c 0.50 mixtures). On the other hand, there was no consistent correlation between MIC_93 and air content with different w/c producing different trend lines. Moreover, the air contents of mixtures containing MIC_93 were lower than those containing MIC_56, except the outlier for 6% MIC_56 in the w/c 0.50 mixture. It means that the effect of MIC_93 may be less critical than MIC_56 which is supported by the preliminary study on the mortar specimens where the strength reduction of mortar was more severe with the addition of MIC_56 than MIC_93.

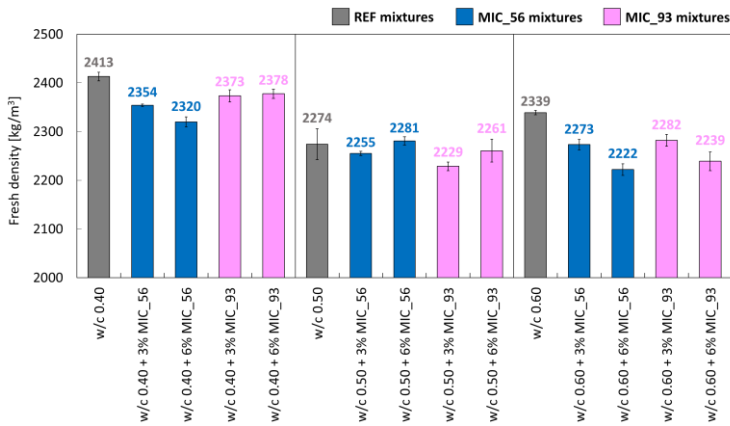


Figure 7-20. Fresh densities of all concrete mixtures (note: three measurements for each mixture)

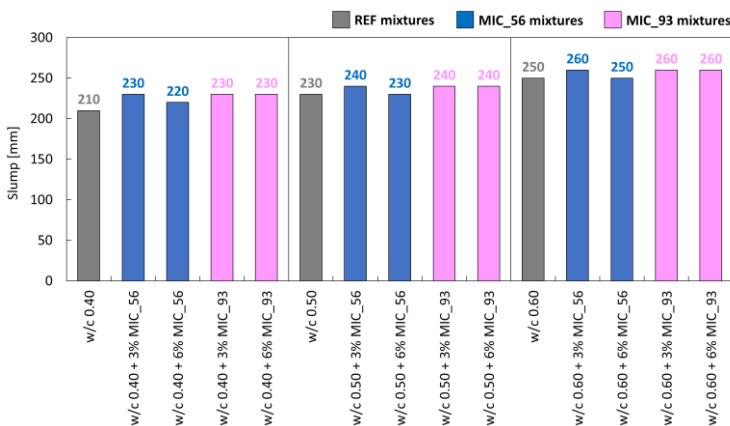


Figure 7-21. Slumps of all concrete mixtures (note: single measurement for each mixture)

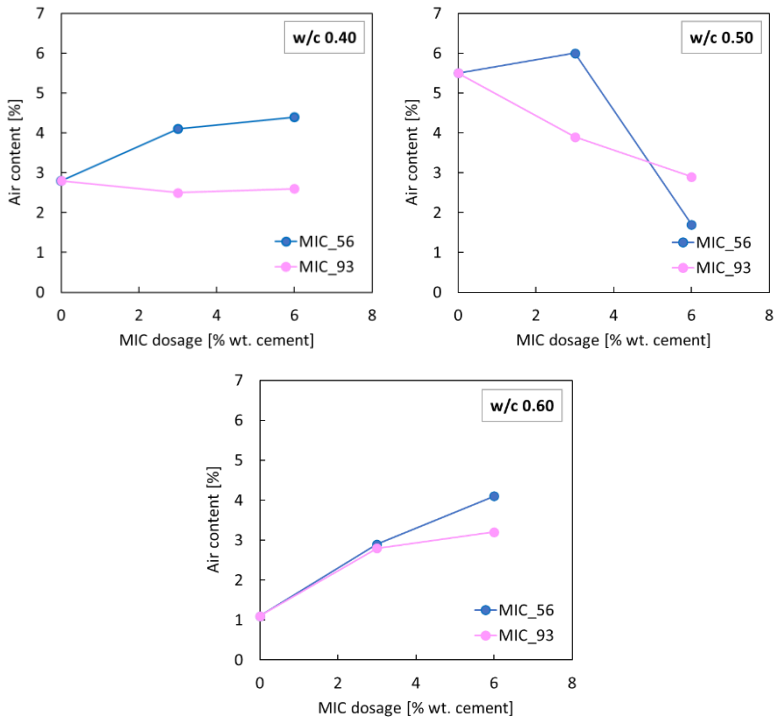


Figure 7-22. Air contents of all concrete mixtures (note: single measurement for each mixture)

7.3.4.5 Hardened properties of MIC concretes

Hardened density

The hardened densities of all concrete mixtures were recorded at the age of 28 days, as shown in Figure 7-23. The density of hardened concrete decreased after the incorporation microcapsules, mimicking the trend seen for fresh density measurements. The reduction of hardened density of capsule-based concrete was in the range of 0.3–3.6% with respect to the hardened density of reference concrete.

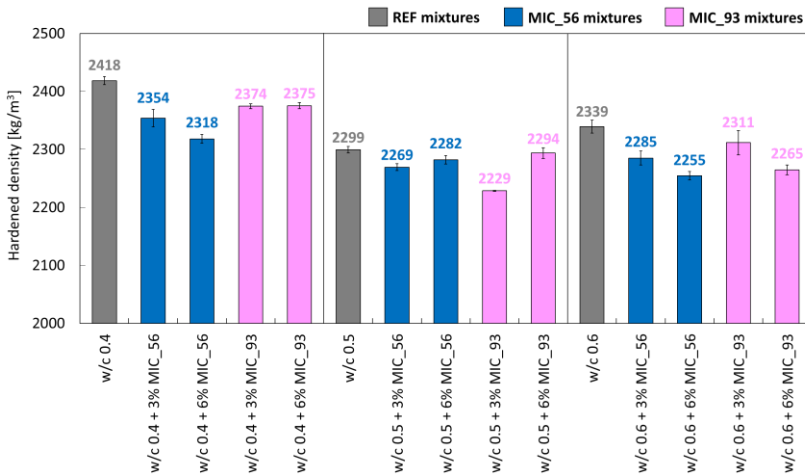


Figure 7-23. Hardened densities of all concrete mixtures (note: three measurements for each mixture)

Compressive strength

Table 7-11 presents the compressive strength, measured at 28 days. For each mixture, measurements were taken in triplicate. The compressive strength in this study ranges from 26.4 to 61.6 MPa. As discussed in Section 7.3.2, the results were processed with Minitab to generate contour plots as shown in Figure 7-24 with selected parameters and hold factors depending on the available factorial designs. Factorial regression was implemented in the contour plots as to the requirements of a statistical full factorial design approach.

Figure 7-24a shows the evolution of compressive strength with running the w/c from 0.40 to 0.60 and MIC dosage from 0 to 6% bwoc with the use of 56- μ m microcapsules. When no microcapsules were incorporated into the concrete mix, the compressive strength decreased with increasing w/c. When the microcapsules were added into the concrete, the performance of the concrete was dependent on both the w/c and MIC dosage. For example, for mixes with a w/c 0.4, the gradual reduction of compressive strength with increasing MIC dosage was more pronounced than for the mixes with a higher w/c. As can be seen in the contour plot (Figure 7-24a), when the w/c was increased to 0.5 or 0.6, the change of contour area was less pronounced for mixes with higher w/c. The strength reductions of capsule-based concretes with 3% and 6% MIC₅₆ were recorded at 20 and 32%, respectively

for w/c 0.50 mixes, and 19 and 33%, respectively for w/c 0.60 mixes, which were identical. Thus, it was concluded that the adverse effect of microcapsules on compressive strength was exacerbated in mixes with lower w/c. It is hypothesised that the physical interaction between the microcapsules and aggregates is the major reasoning behind this trend. In the w/c 0.40 mixes, there was a low volume of cement paste and a high content of aggregates. On the other hand, for mixes with higher w/c, the amount of aggregates was lower with respect to the volume of cement paste. Thus, during mixing, there is a higher chance of collisions between capsules and aggregates in the mixture with lower w/c compared to ones with higher w/c, resulting in a premature breakage of capsules and release of the core into the matrix. This phenomenon contributes to the strength reduction as suggested by previous studies [94,96] although different cargos were used in their case (i.e., epoxy resin/toluene-di-isocyanate). Additionally, this hypothesis is further validated by the effect of mixing procedure on the change in mechanical properties. Consequently, the effect of MIC dosage in terms of compressive strength is found to be less pronounced in the mixtures with a higher w/c.

Table 7-11. Measured values for mechanical properties of hardened concrete (note: the reductions in red are relative to the corresponding reference concrete without capsules)

Mixture	Compressive strength [MPa]	Tensile splitting strength [MPa]	UPV [m/s]
w/c 0.40	61.6 ± 1.4	4.49 ± 0.24	5062 ± 64
w/c 0.40 + 3% MIC_56	43.0 ± 1.2 (↓ 30%)	3.42 ± 0.59 (↓ 24%)	4841 ± 86 (↓ 4%)
w/c 0.40 + 6% MIC_56	40.4 ± 4.5 (↓ 35%)	3.37 ± 0.36 (↓ 25%)	4764 ± 57 (↓ 6%)
w/c 0.40 + 3% MIC_93	46.3 ± 0.3 (↓ 25%)	3.41 ± 0.40 (↓ 24%)	4872 ± 73 (↓ 4%)
w/c 0.40 + 6% MIC_93	40.8 ± 2.3 (↓ 34%)	3.46 ± 0.11 (↓ 23%)	4856 ± 30 (↓ 4%)
w/c 0.50	44.1 ± 2.1	4.00 ± 0.41	4786 ± 45
w/c 0.50 + 3% MIC_56	35.1 ± 1.2 (↓ 20%)	3.37 ± 0.10 (↓ 16%)	4708 ± 85 (↓ 2%)
w/c 0.50 + 6% MIC_56	30.1 ± 0.6 (↓ 32%)	3.46 ± 0.22 (↓ 14%)	4643 ± 90 (↓ 3%)
w/c 0.50 + 3% MIC_93	36.3 ± 1.1 (↓ 18%)	3.26 ± 0.43 (↓ 19%)	4634 ± 32 (↓ 3%)
w/c 0.50 + 6% MIC_93	33.1 ± 0.5 (↓ 25%)	2.82 ± 0.25 (↓ 29%)	4594 ± 40 (↓ 4%)
w/c 0.60	39.3 ± 0.3	3.67 ± 0.52	4776 ± 10
w/c 0.60 + 3% MIC_56	31.8 ± 1.1 (↓ 19%)	3.37 ± 0.25 (↓ 8%)	4625 ± 85 (↓ 3%)
w/c 0.60 + 6% MIC_56	26.4 ± 0.5 (↓ 33%)	2.86 ± 0.22 (↓ 22%)	4473 ± 59 (↓ 6%)
w/c 0.60 + 3% MIC_93	32.7 ± 1.2 (↓ 17%)	3.50 ± 0.19 (↓ 5%)	4646 ± 13 (↓ 3%)
w/c 0.60 + 6% MIC_93	30.7 ± 1.8 (↓ 22%)	3.17 ± 0.38 (↓ 14%)	4566 ± 69 (↓ 4%)

The contour plot for the changes of compressive strength after the addition of MIC_93 is presented in Figure 7-24b. Comparing the contour plots of MIC_56 and MIC_93 (Figure 7-24a,b), the results showed a similar trend except the ones for high MIC dosage and high w/c. According to Table 7-11, the inclusion of 3% and 6% MIC_93 reduced the compressive strength by 25 and 34%, respectively for w/c 0.40 mixes; 18 and 25%, respectively for w/c 0.50 mixes; and 17 and 22%, respectively for w/c 0.60 mixes. In this regard, the larger capsules (MIC_93) demonstrated less reduction in compressive strength compared with smaller sized capsules (MIC_56). This could potentially be because of the amount of capsules added to the mix. Capsule additions were done with respect to mass and, thus, for a given dosage, the number of MIC_56 capsules added would be greater than that of the MIC_93. This can affect the porosity of the cementitious matrix, shifting both the size and the number of pores. Additionally, it may be possible that the presence of microcapsule in the matrix can be seen as tiny spherical shaped bubbles. Hence, the air content of concrete may also increase with a high volume of capsules incorporated. It is evident from Figure 7-22 that the air content of concrete incorporated with MIC_56 was mostly higher than MIC_93, which potentially explains a higher compressive strength reduction on the use of MIC_56 than MIC_93.

The effect of MIC size was further investigated using the 2³ factorial design as discussed in Section 7.3.2. The compressive strength contour plots were depicted in Figure 7-24c and Figure 7-24d. Both figures depict comparable contour lines, meaning that the compressive strength of capsule-based concrete with either a w/c 0.50 or w/c 0.60 was consistent despite different capsule sizes. Based on Figure 7-24c (w/c 0.50 mixes), at a specific MIC size, an increase of MIC dosage gradually decreases the compressive strength. However, the reduction of compressive strength was not very critical as shown by the contour line with the interval of 1 MPa. Furthermore, at a specific MIC dosage, the MIC size did not significantly alter the compressive strength. For instance, for w/c 0.50 mixtures with 3% MIC dosage, the compressive strength was approximately 35–37 MPa for the MIC size of between 56 and 93 μm . This lack of trend is seen in both w/c 0.50 and w/c 0.60 mixes.

A statistical analysis was performed on this data set by means of ANOVA and main effects plots. According to the ANOVA (Table 7-12), the most significant factors affecting the compressive strength were w/c and MIC dosage as indicated with the p-value of zero. The MIC size did not significantly influence the compressive strength results with p-value of 0.06. This was

expected as, according to the contour plots (Figure 7-24c,d), the reduction of compressive strength with increasing MIC size was negligible.

The main effects plot (Figure 7-25) depicted the contribution of each level in each factor. Steep slopes were observed for each factor-level of w/c and MIC dosage, indicating their significance in affecting the response, in this case compressive strength. Although a limited number of levels was observed for MIC size, the increase of MIC size from 56 to 93 μm showed a scant effect as indicated by its gentle slope. Thus, the main effects plot is in agreement with the ANOVA.

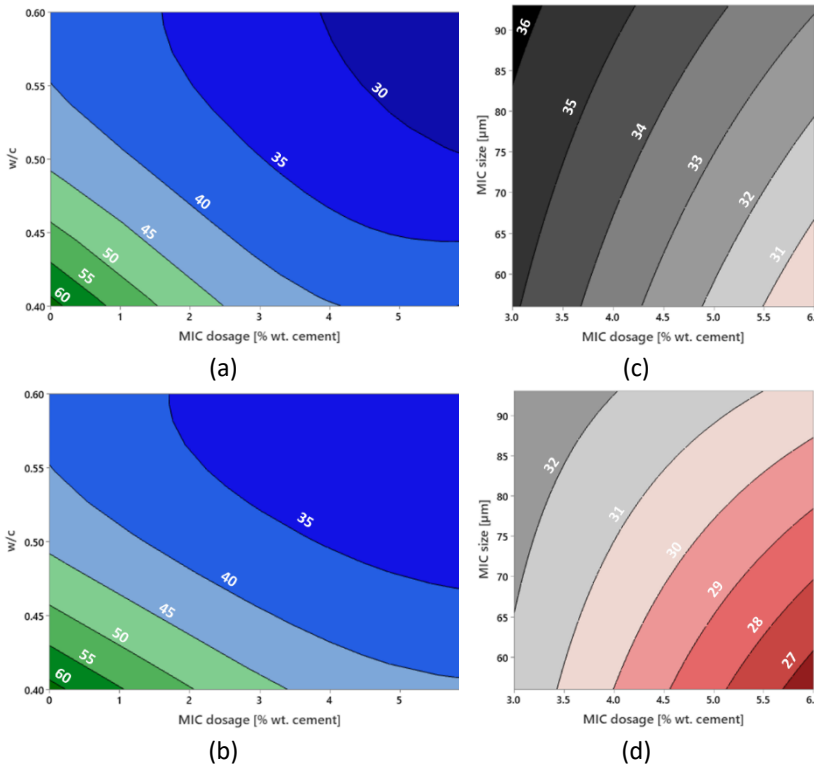


Figure 7-24. Contour plots for the effect of (a) MIC dosage vs w/c for MIC₅₆, (b) MIC dosage vs w/c for MIC₉₃, (c) MIC dosage vs MIC size with a hold factor of w/c 0.50 and (d) MIC dosage vs MIC size with a hold factor of w/c 0.60, on compressive strength

Table 7-12. Analysis of variance for 28d compressive strength (note: DF = degree of freedom, Adj SS = adjusted sum of square, Adj MS = adjusted mean square)

Source	DF	Adj SS	Adj MS	F-value	P-value
w/c	2	2381.96	1190.98	154.65	0.000
MIC size	1	28.81	28.81	3.74	0.059
MIC dosage	2	2105.54	1052.77	136.70	0.000
Error	48	369.66	7.70		
Total	53	4885.97			

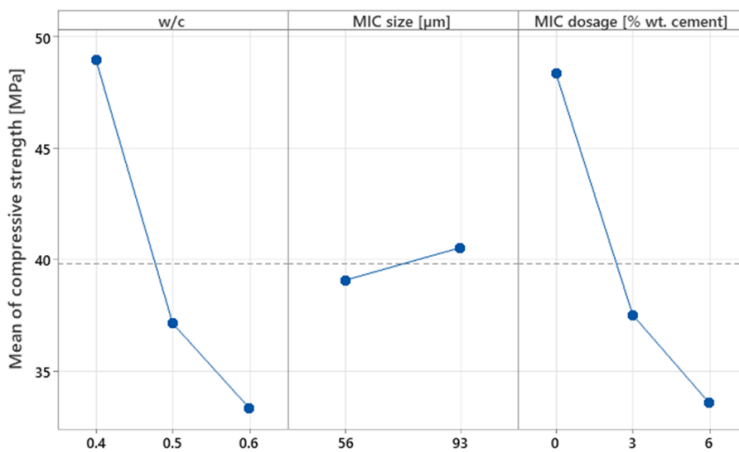


Figure 7-25. Main effects plots for compressive strength

According to the literature, the addition of microcapsules tends to reduce the compressive strength of a cementitious composite. However, there are a wide range of capsule shells (e.g. polyurethane, gelatin gum, urea formaldehyde) and cargo (e.g. sodium silicate, epoxy, IPDI) used, each applied in different cementitious matrices (e.g. concrete, mortar, paste) with various intended applications. Despite this variation, microcapsules are often incorporated into cementitious mixes considering their mean size and dosage. Thus, based on the available data from literature and experimental data from this research, a 3D plot is constructed on the relationship between MIC size, MIC dosage and compressive strength change (see Figure 7-26). The strength change is defined as the percentage increase (positive value) or decrease (negative value) of the compressive strength of MIC composite with respect to the reference composite used in their studies. Green points represent an increase in compressive strength in cementitious systems

containing microcapsules, while red points represent a reduction in compressive strength in microcapsule-based cementitious systems. These data points (85) are obtained from literature [17,19,95–98,190–195,52,61,62,90–94]. The blue points represent 12 data points from this study. The changes in compressive strength span an impressive range, +28% to -77% according to literature. Looking to this study's experimental data, the strength reduction was recorded between 17 and 35%, in line with the general trend seen within literature.

In a few cases, the addition of microcapsules has shown to increase the compressive strength. Research conducted by Du et al. [95,96,98] suggested that an appropriate dosage of microcapsules can fill the internal pores/voids of mortar and small-sized capsules (around 90 μm) can improve the gradation and compactness of concrete. They found 15–28% strength improvement after the addition of 90- μm microcapsules (paraffin shell, TDI / IPDI as cargo) at a dosage of 1.5–3.0% bwoc. Giannaros et al. [17] found 7 and 1% strength increase of cement paste after the addition of 1 and 2% microcapsules (500 μm , gelatin gum shell, sodium silicate cargo), respectively. Also, a 2% strength increase on mortar was found by Kanellopoulos et al. [93] after introducing 0.8% microcapsules (290 μm , gelatin gum shell, sodium silicate cargo). Based on these observations, it was hypothesized that the shell material is responsible to these improvements when used at an appropriate capsule dosage.

In contrast, in most cases, the inclusion of microcapsules has also been shown to considerably decrease the compressive strength. There are several postulates to explain the detrimental effects to the mechanical properties occurring in our mixtures. Firstly, the microcapsules have lower stiffness [92,194] and lower hardness [192] than the cement matrix, thus creating weak spots in the matrix. Secondly, the microcapsule wall may be broken during the mixing due to its low strength and rigidity, hence, releasing the cargo and creating defects similar to pores/holes in the matrix [94,190,193]. Thirdly, an increase of porosity may be expected as many studies [52,97,194,195] confirmed that the volume of pores was found to increase after the addition of microcapsules.

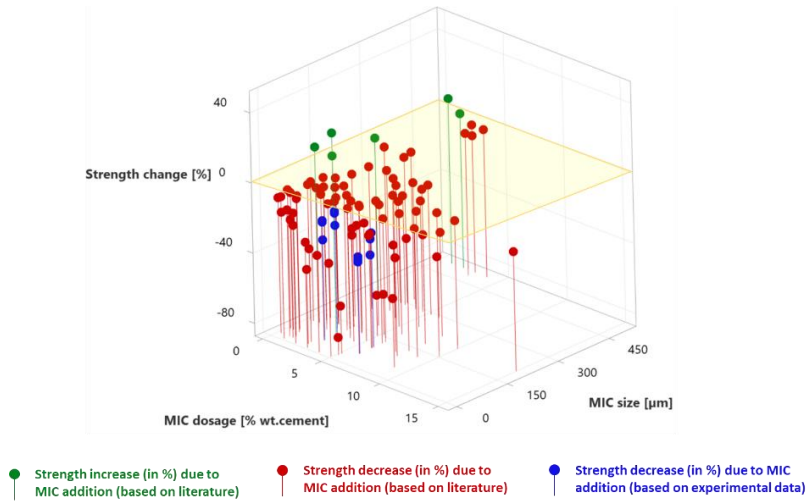


Figure 7-26. 3D plot of the alteration of compressive strength due to the addition of microcapsules in function of MIC size and MIC dosage

Tensile splitting strength

Table 7-11 presents the tensile splitting strength, measured at 28 days. For each mixture, measurements were taken in triplicate. The tensile splitting strength in this study ranges from 2.82 to 4.49 MPa. The changes of tensile splitting strengths due to the inclusion of MIC_56 were elaborated in Figure 7-27a. Concrete mixtures without the addition of microcapsules (0% bwoc) experienced a gradual reduction of tensile splitting strength when increasing the w/c from 0.40 to 0.60. When MIC_56 was added at a variety of dosages (1–6% bwoc), the tensile splitting strength reduced. Reported in Table 7-11, the reduction of tensile splitting strength was expected in the range of 8–25% for the addition of MIC_56 from 3–6% bwoc. Figure 7-27b shows the contour plot of tensile splitting strength on the use of MIC_93. Results suggest that the reduction of tensile splitting strength was more pronounced with MIC_93 than MIC_56, especially at a high capsule dosage (3–6% bwoc) as indicated by the blue contour areas. The effect of MIC size in the range of 56–93 µm was further investigated in Figure 7-27c,d in different w/c. As expected, the tensile splitting strength was not significantly affected by the MIC size. The contour plots - Figure 7-27c (w/c 0.50 mixes) and Figure 7-27d (w/c 0.60 mixes) – only showed minor differences in terms of the strength changes.

Again, a statistical analysis was performed on this data set by means of ANOVA and main effects plots. Based on Table 7-13, the most significant factors were w/c and MIC dosage, mirroring the results seen in the compressive strength data set. MIC size had a large p-value of 0.789, further validating its negligible effect on tensile splitting strength. The main effects plot (Figure 7-28) was in agreement with the ANOVA; the factors - w/c and MIC dosage - considerably affect the tensile splitting strength. There was apparently no effect of MIC size on tensile splitting strength as depicted by a flat slope.

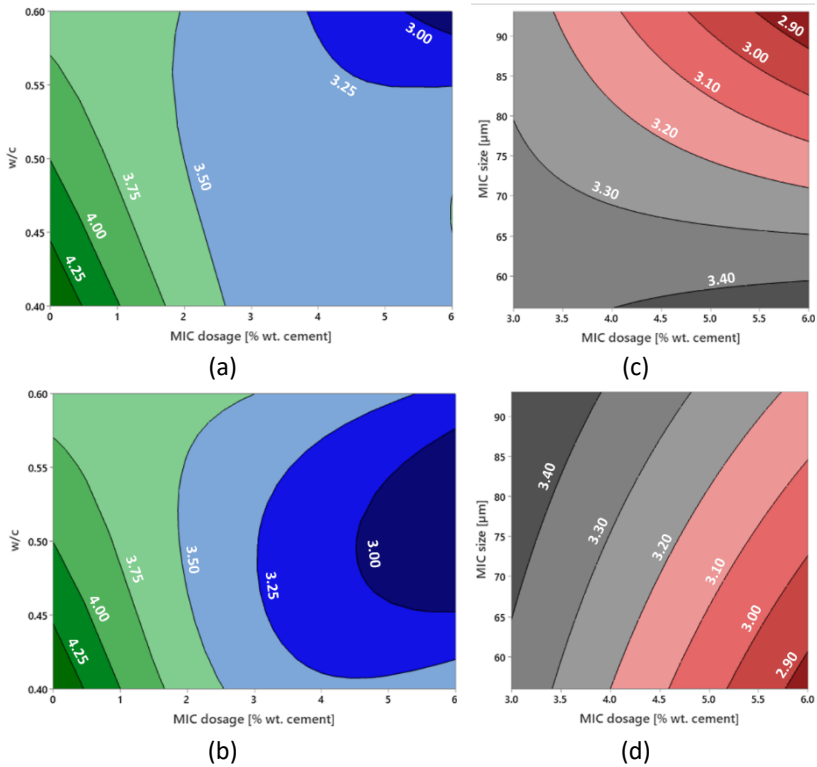


Figure 7-27. Contour plots for the effect of (a) MIC dosage vs w/c for MIC_56, (b) MIC dosage vs w/c for MIC_93, (c) MIC dosage vs MIC size with a hold factor of w/c 0.50 and (d) MIC dosage vs MIC size with a hold factor of w/c 0.60, on tensile splitting strength

Table 7-13. Analysis of variance for 28d tensile splitting strength

Source	DF	Adj SS	Adj MS	F-value	P-value
w/c	2	1.5286	0.76429	5.77	0.006
MIC size	1	0.0096	0.00958	0.07	0.789
MIC dosage	2	7.3720	3.68600	27.82	0.000
Error	48	6.3588	0.13248		
Total	53	15.2690			

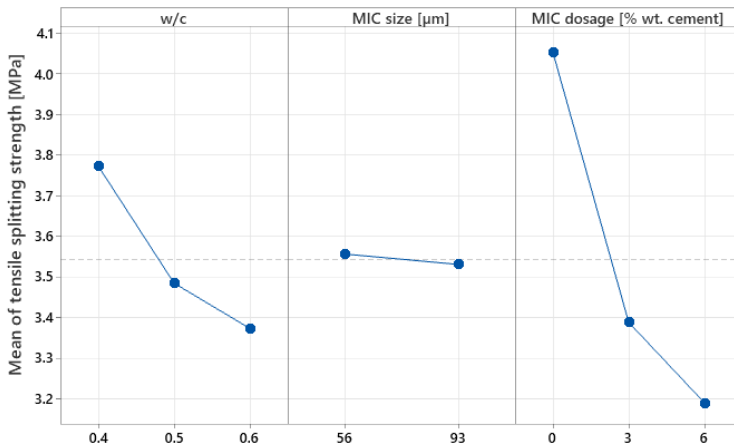


Figure 7-28. Main effects plots for tensile splitting strength

Ultrasonic pulse velocity (UPV)

The measured values of UPV were summarized in Table 7-11. For each mixture, measurements were taken in triplicate. The measured values ranged from 4400 to 5100 m/s. According to Figure 7-29a,b, at any w/c, it is clear that the UPV decreases with increasing the MIC dosage from 0 to 6% bwoc. This may be related to the distribution of the capsules in the matrix since the UPV assessment considers the travelling of longitudinal waves within the concrete matrix. In addition, it may also correlate with the pore size distribution due to the presence of the capsules. However, the distribution of the capsules in the concrete is difficult to be assessed as the fine and coarse aggregates are mainly present in the concrete. Thus, further research is needed to investigate the distribution of the capsules in the concrete. The presence of capsules will be identified later via SEM. As seen in the compressive strength and tensile splitting strength tests, the change

of MIC size from 56 to 93 μm and MIC dosage from 3 to 6% bwoc did not cause a considerable difference in UPV values (see Figure 7-29c,d).

A statistical analysis was conducted on UPV values by means of ANOVA (see Table 7-14) and main effects plots (see Figure 7-30). The trends that were seen for both compressive and tensile splitting strength remained true for UPV with the most influential factors affecting the UPV being w/c and MIC dosage. The MIC size did not significantly influence the UPV values. These results were mirrored in the main effects plots.

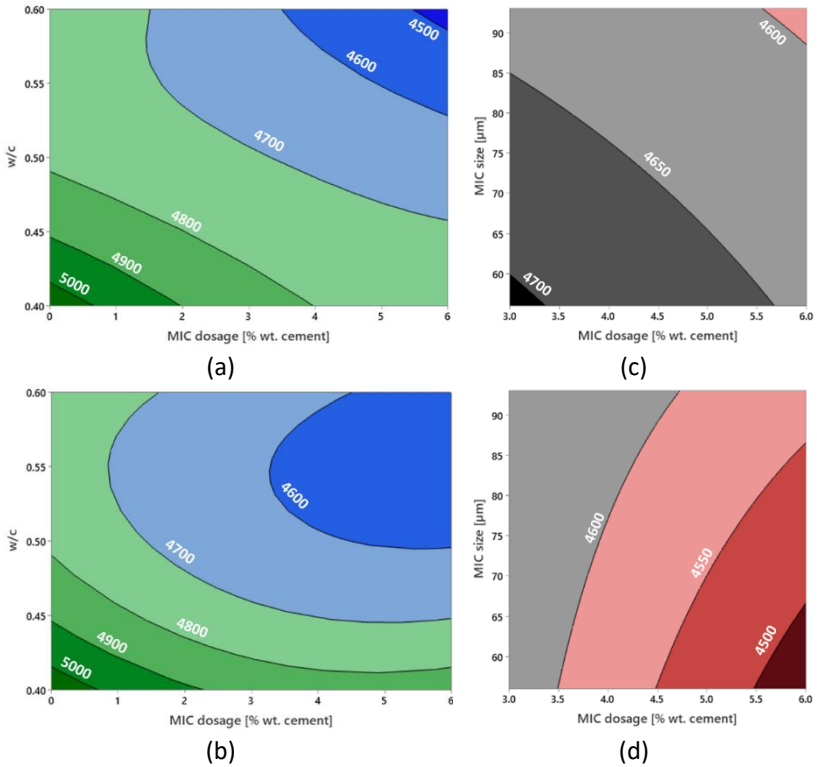


Figure 7-29. Contour plots for the effect of (a) MIC dosage vs w/c for MIC_56, (b) MIC dosage vs w/c for MIC_93, (c) MIC dosage vs MIC size with a hold factor of w/c 0.50 and (d) MIC dosage vs MIC size with a hold factor of w/c 0.60, on UPV

Table 7-14. Analysis of variance for UPV

Source	DF	Adj SS	Adj MS	F-value	P-value
w/c	2	722481	361240	92.04	0.000
MIC size	1	2209	2209	0.56	0.457
MIC dosage	2	477760	238880	60.87	0.000
Error	48	188382	3925		
Total	53	1390831			

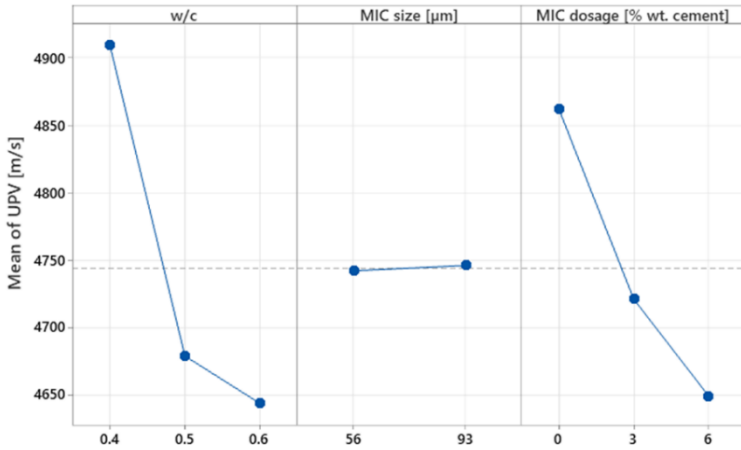


Figure 7-30. Main effects plots for UPV

7.3.4.6 Self-sealing properties of MIC concretes

Figure 7-31 shows the average crack width of all casted mixtures based on three replicates for each mixture (3 specimens × 20 measurements = 60 measurements per mixture). It was originally aimed to obtain the crack width between 200 and 300 µm, while in fact variation was seen. Nevertheless, the average crack widths for all mixtures was within the target crack width boundaries except one mixture (w/c 0.40 + 6% MIC₅₆) which had an average crack width of 174 µm. Considering its standard deviation, however, the mixture was included.

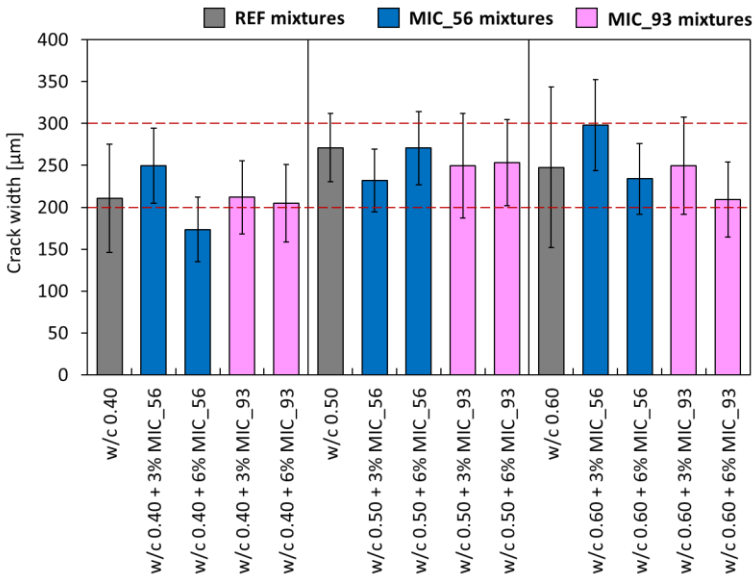


Figure 7-31. Variation of crack width for all mixtures (note: dash lines represent the range of target crack width between 200 and 300 µm)

Figure 7-32 presents the results from the CWA tests, comparing cumulative water uptake and time of water immersion. The water uptake over time of the reference (REF) mixtures, both cracked and uncracked, was distinctly greater than MIC concrete. Moreover, for all mixes both REF and MIC, a higher w/c leads to greater water uptake due to an increased porosity. The effect of microcapsules was also apparent as the water uptake of MIC mixtures was minimal with water uptake equal or less than REF_UNCR. The water uptake of the MIC_CR series was slightly higher than that of the MIC_UNCR. However, when comparing MIC_CR to REF_CR, it is evident that capsules have ruptured, sealing has taken place, and the water absorption has been minimised. This is also evident in Figure 7-33 as the water-mark on the side of the specimen is reduced with increasing microcapsules content. In order to analyse the CWA results, the sorption coefficient (S) was calculated in accordance with EN 13057 and the values are summarized in Figure 7-34.

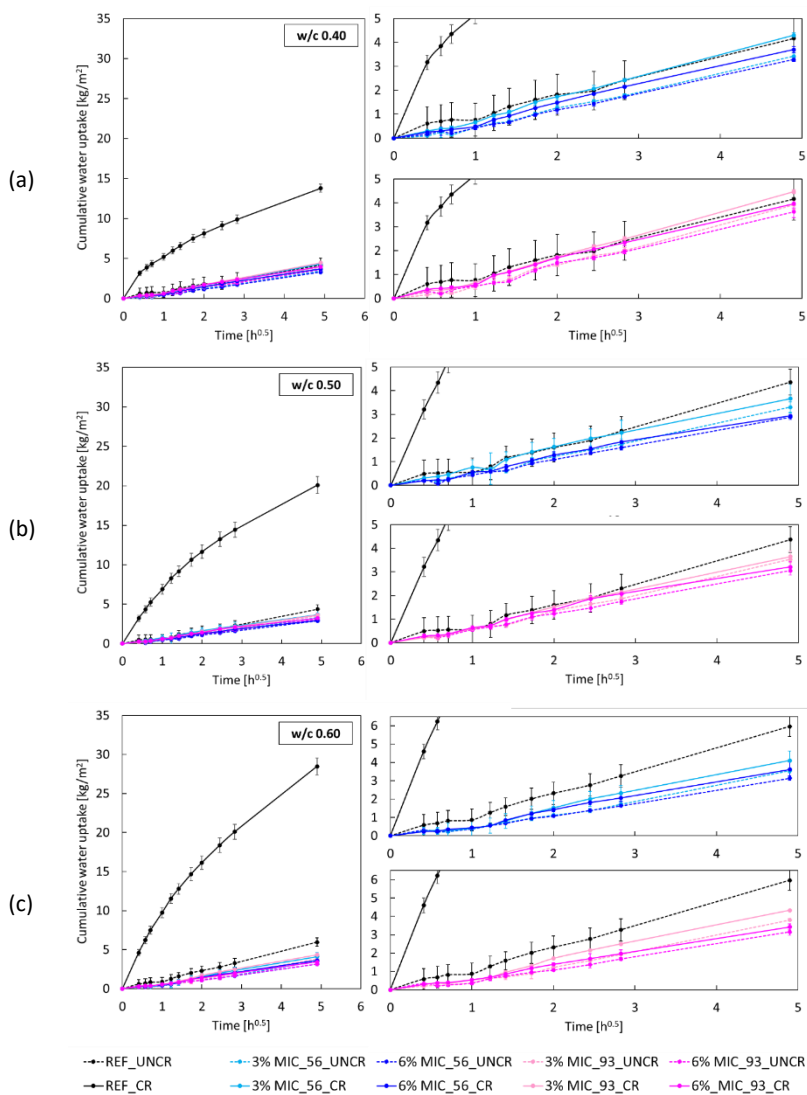


Figure 7-32. Relationship between water uptake and time of water immersion on (a) w/c 0.40 mixtures, (b) w/c 0.50 mixtures and (c) w/c 0.60 mixtures (note: REF = reference (no microcapsules), UNCR = uncracked, CR = cracked)

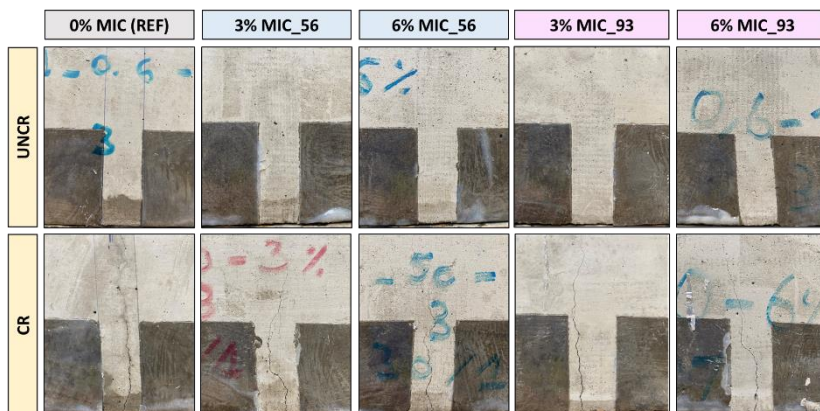


Figure 7-33. Comparison between reference concrete (without microcapsules) and microcapsule-based concretes right after CWA tests

The detailed explanation from Figure 7-34 can be found below:

- *For UNCR series:* In all w/c ratios, it is clear that the S of microcapsule-based concretes is lower than the reference concrete. In addition, the increase of MIC dosage from 3 to 6% gradually reduces the S values. For instance, in mixtures with w/c of 0.50, the average S of reference concrete was $0.89 \text{ kg}/(\text{m}^2\text{h}^{0.5})$ and the inclusion of 3% and 6% MIC_56 lowered the S to 0.68 and $0.59 \text{ kg}/(\text{m}^2\text{h}^{0.5})$, respectively. The same behaviour was found in other mixtures. Concerning the effect of MIC size, in most cases, the S of MIC_93 was slightly higher than MIC_56 with a difference of between 1 and 14%.
- *For CR series:* There was a significant difference between the S values of microcapsule-based concretes and reference concrete. The S values of reference concretes were approximately three to eight times higher than that of the microcapsule-based concretes. When the microcapsules were not present in the cracked concrete, the S increased from 2.81 to $5.81 \text{ kg}/(\text{m}^2\text{h}^{0.5})$ with rising the w/c from 0.40 to 0.60, showing a notable effect of w/c in terms of water absorption. It has been known that a lower w/c leads to a higher improvement in the durability properties and this tendency is confirmed in this observation. The water penetrates through the matrix via the crack with a faster rate in concrete with high w/c than low w/c and this is attributed to the high porosity level [196]. With the incorporation of microcapsules, the S values for CR series stayed at low level around $0.60\text{--}0.90 \text{ kg}/(\text{m}^2\text{h}^{0.5})$ which is basically comparable or, in some cases, slightly higher with respect to the S values of microcapsule-based concretes in UNCR state (approximately $0.60\text{--}0.80 \text{ kg}/(\text{m}^2\text{h}^{0.5})$).

Increasing MIC dosage from 3 to 6% also slightly reduced the S values. For instance, on w/c 0.50 mixture with 3 and 6% MIC₅₆, the S were 0.73 and 0.60 kg/(m²h^{0.5}), respectively. This effect is valid for all mixtures in different w/c. Concerning the effect of MIC size, in most cases, the S of MIC₉₃ was slightly higher than MIC₅₆ with a difference between 0 and 9%.

Both observations on UNCR and CR specimens confirm an improved water tightness of the concrete with the addition of microcapsules, both in uncracked and cracked state.

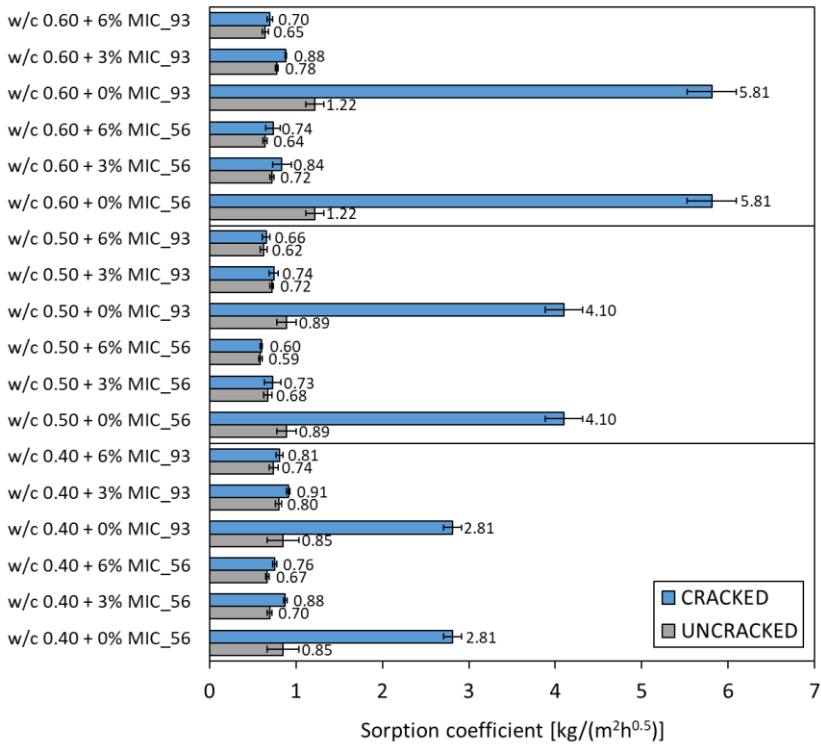


Figure 7-34. Effect of microcapsules on the sorption coefficient of uncracked and cracked concretes

An ANOVA was conducted on the S_{UNCR} and S_{CR} and the results are shown in Table 7-15 and Table 7-16, respectively. In case of S_{UNCR} , w/c and MIC dosage were regarded as the most significant factors affecting the sorption coefficient of uncracked concrete (p -values < 0.05). The same applies to S_{CR} . The factor of MIC size did not show any significant effect on the sorption coefficient both in uncracked and cracked concretes (p -value > 0.05).

Table 7-15. Analysis of variance for S_{UNCR}

Source	DF	Adj SS	Adj MS	F-value	P-value
w/c	2	0.18554	0.092770	7.28	0.002
MIC size	1	0.01612	0.016125	1.26	0.266
MIC dosage	2	1.09967	0.549836	43.13	0.000
Error	48	0.61189	0.012748		
Total	53	1.91322			

Table 7-16. Analysis of variance for S_{CR}

Source	DF	Adj SS	Adj MS	F-value	P-value
w/c	2	8.710	4.3551	10.88	0.000
MIC size	1	0.005	0.0046	0.01	0.915
MIC dosage	2	144.711	72.3557	180.74	0.000
Error	48	19.216	0.4003		
Total	53	172.642			

The sealing efficiency (SE) can be calculated by taking into account the sorption coefficient of CR series from Figure 7-34 with the following formula:

$$SE = \left(1 - \frac{S_{MIC_CR}}{S_{REF_CR}}\right) \times 100\% \quad (7.2)$$

The SE results are depicted in Figure 7-35 with sorting out the x-axis based on the changes of w/c with the same MIC dosage and MIC size to evaluate the effect of mix design parameters. In general, the SE results showed that, regardless of MIC size (either 56 or 93 μm) and MIC dosage (either 3 or 6%), there is a notable effect of the w/c in terms of sealing efficiency. Changing the low w/c (i.e., 0.40) to high w/c (i.e, 0.60) apparently increases the SE. Also, increasing the MIC from 3 to 6% bwoc leads to a further improvement of SE as shown by the upward trend.

In relation to the effect of w/c, in fact, the sorption coefficients of MIC_CR concretes were relatively similar around 0.60–0.80 $\text{kg}/(\text{m}^2\text{h}^{0.5})$ at any w/c, while the sorption coefficients of REF_CR concretes considerably varied depending on the w/c (2.81, 4.10 and 5.81 $\text{kg}/(\text{m}^2\text{h}^{0.5})$ for w/c 0.40, 0.50 and 0.60, respectively). Thus, it was seen that the higher the w/c, the higher the S_{REF_CR} , while the S_{MIC_CR} was comparable for all w/c. Consequently, the SE becomes higher with the higher w/c. Considering the MIC size, the SE for 3% MIC_56 was identical as compared with 3% MIC_93, and the same trend was obtained on the mixtures with MIC dosage of 6% bwoc. This finding is in line

with the observation of the mechanical performance of the MIC concrete where no significant effect of MIC size was attained. This may be attributed to the size of microcapsules used in this study was relatively small (56 and 93 μm), so the effect was not very apparent. Furthermore, the contour plots for SE were developed in Figure 7-36 and the ANOVA was conducted as summarized in Table 7-17. The factors of w/c and MIC dosage, again, showed the most significant factors affecting the sealing efficiency ($p\text{-value} = 0 < 0.05$), confirming that the MIC inclusion is working hand in hand with w/c changes.

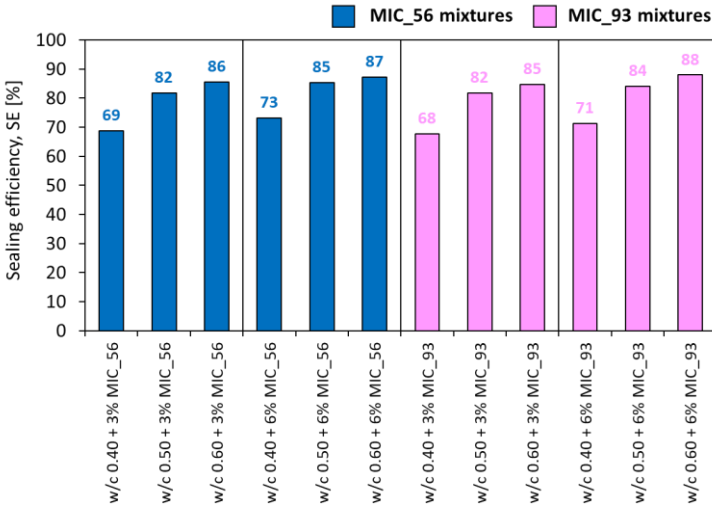


Figure 7-35. Effect of w/c and microcapsules on the sealing efficiency of cracked concretes

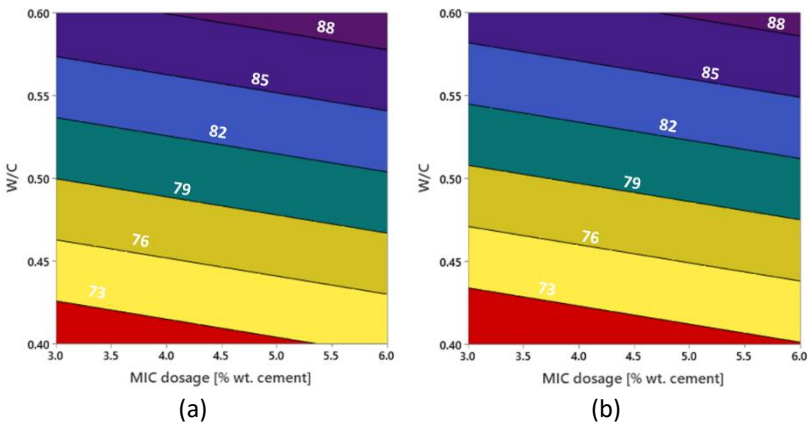


Figure 7-36. Contour plots of SE: (a) MIC₅₆ and (b) MIC₉₃

Table 7-17. Analysis of variance for SE

Source	DF	Adj SS	Adj MS	F-value	P-value
w/c	2	591.500	295.750	540.07	0.000
MIC size	1	1.333	1.333	2.43	0.163
MIC dosage	1	21.333	21.333	38.96	0.000
Error	7	3.833	0.548		
Total	11	618.000			

7.3.5 Microstructural observation

The investigation on the microstructure of microcapsule-based concrete was done by performing scanning electron microscopy (SEM). A fragment from the internal matrix of the concrete was taken and it was coated with gold to ensure conductivity during SEM imaging. Fragments from four representative mixtures were analyzed namely w/c 0.60 + 3% MIC_56, w/c 0.60 + 3% MIC_93, w/c 0.60 + 6% MIC_56, and w/c 0.60 + 6% MIC_93. The SEM micrographs of the concrete matrix are shown in Figure 7-37.

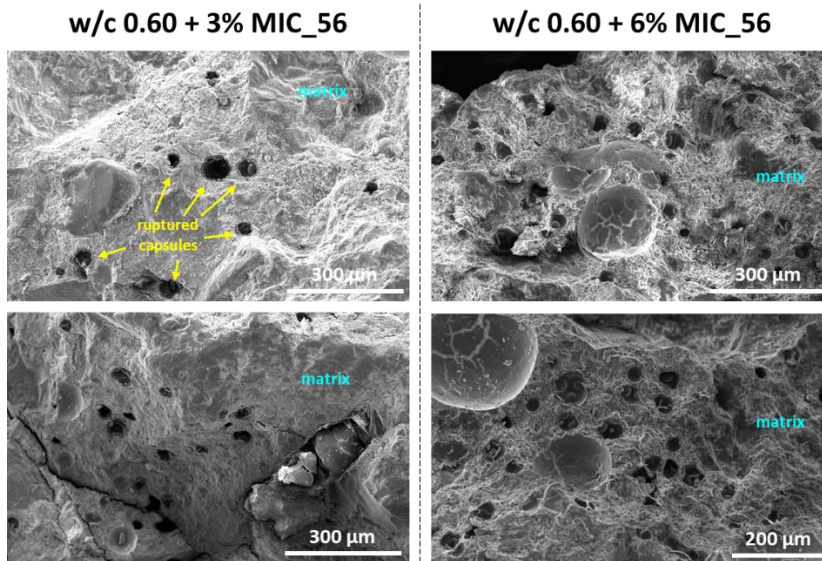


Figure 7-37. The microstructure of the concrete matrix after the inclusion of 3% and 6% MIC_56 observed in mixtures with w/c of 0.60

Ruptured microcapsules adhered to the mortar can clearly be seen in Figure 7-37 with higher microcapsule dosages exhibiting further microcapsule “pores”. This is hypothesised to contribute towards the strength reduction as microcapsules take a partial volume of the concrete matrix, reducing the hardened density in comparison to the reference concretes (see Figure 7-23). Second, as polyurethane microcapsules have less strength and lower stiffness than the concrete materials, they may weaken the concrete matrix causing ‘weak’ spots in the matrix. Third, some capsules may be broken after mixing and some capsules may survive. Although this is very difficult to quantify, the presence of shell or core materials may lead to defects that potentially increase the porosity level. This is also evident from UPV tests where the compactness of microcapsule-based concrete was lower than the reference concrete.

Moreover, energy dispersive X-ray (EDX) spectroscopy was used to study the elemental analysis of the concrete matrix where microcapsules are present. Figure 7-38 shows the EDX mapping analysis on the microcapsules surrounded by the concrete matrix, while Figure 7-39 shows the EDX regional analysis on the capsule and concrete matrix. Both results have the same agreement that the capsules are basically rich in carbon that are very different with the concrete matrix that is rich in calcium, aluminum and silicon.

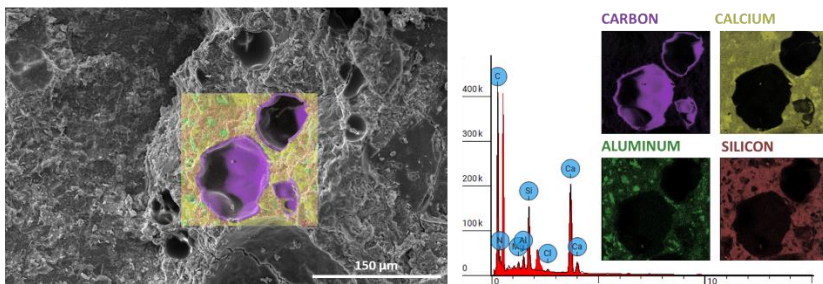


Figure 7-38. EDX mapping analysis on the concrete surface with microcapsules

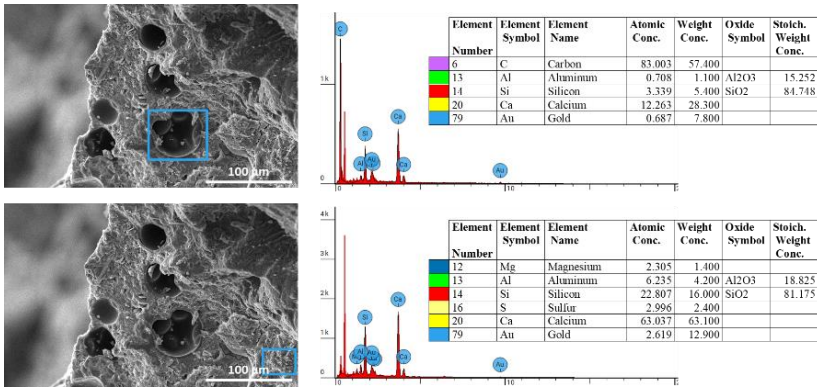


Figure 7-39. EDX regional analysis on the concrete surface with microcapsules

A good bonding between capsule shell and concrete matrix is achieved as depicted in Figure 7-40. A similar observation is also found by Wang et al. [190] in their previous study where the broken capsule shells (melamine-based) still attached to the matrix, indicating a good bond strength between microcapsules and the mortar matrix. As a matter of fact, this good bond is an important indication as Cao et al. [191] suggested that a poor interfacial bond between microcapsules and concrete contributes to the reduction of compressive strength. However, some capsules may experience debonding and delamination in the interface of capsule-matrix. For instance, Figure 7-41 (two images on top) shows that there is a debonding of the capsule shell. However, it is interesting to see that there is a formation of needle-like structures that is presumed to be ettringite. It is obvious that these structures are also formed on the outer shell of the capsule. In other locations (two images on bottom, see Figure 7-41), the ettringite formed on the capsule shell was also found. This may reflect that the microcapsules have a good compatibility with the concrete matrix as they are well attached to the matrix and the hydration products can form on the outer capsule shell.

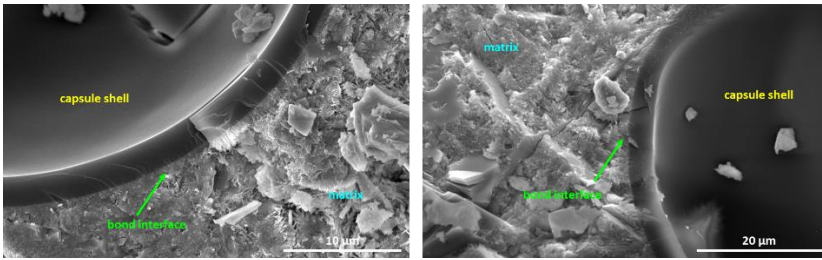


Figure 7-40. SEM micrographs on the bond between capsule shell and concrete matrix

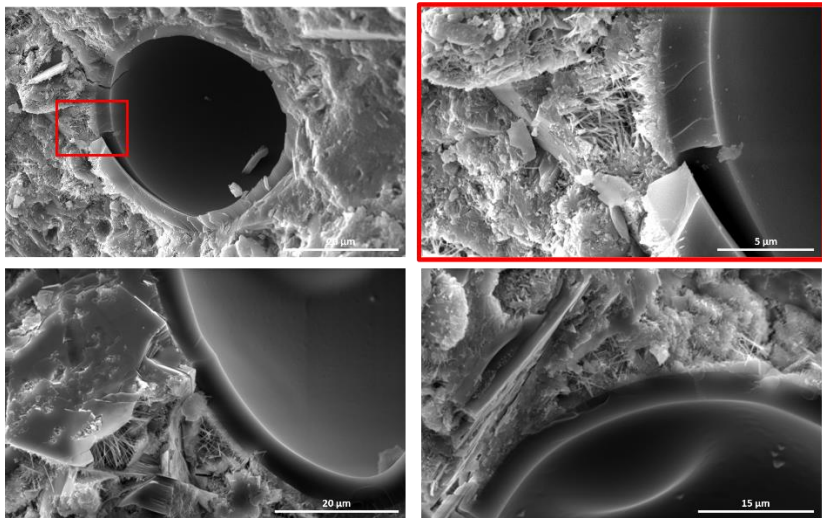


Figure 7-41. SEM micrographs on the delamination between capsule shell and matrix and the formation of crystal needles on the fractured shell

Additionally, based on the visual observation after compressive strength tests on all microcapsule-based concrete cubes, there were ‘wet spots’ found at each concrete face as shown in Figure 7-42a. It suggests that during compression, the embedded microcapsules were burst out and consequently released sealing agent to the matrix via cracks and capillaries. The spread of WRA seems not to be concentrated at one location, but is rather distributed around the surface where the microcracks are present, indicating a good distribution of the capsules. The same observation is later found in cylindrical concrete after being tested by splitting (see Figure 7-42b).

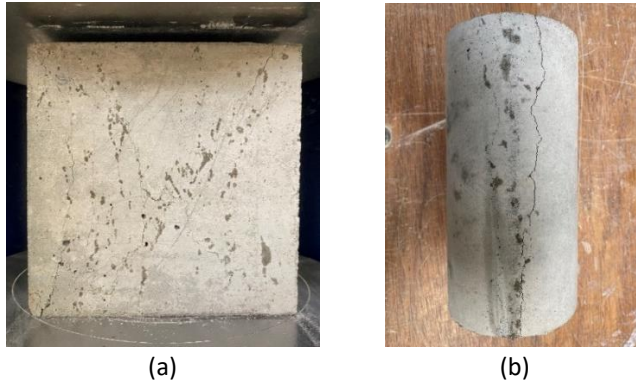


Figure 7-42. Wet spots in concrete indicating a release of sealing agent after mechanical testing on (a) cubical concrete and (b) cylindrical concrete

Based on SEM observation, Figure 7-43 shows that the embedded capsules were ruptured by the micro-cracking during the compression. Since the sealing agent has been released, the broken capsule shells were still left in the matrix. It is interesting to note that some of the capsules have lost their sphericity which is due to the compression test as well as from the mixing process.

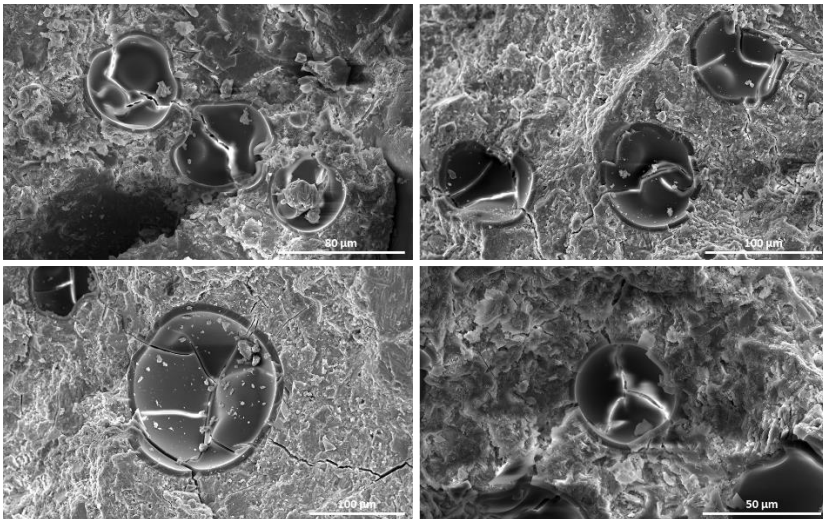


Figure 7-43. Cracking of the embedded microcapsules in the concrete matrix

7.3.6 Conclusions

In this study, the effects of microcapsules (MIC) are further explored starting from the paste to the mortar and concrete levels. At paste level, the fresh properties of cement paste added with microcapsules were investigated. At mortar level, a compatibility study between cement type and microcapsules was performed in terms of the strength performance. Finally, at concrete level, the fresh, hardened and self-sealing properties were examined in detail. The mix designs of MIC concretes were formulated with two full factorial design approaches. Three mix design factors employed with 2-3 levels for each factor were selected namely (1) MIC size (56 and 93 μm), (2) MIC dosage (0, 3 and 6% by weight of cement) and (3) w/c (0.40, 0.50 and 0.60). Microcapsules were added into the fresh mixture during mixing in slurry form. The obtained results related to the concrete properties were optimized with the aid of contour plots and statistical analysis. The key conclusions are listed below:

1. The inclusion of microcapsules did not change the water demand of cement, but caused a retardation in the setting time of cement paste.
2. Mortar made with CEM I 52.5N and microcapsules performed better with the least strength reduction as compared with the other mortars made with different cement types (CEM I 52.5N, CEM III/A 42.5N). However, further investigation is needed to understand the chemical interaction of microcapsules in different cement environments.
3. The performance of microcapsule-based concrete is susceptible to the mixing procedure. Increasing the capsule mixing time from 1 to 5.5 min led to an additional reduction in compressive strength.
4. The workability of fresh concrete mixtures was not affected by the incorporation of microcapsules regardless of their size and dosage. Nevertheless, in most cases, the fresh density of concrete was slightly reduced by the presence of microcapsules in the mixture. Furthermore, in the concrete mixture where superplasticizer was not introduced (i.e., mixes with w/c 0.60), the air content increased with increasing MIC dosage. However, in other mixtures where superplasticizer was introduced (i.e., mixes with w/c 0.40 and 0.50), there were inconsistencies in the trend of air content which may be associated with the interaction of microcapsules with the superplasticizer.
5. Negative effects of incorporating microcapsules into the concrete are related with a reduction in compressive strength, tensile splitting strength and compactness of MIC concrete as tested by UPV.

6. The w/c and MIC dosage were found to be the most significant factors affecting the mechanical properties, while there was no significant effect of changing MIC size from 56 to 93 μm .
7. Based on the contour plots, it was revealed that the negative MIC effect can be reduced with using a high w/c (i.e., 0.60 as compared with 0.40 and 0.50) in the mix design. More strength reduction was attained in the mixture with low w/c than high w/c which may be attributed to the high collision between microcapsules and concrete materials.
8. The capillary water absorption of concrete was significantly improved by the inclusion of microcapsules. The cracked MIC concrete performed as good as the uncracked REF concrete, while the cracked REF concrete experienced a high water uptake in the function of immersion time.
9. The sealing efficiency (SE) of MIC concrete in the uncracked and cracked states was found in the range of 6–47% and 68–88%, respectively. The w/c plays a key role in the sealing efficiency of MIC concrete as the higher the w/c, the higher the SE. Increasing the MIC dosage from 3 to 6% causes a further improvement of SE. In terms of MIC size, the 56- μm microcapsules had a higher SE than 93- μm microcapsules, observed in uncracked concrete. Nevertheless, in the cracked concrete, there was no effect of MIC size as the SE results were identical.
10. SEM and EDX analyses confirm that the capsules are rich in carbon and a good bonding between capsule shell and concrete matrix is showcased, even a formation of hydration products is found on the outer surface of capsule shell. Nevertheless, the presence of the capsules in the matrix is regarded as the presence of internal pores that is responsible for the downgrade of the mechanical performance.

Chapter 8

EFFECT OF MACROCAPSULES IN THE INERT STRUCTURE OF SELF-HEALING CONCRETE: A PROOF OF CONCEPT

8.1 Introduction

Macrocapsules have been used in self-healing applications, as previously discussed in Chapter 2, mainly in the matrices of paste and mortar. However, the application of macrocapsules in the concrete is still in a bottleneck and it is still relatively far to be realized for an actual implementation. It may be attributed to several reasons: (i) the production of macrocapsules is limited to fulfill the demand in lab-scale experiments and (ii) the macrocapsules, in most cases, are manually placed in the paste or mortar specimens with the aid of wire networks glued to the moulds. In fact, it will be more practical to add the capsules in the concrete by incorporating them into the fresh mixture during mixing stage although the position of capsules cannot be predicted. The main challenge of adding capsules during mixing is the capsule robustness toward the harsh mixing condition. The capsules should be robust enough to resist the shear stress during mixing as well as collision with concrete materials and mixing blades, while they also should be brittle enough to rupture whenever cracks occur in the concrete.

) This chapter is based on the following paper: **Hermawan H, Simons A, Teirlynck S, Serna P, Minne P, Anglani G, Tulliani JM, Antonaci P, Gruyaert E. Applicability of cementitious capsules in concrete production: initial assessment on capsule robustness , mechanical and self- sealing properties of concrete. In: MATEC Web of Conferences EDP Sciences; 2023. <https://doi.org/10.1051/mateconf/202337802013>*

This chapter attempts to study the effect of the capsules in the inert structure of the concrete. A particle packing model of Dewar was implemented to evaluate the influence of the capsules in the voids ratio of aggregates. Polymeric and cementitious capsules were used for the modelling, while going into the concrete application, only cementitious capsules were further employed. Capsule size, capsule dosage, aggregate type, aggregate mixture, fine fraction were selected as the main parameters. Based on the modelling part, a modification of concrete mix design for the introduction of macrocapsules was proposed as a proof-of-concept. The outcomes can be a guidance to optimize the mix designs of capsule-based concrete.

8.2 Applicability of cementitious capsules in concrete production: initial assessment on capsule robustness, mechanical and self-sealing properties of concrete

A preliminary study was conducted to develop methodologies of assessing the capsule robustness and mixing capsules with concrete materials to investigate the effects of the macrocapsules in the fresh and hardened concrete. Cementitious capsules with the length of 54 mm (labelled as CEM54) were used in this study. The robustness of capsules toward mixing forces is initially evaluated. The self-sealing properties of capsule-based concrete are assessed by means of a capillary water absorption test. An additional test is conducted to quantify the sealing coverage area as a result of the released sealing agent from the capsules.

8.2.1 Materials

Table 8-1 shows the mix designs of reference concrete (REF) and concrete containing capsules (CAPS). CEM III/A 42.5N, having 52% clinker and 48% blast furnace slag, was used as a binder component. Sea sand 0/2.5 was used as fine aggregate, while two fractions of gravels (4/8 and 8/16) were used as coarse aggregates. The specific gravities of sand 0/2.5, gravel 4/8 and gravel 8/16 were 2.67, 2.59 and 2.60, respectively. The water-cement ratio (w/c) was fixed at 0.50 for all mixtures. Polycarboxylate-ether (PCE) superplasticizer (Fluivicon 801, supplied by CUGLA B.V.) with a 20% solid content was used to improve the workability of the mixes.

Table 8-1. Mix designs

Material	Unit	REF	CAPS
CEM III/A 42.5N	kg/m ³	325	325
Sand 0/2.5	kg/m ³	740	740
Gravel 4/8	kg/m ³	701	678
Gravel 8/16	kg/m ³	378	365
Effective water	kg/m ³	163	163
Superplasticizer	kg/m ³	0.89	0.89
Effective w/c	-	0.50	0.50
Capsules	vol% vs. gravel	-	2

The REF mixture was made without the addition of capsules. In case of CAPS mixture, the cementitious long capsules (CEM54) were added into the concrete mix with a dosage of 2% by the volume of coarse aggregates. The capsules were treated as a partial replacement of gravels (see Table 8-1). The length, outer diameter and inner diameter of cementitious capsules were 54, 9 and 6 mm, respectively. On the outer surface of the capsule, a sand layer was applied in order to provide a good bonding between the capsule and concrete matrix. Water-repellent agent (Sikagard 705L) was selected as a sealing agent that was stored inside each capsule with an approximate amount of 1 mL. The detailed composition and manufacturing process of cementitious capsules can be found in [22,23].

8.2.2 Methods

8.2.2.1 Capsule survivability test

Before incorporating the capsules into the concrete, the capsule survivability test was initially performed to determine the robustness of the capsules during concrete mixing. To realise this test, two types of mixers were employed: a tilting drum mixer (Lescha SM 145 S, see Figure 8-1(a)) and a planetary/rotary pan mixer (Zyklos ZZ 75 HE, see Figure 8-1(b)). In this regard, the REF mixture was used as a preliminary test with a target volume of 20 L. The capsules were added in two different dosages per type of mixing: 40/80 capsules per 20 L of concrete in drum mixer and 20/40 capsules per 20 L of concrete in planetary mixer (note: considering a limited number of capsules, the number of used capsules was varied on each mixer). A normal concrete mixing procedure was implemented. First, the raw materials (i.e.,

cement and aggregates) were mixed for 30 sec in the drum/planetary mixer. Second, the mixing water and superplasticizer were added and the mixing was continued. After 6 min of mixing, capsules were added into the mixer. For the survivability test with the drum mixer, the fresh mixture with the capsules was continuously mixed for another 3 min, while with the planetary mixer, it was only mixed for another 2 min. The survivability test was performed by taking the fresh concrete little-by-little from the mixer onto a sieve (sieve no 8 or 2.35 mm) and then shaking the sieve under water in order to remove the fresh mortar from the aggregates and capsules. In this way, the capsules can be easily found and the number of intact and broken capsules was counted manually. A quick overview of this developed test is depicted in Figure 8-2. The survival ratio was calculated as the total number of intact capsules over the total number of originally added capsules in percentage.

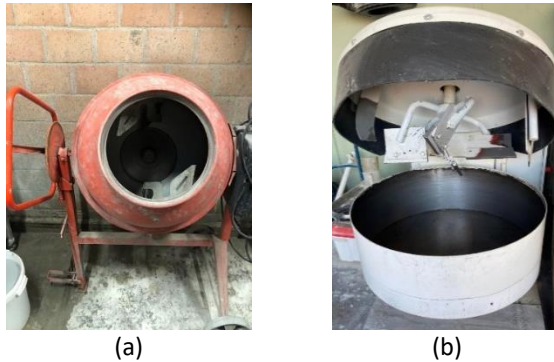


Figure 8-1. (a) Tilting drum mixer (Lescha SM 145 S) and (b) planetary mixer (Zyklus ZZ 75 HE)



Figure 8-2. Capsule survivability test

8.2.2.2 Mixing and casting procedure for capsule-based mixture

A concrete volume of 35 L was aimed both for REF and CAPS mixtures. Especially for the CAPS mixture, a new mixing process was developed. Initially, all dry materials (i.e. cement, sand, gravel) were put into the drum mixer and were mixed for 30 s. Mixing water was then added into the mixer and after 2 min of mixing, the mixer was stopped and the superplasticizer was added. Next, the mixing process was continued. After 6 min of mixing, a big portion of the fresh mix (~20 L) was poured into a bucket and around 15 L of fresh mix remained in the mixer. Fifty-two capsules (corresponding to 2 vol% of gravel in a 15 L fresh mixture) were added into the mixer and the leftover mix (~15 L) was mixed again for 90 s. Hence, the fresh mixture containing capsules was tested by means of slump and air content tests. Fresh concrete from the bucket was then prepared to be combined with capsules and cast into moulds. Three cube moulds (150 mm in side), three cylindrical moulds ($\varnothing 100 \times 200$ mm) and three prismatic moulds (100×100×400 mm) were prepared to cast the capsule-based concrete. It was initially calculated that 2% of capsules by the volume of gravel corresponds with 14 capsules per cube specimen and 6 capsules per cylindrical specimen. A small amount of fresh mix (approximately equivalent to the volume of the mould to be filled) was taken from the bucket into a bowl and depending on the volume of the designated specimens, the desired correct amount of capsules was added into the bowl. Next, the fresh mix and capsules in the bowl were manually mixed by a scoop until a homogeneous mixture was obtained which was then poured into the mould. The fresh mix with capsules was compacted by a vibrating table. In this way, a random distribution of capsules was attained. This method is proposed to have the exact target amount of capsules per specimen. A preliminary test also showed that the capsules were completely intact after concrete mixing in the drum mixer, thus this method can be used to simulate the application of capsules in the concrete and to understand the effects of capsules toward mechanical performance of hardened concrete.

For the prismatic specimens, the capsules were manually placed into the moulds by the following procedure:

- the first layer of fresh mix was poured into the mould with a height of approximately 40 mm,
- on top of the first layer, three capsules were placed in the middle span of the mould (horizontal direction – same direction as rebar),

- the second layer of fresh mix was poured into the mould until reaching a height of 60 mm from the bottom of the mould,
- three capsules were placed again in the middle span of the mould (horizontal direction – same direction as rebars) and finally, the fresh mix was poured until it fully covered the entire mould.

The cross section of the prism can be found in Figure 8-3. Unlike a random distribution of the capsules in cube and cylindrical specimens, the prismatic specimens were not aimed to assess the mechanical performance of the concrete. It was targeted to assess the ability of capsules to break during cracking and at the same time to evaluate the sealing properties. As the point of interest here is a crack that will be generated in the middle span of the prism, it was decided to manually place the capsules instead of adopting a random placement. In order to keep the same condition, the REF mixture was cast in the same way as the CAPS mixture but no capsules were added. One day after casting, the specimens were demoulded. The cube and cylindrical specimens were stored in a water tank at a temperature of $20\pm 2^{\circ}\text{C}$, while the prismatic specimens were stored in a curing chamber at $20\pm 2^{\circ}\text{C}$ and 60% RH.

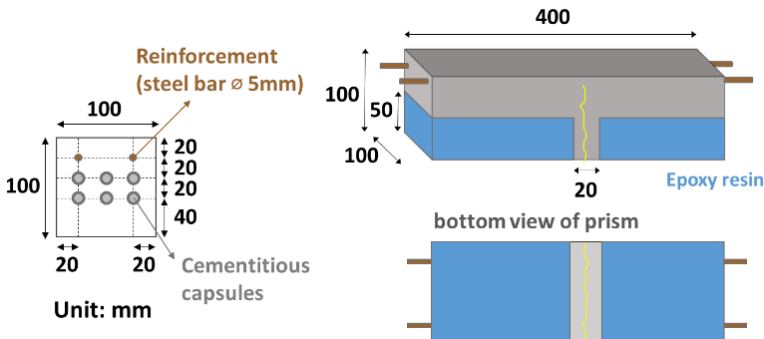


Figure 8-3. Schematic design of the capsule-based prism

8.2.2.3 Test methods

The fresh properties of concrete were assessed by means of slump, air content and fresh density tests (EN 12350-2,6,7), while the hardened properties of concrete were evaluated by means of compression and tensile splitting tests at 28 days (EN 12390-3,6). An ultrasonic pulse velocity (UPV) test based on EN 12504-4 was also conducted on the hardened cube specimens to evaluate the compactness of the specimens with and without the presence of capsules. During the UPV test, the transmitter and receiver were always arranged in the same way for each specimen, either REF or

CAPS, i.e. the UPV probes were placed at the center of two opposite faces of the cube, and the wave propagation direction was perpendicular to the casting direction.

The prisms were subjected to the three-point bending test to induce a crack at the age of 14 days. During the three-point bending test, the loading was manually controlled with a relatively slow loading rate and it was directly unloaded as soon as a crack occurred. Since the rebars were embedded 20 mm from the top of the prisms, the specimens did not experience a sudden failure and after unloading, the crack width slightly reduced due to the rebar relaxation. Upon cracking, the released WRA can be later seen on the crack. After the WRA dried (~4 hours), the cracked prisms were stored in an oven at 40°C for 10 days until constant weight was achieved. All specimens were stored in the same position as to when the three-point bending tests were performed. Constant weight was considered to be achieved when the change in mass over a period of 24 hours was less than 0.2% [99]. Next, the sides and the bottom of the specimens were partially covered with epoxy resin (Episol Designtop SF) as shown in Figure 8-3. The prisms were later returned to the oven for 3 days and the capillary water absorption test was finally conducted. A small area around the crack (20 mm in width) was left uncovered which was assigned as the contact area for this test (see Figure 8-3). The specimens were immersed in water with the water level 3 mm above the bottom surface of the prism. The weight of each specimen was recorded after 10, 20, 30, 60, 90, 120, 180, 240, 360, 480, and 1440 min. During the capillary water absorption test, it was ensured that the water level remained constant. As a note, the capillary water absorption test was performed on 3 uncracked reference prisms (REF_UNCR), 3 cracked reference prisms (REF_CR), and 3 cracked capsule-based prisms (CAPS_CR).

In addition, the water droplet test was later executed on the split cracked specimens. After performing the capillary water absorption tests, all prisms were deliberately cracked until failure, resulting into two parts of prisms per specimen. One part of the specimen was taken and the cross section was tested by the water droplet test. The droplet test was performed by releasing water droplets from the pipette to the crack surface (entire area of the cross section), and the water droplets were remained for approximately one minute. Next, the crack surface was captured by the camera and the area where the water droplets were not absorbed by the matrix indicates a sealed area and the wet area where the water droplets were absorbed by the matrix indicates an unsealed area.

8.2.3 Results and discussion

8.2.3.1 Capsule robustness

The results from the capsule survivability test were summarized in Table 8-2. It was shown that a 100% survival ratio of capsules was achieved during mixing the capsules in a drum mixer, while in case of using a planetary mixer, the survival ratio was attained in the range of 70–95%. A lower survival ratio in a planetary mixer occurred due to the high shear mixing force which eventually damaged a few capsules. Nevertheless, the capsules were considered robust enough to resist the mixing forces. As a proof-of-concept, in order to guarantee no single capsule was broken during the mixing process, the drum mixer was further opted for the final REF and CAPS mixtures.

Table 8-2. Capsule survivability (results based on a single test)

Concrete mixer		Drum mixer		Planetary mixer	
Concrete volume (L)		20	20	20	20
Number of added capsules (pcs)		40	80	20	40
Number of capsules after mixing –manual counting (pcs)	Intact capsules	40	80	14	38
	Broken capsules	0	0	6	2
Survival ratio (%)		100	100	70	95

8.2.3.2 Fresh and hardened properties

The fresh properties of REF and CAPS concretes were summarized in Table 8-3. The slump of REF concrete was 130 mm, while CAPS concrete had a lower slump of 100 mm. Nevertheless, both slump results were categorized in the S3 slump class. The introduction of capsules increased the air content of the fresh mixture from 3% (REF) to 4% (CAPS). This may be due to the fact that the presence of capsules disturbs the packing of the concrete materials (especially on the packing of aggregates). The fresh densities of both mixtures were identical regardless the addition of capsules.

Table 8-3. Fresh properties (note: single measurement for slump and air content tests)

Fresh properties	Unit	REF	CAPS
Slump	mm	130	100
Air content	%	3.0	4.0
Fresh density	kg/m ³	2328 ± 14	2329 ± 6

Figure 8-4 illustrates the mechanical performance of REF and CAPS concretes and the evaluation of UPV results. The REF concrete had a compressive strength of 42.9 MPa and the introduction of 2% capsules caused an 8% strength reduction. Statistical analysis by a t-test revealed that the difference of compressive strengths between REF and CAPS concretes was statistically significant ($p\text{-value} = 0.002 < 0.05$ as significance level). Interestingly, the tensile splitting strength of both mixtures had the same value of 4.1 MPa. Additionally, the UPV of hardened concretes with and without capsules had identical values at roughly 4810 m/s. It can be concluded that the addition of capsules mainly affects the compressive strength and no notable effects are found on the tensile splitting strength and the matrix compactness. It may be attributed to the effect of the random capsule distribution inside the concrete. One possible reason for strength reduction was due to the packing disturbance and the capsules were regarded as ‘weak’ spots in the matrix.

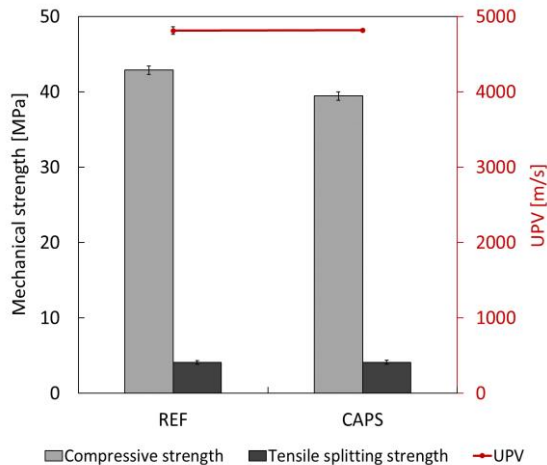


Figure 8-4. Hardened properties of the REF and CAPS concretes (notes: $n = 3$ for compression tests, $n = 3$ for tensile splitting tests and $n = 3$ for UPV tests)

8.2.3.3 Self-sealing properties

The 14-days-old prisms were cracked by means of the three-point bending test. In case of the REF concrete, the average crack width of three cracked prisms was $135 \pm 10 \mu\text{m}$. The CAPS concretes were also cracked, but the average crack width ($184 \pm 17 \mu\text{m}$) was slightly higher than for the REF. When the CAPS prisms were cracked, a release of sealing agent was observed as shown in Figure 8-5. This confirms that the capsules were successfully ruptured during the cracking stage. In this condition, the released water-repellent agent was seen to be rapidly absorbed by the concrete matrix in the crack zone. In order to evaluate the sealing ability, the capillary water absorption was performed on uncracked and cracked specimens. Figure 8-6 shows the relationship between the water uptake and the water immersion time during the test. Based on the REF concretes, it was clear that the presence of a crack caused a significant increase of the water uptake with increasing immersion time with respect to the uncracked specimen. With the cracked CAPS prisms, the progress of water uptake over time was considerably low and it was less dramatic than cracked REF prisms. Nevertheless, the water uptake of cracked CAPS prisms was slightly higher than the uncracked REF prisms. It proves that the released sealing agent seals the concrete matrix by preventing the penetration of water via the crack. According to Figure 8-6, the sorption coefficients (S) were recorded at 1.18, 6.98 and 1.78 $\text{kg}/(\text{m}^2\text{h}^{0.5})$ for uncracked REF, cracked REF and cracked CAPS concretes, respectively. The sealing efficiency (SE) of the CAPS concretes can be calculated by Equation (8.1) and it was found that 75% SE was achieved by the CAPS concrete. A previous study by Anglani et al. [23] showcased a 92% sealing efficiency with the use of the cementitious capsules filled with WRA in the mortar matrix.

$$SE = \left(1 - \frac{S_{CAPS_CR}}{S_{REF_CR}}\right) \times 100\% \quad (8.1)$$



Figure 8-5. Successful rupture of embedded capsules by releasing the sealing agent through the crack

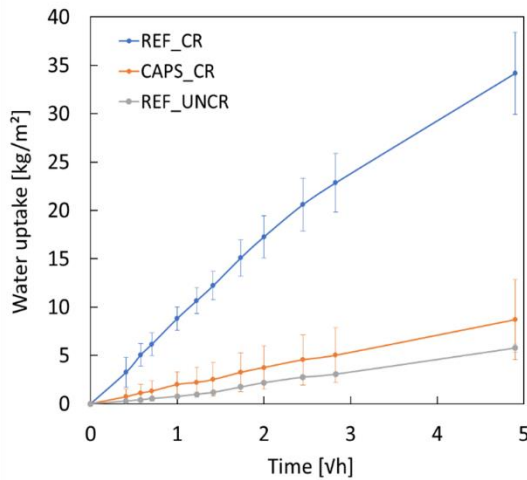


Figure 8-6. Capillary water absorption results (note: $n = 3$ for capillary water absorption tests on each specimen series)

An additional test was performed to assess the sealing coverage area in the crack zone by the water droplet test. Figure 8-7 clearly shows a 100% unsealed area for a REF specimen and a distinction between sealed and unsealed areas for a CAPS specimen. The sealed area represents a hydrophobic coating confirming the presence of the water repellent agent in that area. The AutoCAD software was used to measure the total area of the concrete surface and the total unsealed area. In this way, the sealed area can be quantified. It was found that based on three repetitions, the total sealing coverage area for the CAPS concretes was in the range of 80–88%.

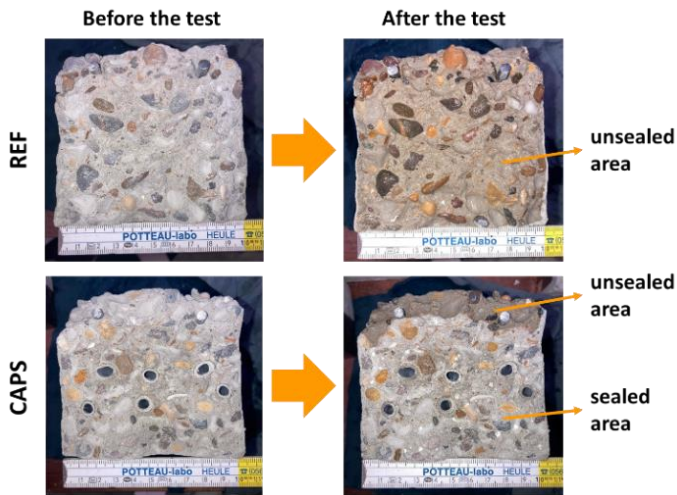


Figure 8-7. Sealing coverage area based on the water droplet test

As a proof-of-concept, a qualitative assessment was made to split the cube and cylindrical specimens, which had been previously tested by compression and tensile splitting tests, respectively, in order to count the amount of broken capsules in a certain crack plane. The specimens were placed in a tensile splitting setup, and they were tested until failure, as shown in Figure 8-8 and Figure 8-9. The number of broken capsules was counted after performing the splitting tests on three cylindrical specimens and three cube specimens containing 2% capsules. Few capsules in a certain plane of specimens broke during the splitting test. As shown in Figure 8-8, based on three repetitions, 2-5 out of 14 embedded capsules were present and broken in the crack plane of the cube specimens. On the other hand, as shown in Figure 8-9, based on three repetitions, 2-3 out of 6 embedded capsules were present and broken in the crack plane of cylindrical specimens. Despite not all the capsules were in the split plane, the fracture surface covered by the sealing agent appears to be quite large with respect to the total fracture surface. This is due to the fact that a single macrocapsule can carry a considerable amount of sealing agent.

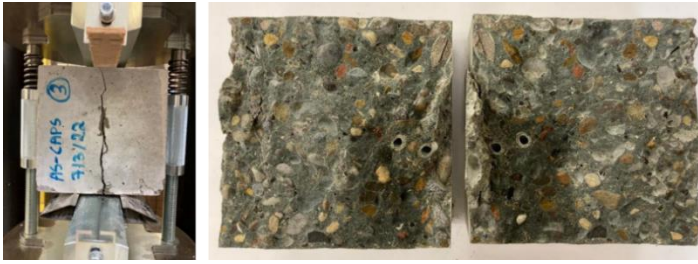


Figure 8-8. Splitting the cube specimens to count the amount of broken capsules in a certain crack plane (note: the darkest concrete surface is the area covered by WRA)

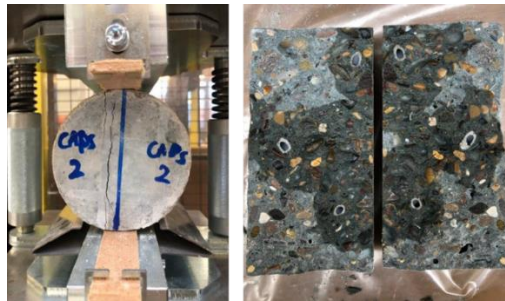


Figure 8-9. Splitting the cylindrical specimens to count the amount of broken capsules in a certain crack plane (note: the darkest concrete surface is the area covered by WRA)

These tendencies occur due to a random distribution of the capsules inside concrete, thus the location of the capsules is not concentrated in one specific location. For the CAPS prisms, the capsules were deliberately placed in the middle span of the specimens, thus when they were split (see Figure 8-7), all embedded capsules were broken. This observation implies that the distribution/placement of the capsules plays a key role on the number of capsules broken when a crack penetrates into the concrete. Pros and cons related to the capsule placement are discussed below:

- In the case of a random distribution of capsules in the concrete, it is not guaranteed that all capsules can be broken when a single crack is introduced. It strongly depends whether the capsules are present in the crack plane and the direction of the capsules. However, it can also be beneficial if the cracks occur in different locations. It will open a high possibility of 'in situ' repair where the capsules in random locations are broken and the release of sealing agent may occur in many places.

- In the case of a specific placement of capsules in the concrete (like CAPS prisms), all capsules are most-likely at the 'right' place when a single crack is introduced. However, if cracks occur in any other location in which the capsules are not present, the 'in situ' repair will not be achieved. This concept of a specific capsules placement might be useful in case the cracks are predicted to occur in a specific location, thus the specific capsules placement can be strived to allow a local repair.

8.2.4 Conclusions

This preliminary study aimed to investigate the introduction of macrocapsules in the concrete production by evaluating the capsules robustness, mechanical and self-sealing properties of hardened concrete. Cementitious capsules with a length of 54 mm and an outer diameter of 9 mm were used and the water-repellent agent was stored inside the capsules. The dosage of capsules was fixed at 2% by the volume of coarse aggregates. Based on this study, the key findings are summarized as follows:

1. The cementitious capsules were found to be robust to resist the mixing forces with 100% survival ratio when tested in a drum mixer and 70–95% when tested in a planetary mixer.
2. The addition of capsules slightly reduced the slump value and resulted in a higher air content.
3. A reduction of compressive strength by 8% was found when the capsules were introduced at 2% by the volume of coarse aggregates which potentially occurs due to the disturbance of the packing and the presence of capsules could be 'weak' spots in the concrete matrix. Furthermore, the presence of capsules did not alter the compactness of concrete matrix measured by UPV and the tensile splitting strength of concrete.

Based on the capillary water absorption test, the water uptake of the cracked CAPS specimens was almost as low as the water uptake of the uncracked REF specimens. This occurred due to the released water-repellent agent from the capsules that sealed the crack. A 75% sealing efficiency was achieved for the capsule-based concrete with the sealing coverage area of 80–88%.

8.3 Prediction of aggregate packing with tubular (macro) capsules based on the Dewar's particle packing method

Following the preliminary study, a modification of the concrete mix design may be necessary to guarantee a good packing of concrete materials after the introduction of capsules. In particular, the packing of solid materials in concrete is of great importance as it governs the fresh and hardened properties as well as the economical aspect of concrete as commercial product. Aggregates, which constitute 60–75% of the total volume of concrete, represent the majority of the material composition. Optimizing the concrete mix design is the key to the production of concrete with the focus of maximizing the packing density (or minimizing the voids ratio). In this research, a particle packing model of Dewar was used and the introduction of macrocapsules in the aggregate mixture was comprehensively studied.

8.3.1 Particle packing model of Dewar

Dewar [145] developed the particle packing method (PPM) based on the voids ratio of materials. The voids ratio is generally defined as the ratio of total void volume to total solid volume and it is a function of shape and surface texture of particles and of the grading in relation to the mean size of particles. A single-sized particle is modelled as a cube having a mean size D as shown in Figure 8-10a. It should be understood that a cube is used merely for convenience in the visual model and there is no assumption that this is a real, common or ideal shape. Each particle is associated with a corresponding void volume where X is the mean size of void. In case of a two-size particle mixture, the mixing of fine and coarse particles dilates the structure of the coarse particles (see Figure 8-10b). The subscripts 0 and 1 are, respectively, the volumetric proportions of the fine component in a two-size particle mixture for the two extreme situations of all coarse and all fine materials. Furthermore, the subscript 0 refers to parameters of the coarse component and the subscript 1 to parameters of the fine component. From Figure 8-10b, the dilation of coarse particle is modelled assuming that the coarse particles move apart to occupy the centers of spaces and the coarse particles are spaced apart m times the mean size of fine particle D_1 . The effective voids ratio of the coarse particles (U_0'') when the structure is dilated is calculated as:

$$U_0'' = (1 + U_0)(1 + mr)^3 - 1 \quad (8.2)$$

where U_0 = voids ratio of coarse particles, m = spacing factor, r = ratio of mean sizes = D_1/D_0 and D_0 = mean size of coarse particles.

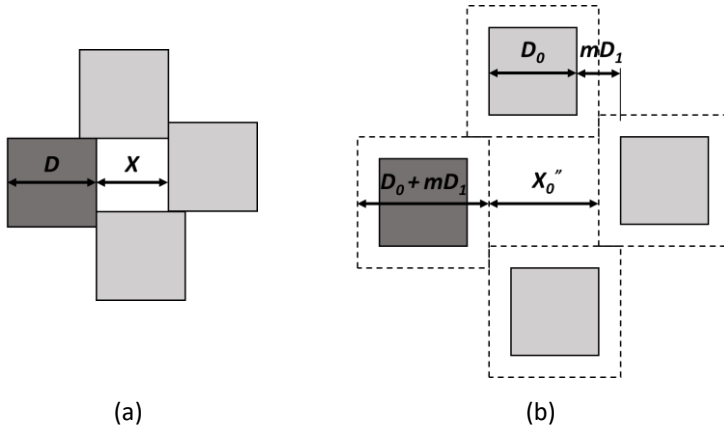


Figure 8-10. (a) Three dimensional model of a particle, associated void and related particles, (b) three-dimensional model of the dilated structure of coarse particles in a mixture containing fine particles

A typical voids ratio or interaction diagram of two materials can be illustrated in Figure 8-11 where the x-axis represents the fine fraction (n) of materials on volumetric basis and the y-axis is the voids ratio (U). The voids ratio of all coarse particles (U_0) is located at the left vertical axis when n equals to 0, while the voids ratio of all fine particles (U_1) is located at the right vertical axis when n equals to 1. The line U_0X represents the theoretical effect on voids ratio of adding fine material without any dilation of the structure of the coarse material. M is the point at which the voids in the coarse material are completely filled with the fine material at its own voids ratio while the coarse particles remain in contact. The line U_1O represents the theoretical effect of addition of coarse material to fine material without increasing the voids ratio of the fine material. The triangular area OMX represents hypothetical mixtures which cannot exist. The triangular area U_0MU_1 represents all practical mixtures (see Figure 8-11, experimental data) that can exist in the presence of particle interference. The lower boundary U_0MU_1 represents the voids ratios for all combinations of the two materials that could exist in the absence of particle interference. The upper boundary U_0U_1 represents the case when the mean sizes of the materials are equal and the particle interference is at maximum. Powers [197] described the particle

interference as the disturbance of the structure of the finer particle by the larger particles which causes an increase of the voids content. De Larrard [198] further elaborates that the 'aggregate wall' effect and 'loosening' effect are responsible for the particle interference, as depicted in Figure 8-12. The aggregate wall effect is a phenomenon when an isolated coarse particle disturbs the packing and increases the voids surrounding its particle, while the loosening effect is a phenomenon when an isolated fine particle in the structure of coarse particles appears to be too large to fit in the space between coarse particles, thus disturbing the packing.

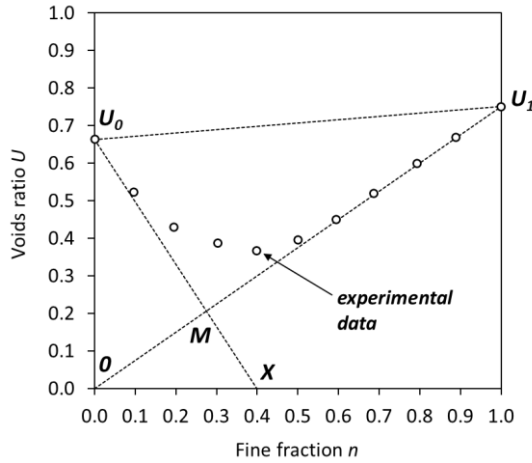


Figure 8-11. Theoretical relationship for voids ratio

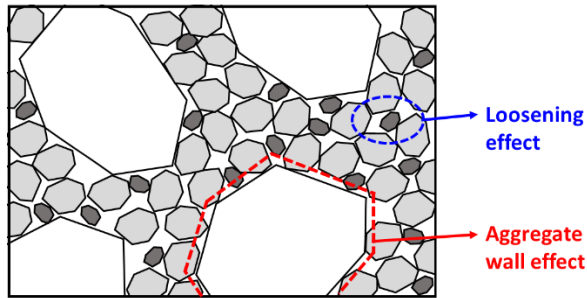


Figure 8-12. Loosening and wall effects

According to the PPM of Dewar, the voids ratio diagram of the combined materials in function of fine fraction can be constructed by using several change points (denoted as A to F) as presented in Figure 8-13. All change points are joined by five straight lines. These change points are associated

with the material properties of certain fractions, the spacing factor m and empirical factors k_{int} and k_p from Table 8-4. The voids ratio (U_n) and fine fraction (n) of each change point can be calculated by following equations:

$$U_n = nU_1'' \quad (8.3)$$

$$U_1'' = \frac{(1+U_1)U_0''}{(1+U_0'')-(1+Z)^3} - 1 \quad (8.4)$$

$$n = \frac{U_0''}{1+U_1''+U_0''} \quad (8.5)$$

$$Z = k_{int} + [(1 + U_0)'^{1/3} - 1 - k_{int}]r^{k_p} \quad (8.6)$$

where U_1'' is the effective voids ratio of fine particles, U_0'' is the effective voids ratio of coarse particles, r = ratio of mean sizes and Z is the notional width factor. The line $A-B$ represents a partial filling of voids of coarse particles by fine particles and the particle interference is minimal. The major interference in the packing of both fine and coarse particles occurs in the lines $B-C$ and $C-D$. The lines $D-E$ and $E-F$ represent a minor interference within fine and coarse particles.

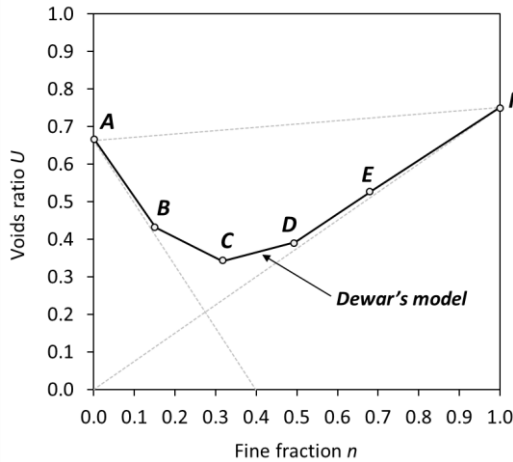


Figure 8-13. Theoretical voids ratio diagram based on Dewar's model

Table 8-4. Parameters for the change points in Dewar’s model

Change point	Parameters		
	m	k_{int}	k_p
A ($n = 0$)	0	-	-
B	0.3	0.12	0.60
C	0.75	0.06	0.65
D	3	0.015	0.8
E	7.5	0	0.9
F ($n = 1$)	∞	-	-

8.3.2 Polymeric and cementitious capsules

In the self-healing technology, capsules are used as vessels for carrying cargo material such as water-repellent agent (WRA), polyurethane (PU), bacterial agent, etc. The capsules should be properly designed to be able to break and release the healing agent when cracks appear in the concrete. In this study, two types of macrocapsules were used namely (1) cementitious capsules and (2) polymeric capsules. Both capsules are used to determine the effect of capsule parameters in the packing of aggregates.

Cementitious capsules

The cementitious capsules were produced by Politecnico di Torino colleagues. The detailed composition and the manufacturing process of these capsules can be found in [22,23,199]. Short cementitious capsules (CEM23) and long cementitious capsules (CEM54) were provided with the length of 23 and 54 mm, respectively. The physical appearance of both capsules is shown in Figure 8-14 and the detailed geometry of the capsules is summarized in Table 8-5. As a note, the volume listed in Table 8-5 considers the full volume of the capsule based on the mean length and the mean outer diameter. The cementitious capsules are mainly made of cement and were externally coated with an epoxy and a sand layer. This external coating improves the shock resistance of the shell and the conservation of the healing agent [23]. WRA (Sikagard 705L) was chosen as a healing agent for encapsulation with an approximate amount of 1 mL stored inside each capsule. This WRA was composed of one-component silane based and solvent free water repellent agent. It was originally used as a water repellent penetrating sealer and due to the sealing effect, the WRA will seal the crack surface so that no harmful substances can penetrate through the crack. The viscosity and density of Sikagard-705 L were 9 mm²/s and 0.900 kg/L, respectively.

Polymeric capsules

The polymeric capsules were prepared from FEP (Fluorinated Ethylene Propylene) polymeric extruded tubes supplied by ZEUS. These tubes were chosen due to their good rigidity and would not deflect when they were combined with aggregates. The extruded tubes were originally used for electrical and medical applications and these tubes can be easily cut into different sizes. The tubes were later cut into three different lengths and were closed with rubber at both ends. The short polymeric tubes with a length of about 35, 50 and 65 mm were further called as POLY35, POLY50 and POLY65 capsules, respectively. The detailed geometry of these capsules is also tabulated in Table 8-5. It should be noted that these polymeric capsules were not intended to be used in the concrete application because in some cases there were incompatibility issues between polymeric capsule shell and the stored healing agent due to premature hardening of healing agent or polymerization. The polymeric capsules were mainly used as a proof-of-concept to further understand the effect of capsules' parameters toward the packing of aggregates, in addition to the cementitious capsules.

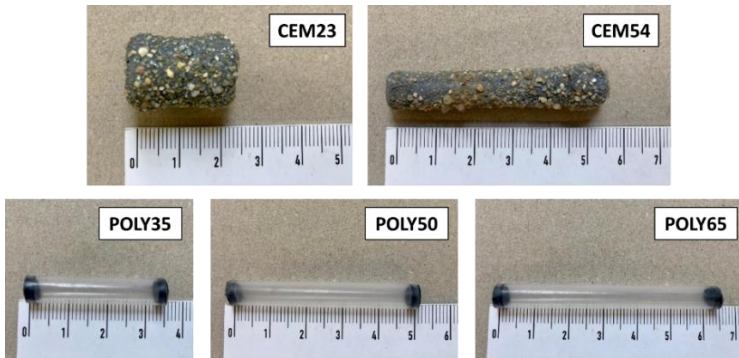


Figure 8-14. Several types of macrocapsules used in this study

Table 8-5. Detailed geometry of the macrocapsules (based on the average values from sampling)

Capsule name	Length, L_{caps} [mm]	Outer diameter, D_{caps} [mm]	Inner diameter [mm]	L_{caps}/D_{caps} ratio	Mass [g]	Volume [mm ³]
CEM23	22.73	14.97	12.00	1.52	6.05	4000
CEM54	54.19	9.06	6.00	5.98	5.98	3490
POLY35	35.61	6.65	6.01	5.35	0.81	1240
POLY50	50.10	6.65	6.01	7.53	1.07	1740
POLY65	65.03	6.65	6.01	9.78	1.33	2260

8.3.3 Physical properties of aggregates

Several types of aggregates were employed in this study starting from the fine to the coarse fractions. The main objective of using various types of aggregates was to combine aggregates and capsules at different dosages in order to analyse the effect of capsules in the packing of a certain aggregate type/fraction. The properties of aggregates can be found in Table 8-6 as determined by particle density and water absorption tests (EN 1097-6) and loose bulk density tests (EN 1097-3); and the particle size distributions (PSD) of all aggregates are depicted in Figure 8-15 as determined by sieving tests (EN 933-1).

Table 8-6. Properties of aggregates

Aggregate	Oven-dry particle density [kg/m ³]	Loose bulk density, ρ_b [kg/m ³]	Water absorption [%]	Voids ratio, U [-]	Mean size [mm]
Sea sand 0/2.5	2670	1520	0.41	0.751	0.40
River sand 0/4	2690	1630	0.43	0.656	0.90
Red sand 0/4	2640	1660	0.79	0.592	0.80
Gravel 4/8	2600	1550	2.05	0.672	6.48
Gravel 8/16	2600	1490	1.89	0.742	12.88
Limestone 2/6	2630	1350	1.17	0.952	4.30
Limestone 6/16	2640	1410	1.10	0.877	8.47
Limestone 16/20	2660	1400	0.79	0.905	18.00

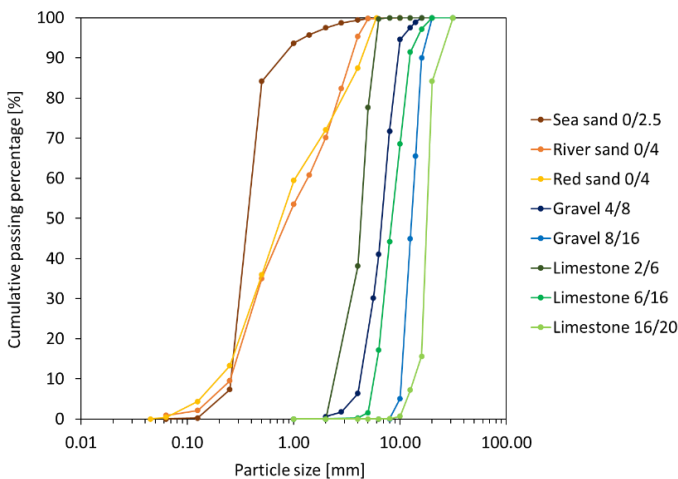


Figure 8-15. PSD of aggregates

8.3.4 Testing program

The voids ratio of aggregate is measured by the loose bulk density test (LBD) in accordance with EN 1097-3. The loose bulk density (ρ_b) and voids ratio (U) of aggregates are calculated as follows:

$$\rho_b = \frac{m_2 - m_1}{V} \times 10^3 \quad (8.7)$$

$$U = \frac{\rho_{rd}}{\rho_b} - 1 \quad (8.8)$$

where ρ_{rd} is the oven-dried density of aggregates [kg/m^3], m_2 is the mass of the container and oven-dried material [kg], m_1 is the mass of the empty container [kg] and V is the volume of the container [dm^3]. In this study, a steel container of 7.5 L was used for all types of aggregates. Furthermore, the capsules were combined with aggregates at specific dosages ranging from 0 to 3.5 % v/v (see Table 8-7). The unit of % v/v is defined as the volume of capsules over the volume of the container (as a note, the volume of the container represents the volume of aggregates + volume of voids + volume of capsules). Considering the physical appearance of CEM and POLY capsules was different, the selection of capsule dosage was slightly varied. For CEM23 and CEM54 capsules, the capsule dosage was fixed at approximately 0, 0.5, 1.0, 2.1 and 3.2 % v/v which means that a different number of capsules was assigned. The same condition was applied for the addition of POLY capsules where the dosage was fixed at approximately 0, 0.1, 0.6, 1.2, 2.5 and 3.5 % v/v. Although the number of capsules was varied depending on the size/volume of the corresponding capsules, the capsule dosage was relatively comparable both for CEM and POLY capsules. In other words, the capsule dosage was here selected as the main parameter. The effect of capsules in the packing system can be identified directly on the changes of the voids ratio of aggregates. Therefore, the loose bulk density of aggregates due to the presence of capsules can be calculated as follows:

$$\rho_b = \frac{m_3 - m_1 - m_{caps}}{V - V_{caps}} \times 10^3 \quad (8.9)$$

where m_3 is the mass of the container, oven-dried test specimen and capsules [kg], m_{caps} is the mass of added capsules [kg] and V_{caps} is the volume of added capsules [dm^3].

Table 8-7. Number of capsules used for LBD tests

CEM23		CEM54		POLY35		POLY50		POLY65	
No. of caps. [pcs]	Caps. dosage [% v/v]	No. of caps. [pcs]	Caps. dosage [% v/v]	No. of caps. [pcs]	Caps. dosage [% v/v]	No. of caps. [pcs]	Caps. dosage [% v/v]	No. of caps. [pcs]	Caps. dosage [% v/v]
0	0	0	0	0	0	0	0	0	0
10	0.535	11	0.513	9	0.149	7	0.163	5	0.151
20	1.069	23	1.073	40	0.661	28	0.651	22	0.664
40	2.138	46	2.145	76	1.255	54	1.255	42	1.267
60	3.207	69	3.218	152	2.511	108	2.510	83	2.504
				212	3.502	151	3.509	116	3.499

A schematic procedure of the LBD test on a specific aggregate type/fraction can be found in Figure 8-16. When a mixture of aggregates (e.g. sand and gravel) was used with a specific fine fraction (n), the procedure is presented in Figure 8-17. The fine fraction was run from 0.1 to 0.9 which was based on volumetric ratio. The voids ratio of mixed fine and coarse aggregates can be calculated by the theoretical oven-dried density of the mixture $\rho_{rd,n}$ (see equation below with the oven-dried density of the fine fraction $\rho_{rd,1}$ and coarse fraction $\rho_{rd,0}$) and the experimental loose bulk density of the mixture.

$$\rho_{rd,n} = n\rho_{rd,1} + (1 - n)\rho_{rd,0} \quad (8.10)$$

In case of capsules being added to the aggregate mixtures, it was ensured that all capsules were present inside the container and no capsules were available as residual materials. As a note, three repetitions were taken for each LBD test and the mean value of the measurements was denoted as the experimental voids ratio.



Figure 8-16. Schematic procedure of LBD test on a single type/fraction of aggregate

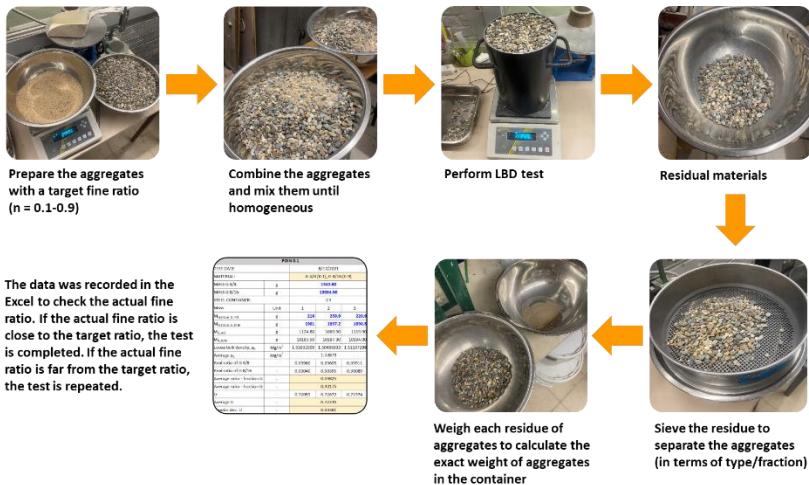


Figure 8-17. Schematic procedure of LBD test on aggregate mixtures

8.3.5 Packing of aggregates with and without macrocapsules

8.3.5.1 Voids ratio of aggregates

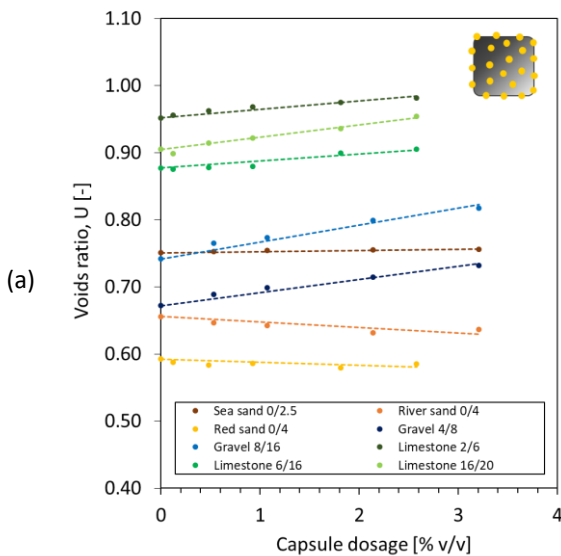
The voids ratio of a single aggregate type/fraction without the addition of macrocapsules was initially measured and the result is tabulated in Table 8-6. It is clear that the voids ratios were different for all aggregates and mainly depend on the fraction or particle size distribution of the respective aggregates, shape and roughness of particles. These initial U values were

regarded as the basis for the evaluation of the changes of U in function of capsule dosage. Specifically here, only cementitious capsules (CEM23 and CEM54) were used for the first assessment. The CEM capsules were added into different types of aggregates (i.e. sea sand, river sand, red sand, gravel and limestone) and different fractions of aggregates (i.e. 0/2.5, 0/4, 2/6, 4/8, 6/16, 8/16 and 16/20). The development of U as a function of capsule dosage is summarized in Figure 8-18 with implementing a linear regression. It is obvious that the voids ratio of fine aggregates (i.e. sea sand, river sand, red sand) did not truly change after the addition of CEM capsules at any dosage (either the case of CEM23 or CEM54) which was shown by a flat linear regression line (nearly zero slope). Contrarily, the voids ratio of coarse aggregates (i.e. gravel and limestone) considerably increased as increasing the capsule dosage. The increase of voids content can be explained due to the secondary loosening and wall effects induced by the capsules, refer as capsule effect, as illustrated in Figure 8-19. This capsule effect generates additional voids surrounding the perimeter of capsule wall/shell when in contact with aggregates and it loosens the packing between each particle.

In order to assess the effect of different CEM capsules, the slope (S) of the regression was recorded and the result is tabulated in Table 8-8. Apparently, the S values with CEM23 were always lower than the S values with CEM54, meaning that the voids ratio of aggregates was more affected with long capsules than short capsules. It is logic that the short capsules are in the shape of short tube or similar like round aggregates, so they can be blended better with aggregates. On the other hand, the long capsules are in rod-like shape. Thus, when these capsules are mixed with aggregates, the capsules will induce extra voids in the packing due to the increased gaps between the long capsules and aggregates as compared with the use of short capsules.

The L_{caps}/D_{caps} ratio may also play a role in the changes of U . The increase of L_{caps}/D_{caps} with a factor 3.9 (from 1.52 (CEM23) to 5.98 (CEM54)) caused an increase of S by 54–56% on all types of gravel and 83–176% on all types of limestone. It is interesting to see that the S of gravel 8/16 with capsules was higher than the S of gravel 4/8 with capsules. This finding was also observed with limestones. It means that the effect of capsules is higher with the coarser fractions of aggregates than the smaller fractions. A bigger size of aggregates in combination with capsules will cause more voids in the packing than a smaller size of aggregates in combination with capsules. Based on Table 8-8, the increment of S was higher on the use of limestones than gravels, showing that the effect of capsules is greater when combined with limestones. The physical characteristic of coarse aggregates apparently

influences the voids ratio of aggregate in the interaction with the capsules. Gravel is typically characterized by its rounded-shape and smooth texture, while limestone is characteristically jagged with sharp and pointy edges and rough surface. The interaction of capsules and limestone apparently seems to generate more voids than a combination of capsules and gravel. Gruyaert et al. [54] stressed that crushed limestone was expected to exert a higher impact on the capsules than gravel in terms of the capsules' resistance during concrete mixing. By taking into account these observations, it was decided to further analyse the effect of capsules in the packing of specific aggregates including sea sand 0/2.5, gravel 4/8 and gravel 8/16.



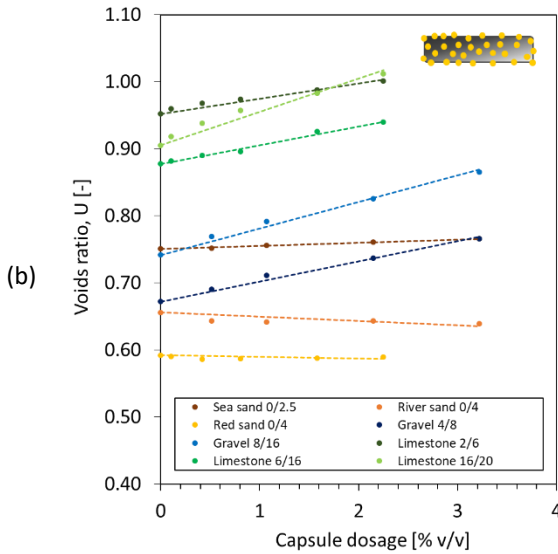


Figure 8-18. Voids ratio of different types and fractions of aggregates in function of the capsule dosage of (a) CEM23 and (b) CEM54

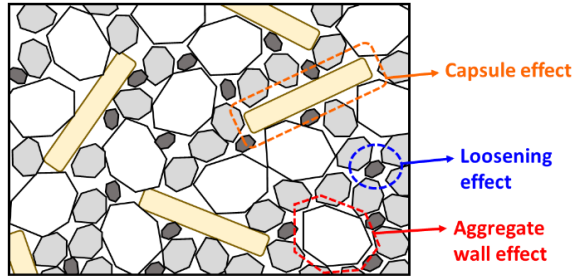


Figure 8-19. Capsule effect in the packing of aggregates

Table 8-8. Assessment on the change of voids ratio of coarse aggregates due to the presence of CEM capsules (note: the increment of S (CEM54 vs CEM23) = $(S_{\text{CEM54}} - S_{\text{CEM23}}) / S_{\text{CEM23}}$)

Aggregate	Slope, S [-/% v/v]		Increment of S [%]
	CEM23	CEM54	
Gravel 4/8	0.0195	0.0300	54
Gravel 8/16	0.0254	0.0395	56
Limestone 2/6	0.0125	0.0229	83
Limestone 6/16	0.0104	0.0281	170
Limestone 16/20	0.0181	0.0500	176

Following the selected aggregates for further analysis, the effect of polymeric capsules with different sizes were also investigated and the results are presented in Figure 8-20 on the relationship between percentage changes in U and capsule dosage. From Figure 8-20a, the effect of POLY capsules on the voids ratio of fine aggregate (sand 0/2.5) was very minor with a maximum increment of U less than 1% with the highest capsule dosage (~3.50% v/v). Moreover, a factor k was introduced as the slope of the percentage change in voids ratio versus the dosage of capsules. The k values for all capsules with sand 0/2.5 were rather identical, ranging from 0.22 to 0.29. It confirms no substantial disturbance of the packing of fine aggregates due to the introduction of any types of capsules. According to Figure 8-20b, increasing the amount of capsules added (up to 3.50% v/v) gradually increases the voids ratio of coarse aggregates, for instance, gravel 4/8 from 0.672 (0% v/v) to 0.745 (3.50% v/v) (equals to 10.8% increment) with the use of POLY50. The k values for POLY35, POLY50, POLY65, CEM23 and CEM54 on gravel 4/8 were 2.45, 3.00, 3.24, 2.91 and 4.47, respectively. On the use of a coarser fraction such as gravel 8/16, the presence of capsules exhibited higher k values than for gravel 4/8. On the other hand, there was a gradual increase of k as increasing the length of POLY capsules from 35 to 65 mm, observed at all dosages.

Regardless the fraction of coarse aggregates, the introduction of CEM54 seems to induce a higher impact than other capsule types as the k value of CEM54 was always the highest. In fact, the length of CEM54 capsules is similar to the POLY50 capsules but they do have different (outer) diameter, surface roughness and volume which makes the distinct changes in U . In order to normalize the different geometric sizes of capsules, a ratio of length over diameter (L_{caps}/D_{caps}) of the capsule was used (see the L_{caps}/D_{caps} values in Table 8-5). A relationship between L_{caps}/D_{caps} ratio and k factor was established as shown in Figure 8-21. It is clear that there is a strong relationship between L_{caps}/D_{caps} and k as observed from the results based on POLY capsules constructed with linear relations. The k values remained constant on sand particles with different L_{caps}/D_{caps} , while the k increased linearly as increasing L_{caps}/D_{caps} on coarse particles. Although there were only two points for CEM capsules (see Figure 8-21 in red), the results can be assumed as linear by taking into account the findings from the POLY capsules. It is guaranteed that the addition of CEM capsules to fine aggregate also did not change the k values at any L_{caps}/D_{caps} ratios and their addition to the coarse aggregates would increase the k values with increasing the L_{caps}/D_{caps} .

Moreover, Figure 8-22 shows that the mean size of aggregates influences the k values where the bigger the mean aggregate size, the higher the k values. The aforementioned results generate information about the relationship of three parameters including k , mean aggregate size (D_{agg}) and L_{caps}/D_{caps} for modelling the effect of capsules in the packing of aggregate. As there is no available model to determine the macrocapsules' effect, the macrocapsules used in this study were seen and modelled as steel fibers. Chu et al. [200] formerly developed a packing model of rigid fibres on aggregate packing using a relationship between factor k and $(G/D_{fibre})^2(L_{fibre}/G)^\alpha$ to set a limit on the aggregate size for avoiding excessive increase in voids ratio when steel fibers are added. G is defined as geometric mean size of aggregate which is slightly changed from the definition of mean size of aggregates (D_{agg}) from Dewar model. The power of 2 was obtained from their analysis considering the proportion of particles in close proximity to the fibers, while the α coefficient was obtained at 1.5 after performing a linear regression with the R^2 of 0.962. The same modelling procedure was followed on the use of current results based on the macrocapsules and the relationship between k and $(G/D_{fibre})^2(L_{fibre}/G)^\alpha$. After several trials, it was found that, in this case, the best fitting of the α coefficient was found at 1.0. However, the linear regression model of steel fibers cannot be implemented in the model of macrocapsules and it seems that a logarithmic regression fits best with our results as shown in Figure 8-23. This may be due to the different physical interaction between the steel fibers and macrocapsules with the aggregate particles. In Figure 8-23, two logarithmic regressions were presented, one for CEM capsules and another one for POLY capsules. Originally, it was aimed to generalize the results based on the change of L_{caps}/D_{caps} , either POLY or CEM capsules. However, the regression result seems not reliable and it was hypothesized that there is a completely different interference level between those capsules and the aggregates. Thus, the regression was split into two parts for the effect of CEM and POLY capsules with the R^2 of 0.89 and 0.98, respectively.

The selection of aggregate and the L_{caps}/D_{caps} ratio of CEM capsules eventually will play key roles in controlling the packing density. In the actual concrete mix design, the paste will first fill into the voids between aggregates and the aggregates-capsules mixture and the excess paste will form paste films surrounding aggregates and capsules to impart workability. Thus, it is notable to avoid excessive decrease in packing density due to the addition of capsules and suitably increase the paste volume to compensate for the increase in voids volume arising from the decrease in packing density due to the addition of capsules.

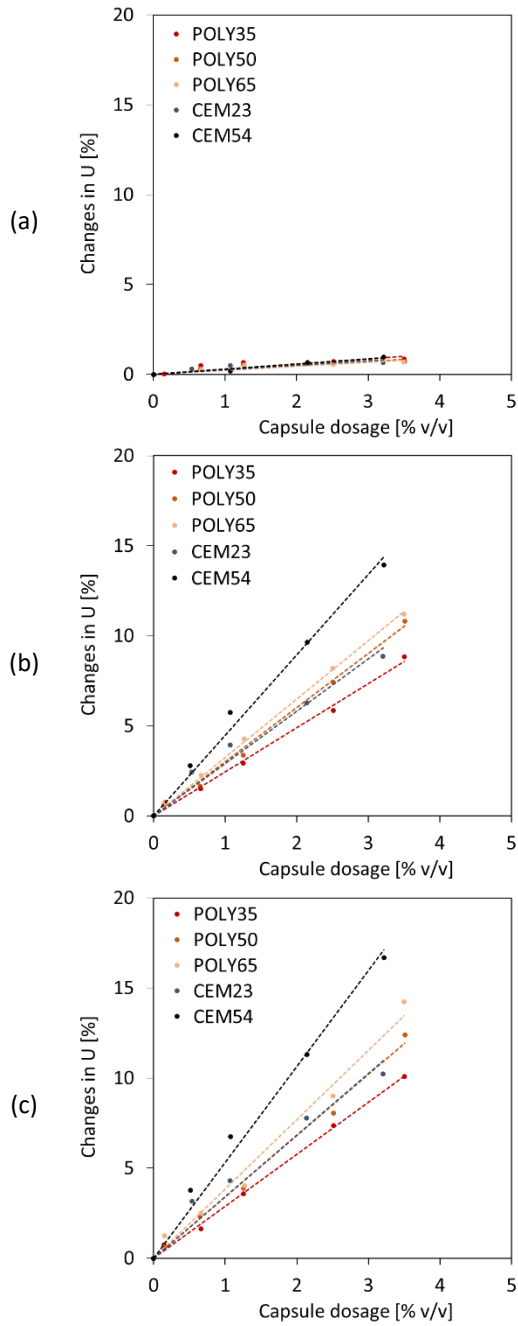


Figure 8-20. Changes in voids ratio due to the increase of capsule dosage with a certain aggregate: (a) sea sand 0/2.5, (b) gravel 4/8 and (c) gravel 8/16

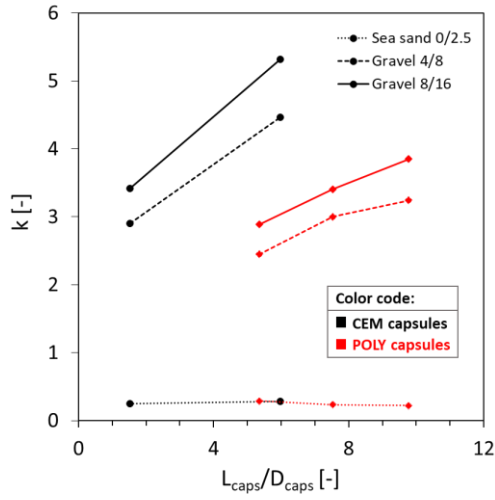


Figure 8-21. Relationship between k and L_{caps}/D_{caps} observed on the use of specific capsule types (note: black line/dot is based on CEM capsules, while red line/dot is based on POLY capsules)

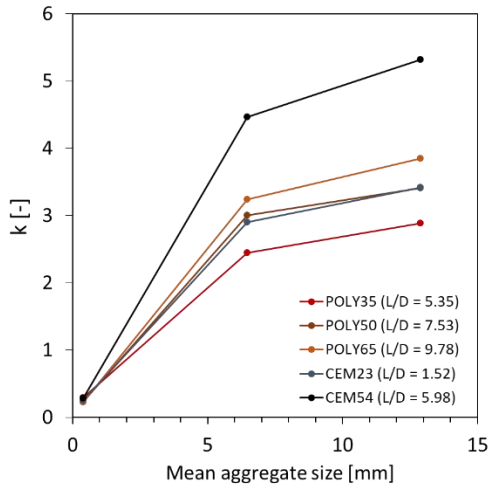


Figure 8-22. Relationship between k and mean aggregate size observed on the use of specific capsule type

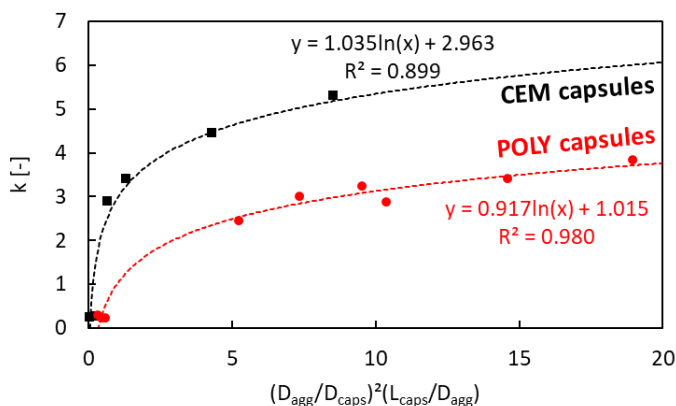


Figure 8-23. Factor k versus $(D_{agg}/D_{caps})^2(L_{caps}/D_{agg})$

8.3.5.2 Interaction diagram of binary aggregate mixture (BAM)

The initial results showed that the presence of capsules did not disturb the packing of fine aggregates and it is more important to assess the effect of capsules in the packing of combined coarse aggregates. Therefore, the interaction of aggregate mixture was started from a mixture of coarse particles (gravel 4/8 + gravel 8/16), further called as binary aggregate mixture (BAM). In the next stage, the ternary aggregate mixture (TAM) was made employing a combination of (sea sand 0/2.5 + (gravel 4/8 + gravel 8/16)).

The BAM was initially made by combining two fractions of gravel and the fine fraction was run from 0.1 (90% gravel 8/16 + 10% gravel 4/8) to 0.9 (10% gravel 8/16 + 90% gravel 4/8). The loose bulk density tests were performed on this BAM and the results were presented in Figure 8-24 with the comparison between the lab result and Dewar model. As shown in Figure 8-24a, the differences between U values of BAM at all fractions were relatively small where the U started from 0.742 ($n=0$) to 0.672 ($n=1$). The lowest U was found at a fine fraction between 0.6 and 0.7. Theoretically, the interaction diagram of BAM closely reaches the straight line of U_0U_1 which means that there is a high particle interference in this aggregate mixture. It is logic that this BAM only consists of coarse particles (gravel-gravel), thus the interference might be higher than the interaction between gravel and sand.

The Dewar model was employed in this BAM in order to analyse the conformity between the experimental (lab) result and Dewar result. Apparently, Figure 8-24a shows that there is a slight mismatch between lab

and Dewar results. The packing theory of Dewar assumes that a graded material can be represented by a single-sized material having the same voids ratio and mean size. In case of combining materials with different fractions, the material shall be arranged from the finest to the coarsest particle. The implementation of single-sized fractions to graded fractions sometimes would inaccurately estimate the fraction mean size and further affect the size ratio r (ratio of the smaller mean size to the bigger mean size of the fractions of an aggregate mixture) [201]. In addition, the accuracy of Dewar's model mainly relies on the basic inputs used in the model. The estimation of mean aggregate size based on the particle size distribution from the sieving test can be inaccurate. Therefore, Dewar [145] proposed an adjustment factor F to improve and calibrate the predicting accuracy of the model on the size ratio r (resulting in $F \times r$). Based on trial and error on different single-sized and multi-sized aggregate mixtures, Dewar [145] set the limit of F between 0.6 and 1.6. In this study, the Dewar's model in BAM was calibrated with an F of 1.3 and the result can be found in Figure 8-24b. The adjustment factor clearly helps to improve the model to fit with the lab result with a good accuracy. Depending on the used mixtures, an adjustment factor may be necessary to avoid discrepancies between the experimental voids ratios and the predictions from Dewar's model as previously discussed by Liu et al. [201].

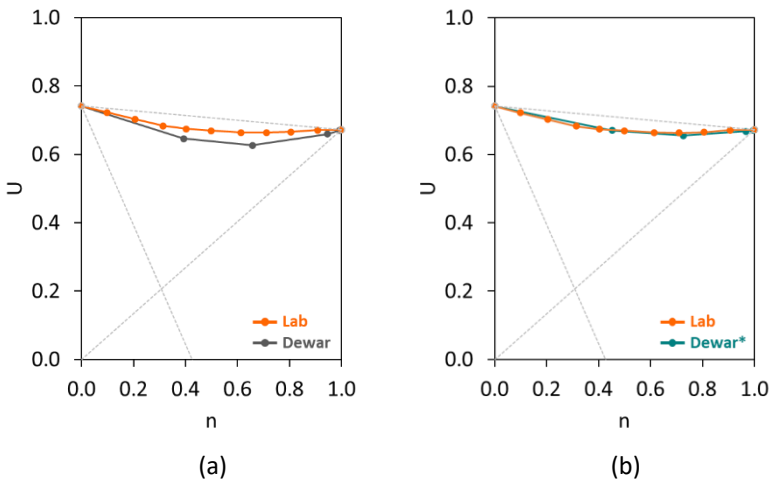


Figure 8-24. Voids ratio of BAM (without capsules): (a) original result, (b) Dewar result with adjustment factor $F = 1.3$

Moreover, the BAM was initially combined with CEM54 capsules at different dosages at 0.51, 1.07, 2.15 and 3.22% v/v. The LBD tests of BAM with CEM54 capsules were performed and the results of voids ratios are

shown in Figure 8-25. Similar to the case of 0% CEM54 capsules, there were minor differences between the experimental results and Dewar results. To increase the predicting accuracy of Dewar's model, the adjustment factor was also applied to all mixtures with CEM54 capsules with an F of 1.1–1.2 (which was similar to the F of BAM without capsules). After implementing the F , the r of each BAM mixture with capsules was corrected and the adjusted Dewar (Dewar*) result showed a good fitting model closely reaching the experimental result. Comparing Figure 8-24b and Figure 8-25, the interaction diagram of BAM without and with capsules possessed similar trend. Due to the fact that the Dewar's model for BAM without capsules (Figure 8-24b) required an adjustment factor, the other BAMs with capsules also followed the same pattern.

To showcase the capsules' effect, the above results were summarized in Figure 8-26a. It is obvious that the addition of CEM54 capsules increased the voids ratio of BAM at any fractions. A high increase of U due to capsules was mainly observed at $n = 0$ and when the n was in the range of 0.4–0.7, the capsules' effect was lower than the one at $n = 0$. This can be explained as within the aforementioned range of n the BAM was well-packed where the U values were the lowest among others. Based on the experimental result, the lowest U occurred at n of 0.60 or 0.70. Next, the Dewar's model was implemented aided with an adjustment factor and the results showed that not all experimental results really fit with the prediction of the Dewar model especially for $n < 0.40$. However, for $n \geq 0.40$, the Dewar's results were relatively reliable. As the objective here is to find the optimal packing of BAM both with and without capsules, it seems that the Dewar model indicated n of 0.70 as the optimal fine fraction with having the lowest U . It shall be noted that Dewar uses few points (i.e. A–F; 6 predicted points) in the interaction diagram to model the packing, while for experimental tests, the n was run from 0 to 1 (11 actual points). Nevertheless, the lowest U predicted by the Dewar model (0.70) was similar to the experimental result (0.6–0.7), showing a good accuracy of Dewar's model to predict the optimal packing with the aid of F . The same analysis was also done on the use of short capsules (CEM23) which is shown in Figure 8-26b. Comparing the results from CEM54 and CEM23 capsules, the interaction diagram between each capsule dosage was less pronounced on CEM23 than CEM54. This reflects that short capsules may induce less disturbance in the packing of BAM than long ones.

In order to further understand the results from Figure 8-26, a relationship between voids ratio at 0% v/v capsules and voids ratio at certain capsule dosage was constructed (see Figure 8-27) by taking into account the

fair comparison of both values at the same fine fraction. The increment of voids ratio of BAM was evident as increasing capsule dosage. On the use of CEM54 capsules, in general, the voids ratio of BAM increased by approximately 2.1, 4.4, 9.0 and 12.4% with the addition of capsules at 0.51, 1.07, 2.15 and 3.22% v/v, respectively. On the other hand, as expected, the addition of CEM23 induced a lower effect than CEM54 as the voids ratio of BAM increased by approximately 1.5, 2.6, 5.3 and 7.7% with the addition of capsules at 0.53, 1.07, 2.14 and 3.21% v/v, respectively. Apparently, the U increased by 1.6 times on the addition of 3.22% v/v CEM54 capsules compared to 3.21% v/v CEM23. The percentage increment of U toward capsule dosage can be established as depicted in Figure 8-28. It was confirmed that the effect of long capsules was more dominant than short capsules. Based on these extensive analyses, the following formulas are proposed to predict the voids ratio of BAM for the addition of capsules as follows:

$$U_{BAM_caps} = U_{BAM_no\ caps}(0.040d_{caps} + 1) \quad (8.11)$$

specifically for CEM54, gravel 4/8, gravel 8/16

$$U_{BAM_caps} = U_{BAM_no\ caps}(0.024d_{caps} + 1) \quad (8.12)$$

specifically for CEM23, gravel 4/8, gravel 8/16

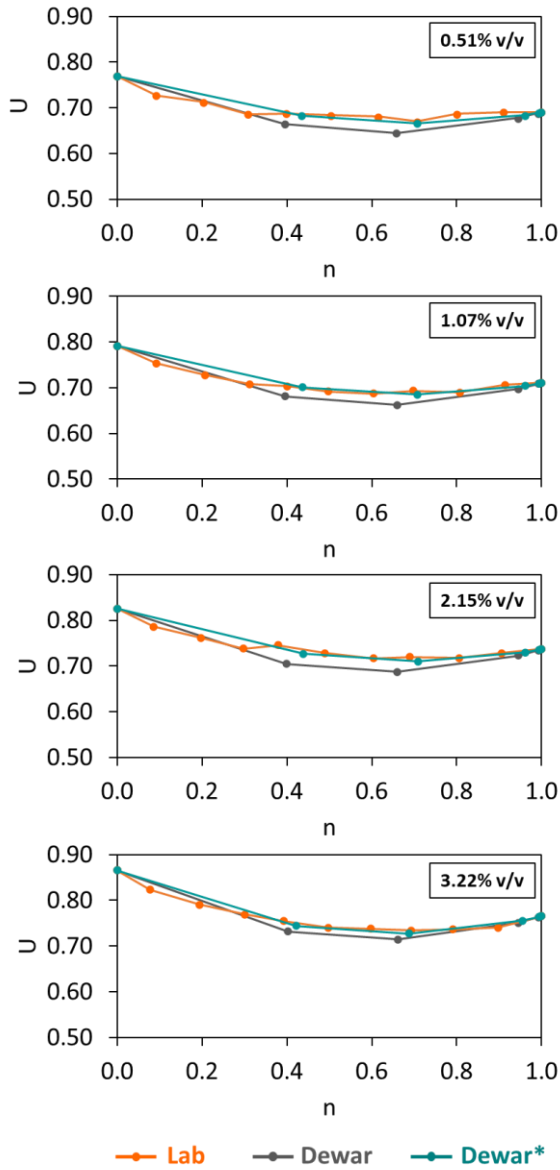


Figure 8-25. Voids ratios of BAM with CEM54 capsules at different dosages (note: Lab is experimental result (orange line), Dewar is Dewar's result without adjustment factor (grey line), Dewar* is Dewar's result with adjustment factor $F = 1.1-1.2$ (green line))

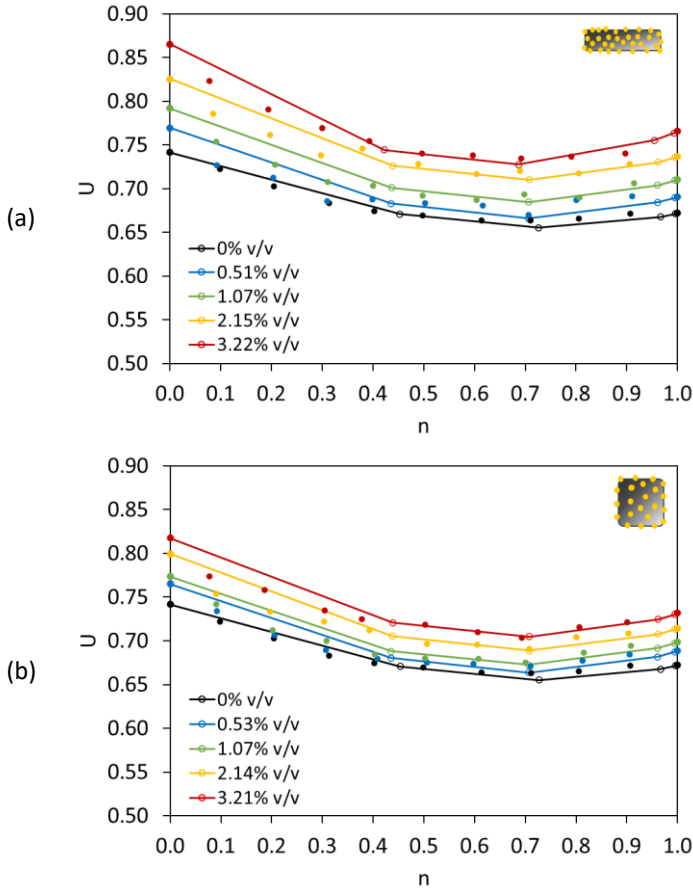


Figure 8-26. Voids ratios of BAM with (a) CEM54 capsules and (b) CEM23 capsules at different fine fraction (note: straight line with hollow dot represents Dewar* result and solid dot represents experimental/lab result)

where U_{BAM_caps} is the voids ratio of BAM after capsules' addition, $U_{BAM_no_caps}$ is the initial voids ratio of BAM without any capsules, d_{caps} is the dosage of capsules [% v/v]. Moreover, the L_{caps}/D_{caps} ratios of CEM54 and CEM23 were 5.98 and 1.52, respectively. The above equations can be normalized into a single equation by assuming a linear relation between the L_{caps}/D_{caps} and the given factors (i.e. 0.040, 0.024) (in the same way as a linear relation between L_{caps}/D_{caps} and k factor in single aggregate type from Figure 8-21) as follows:

$$U_{BAM_caps} = U_{BAM_no\ caps} \left((0.004 \frac{L_{caps}}{D_{caps}} + 0.02) d_{caps} + 1 \right) \quad (8.13)$$

where L_{caps} is the length of the capsule [mm], and D_{caps} is the outer diameter of the capsule [mm]. Figure 8-29 shows that the above equation can be used to predict the voids ratio of BAM in function of capsule dosage and L_{caps}/D_{caps} ratio with a good accuracy. Moreover, further validation of the above model shall be tested with varying capsule geometry.

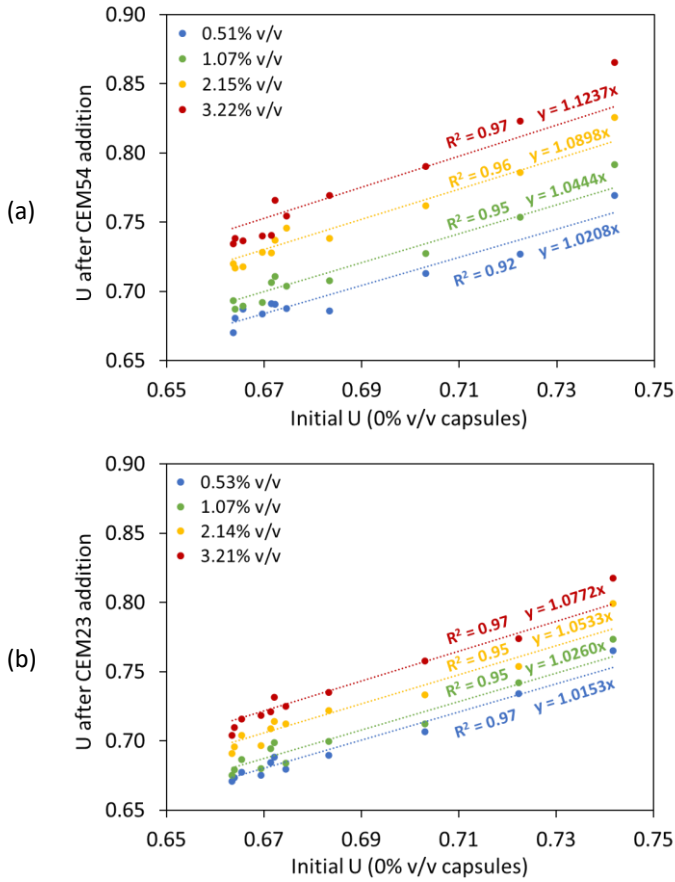


Figure 8-27. Changes of voids ratio of BAM after the addition of (a) CEM54 capsules and (b) CEM23 capsules compared to initial voids ratio of BAM without capsules

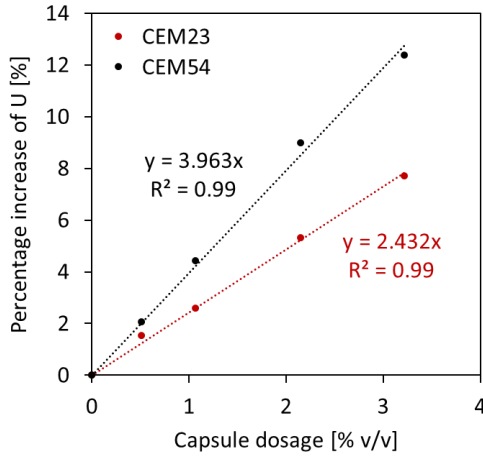


Figure 8-28. Relationship between capsule dosage and percentage increase of voids ratio observed in BAM

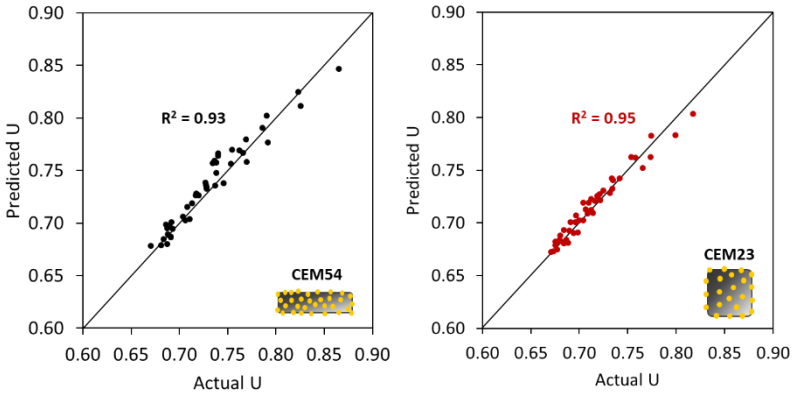


Figure 8-29. Comparison between the actual U values and the predicted U values of BAM in function of capsules dosage and L_{caps}/D_{caps} ratio

8.3.5.3 Interaction diagram of ternary aggregate mixture (TAM)

The TAM was made with employing a combination of (gravel 4/8 + gravel 8/16) and sea sand 0/2.5. A mixture of gravels was selected based on the analysis of BAM. As previously discussed in the interaction diagram of BAM, the lowest voids ratio was found with n in the range of 0.60–0.70 based on the experimental result and at n of 0.70 based on Dewar’s result. It was

decided to take the n of 0.65 as an average fine ratio, meaning that the coarse mixture consisted of 65% gravel 4/8 and 35% gravel 8/16 in volumetric scale. The coarse mixture and sand were gradually mixed starting from the n of 0.1 (90% (gravel 4/8 + gravel 8/16 with $n = 0.65$) + 10% sea sand 0/2.5) to 0.9 (10% (gravel 4/8 + gravel 8/16 with $n = 0.65$) + 90% sea sand 0/2.5). The LBD tests were performed and the interaction diagram of TAM is presented in Figure 8-30. It is clear that the lab result matches very well with the theoretical model of Dewar, even without the aid of an adjustment factor. It should be noted that not all mixtures require an adjustment factor and it depends mainly on the sensitivity of the LBD test and the particle size distribution of the used aggregates. Among all points in Dewar's model, in fact, only point C ($U = 0.373$) showed a slight difference with the lab result ($U = 0.408$). Nevertheless, the remaining points (A, B, D, E, F) fitted with the lab result. Since the U difference at point C was relatively minor and other points followed identical values as the lab result, an adjustment factor was not used as if the U at point C was corrected, the points B, D and E would change and turned far from the lab result. Hence, the reliability of the current Dewar result was good enough to model the packing of TAM.

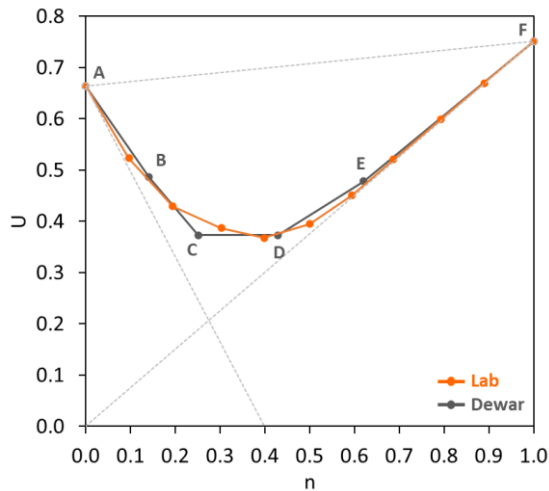


Figure 8-30. Voids ratio of TAM (without capsules) (note: Lab is experimental result (orange line) and Dewar is Dewar's result without adjustment factor (grey line))

Furthermore, the CEM54 capsules were added into the TAM to investigate the effect of long capsules toward the change of U . The dosage of capsules was fixed in the same way as BAM from 0 to 3.22% v/v. Finally, after

performing LBD tests with capsules, the interaction diagrams of TAM with CEM54 at different dosages were constructed as shown in Figure 8-31. Again,

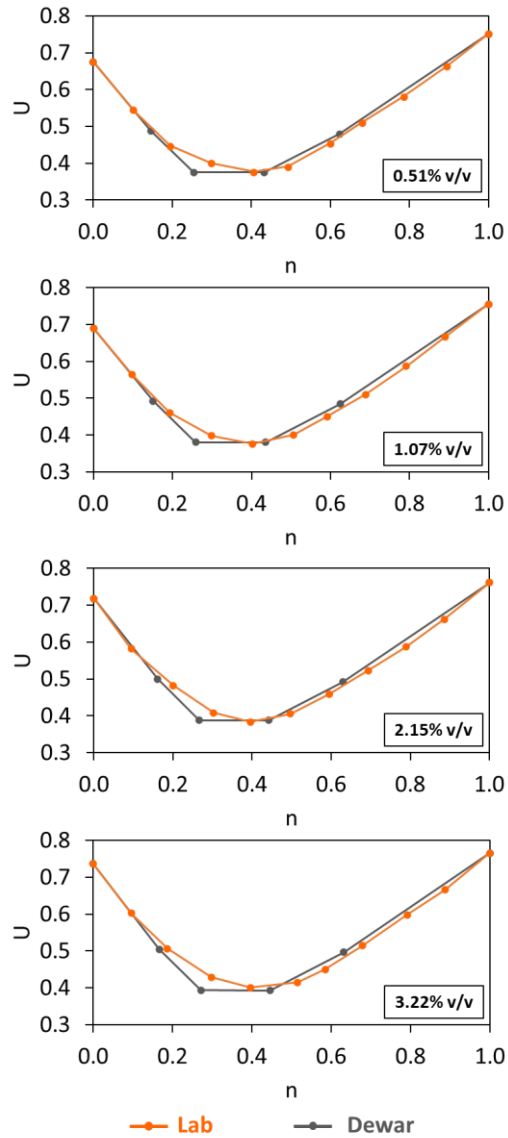


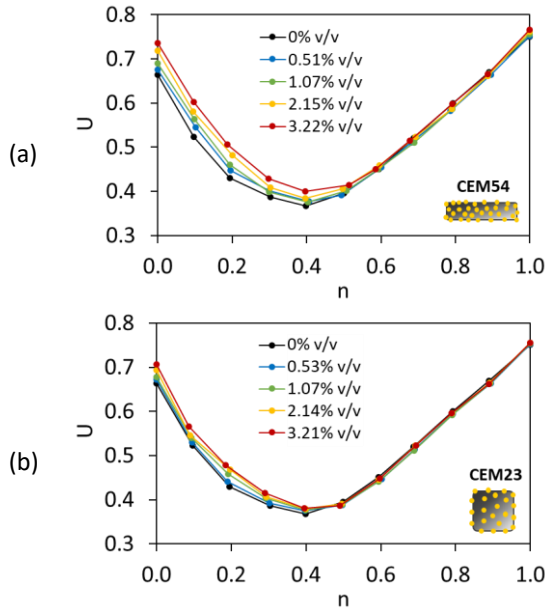
Figure 8-31. Voids ratios of TAM with CEM54 capsules at different dosages (note: Lab is experimental result (orange line) and Dewar is Dewar’s result without adjustment factor (grey line))

there is a good compatibility between the lab and Dewar results although point C from the Dewar results, in all cases, still shows a little difference compared to the lab result.

The interaction diagrams of TAM with CEM54 capsules at different dosages were combined in Figure 8-32a. It is evident that the addition of capsules into the TAM certainly increased the voids ratio of aggregates. The higher the capsule dosage, the higher the voids ratio. Moreover, an interesting fact here was projected at the n of 0.6. TAM with the $n < 0.6$ showed that the gradual addition of capsule tended to increase the voids ratio. In contrast, when the $n \geq 0.6$, the addition of capsules did not affect the voids ratio as the U values were identical with the U of TAM without capsules (Figure 8-32a, black line). These findings suggest that the more coarse aggregates in the mixture ($n < 0.6$), the more disturbance in the packing system due to capsule presence; whereas the more fine aggregates in the mixture ($n \geq 0.6$), the less disturbance in the packing system. To confirm this finding, the other capsule types (CEM23, POLY35, POLY50 and POLY65) were also added to the TAM and the interaction diagrams can be found in Figure 8-32b-e. The use of CEM capsules shared the same behavior as POLY capsules. When the $n \geq 0.6$ (in some cases at 0.5), the disturbance of packing was very minor and all voids ratios were identical, confirming the low impact of capsules in the mixture containing high content of fine particle. On the other hand, as can be seen in the mixture with $n < 0.6$ (or 0.5), the gradual increase of capsule dosage had a gradual increment of voids ratio.

Comparing the influence of CEM23 and CEM54 capsules in the interaction diagram, the difference between U values in function of capsule dosage, specifically at n between 0–0.6, was much bigger with long capsules than with short ones (see Figure 8-32a,b). It may be attributed to the geometry of the short capsules (CEM23) which is comparable with the shape of coarse aggregates, thus these capsules are blended well with other aggregates and exert minor effect in the packing system (or rather similar effect as normal coarse aggregates), indicating the good distribution. Moreover, the use of long capsules (CEM54) induced higher impact on the packing than the short ones. This was due to the geometry of long capsules which was incomparable with the natural coarse aggregates. Hence, when the long capsules are mixed with coarse aggregates, they induce more voids. From Figure 8-32c-e, it is also clear that changing the POLY capsule length from 35 to 50 or 65 mm affected the U values when the TAM was fixed with the n in the range of 0–0.5. To conclude, the use of short capsules is more beneficial than long capsules in terms of reducing the disturbance of the

packing. With using low capsule dosage ($< 0.50\% v/v$), the voids ratio of TAM, either long or short, was relatively similar with the TAM without capsules. This may provide a good indication to carefully select the amount of capsules to be inserted into the concrete without highly disturbing its packing. Moreover, the particle packing model of Dewar was implemented to the TAM with capsules and the comparison of interaction diagrams between experimental and Dewar results can be seen in Figure 8-33. When the capsules were added regardless of its type and dosage, the results showed a good compatibility between the experimental and Dewar results. The lowest U was found at the fine fraction of 0.40 based on lab results (see Figure 8-32) and it is comparable with the Dewar's result with the fine fraction of around 0.43 (see Figure 8-33). Regardless of capsule type and capsule dosage, the lowest U values remained the same as the TAM without capsules, indicating the same optimal aggregate composition in all cases.



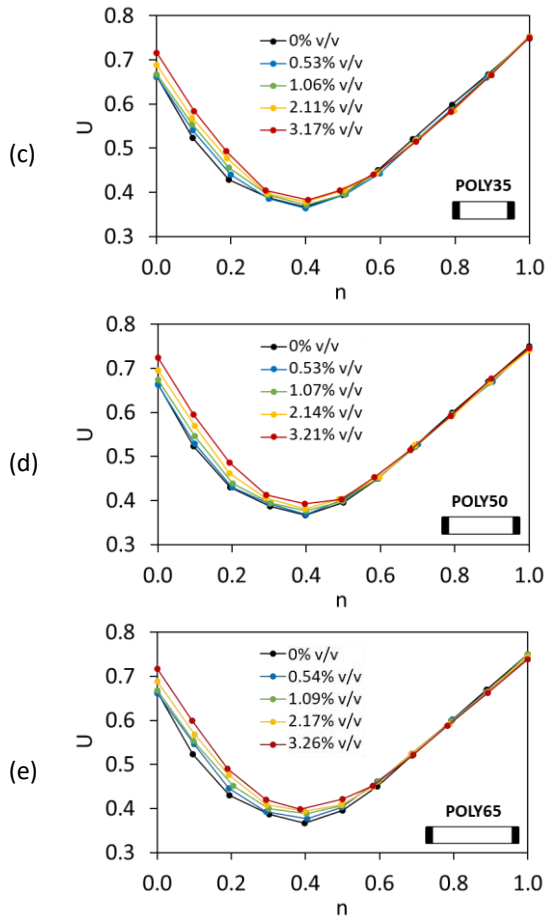
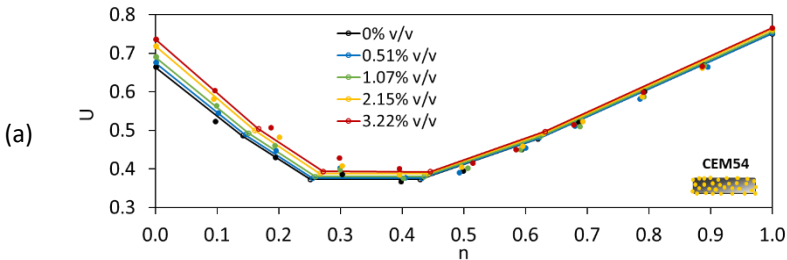


Figure 8-32. Voids ratios of TAM with (a) CEM54 capsules, (b) CEM23 capsules, (c) POLY35 capsules, (d) POLY50 capsules and (e) POLY65 capsules at different fine fraction based on the lab results



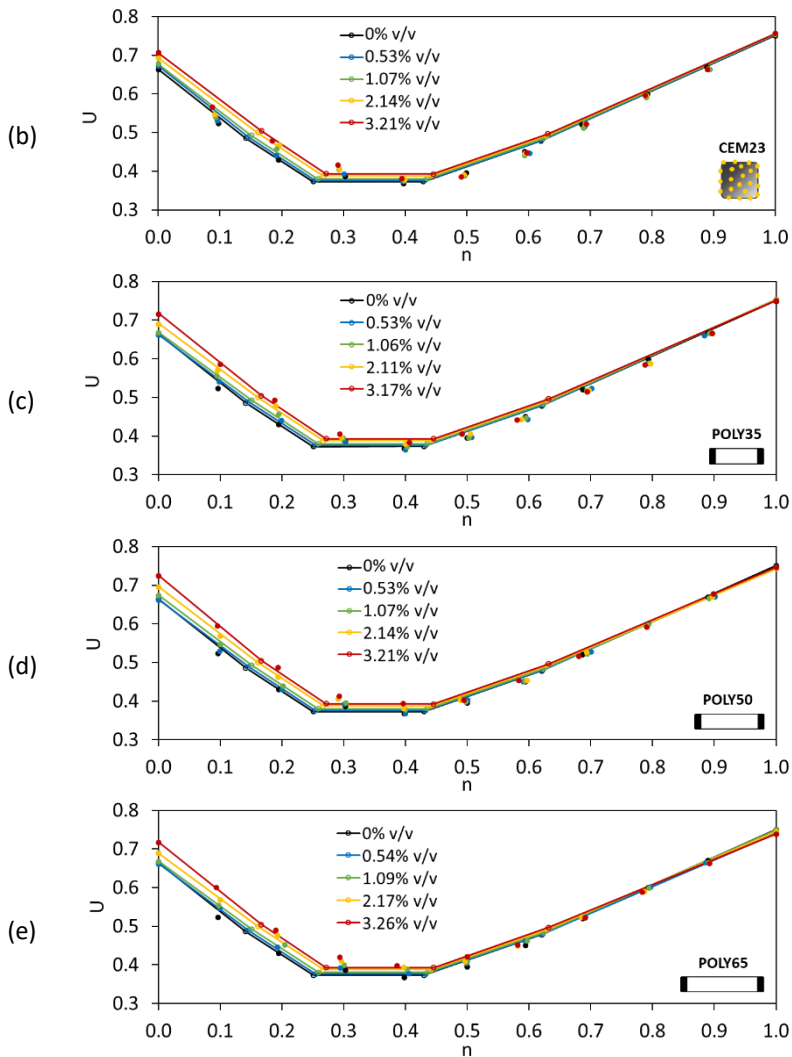


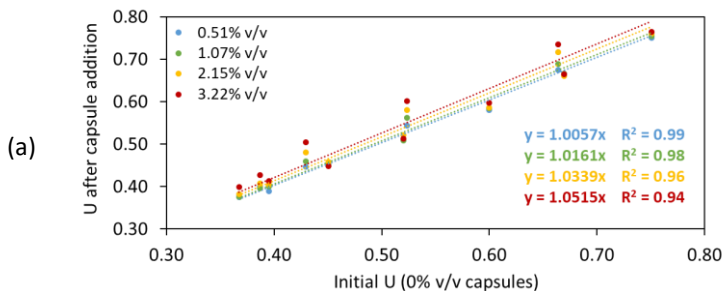
Figure 8-33. Voids ratios of TAM with (a) CEM54 capsules, (b) CEM23 capsules, (c) POLY35 capsules, (d) POLY50 capsules and (e) POLY65 capsules at different fine fraction based on the Dewar results as compared to the lab results (note: straight line with hollow dot represents Dewar result and solid dot represents experimental/lab result)

As a matter of fact, the particle packing model of Dewar does not automatically calculate the effect of capsules as the original model is normally intended for designing the normal concrete. Although there is a good fit between experimental and Dewar results, the model shall be

upgraded for the introduction of the capsules. This can be done by formulating the voids ratio of TAM in function of capsule L_{caps}/D_{caps} ratio and capsule dosage. To realize, the same modelling process from BAM was implemented in TAM. A relationship between voids ratio at 0% v/v capsules and voids ratio at certain capsule dosage was constructed (see Figure 8-34) by taking into account the fair comparison of both values at the same fine fraction. The increment of voids ratio of TAM was evident as increasing capsule dosage. On the use of CEM54 capsules (Figure 8-34a), the voids ratio of TAM increased by approximately 0.57, 1.61, 3.39 and 5.15% with the addition of capsules at 0.51, 1.07, 2.15 and 3.22% v/v, respectively. On the other hand, the addition of other capsule types (i.e. CEM23, POLY35, POLY50, POLY65) induced a lower effect than CEM54 (Figure 8-34b-e). The percentage increment of U toward capsule dosage can be established as depicted in Figure 8-35. It was also confirmed that the effect of long capsules was more dominant than short capsules. The results from Figure 8-35 can be charted out and normalized based on the increment of L_{caps}/D_{caps} ratios. Finally, the following formula is proposed to predict the voids ratio of TAM for the addition of any capsule type with specific aggregates used in this study as follows:

$$U_{TAM_caps} = U_{TAM_no\ caps} \left(\left(0.0004 \frac{L_{caps}}{D_{caps}} + 0.009 \right) d_{caps} + 1 \right) \quad (8.14)$$

where U_{TAM_caps} is the voids ratio of TAM after capsules' addition, $U_{TAM_no\ caps}$ is the initial voids ratio of TAM without any capsules, d_{caps} is the dosage of capsules [% v/v], L_{caps} is the length of capsule [mm], and D_{caps} is the outer diameter of capsule [mm]. Figure 8-36 shows that the above equation can be used to predict the voids ratio of TAM in function of capsule dosage and L_{caps}/D_{caps} ratio with a good accuracy.



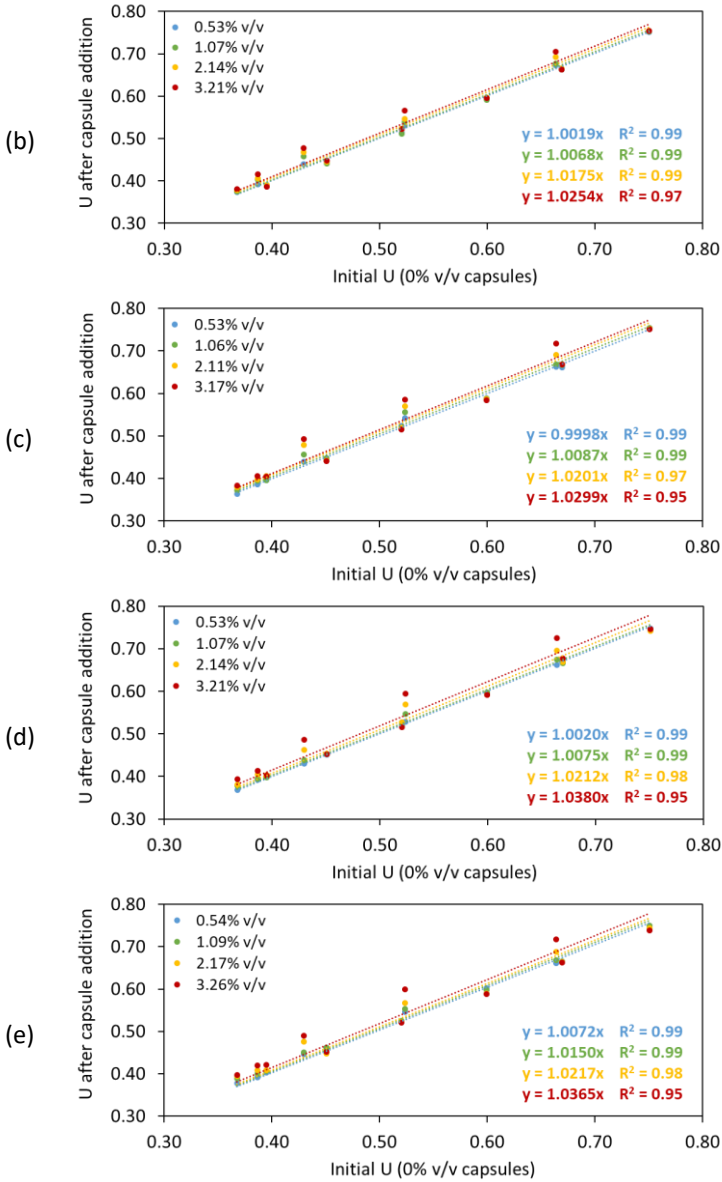


Figure 8-34. Changes of voids ratio of TAM after the addition of (a) CEM54 capsules, (b) CEM23 capsules, (c) POLY35 capsules, (d) POLY50 capsules and (e) POLY65 capsules compared to initial voids ratio of TAM without capsules

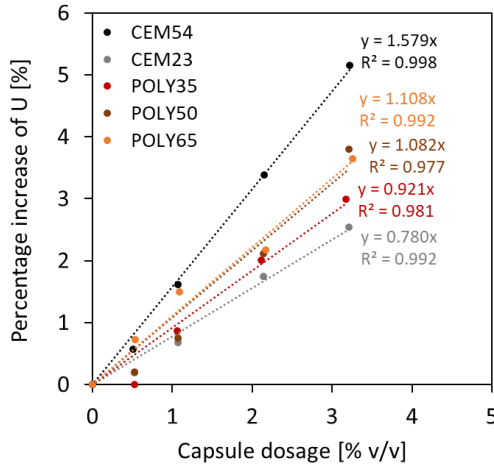


Figure 8-35. Relationship between capsule dosage and percentage increase of voids ratio observed in TAM

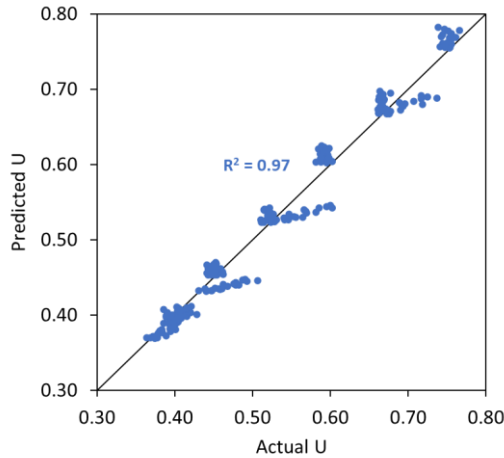


Figure 8-36. Comparison between the actual U values and the predicted U values of TAM in function of capsules dosage and L_{caps}/D_{caps} ratio

Following the analyses of capsules' effect in different aggregate mixtures, the above formulas can be simplified as follow:

$$U_{AM_caps} = U_{AM_no_caps} \left(\left(\alpha \frac{L_{caps}}{D_{caps}} + \beta \right) d_{caps} + 1 \right) \quad (8.15)$$

where U_{AM_caps} is the voids ratio of aggregate mixture (AM) after capsules' addition, $U_{AM_no_caps}$ is the initial voids ratio of AM without any capsules (from

experimental or Dewar result), d_{caps} is the dosage of capsules [% v/v], L_{caps} is the length of capsule [mm], and D_{caps} is the outer diameter of capsule [mm], α and β are empirical constants depending on the number of combined aggregates (only two or three) with the maximum aggregate size (D_{max}) of 20 mm (see Table 8-9).

Table 8-9. Empirical constants for U_{AM_caps}

AM type	α	β
A mixture of two aggregate types/fractions (= BAM) (e.g. gravel 4/8 + gravel 8/16, limestone 2/6 + limestone 6/20, sand 0/2.5 + gravel 4/8, sand 0/4 + limestone 6/20)	0.004	0.02
A mixture of three aggregate types/fractions (= TAM) (e.g. sand 0/2.5 + gravel 4/8 + gravel 8/16, sand 0/1 + limestone 2/6 + limestone 6/20)	0.0004	0.009

According to Table 8-9, it is noteworthy to mention that the effect of capsules in the packing of TAM is much lower than the packing of BAM. It occurs as in the packing of BAM (gravel-gravel), the presence of capsules generated extra voids between capsule and coarse particle. In case of TAM, these extra voids are also present, but since fine particles (sand) is added in the mixture, those extra voids from the capsule-gravel interaction can be (partially) filled with the sand. This notion explains that in the TAM, the effects of capsules are negligible especially in the aggregate mixtures with n above 0.6, while with n below 0.6, there is a slight effect of the capsules as the aforementioned extra voids are not fully filled with the sand. Based on these interaction tests, the interaction of capsules and coarse aggregates is more important than the interaction between capsule and fine+coarse aggregates. It has been clear as well that the packing of fine aggregate is not disturbed by the presence of capsules. Thus, the composition of aggregates in the inert structure of concrete should be modified for the introduction of capsules to compensate the effect of macrocapsules.

8.3.5.4 Validation of the voids ratio model

The U_{AM_caps} formula has been proven to be robust for the aggregates specifically used in the study. A research question comes whether the model will be valid for the other aggregate types and/or capsule types. Hence, in order to validate the model, several aggregate mixtures were assigned with completely different aggregate-capsule formulations than the ones previously used as outlined in Table 8-10.

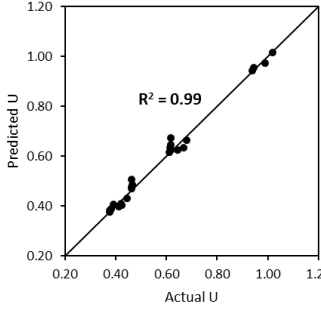
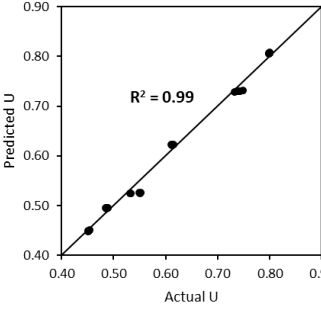
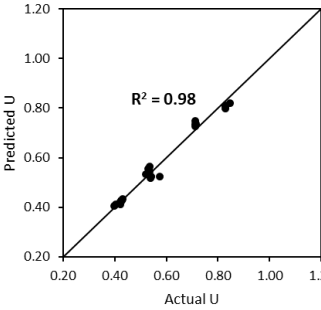
Table 8-10. Composition of new aggregate mixtures for validation

Aggregate mixture (AM)		Fine fraction (n)	Capsule type and dosage (d_{caps})
BAM	Limestone 2/6 + Limestone 6/20	0, 0.2, 0.4, 0.6, 0.8, 1.0	+ CEM23: 0, 0.53, 1.07 % v/v + CEM54: 0, 1.07, 2.15 % v/v
BAM	River sand 0/4 + Limestone 6/20	0, 0.2, 0.4, 0.6, 0.8, 1.0	+ CEM23: 0, 0.53, 1.07 % v/v + CEM54: 0, 1.07, 2.15 % v/v
BAM	Sea sand 0/2.5 + Gravel 4/8	0, 0.2, 0.4, 0.6, 0.8, 1.0	+ CEM23: 0, 1.25 % v/v + CEM54: 0, 1.25% v/v + POLY35: 0, 1.25% v/v + POLY50: 0, 1.25% v/v + POLY65: 0, 1.25% v/v
TAM	Sand 0/1 + (Limestone 2/6 + Limestone 6/20 with $n = 0.4$)	0, 0.2, 0.4, 0.6, 0.8, 1.0	+ CEM54: 0, 0.53, 1.07 % v/v + POLY65: 0, 1.07, 2.15 % v/v

The same procedure for determining the U of AM without and with capsules was followed. The validation results are summarized in Table 8-11, showing the robustness of the model with a good accuracy. The results also proved that the model works well with other combinations of aggregates and capsules. It should be noted that the empirical constants should be applied specifically for the designated mixture. It means that if a mixture of two aggregate types/fractions is used, the empirical constants for BAM should be used and they will not work for TAM (a mixture of three aggregate types/fractions), and vice versa.

Table 8-11. Validation results

Aggregate mixture (AM)		Results
BAM	Limestone 2/6 + Limestone 6/20 + CEM capsules	

BAM	River sand 0/4 + Limestone 6/20 + CEM capsules	
BAM	Sea sand 0/2.5 + Gravel 4/8 + ALL CAPSULES TYPES (CEM and POLY)	
TAM	Sand 0/1 + (Limestone 2/6 + Limestone 6/20 with $n = 0.4$) + ALL CAPSULES TYPES (CEM and POLY)	

8.4 Modification of concrete mix designs for the introduction of macrocapsules

8.4.1 Mix design adaptations

As a proof of concept on the effects of macrocapsules in the packing of concrete, two programs of mix design modifications were proposed:

- (1) The first program is associated with the interaction diagram of the TAM. It has been discussed that the packing of TAM was disturbed by the

presence of CEM54 capsules (see Figure 8-32a). However, the voids ratios of TAM was rather stable when the capsule dosage was increased from 0 to 3.22% v/v for fine fractions limited at 0.6 or above. In contrast, there was a considerable increase of U with increasing capsule dosage and lowering fine fraction below 0.6. A research question comes whether the effect of capsules in different inert structure of concrete (aggregate composition) may lead to different behaviour, especially in terms of compressive strength of concrete. Based on the interaction diagram (Figure 8-32a), it is expected that when the fine fraction is too low, the capsules inside concrete will induce more effects than concrete containing capsules with high fine fraction, as a result of the packing disturbance by capsules. In order to investigate this hypothesis, the aggregate proportion of TAM was considered as an inert skeleton of concrete. The lowest voids ratio of TAM was found at n of 0.40, meaning 40% sea sand 0/2.5 and 60% BAM (gravel 4/8 + gravel 8/16 at $n = 0.65$). The volumetric proportion of BAM was kept the same (at $n = 0.65$) and the fine fraction was set from 0.2 to 0.8 (with interval of 0.1) as shown in Table 8-12. Although some fractions/mixtures were not realistic for the concrete application, they were still considered in order to see the effect of capsules in mixtures with different fine fraction. The other fine fractions of 0, 0.1, 0.9 and 1 were excluded for concrete fabrication. The code of mixture, for instance 1.5CEM54-30, represents 1.5 as capsule dosage at 1.5% v/v, CEM54 as long cementitious capsules with length of 54 mm, 30 as fine fraction at 0.3 (or 30% fine aggregate + 70% coarse aggregate). The first-seven mixtures were regarded as reference mixtures (i.e. 0CEM54-20, ..., 0CEM54-80) without capsules' addition. From the modelling section, the unit of capsule dosage was % v/v previously defined as the volume of capsules over the volume of steel container (7.5 L of steel container was used). Specifically for this program, the volume of steel container was translated to the volume of concrete. Considering the fresh concrete was later cast into 150-mm cube moulds (regarded as container where each cube mould has a volume of 3.375 L), 1.5% v/v CEM54 dosage would need 0.051 L of capsules in each cube mould which was approximately 15 pcs of capsules per cube specimen. As seen in Table 8-12, the aggregate proportion ratio of mixtures containing capsules was not changed compared to reference mixtures. The main objective was to introduce 15 pcs of long capsules (CEM54) in each cube mould with casting different concrete mix designs, in function of fine fraction, to investigate the effect of capsules in the compressive strength of concretes. As a note, three cube specimens

were cast for each mixture. The mix designs from the first program were formulated in Table 8-13. The cement content, w/c, SP dosage and capsule dosage remained constant both for reference and capsule-based mixtures. Especially for capsule-based mixtures, the aggregate proportion was adjusted to compensate the volume of capsules (as compared with reference mixtures). Although the adjustment on the amount of aggregates was made in these mixtures, the aggregate composition ratio was kept same with respect to Table 8-12. It is noteworthy to mention that this adjustment was done to ensure 1 m³ volumetric design based for all mixtures.

Table 8-12. The first proposed aggregate composition ratio for capsule-based mix designs

Mixture	Capsule dosage [% vol. caps / vol. concrete]	w/c	Volumetric aggregate ratio		
			Sand 0/2.5	Gravel 4/8	Gravel 8/16
0CEM54-20	0	0.50	0.200	0.520	0.280
0CEM54-30	0	0.50	0.300	0.455	0.245
0CEM54-40	0	0.50	0.400	0.390	0.210
0CEM54-50	0	0.50	0.500	0.325	0.175
0CEM54-60	0	0.50	0.600	0.260	0.140
0CEM54-70	0	0.50	0.700	0.195	0.105
0CEM54-80	0	0.50	0.800	0.130	0.070
1.5CEM54-20	1.5	0.50	0.200	0.520	0.280
1.5CEM54-30	1.5	0.50	0.300	0.455	0.245
1.5CEM54-40	1.5	0.50	0.400	0.390	0.210
1.5CEM54-50	1.5	0.50	0.500	0.325	0.175
1.5CEM54-60	1.5	0.50	0.600	0.260	0.140
1.5CEM54-70	1.5	0.50	0.700	0.195	0.105
1.5CEM54-80	1.5	0.50	0.800	0.130	0.070

Table 8-13. The first proposed mix designs of capsule-based concrete

Material	Unit	OCEM	OCEM	OCEM	OCEM	OCEM	OCEM	OCEM	1.5CEM	1.5CEM	1.5CEM	1.5CEM	1.5CEM	1.5CEM	
		54-20	54-30	54-40	54-50	54-60	54-70	54-80	54-20	54-30	54-40	54-50	54-60	54-70	54-80
CEM III/A 42.5N	kg/m ³	325	325	325	325	325	325	325	325	325	325	325	325	325	325
Sea sand 0/2.5	kg/m ³	370	555	740	924	1109	1293	1477	362	543	724	904	1085	1265	1445
Gravel 4/8	kg/m ³	937	820	701	585	468	351	234	916	802	686	572	457	343	229
Gravel 8/16	kg/m ³	504	441	378	315	252	189	126	494	432	370	308	246	185	123
Effective water	kg/m ³	163	163	163	163	163	163	163	163	163	163	163	163	163	163
SP Fluivicon 801	kg/m ³	0.00	0.00	0.89	1.00	1.20	1.50	1.80	0.00	0.00	0.89	1.00	1.20	1.50	1.80
Effective w/c	-	0.50	0.50	0.50	0.50	0.50	0.50	0.50	0.50	0.50	0.50	0.50	0.50	0.50	0.50
	% vol. caps. / vol. concrete	-	-	-	-	-	-	-	1.50	1.50	1.50	1.50	1.50	1.50	1.50
CEM54 capsules	... pcs capsules per one 150-mm cube	-	-	-	-	-	-	-	15	15	15	15	15	15	15

- (2) The second program is associated with the interaction diagram of the BAM and the main conclusion of TAM. It is clear that the packing of fine aggregates is not disturbed by the presence of capsules, while the voids ratios of coarse aggregates increase with increasing capsule dosage. Thus, the interaction of capsules and coarse aggregates seems to be more important than the interaction between capsule and all (fine + coarse) aggregates. Although the voids ratio of BAM or TAM is in fact not the same as the voids ratio of 'real' concrete, the packing of BAM can be an interesting point to modify the mix design of capsule-based concrete. Since the packing disturbance mainly occurred in the coarse fraction, the capsule dosage was considered as the replacement of coarse aggregate. Thus, the original unit of capsule dosage (% vol. capsules / vol. container) was translated to the % volume of capsules over volume of coarse aggregates. This approach was strived considering to realize the introduction of capsules, the volume of container could not be used for designing concrete mixtures. Therefore, the capsules were seen as coarse aggregates and the original volume of coarse aggregates shall be adjusted for the introduction of capsules. In this second program, OCEM54-40 from the first program was selected as a reference mixture, considering the fine (sand) fraction of 0.4 based on TAM (sand 0/2.5 + (gravel 4/8 + gravel 8/16)) and another fine (gravel 4/8) fraction of 0.65 based on BAM (gravel 4/8 + gravel 8/16) achieved the lowest voids ratio. Table 8-14 shows the ratio of aggregate composition by taking into account the addition of capsules at different dosage (0, 1, 3, 5 and 7 % vol. capsules/vol. coarse aggregates). The ratio of sand was fixed at 0.4 for all mixtures and the ratio of coarse aggregates (or BAM) was corrected for the inclusion of capsules considered as coarse particles. Nevertheless, the volumetric proportion of BAM was kept same for all mixtures with and without capsules (at $n = 0.65$ corresponding to 65% gravel 4/8 + 35% gravel 8/16). Two cementitious capsules were used namely long capsules (CEM54) and short capsules (CEM23). Both capsules were added with the same dosage in the range of 1–7 % v/v. The same objective as the first program was strived to assess the compressive strength of capsule-based concretes. To realize, the 150-mm cube moulds (3.375 L for each mould) were used for casting the concrete specimens. According to the mix design of reference concrete (OCEM54-40), 69.3% volume of concrete was composed of fine and coarse aggregates where 27.7% belongs to fine aggregates and 41.6% belongs to coarse aggregates. It means that there would be approximately $41.6\% \times 3.375 \text{ L} = 1.40 \text{ L}$ of coarse aggregates in one cube

specimen. As the capsules were considered as a partial replacement of coarse aggregates, the number of capsules to be added into the cube mould can be calculated. Due to the geometrical difference between CEM54 and CEM23 capsules, the number of capsules used slightly differed for long and short capsules. With the specific dosage of 1, 3, 5 and 7% vol. caps/vol. coarse aggregates, there were 5, 13, 21 and 29 CEM54 (long) capsules for each cube specimen, respectively, and on the other hand, there were 4, 11, 18 and 25 CEM23 (short) capsules for each cube specimen, respectively. As a note, three cube specimens were casted for each mixture. The mix designs from the second program were formulated in Table 8-15. The cement content, sand content, w/c, SP dosage and capsule dosage remained constant both for reference (labelled as REF) and capsule-based mixtures. Especially for capsule-based mixtures, the coarse aggregate proportion was adjusted to compensate the volume of capsules (as compared with reference mixtures). Although the adjustment on the amount of coarse aggregates was made in these mixtures, the coarse aggregate composition ratio ($n = 0.65$) was kept the same with respect to Table 8-14. It is noteworthy to mention that this adjustment was done to ensure 1 m³ volumetric design based for all mixtures.

The illustration of these two approaches of capsule-based concrete mix design modifications can be found in Figure 8-37.

Table 8-14. The second proposed aggregate composition ratio for capsule-based mix designs

Mixture	Capsule dosage [% vol. caps / vol. coarse agg.]	w/c	Volumetric aggregate ratio			
			Sand 0/2.5	Gravel 4/8	Gravel 8/16	Capsules
REF	0	0.50	0.400	0.390	0.210	0.000
1CEM54	1	0.50	0.400	0.386	0.208	0.006
3CEM54	3	0.50	0.400	0.378	0.204	0.018
5CEM54	5	0.50	0.400	0.371	0.200	0.030
7CEM54	7	0.50	0.400	0.363	0.195	0.042
1CEM23	1	0.50	0.400	0.386	0.208	0.006
3CEM23	3	0.50	0.400	0.378	0.204	0.018
5CEM23	5	0.50	0.400	0.371	0.200	0.030
7CEM23	7	0.50	0.400	0.363	0.195	0.042

Table 8-15. The second proposed mix designs of capsule-based concrete

Material	Unit	REF	1CEM54	3CEM54	5CEM54	7CEM54	1CEM23	3CEM23	5CEM23	7CEM23
CEM III/A 42.5N	kg/m ³	325	325	325	325	325	325	325	325	325
Sea sand 0/2.5	kg/m ³	740	740	740	740	740	740	740	740	740
Gravel 4/8	kg/m ³	701	694	680	666	652	694	680	666	652
Gravel 8/16	kg/m ³	378	374	366	359	351	374	366	359	351
Effective water	kg/m ³	163	163	163	163	163	163	163	163	163
SP Fluvicon 801	kg/m ³	0.89	0.89	0.89	0.89	0.89	0.89	0.89	0.89	0.89
Effective w/c	-	0.50	0.50	0.50	0.50	0.50	0.50	0.50	0.50	0.50
CEM54 capsules	% vol. caps / vol. coarse agg.	-	1.00	3.00	5.00	7.00	-	-	-	-
	... pcs capsules per one 150- mm cube	-	5	13	21	29	-	-	-	-
CEM23 capsules	% vol. caps / vol. coarse agg.	-	-	-	-	-	1.00	3.00	5.00	7.00
	... pcs capsules per one 150- mm cube	-	-	-	-	-	4	11	18	25

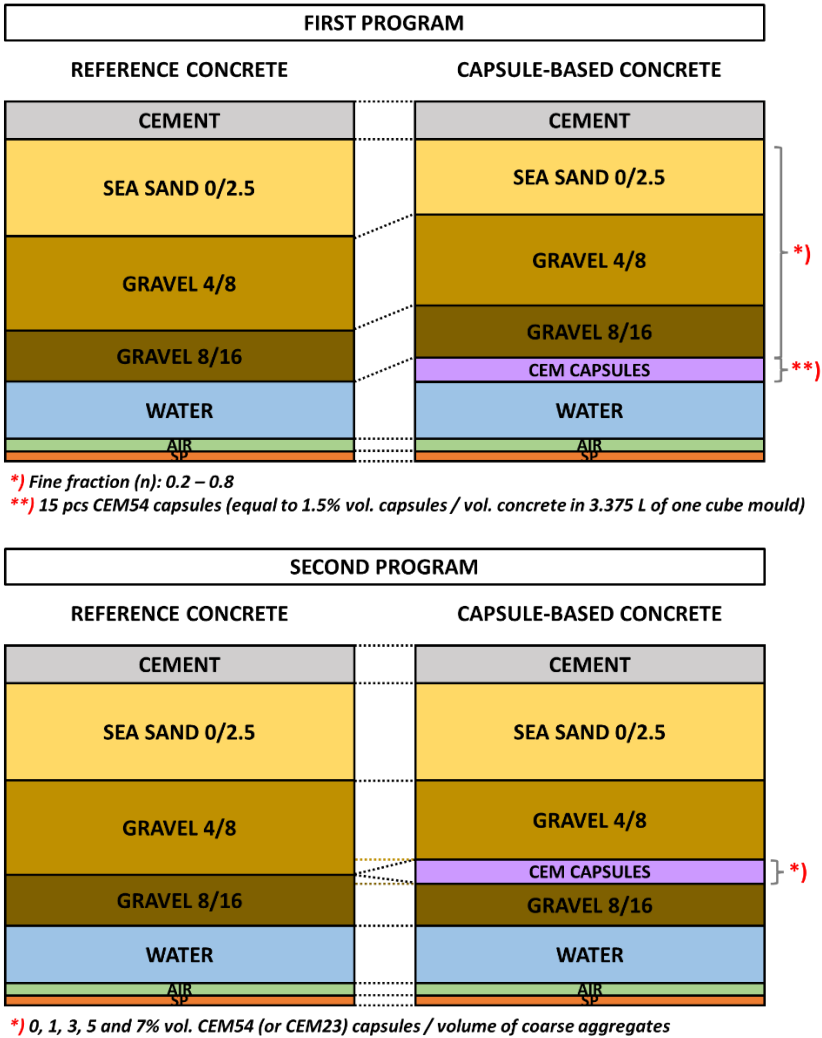


Figure 8-37. Schematic illustration of concrete mix design modifications for the introduction of macrocapsules

8.4.2 Mixing and casting process

A concrete volume of 20 L was aimed for each mixture. Initially, all dry materials (i.e. cement, sand 0/2.5, gravel 4/8, gravel 8/16) were put into the drum mixer and were mixed for 30 s. Mixing water was then added into the

mixer and after 2 min of mixing, the superplasticizer was added. After 5 min of mixing, the mixer was stopped and the fresh mix was taken out from the mixer. Around 10 L of fresh concrete was used for slump and air content tests while another 10 L was put evenly into three bowls with a comparable volume of fresh concrete on each bowl. Depending on the capsule dosage, the exact number of capsules was added into the bowl. Hence, the fresh mix and capsules in all bowls were manually mixed by a scoop until a homogeneous mixture was obtained which was then poured into three cube moulds (150×150×150 mm³) (note: one bowl for one cube mould). It was guaranteed that no capsules were left in each bowl, ensuring the same amount of capsules inside each cube mould. The fresh mix with capsules was compacted by a vibrating table. In this way, a random distribution of capsules was attained. The reference mixtures (without capsules) were cast with the same process as capsule-based mixtures. After 24h of casting, the specimens were demoulded and were transferred to the water tank at 20°C for curing. The casting process of capsule-based concrete is illustrated in Figure 8-38.



Figure 8-38. Procedure of casting capsule-based concrete

8.4.3 Testing program

The fresh tests by means of slump and air content apparatus (based on EN 12350-2,6,7) were conducted only for reference mixtures (OCEM54-20, ..., OCEM54-80) and no fresh tests for capsule-based mixture considering the capsules were not added during mixing. All specimens from twenty-three mixtures, both from the first and second programs, were taken out from the curing tank at the age of 28 days. An ultrasonic pulse velocity (UPV) test

based on EN 12504-4 was also conducted on the hardened cube specimens to evaluate the compactness of the specimens with and without the presence of capsules. During the UPV test, the transducers were placed at the center of two parallel faces of each cube and were repeated at the other faces of each cube. Thus, there were two UPV measurements per specimen (on moulding surfaces) and the average of velocity was considered per specimen. Furthermore, the compression tests were conducted in accordance with EN 12390-3.

8.4.4 Results and discussion

8.4.4.1 Effect of fine ratio in capsule-based concrete mixtures (in relation to the first program)

The fresh properties of all references mixtures (0CEM54-20, ..., 0CEM54-80) were initially evaluated prior to the addition of macrocapsules. As shown in Figure 8-39(a), the slump of reference mixtures with the n between 0.2 and 0.4 was relatively good. However, when the n was increased above 0.4, the slump was close to 0 even when the SP content was slightly adjusted. As a note, when the mixture was put into the mould and was compacted via the vibrating table, the mixture can still spread inside the cube mould until a complete filling. Next, the air content was evaluated as depicted in Figure 8-39(b). The reference mixtures with the n of 0.4–0.7 had an air content in the range of 2.0–3.5%. In case of other mixtures with a lower/higher n , the air content was rather low. The fresh densities of reference and capsule-based mixtures were relatively comparable, except the mixtures with n of 0.5–0.7, as shown in Figure 8-39(c). The fresh density of concrete is not considerably affected by the presence of macrocapsules.

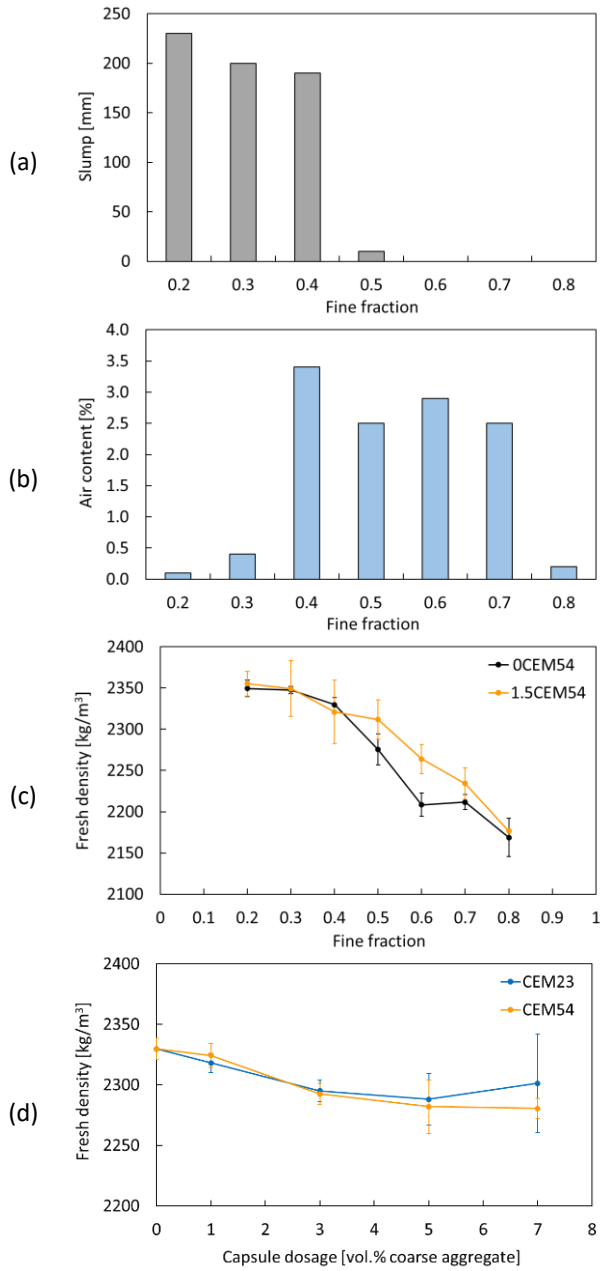


Figure 8-39. (a) Slump, (b) air content and (c) fresh density of all mixtures from the first program; (d) fresh density of all mixtures from the second program

The hardened properties of reference and capsule-based concretes were evaluated at 28 days. The result of hardened density is presented in Figure 8-40(a), while the compressive strength is in Figure 8-40(b). There was no considerable difference between the hardened densities of reference and capsule-based concretes. Nevertheless, the addition of macrocapsules at 1.5 vol.% apparently reduced the compressive strength. The strength reduction was varying depending on the fine fraction. It was found that the concretes with n of 0.2–0.4 experienced a 11–12% strength reduction, as compared with reference concretes with the same n . In case of n between 0.5–0.7, the strength reduction was accounted for 15–18%, while especially with n of 0.8, the strength reduction reached 23% which is the highest among other n . It is obvious that different behavior of the concrete strength is attained with different mix designs. There are two possible reasons that can explain this tendency: (1) the capsules are randomly distributed in all mixtures thus they might induce different effects, and (2) different packing in all mixtures is responsible for the strength downgrade when capsules are present in the matrix. By looking into the variation of strength results in Figure 8-40(b), the standard deviations of mixtures with n of 0.3–0.5 were relatively low. It might indicate that the capsules similarly behave within this range of fine fraction in the mix design. Comparing all fine fractions, n of 0.4 achieved the highest compressive strength, both in the reference and capsule-based concrete. It shows a good agreement with the observation of the lowest voids ratio of TAM at n of 0.4, both with and without capsules. In addition, the UPV results are summarized in Figure 8-40(c). In general, a minor reduction of the matrix compactness is attained after the inclusion of macrocapsules. It was found that the addition of 1.5 vol.% capsules reduced the velocity in the range of 0.2–1.0% within the n of 0.2–0.8, as compared with reference mixtures. All in all, the incorporation of macrocapsules mainly affects the compressive strength of concrete and no considerable effects for the hardened density and the compactness.

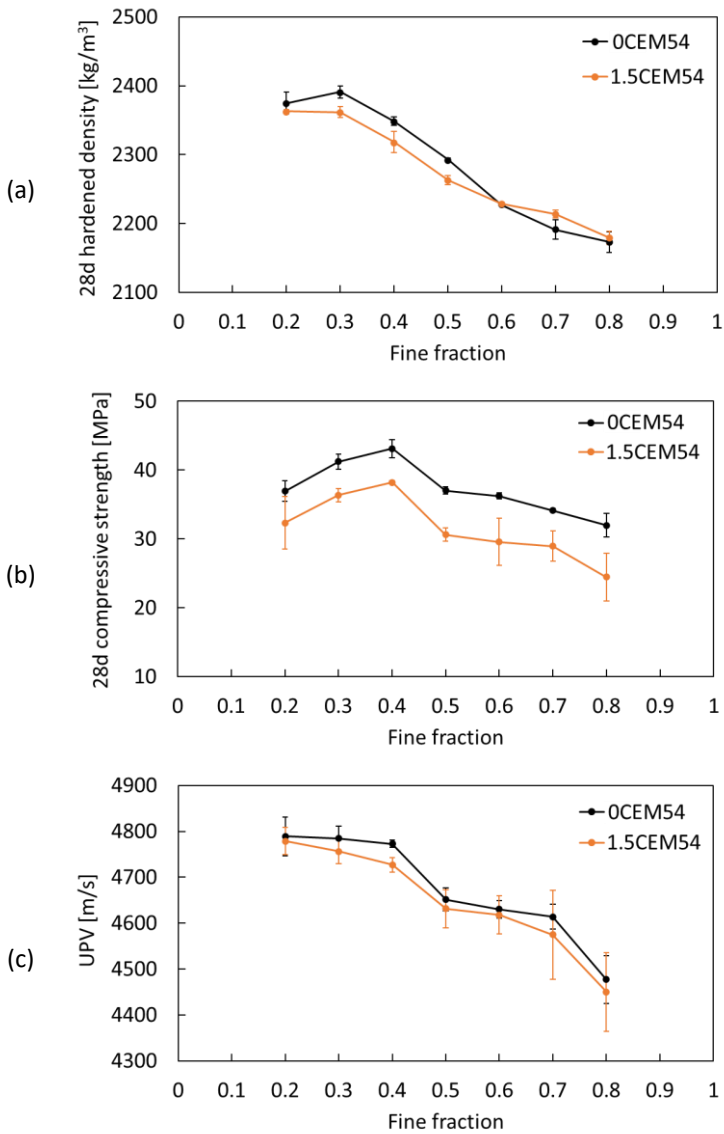


Figure 8-40. Evaluation of (a) hardened density, (b) compressive strength and (c) UPV of reference and capsule-based concretes tested at 28 days from the first program

The results based on the compressive strength, UPV, hardened density and voids ratio of TAM from capsule-based mixtures were normalized by taking into account the ratio of 1.0 at n of 0.4, as presented in Figure 8-41. It is clear that there is a 'reverse' relationship between compressive strength

and voids ratio of TAM. A higher voids ratio of TAM leads to a lower compressive strength and this has been estimated by the Dewar model as the model suggests to use the lowest voids ratio for designing the concrete mixes to achieve a good packing. Consequently, a relationship between compressive strength and voids ratio of TAM is constructed in Figure 8-42. A good coefficient of determination (R^2) was achieved to predict the compressive strength of either reference or capsule-based concrete in function of voids ratio of TAM. It should be noted that only one capsule dosage (1.5 vol.%) was studied in this program to investigate the effect of capsules in different mix designs. Further investigations are needed to continue modelling the compressive strength of concrete in relation to the capsule dosage in different mix designs.

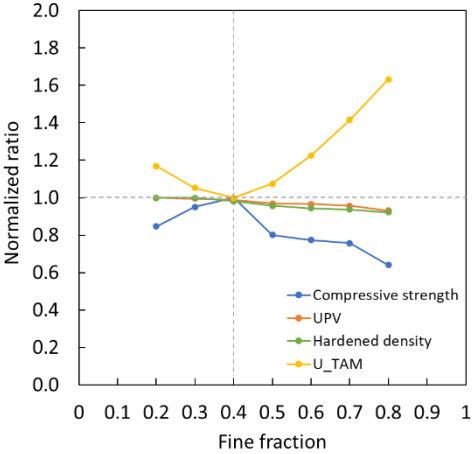


Figure 8-41. Normalized ratio of compressive strength, voids ratio of TAM, UPV, hardened density of capsule-based mixtures (note: the ratio of 1.0 was considered at $n = 0.4$ where the lowest voids ratio was achieved)

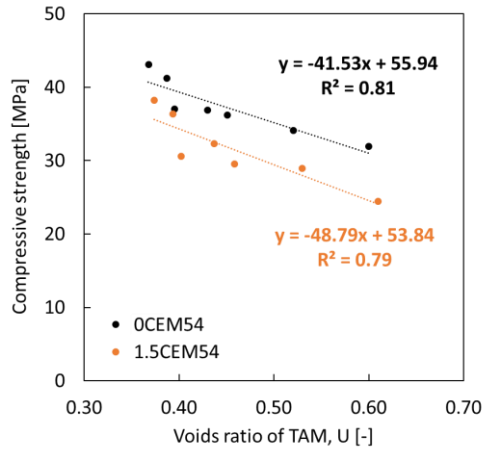


Figure 8-42. Correlation between compressive strength and voids ratio of TAM

8.4.4.2 Effect of capsule size and capsule dosage in capsule-based concrete mixtures (in relation to the second program)

In the second program, the effect of capsule dosage was studied with a representative mix design (OCEM54-40 or n of 0.4) from the first program. The definition of capsule dosage was made different between those programs. In the first program, the capsule dosage is the volume of capsules over volume of concrete. In the second program, the capsules were treated as a replacement of coarse aggregate as they affected the voids ratio of coarse fraction and BAM. Although the definition of capsule dosage is different between those programs, the effect of capsule dosage can be further observed in this scheme. Long capsules (CEM54) and short capsules (CEM23) were used with the same dosage between 0 and 7 vol.%. Initially, the fresh density of the capsule-based mixture was measured as indicated in Figure 8-39(d). The fresh density of concrete slightly reduced with increasing the capsule dosage. It occurs because the capsules are seen as the volumetric replacement of coarse aggregate, thus the higher capsule dosage leads to a lower amount (or mass) of coarse aggregate. There is no considerable difference in the fresh density of capsule-based mixtures on the use of CEM54 and CEM23 capsules.

The hardened properties were evaluated with the same methodology as the first program. Based on Figure 8-43(a), the hardened density of concrete was slightly reduced in the range of 1–3% after the addition of capsules between 1 and 7 vol.%. No considerable difference of hardened density is

found between CEM54 and CEM23 capsules. The compressive strength of capsule-based concrete was mainly evaluated and the result is depicted in Figure 8-43(b). The incorporation of capsules clearly decreases the compressive strength of reference concrete. By fixing the capsule dosage at 1, 3, 5 and 7 vol.%, the strength reduction was recorded at 7, 15, 12 and 15% (on the use of CEM54 capsules), respectively, and at 10, 13, 14 and 18% (on the use of CEM23 capsules), respectively. It is interesting to see that the compressive strength of concrete was similar around 37 MPa with the addition of CEM54 between 3 and 7 vol.%. In contrast, a gradual strength reduction occurred after the addition of CEM23 between 3 and 7 vol.%, but the results were rather comparable with CEM54. Three possible reasons are elaborated with regard to the declined strength: (1) the capsules are regarded as the 'weak' spots in the matrix, (2) the capsules take a partial volume of concrete and (3) the presence of capsules disturbs the packing of concrete. The compactness of concrete tested by UPV was slightly reduced after the incorporation of capsules. The ultrasonic velocity decreased by 1.1–2.6% on the use of 1–7 vol.% CEM54; and 0.5–1.7% on the use of 1–7 vol.% CEM23. CEM23 capsules seem to induce a slightly better compactness as compared with CEM54 capsules. This may be associated with the physical form of the capsules where the CEM23 capsules are designed similar to the size of coarse aggregates thus they can blend well within the mix. In case of CEM54, the capsules are long tubular-shaped, and they might induce more effects in the packing than CEM23. Nevertheless, the differences of velocities are not significant as confirmed by ANOVA (p -values > 0.05).

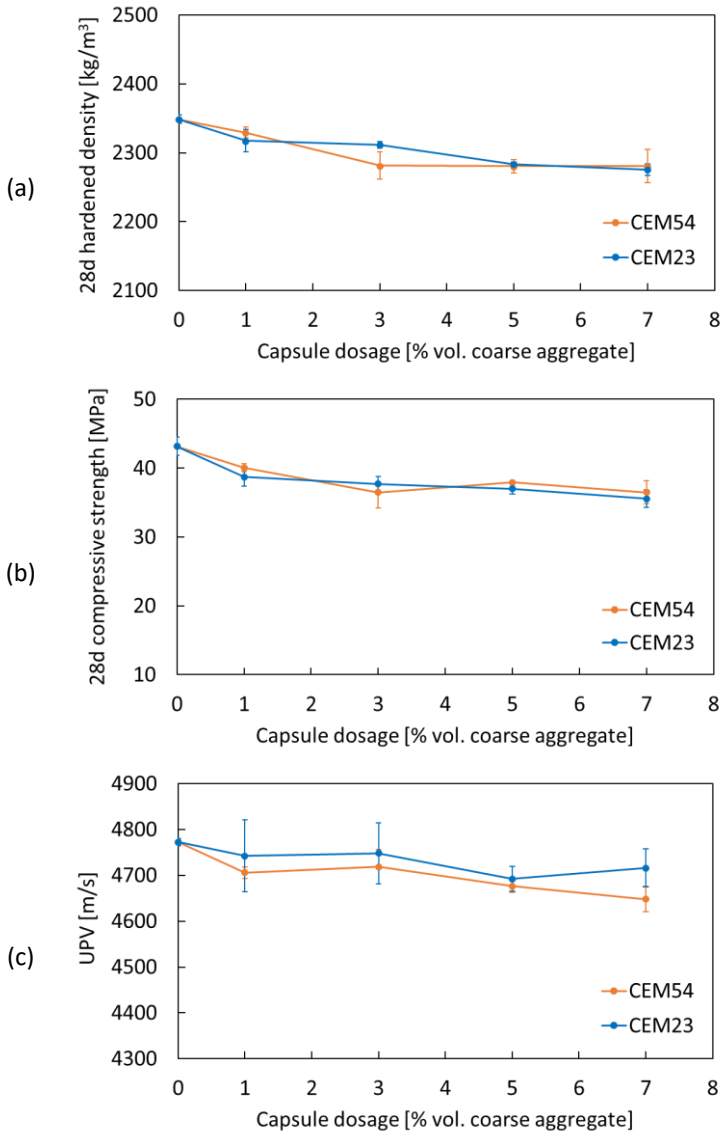


Figure 8-43. Evaluation of (a) hardened density, (b) compressive strength and (c) UPV of reference and capsule-based concretes tested at 28 days from the second program

8.4.5 Qualitative evaluation

8.4.5.1 Capsule breakage

During compression tests, 'wet' spots were found on the concrete surface as shown in Figure 8-45(a). It means that some capsules inside the concrete were broken and consequently releasing WRA via cracks. As it might be difficult to confirm the exact number of broken capsules, at least some capsules are able to rupture due to the high loading. A higher amount of capsules may lead to a higher chance of capsule breakage. Figure 8-45(b) shows a typical spreading of WRA after compression and crazing cracks on the surface were sealed by the WRA as a result of the capsule breakage inside the concrete. In this case, the WRA was released and absorbed by the matrix via cracks and capillary action.

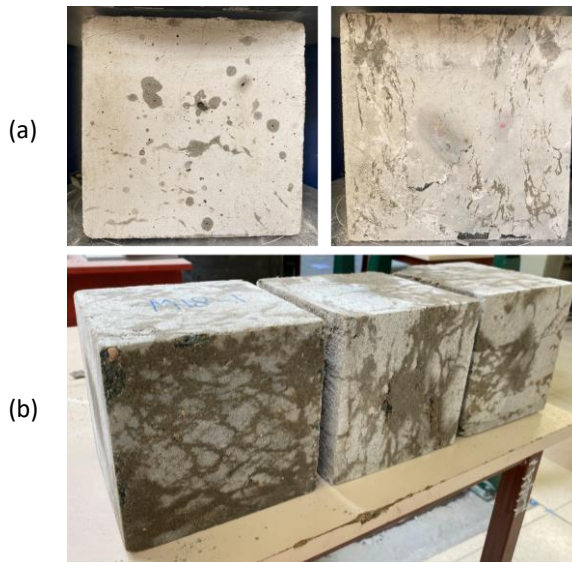


Figure 8-44. (a) Wet spots indicating that some capsules were broken inside the concrete during the compression test by releasing the sealing agent, (b) the spread of WRA via microcracks and capillary action

After all specimens from the second program (e.g., 1CEM54, ..., 7CEM23) were subjected to the compression tests, they were split by the splitting test in order to quantify the amount of broken capsules in a crack plane. As shown in Figure 8-45, the splitting crack was made close to the center position of the cube. Then, the cube was taken out and opened to count the amount of broken capsules. Table 8-16 summarizes the total amount of embedded

capsules as well as the ruptured capsules with employing three repetitions per mixture. Among CEM54 mixtures, 7CEM54 showed the highest amount of broken capsules in a crack plane due to the high capsule dosage. With a low capsule dosage, a low probability of the capsule breakage is also attained. In case of CEM23 mixtures, the probability of capsule breakage is apparently much lower than CEM54 mixtures. It may occur due to the shape of the capsules. CEM23 capsules are rather short and they are similar to the size of coarse aggregates, thus the broken capsules in a crack plane are strongly dependent on the position of the capsules and crack itself. In contrast, since the CEM54 capsules are rather long, they may have a higher probability for the capsule breakage when cracks occur.

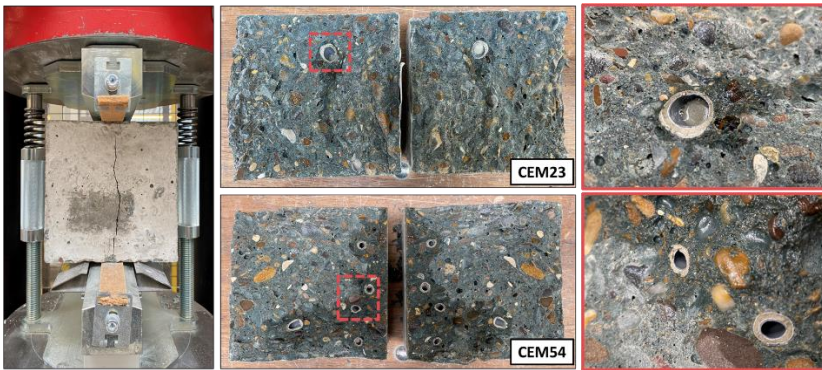


Figure 8-45. Observation of the broken capsules in a certain crack plane after splitting the cubes

Table 8-16. Probability of capsule breakage in a certain crack plane

Mixture	Number of embedded capsules per cube	Number of broken capsules in a certain crack plane			Probability of capsule breakage
		Cube 1	Cube 2	Cube 3	
1CEM54	5	2	0	0	0–40%
3CEM54	13	1	0	0	0–8%
5CEM54	21	5	4	2	10–24%
7CEM54	29	5	2	7	7–24%
1CEM23	4	0	0	1	0–25%
3CEM23	11	0	0	0	0%
5CEM23	18	0	0	0	0%
7CEM23	25	0	0	2	0–8%

8.4.5.2 Bond between capsule shell and concrete matrix

The broken capsules from the split cube were observed by means of optical microscopy (TOOLCRAFT USB microscope 5MP, Germany) at the interface. Figure 8-46 shows the microscopic observation on the bond between capsule shell and concrete matrix. It shows that the capsules were well attached to the concrete matrix. From the microscopy observation, it seems that there is no delamination in the interface of capsule-matrix even after cracking the specimen. The bond between capsule and concrete matrix will also influence the mechanical performance of the concrete. However, in this study, the bond strength between capsule and concrete is not quantitatively measured and it needs to be further investigated in a future research. Furthermore, in order to confirm the bond of capsules, scanning electron microscopy (SEM) (PhenomXL, Thermo Fisher Science, US) was performed on a capsule-matrix fragment (which was previously coated with gold for the imaging) and the microstructure images based on the secondary electron detector (SED) were produced as presented in Figure 8-47. The SEM investigation also revealed that the capsule shell is well attached to the concrete matrix without a sign of delamination. As shown in Figure 8-47, there is a distinction between concrete matrix and outer capsule shell and this is confirmed by the energy dispersive X-ray (EDX) spectroscopy analysis from Figure 8-48 where the outer capsule shell is rich in carbon due to the epoxy coating while the concrete matrix itself is rich in calcium.

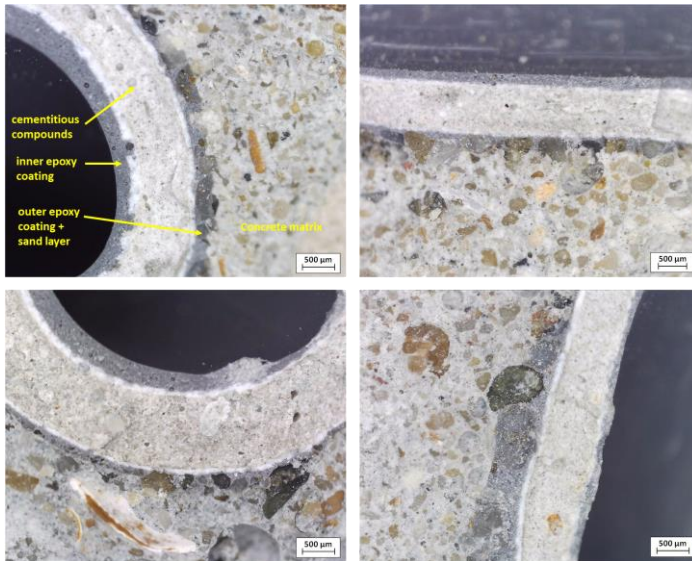


Figure 8-46. Bond observation between the capsule shell and concrete matrix

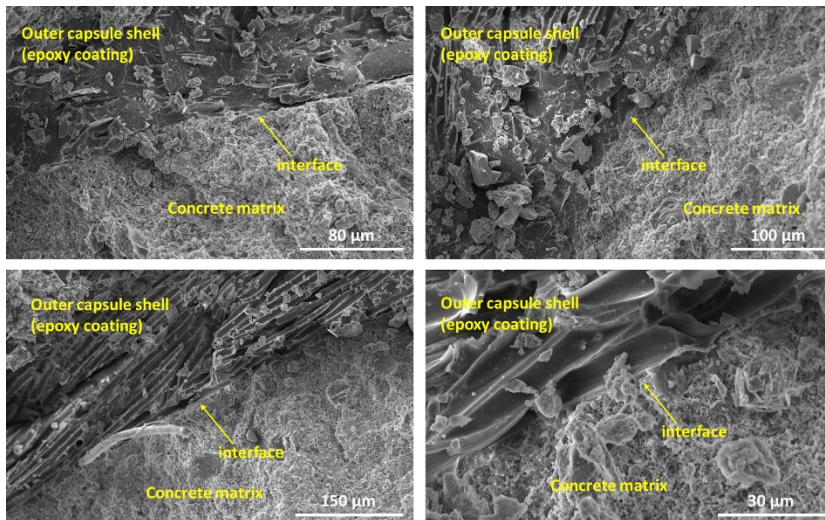


Figure 8-47. Microstructure images at the interface between outer capsule shell and concrete matrix

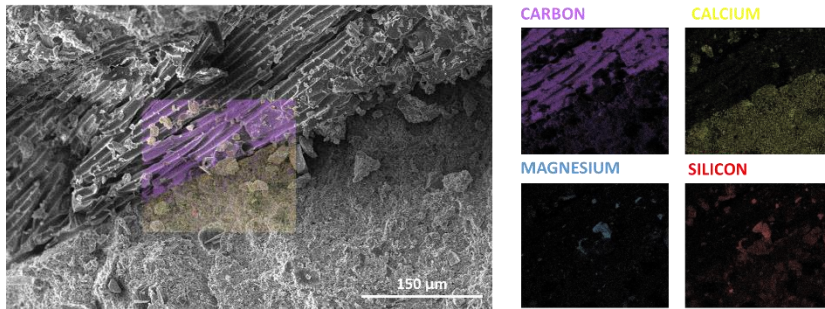


Figure 8-48. EDX analysis on the interface of concrete matrix–outer capsule shell

8.4.6 Conclusions

This study aims to evaluate the effect of macrocapsules in the different concrete mix designs in relation to the packing model as previously elaborated in Section 8.3.5. Two cementitious capsules were used namely CEM54 (54 mm in length and 9 mm in outer diameter) and CEM23 (23 mm in length and 15 mm in outer diameter). The water-repellent agent (WRA) was stored inside the capsules. The modification of mix designs was split into two programs: (1) the first program involves the incorporation of 1.5% volume of CEM54 capsules over the volume of concrete in seven concrete mix designs with different fine fraction (n) from 0.2 to 0.8; and (2) the second program investigates the use of capsules as the replacement of coarse aggregates, as the capsules strongly affect the voids ratio of coarse fractions. Thus, the effect of capsule dosage (both CEM54 and CEM23) ranging from 1 to 7% volume of capsules over volume of coarse aggregates is evaluated. All reference and capsule-based concretes are subjected to the compression and UPV tests for the assessment. The main findings are presented as follows:

1. The incorporation of 1.5% vol. capsules decreased the compressive strength of the concrete in which the reduction depends on the fine fraction. When the n was fixed in the range of 0.2–0.4 and 0.5–0.8, 11–12% and 15–23% strength reductions were observed, respectively.
2. The highest compressive strength was achieved by the reference and capsule-based concretes with the n of 0.4, which is in a good agreement with the lowest voids ratio of TAM at n of 0.4 based on experimental and Dewar results. A strong relationship between compressive strength and

voids ratio of TAM was established where a higher voids ratio of TAM leads to a lower compressive strength and vice versa.

3. No considerable effects of the capsules' addition were observed for the hardened density and the compactness of the concrete.
4. Increasing the capsule dosage from 1 to 7 vol.% gradually reduced the compressive strength of concrete. On the use of CEM54 and CEM23 capsules, the strength reduction was found in the range of 7–15% and 10–18%, respectively.
5. During compression test, some capsules were broken as indicated by wet spot on the concrete surface. Furthermore, the released sealing agent was able to widely spread in the matrix via cracks and capillary action.
6. Based on the microscopic and microstructure observations, a good bond was achieved in the interface of capsule shell and concrete matrix.

Chapter 9

VALORIZATION PLANS

9.1 Identification of key exploitable results

The main objective of this PhD research was to optimise the mix design of self-healing concrete to be readily used in the ready-mix concrete applications. Several methodologies have been used as explained in the previous chapters in order to understand the contribution of mix design parameters affecting the concrete properties. The key findings obtained in this PhD can help researchers/engineers in order to formulate their concrete mixtures for self-healing application. By looking at several strategies to optimize the designs, there are two items that can potentially be exploited in the future as follows:

- *An optimization guideline for self-healing concrete production.* This will include (1) a state-of-the-art about the impact of healing agents on concrete properties, (2) recommendations for using specific healing agents for specific applications or environments, (3) mitigation plans to overcome negative impacts on the use of healing agents and (4) detailed procedures for optimizing the mix designs.
- *An optimization tool.* This tool will enable the user to formulate the mix designs of concrete based on their preferences and desired projects. The tool will help to decide which mixture is suitable for the user's application and the theoretical background behind the tool will optimise the results based on the user's input.

In this proposal, services to the industry could be offered for projects related to concrete technology. Serving as a technical expert or engineer in this research area may attract clients to provide a consultation especially for self-healing application. This is because self-healing concrete can be

considered a new breakthrough in the domain of concrete technology and there are only few demonstration projects that make use of it. It is important to note that not all healing/sealing agents can be used for all concrete applications. It greatly depends on certain requirements. For instance, the self-healing technologies by bacteria and crystalline admixture need a presence of water for the healing activation when a crack is present in the structure. Thus, concrete structures that have a close contact with water such as dams and water reservoirs might be fitted in this case. Other self-healing technologies on the use of micro- or macro-encapsulated sealing agent (e.g. water repellent agent) do not require moisture/water for the activation and it will give a water barrier effect as a result of capsules breakage when a crack occurs. This can be potentially applied for instance in concrete bridges where the self-sealing technology can be introduced in the cover zone of concrete bridge deck with micro-/macro-capsules containing sealing agent. Consequently, the potential cracks on the bottom part of the deck due to the tension can be sealed as a result of capsule triggering, preventing the ingress of water into the crack and concrete matrix. So, the concept of self-healing concrete and its benefits yet drawbacks should be well understood by the clients. The stakeholders who are concrete and self-healing material producers are most likely to be the 'foundation' to create the business and mainly exploit our results.

9.2 Brief market analysis

To date, there are no available services/tools to optimize the mix design of self-healing concrete in the market because the advancement is often done on the self-healing products with regards to the effectiveness of healing efficiency, not on the mix design itself. One of the current demands of the market is the development of a methodology to introduce the healing agents in the concrete without affecting its fresh and hardened properties. The creation of a mix design tool will potentially help to overcome this demand. The first input for the tool can be based on the current PhD works where optimization of mix designs was performed on the use of specific agents, as well as the other promising results from the SMARTINCS project. Despite a limited number of types of self-healing materials being used now, the market size will grow as self-healing concrete is further accepted and introduced in the market. As this (hopefully) will grow, the interest in the mix design tool will increase.

9.3 Strategy for valorization

Following the proposed service to industry via the development of a mix design tool and optimization guideline, a good penetration strategy for valorization is required.

First of all, it can be done by advertising the consultancy/service to the public aiming to create a brand awareness. This can be achieved by attending several conferences and workshops to disseminate the service with the hope of attracting many clients from different sectors (e.g. concrete plant, university, private sector).

Next, finding investors to get funding for further development. In this case, the intellectual protection right (IPR) strategy can be proposed in Table 9-1. Consultancy services in self-healing concrete mix design do not apply in terms of IPR registered. The tool can be kept private and be used for internal use/via contract research. The guideline containing several methodologies to optimize the mix design of self-healing concrete can be made 'open'.

In fact, there are some risks that may be encountered during the valorization. Thus, a PEST analysis and risk analysis for the valorization of the results are elaborated as shown in Table 9-2 and Table 9-3, respectively, together with some possible preventive actions.

Table 9-1. IPR strategy proposed

No	Main exploitable results	IPR strategy	Target group
1	Strategy/tool for self-healing concrete mix design	Contract research	+ Construction companies + Ministries + Project manager + Self-healing materials producers + Etc
2	Optimization guideline	Open	+ Construction industries + Universities + Ministries of public works + Etc

Table 9-2. PEST analysis for valorization

Political (P)	<ul style="list-style-type: none"> ▪ Construction policies are mainly focused on green deal and sustainability, which can be an opportunity for self-healing technologies to reach the market
Economical (E)	<ul style="list-style-type: none"> ▪ The cost of buying a software or paying a subscription for a concrete mix design tool is relatively pricey ▪ Economic growth is decreasing due to other crises
Social (S)	<ul style="list-style-type: none"> ▪ A large awareness about sustainability, which may benefit the penetration of self-healing products in the market ▪ People want to buy a tool with a cheap price but with a high quality
Technological (T)	<ul style="list-style-type: none"> ▪ There is still no availability of mix design tools for self-healing concrete in the market and cloud ▪ The development of new technologies and various optimization approaches may become a threat

Table 9-3. Risks identified

Risk event	Preventive / corrective actions
Customers show less interest to use the service (tool/guideline/consultancy) because they have their own way to produce concrete or they are not convinced to use self-healing concrete	Spreading information towards society regarding the service by promoting it in the conference, workshop, expo, etc.
Limited applicability of the tool (related to specific healing agents)	Further research and development needed and rising it as another PhD topic / hiring a postdoc (also search for additional funding)
Incompatibility between partners (during exploitation) once under way	Define the scope of service and work on relationships (or terminate ineffective partnership)
Documentation (i.e. guideline) does not provide sufficient or adequate knowledge for readers	Assess adequacy of documentation and provide a state-of-the-art
Necessity to update the optimization tool in the future based on new standard regulations	Identify the changes and adapt the content

All in all, this PhD research can be seen as a promising contribution to the state-of-the-art for the creation of the new mix design tool and/or for the possible improvement of the available mix design tools with integrating an option to include the healing/sealing agents in their program. Thus, the coding/program for designing the concrete mixes shall be updated considering the alteration of the concrete properties due to the effect of certain agents. The first attempt was done with adapting an existing mix design tool from KU Leuven with the introduction of 'powdery' healing agents (i.e., Penetron crystalline admixture and Basilisk bacteria healing agent) for the internal use of SMARTINCS consortium. Nevertheless, the tool shall be upgraded in the future with introducing the other healing and sealing agents, also with offering optimization feature for certain concrete properties. In addition, this PhD work has been (partially) disseminated in various platforms such as international peer-reviewed publications; oral presentations in conferences, workshops and seminars; internal reports of the project and social media of SMARTINCS. Those activities are expected to increase public awareness towards the functionalities of self-healing concrete that can hopefully transform the construction industries.

Chapter 10

CONCLUSIONS AND RECOMMENDATIONS FOR FUTURE RESEARCH

10.1 Summary

This PhD research aimed to optimize the mix design for self-healing concrete considering the fresh, hardened, self-healing and self-sealing properties of normal concrete due to the incorporation of specific healing/sealing agents. This chapter summarizes the most important conclusions of the present work and presents some suggestions for further research.

Self-healing concrete gains an immense popularity within the academic and industrial sectors thanks to its ability to heal and seal the cracks autonomously. The main purpose of using self-healing concrete is to prolong the service life of concrete structures and to improve the durability with the aid of smart materials often called as healing/sealing agents. As a matter of fact, it has been more than a decade that researchers attempt to develop self-healing concrete both in small- and large-scale studies which are found in many publications. However, the realization of self-healing concrete in field applications is still minimal and it implies that there are still issues that need to be solved by researchers to convince the owner or contractor of the project. Based on an intensive literature review, it is clear that one of the main issues in the development of self-healing concrete is that the healing/sealing agent is often added on top of the normal concrete, meaning that no adaptations in mix design are made after the inclusion of any agents. Moreover, although the agents have been technologically well-developed, not all agents are compatible with (all types of) cementitious materials. Some

agents may induce negative effects to the concrete properties and other agents may not be harmful or even beneficial for the concrete. In addition, there is a stereotype for the research in the area of self-healing concrete, where many past studies strongly focused on the healing and sealing abilities of concrete and the evaluation of fresh and hardened properties (workability, strength, durability, etc.) was often neglected. Thus, there was a demand to do research focused on the alteration of the fresh and hardened properties of self-healing concrete due to the introduction of healing/sealing agents; which was basically the objective of this PhD dissertation.

A wide range of healing/sealing agents has been used in this research: commercial agents (Penetron crystalline admixture (CA), Basilisk bacteria healing agent (BAC)), biomasses (HTN, YEAST), micro-encapsulated agent (microcapsules with PU shell and water repellent agent cargo having the mean size of 56 and 93 μm (MIC_56, MIC_93)) and lastly macro-encapsulated agent (cementitious capsules containing water repellent agent). As a note, HTN, YEAST, MICs were agents developed within the SMARTINCS project and these materials were kindly provided by the producers (i.e. Avecom b.v., Micropore Technologies Ltd) for the collaborative works. Macrocapsules were also provided by colleagues from Politecnico di Torino. Short and long cementitious capsules having a length of 23 and 54 mm, respectively, were used (labelled as CEM23 and CEM54). Both CA and BAC were available in the form of powder and they were used with the recommended dosages as suggested by producers (1% and 2% by weight of cement (bwoc) for CA and BAC, respectively). HTN and YEAST were available in solution and the active content of microorganisms from each biomass has been optimally fixed by the producer (0.05% and 0.45% bwoc for HTN and YEAST, respectively). On the other hand, microcapsules were available also in the form of slurry while macrocapsules were present in the form of rigid tubes. There were no recommended dosages for these capsules to be added into the concrete, but after consultation with producers and from literature review, the dosage of microcapsules for optimization ranged between 0 and 6% bwoc. Specifically for macrocapsules, unlike the other 'powdery' and 'slurry' agents, they were not added by the weight of cement, instead added by volume of concrete or aggregates (in the range of 0–7 vol%).

On the compatibility of healing agents with concrete components:

Prior to introducing these agents into the concrete mixture, effects of the incorporation of CA and BAC on the paste level were investigated and the following main conclusions could be drawn:

- The water demand of cement increased after the addition of CA, while no considerable effect was found with the BAC, MIC_56 and MIC_93.
- Inclusion of these agents (i.e. BAC, MIC_56 and MIC_93) prolonged the setting time of cement paste, while a rapid initial setting was found on the use of CA.
- A reduced consistency and high viscosity of the CA paste were identified. When chemical admixture such as polycarboxylate ether (PCE) superplasticizer was added into the paste, it was interestingly found that the SP could adsorb on CA particles. In contrast, no negative interaction was observed between superplasticizer and BAC. The details can be found in Chapter 3 and 7.

On the mix design optimization using CA:

After understanding the effect of healing/sealing agents in cement paste, the agents were finally applied to the concrete mixtures to assess the fresh, hardened and self-healing or self-sealing properties. The key research findings from all experiments are summarized here, and are related to the mix designs and experimental programs adopted in this PhD, for which the details can be found in the respective chapters of this thesis. On the use of CA, the optimization of mix design might be difficult considering the recommended dosage of this agent is only 1% bwoc which is very low. Thus it was decided to modify the mix design of self-healing concrete with employing three parameters namely CA dosage (0, 1 and 2% bwoc), water-cement (w/c) ratio (0.46, 0.49 and 0.52 – all with 1% CA) and cement content (320, 340 and 360 kg/m³ – all with 1% CA).

- Focusing on the utilization of 1% and 2% CA, apparently, the introduction of 1% CA had a similar workability as reference concrete (0% CA). However, increasing the CA dosage from 1 to 2% caused a considerable reduction in workability even after increasing the SP demand. This observation was in line with the previous

finding that the CA interfered the adsorption capacity of SP on cement particles.

- Furthermore, the addition of 1% and 2% CA caused a slight reduction in air content of fresh concrete.
- In term of compressive strength, the higher the CA dosage, the higher the mean compressive strength observed at 28 and 91 days although the strength difference relative to the reference (0% CA) was not significant.

The modification of mix design was actually targeted to evaluate whether changing these parameters will allow improving the healing and sealing efficiency. Healing efficiency was referred to crack closure by precipitation, while sealing efficiency was referred to the reduction of water permeability rate. The results showed that:

- The healing efficiency increased with increasing the CA dosage and as a result of doubling the CA dosage from 1 to 2% bwoc, the improvement of healing efficiency was almost doubled observed after a short healing period (i.e., 21 days under water). Moreover, only the addition of 2% CA gave a considerable improvement on sealing efficiency.
- The variation of w/c did not give a clear picture on the improvement of healing and sealing efficiency.
- In contrast, a gradual increase of cement content from 320 to 360 kg/m³ led to a continuous improvement on both healing and sealing efficiency. The details can be found in Chapter 4.

On the effect of healing agents on the rebar-bond capability:

One of the main and novel contributions of this PhD research is the investigation on the bond behavior of reinforcement in self-healing concrete. This contribution is considered novel because at the time this thesis is written, almost no studies have been conducted related to this topic and past studies, in most cases, cast self-healing concretes in an unreinforced condition.

Nevertheless, in reality, the concrete shall be casted in a reinforced condition for structural applications. Thus, the bond properties between steel reinforcement and self-healing concrete are very important.

Four healing agents were used in the current study including HTN, YEAST, CA and BAC, and they were added on top of the normal concrete (no optimization). A short pull-out test was designed and developed with a series of uncracked, cracked and healed specimens. Prior to this investigation, the fresh and mechanical properties of the concretes were also assessed.

- Based on short pull-out tests, the ultimate bond strength of reinforcement in uncracked concrete was greatly improved (7–57%) after the addition of any healing agents.
- A splitting crack with a width between 200 and 500 μm on pull-out specimens caused a severe reduction in bond strength of approximately 60–80%.
- A limited bond strength restoration can be achieved when the cracked specimens were healed under water for 28 days. When the healing was prolonged to 112 days, no clear self-healing recovery was further detected.
- Despite the fact that the bond strength was not significantly recovered after healing, the splitting crack was able to be fully closed by the precipitation of calcium carbonates near the crack mouth and the formation of healing products inside the crack was also evident. This advances a possible improvement against corrosion effects. The details can be found in Chapter 5.

Considering the potential benefit of healing agents in the bond properties as explained above, an optimization of concrete mix designs was proposed. Three mix design parameters were employed for optimisation including w/c (0.40, 0.50 and 0.60), fine ratio (FR) (0.34, 0.44 and 0.54) and healing agent (HA) (REF, CA, BAC). Those factors were analysed in a broad range to cover most of the possible concretes used in practice. It is assumed that other factors like cement type or dosage, type of aggregate, etc., can also influence the bond properties, but it was decided to keep it out of this study.

Nine concrete mixtures were finally developed with the fractional factorial design and the analysis was done via the Taguchi method where it

analyses the results based on the signal-to-noise (SN) ratio for process optimization.

- Based on an extensive analysis, the advantage of using healing agents was found in the compressive strength and bond properties of rebars in uncracked concrete.
- The compressive strength of concrete considerably increased when lowering the w/c, increasing the FR and incorporating the healing agents. This finding is in line with the observation from the previous chapters.
- The bond of steel reinforcement with the concrete matrix in the uncracked state improved after the BAC or CA was added into the concrete. Furthermore, the effect of mix design factors and levels was only evident in the ultimate bond strength specifically for small cracks (200–300 μm) and the effect of w/c is more superior than all other factors (FR, HA). The details can be found in Chapter 6.

On the use of microcapsules as self-healing technology:

Aside from the healing agents discussed above, microcapsules (MIC) with water repellent agent (as sealing agent) were also used for self-sealing concrete application. The shell and cargo of the microcapsules were polyurethane (PU) and water repellent agent (WRA), respectively. Based on the preliminary study, it was revealed that:

- The microcapsules caused a severe reduction in concrete mechanical properties.
- The sealing ability of concrete mixed with microcapsules was significantly improved.

These observations were generally in line with the results from literature. In order to mitigate the negative effects of the microcapsules, especially in terms of mechanical performance, a mix design optimization was performed via full factorial design approach. Three mix design parameters were selected namely MIC size (56 and 93 μm), MIC dosage (0, 3 and 6% bwoc) and w/c (0.40, 0.50 and 0.60). Fifteen concrete mixtures were developed for the optimization. The key findings were:

- The w/c and MIC dosage were found to be the most significant factors affecting the mechanical properties, while there was no significant effect of changing MIC size from 56 to 93 μm .
- The strength reduction due to MIC was higher in the mixture with low w/c (i.e., 0.40) than in the mixture with high w/c (i.e., 0.50, 0.60). Hence, changing the w/c may reduce the negative effect of MIC.
- The sealing efficiency of cracked concrete tested via capillary water absorption tests was in the range of 68–88% as a result of the addition of microcapsules.
- Furthermore, the sealing efficiency was found to be higher in the mixture with higher w/c. Increasing the MIC dosage from 3 to 6% bwoc also caused a sealing improvement. The effect of MIC size was found to be insignificant on sealing efficiency. The details can be found in Chapter 7.

On the use of macrocapsules as self-healing technology:

Macrocapsules were lastly researched in this study to understand their effect in the packing of self-healing concrete. Initially, the used materials (i.e., aggregates) were characterized via particle density, sieving and loose bulk density tests. Furthermore, the interaction between aggregates and macrocapsules was analyzed from the changes of voids ratio of aggregates, tested via loose bulk density test.

- The results showed that voids ratio of fine aggregates was not affected by the addition of capsules, while the voids ratio of coarse aggregates increased with increasing the capsule dosage (from 0.5 to 3.2 vol%) due to the loosening effect, wall effect and capsule effect.

As a proof-of-concept, the effect of macrocapsules on aggregate packing was initially modelled for the voids ratio of single aggregate type/fraction. Furthermore, the interaction tests were employed on a binary aggregate mixture (BAM) and ternary aggregate mixture (TAM) with macrocapsules. Several formula were proposed to predict the voids ratio of either BAM or TAM with capsules (from the voids ratio of mixture without capsules) in function of capsule dosage and capsule geometry. However, it should be

noted that the voids-ratio model for the packing of aggregates-capsules is developed based on restricted materials (e.g., 20-mm maximum size of aggregate and tubular macrocapsules). If these requirements are not fulfilled (e.g. aggregate > 20 mm, spherical capsules, ...), further validation tests are necessary.

Preliminary study was conducted to assess the capsule robustness toward mixing and the effect of macrocapsules in the fresh, hardened and self-sealing properties of concrete. The key findings are:

- CEM54 capsules were found to be robust to resist the mixing forces with 100% survival ratio when tested in a drum mixer and 70–95% when tested in a planetary mixer.
- The addition of 2 vol% CEM54 capsules slightly reduced the workability and increased the air content.
- As a result of a random distribution of capsules in the matrix, a reduction of compressive strength was found. When the mix design was modified in terms of fine fraction, the strength reduction was still noticed in the range of 11–23% using 1.5 %vol CEM54 capsules. A higher the capsule dosage led to a higher strength reduction.
- A relationship between compressive strength and voids ratio of TAM was established where the higher the voids ratio, the lower the compressive strength. The details can be found in Chapter 8.

10.2 Suggestions for future research

The optimization of mix designs is relatively complex and very dependent on the objectives and selected variables. There are many parameters to be considered while composing the concrete mix designs such as concrete type, cement type, cement content, water content (w/c), aggregate type, aggregate size/fraction, grading and admixture. Also, to what extent the optimization is performed in terms of workability, strength, durability, self-healing performance, etc. It is literally very challenging to consider all of these parameters to fit in the scope of optimization of mix designs for self-healing concrete because in this new type of concrete, other parameters should also be considered such as type of healing/sealing agent, dosage of agent and particle size of agent (e.g. capsules – in terms of capsule shell material, capsule shell thickness, core content, etc.). Combination of all

these parameters would make a very large number of experiments which is quite impossible to do. Thus, only selected prospective parameters could be considered for the optimization. In this PhD research, some parameters have been used while other basic parameters such concrete type, cement type, aggregate type, aggregate size, grading and admixture are not explored yet. These parameters will also influence the healing and sealing abilities of the concrete, thus it might be interesting to be considered for future research.

Besides the basic parameters of concrete mix designs, the healing/sealing agent itself can be further optimized. In this study, the commercial healing agents such CA and BAC have been mostly added at recommended dosages. However, depending on the objectives, the normal dosage can be further increased for specific application. As an example, for the application of a thin-layered concrete cover zone, the BAC can be increased up to 5% bwoc [38]. For the grouting application and repair products, the CA has been used at 3% bwoc [202] above the normal dosage for concrete. Of course, increasing the dosage of healing agent may also influence the fresh and hardened properties, thus more investigations are needed.

Regarding specific studies done in this research, some suggestions are elaborated below for the future works.

Firstly, compatibility between cement type, CA, BAC and superplasticizer on cement paste has been investigated. However, the compatibility between cement type, superplasticizer and biomass/microcapsules is not yet investigated due to limitation in time. As previously explained in Chapter 5, the workability of fresh concrete mixed with HTN showed a declined trend. Additional research can be interesting regarding the effects of biomasses, starting from the paste level. In Chapter 7, there was an inconsistency on the air content results after the addition of microcapsules. Concrete mixtures with microcapsules without SP addition (referring to the mixes with w/c 0.60) showed a clear trend where the increase of microcapsules' dosage tends to increase the air content, while for other mixtures with SP addition (referring to the mixes with w/c 0.40, 0.50), there is no clear trend of air content with increasing microcapsules' dosage as sometimes it increases, decreases or remains constant. It seems that there is an interaction between microcapsules and superplasticizer that may generate unstable results on fresh concrete mixtures. This interaction is not yet proven and future works might be useful to confirm the compatibility of microcapsules.

Secondly, in relation to the bond behavior research (Chapter 5), the longitudinal crack along the direction of rebar is previously made on pull-out specimens. If a pull-out test is conducted on specimens with cracks induced in the transverse direction (perpendicular with rebar direction), the effect of self-healing materials on the tension-stiffening of concrete which plays an important role in the mechanical behavior of RC structures, can be studied. The bond recovery was found to be limited due to the self-healing effects that promote crack closure via precipitated products. Another approach can be considered by using macrocapsules or vascular networks (acting as vessels) where the capsules/networks are filled with polymerizing agent (e.g. polyurethane). In that way, when the crack occurs and the vessel breaks with releasing the agent, polymerization may take place in the crack zone and it seems that in this way, the bond between the concrete matrix, reinforcement and polymerized product may be stronger than the precipitated healing products.

Thirdly, in relation to the optimization technique (Chapter 6), the Taguchi design of experiment on the selection of three mix design factors and three levels is found to be robust in optimizing the concrete properties based on the main effects plot. With this plot, the trend of changing mix design factor-level can be easily seen. Thus, it is interesting to broaden the design with employing more than three mix design factors and more than three mix design levels. For instance, with the Taguchi design, five factors with three levels for each factor can be performed with L_{27} orthogonal array, meaning 27 mixtures for optimization. If the full factorial design is used, the number of experiments is very large with $3^5 = 243$ experiments. Consequently, it is very interesting to look into other parameters other than those have been researched in this study to gain more knowledge about the mix design optimization.

Fourthly, although the negative effect of microcapsules can be minimized as demonstrated in this current study (Chapter 7), the strength reduction is still there. Thus, the optimization of concrete mix designs should be further explored for instance by looking into certain admixtures that can prevent the negative impact of microcapsules with the concrete matrix. Also, since the microcapsules are composed of several materials, here polyurethane in shell and water repellent agent in cargo, the pure effect of such polyurethane and empty shell equivalent to the dosage of microcapsules can be studied in order to trace back or quantify the biggest contributor of strength reduction, related to the specific capsule composition.

Lastly, the packing model of macrocapsules may serve as a guidance to design the inert structure of self-healing concrete (Chapter 8). Nevertheless, it should be noted that the model is designed to distribute the macrocapsules randomly in the packing. One of the possible applications is to make a concrete cover zone with the randomly distributed macrocapsules as the cracks will normally occur starting from the cover zone. Thus, the distributed capsules may help to promote local repair at random places if cracks are present. However, this is not yet proven for the large-scale application and this can be considered for future research. Additionally, more repetitions on the capsule robustness test are needed to give a confidence level on the obtained results. More investigations are also needed on the use of different size/geometry of macrocapsules and different aggregates to accurately predict the effect of macrocapsules in the packing and toward the compressive strength.

The current PhD research has explored several approaches to optimize the mix design of self-healing concrete. However, there are still many challenges that need to be addressed to fully understand the influence of many mix design parameters and to assess the effectiveness of healing/sealing agent in different mix designs. As the research about self-healing concrete is continuously growing, it may be hoped that more investigations and more interesting results can be generated to propose optimal mix designs, so the concept of self-healing concrete can be easily accepted in the market.

REFERENCES

- [1] ACI Committee 212. Report on chemical admixtures for concrete. *Am Concr Inst* 2010;1(631).
- [2] Sisomphon K, Copuroglu O, Koenders EAB. Self-healing of surface cracks in mortars with expansive additive and crystalline additive. *Cem Concr Compos* 2012;34(4):566–74. doi: 10.1016/j.cemconcomp.2012.01.005.
- [3] Li D, Chen B, Chen X, Fu B, Wei H, Xiang X. Synergetic effect of superabsorbent polymer (SAP) and crystalline admixture (CA) on mortar macro-crack healing. *Constr Build Mater* 2020;247. doi: 10.1016/j.conbuildmat.2020.118521.
- [4] García-Vera VE, Tenza-Abril AJ, Saval JM, Lanzón M. Influence of crystalline admixtures on the short-term behaviour of mortars exposed to sulphuric acid. *Materials (Basel)* 2018;12(1). doi: 10.3390/ma12010082.
- [5] Ferrara L, Krelani V, Moretti F. On the use of crystalline admixtures in cement based construction materials: From porosity reducers to promoters of self healing. *Smart Mater Struct* 2016;25(8):1–17. doi: 10.1088/0964-1726/25/8/084002.
- [6] Jonkers HM, Thijssen A, Muyzer G, Copuroglu O, Schlangen E. Application of bacteria as self-healing agent for the development of sustainable concrete. *Ecol Eng* 2010;36(2):230–5. doi: 10.1016/j.ecoleng.2008.12.036.
- [7] Palin D, Wiktor V, Jonkers HM. A bacteria-based bead for possible self-healing marine concrete applications. *Smart Mater Struct* 2016;25(8). doi: 10.1088/0964-1726/25/8/084008.
- [8] Palin D, Wiktor V, Jonkers HM. A bacteria-based self-healing cementitious composite for application in low-temperature marine environments. *Biomimetics* 2017;2(3). doi: 10.3390/biomimetics2030013.
- [9] Wang J, Mignon A, Trensou G, Van Vlierberghe S, Boon N, De Belie N.

A chitosan based pH-responsive hydrogel for encapsulation of bacteria for self-sealing concrete. *Cem Concr Compos* 2018;93:309–22. doi: 10.1016/j.cemconcomp.2018.08.007.

- [10] Seifan M, Sarmah AK, Samani AK, Ebrahimezhad A, Ghasemi Y, Berenjia A. Mechanical properties of bio self-healing concrete containing immobilized bacteria with iron oxide nanoparticles. *Appl Microbiol Biotechnol* 2018;102(10):4489–98. doi: 10.1007/s00253-018-8913-9.
- [11] Alazhari M, Sharma T, Heath A, Cooper R, Paine K. Application of expanded perlite encapsulated bacteria and growth media for self-healing concrete. *Constr Build Mater* 2018;160:610–9. doi: 10.1016/j.conbuildmat.2017.11.086.
- [12] Wu M, Hu X, Zhang Q, Cheng W, Xue D, Zhao Y. Application of bacterial spores coated by a green inorganic cementitious material for the self-healing of concrete cracks. *Cem Concr Compos* 2020;113(579):103718. doi: 10.1016/j.cemconcomp.2020.103718.
- [13] Mondal S, Ghosh A (Dey). Investigation into the optimal bacterial concentration for compressive strength enhancement of microbial concrete. *Constr Build Mater* 2018;183:202–14. doi: 10.1016/j.conbuildmat.2018.06.176.
- [14] Pei R, Liu J, Wang S, Yang M. Use of bacterial cell walls to improve the mechanical performance of concrete. *Cem Concr Compos* 2013;39:122–30. doi: 10.1016/j.cemconcomp.2013.03.024.
- [15] Schreiberová H, Bílý P, Fládr J, Šeps K, Chylík R, Trtík T. Impact of the self-healing agent composition on material characteristics of bio-based self-healing concrete. *Case Stud Constr Mater* 2019;11. doi: 10.1016/j.cscm.2019.e00250.
- [16] White SR, Sottos NR, Geubelle PH, Moore JS, Kessler MR, Sriram SR, et al. Autonomic healing of polymer composites. *Nature* 2001;409:794–817.
- [17] Giannaros P, Kanellopoulos A, Al-Tabbaa A. Sealing of cracks in cement using microencapsulated sodium silicate. *Smart Mater Struct* 2016;25(8):1–12. doi: 10.1088/0964-1726/25/8/084005.
- [18] Kanellopoulos A, Giannaros P, Palmer D, Kerr A, Al-Tabbaa A. Polymeric microcapsules with switchable mechanical properties for self-healing concrete: Synthesis, characterisation and proof of concept. *Smart Mater Struct* 2017;26(4). doi: 10.1088/1361-665X/aa516c.

- [19] Wang X, Sun P, Han N, Xing F. Experimental study on mechanical properties and porosity of organic microcapsules based self-healing cementitious composite. *Materials (Basel)* 2017;10(1). doi: 10.3390/ma10010020.
- [20] Hilloulin B, Van Tittelboom K, Gruyaert E, De Belie N, Loukili A. Design of polymeric capsules for self-healing concrete. *Cem Concr Compos* 2015;55:298–307. doi: 10.1016/j.cemconcomp.2014.09.022.
- [21] Van Tittelboom K, De Belie N, Van Loo D, Jacobs P. Self-healing efficiency of cementitious materials containing tubular capsules filled with healing agent. *Cem Concr Compos* 2011;33(4):497–505. doi: 10.1016/j.cemconcomp.2011.01.004.
- [22] Anglani G, Tulliani JM, Antonaci P. Behaviour of pre-cracked self-healing cementitious materials under static and cyclic loading. *Materials (Basel)* 2020;13(5):16–23. doi: 10.3390/ma13051149.
- [23] Anglani G, Van Mullem T, Zhu X, Wang J, Antonaci P, De Belie N, et al. Sealing efficiency of cement-based materials containing extruded cementitious capsules. *Constr Build Mater* 2020;251:119039. doi: 10.1016/j.conbuildmat.2020.119039.
- [24] Formia A, Terranova S, Antonaci P, Pugno NM, Tulliani JM. Setup of extruded cementitious hollow tubes as containing/releasing devices in self-healing systems. *Materials (Basel)* 2015;8(4):1897–923. doi: 10.3390/ma8041897.
- [25] Formia A, Irico S, Bertola F, Canonico F, Antonaci P, Pugno NM, et al. Experimental analysis of self-healing cement-based materials incorporating extruded cementitious hollow tubes. *J Intell Mater Syst Struct* 2016;27(19):2633–52. doi: 10.1177/1045389X16635847.
- [26] Park B, Choi YC. Self-healing capability of cementitious materials with crystalline admixtures and super absorbent polymers (SAPs). *Constr Build Mater* 2018;189:1054–66. doi: 10.1016/j.conbuildmat.2018.09.061.
- [27] Xue C, Li W, Qu F, Sun Z, Shah SP. Self-healing efficiency and crack closure of smart cementitious composite with crystalline admixture and structural polyurethane. *Constr Build Mater* 2020;260. doi: 10.1016/j.conbuildmat.2020.119955.
- [28] Pazderka J, Hájková E. Crystalline admixtures and their effect on selected properties of concrete. *Acta Polytech* 2016;56(4):306–11. doi: 10.14311/AP.2016.56.0306.

- [29] Jafarnia MS, Khodadad Saryazdi M, Moshtaghioun SM. Use of bacteria for repairing cracks and improving properties of concrete containing limestone powder and natural zeolite. *Constr Build Mater* 2020;242. doi: 10.1016/j.conbuildmat.2020.118059.
- [30] Andalib R, Abd Majid MZ, Hussin MW, Ponraj M, Keyvanfar A, Mirza J, et al. Optimum concentration of *Bacillus megaterium* for strengthening structural concrete. *Constr Build Mater* 2016;118:180–93. doi: 10.1016/j.conbuildmat.2016.04.142.
- [31] Madhu Sudana Reddy B, Revathi D. An experimental study on effect of *Bacillus sphaericus* bacteria in crack filling and strength enhancement of concrete. *Mater Today Proc* 2019;19:803–9. doi: 10.1016/j.matpr.2019.08.135.
- [32] Vijay K, Murmu M. Self-repairing of concrete cracks by using bacteria and basalt fiber. *SN Appl Sci* 2019;1(11):1–10. doi: 10.1007/s42452-019-1404-5.
- [33] Khaliq W, Ehsan MB. Crack healing in concrete using various bio influenced self-healing techniques. *Constr Build Mater* 2016;102:349–57. doi: 10.1016/j.conbuildmat.2015.11.006.
- [34] Nguyen TH, Ghorbel E, Fares H, Cousture A. Bacterial self-healing of concrete and durability assessment. *Cem Concr Compos* 2019;104. doi: 10.1016/j.cemconcomp.2019.103340.
- [35] Siddique R, Jameel A, Singh M, Barnat-Hunek D, Kunal, Ait-Mokhtar A, et al. Effect of bacteria on strength, permeation characteristics and micro-structure of silica fume concrete. *Constr Build Mater* 2017;142:92–100. doi: 10.1016/j.conbuildmat.2017.03.057.
- [36] Mors RM, Jonkers HM. Bacteria - based self - healing concrete : evaluation of full scale demonstrator projects. *RILEM Tech Lett* 2019;4(2019):138–44.
- [37] Mors R, Jonkers H. Effect on concrete surface water absorption upon addition of lactate derived agent. *Coatings* 2017;7(4). doi: 10.3390/coatings7040051.
- [38] He S, Zhang S, Luković M, Schlangen E. Effects of bacteria-embedded polylactic acid (PLA) capsules on fracture properties of strain hardening cementitious composite (SHCC). *Eng Fract Mech* 2022;268(October 2021). doi: 10.1016/j.engfracmech.2022.108480.
- [39] Cappellesso VG, Van Mullem T, Gruyaert E, Van Tittelboom K, De Belie N. Bacteria-based self-healing concrete exposed to frost salt

- scaling. *Cem Concr Compos* 2023;139(December 2022):105016. doi: 10.1016/j.cemconcomp.2023.105016.
- [40] Chahal N, Siddique R, Rajor A. Influence of bacteria on the compressive strength, water absorption and rapid chloride permeability of fly ash concrete. *Constr Build Mater* 2012;28(1):351–6. doi: 10.1016/j.conbuildmat.2011.07.042.
- [41] Chahal N, Siddique R, Rajor A. Influence of bacteria on the compressive strength, water absorption and rapid chloride permeability of concrete incorporating silica fume. *Constr Build Mater* 2012;37:645–51. doi: 10.1016/j.conbuildmat.2012.07.029.
- [42] Ameri F, Shoaie P, Bahrami N, Vaezi M, Ozbakkaloglu T. Optimum rice husk ash content and bacterial concentration in self-compacting concrete. *Constr Build Mater* 2019;222:796–813. doi: 10.1016/j.conbuildmat.2019.06.190.
- [43] Mohammed H, Ortoneda-Pedrola M, Nakouti I, Bras A. Experimental characterisation of non-encapsulated bio-based concrete with self-healing capacity. *Constr Build Mater* 2020;256. doi: 10.1016/j.conbuildmat.2020.119411.
- [44] Van Mullem T, Gruyaert E, Caspeepe R, Belie N De. First large scale application with self-healing concrete in belgium: Analysis of the laboratory control tests. *Materials (Basel)* 2020;13(4). doi: 10.3390/ma13040997.
- [45] Jiang L, Lu W, Wang W, Zhang Y, Han Q, Li Z. Mechanical properties and frost resistance of self-healing concrete based on expended perlite immobilized bacteria. *Constr Build Mater* 2022;348(May):128652. doi: 10.1016/j.conbuildmat.2022.128652.
- [46] Wang X, Xu J, Wang Z, Yao W. Use of recycled concrete aggregates as carriers for self-healing of concrete cracks by bacteria with high urease activity. *Constr Build Mater* 2022;337(December 2021):127581. doi: 10.1016/j.conbuildmat.2022.127581.
- [47] Xiao X, Tan ACY, Unluer C, Yang EH. Development of a functionally graded bacteria capsule for self-healing concrete. *Cem Concr Compos* 2023;136(November 2022):104863. doi: 10.1016/j.cemconcomp.2022.104863.
- [48] Zamani M, Nikafshar S, Mousa A, Behnia A. Bacteria encapsulation using synthesized polyurea for self-healing of cement paste. *Constr Build Mater* 2020;249:118556. doi: 10.1016/j.conbuildmat.2020.118556.

- [49] Sidiq A, Gravina RJ, Setunge S, Giustozzi F. Microstructural analysis of healing efficiency in highly durable concrete. *Constr Build Mater* 2019;215:969–83. doi: 10.1016/j.conbuildmat.2019.04.233.
- [50] Mostavi E, Asadi S, Hassan MM, Alansari M. Evaluation of Self-Healing Mechanisms in Concrete with Double-Walled Sodium Silicate Microcapsules. *J Mater Civ Eng* 2015;27(12). doi: 10.1061/(asce)mt.1943-5533.0001314.
- [51] Hassan MM, Milla J, Rupnow T, Al-Ansari M, Daly WH. Microencapsulation of calcium nitrate for concrete applications. *Transp Res Rec* 2016;2577:8–16. doi: 10.3141/2577-02.
- [52] Wang X, Huang Y, Huang Y, Zhang J, Fang C, Yu K, et al. Laboratory and field study on the performance of microcapsule-based self-healing concrete in tunnel engineering. *Constr Build Mater* 2019;220:90–101. doi: 10.1016/j.conbuildmat.2019.06.017.
- [53] Gilford J, Hassan MM, Rupnow T, Barbato M, Okeil A, Asadi S. Dicyclopentadiene and Sodium Silicate Microencapsulation for Self-Healing of Concrete. *J Mater Civ Eng* 2014;26(5):886–96. doi: 10.1061/(asce)mt.1943-5533.0000892.
- [54] Gruyaert E, Van Tittelboom K, Sucaet J, Anrijs J, Van Vlierberghe S, Dubruel P, et al. Capsules with evolving brittleness to resist the preparation of self-healing concrete. *Mater Constr* 2016;66(323). doi: 10.3989/mc.2016.07115.
- [55] De Belie N, Gruyaert E, Al-Tabbaa A, Antonaci P, Baera C, Bajare D, et al. A Review of Self-Healing Concrete for Damage Management of Structures. *Adv Mater Interfaces* 2018;5(17):1–28. doi: 10.1002/admi.201800074.
- [56] Araújo M, Chatrabhuti S, Gurdebeke S, Alderete N, Van Tittelboom K, Raquez JM, et al. Poly(methyl methacrylate) capsules as an alternative to the proof-of-concept'' glass capsules used in self-healing concrete. *Cem Concr Compos* 2018;89:260–71. doi: 10.1016/j.cemconcomp.2018.02.015.
- [57] Van Tittelboom K, Tsangouri E, Van Hemelrijck D, De Belie N. The efficiency of self-healing concrete using alternative manufacturing procedures and more realistic crack patterns. *Cem Concr Compos* 2015;57:142–52. doi: 10.1016/j.cemconcomp.2014.12.002.
- [58] Tsangouri E, Gilabert FA, De Belie N, Van Hemelrijck D, Zhu X, Aggelis DG. Concrete fracture toughness increase by embedding self-healing capsules using an integrated experimental approach. *Constr Build*

Mater 2019;218:424–33. doi: 10.1016/j.conbuildmat.2019.05.138.

- [59] Milla J, Hassan MM, Rupnow T, Daly WH. Measuring the crack-repair efficiency of steel fiber reinforced concrete beams with microencapsulated calcium nitrate. *Constr Build Mater* 2019;201:526–38. doi: 10.1016/j.conbuildmat.2018.12.193.
- [60] Van Tittelboom K, Wang J, Araújo M, Snoeck D, Gruyaert E, Debbaut B, et al. Comparison of different approaches for self-healing concrete in a large-scale lab test. *Constr Build Mater* 2016;107:125–37. doi: 10.1016/j.conbuildmat.2015.12.186.
- [61] Al-Tabbaa A, Litina C, Giannaros P, Kanellopoulos A, Souza L. First UK field application and performance of microcapsule-based self-healing concrete. *Constr Build Mater* 2019;208:669–85. doi: 10.1016/j.conbuildmat.2019.02.178.
- [62] Milla J, Hassan MM, Rupnow T. Evaluation of Self-Healing Concrete with Microencapsulated Calcium Nitrate. *J Mater Civ Eng* 2017;29(12). doi: 10.1061/(asce)mt.1943-5533.0002072.
- [63] Kanellopoulos A, Qureshi TS, Al-Tabbaa A. Glass encapsulated minerals for self-healing in cement based composites. *Constr Build Mater* 2015;98:780–91. doi: 10.1016/j.conbuildmat.2015.08.127.
- [64] Ferrara L, Van Mullem T, Alonso MC, Antonaci P, Borg RP, Cuenca E, et al. Experimental characterization of the self-healing capacity of cement based materials and its effects on the material performance: A state of the art report by COST Action SARCOS WG2. *Constr Build Mater* 2018;167:115–42. doi: 10.1016/j.conbuildmat.2018.01.143.
- [65] Roig-Flores M, Pirritano F, Serna P, Ferrara L. Effect of crystalline admixtures on the self-healing capability of early-age concrete studied by means of permeability and crack closing tests. *Constr Build Mater* 2016;114:447–57. doi: 10.1016/j.conbuildmat.2016.03.196.
- [66] Roig-Flores M, Moscato S, Serna P, Ferrara L. Self-healing capability of concrete with crystalline admixtures in different environments. *Constr Build Mater* 2015;86:1–11. doi: 10.1016/j.conbuildmat.2015.03.091.
- [67] Escoffres P, Desmettre C, Charron JP. Effect of a crystalline admixture on the self-healing capability of high-performance fiber reinforced concretes in service conditions. *Constr Build Mater* 2018;173:763–74. doi: 10.1016/j.conbuildmat.2018.04.003.
- [68] Azarsa P, Gupta R, Biparva A. Assessment of self-healing and

- durability parameters of concretes incorporating crystalline admixtures and Portland Limestone Cement. *Cem Concr Compos* 2019;99:17–31. doi: 10.1016/j.cemconcomp.2019.02.017.
- [69] Wang XF, Yang ZH, Fang C, Wang W, Liu J, Xing F. Effect of carbonate-containing self-healing system on properties of a cementitious composite: Fresh, mechanical, and durability properties. *Constr Build Mater* 2020;235. doi: 10.1016/j.conbuildmat.2019.117442.
- [70] Chandraiah M, Reddy TCS. Study on Strength Characteristics of Self-Healing Concrete with Crystalline Admixture. *Int J Innov Res Sci Eng Technol* 2020;6(1):1312–9. doi: 10.1016/j.matpr.2020.08.665.
- [71] Sideris KK, Chatzopoulos A, Tassos C, Manita P. Durability of concretes prepared with crystalline admixtures. *MATEC Web Conf* 2019;289. doi: 10.1051/mateconf/201928909003.
- [72] Xypex Concrete Waterproofing by Crystallization™. Available online: https://www.xypex.com/docs/default-source/default-document-library/english/xypex-catalogue.pdf?sfvrsn=e9df0169_66 (accessed on 24th March 2021).
- [73] Durable Concrete Starts with Penetron Admix. Available online: https://www.penetron.com/uploads/Penetron_Admix_Brochure.pdf (accessed on 12th February 2021).
- [74] Nasim M, Dewangan UK, Deo S V. Effect of crystalline admixture, fly ash, and PVA fiber on self-healing capacity of concrete. *Mater Today Proc* 2020; doi: 10.1016/j.matpr.2020.04.062.
- [75] Kannikachalam NP, Asensio EC, Brac EMG, Rosignoli R, De Belie N, Ferrara L. An Experimental Methodology To Assess Effects of Healing on Freeze-Thaw Damaged Ultra High-Performance Concrete. *fib Symp* 2022;280–7.
- [76] Kannikachalam NP, Summa D, Borg RP, Cuenca E, Parpanesi M, Belie N De, et al. Assessment of Sustainability and Self-Healing Performances of Recycled Ultra-High-Performance Concrete. *ACI Mater J* 2023;120(1). doi: 10.14359/51737336.
- [77] Niranjana Prabhu K, Vela DAC, Pacheco YGO, Monte F Lo, De Belie N, Ferrara L. Fatigue behavior and effect of stimulated autogenous self-healing in Ultra High-Performance Concrete. *fib Symp* 2022;297–304.
- [78] Wang X, Fang C, Li D, Han N, Xing F. A self-healing cementitious composite with mineral admixtures and built-in carbonate. *Cem Concr Compos* 2018;92:216–29. doi:

10.1016/j.cemconcomp.2018.05.013.

- [79] Rossi E, Vermeer CM, Mors R, Kleerebezem R, Copuroglu O, Jonkers HM. On the Applicability of a Precursor Derived from Organic Waste Streams for Bacteria-Based Self-Healing Concrete. *Front Built Environ* 2021;7(January):1–14. doi: 10.3389/fbuil.2021.632921.
- [80] Sadeghpour M, Baradaran M. Effect of bacteria on the self-healing ability of fly ash concrete. *Constr Build Mater* 2023;364(November 2022):129956. doi: 10.1016/j.conbuildmat.2022.129956.
- [81] Nezafat Tabalvandani M, Tajabadi-Ebrahimi M, Esfandi Sarafranz M, Akhavan Sepahi A. Investigation of self-healing properties in concrete with *Bacillus licheniformis* isolated from agricultural soil. *J Build Eng* 2023;67(January):106057. doi: 10.1016/j.jobe.2023.106057.
- [82] Shaheen N, Khushnood RA, Memon SA, Adnan F. Feasibility assessment of newly isolated calcifying bacterial strains in self-healing concrete. *Constr Build Mater* 2023;362(July 2022):129662. doi: 10.1016/j.conbuildmat.2022.129662.
- [83] Scrivener KL, Crumbie AK, Laugesen P. The interfacial transition zone (ITZ) between cement paste and aggregate in concrete. *Interface Sci* 2004;12(4):411–21. doi: 10.1023/B:INTS.0000042339.92990.4c.
- [84] Akhtar MK, Kanwal M, Khushnood RA, Khan MBE. Assessment of mechanical attributes and microstructural densification of self-healing recycled coarse aggregate concrete using various bacterial immobilizers. *J Build Eng* 2023;69(November 2022):106229. doi: 10.1016/j.jobe.2023.106229.
- [85] Chuo SC, Mohamed SF, Setapar SHM, Ahmad A, Jawaid M, Wani WA, et al. Insights into the current trends in the utilization of bacteria for microbially induced calcium carbonate precipitation. *Materials (Basel)* 2020;13(21):1–28. doi: 10.3390/ma13214993.
- [86] Chaerun SK, Syarif R, Wattimena RK. Bacteria incorporated with calcium lactate pentahydrate to improve the mortar properties and self-healing occurrence. *Sci Rep* 2020;10(1):1–9. doi: 10.1038/s41598-020-74127-4.
- [87] Vijay K, Murmu M. Effect of calcium lactate on compressive strength and self-healing of cracks in microbial concrete. *Front Struct Civ Eng* 2019;13(3):515–25. doi: 10.1007/s11709-018-0494-2.
- [88] Chen X, Yuan J, Alazhari M. Effect of Microbiological Growth Components for Bacteria-Based Self-Healing on the Properties of

Cement Mortar. *Materials (Basel)* 2019;12(8):1303.

- [89] Norambuena-Contreras J, Liu Q, Zhang L, Wu S, Yalcin E, Garcia A. Influence of encapsulated sunflower oil on the mechanical and self-healing properties of dense-graded asphalt mixtures. *Mater Struct Constr* 2019;52(4). doi: 10.1617/s11527-019-1376-3.
- [90] Al-Ansari M, Abu Taqa AG, Senouci A, Hassan MM, Shaat A. Effect of calcium nitrate healing microcapsules on concrete strength and air permeability. *Mag Concr Res* 2019;71(4):195–206. doi: 10.1680/jmacr.17.00435.
- [91] Litina C, Cao B, Chen J, Li Z, Papanikolaou I, Al-Tabbaa A. First UK Commercial Deployment of Microcapsule-Based Self-Healing Reinforced Concrete. *J Mater Civ Eng* 2021;33(6):1–15. doi: 10.1061/(asce)mt.1943-5533.0003702.
- [92] Mao W, Litina C, Al-Tabbaa A. Development and application of novel sodium silicate microcapsule-based self-healing oil well cement. *Materials (Basel)* 2020;13(2). doi: 10.3390/ma13020456.
- [93] Kanellopoulos A, Giannaros P, Al-Tabbaa A. The effect of varying volume fraction of microcapsules on fresh, mechanical and self-healing properties of mortars. *Constr Build Mater* 2016;122:577–93. doi: 10.1016/j.conbuildmat.2016.06.119.
- [94] Han T, Wang X, Li D, Li D, Xing F, Han N. Influence of strain rate on mechanical characteristic and pore structure of self-healing cementitious composites with epoxy/urea-formaldehyde microcapsules. *Constr Build Mater* 2021;268(xxxx):121138. doi: 10.1016/j.conbuildmat.2020.121138.
- [95] Du W, Yu J, He B, He Y, He P, Li Y, et al. Preparation and characterization of nano-SiO₂/paraffin/PE wax composite shell microcapsules containing TDI for self-healing of cementitious materials. *Constr Build Mater* 2020;231. doi: 10.1016/j.conbuildmat.2019.117060.
- [96] Du W, Yu J, Gu Y, Li Y, Han X, Liu Q. Preparation and application of microcapsules containing toluene-di-isocyanate for self-healing of concrete. *Constr Build Mater* 2019;202:762–9. doi: 10.1016/j.conbuildmat.2019.01.007.
- [97] Wang X, Liang J, Ren J, Wang W, Liu J, Xing F. Constitutive relations, mechanical behaviour, and failure criterion of microcapsule-based self-healing concrete under uniaxial and triaxial compression. *J Build Eng* 2023;65(November 2022):105773. doi:

10.1016/j.jobe.2022.105773.

- [98] Du W, Lin R, Liu Q. Investigation of isophorone diisocyanate microcapsules to improve self-healing properties and sulfate resistance of concrete. *Constr Build Mater* 2021;300(July):124438. doi: 10.1016/j.conbuildmat.2021.124438.
- [99] Van Mullem T, Anglani G, Dudek M, Vanoutrive H, Bumanis G, Litina C, et al. Addressing the need for standardization of test methods for self-healing concrete: an inter-laboratory study on concrete with macrocapsules. *Sci Technol Adv Mater* 2020;21(1):661–82. doi: 10.1080/14686996.2020.1814117.
- [100] Siahkouhi M, Han X, Wang M, Manalo A, Jing G. Development and performance evaluation of self-healing concrete railway sleepers using different size PU tubes. *Eng Struct* 2023;283(January):115920. doi: 10.1016/j.engstruct.2023.115920.
- [101] Sinha A, Lim DZH, Wei J. A lignin-based capsule system with tunable properties tailored for robust self-healing concrete. *Cem Concr Compos* 2022;132(June):104643. doi: 10.1016/j.cemconcomp.2022.104643.
- [102] Sinha A, Wang Q, Wei J. Feasibility and compatibility of a biomass capsule system in self-healing concrete. *Materials (Basel)* 2021;14(4):1–24. doi: 10.3390/ma14040958.
- [103] Hu ZX, Hu XM, Cheng WM, Zhao YY, Wu MY. Performance optimization of one-component polyurethane healing agent for self-healing concrete. *Constr Build Mater* 2018;179:151–9. doi: 10.1016/j.conbuildmat.2018.05.199.
- [104] Hermawan H, Minne P, Serna P, Gruyaert E. Understanding the Impacts of Healing Agents on the Properties of Fresh and Hardened Self-Healing Concrete: A Review. *Processes* 2021;9(12):2206. doi: 10.3390/pr9122206.
- [105] Alonso MM, Palacios M, Puertas F. Compatibility between polycarboxylate-based admixtures and blended-cement pastes. *Cem Concr Compos* 2013;35(1):151–62. doi: 10.1016/j.cemconcomp.2012.08.020.
- [106] Liu J, Wang K, Zhang Q, Han F, Sha J, Liu J. Influence of superplasticizer dosage on the viscosity of cement paste with low water-binder ratio. *Constr Build Mater* 2017;149:359–66. doi: 10.1016/j.conbuildmat.2017.05.145.

- [107] Pereira P, Evangelista L, de Brito J. The effect of superplasticizers on the mechanical performance of concrete made with fine recycled concrete aggregates. *Cem Concr Compos* 2012;34(9):1044–52. doi: <https://doi.org/10.1016/j.cemconcomp.2012.06.009>.
- [108] Bonen D, Sarkar SL. The superplasticizer adsorption capacity of cement pastes, pore solution composition, and parameters affecting flow loss. *Cem Concr Res* 1995;25(7):1423–34. doi: 10.1016/0008-8846(95)00137-2.
- [109] Kipkemboi B, Zhao T, Miyazawa S, Sakai E, Nito N, Hirao H. Effect of C3S content of clinker on properties of fly ash cement concrete. *Constr Build Mater* 2020;240:117840. doi: 10.1016/j.conbuildmat.2019.117840.
- [110] Andrade Neto J da S, De la Torre AG, Kirchheim AP. Effects of sulfates on the hydration of Portland cement – A review. *Constr Build Mater* 2021;279. doi: 10.1016/j.conbuildmat.2021.122428.
- [111] Ma Y, Qian J. Influence of alkali sulfates in clinker on the hydration and hardening of Portland cement. *Constr Build Mater* 2018;180:351–63. doi: 10.1016/j.conbuildmat.2018.05.196.
- [112] RESHEALIENCE. D4.1 – Recommendation on the use of crystalline admixtures, nanofibers, and nanocellulose for production of UHDC (accessed on 3rd September 2022). 2018.
- [113] Rodríguez CR, de Mendonça Filho FF, Mercuri L, Gan Y, Rossi E, Anglani G, et al. Chemo-physico-mechanical properties of the interface zone between bacterial PLA self-healing capsules and cement paste. *Cem Concr Res* 2020;138(September):106228. doi: 10.1016/j.cemconres.2020.106228.
- [114] Vasanelli E, Colangiuli D, Calia A, Sileo M, Aiello MA. Ultrasonic pulse velocity for the evaluation of physical and mechanical properties of a highly porous building limestone. *Ultrasonics* 2015;60:33–40. doi: 10.1016/j.ultras.2015.02.010.
- [115] Zhang Y, Zhang W, She W, Ma L, Zhu W. Ultrasound monitoring of setting and hardening process of ultra-high performance cementitious materials. *NDT E Int* 2012;47:177–84. doi: 10.1016/j.ndteint.2009.10.006.
- [116] Ye G, Lura P, Van Breugel K, Fraaij ALA. Study on the development of the microstructure in cement-based materials by means of numerical simulation and ultrasonic pulse velocity measurement. *Cem Concr Compos* 2004;26(5):491–7. doi: 10.1016/S0958-9465(03)00081-7.

- [117] Wallevik OH, Feys D, Wallevik JE, Khayat KH. Avoiding inaccurate interpretations of rheological measurements for cement-based materials. *Cem Concr Res* 2015;78:100–9. doi: 10.1016/j.cemconres.2015.05.003.
- [118] Alonso MM, Puertas F. Adsorption of PCE and PNS superplasticisers on cubic and orthorhombic C3A. Effect of sulfate. *Constr Build Mater* 2015;78:324–32. doi: 10.1016/j.conbuildmat.2014.12.050.
- [119] Yoshioka K, Tazawa EI, Kawai K, Enohata T. Adsorption characteristics of superplasticizers on cement component minerals. *Cem Concr Res* 2002;32(10):1507–13. doi: 10.1016/S0008-8846(02)00782-2.
- [120] Mourabet M, El Boujaady H, El Rhilassi A, Ramdane H, Bennani-Ziatni M, El Hamri R, et al. Defluoridation of water using Brushite: Equilibrium, kinetic and thermodynamic studies. *Desalination* 2011;278(1–3):1–9. doi: 10.1016/j.desal.2011.05.068.
- [121] Jun Y, Ahn YR, Jeon D, Yim HJ. Nondestructive Evaluation for Hydration and Setting Time of Gypsum Modified Calcium Sulfoaluminate Cement Paste. *Materials (Basel)* 2023;16(3). doi: 10.3390/ma16030920.
- [122] Lin YC, Lin Y, Cheng CC. A Unified Equation for Prediction of Concrete Strength at Various Ages Using the Ultrasonic Pulse Velocity. *Appl Sci* 2022;12(17). doi: 10.3390/app12178416.
- [123] Lothenbach B, Winnefeld F, Figi R. The influence of superplasticizers on the hydration of Portland cement B. Lothenbach, F. Winnefeld, R. Figi Empa, Dübendorf, Switzerland; In: International Congress on the Chemistry of Cement (ICCC) 2007. p. 1–12.
- [124] Paine K, Alazhari M, Sharma T, Cooper R, Heath A. Design and performance of bacteria-based self-healing concrete. In: The 9th International Concrete Conference 2016: Environment, Efficiency and Economic Challenges for Concrete 2016. p. 545–54.
- [125] Belgium Bureau for Standardisation, NBN B 15-001:2018 - Concrete - Specification, performance, production and conformity - National supplement to NBN EN 206:2013+A1:2016. Belgium, 2018.
- [126] European Committee for Standardization, EN 206:2014 - Concrete - Specification, performance, production and conformity. Brussels, Belgium: European Committee for Standardization, 2014.
- [127] Action CA15202 — Self-Healing as Preventive Repair of Concrete Structures. 2016 – 2021 European Cooperation in Science and

Technology (COST) (accessed on 6th September 2022) [Internet]. 2021.

- [128] Manhanga FC, Rudžionis Ž, Ivanauskas E, Augonis A. The investigations on properties of self-healing concrete with crystalline admixture and recycled concrete waste. *MATEC Web Conf* 2022;364:05002. doi: 10.1051/mateconf/202236405002.
- [129] Kirby DM, Biernacki JJ. The effect of water-to-cement ratio on the hydration kinetics of tricalcium silicate cements: Testing the two-step hydration hypothesis. *Cem Concr Res* 2012;42(8):1147–56. doi: 10.1016/j.cemconres.2012.05.009.
- [130] Tsukamoto M., J.-D. W. Permeability of cracked fibre-reinforced concrete. *Darmstadt Concr* 1991;(6):123–35.
- [131] Li X, Li D, Xu Y. Modeling the effects of microcracks on water permeability of concrete using 3D discrete crack network. *Compos Struct* 2019;210(November 2018):262–73. doi: 10.1016/j.compstruct.2018.11.034.
- [132] Lee KM, Kim HS, Lee DK, Shin KJ. Self-healing performance evaluation of concrete incorporating inorganic materials based on a water permeability test. *Materials (Basel)* 2021;14(12). doi: 10.3390/ma14123202.
- [133] Galván-Ruiz M, Hernández J, Baños L, Noriega-Montes J, Rodríguez-García ME. Characterization of Calcium Carbonate, Calcium Oxide, and Calcium Hydroxide as Starting Point to the Improvement of Lime for Their Use in Construction. *J Mater Civ Eng* 2009;21(11):694–8. doi: 10.1061/(asce)0899-1561(2009)21:11(694).
- [134] Kusuktham B. Spinning of PET Fibres Mixed with Calcium Carbonate. *Asian J Text* 2011;1(2):106–13.
- [135] Munawaroh F, Muharrami LK, . T, Arifin Z. Synthesis and Characterization of Precipitated CaCO₃ from Ankerite Prepared by Bubbling Method. *KnE Eng* 2019;1(2):98. doi: 10.18502/keg.v1i2.4435.
- [136] Chakrabarty D, Mahapatra S. Aragonite crystals with unconventional morphologies. *J Mater Chem* 1999;9(11):2953–7. doi: 10.1039/a905407c.
- [137] Wada N, Horiuchi N, Nakamura M, Nozaki K, Nagai A, Yamashita K. Controlled crystallization of calcium carbonate via cooperation of polyaspartic acid and polylysine under double-diffusion conditions in

- agar hydrogels. *ACS Omega* 2018;3(12):16681–92. doi: 10.1021/acsomega.8b02445.
- [138] El-Shahate Ismaiel Saraya M, Hassan Abdel Latif Rokbaa H. Preparation of Vaterite Calcium Carbonate in the Form of Spherical Nano-size Particles with the Aid of Polycarboxylate Superplasticizer as a Capping Agent. *Am J Nanomater* 2016;4(2):44–51. doi: 10.12691/ajn-4-2-3.
- [139] Siva T, Muralidharan S, Sathiyarayanan S, Manikandan E, Jayachandran M. Enhanced Polymer Induced Precipitation of Polymorphous in Calcium Carbonate: Calcite Aragonite Vaterite Phases. *J Inorg Organomet Polym Mater* 2017;27(3):770–8. doi: 10.1007/s10904-017-0520-1.
- [140] Matei C, Berger D, Dumbrava A, Radu MD, Gheorghe E. Calcium carbonate as silver carrier in composite materials obtained in green seaweed extract with topical applications. *J Sol-Gel Sci Technol* 2020;93(2):315–23. doi: 10.1007/s10971-019-05145-6.
- [141] Ghosh I, Sharma C, Tandon R. Structural evaluation of chitosan-modified precipitated calcium carbonate composite fillers for papermaking applications. *SN Appl Sci* 2020;2(9):1–14. doi: 10.1007/s42452-020-03313-w.
- [142] Mousavi SS, Ouellet-Plamondon CM, Guizani L, Bhojaraju C, Brial V. On mitigating rebar–concrete interface damages due to the pre-cracking phenomena using superabsorbent polymers. *Constr Build Mater* 2020;253:119181. doi: 10.1016/j.conbuildmat.2020.119181.
- [143] Mousavi SS, Guizani L, Bhojaraju C, Ouellet-Plamondon C. The effect of air-entraining admixture and superabsorbent polymer on bond behaviour of steel rebar in pre-cracked and self-healed concrete. *Constr Build Mater* 2021;281:122568. doi: 10.1016/j.conbuildmat.2021.122568.
- [144] Mousavi SS, Guizani L, Bhojaraju C, Ouellet-Plamondon CM. Application of Superabsorbent Polymer as Self-Healing Agent in Self-Consolidating Concrete for Mitigating Precracking Phenomenon at the Rebar–Concrete Interface. *J Mater Civ Eng* 2021;33(10).
- [145] Dewar J. Computer Modelling of Concrete Mixtures. *Computer Modelling of Concrete Mixtures*. 1999. doi: 10.4324/9780203031148.
- [146] Concrete B. Basilisk info, no. 1 - crystalline products EN (accessed on 17th August 2022) [Internet].

- [147] Roy R, Rossi E, Silfwerbrand J, Jonkers H. Self-healing capacity of mortars with added-in bio-plastic bacteria-based agents: Characterization and quantification through micro-scale techniques. *Constr Build Mater* 2021;297:123793. doi: 10.1016/j.conbuildmat.2021.123793.
- [148] Desnerck P, Lees JM, Morley CT. Bond behaviour of reinforcing bars in cracked concrete. *Constr Build Mater* 2015;94(10):126–36. doi: 10.1016/j.conbuildmat.2015.06.043.
- [149] Brantschen F, Faria DMV, Fernández Ruiz M, Muttoni A. Bond behaviour of straight, hooked, U-shaped and headed bars in cracked concrete. *Struct Concr* 2016;17(5):799–810. doi: 10.1002/suco.201500199.
- [150] RILEM TC. Bond test for reinforcing steel: 2. Pull-out test. *Mater Struct* 1970;3(15):175–8.
- [151] Mousavi SS. Effect of concrete composition and self-healing method on bond behaviour of cracked normal concrete and self-consolidating concrete. *École de technologie supérieure*; 2020.
- [152] Mousavi SS, Dehestani M, Mousavi KK. Bond strength and development length of steel bar in unconfined self-consolidating concrete. *Eng Struct* 2017;131:587–98. doi: 10.1016/j.engstruct.2016.10.029.
- [153] Wu Y-F, Zhao X-M. Unified Bond Stress–Slip Model for Reinforced Concrete. *J Struct Eng* 2013;139(11):1951–62. doi: 10.1061/(asce)st.1943-541x.0000747.
- [154] Esfahani MR, Kianoush MR. Development/splice length of reinforcing bars. *ACI Struct J* 2005;102(1):22–30. doi: 10.14359/13527.
- [155] Idda K. *Verbundverhalten von Betonrippenstählen bei Querkzug*. Institut für Massivbau und Baustofftechnologie (IMB); 1999.
- [156] Purainer R. *Last- und Verformungsverhalten von Stahlbetonflächentragwerken unter zweiachsender Zugbeanspruchung*. Universität der Bundeswehr München; 2005.
- [157] Gambarova PG, Rosati GP, Zasso B. Steel-to-concrete bond after concrete splitting: test results. *Mater Struct* 1989;22(1):35–47. doi: 10.1007/BF02472693.
- [158] Gambarova PG, Rosati GP, Zasso B. Steel-to-concrete bond after concrete splitting: constitutive laws and interface deterioration.

Mater Struct 1989;22(5):347–56. doi: 10.1007/BF02472505.

- [159] Mahrenholtz C. Seismic Bond Model for Concrete Reinforcement and the Application to Column-to Foundation Connections. Universität Stuttgart; 2012.
- [160] Mousavi SS, Guizani L, Ouellet-Plamondon CM. On bond-slip response and development length of steel bars in pre-cracked concrete. Constr Build Mater 2019;199:560–73. doi: 10.1016/j.conbuildmat.2018.12.039.
- [161] Mousavi SS, Guizani L, Ouellet-Plamondon CM. Simplified Analytical Model for Interfacial Bond Strength of Deformed Steel Rebars Embedded in Pre-cracked Concrete. J Struct Eng 2020;146(8):1–15. doi: 10.1061/(asce)st.1943-541x.0002687.
- [162] Taguchi G. Introduction to Taguchi methods. Eng 1988;228(1).
- [163] Peace GS. Taguchi Methods: A Hands-on Approach. New York: Addison-Wesley; 1993.
- [164] Lochner RH, Matar JE. Designing for quality: an introduction to the Best of Taguchi and Western methods of statistical experimental design. London: Chapman and Hall; 1990.
- [165] Dhemia P, Somani P, Swami BL, Gaur A. Optimizing the design of sintered fly ash light weight concrete by Taguchi and ANOVA analysis. Mater Today Proc 2022;62:495–503. doi: 10.1016/j.matpr.2022.03.573.
- [166] Panda S, Sarkar P. Abrasion resistance of copper slag aggregate concrete designed by Taguchi method. Mater Today Proc 2022;65:434–41. doi: 10.1016/j.matpr.2022.02.545.
- [167] Durgun MY, Sevinç AH. Determination of the effectiveness of various mineral additives against sodium and magnesium sulfate attack in concrete by Taguchi method. J Build Eng 2022;57(June):104849. doi: 10.1016/j.jobe.2022.104849.
- [168] Zhang G, Ying W, Li G, Yang Y, He T. Study of the defrosting behavior of concrete by using Taguchi-based grey relational analysis method. Constr Build Mater 2022;321(April 2021):126324. doi: 10.1016/j.conbuildmat.2022.126324.
- [169] Chokkalingam P, El-Hassan H, El-Dieb A, El-Mir A. Development and characterization of ceramic waste powder-slag blended geopolymer concrete designed using Taguchi method. Constr Build Mater

2022;349(August):128744. doi: 10.1016/j.conbuildmat.2022.128744.

- [170] Bakhbergen U, Shon CS, Zhang D, Ryeol Kim J, Liu J. Optimization of mixture parameter for physical and mechanical properties of reactive powder concrete under external sulfate attack using Taguchi method. *Constr Build Mater* 2022;352(August):129023. doi: 10.1016/j.conbuildmat.2022.129023.
- [171] Sharifi E, Sadjadi SJ, Aliha MRM, Moniri A. Optimization of high-strength self-consolidating concrete mix design using an improved Taguchi optimization method. *Constr Build Mater* 2020;236:117547. doi: 10.1016/j.conbuildmat.2019.117547.
- [172] Kamalakannan R, Pradeep GM, NaveenKumar T, Elango M. Machining parameters in WEDM of EN31 steel using Taguchi technique optimization. *Mater Today Proc* 2021;50:1781–5. doi: 10.1016/j.matpr.2021.09.196.
- [173] Dhote N, Khond M, Sankpal R. Wear material determination and parameters optimization of an external gear pump by Taguchi technique. *Mater Today Proc* 2022;c(xxxx). doi: 10.1016/j.matpr.2022.08.374.
- [174] Lagzian M, Ehsan Razavi S, Goharimanesh M. Investigation on tumor cells growth by Taguchi method. *Biomed Signal Process Control* 2022;77(May 2021):103734. doi: 10.1016/j.bspc.2022.103734.
- [175] Madian HR, Hamouda HI, Hosny M. Statistical optimization of bioethanol production from giant reed hydrolysate by *Candida tropicalis* using Taguchi design. *J Biotechnol* 2022;360(October):71–8. doi: 10.1016/j.jbiotec.2022.10.007.
- [176] Vu VD, Nguyen TT, Chu NH, Ngo QH, Ho KT, Nguyen V Du. Multiresponse optimization of cutting force and cutting power in chopping agricultural residues using grey-based Taguchi method. *Agric* 2020;10(3). doi: 10.3390/agriculture10030051.
- [177] Gabryelczyk A, Ivanov S, Bund A, Lota G. Taguchi method in experimental procedures focused on corrosion process of positive current collector in lithium-ion batteries. *Electrochim Acta* 2020;360:137011. doi: 10.1016/j.electacta.2020.137011.
- [178] de Souza Oliveira A, da Fonseca Martins Gomes O, Ferrara L, de Moraes Rego Fairbairn E, Toledo Filho RD. An overview of a twofold effect of crystalline admixtures in cement-based materials: from permeability-reducers to self-healing stimulators. *J Build Eng* 2021;41(November 2020). doi: 10.1016/j.jobe.2021.102400.

- [179] Mousavi SS, Mousavi Ajarostaghi SS, Bhojaraju C. A critical review of the effect of concrete composition on rebar–concrete interface (RCI) bond strength: A case study of nanoparticles. *SN Appl Sci* 2020;2(5):1–23. doi: 10.1007/s42452-020-2681-8.
- [180] Hermawan H, Wiktor V, Gruyaert E, Serna P. Experimental investigation on the bond behaviour of steel reinforcement in self-healing concrete. *Constr Build Mater* 2023;383(April):131378. doi: 10.1016/j.conbuildmat.2023.131378.
- [181] Hermawan H, Wiktor V, Serna P, Gruyaert E. Experimental Investigation on the Novel Self-healing Properties of Concrete Mixed with Commercial Bacteria-Based Healing Agent and Crystalline Admixtures. In: *International RILEM Conference on Synergising Expertise towards Sustainability and Robustness of Cement-based Materials and Concrete Structures SynerCrete 2023* Springer; 2023. p. 841–52. doi: 10.1007/978-3-031-33187-9.
- [182] Hermawan H, Beltran GS, Wiktor V, Serna P, Gruyaert E. Effect of healing agents on the rheological properties of cement paste and compatibility with superplasticizer. *MATEC Web Conf* 2022;5008(361).
- [183] Hermawan H, Minne P, Brac EG, Wiktor V, Serna Ros P, Gruyaert E. Influence of Crystalline Admixtures and Bacteria on the Fresh Properties of Self-healing Concrete. In: *Proceedings of the 75th RILEM Annual Week 2021, RW 2021* Springer International Publishing; 2023. p. 451–60. doi: 10.1007/978-3-031-21735-7_50.
- [184] Cadessa AS, Zephir D. Effect of Penetron Admix on the Properties of Concrete. *Univ Mauritius Res J* 2014;20. doi: 10.3390/polym9120672.
- [185] Neverkovic D, Korjakins A. Influence of Additives on Reinforced Concrete Durability. *Constr Sci* 2015;16(1):21–6. doi: 10.1515/cons-2014-0009.
- [186] Ferrara L, Krelani V, Carsana M. A “fracture testing” based approach to assess crack healing of concrete with and without crystalline admixtures. *Constr Build Mater* 2014;68:535–51. doi: 10.1016/j.conbuildmat.2014.07.008.
- [187] Dong B, Fang G, Ding W, Liu Y, Zhang J, Han N, et al. Self-healing features in cementitious material with urea-formaldehyde/epoxy microcapsules. *Constr Build Mater* 2016;106:608–17. doi: 10.1016/j.conbuildmat.2015.12.140.

- [188] Xue C, Li W, Li J, Tam VWY, Ye G. A review study on encapsulation-based self-healing for cementitious materials. *Struct Concr* 2019;20(1):198–212. doi: 10.1002/suco.201800177.
- [189] Riordan C, Palmer D, Al-tabbaa A. Investigation of Membrane Emulsification for the Scaled Production of Microcapsules for Self-sealing Cementitious Systems. In: *MATEC Web of Conferences EDP Sciences*; 2023.
- [190] Wang JY, Soens H, Verstraete W, De Belie N. Self-healing concrete by use of microencapsulated bacterial spores. *Cem Concr Res* 2014;56:139–52. doi: 10.1016/j.cemconres.2013.11.009.
- [191] Cao VD, Pilehvar S, Salas-Bringas C, Szczotok AM, Valentini L, Carmona M, et al. Influence of microcapsule size and shell polarity on thermal and mechanical properties of thermoregulating geopolymer concrete for passive building applications. *Energy Convers Manag* 2018;164(February):198–209. doi: 10.1016/j.enconman.2018.02.076.
- [192] Zhou G, Jiang W, Li S, Liu R, Zhang Q, Qi G, et al. Preparation and performance analysis of dopamine hydrochloride functionalized E-51@MPF/SiO₂ double-wall microcapsules for microcracks self-healing in cement-based materials. *Constr Build Mater* 2022;325(November 2021):126622. doi: 10.1016/j.conbuildmat.2022.126622.
- [193] Ma Y, Ge Y, Wu R, Huang H, Chen G, Xu Y, et al. Mechanical behavior and self-healing mechanism of force-chloride ion triggered double-walled microcapsule/cement-based composites. *Constr Build Mater* 2022;340(January):127765. doi: 10.1016/j.conbuildmat.2022.127765.
- [194] Li X, Liu R, Li S, Zhang C, Yan J, Liu Y, et al. Properties and mechanism of self-healing cement paste containing microcapsule under different curing conditions. *Constr Build Mater* 2022;357(September):129410. doi: 10.1016/j.conbuildmat.2022.129410.
- [195] Dong B, Fang G, Wang Y, Liu Y, Hong S, Zhang J, et al. Performance recovery concerning the permeability of concrete by means of a microcapsule based self-healing system. *Cem Concr Compos* 2017;78:84–96. doi: 10.1016/j.cemconcomp.2016.12.005.
- [196] Zhang SP, Zong L. Evaluation of relationship between water absorption and durability of concrete materials. *Adv Mater Sci Eng* 2014;2014. doi: 10.1155/2014/650373.

- [197] Powers TC. *The Properties of Fresh Concrete* [Internet]. New York: John Wiley & Sons; 1968.
- [198] De Larrard F. *Concrete mixture proportioning: a scientific approach*. Taylor and Francis; 1999.
- [199] Anglani G, Van Mullem T, Tulliani J-M, Van Tittelboom K, De Belie N, Antonaci P. Durability of self-healing cementitious systems with encapsulated polyurethane evaluated with a new pre-standard test method. *Mater Struct* 2022;55(5):1–16. doi: 10.1617/s11527-021-01818-3.
- [200] Chu SH, Jiang Y, Kwan AKH. Effect of rigid fibres on aggregate packing. *Constr Build Mater* 2019;224:326–35. doi: 10.1016/j.conbuildmat.2019.07.072.
- [201] Liu S, Minne P, Lulić M, Li J, Gruyaert E. Implementation and validation of Dewar’s particle packing model for recycled concrete aggregates. *Constr Build Mater* 2021;294. doi: 10.1016/j.conbuildmat.2021.123429.
- [202] da Rocha Gomes S, Kumar PA, Rengaraju S, Al-Tabbaa A, Ferrara L, Sánchez L, et al. Assessment of autonomous and autogenous healing on cementitious grouts promoted by additions of microcapsules and crystalline admixtures. *MATEC Web Conf* 2023;378:07001. doi: 10.1051/mateconf/202337807001.

CURRICULUM VITAE

Harry Hermawan
23rd October 1993, Sumedang, Indonesia

Education

PhD in Engineering Technology (KU Leuven, Belgium)
PhD in Construction Engineering (UPV, Spain)
September 2020 – December 2023

MSc in Civil and Construction Engineering (NTUST, Taiwan)
September 2016 – September 2018

BSc in Civil Engineering (Parahyangan Catholic University, Indonesia)
August 2011 – February 2015

Professional experience

Research Associate at Department of Civil Engineering, Materials and
Constructions, KU Leuven – Ghent, Belgium
September 2020 – September 2023

Supervisor Engineering at PT. Surya TOTO Indonesia Tbk., Indonesia
February – June 2019

Estimator at PT. Total Bangun Persada Tbk., Indonesia
April 2015 – July 2016

Foreign research visit

Visiting researcher at Buzzi Unicem (BUILT), Italy
April – May 2023

Guest lecturer at Parahyangan Catholic University, Indonesia
January 2023

Visiting researcher at UPV, Spain
May – July 2021, May – July 2022

Visiting researcher at Cugla b.v., the Netherlands
September – October 2021

Teaching experience

Co-supervisor of 2 MSc theses, Department of Civil Engineering, KU Leuven – Ghent
September 2020 – December 2023

Teaching assistant of 17 BSc students in the course of *Seminars Professional Competences (Introduction to Research)*, Department of Civil Engineering, KU Leuven – Ghent
September 2020 – December 2023

English teacher of NTUST Digital Learning Partnership (DLP) project in Taiwan
April – June 2018

Grants and awards

Best Interdisciplinary Research Award at International SynerCrete'23 conference in Milos, Greece
June 2023

Marie Skłodowska-Curie Actions – Innovative Training Networks (MSCA-ITN) Fellowship, European Commission
September 2020 – September 2023

Best Paper Presentation at International Conference on Civil Engineering in
Danang, Vietnam
May 2018

NTUST College of Engineering Excellent Youth
December 2017

Publications

Journal papers

- [1] Hermawan H, Wiktor V, Gruyaert E, Serna P. Optimization of concrete mix designs toward the bond properties of steel reinforcement in self-healing concrete by Taguchi method. *J Build Eng* 2023. <https://doi.org/10.1016/j.jobe.2023.107294>
- [2] Hermawan H, Wiktor V, Gruyaert E, Serna P. Experimental investigation on the bond behaviour of steel reinforcement in self-healing concrete. *Constr Build Mater* 2023;383:131378. <https://doi.org/10.1016/j.conbuildmat.2023.131378>
- [3] Hermawan H, Minne P, Serna P, Gruyaert E. Understanding the Impacts of Healing Agents on the Properties of Fresh and Hardened Self-Healing Concrete: A Review. *Processes* 2021;9(12):2206. <https://doi.org/10.3390/pr9122206>
- [4] Hermawan H, Wiktor V, Serna P, Gruyaert E. Modification of concrete mix design with crystalline admixture for self-healing improvement. *J Adv Concr Technol* 2023. (*submitted*)
- [5] Hermawan H, Serna P, Van Der Sichel S, Lust L, Riordan C, Palmer D, Al-Tabbaa A, Gruyaert E. Mix design optimisation of self-sealing concrete containing microcapsules with PU shell and water repellent cargo. 2023. (*under review*)
- [6] Hermawan H, Simons A, Teirlynck S, Serna P, Minne P, Anglani G, Tulliani JM, Antonaci P, Gruyaert E. Prediction of aggregate packing with tubular macrocapsules in the inert structure of self-healing concrete based on the Dewar's particle packing model. 2023. (*under review*)

Conference papers

- [1] Hermawan H, Wiktor V, Serna P, Gruyaert E. Experimental investigation on the novel self-healing properties of concrete mixed with commercial bacteria-based healing agent and crystalline admixtures. In: Proceedings of the SynerCrete'23, Springer International Publishing; 2023. https://doi.org/10.1007/978-3-031-33187-9_77
- [2] Hermawan H, Simons A, Teirlynck S, Serna P, Minne P, Anglani G, Tulliani JM, Antonaci P, Gruyaert E. Applicability of cementitious capsules in concrete production: initial assessment on capsule robustness , mechanical and self- sealing properties of concrete. In: MATEC Web of Conferences EDP Sciences; 2023. <https://doi.org/10.1051/matecconf/202337802013>
- [3] Hermawan H, Tezer MM, Verstraete W, Belie N De, Serna P, Gruyaert E. Bond behaviour evaluation between steel reinforcement and self-healing concrete containing non-axenic biomasses. In: MATEC Web of Conferences EDP Sciences; 2023. <https://doi.org/10.1051/matecconf/202337802009>
- [4] Hermawan H, Beltran GS, Wiktor V, Serna P, Gruyaert E. Effect of healing agents on the rheological properties of cement paste and compatibility with superplasticizer. MATEC Web Conf 2022;5008(361). <https://doi.org/10.1051/matecconf/202236105008>
- [5] Hermawan H, Minne P, Brac EG, Wiktor V, Serna Ros P, Gruyaert E. Influence of Crystalline Admixtures and Bacteria on the Fresh Properties of Self-healing Concrete. In: Proceedings of the 75th RILEM Annual Week 2021, RW 2021 Springer International Publishing; 2023. p. 451–60. https://doi.org/10.1007/978-3-031-21735-7_50
- [6] Hermawan H, Ta-Peng C, Yu-Chen W. Strengths development of slag-based paste with CFBC fly ash under different curing conditions. In: Proceedings of the Structures18; 2018. http://www.iasem.org/publication_conf/structures18/7.ICACC18/T5E.1.CC1502_464_8F1.pdf
- [7] Hermawan H, Ta-Peng C, Djayaprabha HS, Hoang-Anh N. Effect of elevated temperature on engineering properties of ternary blended no-cement mortar. In: MATEC Web of Conferences EDP Sciences; 2018. <https://doi.org/10.1051/matecconf/201820602008>

Active conference participations

- [1] Oral presentation at International Conference on Advances in Sustainable Construction Materials and Structures – 75th RILEM Annual Week 2021 on 29 August – 3 September 2021, Merida, Mexico.
- [2] Oral presentation at 8th International Conference on Self-Healing Materials (ICSHM) 2022 on 20–22 June 2022, Milan, Italy.
- [3] Oral presentation at 8th International Conference on Concrete Repair, Technology and Durability – Concrete Solutions 2022 on 11–13 July 2022, Leeds, UK.
- [4] Oral presentation at SMARTINCS'23 Conference on Self-Healing, Multifunctional and Advanced Repair Technologies in Cementitious Systems on 22–23 May 2023, Ghent, Belgium.
- [5] Oral presentation at International RILEM Conference on Synergizing Expertise towards Sustainability and Robustness of Cement-based Materials and Concrete Structures (SynerCrete'23) on 14–16 June 2023, Milos, Greece.

Contributions in internal SMARTINCS reports

- [1] Deliverable 1.1: Self-healing mix design optimization tool
- [2] Deliverable 1.2: Report and models on the improved self-healing concrete developments
- [3] Deliverable 1.3: Report and models on the performance of improved self-healing concrete systems
- [4] Deliverable 1.5: Report summarizing the PhD project works of WP 1 + PhD degrees ESR1-5
- [5] Deliverable 4.1: Valorization opportunity identification after screening of the research projects
- [6] Deliverable 4.2: Determination of commercialization routes for self-healing, multifunctional, advanced, repair technologies in cementitious systems
- [7] Deliverable 4.3: Final exploitation plan and practitioner's guideline
- [8] Deliverable 5.2: Personal career development plan (PCDP) for each ESR
- [9] Deliverable 5.3: Yearly ESR progress (I)

- [10] Deliverable 5.4: Yearly ESR progress (II)
- [11] Deliverable 5.5: Yearly ESR progress (III)
- [12] Deliverable 7.9: Update of the data management plan
- [13] Milestone 9: Scaled up production of newly developed self-healing systems
- [14] Milestone 10: Mix design tool ready for use by consortium partners
- [15] Milestone 13: Identification of optimum systems for exploration in full scale trial application